ANTIBACTERIAL, ANTIDERMATOPHYTIC AND CYTOTOXIC SECONDARY METABOLITES FROM *Bersama abyssinica* subsp. *abyssinica*, subsp. *paulliniodes* AND THEIR ENDOPHYTIC FUNGI

DIVINAH KWAMBOKA NYAMBOKI

A Thesis Submitted to the Graduate School in Partial Fulfillment of the Requirements for the Doctor of Philosophy Degree in Chemistry of Egerton University

EGERTON UNIVERSITY

JUNE, 2024

DECLARATION AND RECOMMENDATION

Declaration

This thesis is my original work and has not been presented in this university or any other for the award of a degree

Signature: ----  ---------- Date: 24/05/2024 ----------

Divinah Kwamboka Nyamboki

SD11/22005/18

Recommendation

This thesis has been submitted with our approval as University supervisors

Signature: --  -------- Date**:** 27/05/2024 ----------

Prof. Josphat C. Matasyoh

Department of Chemistry

Egerton University

Signature: -----  ---------- Date**:** 27/05/2024 ----------

Prof. Dr. Michael Spiteller

Department of Chemistry and Chemical Biology

Technical University of Dortmund

COPYRIGHT

.

DEDICATION

I dedicate this work to my parents, Mr. Duncan Nyamboki and Mrs. Teresah Nyamboki.

ACKNOWLEDGEMENTS

First and above all, I want to praise the Almighty God for His blessings and for giving me the ability and good health to complete this research successfully. My sincere gratitude goes to my supervisors Professor Josphat Matasyoh and Prof. Dr. Michael Spiteller for their guidance and support throughout this research. I would like to express my gratitude to the German Academic Exchange Service (DAAD) and the German Ministry of Education and Research (BMBF) under the "Partnership for Sustainable Solution in Sub-Saharan Africa" grant number SSA2015-33-074 for financing part of this research. Gratitude to Horizon 2020 Framework Programme Grant number 101008129 –Mycobiomics for financing part of this research. My appreciation to Egerton University for giving me the opportunity to undertake my P.h.D studies. My heartfelt appreciation goes to the Chemistry department of Egerton University for the help and guidance I received during my P.h.D studies. I acknowledge the Alexander von Humboldt Foundation for the fellowship award they granted me to do this research. My profound gratitude also goes to Dortmund University where part of the work was carried out including NMR, X-ray, and mass analysis of the isolated secondary metabolites in this study. I am grateful to the Department of Microbial Drugs, Helmholtz Centre for Infection Research, Braunschweig, Germany and the German Centre for Infection Research (DZIF), partner site Hannover-Braunschweig, Braunschweig, Germany where the antibacterial and cytotoxicity assays were carried out. I am also grateful to the Institute of Microbiology (IMIC), Czech Academy of Sciences, Prague, where the antifungal assays were carried out. A lot of thanks to Dr. Kibrom Gebreheiwot Bedane for the guidance and assistance he gave during my stay at Dortmund University. I am grateful to the late Prof. S.T. Kariuki, Department of Biological Sciences, Egerton University for his taxonomic expertise in the identification of the plant specimens used in this research. I finally thank my friends and colleagues, Lucy Wanga, Dr. Caroline Kosgei, and David Muthama for their support during this research.

ABSTRACT

Infectious and non-infectious diseases have caused a huge burden to the affected people as well as the healthcare systems across the globe. Antimicrobial resistance is on the rise and becoming a major threat in the efforts to treat diseases. Medicinal plants and fungi offer alternative solutions to this challenge and *Bersama abyssinica* is one of the plants used for treatment of various diseases such as tumors, dysentery, and roundworm infestation. This study aimed to isolate secondary metabolites from the stem barks and leaves of two subsp. of *B. abyssinica* and their endophytic fungi. The stem bark and leaves of the two subsp. of *B. abyssinica* were collected from Mt. Elgon National Forest. A portion of the collected plant materials was used for fungal endophyte isolation while the other portion was dried for extraction of secondary metabolites. The isolated pure fungal endophytes were subjected to fermentation on solid media followed by subsequent extraction of secondary metabolites. The extracts from both plant material and endophytic fungi were subjected to fractionation using column chromatography over silica gel and Sephadex LH-20 followed by further purification by High-Performance Liquid Chromatography (HPLC). Structure elucidation of pure compounds was done using a combination of spectroscopic techniques that include 1D and 2D NMR spectroscopy and Liquid Chromatography Mass Spectrometry. The relative configurations were defined by single-crystal X-ray crystallography and Nuclear Overhauser Effect Spectroscopy (NOESY) correlations. Structures for thirty compounds (**17** – **46**) were successfully elucidated with eight previously undescribed compounds (**17** – **19**, **33** – **36**, and **41**). Paulliniogenin A (**17**), 16*β*-hydroxybersamagenin 1,3,5-orthoacetate (**20**), 1*β*-acetoxy-3*β*,5*β*-dihydroxy-15-methoxy-16,19-dioxobufa-14(15),20,22-trienolide (**35**), epicocconigrone A (**44**) showed cytotoxic activities against Hela (KB3.1) cell lines with IC_{50} in the range of 1.4 ± 0.77 µM and 5.9 ± 1.89 µM. 1,2,3,6-tetra-*O*-galloyl-β-D-glucose (**24**), epicoccolide B (**43**), epicocconigrone A (**44**) and eleganketal A (**45**) showed weak cytotoxicity ranging between 11.7 ± 6.78 µM and 35.82 ± 5.40 µM for mouse fibroblast (L929) cell lines. Compounds **24**, **43,** and **45** exhibited antibacterial activity against *E. coli* and *B. subtilis* with an MIC value of 33.3 µg/mL. Moreover, **45** exhibited antifungal activity against *T. tonsurans* with an MIC value of 18.75 µg/mL. The bioactive compounds are potential lead compounds for the development of new drugs.

TABLE OF CONTENTS

LIST OF FIGURES

LIST OF TABLES

LIST OF ABBREVIATIONS AND ACRONYMS

AIDS	Acquired immunodeficiency syndrome
AMR	Antimicrobial resistance
BLAST	Basic local alignment search tool
^{13}C NMR	Carbon-13 nuclear magnetic resonance
CC	Column chromatography
CCDC	Cambridge crystallographic data centre
CFU	Colony forming unit
CMA	Corn meal agar
CO_2	Carbon (iv) oxide
COSY	Correlation spectroscopy
DEHP	Di-(2-ethylhexyl)phthalate
DEPT	Distortionless enhancement by polarization transfer
DMSO	Dimethyl sulphoxide
ESBL	Extended spectrum beta-lactamase
ESI	Electrospray ionization
EtOAc	Ethyl acetate
FDA	Food and drug administration
FTIR	Fourier transform infrared spectroscopy
^{1}H NMR	Proton nuclear magnetic resonance
HIV	Human immunodeficiency virus
HMBC	Heteronuclear multiple bond correlation

HPLC	High performance liquid chromatography
HRESIMS	High-resolution electrospray ionization mass spectrometry
HSQC	Heteronuclear single quantum correlation experiment
IC_{50}	Half-maximal inhibitory concentration
ITS	Internal transcribed spacer
LC-MS	Liquid chromatography mass spectrometry
LF	Liquid state fermentation
LPS	Lipoposaccharides
MDR	Multi-drug resistance
MeOH	Methanol
MIC	Minimum inhibitory concentration
MRSA	Methicillin-resistant *Staphylococcus aureus*
MS	Mass spectrometry
MTT	(3-(4,5-dimethylthiazol-2-yl)-2,5-diphenyltetrazolium bromide
NCBI	National center for biotechnology information
NCCLS	National committee for clinical laboratory standards
NCI	National cancer institute
NMR	Nuclear magnetic resonance
OD	Optical density
OMA	Oatmeal agar
ORTEP	Oak ridge thermal ellipsoid plot
PBPs	Penicillin-binding proteins

PCR	Polymerase chain reaction
PDA	Potato dextrose agar
pH	Potential of hydrogen
PVP	Polyvinylpyrrolidone
rDNA	Ribosomal deoxyribonucleic acid
SDA	Sabouraud dextrose agar
SmF	Submerged fermentation
SSF	Solid state fermentation
TLC	Thin layer chromatography
TMS	Tetramethylsilane
UV-VIS	Ultraviolet-visible spectroscopy
WHO	World health organization
XRD	X-Ray diffraction
YMA	Yeast malt extract

CHAPTER ONE
INTRODUCTION

1.1 Background Information

Microbial infections continue to be a growing concern in the world due to resistance to the available antimicrobial agents. Infectious diseases caused by bacteria, viruses, fungi and parasites are among the top 10 causes of mortality across the globe (WHO, 2017). Globally, approximately 700,000 deaths are reported every year as a result of infections caused by antimicrobial resistant pathogens. Further, antimicrobial resistance (AMR) contributes directly to the decline in the global economy (Dadgostar, 2019), and increase in poverty especially in middle and low income countries (Ahmad & Khan, 2019; Mattar *et al*., 2020). According to the antimicrobial resistance report by the Center for Disease Control and Prevention (CDC), about 2.8 million antibiotic-resistant infections occur in the United States every year with approximately 35,000 deaths (CDC, 2019). Most of the developing countries are affected by the morbidity and mortality resulting from infectious diseases with infants and children being the most vulnerable group (UNICEF, 2004). In the year 2011, severe bacterial infections were reported to account directly for about one-third of neonatal deaths in sub-Saharan Africa, South Asia (SA), Latin America, and the Caribbean (Liu *et al*., 2012).

The skin is the largest organ of the body with the function of protecting the body from infection (Baroni *et al*., 2012). However, the skin itself may get infected, leading to destruction of the skin structure. Dermatological infections are classified into; fungal skin infections, bacterial skin infections, viral skin infections and parasitic skin infections (Russell, 2013). According to the World Health Organization (WHO), skin diseases contribute to 1.79% of the disease burden in the world measured disability adjusted life years (DALYs) (Karimkhani *et al*., 2017). Fungal and bacterial skin diseases are among the dermatological conditions that contribute to the high disability adjusted life years (Karimkhani *et al*., 2017). Havlickova *et al*. (2009), estimates that 20-25% of the population in the world is affected by fungal skin infections. Fungal infections of the skin due to dermatophytoses are a common problem across the globe (Bitew, 2018). *Trichophyton* species is the most common causative fungi for ringworm infections such as *Tinea capitis*, ringworm of the scalp (Bongomin *et al*., 2020), *Tinea cruris*, fungal infection of the groin region, *Tinea pedis*, ringworm of the feet and toes and *Tinea unguium*, nail fungus (Sahoo & Mahajan,

2016). *T. capitis* and *T. corporis* are the most frequent forms of dermatophytoses in the tropical areas (Havlickova *et al*., 2009).

About 70-95% of the developing countries' population depends on plants for primary healthcare (Kaneria *et al*., 2017). Besides, in a number of rural areas, traditional medicine is the only healthcare system available. According to Madzinga *et al*. (2018), medicinal plants have the ability to treat a range of diseases including fungal and bacterial skin diseases. *Bersama abyssinica* has been used by several communities in East Africa to treat several conditions (Kokwaro, 1993). The plant has been used in the treatment of diseases such as, male infertility, skin infections, diabetes (Kuete *et al*., 2007), syphilis, intestinal worms, cholera, gonorrhea, fatigue and malaria (Zekeya *et al*., 2014). These properties are attributed to the presence of bioactive secondary metabolites (Amuka *et al*., 2015). The genus *Bersama* (family Melianthaceae) are widely distributed in tropical and subtropical Africa (Kuete *et al*., 2007). Pharmacological studies on plants of this genus revealed antitumor, antioxidant, antispasmodic, and antimicrobial activities (Asres *et al*., 2006; Kuete *et al*., 2007; Lock, 1962). Previous phytochemical studies on the genus led to the identification of different bufadienolides (Steyn & van Heerden, 1998) and several derivatives of this class have been reported from *B. abyssinica* including abyssinin (Kubo & Matsumoto, 1984) abyssinol (Kubo & Matsumoto, 1985b) and bersamagenin (Kupchan *et al*., 1971). Recent updates are unavailable on phytochemical investigation on *B. abyssinica* and decades have passed since the last report on the plants.

The main focus of this research was on phytochemical investigation of extracts of the barks and leaves of two subsp. of *B. abyssinica*, collected from Mt. Elgon National Forest. Further, the endophytic fungi from these plants was also investigated. The investigation led to the isolation and identification of eight new compounds and twenty two known compounds. The isolation and structure elucidation of these compounds is described. Eight of the described compounds are bufadienolides while the rest are phenolic compounds. To evaluate the bioactivities of the isolated compounds, antibacterial assay was done against *Escherichia coli*, *Mycobacterium smegmatis*, *Staphylococcus aureus* and *Bacillus subtilis*. The cytotoxicity assay was done against HeLa (KB3.1) and mouse fibroblast (L929) cell lines. The antidermatophytic assay was done against *Trichophyton mentagrophytes*, *Trichophyton rubrum*, *Trichophyton rubrum* resistant, *Trichophyton benhamiae* var. *luteum* and *Trichophyton tonsurans.*

1.2 Statement of the Problem

The discovery of antimicrobial drugs implied that the problem of infectious diseases would be solved, creating a false sense of security. Besides pathogenic microbes for which there is no current treatment option, emergence of multidrug resistant organisms compromises the use of antibiotic and antifungal drugs. The adaptability and resistance of infectious agents to drugs designed to kill them is incredibly fast-moving. For example, sulfonamide-resistant organisms, such as *Streptococcus pyrogenes*, emerged shortly after the introduction of the first sulfonamide drug, the azo compound that was developed in the 1930s as a solution for broad spectrum antimicrobial therapy. Bacterial resistance has, thus, become one of the main factors in triggering a global, urgent search for novel antimicrobial agents. Resistance associated with known pathogens such as methicillin-resistant *S. aureus* (MRSA) and respiratory pathogens such as *Streptococcus pneumoniae*, are increasingly often described in epidemiological analyses, impacting all fields of medicine and representing a threat to public health. Futhermore, antifungal resistance especially *T. rubrum*, a skin disease causing pathogen is on the rise. Antimicrobial resistance (AMR) is a major problem in the treatment of patients with immunocompromised immunity such as cancer and HIV/AIDS patients. This is partly because most of these pathogens are opportunistic and occur severely and frequently in immunosuppressed individuals. The world health organization report indicates that cancer is the leading cause of mortality worldwide. In Kenya, from 2012 to 2018, the annual incidence of cancer increased from 37,000 to 47,887 new cases. Furthermore, the number of new cancer cases is expected to rise by more than 120% over the next 2 decades. It is therefore, important to search for alternative drugs to mitigate this problem.

1.3 Objectives

1.3.1 General Objective

To investigate antimicrobial and anticancer secondary metabolites from *B. abyssinica* subsp. *abyssinica*, subsp. *paullinioides* and their endophytic fungi

1.3.2 Specific Objectives

i. To isolate endophytic fungi from the stem barks and leaves of *B. abyssinica* subsp. *abyssinica* and subsp. *paullinioides*

ii. To isolate secondary metabolites from the stem barks and leaves of *B. abyssinica* subsp. *abyssinica*, subsp. *paullinioides* and their endophytic fungi

iii. To investigate the bioactivities of secondary metabolites isolated from the stem barks and leaves of *B. abyssinica* subsp. *abyssinica* and subsp. *paullinioides* and their endophytic fungi

iv. To determine the structures of the secondary metabolites isolated from *B. abyssinica* subsp. *abyssinica*, subsp. *paullinioides* and their endophytic fungi

1.4 Hypotheses

i. Endophytic fungi isolated from the stem barks and leaves of *B. abyssinica* subsp. *abyssinica* and subsp. *paullinioides* have similar molecular characteristics.

ii. Secondary metabolites in crude form do not exhibit any antimicrobial and cytotoxic activities.

iii. The isolated pure compounds show no antimicrobial and cytotoxic activities against controls

iv. The chemical structures of the isolated compounds cannot be conclusively elucidated using the available spectroscopic tools

1.5 Justification

Natural products have been used by humans as remedies for various diseases over time. Antimicrobials from plant extracts and decoctions recorded in ethnobotanical studies have shown potency against microbial pathogens and tumors that affect both human beings and plants. The frequent misuse and overuse of available drugs has led to emergence of resistant strains of microbial pathogens. Furthermore, some of these pathogens are opportunistic and pose a serious threat to cancer patients because of the compromised immune system. The trends of new antimicrobials that are being introduced into the market have remained insignificant. This is because resistance towards the drug being introduced has apparently increased, especially in patients undergoing long-term treatment. There has been increased enthusiasm to search for bioactive secondary metabolites from natural sources that can effectively manage and treat both infectious and noninfectious diseases with the aim of improving people's quality of life. Melianthaceae family plant extracts and decoctions have been used in the past by traditional medicinal practitioners for the treatment of tumors, skin infections, wounds, dysentery, and roundworm infestation. Furthermore, natural drugs obtained from plants and their endophytic fungi have gained popularity because they have

better patient tolerance, are relatively less costly and have fewer side effects. This study seeks to investigate secondary metabolites in *B. abyssinica* subsp. *abyssinica* and subsp. *paullinioides* with antibacterial, antifungal and anticancer properties. Medicinal plants such as *B. abyssinica* can be propagated while endophytes can be cultured providing potential new antimicrobial and anticancer compounds. The compounds derived adds to the library of existing ones and may form a basis for future discovery of new or alternative antimicrobial and anticancer compounds through structure activity relationship (SAR) techniques. This study contributes to the sustainable development goal (SDG 3) on health and wellbeing.

CHAPTER TWO
LITERATURE REVIEW

2.1 An overview of Infectious diseases

Infectious diseases are also known as communicable diseases or transmissible diseases. They comprise clinically evident illnesses that result from an infection in the presence of a pathogenic bacterial agent in a host organism. Infectious diseases may be asymptomatic in a given host for a long time. Infectious pathogens are the cause of disease epidemics and include; bacteria, fungi, viruses, protozoa, and parasites (Mirzaei *et al*., 2020; Pirofski & Casadevall, 2020). Infectious diseases are the biggest cause of death amongst both children and adults across the globe. Each year, 13 million deaths are attributed to infectious diseases, translating to one in two deaths in developing countries. The majority of deaths due to infectious diseases occur in low and middle income countries. This is partly because developing countries spend little money in health care systems (Engels & Savioli, 2006; Lindahl *et al*., 2015). However, infectious diseases are not just a problem of the underdeveloped countries but a global problem, especially with increased air travel leading to the transportation of pathogens from continent to continent. Furthermore, drugs that are available for the treatment of infectious diseases are progressively being depleted because of the increasing resistance of microbes to antimicrobial drugs (Shinu *et al*., 2022).

Organisms that cause human infections are divided into two categories; primary and opportunistic pathogens. Primary pathogens are those organisms that cause disease in healthy people while opportunistic pathogens mainly infect immunocompromised people or people with underlying diseases such as cancer and HIV / AIDS patients (Martínez, 2007). Opportunistic diseases are sometimes caused by microbes that the host is ordinarily in contact with, such as pathogenic bacteria or fungi in the gastrointestinal or the upper respiratory tract. They may also be due to microbes acquired from other hosts as in the case of *Clostridium difficile* colitis or from the environment because of traumatic introduction for instance surgical wound infections or an open fracture (Kumpitsch *et al*., 2019; Prabhu, 2023). Primary pathogens may also cause more severe disease in a host with depressed resistance than would normally occur in an immunosufficient host (Chahal, 2021). In addition, many diseases once thought unrelated to infectious diseases especially cancers are now known to be the result of chronic infections. Cervical cancer, for instance is now associated with human papillomavirus infection and is one of the most common type of cancer in the developing world among women (Almeida *et al*., 2019; Chan *et al*., 2019; Sivars *et al*., 2023).

2.2 Bacteria and common bacterial infections

Bacteria are very small microorganisms that only have one cell. While most bacteria do not cause illness, infectious bacteria can cause severe illness because they reproduce quickly in the body and give off toxins that can damage the host tissue. Bacterial reproduction is by binary fission and they multiply very fast under optimal conditions (Koch, 2002). Bacteria that cause infections include; *Escherichia coli*, *Streptococcus* and *Staphylococcus*. Bacteria are classified into gram-positive and gram-negative based on gram staining. Gram staining differentiates bacterial species based on chemical and physical properties of their cell walls peptidoglycan, which is present in a thick layer in gram-positive bacteria (Kristensen *et al*., 2023). Gram-positive bacteria stain blue while gram-negative bacteria stain red. Further, they cause different types of infections and hence are treated using different types of antibiotics.

A range of gram-negative microorganisms cause various infections. For instance, *Escherichia coli* infections in the digestive tract; *brucellosis*, an infection caused by several species of *Brucella* and characterized by fever, lower back pain, severe headache, chills, bone and joint pain. Cholera, an infection of the intestine caused by *vibrio cholerae* bacteria. *Pseudomonas aeruginosa* can infect any type of the body such as lungs, heart valves or blood stream. *Salmonella* infections due to contaminated food and fluids causing diarrhea and typhoid fever. *Legionella* infections caused by *Legionella pneumophila* often affect the lungs causing pneumonia, fever, muscle aches, painful and difficult breathing. *Klebsiella*, *Enterobacter* and *serratia* infections infect respiratory tract and urinary tract of people in health care facilities (Syed, 2021). Similarly, gram-positive microorganisms cause various infections. For instance, Enterococcal infections caused by *Enterococcus faecalis* and *Enterococcus faecium.* Erysipelothricosis, a skin infection caused by *Erysipelothrix rhusiopathiae* characterized by hardened, itchy rash. Pneumococcal infections caused by *Streptococcus pneumoniae* (pneumococci) leading to pneumonia, ear infection, meningitis and sinusitis. *Staphylococcus aureus*, the most dangerous of staphylococcal bacteria causes skin infections, pneumonia, bone infections and heart valve infections. Streptococcal infections also lead to blood stream infections, pneumonia, skin and heart valve infections (Shrestha *et al*., 2019).

2.3 Overview of bacterial pathogens used in this study

Gram-positive bacteria *Staphylococcus aureus*, *Mycobacterium smegmatis* and *Bacillus subtilis* as well as gram-negative *Escherichia coli* were used in this study.

2.3.1 *Staphylococcus aureus*

Staphylococcus aureus is a gram-positive bacteria whose cells occur in clusters and is spherical shaped in appearance (Gnanamani *et al*., 2017). Bacteria in the genus *Staphylococcus* are pathogens that affect both man and other mammals. It causes a range of infections due to the virulence factors and hence an important human pathogen. *S. aureus* has been reported to have the ability to acquire resistance to various classes of antibiotics, making it a challenging pathogen to treat. *S. aureus* is a major cause of hospital acquired infections of surgical wounds, deep-seated infections such as osteomyelites and endocarditis and a number of skin infections. The emergence of antimicrobial resistance in *S. aureus* is a threat in the public health sectors across the world. Further, methicillin-resistant *S. aureus* (MRSA) strains, are often multi-drug resistant in both hospitals and communities accounting for the large numbers of mortality and morbidity (Dilnessa & Bitew, 2016). In humans, *S. aureus* causes a wide range of infections which, based on the origin of the infection are classified into nosocomial and community categories. *S. aureus* is a leading cause of mortality and morbidity in hospitals, being a predominantly nosocomial pathogen for decades. Community infections from *S. aureus* are also on the rise. Nosocomial and community infections are distinct in antibiotic susceptibility, clinical manifestation of infection and genetic background of *S. aureus* strain leading to the infection. The most common *S. aureus* clinical infections include; skin and soft tissue infections, bacteraemia, pleuropulmonary and osteoarticular infections, meningitis, urinary tract infections, epidural abscess and toxic shock syndrome (Bitrus *et al*., 2018). Methicillin resistant *S. aureus* (MRSA) causes outbreaks in hospitals and can be problematic in the community (Rossney *et al*., 2007). It is reported that, inappropriate use of penicillin could lead to mutant forms of *S. aureus* causing more serious infection in the host and other people that the host is in contact with and hence could pass the resistant microbe (Sefton, 2002).

2.3.2 *Mycobacterium smegmatis*

Mycobacterium smegmatis is a gram positive bacteria with a thick cell wall and inner membrane. It is reported to have low response to antibiotics because of the slow cell growth and irregularly thick cell wall in comparison to the other gram positive bacteria. *M. smegmatis* is a rapid growing bacteria and multiplies very fast in the affected host (Alqurashi *et al*., 2019). *M. smegmatis* usually causes skin infections such as abscesses, erythema, subcutaneous nodules and

papules. These infections are mostly opportunistic and occur after cosmetic related procedures due to the open wounds (Wang *et al*., 2022).

2.3.3 *Bacillus subtilis*

Bacillus subtilis is a rod-shaped ubiquitous organism that is found in water, soil, air and even decaying matter. It produces endospheres which allow it to survive the extreme environmental conditions such as desiccation and heat. *B. subtilis* can be grown in the laboratory and is easy to manipulate. *B. subtilis* inhabits aquatic environments, plants, soil and roots in nature and can also inhabit the gastrointestinal tract of animals including humans. *B. subtilis* has generally been reported to be non-pathogenic to human beings. However, it has been linked to food poisoning because the bacteria are able to survive the heat that is applied during cooking. This leads to diarrhea and acute vomiting in affected patients and can be life threatening (Ali *et al*., 2022; Parija, 2023).

2.3.4 *Escherichia coli*

Escherichia coli are a group of gram negative bacteria that are rod-shaped and facultative anaerobic. *E. coli* commonly resides in the intestines of warm-blooded organisms such as humans causing no disease (Ramos *et al*., 2020). Some strains however, can cause infection in many other parts of the body. There are many types of *E. coli* most of which are harmless while some strains cause severe infections. The bacteria are mainly acquired through drinking contaminated water, meat and leafy vegetables (Heiman *et al*., 2015). Antibacterial resistant *E. coli* of animal origin poses human health hazards. This is due to intensive use of antibacterial agents in food production: Meat and milk is frequently contaminated with antibacterial resistant *E. coli* (Hammerum & Heuer, 2009). While most *E. coli* strains are harmless, some strains are pathogenic because they acquire invasion factors, bacteriophage or plasmid DNA-encodingenterotoxins. The pathogenic strains are responsible for various infections across the globe. These infections include; diarrhea, urinary tract infections, neonatal meningitis and septicemia. People may develop intestinal infection by ingesting contaminated food, drinking contaminated food or touching infected animals. Infections with multidrug resistant *E. coli* are an increasing concern, with resistance mediated by extended-spectrum β-lactamase (ESBL) production. These isolates are most often obtained from hospitalized patients but are becoming an increased cause of community acquired infections as well (Soltani *et al*., 2018; Sousa, 2006).

2.4 Overview of antibiotics

Antibiotics are drugs used to either destroy bacterial or slow down the rate at which bacteria undergoes multiplication. They are not effective against viral infections and most other infections. Antibiotics either kill bacteria or stop them from reproducing, allowing the body's natural defenses to eliminate them (Morris & Cerceo, 2020; Paterson *et al*., 2016). Doctors try to use antibiotics for specific bacterial infections, but they sometimes start antibiotics that can treat many different bacteria while waiting for results of tests that identify the specific bacteria. Taking the antibiotics as prescribed is important, and antibiotics should be taken in the dose, frequency, and number of days that are most effective to treat a specific infection (Guilhaumou *et al*., 2019). Bacteria can develop resistance to the effects of antibiotics, especially if they are not taken as directed. Antibiotics can have side effects, such as upset stomach, diarrhea, and, in women, vaginal yeast infections. Some people are allergic to certain antibiotics (Kopacz & Phadtare, 2022). Antibiotics are grouped into classes based on their chemical structure. However, antibiotics within each class often affect the body differently and may be effective against different bacteria. Classes of antibiotics include the following: aminoglycosides, carbapenems, cephalosporins, fluoroquinolones, glycopeptides and lipoglycopeptides, macrolides, monobactams, oxazolidinones, penicillins, polypeptides, rifamycins, sulfonamides, streptogramins and tetracyclines (Hutchings *et al*., 2019; Lima *et al*., 2020).

2.4.1 Antibiotic resistance

Antibiotics are medicines used to prevent and treat bacterial infections. Antibiotic resistance (AMR) occurs when bacteria undergoes genetic mutation that allows it to resist the action of an antibacterial drug. Antibiotic resistance arises when bacteria is no longer susceptible to the antibiotics that designed to kill or slow down their cell division (Nadeem *et al*., 2020). While strains that have not undergone mutation are wiped out by the antibiotic, the strain that has undergone mutation survives antibiotic exposure. The genetic advantage is then passed on when the strain undergoes replication. The infected host spreads the resistant strain to others and with time it becomes the most prevalent strain and renders the antibiotic widely ineffective (Jian *et al*., 2021). Antibiotic resistance is rising to dangerously high levels in all parts of the world. New resistance mechanisms are emerging and spreading globally, threatening our ability to treat common infectious diseases. A growing list of infections such as pneumonia, tuberculosis, blood

poisoning, gonorrhea, and foodborne diseases are becoming harder, and sometimes impossible, to treat as antibiotics become less effective (Chen *et al*., 2019).

Multidrug resistance (MDR) arises when a microbe is resistant to multiple antimicrobial medicines that are normally effective against it. For instance, the emergence and spread of methicillin-resistant *S. aureus* (MRSA) strains which are often multi-drug resistant in hospitals and subsequently in community resulted in significant mortality and morbidity. The epidemiology of MRSA has been evolving since its initial outbreak which necessitates a comprehensive medical approach to tackle this pathogen. Vancomycin has been the drug of choice for years but its utility was challenged by the emergence of resistance (Kumar *et al*., 2021). In the last 10 years or so, newer anti-MRSA antibiotics were approved for clinical use. However, being notorious for developing antibiotic resistance, there is a continuous need for exploring novel anti- MRSA agents from various sources including plants and evaluation of non-antibiotic approaches such as phytomedicines and probiotics (Bassetti *et al*., 2019).

2.4.2 Antifungal resistance

Antifungal drugs are used in the treatment of fungal infections stopping the growth of dangerous fungi in or on the body. Fungi can develop resistance to antifungal drugs the same way bacteria can develop resistance to antibiotics. The resistance happens when germs develop the ability to survive exposure to the drugs designed to kill them (McDermott, 2022). Currently, only a small number of antifungal drug types exist, so resistance can severely limit treatment options. Some types of fungi, like *candida auris*, can become resistant to all the antifungal drugs normally used to treat these infections. Resistance is especially concerning for patients with invasive fungal infections where severe infections affect the blood, heart, brain, eyes, or other parts of the body. Resistant fungi include *Aspergillus*, certain *Candida* species, and certain dermatophytes such as *Trichophyton rubrum* (Maji *et al*., 2023).

2.5 Mechanism of antimicrobial resistance

Microbes use a lot of ways to survive the effect of antibacterial and antifungal drugs. The mechanisms of antimicrobial resistance include, limiting the uptake of the antibiotic, modifying the target of the antibiotic, inactivating the antibiotic and active drug efflux. Bacteria with intrinsic or natural resistance can utilize the ability to limit the uptake of the antibiotic, modify the target of the antibiotic and drug efflux. Acquired resistance mechanisms used may be modification of the

drug target, inactivation of the drug, and drug efflux. Gram negative bacteria and gram positive bacteria use varying mechanisms due to the differences in structure of the bacteria among other factors. Gram positive bacteria don't have the lipopolysaccharide outer membrane and therefore, rarely uses the ability to limit the uptake of a drug. Furthermore, they do not possess the capacity for certain types of drug efflux mechanisms. On the other hand, Gram negative bacteria utilizes all the mechanisms mentioned earlier (Abushaheen *et al*., 2020; Reygaert, 2018).

2.5.1 Limiting drug uptake

Gram negative bacteria have the lipopolysaccharide (LPS) layer which acts as a barrier to some drug molecules. This layer allows those bacteria to develop natural resistance to some antibacterial drugs (Blair *et al*., 2014). Bacteria with an outer membrane possess high lipid content allowing hydrophobic drugs like rifampicin and fluoroquinolones to infiltrate the cell easily. However, hydrophilic drugs cannot access the cell (Ayush & Schweizer, 2005; Lambert, 2002). Bacteria that lack a cell wall, such as *Mycoplasma* and related species, are therefore intrinsically resistant to all drugs that target the cell wall including β-lactams and glycopeptides. *S. aureus*, a gram positive bacteria, developed resistance to vancomycin over a decade ago (Cong *et al*., 2020). The bacteria produces thickened cell wall making it difficult for the drug go into the cell, and hence providing resistance to vancomycin (Lambert, 2002; Miller *et al*., 2014). Bacterial communities also form biofilm to protect themselves from antibiotics. The biofilms contain different kinds of organisms but may have a predominant organism. Biofilms are thick, sticky matrix consisting of polysaccharides, proteins and DNA from the bacteria, making it difficult for antimicrobial agents to attack the bacteria (Acker *et al*., 2014; Mah, 2012; Soto, 2013).

2.5.2 Modification of drug targets

Bacteria has multiple cells that can be a target for antimicrobial agents and these targets can also be modified by the bacteria to enable resistance to those drugs. For instance, β-lactam drugs are mostly used for gram positive bacteria, the mechanism of resistance to these drugs is by altering the number or structure of penicillin-binding proteins (PBPs). The change in the number of binding proteins has an impact on the quantity of the drug that can bind to that target and hence decreasing or totally inhibiting drug binding (Beceiro *et al*., 2013; Reygaert, 2009). Gram negative bacteria have thick LPS and hence have intrinsic resistance to glycopeptides such as vancomycin and lipopeptides such as daptomycin. This is because glycopeptides also work by inhibiting cell

wall synthesis and lipopeptides work by depolarizing the cell membrane (Randall *et al*., 2013). Resistance to vancomycin has become a major issue in the enterococci and methicillin resistant *S. aureus* (MRSA) (Beceiro *et al*., 2013; Cox & Wright, 2013).

2.5.3 Drug inactivation

Bacteria inactivates antibacterial drugs in two major ways. This includes; actual degradation of the drug and transfer of a chemical group to the antibiotic. The β-lactams and tetracycline are examples of drugs that are inactivated by degradation. Tetracyclines are inactivated by hydrolyzation through the *tetX* gene while β-lactams can be hydrolyzed by enzymes produced by the bacteria (Blair *et al*., 2015). Drug inactivation through the transfer of a chemical group to the antimicrobial agent mostly utilizes transfer of three major groups; acetyl, adenyl and phosphoryl groups. Acetylation is the most diversely used transferase mechanism against chloramphenicol, aminoglycosides, streptogramins, and fluoroquinolones. Transferases involving phosphorylation and adenylation are commonly used against the aminoglycosides (Blair *et al*., 2015; Ramirez & Tolmasky, 2010; Robicsek *et al*., 2006; Schwarz *et al*., 2004).

2.5.4 Drug efflux

Efflux pumbs are transporters in the inner membrane of bacteria whose function is to export antibiotics from the inside to the outside of the bacterial cells. These has contributed to multidrug resistance (MDR) because one multidrug efflux pump has the ability to move multiple antibiotics out of the bacterial cells. It is therefore, important to develop efflux pump inhibitors so as to overcome infectious diseases resulting from multi-drug resistant bacteria (Nishino *et al*., 2021). Bacteria possess chromosomally encoded genes for efflux pumps. Some are expressed constitutively, and others are induced or overexpressed under certain environmental stimuli or when a suitable substrate is present. This implies that, the high level of resistance is usually through a mutation that modifies the transport channel. The efflux pumps function primarily to rid the bacterial cell of toxic substances, and many of these pumps will transport a large variety of compounds including antibiotic drugs. The resistance capability of many of these pumps is influenced by the available carbon source (Blair *et al*., 2015; Thakur *et al*., 2021; Villagra *et al*., 2012).

2.6 Dermatophytes and common dermatophytic infections

The skin is the largest organ in the body and its major functions are regulation, sensation and protection of the underlying organs (Lefèvre-Utile *et al*., 2021). Skin diseases can be caused by fungi, bacteria, viruses and parasites (Nahar *et al*., 2020). Skin infections are classified into either; primary or secondary. Primary infections occur in normal skin, are initiated by a single organism and have characteristic causes and morphologies. Secondary skin infections, on the other hand, originate in diseased skin as a superimposed condition (Burstein *et al*., 2020). Fungal skin infections are classified into two; dermatophytes and yeasts. Dermatophytes are caused by species belonging to *Trichophyton*, *Epidermophyton* and *Microsporum* genera. In a study by Tiwari *et al*. (2023), it is reported that, *T. rubrum* is the most prevalent causative agent of dermatophytes. The prevalence of dermatophytes in developing countries is high because of high population densities, poor social economic status and poor sanitary conditions (Nweze & Eke, 2018). Dermatophytes commonly affecting human beings include; *Tinea capitis*, *Tinea corporis*, *Tinea cruris* (Nagaral *et al*., 2018), *Tinea barbae*, *Tinea faciei*, *Tinea manuum*, *Tinea pedis* and *Tinea unguium* (Chadeganipour *et al*., 2016). Furthermore, infections caused by dermatophytes are named according to the anatomic location involved, for instance, *tinea barbae* (beard and moustache), *tinea capitis* (scalp, eyebrows, and eyelashes), *tinea corporis* (face, trunk and major limbs), *tinea cruris* (groin, perineal, and perianal areas), *tinea pedis* (soles and toe webs), *tinea manuum* (palms) and *tinea unguium* (nails). Different dermatophyte species may produce clinically identical lesions; conversely, a single species may infect many anatomic sites (Ahmad *et al*., 2021).

2.7 Overview of dermatophytes used in this study

The dermatophytes used in this study include: *Trichophyton mentagrophytes, Trichophyton rubrum, Trichophyton rubrum* resistant, *Trichophyton benhamiae* var. *luteum* and *Trichophyton tonsurans.* These strains are amongst the most common causative agents of most of the tinea infections in humans (Moto *et al*., 2015). Statistics indicate that Trichophyton genus account for 93% of dermatophytoses, which was shared by *Trichophyton rubrum* (73.3%) and *Trichophyton mentagrophytes* (19.7%), followed by *Epidermophyton floccosum* (4.2%) and *Microsporum gypseum* (2.8%) (Venkatesan *et al*., 2007).

2.7.1 *Trichophyton mentagrophytes*

Trichophyton mentagrophytes is primarily a zoophilic dermatophyte that attacks humans. Infections by zoophilic species result from animal-to-human contact such as cats, dogs, cattle, and

laboratory animals (Samanta, 2015). It is the most common dermatophyte and may also survive saprophytically in the soil. Infections caused by *T. mentagrophytes* have been reported in a large number of both wild animals and domesticated animals (Gnat *et al*., 2019; Tang *et al*., 2021). Most rodents carry *T. mentagrophytes* as normal flora without signs of disease (Tamura, 2010). *T. mentagrophytes* colonies are powdery or granular, light buff to rose-tan with a buff to deep wine or brown reverse. Macroaleuriospores are 3–5-celled, thin-walled, clavate, and not too abundant. The most consistent microscopic feature is the production of large numbers of microaleuriospores in grapelike clusters, especially in the zoophilic strains. *T. mentagrophytes* typically cause suppurative inflammation with very itchy blisters followed by scaly, focal, or multifocal circular and painful lesions with hair loss on the skin (Coyner, 2019; Rook & Abraham, 2022). This dermatophyte is part of the natural skin flora of hedgehogs where it asymptomatically resides on the skin and quills (Chermette *et al*. 2008; Connole 1968; Hata *et al*. 2000;). Several reports have identified hedgehogs as a potential risk for the transmission of this species to human and dogs through direct or indirect contact (Gnat *et al*., 2022; Jota Baptista *et al*., 2023; Ruszkowski *et al*., 2021). Ringworm lesions on humans such as inflammatory *T. pedis* can be caused by *T. mentagrophytes* (Sharquie & Jabbar, 2021).

2.7.2 *Trichophyton rubrum*

The *Trichophyton rubrum* is the most commonly encountered dermatophytic fungi with a worldwide distribution with high keratinase activity. Dermatophytes with reduced sensitivity have emerged across the world. *T. rubrum* is one of the most predominant fungi especially in developing countries with reported antimicrobial resistance. The major predisposing factors include excessive sweating, diabetes, and obesity (Chanyachailert *et al*., 2023). *T. rubrum* is one of the major causative agent for ringworms such as *T. capitis*, *T. cruris*, *T. pedis,* and *T. unguium* (Duarte *et al*., 2019). *T. cruris* commonly referred to as jock itch is usually caused by *T. rubrum* or *Epidermophyton floccosum*. It typically appears as scaly, erythematous to tawny brown, bilateral and asymmetric lesions extending down to the inner thigh and exhibiting a sharply marginated border frequently studded with small vesicles. *T. pedis* varies in appearance, however, the most common manifestation is maceration, peeling, itching, and painful fissuring between the fourth and fifth toes. Acute inflammation conditions with vesicles and pustules and hyperkeratotic chronic infection of the sole can also occur in *T. pedis*. Members of the *T. mentagrophytes* complex frequently cause the more inflammatory type of infections, whereas *T. rubrum* usually

causes the more chronic type (Cañete-Gibas & Wiederhold, 2023). Dermatophytic nail infection, *T. unguium*, is also most often caused by *T. rubrum*, and usually appears as thickened, deformed, friable, discolored nails with accumulated subungual debris. This infection, in which the nail is subungually infected beginning near its point of origin in the area of the lunula, is usually caused by *T. rubrum* and often signals immunosuppression such as HIV / AIDS and *diabetes mellitus* (Amaewhule, 2022).

2.7.3 *Trichophyton tonsurans*

Trichophyton tonsurans is an anthropophilic dermatophyte, responsible for infections of the scalp and sometimes of the glabrous skin or nails (Havlickova *et al*., 2009). Unlike dermatophytosis caused by other dermatophytes, the clinical features of infection due to *T. tonsurans* are not very apparent initially. *T. corporis* due to *T. tonsurans* appears as small, erythematous, scaly plaques, often measuring only 1-2 cm in diameter, have no central clearing, and are similar in appearance to eczema. *T. capitis* due to *T. tonsurans* can be subdivided into three types: the seborrheic subtype, which is primarily characterized by the presence of dandruff and crusts; the kerion celsi subtype, which shows as acute inflammation; and the black dot subtype which results from discolored patches and is exhibited mostly among sports players (Lee *et al*., 2016). *T. tonsurans*, is the most common cause for *T. capitis* in North America. Other causes include: *Microsporum canis* (more often than not from pets), *Microsporum audouinii*, *T. mentagrophytes*, and *Trichophyton violaceum. T. capitis* is most prevalent in young children, especially school going children. This poses a danger to family members and postmenopausal caretakers can be infected. *T. tonsurans* is transmitted from human to human while *M. canis* is transmitted from pets to humans (Romano *et al*., 2001).

T. corporis is a shallow skin disease that happens worldwide and influences all age groups. Around half of the cases happen in age groups of 15-year old individuals and above. While all dermatophytes cause skin disease, the prevalent pathogens differ topologically. *T. rubrum*, *T. tonsurans*, *T. mentagrophytes*, *M. canis*, and *E. floccosum* are the most widely recognized reasons for *tinea corporis* (Nenoff *et al*., 2014). *T. unguium* causes infections of the nails and is mostly connected with *T. pedis*. It is more common in older individuals than children with overall predominance ranging from 0.1% to 1%. Adults have a higher predominance at 2% to 14%, and pervasiveness in old individuals approaches 40% (Alshehri *et al*., 2021). *T. rubrum*, *T.*

mentagrophytes, and *E. floccosum* are the essential pathogens of *tinea unguium* (Chowdhry *et al*., 2009).

2.7.4 *Trichophyton benhamiae* var. *luteum*

T. benhamiae var. *luteum* is a dermatophyte that is widely reported in guinea pigs, cats and dogs. It is a zoonotic pathogen and therefore can spread to humans who are in contact with the hosts (Čmoková *et al*., 2020; Maldonado *et al*., 2021; Scarpa *et al*., 2021; Spanamberg *et al*., 2023). *T. benhamiae* var. *luteum* is most prevalent in Europe because most homesteads rear pets which are the major carriers of the fungi (Čmoková *et al*., 2020). *T. benhamiae* causes *Tinea* infections in both animals and humans. *T. benhamiae* infections in humans often result in severe skin lesions like *Tinea corporis*, *Tinea faciei* and *Tinea capitis* (Baert *et al*., 2021; Nenoff *et al*., 2014)

2.8 The impact of skin conditions

The impact associated with both visible and hidden skin conditions is considerable and often has negative impact on the life of the patients (Blome *et al*., 2016). People with skin problems are at a higher risk of developing psychological and emotional stress, as well as, poor psychosocial health. Patients with conditions such as eczema, skin cancer and psoriasis encounter psychological challenges and hence their social life are affected negatively (Blome *et al*., 2016). Chronic skin disorders lead to major depression, social withdrawal, and lack of confidence, anger and frustration. The American academy of dermatology reports that, about 5% of American adults suffering from chronic psoriasis experience suicidal thoughts. Further, 26% of individuals suffering from mild psoriasis have been forced to change their lifestyle or discontinue their normal daily activities and thereby, increasing the dependency rates (Luca *et al*., 2020). Besides, skin disorders and the resulting consequences do not affect adults only, children also suffer with two out of five of these children having psychosocial impairment (Xu *et al*., 2019).

2.9 Cancer

Cancer is the uncontrolled growth of abnormal cells anywhere in the body and it is one of the most devastating disease and major cause of death in the world (Baskar *et al*., 2012). These abnormal cells are termed cancer cells, malignant cells, or tumor cells and these cells can infiltrate normal body tissues. Many cancers and the abnormal cells that compose the cancer tissue are further identified by the name of the tissue that the abnormal cells originated from, for instance, breast cancer, lung cancer, and colorectal cancer (Li *et al*., 2021). When damaged and unrepaired

cells stay alive and become cancer cells, they show uncontrolled division and growth leading to the development of a mass of cancer cells. Cancer cells break away frequently from the original mass of cells, travel through the blood and lymph systems, and lodge in other organs where they can again repeat the uncontrolled growth cycle. This process of cancer cells leaving an area and growing in another body area is termed metastatic spread or metastasis. For example, if breast cancer cells spread to a bone, it implies that the patient has metastatic breast cancer to bone (Fares *et al*., 2020).

The cancer burden is on a steady rise and is further expected to rise, with over the predicted 20 million new cancer cases expected globally by 2025. In the low- and middle-income countries, the picture is even darker, where approximately 70% of deaths are due to cancer diseases and where only one in five countries have the necessary data to drive cancer policy (Mccormack & Boffetta, 2011; Sankaranarayanan, 2014). Advancing the fight against cancer requires both increased investment in cancer pathology research and in new safe, effective, inexpensive and minimal side effect anticancer agents. Throughout history, many cultures across the globe have used traditional herbal medicine to treat a myriad of diseases and disorders. Plants constitute a common alternative for cancer treatment in many countries, and more than 3000 plants worldwide have been reported to have anticancer properties (Alves-Silva *et al*., 2017; Tariq *et al*., 2017). In the last two decades, the use of herbal remedies has also been widely embraced in many developed countries as complementary and alternative medicine, but following tight legislation and under surveillance (Enioutina *et al*., 2017). Natural products have garnered increasing attention in cancer chemotherapy because they are viewed as more biologically friendly and consequently more co-evolved with their target sites and less toxic to normal cells (Mishra & Tiwari, 2011). Moreover, there is evidence that natural product derived anticancer drugs have alternative modes of promoting cell death (Gali-Muhtasib *et al*., 2015; Khalid *et al*., 2016). Based on these facts, many researchers are now centering their investigations on natural products sources such as plants, fungi and bacteria with potential compounds for use in the pharmaceutical industry (Bernardini *et al*., 2018; Huang *et al*., 2021; Katz & Baltz, 2016). From small molecules approved for cancer chemotherapy between 1940 and 2014, around 49% are derived from natural products (Newman & Cragg, 2016).

2.10 Overview of cancer cell lines used in this study

Two mammalian cell lines namely; HeLa (KB3.1) and mouse fibroblast (L929) cell lines were used in this study

2.10.1 KB3.1 cell line

KB3.3 cell line is human cervix carcinoma. It is a subclone of the parental KB cell line which is a HELA subclone. The cell line was used to establish several drug resistance subclones like the multi-drug resistant KB-V1 resistant to vinblastine (Akiyama *et al*., 1985).

2.10.2 L929 cell line

L929 Cell Line is a mouse subcutaneous connective tissue. L-929 is an adherent type of mouse fibroblast cell line known as an alternate test system for toxicity assessment. L929 cells can be used in the development of novel anti-cancer treatments. Resistance can be circumvented by modulating agents such as verapamil and quinine. The parent cell line L929 was derived from normal subcutaneous areolar adipose tissue (Cadagan & Merry, 2013).

2.11 Medicinal plants

Traditional medicine plays a major role in the healthcare of most communities particularly in Africa and Asia (Ashworth & Cloatre, 2022). According to the World Health Organization (WHO), approximately 80% of the human population relies on medicinal plants for therapy and treatment of various diseases. Statistically, approximately 40,000 to 70,000 medicinal plant species are utilized across the world as traditional medicines (Uttpal *et al*., 2019, 2022). It is reported that approximately 25% of pharmaceuticals are also derived from plants either directly or indirectly from plants and are effective in the management of illnesses. Plants, evolve and adapt to their environment producing secondary metabolites that act as defense system towards the hostile environments. These natural products are chemically complex molecules more often due to their multiple chiral centers. It therefore, becomes a challenge to chemically synthesize these molecules and where it is possible, the process is not commercially viable due to the costs involved. The structural complexity of natural products contributes to their vast range of therapeutic activities (Datta *et al*., 2021; Mohammed *et al*., 2021; Uttpal *et al*., 2019, 2022). It is therefore, imperative that medicinal plants are the major sources of these medically important natural products (Halder

et al., 2021; Khare *et al*., 2021). In this study, two subspecies of a medicinal plant, *B. abyssinica* subsp. *abyssinica* and *B. abyssinica* subsp. *paullinioides* were selected for investigation of their bioactive secondary metabolites.

2.12 *Bersama abyssinica*

The genus *Bersama* comprises of four species and belong to Melianthaceae family including *B. abyssinica, B. swinnyi, B. yangambiensis,* and *B. engleriana* (Djemgou *et al*., 2010; Kifle & Enyew, 2020). *B. abyssinica* consists of two subspecies, namely, *B. abyssinica* subsp. *abyssinica* (Figure 2.1) and *B. abyssinica* subsp. *paullinioides* (Figure 2.2) (photos courtesy of Prof. I. Wagara). The leaf of *B. abyssinica* subsp. *abyssinica* Verdc. has a wingless rachis with a pointed apex and is usually hairy, whereas that of *B. abyssinica* subsp. *paullinioides* (Gurke) F. White has a wingless or only slightly winged rachis that is spherical. Another distinguishing character between the two is that the capsule of the latter is smoother than that in the former (Beentje *et al*., 1994). *B. abyssinica* is localy known as morgenet and sigirwo by the Sabaot community; omubamba by the Kisii community and olobayie tiang'ata by the Maasai.

Figure 2.1: *Bersama abyssinica* subsp. *abyssinica* plant

Figure 1.2: *Bersama abyssinica* subsp. *paulliniodes* plant

2.12.1 Geographical distribution of *Bersama abyssinica*

The genus *Bersama* is widely distributed in tropical and subtropical Africa (Kuete *et al*., 2007). It grows in lowland bush savanna, gallery forests and montane forests, from sea-level up to 2700 m altitude. In East Africa, there are two subspecies of *B. abyssinica* namely; *B. abyssinica* Fresen. subsp. *abyssinica* and *B. abyssinica* subsp. *paullinioides*. It is distributed in Democratic Republic of Congo, Tanzania, Mozambique, Zambia, Zimbabwe, Angola, Nigeria, Ethiopia, Kenya, Sudan and Uganda (Mikkelsen & Seberg, 2001). Figure 2.3 shows the growing areas of *B. abyssinica* across Africa.

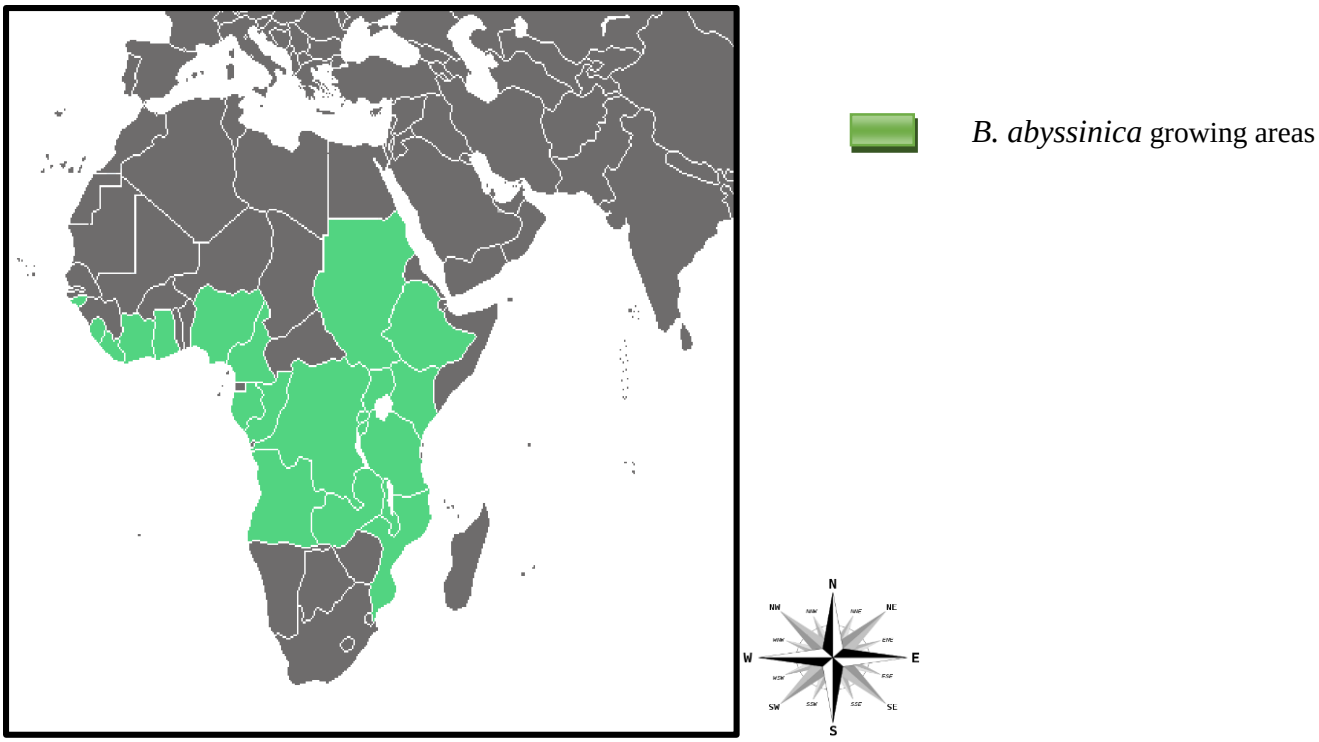

Figure 2.3: Map showing the geographical distribution of *B. abyssinica* in Africa

2.12.2 Medicinal Uses of *Bersama abyssinica*

The majority of *Bersama* species are used traditionally as remedies to manage various diseases. The leaf extracts of *B. abyssinica* are administered orally for treating dysentery and roundworm infestations (Birhanu, 2013; Seyoum & Zerihun, 2014), and the aqueous extract of the plant is also used to treat tumors (Schmelzer & Gurib-Fakim, 2013). The leaves extracts of *B. abyssinica* are administered orally to treat stomach disorders such as abdominal pain, colic, cholera (Regassa, 2013) and diarrhea (Lulekal *et al*., 2014). The stem bark and root bark decoctions are used to treat amoebiasis, rabies, syphilis, gonorrhoea and malaria (Fenetahun & Eshetu, 2017). The bark and leaves of *B. abyssinica* has been used against malaria and fever in humans (Guédé *et al*., 2010). The stem and leaves has been used in the management of blackwater east coast fever and rift valley fever in cattle by the Ogiek and Maasai communities (Amuka *et al*., 2015).

2.12.3 Phytochemistry and Pharmacological Activities of *B. abyssinica*

Phytochemical studies of *B. abyssinica* have been reported in various studies. *B. abyssinica* fresen is rich in various secondary metabolites responsible for the drug's effects in the treatment of various ailments. The stem bark of *B. abyssinica* is rich in phenols, flavonoids, and saponins (Sinan *et al*., 2020). Gas chromatography-mass spectrometry of the methanolic fraction

of leaf, stem bark, and root bark of *B. abyssinica* revealed the presence of flavonoids, terpenes, steroid, carotenoid, unsaturated, and saturated fatty acids (Zekeya *et al*., 2014). The class of compounds identified in the study by Mathewos *et al*., (2018) reported that *B. abyssinica* possess antioxidant, antimicrobial, insecticidal and antitumor properties. The methanolic and chloroform extracts of the leaves of the plant are rich in alkaloids, glycosides, and flavonoids, while the methanolic extract of the leaves contained; steroids, phenols, tannins, triterpenes, anthraquinones, polysterols, and coumarin (Mathewos *et al*., 2018). The aqueous extract of the leaves contains phenolic compounds such as; flavonoids and tannins (Sinan *et al*., 2021). In another study by Amuka *et al*. (2015), it is reported that extracts from *B. abyssinica* are effective against various fungal and bacterial pathogens such as *C. albicans*, *Escherichia coli* and *Klebsiella pneumonia*. Furthermore, the aqueous extract of *B. abyssinica* stem bark was tested against six multi-resistant strains of *S. aureus*. All the multi-resistant strains were sensitive to the extract with an inhibition zone of more than 10 mm (Bene *et al*., 2016).

2.12.4 Secondary metabolites previously reported in *Bersama abyssinica*

Plants of the genus *Bersama* have proved to be a rich source of bufadienolides (Steyn & Van Heerden, 1998). A number of secondary metabolites (**1-16**) have been isolated from *Bersama abyssinica* (figure 2.4). A study by Kupchan *et al*., (1968) led to the isolation of hellebrigenin 3-acetate (**5**) and hellebrigenin 3, 5-diacetate (**2**) which showed antitumor properties. In another study, bersaldegenin 1,3,5-orthoacetate (**12**) and 16β-hydroxy-bersaldegenin 1,3,5-orthoacetate (**13**) were found to be cytotoxic against KB cell lines (Kupchan *et al*., 1971). Compounds **1-13** are bufadienolides, a class of C-24 steroids consisting of a characteristic α-pyrone ring at C-17. Three structures are drawn as a template of the common part of the compounds **1-13** and the varying substituents are shown below. Compounds **14** – **16** are flavonoid glycosides and have been previously reported from the leaves of *B. abyssinica* (Asres *et al*., 2006).

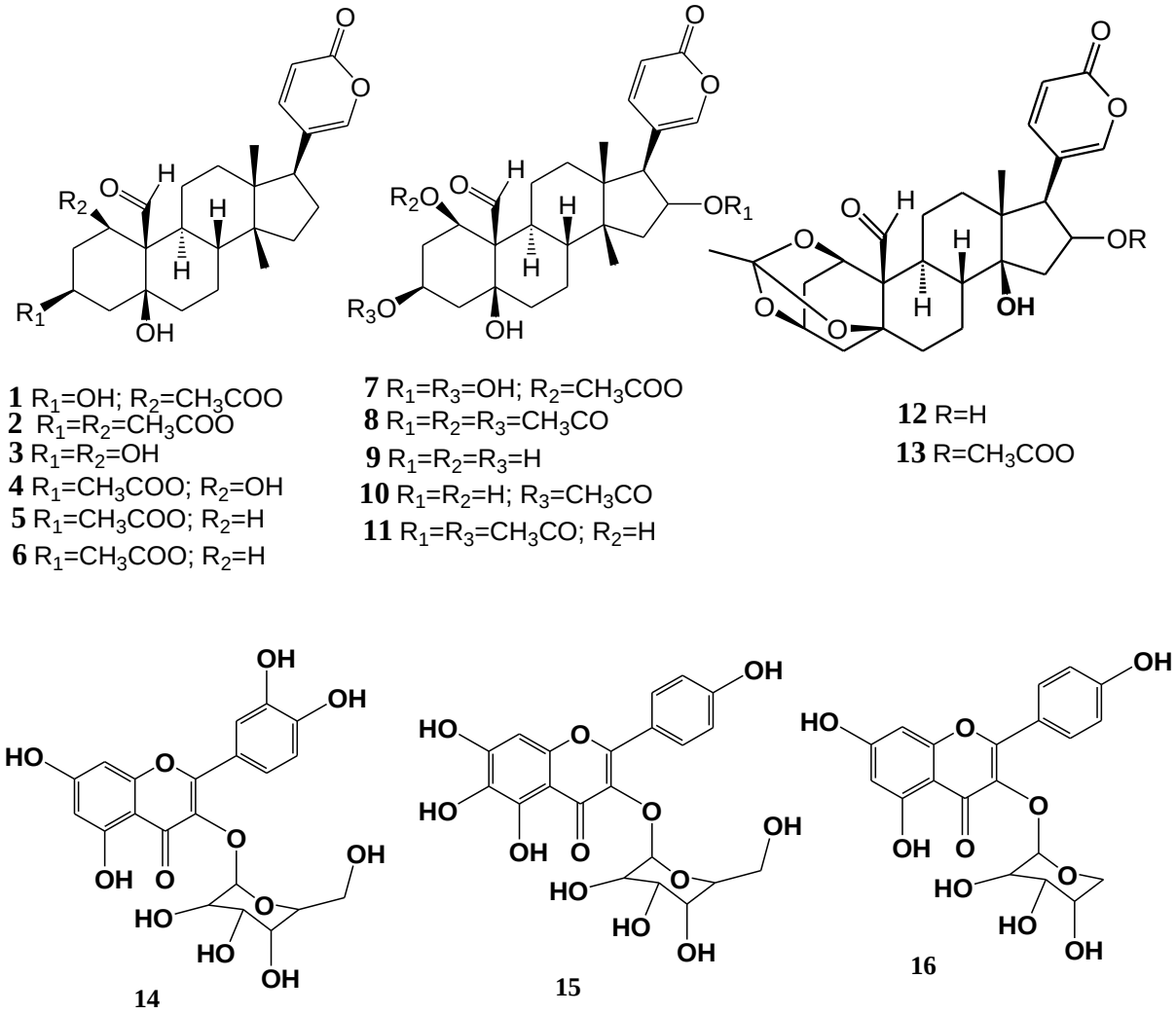

Figure 2.4: Chemical structures of secondary metabolites isolated from *Bersama abyssinica*

2.13 Medicinal plants as sources of antibacterial and antifungal agents

Medicinal plants have been part of the integral culture of many communities for the treatment of various ailments including bacterial and fungal infections (Mahomoodally, 2013). In the recent past, scientists have reported various antimicrobial properties of extracts and compounds from plants. Plant derived antibacterial and antifungal agents have generated a lot of interest for the improvement of human health (Ververidis *et al*., 2007). Studies on clinical efficacy and

antimicrobial effects as well as the chemistry of commercially available antibacterial and antifungal agents of plant origin currently used in the prevention and treatment of infections have been done. These infections include: skin infections, gastrointestinal infections, oral infections, urinary tract infections and respiratory infections (Omwenga *et al*., 2015). More than 40 plant-derived over the counter pharmaceuticals, cosmetics, herbal medicines and dietary supplements are currently in use. Examples include extracts such as, *Glycyrrhiza glabra* extract, *Melaleuca alternifolia* essential oil, and *Pistacia lentiscus* resin; pure compounds such as benzoic acid, eucalyptol, salicylic acid, berberine and thymol; and derivatives such as, bismuth zinc pyrithione, and subsalicylate. In vitro antimicrobial data supporting the efficacy of these products have been illustrated through clinical trials. These data, as well as, the broad spectrum of various commercial products currently available on the market indicate that medicinal plants are expected sources of antibacterial and antifungal agents. Furthermore, medicinal plants are alternative sources of secondary metabolites that could be effective against microbial human diseases that are recently emerging. They also offer prospective solutions to the challenges of antimicrobial resistance (Kokoska *et al*., 2019).

2.14 Medicinal plants as sources of anticancer agents

Plants have a long history of use in the treatment of cancer with more than 3000 plant species reported to have been used in the treatment of cancer. It is significant that over 60% of currently used anticancer agents are derived in one way or another from natural sources, including plants, marine organisms and micro-organisms (Abbott *et al*., 1967; Graham *et al*., 2000; Shoeb, 2008; Talib *et al*., 2022). Secondary metabolites of plant origin are often excellent leads for drug development. Scientists therefore modify the chemical structure of more promising compounds in one strategic way to increase their anticancer action and selectivity, improve their absorption, distribution, metabolism and excretion properties and decrease their toxicity and side effects (Guo, 2017; Yao *et al*., 2017). Some plant secondary metabolites and their derivatives obtained by structural modifications, have made great achievements as anticancer agents. For instance, vincristine, is one of the first anticancer agents of plant origin to be approved in clinical use. It is a naturally-occurring alkaloid extracted from the leaves of *Catharanthus roseus* (L.) G. Don and has been used in chemotherapy against acute lymphoblastic leukemia. Furthermore, it has been used to treat other cancers such as rhabdomyosarcoma, lymphomas, neuroblastoma and nephroblastoma (Almagro *et al*., 2015; Moore & Pinkerton, 2007).

Another chemotherapy drug of plant origin is paclitaxel, a tricyclic diterpenoid. It was isolated from the bark of *Taxus brevifolia* Nutt. (Pacific Yew) and sold under the brand name Taxol® since 1993. Paclitaxel is a complex molecule that has become one of the most active cancer chemotherapeutic drugs known (Bernabeu *et al*., 2017; Weaver, 2014). Traditional medicine uses the bark extracts of *Cephalotaxus harringtonii* (Knight ex J.Forbes) K. Koch and *Cephalotaxus fortunei* Hook. trees to treat cancer. Furthermore, homoharringtonine, is an alkaloid and was first isolated from these plants and exhibits potent antiproliferative activity against leukemia cells. After a series of clinical trials, the Food and Drug Administration (FDA) in 2014 approved homoharringtonine for self administration at home and therapy by the patients or caregivers (Shen *et al*., 2014). Cephalotaxine, a compound that is naturally occurring in the leaves of *Cephalotaxus* species can be transformed into homoharringtonine by esterification (Butler *et al*., 2014; Xiao *et al*., 2016).

2.15 Modes of action of plant secondary metabolites

Plants produce secondary metabolites which act as defense compounds against microbes, as well as, signal compounds. These secondary metabolites exhibit a wide range of biological and pharmacological properties (Wink, 2015). Because of this, some plant products have been and still are used to treat infections and various health disorders. Secondary metabolites interact with the main target in the cells such as proteins, biomembranes or nucleic acids. Secondary metabolites specifically modulate a corresponding molecular target in animals or humans. Such targets are often neuroreceptors, enzymes which degrade neuroreceptors, ion channels, ion pumps or members of the cycloskeleton (Wink, 2015; Wink & Schimmer, 2010). Secondary metabolites have been presently extracted from plants and endophytes and are used in modern medicine as chemical entities with established applications. These secondary metabolites are specific for a given target. Table 2.1 provides examples of secondary metabolites isolated from plants and their mode of action as well as their medicinal application (Wink, 2015).

Table 2.1: Mode of action of secondary metabolites isolated from medicinal plants

Secondary metabolites	Plant species	Mode of action	Application
Morphine	*Papaver somniferum*	agonist of endorphine receptors	analgesic, hallucinogen
Cocaine (A)	*Erythroxylum coca*	inhibits Na^+ channels and reuptake of noradrenaline and dopamine	analgesic; stimulant
Digitoxin, digoxin (T)	*Digitalis lanata*	inhibits Na^+,K^+-ATPase	heart insufficiency
Dimeric Vinca alkaloids	*Cannabis sativa*	inhibit microtubule assembly	tumor therapy
Colchicine	*Colchicum autumnale*	inhibits microtubule assembly	gout treatment
Huperzine A	*Lycopodium clavatum*	Inhibits AChE (anti-cholinesterases)	Alzheimer treatment
Pilocarpine	*Pilocarpus joborandi*	agonist of mAChR (Muscarinic acetylcholine receptor)	glaucoma treatment

2.16 Endophytes

Plants are reservoirs for an enormous number of bacterial and fungal microorganisms known as endophytes (Tanvir *et al*., 2017). Endophytes colonize the internal tissues of plants without causing any harm. Endophytes impact the mechanisms of the metabolism of host plants by employing pathways such as; endophyte self-metabolizing, endophyte and host co-metabolizing and signaling. Further, the introduction of secondary metabolites could be one of the mechanisms endophytes influence the metabolism in the host plants (Huang *et al*., 2018). Endophytes produce many bioactive secondary metabolites in plants and have proven to be good sources of drugs for the treatment of various diseases (Kaul *et al*., 2012). Secondary metabolites that have been isolated from endophytes include; quinones, alkaloids, flavonoids, benzopyrones, saponins, terpenoids, xanthones, steroids, and tannins. Endophytes therefore, are potential sources

of novel compounds for exploitation in the pharmaceutical industry (Pimentel *et al*., 2011). In another study by Nisa *et al*. (2015), it is reported that the use of medicinal plants as source of novel compounds may lead to the deterioration of species and hence loss of biodiversity. Therefore, microorganisms residing inside the medicinal plants offer an alternative to the process of drug discovery while conserving the biodiversity.

A number of fungi have been isolated from medicinal plants and screened for biological activities against various pathogens (Kaul *et al*., 2017; Vasundhara *et al*., 2016). Secondary metabolites produced by different endophytic fungi from medicinal plants possess unusual chemical structures with interesting bioactivities (Lunardelli *et al*., 2016). Endophytic fungi should therefore, be exploited for lead compounds of pharmaceutical importance. Endophytes are beneficial to the plants by producing secondary metabolites which prevent the host from being attacked by pathogenic fungi, bacteria, and pests (Kusari *et al*., 2013). Endophytes have shown to produce a variety of secondary metabolites with structures such as alkaloids, lipids, polyketides, terpenoids and glycosides (Suresh & Sona, 2021). Several other studies report a wide range of various classes of compounds such as steroids, xanthones, phenols, isocoumarins, perylene derivatives, quinines, furandiones, terpenoids, depsipeptides, and cytochalasins. These secondary metabolites exhibit pharmacological activities which include: antibacterial, antiviral, anticancer, antioxidant, antifungal, insecticidal, antidiabetic, and immunosuppressive properties (Deshmukh & Verekar, 2012; Gunatilaka, 2006; Hridoy *et al*., 2022; Manganyi & Ateba, 2020; Silva-Hughes *et al*., 2015).

2.16.1 Fungal endophytes as sources of antibacterial agents

The potential of endophytic microorganisms to produce a range of secondary metabolites makes them an interesting source in the search for new antimicrobial agents, and their application in the food and cosmetics industry can contribute to several biotechnological applications. Some of the metabolites produced by endophytes are terpenes, alkaloids, phenols, tannins, quinones, saponins, steroids (Sharma *et al*., 2020). Several compounds have been isolated from various endophytic fungi with interesting antimicrobial activities. For instance, sesquiterpenoids and terpenes were isolated from endophytic fungus *Leptosphaeria sp*. isolated from the leaves of *Panax notoginseng*. These molecules showed antibacterial activity against *E. coli*, *P. aeruginosa*, and *Salmonella typhimurium* strains, with MIC ranging from 12.5 to >100 µg/mL (Chen *et al*., 2019). An anthraquinone, altersolanol was isolated from endophytic fungus *Phomopsis longicolla*

obtained from the leaves of *Bruguiera sexangular* var. *rhynchopetala*. The compound was active against *Vibrio parahaemolyticus* and *Vibrio anguillarum* with MIC values of 2.5 and 5.0 µg/mL, respectively (Li *et al*., 2017). Alkaloids namely, indol-3-acetic acid, methyl indolyl-3- acetate, and bassiatin from *Fusarium proliferatum* isolated from green Chinese onion showed activity against *E. coli* with MIC above 100 µg/mL (Jiang *et al*., 2019). Further, di-(2-ethylhexyl) phthalate (DEHP) was isolated from the endophytic fungus *Diaporthe phaseolorum* obtained from *Paullinia cupana* var. *sorbilis* (Mart.). The compound showed antibacterial activity against multi resistant and sensitive *E. coli* and *P. aeruginosa* strains, with MIC values of >30 µg/mL for *E. coli* and 0.23 µg/mL for *P. aeruginosa* (Silva *et al*., 2018).

2.16.2 Fungal endophytes as sources of antifungal agents

Endophytic fungi is reported to have the potential to produce secondary metabolites that are active against fungal pathogens. In a study by Wu *et al*. (2016) compounds isolated from *Pestalotiopsis* sp. obtained from *Dendrobium officinale* were tested for antifungal activities. They exhibited anti-fungal activities against *C. albicans*, *Cryptococcus neoformans*, *T. rubrum*, and *Aspergillus fumigatus* with MIC values ≤ 50 µg/mL (Wu *et al*., 2016). In another study, endophytic fungus *Pestalotiopsis fici* obtained from *Camellia sinensis* was a source of ficipyrone A. This compound showed antifungal activity against *Gibberella zeae*, a fungal plant pathogen with, an IC_{50} value of 15.9 µM (Liu *et al*., 2013). A phenolic compound was isolated from endophytic fungus *Pestalotiopsis mangiferae* associated with *Mangifera indica* Linn. The compound exhibited strong antifungal activity against *C. albicans* with an MIC value of 0.039 µg/mL, while nystatin showed an MIC of 10.0 µg/mL (Subban *et al*., 2013). Further, compounds isolated from endophytic fungus *Rhizopycnis vagum* obtained from *Nicotiana tabacum* showed strong inhibition of *Magnaporthe oryzae* with IC_{50} values ranging from 9.9 µg/mL and 12.0 µg/mL (Lai *et al*., 2016).

2.16.3 Fungal endophytes as sources of anticancer agents

Pacilitaxel is an important anticancer drug that is used for the treatment of ovarian cancer, breast cancer, and lung cancer (Wood *et al*., 1995). It was initially isolated from a medicinal plant *Taxus brevifolia* as discussed earlier. Later on the compound was isolated from an endophytic fungal culture of *Pestalotiopsis* sp. The fungal culture was obtained from the stem bark of a medicinal plant, *Tabebuia pentaphylla* (Visalakchi & Muthumary, 2010). The derivative of pacilitaxel named docetaxel was also invented and the mechanism of these drugs is through the

blockage of cell mitosis by stabilization of the microtubule polymer and consequently cell death (Żwawiak & Zaprutko, 2014). More anticancer agents have been discovered from fungal endophytes over time. Vinblastine and vincristine, was originally isolated from the plant *Catharanthus roseus* and later found from the culture of *Alternaria* sp. (Guo *et al*., 1998) and *Fusarium oxysporum* (Kumar *et al*., 2013). *Alternaria* sp. and *F. oxysporum* endophytic fungi were obtained from the same plant host. Derivatives of camptothecin, topotecan and irinotecan were isolated from the stem bark of *Camptotheca acuminate* plant. They exhibit cytotoxicity against several cell lines including lung cancer, ovarian cancer and liver cancer and have also been found in the culture of endophytic fungi such as *Neuropsora* sp., *Fusarium solani* and *Entrophospora infrequens* (Kharwar *et al*., 2011).

2.17 Overview of fungal endophytes isolated from *Bersama abyssinica* in this study

Endophytic fungi have a great influence on plant health and growth, and are an important source of bioactive natural compounds. These endophytic fungi belong to the phylum Ascomycota and produce various classes of bioactive secondary metabolites (Gakuubi *et al*., 2022; Helaly *et al*., 2018). In this study, six endophytic fungi were isolated from the plant tissues of *B. abyssinica* subsp. *abyssinica* and subsp. *paulliniodes*. They include *Epicoccum nigrum, Hypoxylon lividipigmentum and Talaromyces pinophilus, Purpureocillium lilacinum, Clonostachys rosea, Scopulariopsis fusca*.

2.17.1 *Epicoccum nigrum*

Epicoccum nigrum is an endophytic fungi that has been isolated from terrestrial microorganisms such as *Salix sp*. (Harwoko *et al*., 2019), *Cordyceps sinensis* (Guo *et al*., 2009), *Lysidice rhodostegia* (Wang *et al*., 2010) and *Mentha suaveolens* (Amrani *et al*., 2014). *E. nigrum* has also been isolated from *Theobroma cacao* L. (Sterculiaceae), commonly known as cocoa tree. It is an economically important crop cultivated in several tropical and subtropical parts of the world for the manufacture of chocolate, and for pharmaceutical and cosmetic purposes (Talontsi *et al*., 2013a). In this study, the fungus *E. nigrum* was isolated from the fresh leaves of *B. abyssinica* subsp. *abyssinica*. Previous studies reveal that the endophytic fungi *E. nigrum* is rich in isobenzofuran derivatives, polyketides, thiodiketopiperazines and diketopiperazines (Amrani *et al*., 2014; Guo *et al*., 2009; Harwoko *et al*., 2019; Wang *et al*., 2010).

2.17.2 *Hypoxylon lividipigmentum*

Hypoxylon lividipigmentum has been reported as fungus from both medicinal plants and lichens tissues. Ethyl acetate extract of the fungus has been reported to possess antioxidant, anti-inflammatory, tyrosinase inhibitory and antibacterial potency. LC-MS dereplication was conducted on the crude extract to identify the secondary metabolites. The secondary metabolites in *H. lividipigmentum* include: ochrindole C, 2,5-Dihydroxybenzenemethanol, epoformin, isoepiepoformin, 2,3,6-Trihydroxytoluene, aurantiomide A, jiangolide, cinatrin B, 5-Methylpyrogallol and 2-Methylene-3-oxocyclopentanecarboxylic acid (Weerasinghe *et al*., 2021a; Weerasinghe *et al*., 2021b).

2.17.3 *Talaromyces pinophilus*

Talaromyces pinophilus is an endophytic fungus from the genus *Talaromyces* and the family *Trichocomaceae*. *T. pinophilus* is known for producing some essential bioactive secondary metabolites, including terpenoids, alkaloids, polyketides, tetraene, esters, lactones, and furanosteroids (Adelusi *et al*., 2022; Lan & Wu, 2020). Organic extracts obtained from the culture filtrate of an endophytic strain of *Talaromyces pinophilus* isolated from strawberry tree (*Arbutus unedo*) were studied. The analysis of secondary metabolites revealed the presence of bioactive metabolites including; siderophore ferrirubin, the platelet-aggregation inhibitor herquline B and 3-O-methylfunicone with antibacterial activity (Vinale *et al*., 2017).

2.17.4. *Purpureocillium lilacinum*

Purpureocillium lilacinum belongs to the genus *Purpureocillium* and family *Ophiocordycipitaceae*. A number of secondary metabolites have been isolated from the fungus *P. lilacinum* including, acremoxanthone, acremonidin, paecilomide, pyrones, ergosterols, cerebrosides and leucinostatins (Wei & Hu, 2022). *P. lilacinum* is an important fungus which has been previously used in the development of pesticide products in China, USA and Europe. Furthermore, *P. lilacinum* has been reported to be effective against *Phyllotreta striolata, Thrips palmi,* and predatory mite (Hotaka *et al*., 2015; Yoder *et al*., 2018). Studies have reported that, healthy crops and plants can be achieved by treatment with symbiotic fungi (Colla *et al*., 2015; Hyde & Soytong, 2008; Strobel & Daisy, 2003). Endophytic fungi and mycorrhizal fungi are the major groups of fungi in which such plant-fungus associations have been established (Bonfante & Genre, 2010). *P. lilacinum* has been reported to be potential plant growth hormone. The fungus

was used as a bioinoculant in beans, soybean and maize. The findings showed an increase in vegetation growth and plant height were associated with the fungus *P. lilacinum* (Baron *et al*., 2020). These findings can be attributed to the presence of growth promoting secondary metabolites in this fungus (Erb & Kliebenstein, 2020; Selim *et al*., 2021).

2.17.5. *Clonostachys rosea*

The fungus *Clonostachys rosea* has been reported in mangrove plants, strawberry, onion plants, lettuce cocoa trees, tomato and medicinal plants such as *Blumea balsamifera* among others (Costa *et al*., 2012; Meng *et al*., 2022; Muvea *et al*., 2014; Shu *et al*., 2020; Supratman *et al*., 2019). New secondary metabolites isolated from the fungus, *C. rosea* obtained from mangrove plants have been described. These secondary metabolites include (-)-dihydrovertinolide, and clonostach acid A, clonostach acid B, and clonostach acid C. Further, previously described compound (-)-vertinolide was also isolated (Supratman *et al*., 2019). In another study, *C. rosea* was obtained from the medicinal plant *Blumea balsamifera*. Secondary metabolites described as verticillin A, (S)-(+)-fusarinolic acid, 8-hydroxyfusaric acid, cerebroside C, 3-Maleimide-5-oxime, and bionectriol A were isolated from *C. rosea*. The compounds exhibited antibacterial activities against a range of bacterial pathogens that include: *E. coli*, *S. aureus*, *B. subtilis* and *P. aeruginosa* (Shu *et al*., 2020).

2.17.6. *Scopulariopsis fusca*

Scopulariopsis fusca has been reported as both endophytic marine fungus and endophytic fungus from medicinal plants. It is one of the fungus with untapped potential and posses secondary metabolites with a wide range of biological activities (Hawas & Al-Farawati, 2017; Manganyi & Ateba, 2020). *S. fusca* is among the fungi that improve the resistance of the host marine organisms to the harsh environment through the production of bioactive metabolites. The fungus produce secondary metabolites that belong to various structural groups such as tannins, flavonoids, quinones, alkaloids and steroids. These classes of compounds have been reported with antimicrobial and insecticidal activities (Hawas & Al-Farawati, 2017).

2.18 Effect of ecological differences on production of plant secondary metabolites

Medicinal plants are a source of all kinds of secondary metabolites and are subjected to various environmental stresses through the process of growth and development. Ecologically limiting factors include temperature or heat, carbon dioxide, lighting in the area the plant grows,

the nature of the soil in terms of fertility, humidity and salinity. These factors have significant influence on the physiological and biochemical responses of medicinal plants′ which in turn impact the synthesis of secondary metabolites (Mahajan *et al*., 2020; Pant *et al*., 2021). Secondary metabolites are important for assessing the therapeutic ingredients of plants and their quality which are natural derived drugs such as antimicrobials, immunosuppressant, anti-diabetic, and anti-cancer (Nandy *et al*., 2020). Plants have the ability to synthesize a variety of secondary metabolites to cope with the negative effects of stress. The environmental factor is the major limiting factor for the survival and growth of medicinal plants. Studies have revealed that plants of the same species grown in a different environment have a different concentration of a particular secondary metabolite. This is because the plant has to produce a specified quantity and quality of secondary metabolite to counter the environmental stress (Radušienė *et al*., 2013; Ramakrishna & Ravishankar, 2011).

2.18.1 Temperature stress

The growth of plants and their metabolic pathways that signal defense responses and physiological regulation change with temperature change. Temperature is a weather variable and can influence the production and composition of secondary metabolites significantly due to the disruption in the photosynthesis process to tolerate stressful environments (Mahajan *et al*., 2020; Pant *et al*., 2021). For instance, the appearance of vegetative development increases as temperature rise to the plants' optimum level while growth and development are limited during cold temperatures. It is reported that, the composition of alkaloids in *Duboisia myoporoides* R. Br. increased slightly with a temperature increase of 4 °C (Ullrich *et al*., 2017). In another study, an increase in the accumulation of tanshinones from *Salvia miltiorrhiza* Bunge was observed with an increase in temperature (Zhang *et al*., 2019). Likewise, in *Tithonia diversifolia* A. Gary, there is an increase in phenolic compounds at 22 °C and a decrease afterward (Sampaio *et al*., 2016). *Camellia japonica* L. global gene regulation of unsaturated fatty acid and jasmonic biosynthesis pathways were deduced in the low temperature (Li *et al*., 2016). On contrary, high temperature reduce silymarin content in *Silybum marianum* L. roots showing secondary metabolites accumulation is a temperature-dependent process (Rahimi & Hasanloo, 2016).

2.18.2 Carbon (iv) oxide (CO_2) Stress

Carbon (iv) oxide is a greenhouse gas hindering the physiology of medicinal plants. The concentration of this gas is increasing rapidly due to the industrial revolution (WMO, 2019). The

metabolic plasticity in plants enables them to adapt to the changing environment. However, these affect the production of secondary metabolites which are the basis of the plant's medicinal activity (Yang *et al*., 2018). For example, *Hypericum perforatum* L. is known for its use in moderate depression. It was treated with CO_2 and its growth increased after 4 months compared to ambient conditions. Furthermore, the bud and flower formation advanced by 4 days. Hypericin, a compound in *H. perforatum* L. decreased significantly under the combined effects of elevated CO_2 and temperature (Sharma *et al*., 2020). *Paris polyphylla* var. *yunnanensis*, a traditional Chinese medicinal plant, showed stronger photosynthetic activity and higher content of bioactive compounds in western Yunnan than in a cultivar from central Yunnan under elevated CO_2. In western Yunnan, the growth rate increases at first and decreases with further CO_2 increase. On the contrary, in central Yunnan growth rate is lower at first and increases afterward suggesting western Yunnan cultivars are sensitive to atmospheric CO_2 concentration. Contents of bioactive compound diosgenin of western Yunnan cultivars increased under elevated CO_2 suggesting *Paris polyphylla* var. *yunnanensis* a potential candidate for industrial cultivation in a high CO_2 environment (Qiang *et al*., 2020). A similar study conducted on *Mentha piperita* L. showed an increase in flavonoids concentration with the application of elevated CO_2 (Siavash *et al*., 2017).

2.18.3 Light Stress

Light is essential for plant metabolism and life due to its role in photosynthesis process. Therefore, the survival of plants depends on their ability to sense different light spectra present in solar radiation. Also, the light at different intensity impacts the levels of a broad range of secondary metabolites in the complex biochemical interaction (Kazan & Manners, 2011). A study on plants of the genus *Mahonia* (*Mahonia bodinieri* (Gagnep.) Laferr and *Mahonia breviracema* Y.S. Wang & P.K. Hsiao) popularly known traditional Chinese medicine used for the treatment of tuberculosis, dysentery, periodontitis, pharyngolaryngitis, eczema and wounds showed a higher yield of alkaloids under I_{50} (50 % of sunlight) followed by I_{30} (30 % of sunlight) than under I_{10} (10 % of sunlight) and I_{100} (Full sunlight) (Kong *et al*., 2016). Therefore, I_{30} and I_{50} were beneficial for the synthesis and accumulation of secondary metabolites indicating noticeable effects of light intensity and duration of light exposure. Rarely, the opposite situation was also reported like in *Flourensia cernua* DC, a Mexican traditional medicine used to treat indigestion, respiratory tract infection, tuberculosis which showed higher total phenolic compounds under partial shade than on fully irradiated conditions (Estell *et al*., 2016).

2.19 Fermentation techniques and crude extract production

In the microbial growth phase, secondary metabolite production begins at the stationary phase; these are usually compounds with unique chemical structures. Their production begins when a vital source of nutrient such as carbon, nitrogen or phosphate are depleted. Fungal endophytes should be obtained in pure culture and optimal media. Growth conditions must be determined before fermentation begins as this will determine crude extract production. Factors that quantitatively and qualitatively affect production of secondary metabolites include: degree of aeration, temperature, media composition, pH and culture duration (Barrios-González & Mejía, 1996; Hwang *et al*., 2014; Robinson *et al*., 2001). Different types of media can be used to cultivate fungi, these are; Potato Dextrose Agar (PDA), Yeast Malt Agar (YMA), Oatmeal Agar (OMA), Corn Meal Agar (CMA) among others. The type of media is dependent on the purpose and type of species (Hölker *et al*., 2004). Fermentation techniques used in the cultivation of fungal endophytes include submerged fermentation (SmF) or liquid fermentation and solid state fermentation (SSF) (Barrios-González & Mejía, 1996; Udo Hölker & Lenz, 2005). Although the two techniques are different in terms of operation both can be used to identify secondary metabolites produced by fungal endophyte. The appropriateness of a given procedure is usually evaluated based on the objective of the study and available resources.

2.19.1 Solid State Fermentation

Solid state fermentation is the cultivation of microorganisms under controlled conditions in the absence of free water. The advantages of solid state fermentation have attracted researchers and industrialists. These advantages include; the high volume of productivity of secondary metabolites, the simplicity of the process which requires low energy for production, meeting aeration requirement is easier for solid state fermentation than liquid state fermentation and it resembles the natural habitat of some microorganisms such as fungi and bacteria. The solid state fermentation utilizes solid substrates such as rice bran, saw dust, sugar beet pulp, maize bran, wheat straw, rice straw and banana (Naik *et al*., 2019; Pandey *et al*., 2000)

2.19.2 Liquid State Fermentation

Liquid state fermentation (LF) also referred to as submerged fermentation (SmF) is a technique that utilizes free flowing substrates such as broths, vegetable and fruit juices and molasses. The bioactive compounds are secreted into the fermentation broth and mycelial growths. The substrates are utilized rapidly and hence constant supplementation of nutrients is required.

Liquid fermentation technique is best for microorganisms that require high moisture content for better production of secondary metabolites (Subramaniyam & Vimala, 2012).

2.20 Structure elucidation of the isolated compounds

Structure determination is often carried out using a combination of spectrometric and spectroscopic techniques. Spectrometric methods such as mass spectrometry (MS) and tandem mass spectrometry (MS^n) provide information linked to the structure of the molecule including the molecular weight of the analyzed material and the nature of the bonds. Spectroscopic methods of structure determination include; X-ray crystallography, cryo-electron microscopy, NMR spectroscopy, ultra-violet visible (UV/Vis) spectroscopy, and Infrared spectroscopy (IR) (Karlsson *et al*., 2023; Letourneau & Volmer, 2023).

2.20.1 Mass spectrometry

A typical LC-MS system is a combination of HPLC or UPLC with MS using an interface. High performance liquid chromatography coupled to mass detection (HPLC–MS) is the most frequently used technique for analyzing secondary metabolites. This is an important tool in the identification, quantitation, and mass analysis of components. It is also used in determining the purity as well as the composition of the analyte. HPLC-MS has high sensitivity and is optimal for performing precise and reproducible quantitative analyses. Reversed-phase HPLC coupled with mass spectrometry (HPLC-MS) is a popular analytical technique for semi-polar compounds and a powerful platform for both targeted and untargeted profiling of secondary metabolites (Li *et al*., 2013; Nahar *et al*., 2020; Parasuraman *et al*., 2014). High-resolution LCMS with exact mass determination provides comprehensive mass and retention time fingerprints representing hundreds of known and unknown metabolites. The combination with mass spectrometry fragmentation abilities and / or UV / Vis detection also provides valuable structural information about the compounds detected (Alvarez-Rivera *et al*., 2019). Liquid chromatography - mass spectrometry (LC-MS) with electrospray ionization (ESI) can be performed in either negative mode or positive mode, usually depending on the compounds of primary interest. The classes of compounds readily detected in ESI-negative mode include; phenylpropanoids, flavonoids, terpenoids, and glycosylated compounds (Ramabulana *et al*., 2021; Yahia *et al*., 2020). On the other hand, polyamines and other compounds comprising chemical structures that easily form proton adducts, e.g., alkaloids and anthocyanins, can be better detected in ESI-positive mode. Thus, analysis of

samples in both positive and negative ionization modes provides the most comprehensive insight into their metabolic composition. Nevertheless, profiling in just a single ionization mode may already be sufficient to obtain an overview of the differences and similarities

2.20.2 Nuclear magnetic resonance spectroscopy (NMR)

For nuclei with I = 1/2, when placed in a magnetic field, two spin states exist, +1/2 and -1/2, with the magnetic moment of the lower energy aligned with the external field and the higher energy spin state opposed to the external field. The difference between the two spin states is responded to the external magnetic field. The low state of nuclei will be excited to upper state by absorbing energy from radiation, whereas the upper state nuclei will return to low state by releasing the energy. If the population of the upper and lower energy spin states is not the same, there is a Boltzmann distribution of the nuclei with a slight excess in the lower state, hence, the slight excess of nuclei is observed (Atta-Ur-Rahman, 2012; Bovey *et al*., 1988). One dimentional NMR (^{1}H NMR, ^{13}C NMR, DEPT) and two dimentional NMR (^{1}H–^{1}H COSY, HMBC, HSQC, NOESY, spectroscopy are frequently used to elucidate structures. ^{1}H NMR spectroscopy is a well-established and important application during isolation: chemical shifts give the information about the chemical environment of the protons; integrations show the number of protons; and *J*-coupling constants provide detailed connectivity of adjacent protons. ^{13}C NMR and Distortionless enhancement by Polarization Transfer (DEPT) display the information of carbons involved in the structures including C, CH, CH_2 or CH_3. ^{1}H–^{1}H COSY (Correlation Spectroscopy) and NOESY (Nuclear Overhauser Effect Spectroscopy) give the different relationship of neighboring protons (adjacent connection for COSY and adjacent in space for NOESY), while HMBC (Heteronuclear Multiple-Bond Correlation Spectroscopy) and HSQC (Heteronuclear Single-Quantum ^{1}H–Correlation Spectroscopy) provide the different relationship between protons and carbons (HMBC detects C correlations over longer ranges of about 2 – 4 bonds, while HSQC detects direct correlations between ^{1}H and ^{13}C nuclei). The samples for NMR are dissolved in deuterated solvents, while tetramethylsilane (TMS) is the internal standard (Anand *et al*., 2022; Topcu & Ulubelen, 2007).

CHAPTER THREE
MATERIALS AND METHODS

3.1 Plant material

The leaves and stem barks of two subspecies of *B. abyssinica*, subspecies *abyssinica*, and subspecies *paullinioides* were collected from Mt. Elgon national forest (1.1493° N, 34.5418° E). The plants were identified by a taxonomist (the late Prof. S.T. Kariuki) at the Department of Biological Sciences, Egerton University. The plant materials were dried under shade and at room temperatures to prevent the loss of labile compounds and to retain their natural active compounds. The plant materials were turned over periodically during drying to avoid growth of moulds. Voucher specimens BW12 and PSK245 were deposited at the department of biological sciences, Egerton University. Figure 3.1 is the map of Kenya indicating the sample collection site.

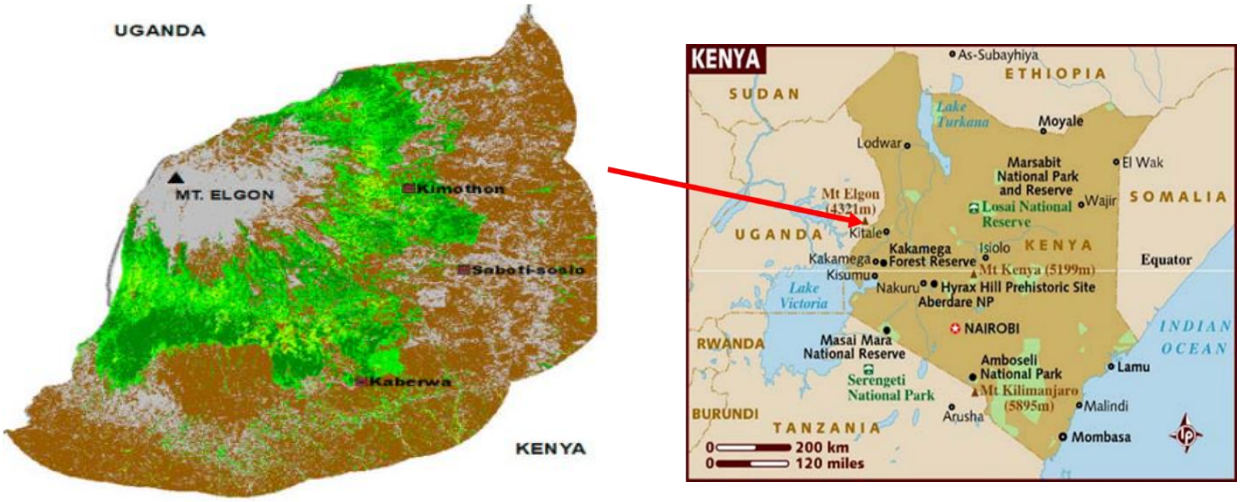

Figure 3.1: Map of Kenya showing Mt. Elgon national park

3.2 General Experimental Procedures

Optical rotations were determined using a Kruss P8000-T polarimeter in methanol at 25 °C. IR spectra were recorded by Bruker Tensor-27 FT-IR spectrometer using a diffuse reflection apparatus (Cricket, Harrick Scientific). UV spectra were measured using UV-1602 UV-VIS spectrometry (Shimadzu). NMR experiments were performed with a Bruker Avance III spectrometer operating at 700 MHz (^{1}H) and 175 MHz (^{13}C). High-resolution mass spectra (HRESIMS) were carried out using LTQ Orbitrap spectrometer (Thermo Scientific, USA)

equipped with a HESI-II ion source. For column chromatography, silica gel 60 (0.063 – 0.2 mm, Macherey-Nagel) and Sephadex LH–20 (18 – 111 μm, GE Healthcare) were used. TLC was carried out on pre-coated silica gel 60 plates (0.20 mm, Macherey-Nagel). Semi-preparative HPLC was conducted using a Shimadzu LC-20AP pump equipped with DGU-20A5R degassing unit, a Shimadzu SPD-M20A detector and a Shimadzu SIL-20ACHT auto-sampler, using LabSolutions software.

3.3 Extraction of secondary metabolites from dried plant materials

Extraction for secondary metabolites from dried plant materials was carried out on three samples separately; the stem bark of *B. abyssinica* subsp. *paullinioides*, the stem bark of *B. abyssinica* subsp. *abyssinica*, the leaves of *B. abyssinica* subsp. *abyssinica*.

3.3.1 Extraction of secondary metabolites from the stem bark of *B. abyssinica* subsp. *paullinioides*

The air-dried bark of *B. abyssinica* subsp. *paullinioides* (1300 g) was soaked with MeOH for 24 h, twice at room temperature. The extracts were concentrated under reduced pressure to give brown residues (135 g) and about 130 g of the extract was applied to column chromatography (CC) over silica gel 60 and eluted with cyclohexane/EtOAc and then EtOAc/MeOH mixtures of increasing polarities. Fractions were combined into eight fractions based on similar LC-MS profile. Fraction 4 (EtOAc 100 %), fraction 5 (EtOAc/MeOH 90:10), and fraction 6 (EtOAc/MeOH 80:20) were identified as potential fractions for HPLC separation because of their interesting masses. The fractions were passed through Sephadex LH-20 prior to separation by semi-preparative HPLC and a Gemini C_{18} column (10 × 250 mm, 10 μm particle size, Phenomenex) was used for reversed-phase preparative HPLC. Double distilled water (A) (0.1 % formic acid) and MeOH (B) were used as a mobile phase. The elution gradient used 45−65% solvent B over 25 min and thereafter isocratic conditions at 100% solvent B for 10 min, and then the system returned within 0.5 min to the initial conditions of 45% B and was equilibrated for 10 min. UV monitoring was carried out at 254, 275, and 350 nm, and the flow rate was 4 mL/min. Six fractions (F4A-F4F) were collected from fraction 4, four fractions (F5A-F5D) from fraction 5 and five fraction (F6A-F6E) from fraction 6 were collected. Fraction F4D was further purified by a reverse-phase preparative HPLC using VP 125/10 NUCLEODUR PolarTec column (10×125 mm, 5 μm, Macherey-Nagel) as a stationary phase and flow rate of 4 mL/min, elution gradient:

65% isocratic conditions for 10 min, to afford compound **17** (2.4 mg). Unless stated otherwise, the same column was used for the purification of the other fractions. Compound **18** (2.0 mg) was obtained from fraction F4E using 65% isocratic condition. Application of the elution gradient 47-50% solvent B for 10 min followed by isocratic condition at 50% for 5 min afforded **19** (2.5 mg) from fraction F4C. Compound **20** (3.2 mg) and compound **21** (2.2 mg) were purified from fraction F6D with elution gradient 10-50% of solvent B for 20 min and then isocratic condition at 50% for 5 min.

3.3.2 Extraction of secondary metabolites from the stem bark of *B. abyssinica* subsp. *abyssinica*

The air-dried bark of *B. abyssinica* subsp. *abyssinica* (1300 g) was soaked with MeOH for 24 h, twice at room temperature. The extracts were concentrated under reduced pressure to give brown residues (135 g) and applied to CC over silica gel 60, eluted with cyclohexane/EtOAc and then EtOAc/MeOH mixtures of increasing polarities. Fraction 5 (EtOAc/MeOH 90:10), fraction 6 (EtOAc/MeOH 80:20) and fraction 7 (EtOAc/MeOH 80:30) were identified for further purification after LCMS profiling. The fractions were passed through Sephadex LH-20 prior to separation by semi-preparative HPLC and a Gemini C_{18} column (10 × 250 mm, 10 μm particle size, Phenomenex) was used for reversed-phase preparative HPLC. Double distilled water (A) (0.1 % formic acid) and MeOH (B) were used as a mobile phase. Four fractions (5A-5D) from fraction 5, five fraction (6A-6E) from fraction 6 and four fractions (7A-7D) from fraction 7 were collected. Compound **22** (3.7 mg) was purified from fraction 6D with elution gradient 10-50% of solvent B for 20 min and then isocratic condition at 50% for 5 min. The same gradient was used to isolate compounds **23** (2.2 mg) and **24** (3.2 mg) from fraction 6C and 6B, respectively. Three elagic acid derivatives ellagic acid (**25**) (1.4 mg), elagic acid (**26**) and ellagic acid-4-*O*-*β*-D-xylopyranoside (**27**) (2.0 mg) and were obtained from fraction F6A with isocratic elution of 50% solvent B for 15 min. Compound **28** (2.5 mg) was obtained from fraction 7A with isocratic elution of 45% solvent B for 15 min. Compounds **29** (2.7 mg) and **32** (4.8 mg) were purified from fraction 7B with elution gradient 10-50% of solvent B for 20 min and then isocratic condition at 50% for 5 min. Compounds **30** (3.9 mg) and **31** (2.1 mg) were obtained from fraction 7C and fraction 7D respectively using a gradient elution of 10-45% of solvent B for 20 min and then isocratic condition at 45% for 5 min. Figure 3.2 shows a flow diagram on the isolation and extraction procedure.

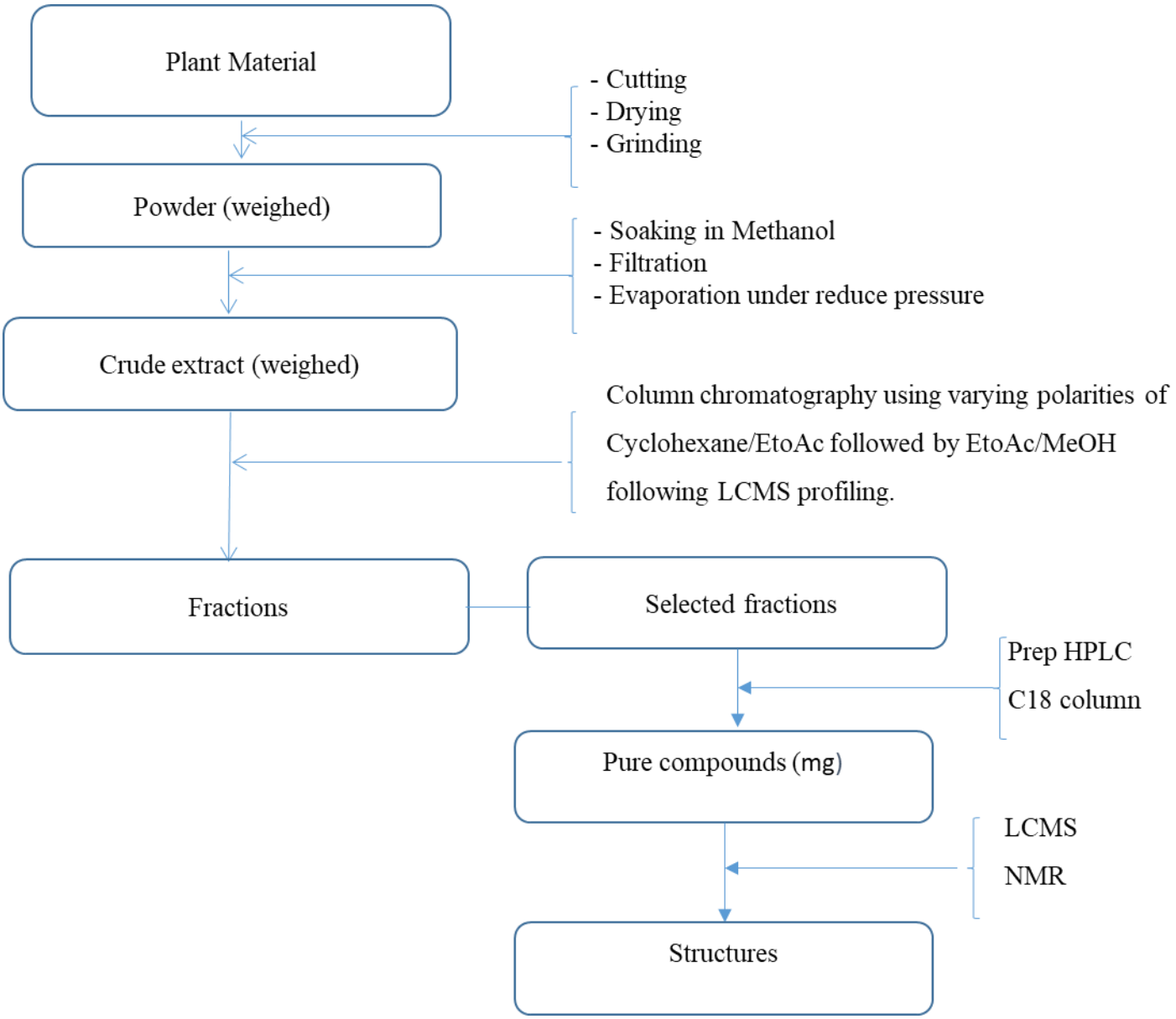

Figure 3.2: Flow chart showing extraction and isolation procedure

3.3.3 Extraction of secondary metabolites from the leaves of *B. abyssinica* subsp. *abyssinica*

The air-dried leaves of *B. abyssinica* subp. *abyssinica* (1642.9 g) was soaked with MeOH for 24 h, thrice at room temperature. The extract was concentrated under reduced pressure to give brown residue (194 g). About 190 g of the extract was applied to column chromatography (CC) over silica gel 60 and eluted with cyclohexane/EtOAc and then EtOAc/MeOH mixtures of increasing polarities. Fractions were combined into nine fractions based on similar LCMS profile. Fraction 7 (EtOAc 100 %) and fraction 9 (EtOAc/MeOH 80:20) were subjected to further HPLC separation. The fractions were passed through Sephadex LH-20 prior to separation by preparative HPLC.

Compounds were separated on a Gemini C18 column (10 × 250 mm, 10 μm particle size, Phenomenex) using the following gradient programme: 45% to 65% MeOH (B) over 25 min and thereafter isocratic conditions at 100% solvent B for 10 min, the system returned within 0.5 min to initial conditions of 55% water (A) (0.1 % formic acid) and was equilibrated for 10 min; flow rate: 4 mL/min, detection: UV at λ 254, 275, and 350 nm. Eleven fractions (F7A-F7K) were collected from fraction 7 and fourteen fractions (F9-1-F9-14) from fraction 9. Fraction F7K was further purified by a reverse-phase preparative HPLC using VP 125/10 NUCLEODUR PolarTec column (10×125 mm, 5 μm, Macherey-Nagel) as a stationary phase with a flow rate of 4 mL/min, elution gradient: 55% isocratic conditions for 10 min compound **33** (1.0 mg). The same column was used for the purification of the other fractions. Compound **34** (2.1 mg) was obtained from fraction F7H using 50% isocratic condition for 10 min. Fraction F7J was purified using 55 % isocratic condition for 12 min to afford compound **35** (1.3 mg). Compound **36** (1.8 mg) and **36** (2.6 mg) were obtained from fraction F7D using 40% isocratic condition for 15 min. Compound **38** (1.3 mg) was purified from fraction F9-4 with isocratic elution of 40% solvent B for 10 min. Compound **39** (3.4 mg) and compound **40** (1.6 mg) were purified from fraction F9-13 and fraction F9-14 respectively with isocratic conditions of 50% solvent B for 10 min.

3.4 Fungal endophytes

3.4.1. Fungal endophytes isolation

Endophytic fungi was isolated from fresh leaves and stem bark of *B. abyssinica* subsp. *abyssinica* and subsp. *paullinioides* using a method described by Zinniel *et al*., (2002), with slight modification. In this method, the leaves and stem barks of *B. abyssinica* subsp. *abyssinica* and subsp. *paullinioides* were washed separately under running tap water to remove any soil or other

foreign materials. Afterwards, they were surface sterilized for three minutes using 70% ethanol followed by soaking in 1% sodium hypochlorite for one minute and washing three times with sterile distilled water to remove any traces of the disinfectant. The surface sterilized leaves were then cut aseptically into sections approximately 1 mm by 4 mm and inoculated in petri dishes containing PDA (39 g/L) amended with streptomycin sulphate (250 mg/L). The inoculated plates were placed in an incubator at 25 ± 2ºC for 1- 4 weeks. The petri dishes were monitored after every three days to check for fungal growth. Sub-culturing of fungal mycelia of each endophyte isolate into sterile petri dishes containing PDA without antibiotics was then done to prepare pure cultures. The plates were incubated at 25 ± 2ºC for 1- 4 weeks. Three pure strains, BAPB_2, BAPB_B, BAPB_D were obtained from the stem bark of *B. abyssinica* subsp. *paullinioides*, two strains, BAPLC, BAPLC_1 were obtained from the leaf of *B. abyssinica* subsp. *paullinioides* and one strain, BAAL_A2 was obtained from the leaf of *B. abyssinica* subsp. *abyssinica*.

3.4.2. Ribosomal DNA (rDNA) isolation

Genomic DNA was isolated using the ArchivePure DNA Yeast and Gram- + wKit (5 PRIME, Hamburg, Germany) according to Kolařík *et al*., (2017) with slight modification. Briefly, approximately 100 mg (wet weight) of fungal cells were suspended in 200 µL distilled water in a ZR BashingBead™ lysis tube. About 750 µL BashingBead™ buffer was added to the tube. The mixture was then mixed for 10 minutes followed by 1 minute centrifugation at 10000 rpm. Up to 400 µL of the supernatant was transferred to a Zymo-Spin™ III-F filter in a collection tube followed by centrifugation at 8000 rpm for 1 min. Genomic lysis buffer (1200 µL) was added to the filter in the collection tube to open up the cells and make them more permeable for DNA extraction. About 800 µL of the mixture was transferred to a Zymo-Spin™ IICR column and centrifuged at 10000 rpm. The solution in the collection tube was discarded and the process was repeated. About 200 µL of DNA pre-wash buffer was added to the Zymo-Spin™ IICR column in a new collection tube and centrifuged at 10000 rpm for 1 min. About 500 µL of g-DNA wash buffer was added to the Zymo-Spin™ IICR column in a new collection tube and centrifuged at 10000 rpm for 1 min. Ultra-pure DNA was eluted from Zymo-Spin™ IICR column using 100 µL DNA elution buffer and stored at 4°C for further analysis.

3.4.3. Polymerase Chain Reaction (PCR) amplification

The Internal Transcribed Spacer (ITS) region of the ribosomal DNA (rDNA) was amplified by conducting a Polymerase Chain Reaction (PCR). Polymerase Chain Reaction amplification was done in a final volume of 20 µL by mixing 1 µL of the genomic DNA with 19 µL of the master mix. The master mix was prepared by adding 0.3 µL of the forward primer ITS1 (CTTGGTCATTTAGAGGAAGTAA) (Bruns & Gardes, 1993) into a 2 mL eppendorf tube, followed by 0.3 µL of the reverse primer ITS4 (TCCTCCGCTTATTGATATGC) (White *et al*., 1990), 4.0 µL of MyTaq™ Reaction Buffer, 14.2 µL of RNA free PCR water and 0.2 µL of MyTaq DNA polymerase. The mixture was vortexed for 30 seconds. About 1 µL of distilled water mixed with 19 µL of the master mix was used as the negative control. Amplification was done in a thermal cycler (Mastercycler pro S) with an initial denaturation of 5 minutes at 94 ºC, followed by 35 cycles of denaturation for 1 munute at 95 ºC, 35 seconds for annealing at 52 ºC, 1 minute for elongation at 72 ºC and a final elongation of 5 minutes at 72 ºC. The quality and quantity of PCR products were checked by agarose gel electrophoresis on a 0.8% agarose gel. The PCR products were mixed with 2 µl ethidium bromide (EtBr) and loaded in the already prepared gel and 60 mL Tris/Borate/EDTA (TBE) buffer. It was then run for 30 minutes at 100 volts and visualization was done by use of UV transilluminator. PCR products were purified with ExoSAP Cleanup Reagent (Thermo Fisher Scientific, Waltham, MA, USA) according to manufacture's instructions and both strand sequenced at Macrogen Europe (Amsterdam, The Netherlands). The sequences obtained were manually cut from unreadable sections and the highest sequence probability was searched for in the GenBank database using BlastN similarity search. The sequences were compared with those from reference strains published by taxonomic studies (Hernández-Gómez *et al*., 2017; Réblová *et al*., 2016).

3.5 Fermentation of endophytic fungi

Solid fermentation was carried out in ten 500 mL Erlenmeyer flasks containing 90 g of parboiled rice in 90 mL distilled water per flask, previously twice autoclaved at 120 ºC for 40 min for each fungal strain. Agar plugs approximately 7 mm were cut using a sterile cork borer from 7 day old endophytic cultures on PDA media and inoculated. One flask, without inoculum was used as the control. After 21 days incubation at 30 ºC, 150 mL of methanol was added to each flask and the contents allowed to stand overnight at room temperature. The methanol extract was filtered and evaporated at reduced pressure. Methanol extract was partitioned between hexane and ethyl

acetate. The resulting organic layers were evaporated under reduced pressure to produce hexane and ethyl acetate extracts (Nascimento *et al*., 2012).

3.6 Extraction of secondary metabolites from endophytic fungus *Epicoccum nigrum*

The ethyl acetate extract (95 g) was applied to column chromatography over silica gel 60 and eluted with cyclohexane/EtOAc and then EtOAc/MeOH mixtures of increasing polarities. Fraction 10 (cyclohexane/EtOAc 10:90), fraction 11 (100% EtOAc), fraction 12 (EtOAc/MeOH 90:10) and fraction 13 (EtOAc/MeOH 80:20) were identified for further purification after LCMS profiling. The fractions were passed through Sephadex LH-20 prior to separation by semi-preparative HPLC and a Gemini C_{18} column (10 × 250 mm, 10 μm particle size, Phenomenex) was used for reversed-phase preparative HPLC, detection: UV at wavelengths (λ) 254 275, 300 and 350 nm. Double distilled water (A) (0.1 % formic acid) and MeOH (B) were used as a mobile phase. Two fractions (10A and 10B) from fraction 10, four fractions (11A-11D) from fraction 11, three fractions (12A-12C) from fraction 12, two fractions (13A and 13B) were collected. Compound **41** (3.1 mg) was obtained from fraction 10A with isocratic elution of 55% solvent B for 15 min using VP 125/10 NUCLEODUR PolarTec column (10×125 mm, 5 μm, Macherey-Nagel) as a stationary phase with a flow rate of 4 mL/min. The same column was used for the purification of the other fractions. Compound **42** (3.7 mg) was purified from fraction 11B with isocratic elution condition at 50% for 8 min. Compounds **43** (2.2 mg) and **44** (3.2 mg) were purified using gradient elution of 10-50% of solvent B for 20 min and then isocratic condition at 50% for 5 min from fractions 12B and 12C, respectively. Compounds **45** (2.5 mg) was obtained from fraction 13A with isocratic elution of 45% solvent B for 15 min. The same gradient was used to purify compound **46** (2.5 mg) from fraction 13B.

3.7 Nuclear magnetic resonance (NMR) spectroscopy

The ^{1}H, ^{13}C, DEPT, HSQC, COSY and HMBC NMR spectra were recorded on the Bruker Advance 600 MHz and 700 MHz NMR spectrometer at the Technical University of Dortmund, Germany. The measurements were done in deuterated DMSO, chloroform or methanol and chemical shifts assigned by comparison with the residue proton and carbon resonance of the solvent. Tetramethylsilane (TMS) was used as an internal standard and chemical shifts were given as δ (ppm). The off - diagonal elements was used to identify the spin – spin coupling interactions in the ^{1}H –^{1}H COSY (Correlation spectroscopy). The proton-carbon connectivity,

up to three bonds away, was identified using $^{1}H–^{13}C$ HMBC (Heteronuclear Multiple Bond Correlation) spectrum. The $^{1}H–^{13}C$ HSQC spectrum (Heteronuclear Single Quantum Coherence) was used to determine the connectivity of hydrogen to their respective carbon atoms.

3.8 Mass spectrometry

The compounds' mass high-resolution mass spectra (HRESIMS) were carried out using LTQ Orbitrap spectrometer (Thermo Scientific, USA) equipped with a HESI-II ion source. Thermo Xcalibur Qual computer software was used in the analysis of the mass chromatograms. The masses of the compounds and molecular formula were obtained and used to determine the structure of the compounds.

3.9 Bioassays

3.9.1 Antidermatophytic assays

Five dermatophytic strains; *Trichophyton mentagrophytes* CCF 6579, *Trichophyton rubrum* IDE 241/20, *Trichophyton rubrum resistant* LY 8, *Trichophyton benhamiae* var. *luteum* (CCF 6474) and *Trichophyton tonsurans* CCIS 5356 were used in the study. These strains were obtained from the Institute of Microbiology - Czech Academy of Sciences. The MIC of the secondary metabolites was assessed by broth microdilution assay according to the Clinical and Laboratory Standards Institute (CLSI) M38-A2 guidelines (Wayne, 2008), with slight modification. Briefly, the inoculum suspension of each test dermatophyte isolate was prepared by scrapping the surface of 10-day-old cultures and suspended in sterile 0.1% (v/v) tween 80 in PBS to make the stock solution. One mL of the stock solution was further diluted in 60 mL of yeast malt broth and colony-forming units (CFU/mL) were confirmed microscopically using a hemocytometer by counting the emerged colonies from 10 mL of the already prepared suspension. Spore suspension (150 µL) containing 10^5 of each dermatophyte was inoculated into 96 well microdilution plates. In the first row of each plate, an additional 130 µL of yeast malt broth and 20 µL of 4 mg/mL concentration of the test compounds were added in three replicates and mixed thoroughly. In this experiment, methanol was used as a negative control while amphotericin B antifungal was used as a positive control. The mixture was serially diluted by transferring 150 µL from the first row into the subsequent row until the last row where the excess 150 µL of the mixture was discarded after the last mixing making the final concentration of 300, 150, 75, 37.5, 18.75, 9.38, 4.69, 2.69 µg/mL. The mixture was incubated at 30°C for 3 to 7 days with continuous

monitoring for growth. The least concentration in which no visible growth was observed was defined as their MIC and reported in µg/mL.

3.9.2 Antibacterial assays

Four bacterial pathogens: *E. coli* DSM1116, *M. smegmatis* DSM ATCC 700084, *S. aureus* DSM346 and *B. subtilis* DSM10 were used in this study. The bacterial strains were obtained from Leibniz Institute DSMZ - German Collection of Microorganisms and Cell Cultures GmbH, Braunschweig, Germany. Compounds were dissolved in MeOH (1 mg/mL) for the antibacterial activity assay. The assays were carried out in 96 well microtitre plate in MH media. The stock solution concentration was 300 µg/mL. Minimum inhibitory concentration (MIC), against different test organisms were determined in serial dilution assay as described by Chepkirui *et al*. (2018). Inhibition of growth was visually evaluated the next day. The MIC is defined as the lowest concentration of the test compound where no growth of the test organism was observed. Methanol was used as a negative control while oxytetracyclin and kanamycin were used as the positive controls.

3.9.3 Anticancer assays

In vitro cytotoxicity (IC_{50}) of the isolated natural products was determined against two mammalian cell lines; HeLa (KB3.1) and mouse fibroblast L929. The cell lines were obtained from the Leibniz Institute DSMZ - German Collection of Microorganisms and Cell Cultures GmbH, Braunschweig, Germany. The cell lines were cultured in DMEM (Gibco, ThermoFisher Scientific Hilden, Germany) media, supplemented with 10% of fetal bovine serum (Gibco) under 10% CO_2 at 37 ˚C. The cytotoxicity assay was performed according to the MTT (3-(4,5-dimethylthiazol-2-yl)-2,5 diphenyltetrazolium bromide) method in 96-well microplates (Mossmann, 1983). Briefly 60 µL aliquots of serial dilutions from an initial stock of 1 mg/mL in MeOH of the test compounds were added to 120 µL aliquots of a cell suspension in 96-well microplates. After 5 days incubation, a MTT assay was performed, and the absorbance measured at 590 nm using an ELISA plate reader (Victor, PerkinElmer, Überlingen, Germany). The concentration at which the growth of cells was inhibited to 50% of the control (IC_{50}) was obtained from the dose response curves. The negative control was methanol. The positive control was epithilon B with IC_{50} values of 0.000056 ± 000001 and 0.001 081 ± 0.000 776 µM for KB3.1 and L929 cells, respectively.

3.10. Data analysis

NMR spectra was obtained in 1D and 2D NMR data and was analyzed using mestrenova NMR software version 14.2.0. High resolution electrospray ionization mass spectrometry spectral data was analyzeded using Thermo Xcalibur Qual computer software. The X-ray diffraction data was analyzed on a Bruker D8 VENTURE area detector diffractometer according to the method described by Kamtcha *et al*. (2018). The crystal was kept at 100.0 K during data collection. Using Olex2 (Dolomanov *et al*., 2009), the structure was solved with the XT (Sheldrick, 2015) structure solution program using Intrinsic Phasing and refined with the XL (Sheldrick, 2008) refinement package using Least Squares minimisation.

CHAPTER FOUR

RESULTS AND DISCUSSION

4.1 Secondary metabolites isolated from the stem bark of *B. abyssinica* subsp. *paullinioides*

The MeOH extract of the stem bark of *B. abyssinica* subsp. *paullinioides* was subjected to successive column chromatography over silica gel and Sephadex LH-20 followed by preparative HPLC to afford five compounds **17** – **21**. Compounds **17**, **18**, and **19** were found to be new while **20** and **21** have been reported previously. Compound **17** (figure 4.1) was isolated as a colorless needle. Its molecular formula $C_{26}H_{30}O_6$ was determined from its HRESIMS (appendix 1) at *m/z* 439.2117 $[M + H]^+$ (calcd for $C_{26}H_{31}O_6$, 439.2115). IR spectral cm^{-1}: 2944, 1746, 1721 (appendix 2). The ^1H (appendix 3) and ^{13}C NMR (appendix 4) spectroscopic data (Table 4.1) suggested that **17** has a bufadienolide steroidal structure with α-pyrone ring system. The presence of this characteristic α-pyrone ring was evidenced from ^1H NMR data at δ_H 7.30 (H-21, d, J = 2.5 Hz), 7.02 (H-22, dd, J = 9.7 Hz, 2.5 Hz), and 6.32 (H-23, d, J = 9.7 Hz), and from the ^{13}C NMR at δ_C 151.2 (C-21), δ_C 145.1 (C-22) and δ_C 116.4 (C-23) (Tian *et al*., 2010). The NMR data assignment of the tetracyclic moiety was done by comparison with reported bufadienolides (Nogawa *et al*., 2001) and by an extensive analysis of COSY (appendix 5), HSQC (appendix 6) and HMBC (appendix 7) data. The compound has an orthoacetate group on ring A, confirmed from the presence of a characteristic orthoacetate singlet methyl protons at H_3-26 (δ_H 1.45), which showed a strong HMBC correlation with C-25 (δ_C 110.5) (Kupchan *et al*., 1971b).

Long range HMBC correlations of H-1 (δ_H 3.96) with C-25 (δ_C 110.5) also supporting the orthoacetate structure. Further, COSY correlations of H-2 with H-1 and H-3 then H-3 with H-2 and H-4 identified the connectivity sequence in ring A. Signals for 26 carbon atoms were observed in the ^{13}C NMR spectrum. Of these, signals at δ_C 188.7 (C-14), δ_C 124.2 (C-15), and δ_C 204.5 (C-16) were due to the presence of α-β unsaturated carbonyl group in ring D, comparable to ring D of that of abyssinol A (Kubo & Matsumoto, 1985). HMBC correlations from H-15 (δ_H 4.28) to C-13 (δ_C 48.0), C-14 (δ_C 188.7), C-16 (δ_C 204.5), and C-17 (δ_C 61.2) as well as from H-17 (δ_H 3.11) to C-13, C-14, C-15, and C-16 are important correlations found in ring D. Singlet methyl groups at δ_H 0.98 (δ_C 23.1) and δ_H 1.40 (δ_C 14.9) are typical steroidal methyl groups and were assigned C-18 and C-19 respectively based on their HMBC correlations: H_3-18 to C-12, C-13, C-14, and C-17; H_3-19 to C-1, C-5, C-9, and C-10. Moreover, the connectivity of the pyrone ring to C-17 was deduced from HMBC correlations of H-17 to C-20, C-21 and C-22. The NOESY (appendix 8)

correlations between H_3-19 and H-8 and between H-8 and H_3-18 suggested the β-orientation of H_3-18, H_3-19, and H-8. Additional NOESY correlations from H_3-18 to H-21 and H-22 resonances confirmed the β-orientation of the α-pyrone ring. In order to determine the full configuration in **17**, the sample was re-crystallized from methanol-water and subjected to single-crystal X-ray diffraction analysis. The result showed that the orthoacetate group occupied the axial positions (β-orientation) in ring A. Therefore, the structure of the new compound **17** was determined as (1β,3β,5β)-ethylidynetris(oxy)-16-oxobufa-14(15),20,22-trienolide and was given the trivial name paulliniogenin A.

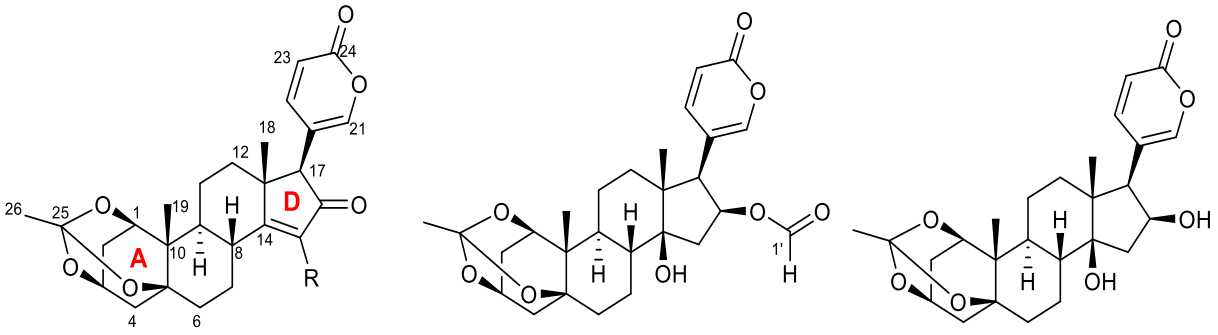

17 R = H
18 R = OCH_3

19

20

Figure 4.1: Chemical structures of compounds **17** - **20**

Compound **18** (figure 4.1) was isolated as colorless powder with a molecular formula $C_{27}H_{32}O_7$ that was determined from HRESIMS (appendix 9) at *m/z* 469.2220 $[M + H]^+$ (calcd for $C_{27}H_{33}O_7$, 469.2220). IR spectral cm^{-1}: 2945, 1736, 1707 (appendix 10). Its NMR data were very similar to those of **17** except the presence of a methoxy group at C-15. This was deduced from methoxy signals at δ_H 3.82 (δ_C 58.9) and in effect the chemical shift of C-15 appeared further downfield at δ_C 150.1 compared to δ_C 124.3 in **17**. HMBC correlations from the methoxy protons OMe-15 (δ_H 3.82) to C-15, from H-8 to C-15, and H-17 to C-15 also supporting the attachment of the methoxy at C-15. Comparison of its NMR data with literature revealed that ring D of **18** is the same as those in abyssinin, which was isolated previously from *B. abyssinica* (Kubo & Matsumoto, 1984). The complete ^1H (appendix 11) and ^{13}C NMR (appendix 12) signal assignments and connectivity were determined from a combination of ^1H-^1H COSY (appendix 13), HSQC (appendix 14) and HMBC (appendix 15) data. The relative configuration of **18** was established from the observed identical coupling constants and NOESY (appendix 16) correlations as in **17**.

Therefore, the structure of **18** was elucidated for the first time as (1β,3β,5β)-ethylidynetris(oxy)-15-methoxy-16-oxobufa-14(15),20,22-trienolide and was given the trivial name paulliniogenin B.

Table 4.1: ^{1}H NMR (700 MHz) and ^{13}C NMR (175 MHz) Spectroscopic Data[a] of Compound **17–19**

no.	**17**[b]		**18**[b]		**19**[c]	
	^{13}C, Type	^{1}H, mult.(*J* in Hz)	^{13}C, Type	^{1}H , mult.(*J* in Hz)	^{13}C, Type	^{1}H , mult. (*J* in Hz)
1α	74.7, CH	3.96, brs	74.8, CH	3.94, brs	74.3, CH	3.81, brs
2α	28.0, CH_2	1.69	28.0, CH_2	1.70, d (14.0)	27.2, CH_2	1.95, d (13.4)
2β		2.45, dt (13.4, 3.5)		2.42		2.12, m
3α	67.8, CH	4.32, brs	67.9, CH	4.32, brs	67.3, CH	4.19, brs
4α	33.2, CH_2	2.00, dt (13.5, 3.2)	33.2, CH_2	2.01, dt (13.5, 3.0)	32.6, CH_2	2.32, d (13.0)
4β		2.25, dd (13.5, 2.0)		2.32		1.76, m
5	74.9, C		74.9, C		74.9, C	
6α	31.6, CH_2	1.86, dd (13.5, 5.0)	32.0, CH_2	1.80, dt (13.5, 5.0)	31.7, CH_2	1.54, m
6β		1.45, m		1.41, m		1.20, m
7α	24.1, CH_2	1.69	23.6, CH_2	1.98	21.0, CH_2	1.11, m
7β		1.91, m		2.31, m		1.90, m
8β	36.6, CH	2.70, m	36.9, CH	2.74, td (12.0, 4.4)	40.5, CH	1.64
9α	45.3, CH	1.60, m	44.7, CH	1.65, td (12.0, 3.2)	38.3, CH	1.56
10	40.3, C		40.4, C		40.0, C	
11α	20.6, CH_2	1.47	20.5, CH_2	1.43	20.3, CH_2	1.10
11β		1.60		1.54		1.12
12α	39.9, CH_2	2.06, m	39.3, CH_2	1.98	38.7, CH_2	1.34, m
12β		1.51, m		1.43		1.40, m
13	48.0, C		43.3, C		49.2, C	
14	188.7, C		161.3, C		82.2, C	
15α	124.2, CH	5.91, s	150.1, C		39.8, CH_2	1.74
15β						2.74, dd (15.4, 9.1)
16α	204.5, C		200.6, C		73.5, CH	5.46, t (9.1)
17α	61.2, CH	3.11, s	58.7, CH	3.00, s	55.5, CH	2.93, d (9.0)
18	23.1, CH_3	0.98, s	23.6, CH_3	0.94, s	16.2, CH_3	0.67, s
19	14.9, CH_3	1.40, s	15.1, CH_3	1.36, s	14.5, CH_3	1.12, s
20	114.5, C		114.2, C		117.0, C	

21	151.2, CH	7.30, d (2.5)	151.1, CH	7.30, d (2.5)	151.4, CH	7.53, s
22	145.1, CH	7.02, dd (9.7, 2.5)	145.0, CH	7.04, dd (9.7, 2.5)	149.9, CH	8.13, d (9.5)
23	116.4, CH	6.32, d (9.7)	116.4, CH	6.32, d (9.7)	111.9, CH	6.21, d (9.5)
24	161.2, C		161.3, C		161.0, C	
25	110.5, C		110.5, C		109.5, C	
26	26.1, CH_3	1.45, s	26.1, CH_3	1.45, s	25.9, CH_3	1.24, s
12					161.3	8.00, s
OMe-15			58.9	3.82, s		

[a]Signals without multiplicity are overlapping signals deduced by HSQC.

[b]Recorded in $CDCl_3$. [c]Recorded in DMSO-*d*6

Compound **19** (figure 4.1) was isolated as colorless powder with molecular formula of $C_{27}H_{34}O_8$, determined from its HRESIMS (appendix 17) at *m/z* 487.2328 $[M + H]^+$ (calcd for $C_{27}H_{35}O_8$, 487.2326). IR spectral cm^{-1}: 3480, 2947, 1715 (appendix 18). Like the previous compounds, signals for the α-pyrone ring and the orthoacetate ring were observed in ^1H (appendix 19) and ^{13}C NMR (appendix 20) spectrum (Table 4.1). However, compound **19** differ from the previous compounds on ring D where a hydroxyl and a formyloxy group are present instead of α, β-unsaturated group. Comparison of its NMR data with literature indicated compound **19** is a derivative of 16β-hydroxybersamagenin 1,3,5-orthoacetate (**20**), which was isolated previously from *B. abyssinica* (Kupchan *et al*., 1971). The only difference involved was the presence of formyloxy group at C-16 in **19**. ^1H-^1H COSY (appendix 21), HSQC (appendix 22) and HMBC (appendix 23) correlations were important in determining the structure of **19**. This formyloxy was deduced from a formyl proton at δ_H 8.00 which correlated with δ_C 161.3 (C-12) in the HSQC (Nogawa *et al*., 2001). In the HMBC spectrum, H-16 (δ_H 5.46) correlated with C-12 (δ_C 161.3) and H-12 (δ_H 8.00) correlated with C-16 (δ_C 73.5), suggested the position of the formyloxy to be at C-16. Further, COSY correlations of H-16 with H_2-15 and H-17 supporting ring-D NMR assignments. The relative configuration of the formyloxy group assigned β-position based on the observed NOESY correlations of H-16 with H-17 and H-16 with H-15α (δ_H 1.74). Thus, the structure of compound **19** was elucidated as 16*β*-formyloxybersamagenin 1,3,5-orthoacetate.

Compound **20** (figure 4.1) was isolated as colorless powder with molecular formula of $C_{26}H_{34}O_7$, determined from its HRESIMS (appendix 24) at *m/z* 459.2372 $[M + H]^+$ (calcd for $C_{27}H_{35}O_8$, 459.2372). IR spectral cm^{-1}: 3410, 2947, 1725, 1706 (appendix 25). Like the previous

compounds, signals for the α-pyrone ring and the orthoacetate ring were observed in ^{1}H (appendix 26) and ^{13}C NMR (appendix 27) spectrum (Table 4.2). However, compound **20** differered from compound **19** on ring D where formyloxy group at C-16 is replaced by the hydroxyl group. Comparison of its NMR data with literature indicated compound 16β-hydroxybersamagenin 1,3,5-orthoacetate, which was isolated previously from *B. abyssinica* (Kupchan *et al*., 1971). The NMR data assignment of the tetracyclic moiety was done by comparison with reported bufadienolide (Kupchan *et al*., 1971) and by an extensive analysis of COSY (appendix 28), HSQC (appendix 29) and HMBC (appendix 30) data. The COSY correlations of H-16 with H_2-15 and H-17 were important in determining the connectivity in ring D. Furthermore, HMBC correlations from H-16 (δ_H 4.44) correlated with C-13 (δ_C 49.7), C-14 (δ_C 83.3), C-15 (δ_C 42.9) and C-20 (δ_C 119.1), suggested the position of the hydroxyl to be at C-16 and were important in establishing the connectivity in ring D. The relative configuration of the hydroxyl group assigned β-position based on the observed NOESY correlations of H-16 with H-17 and H-16 with H-15α (δ_H 1.62) (appendix 31). Thus, the structure of compound **20** was elucidated as 16β-hydroxybersamagenin 1,3,5-orthoacetate.

Table 4.2: ^{1}H NMR (700 MHz) and ^{13}C NMR (175 MHz) Spectroscopic Data[a] of Compound **20** and **22**

no.	**20**		**22**	
	^{13}C, Type	^{1}H, mult. (*J* in Hz)	^{13}C, Type	^{1}H, mult. (*J* in Hz)
1α	74.8, CH	3.82, brs	70.2, CH	4.31, brs
2α	27.8, CH_2	1.91, m	30.4, CH_2	1.89
2β		2.13, m		1.93, dt (13.4, 3.5)
3α	67.8, CH	4.20, brs	64.9, CH	4.10, brs
4α	33.2, CH_2	2.34, d (13.0)	37.3, CH_2	1.54, dt (13.5, 3.2)
4β		1.75, m		2.22, dd (13.5, 2.0)
5	75.4, C		73.0, C	
6α	32.3, CH_2	1.21, m	35.8, CH_2	1.61, dd (13.5, 5.0)
6β		1.53, m		2.61, m
7α	21.7, CH_2	1.11, m	23.5, CH_2	1.17
7β		1.90, m		2.08, m
8β	40.5, CH	1.62	42.1, CH	1.32, m

9α	39.0, CH	1.51	40.7, CH	1.51, m
10	49.5, C		56.4, C	
11α	20.8, CH_2	1.10	21.3, CH_2	1.15
11β		1.12		1.42
12α	39.5, CH_2	1.29, m	38.7, CH_2	1.20, m
12β		1.38, m		1.37, m
13	49.7, C		48.6, C	
14	83.3, C		82.6, C	
15α	42.9, CH_2	1.62	42.2, CH_2	1.54, s
15β		2.55, m		2.45
16α	70.9, CH	4.44, t (8.3)	70.2, CH	5.48
17α	57.8, CH	2.65, d (8.2)	57.2, CH	2.63, s
18	17.3, CH_3	0.66, s	16.4, CH_3	0.54, s
19	15.0, CH_3	1.13, s	206.6, CH	9.99, s
20	119.1, C		118.5, C	
21	150.8, CH	7.48, s	150.3, CH	7.47, dd (2.5, 1.1)
22	152.0, CH	8.08, d (9.5)	151.4, CH	8.06, dd (9.8, 2.5)
23	111.4, CH	6.14, d (9.5)	111.0, CH	6.12, dd (9.8, 1.0)
24	162.1, C		161.6, C	
25	110.0, C		169.4, C	
26	26.4, CH_3	1.25, s	21.2, CH_3	1.84, s

Compound **21** (figure 4.2) was isolated as a yellow powder with a molecular formula of $C_{19}H_{20}O_{10}$, determined from its HRESIMS (appendix 32) m/z 409.1129 $[M + H]^+$ (calcd for $C_{19}H_{21}O_{10}$, 409.1129). The NMR data assignment was done by analysis of 1D and 2D NMR spectra and by comparison with benzophenone compounds reported in literature data (Nedialkov & Kitanov, 2002). The ^1H NMR spectrum (appendix 33) displayed signals at δ_H 7.62 (2H, m, H-2', H-6'), 6.79 (2H, m, H-3', H-5'), 5.97 (1H, s, H-5), 4.88 (1H, H-1) and sugar protons appeared at chemical shift ranging between δ_H 3.19 and δ_H 3.58; ^{13}C NMR spectrum (appendix 34) indicated the presence of nineteen carbon signals at δ_c 105.8 (C-1), 159.4 (C-2), 157.4 (C-3), 159.9 (C-4), 94.9 (C-5), 161.3 (C-6), 197.5 (C-7), 131.8 (C-1'), 131.4 (C-2', C-6'), 114.1 (C-3', C-5'), 161.4 (C-4'), 75.1 (C-1"), 72.2 (C-2"), 78.5 (C-3"), 70.0 (C-4"), 81.0 (C-5"), 61.1 (C-6"). The complete ^1H

and ^{13}C NMR signal assignments and connectivity were determined from a combination of ^{1}H-^{1}H COSY (appendix 35), HSQC (appendix 36) HMBC (appendix 37) and NOESY (appendix 38) data. HMBC correlations from H-1" to C-2, C-3 and C-4 established the connectivity between the glycone moiety and aglycone moiety. Compound **21** was determined as 3-C-β-D-glucopyranosyl-2,4,6,4¢- tetrahydroxybenzophenone (Severi *et al*., 2009; Shahat *et al*., 2003). 3-C-β-D-glucopyranosyl-2,4,6,4¢- tetrahydroxybenzophenone is reported to be an effective anti-inflammatory, immunomodulator analgesic and antioxidant which has been used traditionally in the treatment of obesity (Shinde *et al*., 2010).

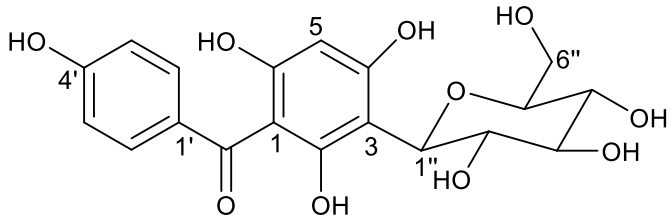

21

Figure 4.2: Chemical structure of compounds **21**

4.2 Secondary metabolites isolated from the stem bark of *B. abyssinica* subsp. *abyssinica*

The MeOH extract of the stem bark of *B. abyssinica* subsp. *abyssinica* was subjected to successive column chromatography over silica gel and Sephadex LH-20 followed by preparative HPLC to afford eleven compounds **22** – **32**. Compound **22** (figure 4.3) was isolated as a colorless crystal with molecular formula of $C_{26}H_{34}O_9$, determined from its HRESIMS (appendix 39) m/z 491.2274 $[M + H]^+$ (calcd for $C_{26}H_{35}O_9$, 491.2275). IR spectral cm^{-1}: 3436, 2877, 1711, 1632 (appendix 40). Like the bufadienolides from the stem bark of *B. abyssinica* subsp *paulliniodes*, signals for the α-pyrone ring were observed in ^{1}H (appendix 41) and ^{13}C NMR (appendix 42) spectrum (Table 4.2). ^{1}H NMR data at δ_H 7.47 (H-21, dd, J = 2.5 Hz, 1.1 Hz), 8.06 (H-22, dd, J = 9.7 Hz, 2.5 Hz), and 6.12 (H-23, d, J = 9.8 Hz, 1.0 Hz), and from the ^{13}C NMR at δ_C 150.3 (C-21), δ_C 151.4 (C-22) and δ_C 111.0 (C-23). The major difference in the bufadienolides obtained from the stem barks of *B. abyssinica* subsp *abyssinica* and *B. abyssinica* subsp *paulliniodes* occurred on ring A. Compound **22** lacked the orthoacetate ring which was observed on ring A of all the bufadienolides from the stem of *B. abyssinica* subsp *paulliniodes*. Further, the methyl group at C-

19 was oxidized to form an aldehyde in compound **22**. The complete ^{1}H and ^{13}C NMR signal assignments and connectivity were determined from a combination of ^{1}H-^{1}H COSY (appendix 43), HSQC (appendix 44) and HMBC (appendix 45) data. Further, COSY correlations of H-2 with H-1 and H-3 then H-3 with H-2 and H-4 identified the connectivity sequence in ring-A. Signals for 26 carbon atoms were observed in the ^{13}C NMR spectrum. Furthermore, compound **22** was similar to compound **20** on ring D where hydroxyl groups were observed at C-14 and C-16.

HMBC correlations from H-16 (δ_H 4.48) to C-14 (δ_C 82.6), C-15 (δ_C 42.2), and C-17 (δ_C 57.2) as well as from H-17 (δ_H 2.63) to C-13 (δ_C 48.6), C-14 (δ_C 82.6), C-15 (δ_C 42.2) and C-16 (δ_C 70.2) are important correlations found in ring D. Singlet methyl group at δ_H 0.54 (δ_C 16.4) typical of steroidal methyl groups was assigned to C-18 based on their HMBC correlations: H_3-18 to C-12, C-13, C-14, and C-17. Moreover, the connectivity of the pyrone ring to C-17 was deduced from HMBC correlations of H-17 to C-20, C-21 and C-22. In order to determine the full configuration in **22**, the sample was re-crystallized from methanol-water and subjected to single-crystal X-ray diffraction analysis. The result showed that the orthoacetate group occupied the axial positions (β-orientation) in ring A. Therefore, the structure of compound **22** was determined as 16*β*-hydroxybersaldegenin-1-acetate (**22**).

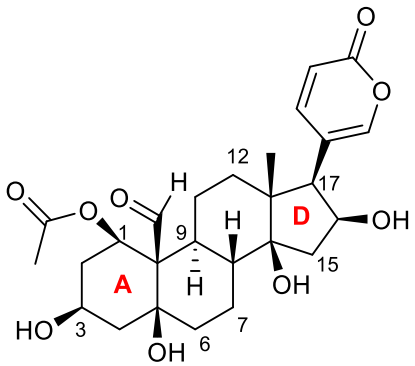

22

Figure 4.3: Chemical structure of compounds **22**

Compound **23** (figure 4.4) was obtained as a white powder with molecular formula of $C_{27}H_{24}O_{18}$, determined from its HRESIMS (appendix 46) m/z 637.1041 $[M + H]^+$ (calcd for $C_{27}H_{25}O_{18}$, 637.4790). The ^{1}H (appendix 47) and ^{13}C NMR (appendix 48) spectroscopic data (Table 4.3) suggested that **23** has a glucose structure with three galloyl groups (Lavoie *et al*., 2016). Singlet signals for the galloyl groups were observed in the ^{1}H spectrum at δ_H 6.97 (H-2' and H-6'), δ_H 6.92 (H-2'' and H-6'') and δ_H 6.87 (H-2''' and H-6'''), and from the ^{13}C NMR at δ_C 119.2 (C-

1'), δ_C 108.6 (C-2'), δ_C 145.5 (C-3'), δ_C 138.5 (C-4'), δ_C 145.5 (C-5'), δ_C 108.6 (C-6'), δ_C 165.7 (CO); 119.0 (C-1"), δ_C 108.8 (C-2"), δ_C 145.4 (C-3"), δ_C 138.6 (C-4"), δ_C 145.4 (C-5"), δ_C 108.8 (C-6"), δ_C 164.9 (CO); 117.7 (C-1'"), δ_C 108.9 (C-2'"), δ_C 145.6 (C-3'"), δ_C 139.4 (C-4'"), δ_C 145.6 (C-5'"), δ_C 108.9 (C-6'"), δ_C 164.1 (CO). The anomeric signals at δ_H 5.90 (H-1) and δ_C 92.2 (C-1) suggested the presence of a glucose substructure (Pomin, 2012). Signals of the glucose moiety were observed in ^{1}H and ^{13}C NMR spectra at δ_H 5.90 (H-1, d, J = 3.83 Hz), δ_H 5.04 (H-2, t, J = 9.0 Hz), δ_H 3.70 (H-3, t, J = 9.59 Hz), δ_H 3.52 (H-4, J = 9.5 Hz), δ_H 3.81 (H-5, m), δ_H 4.32 (H_2-6, dd, J = 12.2 Hz, 4.7 Hz) and δ_C 92.2 (C-1), δ_C 72.7 (C-2), δ_C 73.6 (C-3), δ_C 69.8 (C-4), δ_C 74.8 (C-5), δ_C 62.9 (C-6).

The complete ^{1}H and ^{13}C NMR signal assignments and connectivity were determined from a combination of ^{1}H-^{1}H COSY (appendix 49), HSQC (appendix 50) and HMBC (appendix 51) data. COSY correlations of H-2 with H-1 and H-3; H-3 with H-2 and H-4; H-5 with H-4 and H-6 identified the connectivity sequence in the glucose moiety. HMBC correlations from δ_H 4.32 (H_2-6) to δ_C 165.7 (CO); from δ_H 5.04 (H-2) to δ_C 164.9 (CO) and from δ_H 5.90 (H-1) to δ_C 164.1 (CO) established the links between the glucose moiety and the three galloyl groups. Compound **23** was determined as 1,2,6-tri-*O*-galloyl-β-D-glucose. Compound **23** has been isolated previously from traditional Chinese medicine, *Galla Chinese* and is described to exhibit antiviral activities (Duan *et al*., 2004).

Table 4.3: ^{1}H NMR (700 MHz) and ^{13}C NMR (175 MHz) Spectroscopic Data of Compound **23** and **24**

	23		**24**	
	^{13}C, Type	^{1}H, mult.(*J* in Hz)	^{13}C, Type	^{1}H , mult.(*J* in Hz)
Glucose				
1	92.1, CH	5.90, d (8.38)	92.3, CH	6.13, d (8.30)
2	72.7, CH	5.04, t (9.0)	71.1, CH	5.27, dd (9.90, 8.30)
3	73.6, CH	3.70, t (9.59)	74.8, CH	5.52, t (9.50)
4	69.8, CH	3.52, d (9.50	68.1, CH	3.81, t (9.50)
5	74.8, CH	3.81, m	75.0, CH	4.09, m
6	62.9, CH_2	4.32, dd (12.2, 4.7)	63.1, CH_2	4.39, dd (12.2, 4.5)
				4.44, d (11.0)
Galloyl				
1'	119.2, C		119.5	

2'	108.6, CH	6.97, s	109.1, CH	6.99, s
3'	145.5, C		146.1, C	
4'	138.5, C		139.2, C	
5'	145.5, C		146.1, C	
6'	108.6, CH	6.97, s	109.1, CH	6.99, s
C═O	165.7, C		166.1, C	
1"	119.0, C		119.4, C	
2"	108.8, CH	6.92, s	109.3, CH	6.92, s
3"	145.4, C		145.9, C	
4"	138.6, C		139.1, C	
5"	145.4, C		145.9, C	
6"	108.8, CH	6.92, s	109.3, CH	6.92, s
C═O	164.9, C		165.5, C	
1"'	117.7, C		118.5, C	
2"'	108.9, CH	6.87, s	109.2, CH	6.81, s
3"'	145.6, C		145.9, C	
4"'	139.4, C		139.5, C	
5"'	145.6, C		145.9, C	
6"'	108.9, CH	6.87, s	109.2, CH	6.81, s
C═O	164.1, C		165.1, C	
1""			117.8, C	
2""			109.4, C	
3""			146.1, C	
4""			140.2, C	
5""			146.1, C	
6""			109.4, CH	6.89, s

C═O	164.4, C

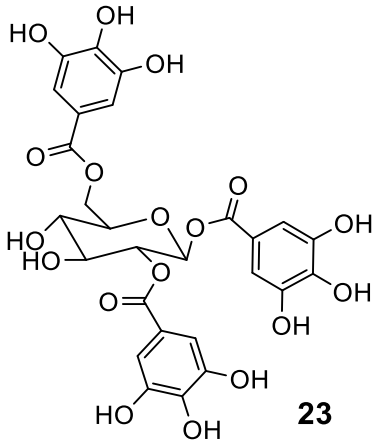

23

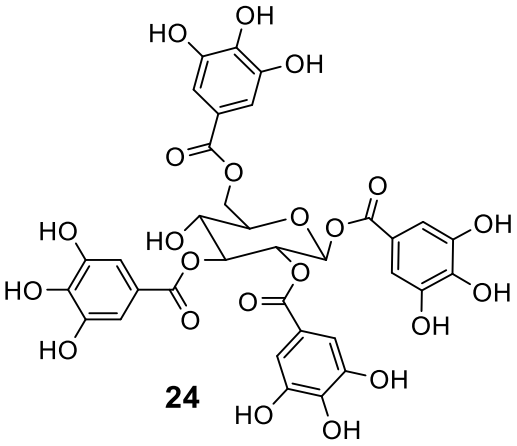

24

Figure 4.4: Chemical structures of compounds **23** and **24**

Compound **24** (figure 4.4) was obtained as a white powder with molecular formula of $C_{34}H_{28}O_{22}$, determined from its HRESIMS (appendix 52) m/z 689.1150 $[M + H]^+$ (calcd for $C_{34}H_{29}O_{22}$, 789.1150). Like compound **23**, the ^1H (appendix 53) and ^{13}C NMR (appendix 54) spectroscopic data (Table 4.3) suggested that **24** has a glucose structure except with four galloyl groups. Singlet signals for four galloyl groups were observed in the ^1H spectrum at δ_H 6.99 (H-2' and H-6'), δ_H 6.92 (H-2'' and H-6''), δ_H 6.81 (H-2''' and H-6''') and), δ_H 6.89 (H-2'''' and H-6'''') and from the ^{13}C NMR signals appeared at δ_C 119.5 (C-1'), δ_C 109.1 (C-2'), δ_C 146.1 (C-3'), δ_C 139.2 (C-4'), δ_C 146.1 (C-5'), δ_C 109.1 (C-6'), δ_C 166.1 (CO); 119.4 (C-1''), δ_C 109.3 (C-2''), δ_C 145.9 (C-3''), δ_C 139.1 (C-4''), δ_C 145.9 (C-5''), δ_C 109.3 (C-6''), δ_C 165.5 (CO); 118.5 (C-1'''), δ_C 109.2 (C-2'''), δ_C 145.9 (C-3'''), δ_C 139.5 (C-4'''), δ_C 145.9 (C-5'''), δ_C 109.2 (C-6'''), δ_C 165.1 (CO). δ_C 117.8 (C-1''''), δ_C 109.4 (C-2''''), δ_C 146.1 (C-3''''), δ_C 140.2 (C-4''''), δ_C 146.1 (C-5''''), δ_C 109.4 (C-6''''), δ_C 165.4 (CO). The anomeric signals at δ_H 6.13 (H-1) and δ_C 92.3 (C-1) suggested the presence of a glucose substructure (Pomin, 2012). Signals of the glucose moiety were observed in ^1H and ^{13}C NMR spectra at δ_H 6.13 (H-1, d, J = 8.3 Hz), δ_H 5.27 (H-2, dd, J = 9.9 Hz, 8.3 Hz), δ_H 5.52 (H-3, t, J = 9.5 Hz), δ_H 3.81 (H-4, t, J = 9.5 Hz), δ_H 4.09 (H-5, m), δ_H 4.39 (H_2-6, dd, J = 12.2 Hz, 4.5 Hz), δ_H 4.44 (H_2-6, d, J = 11.0 Hz) and δ_C 92.3 (C-1), δ_C 71.1 (C-2), δ_C 74.8 (C-3), δ_C 68.1 (C-4), δ_C 75.0 (C-5), δ_C 63.1 (C-6). The complete ^1H and ^{13}C NMR signal assignments and connectivity

were determined from a combination of ^{1}H-^{1}H COSY (appendix 55), HSQC (appendix 56) and HMBC (appendix 57) data. COSY correlations of H-2 with H-1 and H-3; H-3 with H-2 and H-4; H-5 with H-4 and H-6 identified the connectivity sequence in the glucose moiety. HMBC correlations from δ_H 4.32 (H_2-6) to δ_C 166.1 (CO); from δ_H 5.27 (H-2) to δ_C 165.5 (CO); from δ_H 6.13 (H-1) to δ_C 165.1 (CO) and from δ_H 5.52 (H-3) to δ_C 164.4 (CO) established the links between the glucose moiety and the four galloyl groups. Compound **24** was determined as 1,2,3,6-tetra-*O*-galloyl-β-D-glucose. Compound **24** has also been isolated previously in *Galla Chinese* with antiviral properties (Duan *et al*., 2004).

Compound **25** (figure 4.5) was obtained as a white powder with molecular formula of $C_{14}H_6O_8$, determined from its HRESIMS (appendix 58) m/z 303.0135 $[M + H]^+$ (calcd for $C_{14}H_7O_8$, 303.0141). The NMR data assignment was done by analysis of 1D and 2D NMR spectra (table 4.4) and by comparison with elagic acid derivatives reported in literature data (Ito *et al*., 2002; Ye *et al*., 2007). The ^{1}H NMR spectrum (appendix 59) displayed a single singlet signal at δ_H 7.44 (H-3/H-3') which upon integration showed the presence of two protons. The ^{13}C NMR spectrum (appendix 60) indicated six quartenary carbon signals at δ_C 107.2 (C-1/C-1'), δ_C 113.0 (C-2/C-2'), δ_C 148.7 (C-4/C-4'), δ_C 141.1 (C-5/C-5'), δ_C 136.8 (C-6/C-6'), δ_C 159.7 (C-7/C-7') and one methine carbon at δ_C 110.3 (C-3/C-3'). The complete ^{1}H and ^{13}C NMR signal assignments and connectivity were determined from a combination of ^{1}H-^{1}H COSY (appendix 61), HSQC (appendix 62) and HMBC (appendix 63) data. The HMBC correlation from δ_H 7.44 (H-3) to δ_C 107.2 (C-1), δ_C 113.0 (C-2), δ_C 148.7 (C-4), δ_C 141.1 (C-5), δ_C 136.8 (C-6), δ_C 159.7 (C-7) and from δ_H 7.44 (H-3') to δ_C 107.2 (C-1'), δ_C 113.0 (C-2'), δ_C 148.7 (C-4'), δ_C 141.1 (C-5'), δ_C 136.8 (C-6'), δ_C 159.7 (C-7') led to the establishment in the connectivities in compound **25**. Compound **25** was determined as ellagic acid.

Compound **26** (figure 4.5) was obtained as a white powder with molecular formula of $C_{14}H_6O_8$, determined from its HRESIMS (appendix 64) m/z 303.0135 $[M + H]^+$ (calcd for $C_{14}H_7O_8$, 303.0141). Compound **26** is similar to **25** except for the shift in the position of the carbonyl ester and oxygen which in turn led to a shift in the carbon chemical shifts downfield. The 1D NMR data is shown in (table 4.4). The ^{1}H NMR spectrum (appendix 65) displayed a single singlet signal at δ_H 7.36 (H-5/H-5') which upon integration showed the presence of two protons. The ^{13}C NMR spectrum (appendix 66) indicated six quartenary carbon signals at δ_C 113.5 (C-1/C-1'), δ_C 136.6 (C-2/C-2'), δ_C 160.1 (C-3/C-3'), δ_C 149.1 (C-4/C-4'), δ_C 143.6 (C-6/C-6') δ_C 163.6 (C-

7/C-7') and one methine carbon at δ_C 109.1 (C-5/C-5'). The complete ^1H and ^{13}C NMR signal assignments and connectivity were determined from a combination of ^1H-^1H COSY (appendix 67), HSQC (appendix 68) and HMBC (appendix 69) data. The HMBC correlation from δ_H 7.36 (H-5) to δ_C 113.5 (C-1), δ_C 136.6 (C-2), δ_C 160.1 (C-3), δ_C 149.1 (C-4), δ_C 143.6 (C-6), δ_C 163.6 (C-7) and from δ_H 7.36 (H-5') to δ_C 113.5 (C-1'), δ_C 136.6 (C-2'), δ_C 160.1 (C-3'), δ_C 149.1 (C-4'), δ_C 143.6 (C-6'), δ_C 163.6 (C-7') led to the establishment in the connectivities in compound **26**. Compound **26** was also determined as ellagic acid.

Table 4.4: ^1H NMR (600 MHz) and ^{13}C NMR (175 MHz) Spectroscopic Data of Compound **25 - 27**

	25[a]		**26**[a]		**27**[a]	
No.	^{13}C, Type	^1H, mult.(*J* in Hz)	^{13}C, Type	^1H , mult.(*J* in Hz)	^{13}C, Type	^1H , mult.(*J* in Hz)
1	107.2, C		113.5, C		108.0, C	
2	113.0, C		136.6, C		115.3, C	
3	110.3, CH	7.44, s	160.1, C		111.9, CH	7.70, s
4	148.7, C		149.1, C		147.4, C	
5	141.1, C		109.1, CH	7.36, s	141.4, C	
6	136.8, C		143.6, C		136.6, C	
7	159.7, C		163.6, C		159.4, C	
1'	107.2, C		113.5, C		108.7, C	
2'	113.0, C		136.6, C		112.2, C	
3'	145.5, C		160.1, C		110.9, CH	7.49, s
4'	110.3, CH	7.44, s	149.1, C		149.2, C	
5'	141.1, C		109.1, CH	7.36, s	140.1, C	
6'	136.8, C		143.6, C		137.2, C	
7'	159.7, C		163.6, C		159.5, C	
1"					103.3, CH	5.00, d
2"					73.5, CH	3.40
3"					76.0, CH	3.31
4"					67.8, CH	3.43
5"					66.3, CH_2	3.37
						3.85

[a]Recorded in DMSO-*d*6

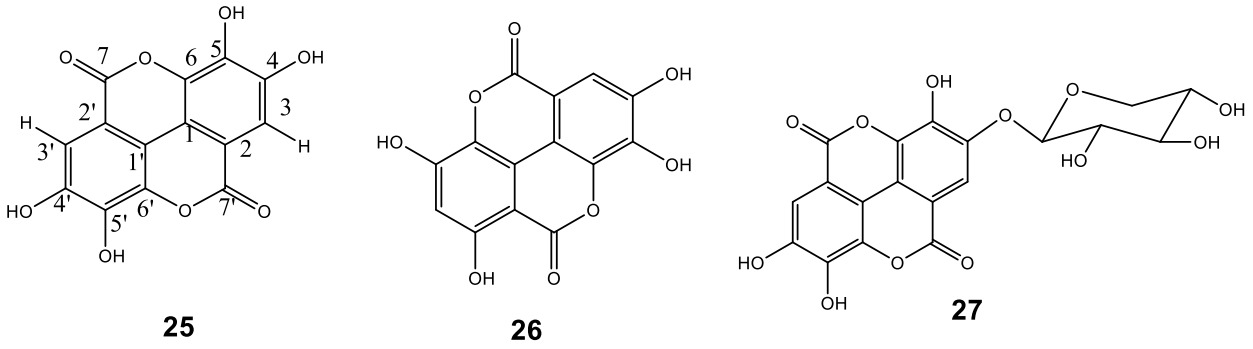

Figure 4.5: Chemical structures of compounds **25, 26** and **27**

Compound **27** (figure 4.5) was obtained as a white powder with molecular formula of $C_{19}H_{14}O_{12}$, determined from its HRESIMS (appendix 70) m/z 435.0914 $[M + H]^+$ (calcd for $C_{19}H_{15}O_{12}$, 435.0923). Compound **27** was similar to **25** except the presence of xylopyranoside ring. The NMR data assignment was done by analysis of 1D and 2D NMR spectra (table 5) and by comparison with ellagic acid derivatives reported in literature data (Ito *et al*., 2002; Ye *et al*., 2007). The ^{1}H NMR spectrum (appendix 71) displayed singlet signal at δ_H 7.70 (H-3) and δ_H 7.49 (H-3') which were attributed to the presence of ellagic acid. Proton signals for the xylopyranoside ring were observed at δ_H 5.0 (H-1"), δ_H 3.40 (H-2"), δ_H 3.31 (H-3"), δ_H 3.43 (H-4"), δ_H 3.37, 3.85 (H_2-5"). The ^{13}C NMR spectrum (appendix 72) indicated signals for twelve quartenary carbon at δ_C 108.0 (C-1), δ_C 115.3 (C-2), δ_C 147.4 (C-4), δ_C 141.4 (C-5), δ_C 136.6 (C-6), δ_C 159.4 (C-7) δ_C 108.7 (C-1'), δ_C 112.2 (C-2'), δ_C 149.2 (C-4'), δ_C 140.1 (C-5'), δ_C 137.2 (C-6'), δ_C 159.5 (C-7'); six methine carbon signals at δ_C 111.9 (C-3), δ_C 110.9 (C-3'), δ_C 103.3 (C-1"), δ_C 73.5 (C-2"), δ_C 76.0 (C-3"), δ_C 67.8 (C-4"); and one methylene carbon signal at δ_C 66.3 (C-5"). The complete ^{1}H and ^{13}C NMR signal assignments and connectivity were determined from a combination of ^{1}H-^{1}H COSY (appendix 73), HSQC (appendix 74) and HMBC (appendix 75) data. The HMBC correlation from δ_H 7.70 (H-3) to δ_C 108.0 (C-1), δ_C 115.3 (C-2), δ_C 147.4 (C-4), δ_C 141.4 (C-5), δ_C 136.6 (C-6), δ_C 159.4 (C-7) and from δ_H 7.49 (H-3) to δ_C 108.7 (C-1'), δ_C 112.2 (C-2'), δ_C 149.2 (C-4'), δ_C 140.1 (C-5'), δ_C 137.2 (C-6'), δ_C 159.5 (C-7') led to the establishment of the connectivities in the ellagic acid moiety. HMBC correlations from δ_H 5.0 (H-1") to δ_C 73.5 (C-2"), δ_C 76.0 (C-3"), δ_C 66.3 (C-5"); from δ_H 3.31 (H-3") to δ_C 73.5 (C-2"), δ_C 67.8 (C-4"), δ_C 66.3 (C-5") were some of the important correlations in determining the xylopyranoside moiety. Furthermore, COSY

correlations of H-2" with H-1" and H-3"; H-3" with H-2" and H-4"; H-4" with H-5" identified the connectivity sequence in the xylopyranoside moiety. The link between the ellagic acid moiety and xylopyranoside moiety was established by HMBC correlation from δ_H 5.0 (H-1") to δ_C 147.4 (C-4). Compound **27** was determined as ellagic acid-4-*O*-β-D-xylopyranoside. Ellagic acid-4-*O*-β-D-xylopyranoside is reported to exhibit antimicrobial properties to both human and plant pathogens (Fogliani *et al*., 2005).

Table 4.5: ^{1}H NMR (600 MHz) and ^{13}C NMR (175 MHz) Spectroscopic Data of Compound **28**

	28		**28***	
no.	^{13}C, Type	^{1}H, mult.(*J* in Hz)	^{13}C, Type	^{1}H, mult.(*J* in Hz)
1	162.2, C		161.3, C	
2	108.0, C		108.1, C	
3	164.3, C		161.3, C	
4	93.8, CH		108.1, CH	
4a	156.6, C		156.7, C	
4b	151.4, C		151.2,C	
5	108.1, CH	6.41	101.8, CH	
6	155.3, C		154.5, C	6.42
7	144.4, C		144.6, C	
8	108.1, CH	6.22	108.5, CH	6.22
8a	111.7, C		112.2, C	
8b	101.7, C		103.1, C	
9	179.4, C		179.6, C	
1'	82.1, CH		82.3, CH	
2'	73.6, CH	7.60	73.5, CH	7.61
3'	71.1, CH	6.89	71.1, CH	6.89
4'	70.7, CH		70.6, CH	
5'	79.5, CH		79.4, CH	
6'	62.0, CH_2	7.76	62.0, CH	7.73

Compound **28** (figure 4.6) was isolated as a yellow powder with molecular formula of $C_{19}H_{18}O_{11}$, determined from its HRESIMS (appendix 76) m/z 423.0918 $[M + H]^+$ (calcd for $C_{19}H_{19}O_{11}$, 423.0924). The NMR data assignment was done by analysis of 1D and 2D NMR spectra (table

4.5) and by comparison with xanthone compounds reported in literature data (Sun *et al*., 2013). The ^{1}H NMR spectrum (appendix 77) displayed a total of nine signals of which signals at δ_H 6.37 (s, H-4), δ_H 6.83 (s, H-5), δ_H 7.36 (s, H-8) were attributed to the xanthonoid moiety. The rest of the protons were attached to the glucopyranosyl moiety. A total of ninteen carbon signals were observed in the ^{13}C NMR spectrum (appendix 78). The complete ^{1}H and ^{13}C NMR signal assignments and connectivity were determined from a combination of ^{1}H-^{1}H COSY (appendix 79), HSQC (appendix 80) and HMBC (appendix 81) data. Compound **28** was determined as mangferin, a *C*-glucopyranoside of 1,3,6,7-tetrahydroxyxanthone (Severi *et al*., 2009; Shahat *et al*., 2003). Mangiferin is reported to be an effective anti-inflammatory, immunomodulator analgesic and antioxidant which has been used traditionally in the treatment of obesity (Shinde *et al*., 2010)

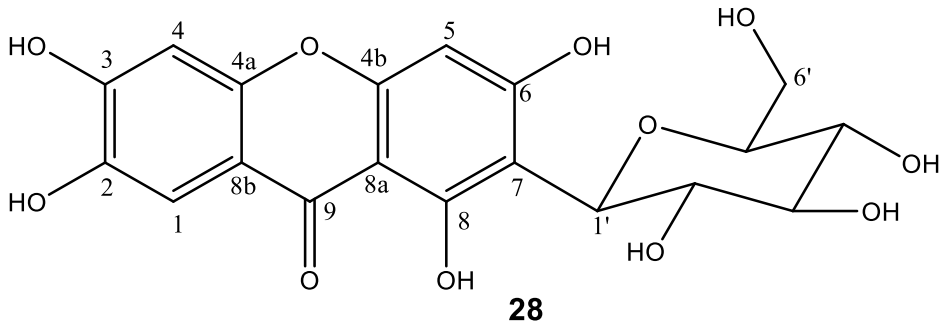

28

Figure 4.6: Chemical structure of compound **28**

Compound **29** (figure 4.7) was isolated as colorless powder with a molecular formula $C_{15}H_{10}O_5$, which was determined from its HRESIMS (appendix 82) at *m/z* 271.0602 $[M + H]^+$ (calcd for $C_{15}H_{11}O_5$, 271.0606). The NMR data assignment was done by analysis of 1D and 2D NMR spectra (table 4.6) and by comparison with isoflavone analogues reported in literature data (Lv *et al*., 2011; Zielińska *et al*., 2008). The ^{1}H NMR spectrum (appendix 83) displayed methine signals at H-2 (δ_H 8.22), H-6 (δ_H 6.10), H-8 (δ_H 6.25), H-2′ / H-6′ (δ_H 7.36), H-3′ / H-5′ (δ_H 6.81). ^{13}C NMR spectrum (appendix 84) confirmed the presence of 15 carbon atoms including one carbonyl group; C-4 (δ_c 180.1) seven methine carbons; C-2 (δ_c 153.8), C-6 (δ_c 100.2), C-8 (δ_c 94.6), C-2′ / C-6′ (δ_c 130.6), C-3′ / C-5′ (δ_c 115.5) and seven quartenary carbons; C-3 (δ_c 122.4), C-4a (δ_c 103.7), C-5 (δ_c 162.3), C-7 (δ_c 165.6), C-8a (δ_c 158.3), C-1′ (δ_c 122.0) and C-4′ (δ_c 157.8). The complete structure of **29** was determined by analysis of COSY (appendix 85), HSQC (appendix 86) and HMBC (appendix 87), spectra. ^{1}H-^{1}H COSY correlations between H-2′ / H-6′ (δ_H 7.36), H-3′ / H-5′ (δ_H 6.81) were observed. The link between the carbon skeleton was

established by HMBC correlations from H-2 (δ_H 8.22) to C-3 (δ_c 122.4), C-4 (δ_c 180.1), C-8a (δ_c 158.3), C-1′ (δ_c 122.0); from H-6 (δ_H 6.10) to C-4a (δ_c 103.7), C-5 (δ_c 162.3), C-8 (δ_c 94.6); from H-8 (δ_H 6.25) to C-2 (δ_c 153.8), C-4a (δ_c 103.7); from H-2′ (δ_H 7.36) to C-1′ (δ_c 122.0), C-3′ (δ_c 115.5), C-4′ (δ_c 157.8), C-6′ (δ_c 130.6) and from H-3′ (δ_H 6.81) to C-2′ (δ_c 130.6), C-4′ (δ_c 157.8), C-5′ (δ_c 115.5). From the NMR analysis and comparisons with reported flavonoids (Zielińska *et al*., 2008) compound **29** was determined as genistein.

Compound **30** (figure 4.7) was isolated as colorless powder with a molecular formula $C_{17}H_{14}O_5$, which was determined from its HRESIMS (appendix 88) at *m/z* 299.0915 $[M + H]^+$ (calcd for $C_{17}H_{15}O_5$, 299.0919). The NMR data assignment was done by analysis of 1D and 2D NMR spectra (table 4.6) and by comparison with isoflavone analogues reported in literature data (Babu *et al*., 2023). Compound **30** was similar to compound **29** except for the methoxylation at C-7 and C-4′ in **30**. The ^{1}H NMR spectrum (appendix 89) displayed methine signals at H-2 (δ_H 8.40), H-5 (δ_H 7.70), H-8 (δ_H 6.27), H-2′ / H-6′ (δ_H 7.51), H-3′ / H-5′ (δ_H 6.99) and methoxy signals at 7-OCH_3 (δ_H 3.87) and 4′-OCH_3 (δ_H 3.80). ^{13}C NMR spectrum (appendix 90) confirmed the presence of 17 carbon atoms including one carbonyl group; C-4 (δ_c 175.1) and two methoxy signals at 7-OCH_3 (δ_c 61.1) and 4′-OCH_3 (δ_c 55.6). Seven methine carbons were also observed at C-2 (δ_c 153.4), C-5 (δ_c 121.2), C-8 (δ_c 96.0), C-2′ / C-6′ (δ_c 130.6), C-3′ / C-5′ (δ_c 114.1) and seven quartenary carbons; C-3 (δ_c 123.3), C-4a (δ_c 131.8), C-6 (δ_c 156.1), C-7 (δ_c 135.2), C-8a (δ_c 151.2), C-1′ (δ_c 124.8) and C-4′ (δ_c 159.4). The complete structure of **30** was determined by analysis of COSY (appendix 91), HSQC (appendix 92), and HMBC (appendix 93), spectra. ^{1}H-^{1}H COSY correlations between H-2′ / H-6′ (δ_H 7.51), H-3′ / H-5′ (δ_H 6.99) were observed. The link between the carbon skeleton was established by HMBC correlations from H-2 (δ_H 8.40) to C-3 (δ_c 123.3), C-4 (δ_c 175.1), C-8a (δ_c 151.2), C-1′ (δ_c 124.8); from H-5 (δ_H 7.70) C-4a (δ_c 131.8), C-6 (δ_c 156.1), C-8a (δ_c 151.2); from H-2′ (δ_H 7.36) to C-1′ (δ_c 124.8), C-3′ (δ_c 114.1), C-4′ (δ_c 159.4), C-6′ (δ_c 130.6) and from H-3′ (δ_H 6.99) to C-2′ (δ_c 130.6), C-4′ (δ_c 159.4), C-5′ (δ_c 114.1). From the NMR analysis and comparisons with reported flavonoids (Babu *et al*., 2023) compound **30** was determined as apigenin-7,4'-diethylether.

Compound **31** (figure 4.7) was isolated as a yellow powder with molecular formula of $C_{16}H_{14}O_4$, determined from its HRESIMS (appendix 94) m/z 271.0970 $[M + H]^+$ (calcd for $C_{16}H_{15}O_4$, 271.0970). The NMR data assignment was done by analysis of 1D and 2D NMR spectra (table 4.6) and by comparison with isoflavone analogues reported in literature data (Babu *et al*.,

2023). The ^{1}H NMR spectrum (appendix 95) displayed a total of nine signals. A total of sixteen carbon signals were observed in the ^{13}C NMR spectrum (appendix 96). The complete structure of **31** was determined by analysis of COSY (appendix 97), HSQC (appendix 98), and HMBC (appendix 99) spectra. ^{1}H-^{1}H COSY correlations between H-5 and H-6; H-2′ / H-6′ and H-3′ / H-5′ (δ_H 6.81) were observed. The link between the carbon skeleton was established by HMBC correlations from H-2 (δ_H 8.29) to C-3 (δ_c 124.9), C-4 (δ_c 175.0), C-8a (δ_c 158.1), C-1′ (δ_c 123.5); from H-6 (δ_H 6.89) to C-4a (δ_c 111.6), C-5 (δ_c 127.5), C-8 (δ_c 102.5); from H-8 (δ_H 6.80) to C-2 (δ_c 153.4), C-4a (δ_c 111.6); from H-2′ (δ_H 7.51) to C-1′ (δ_c 130.5), C-3′ (δ_c 114.0), C-4′ (δ_c 159.4), C-6′ (δ_c 130.5) and from H-3′ (δ_H 6.98) to C-2′ (δ_c 130.5), C-4′ (δ_c 159.4), C-5′ (δ_c 114.0). From the NMR analysis and comparisons with reported isoflavones (Zielińska *et al*., 2008) compound **31** was determined as formononetin with IUPAC name 7-hydroxy-3-(4-methoxyphenyl)-4H-chromen-4-one.

Table 4.6: ^{1}H NMR (600 MHz) and ^{13}C NMR (175 MHz) Spectroscopic Data of Compound **30 - 32**

	29		**30**		**31**		**32**	
No.	^{13}C, Type	^{1}H	^{13}C, Type	^{1}H	^{13}C, Type	^{1}H	^{13}C, Type	^{1}H
2	153.8, CH	8.22, s	153.4, CH	8.40, s	153.4, CH	8.29, s	153.0, CH	8.20, s
3	122.4, C		123.3, C		124.9, C		123.8, C	
4	180.1, C		175.1, C		175.0, C		175.1, C	
4a	103.7, C		131.8, C		111.6, C		116.1, C	
5	162.3, C		121.2, CH	7.70	127.5, CH	7.92	127.4, CH	7.90
6	100.2, CH	6.10, s	156.1, C		116.3, CH	6.89	116.4, CH	6.87
7	165.6, C		135.2, C		164.7, C		165.7, C	
8	94.6, CH	6.25, s	96.0, CH	6.27	102.5, CH	6.80	102.4, CH	6.79
8a	158.3, C		151.2, C		158.1, C		158.1, C	
1′	122.0, C		124.8, C		123.5, C		123.1, C	
2′	130.6, CH	7.36	130.6, CH	7.51	130.5, CH	7.51	130.4, CH	7.37
3′	115.5, CH	6.81	114.1, CH	6.99	114.0, CH	6.98	115.4, CH	6.81
4′	157.8, C		159.4, C		159.4, C		157.6, C	
5′	115.5, CH	6.81	114.1, CH	6.99	114.0, CH	6.98	115.4, CH	6.81
6′	130.6, CH	7.36	130.6, CH	7.51	130.5, CH	7.51	130.4, CH	7.37
7-OMe			61.1, CH_3	3.87, s				

4′-OMe	55.6, CH_3	3.80, s	55.6, CH_3	3.79, s

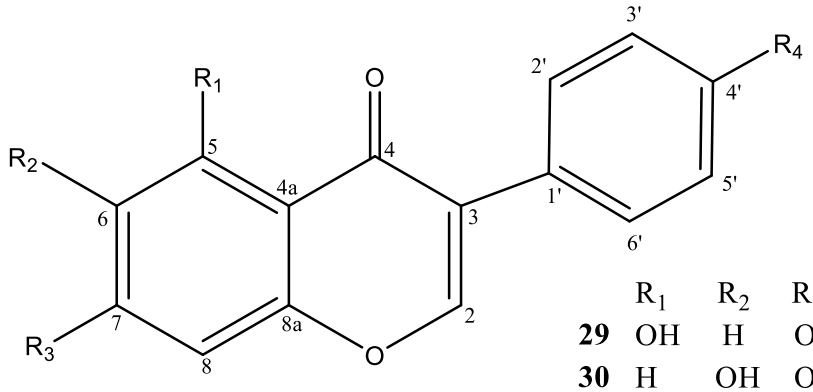

	R_1	R_2	R_3	R_4
29	OH	H	OH	OH
30	H	OH	OCH_3	OCH_3
31	H	H	OH	OCH_3
32	H	H	OH	OH

Figure 4.7: Chemical structures of compounds **29 - 32**

Compound **32** (figure 4.7) was isolated as colorless powder with a molecular formula $C_{15}H_{10}O_4$, which was determined from its HRESIMS (appendix 100) at *m/z* 255.0653 $[M + H]^+$ (calcd for $C_{15}H_{11}O_4$, 255.0657). The difference between compounds **32** and **29** is hydroxylation at C-5 in **29**. The NMR data assignment was done by analysis of 1D and 2D NMR spectra (table 4.6) and by comparison with isoflavone analogues reported in literature data (Yi *et al*., 2019). The ^1H NMR spectrum (appendix 101) displayed methine signals at H-2 (δ_H 8.20), H-5 (δ_H 7.90), H-6 (δ_H 6.87), H-8 (δ_H 6.79), H-2′ / H-6′ (δ_H 7.37), H-3′ / H-5′ (δ_H 6.81). ^{13}C NMR spectrum (appendix 102) confirmed the presence of 15 carbon atoms including one carbonyl group; C-4 (δ_c 175.1), seven methine carbons; C-2 (δ_c 153.0), C-5 (δ_c 127.4), C-6 (δ_c 116.4), C-8 (δ_c 102.4), C-2′ / C-6′ (δ_c 130.4), C-3′ / C-5′ (δ_c 115.4) and seven quartenary carbons; C-3 (δ_c 123.8), C-4a (δ_c 116.1), C-7 (δ_c 165.7), C-8a (δ_c 158.1), C-1′ (δ_c 123.1) and C-4′ (δ_c 157.6). The complete structure of **32** was determined by analysis of COSY (appendix 103), HSQC (appendix 104), and HMBC (appendix 105), spectra. ^1H-^1H COSY correlations between H-2′ / H-6′ (δ_H 7.37), H-3′ / H-5′ (δ_H 6.81) were observed. The link between the carbon skeleton was established by HMBC correlations from H-2 (δ_H 8.20) to C-3 (δ_c 123.8), C-4 (δ_c 175.1), C-8a (δ_c 158.1), C-1′ (δ_c 123.1); from H-6 (δ_H 6.87) to C-4a (δ_c 116.1), C-5 (δ_c 127.4), C-8 (δ_c 102.4); from H-8 (δ_H 6.79) to C-2 (δ_c 153.0), C-4a (δ_c 116.1); from H-2′ (δ_H 7.37) to C-1′ (δ_c 123.1), C-3′ (δ_c 115.4), C-4′ (δ_c 157.6), C-6′ (δ_c 130.4) and

from H-3′ (δ_H 6.81) to C-2′ (δ_c 130.4), C-4′ (δ_c 157.6), C-5′ (δ_c 115.4). From the NMR analysis and comparisons with reported flavonoids (Yi *et al*., 2019), compound **32** was determined as daidzein with IUPAC name 7,4'-dihydroxyisoflavone. Genistein (**29**) apigenin-7,4'-diethylether (**30)**, formononetin (**31**), daidzein (**32**) are isoflavone compounds which are reported to be chemopreventive for various types of cancers (Křížová *et al*., 2019; Murata *et al*., 2004; Zhang *et al*., 2018). These molecules are also active antioxidants mostly present in medicinal plants, fruits and vegetables (Dasbasi, 2020; Yi *et al*., 2019).

4.3 X-ray Diffraction Analysis (XRD)

Compounds **17**, **18**, and **22** were crystallized from methanol and water in the ratio 2:1. (Figure 4.8). The suitable crystals were selected and analyzed on a Bruker D8 VENTURE area detector diffractometer according to the method described by Kamtcha *et al*. (2018). The crystal was kept at 100.0 K during data collection. Using Olex2 (Dolomanov *et al*., 2009), the structure was solved with the XT (Sheldrick, 2015) structure solution program using Intrinsic Phasing and refined with the XL (Sheldrick, 2008) refinement package using Least Squares minimisation. Crystal data of compound **17**, **18**, and **22** have been deposited at the Cambridge Crystallographic Data Centre with deposition number CCDC 2007927 (**17**), 2007929 (**18**), and 2007931 (**22**). A copy of the data can be obtained free of charge from https://www.ccdc.cam.ac.uk/ after registration or by e-mailing to deposit@ccdc.cam.ac.uk.

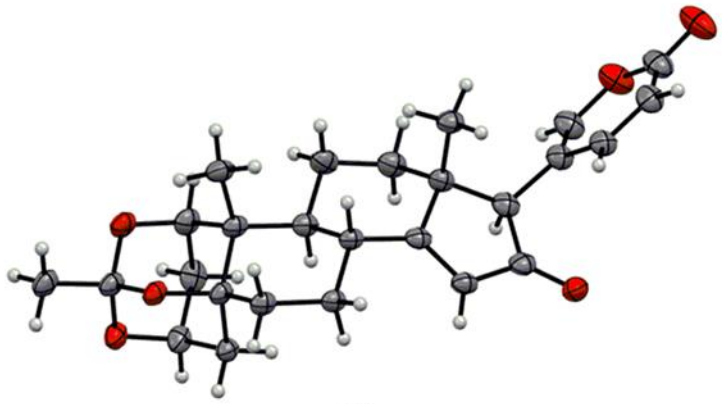

17

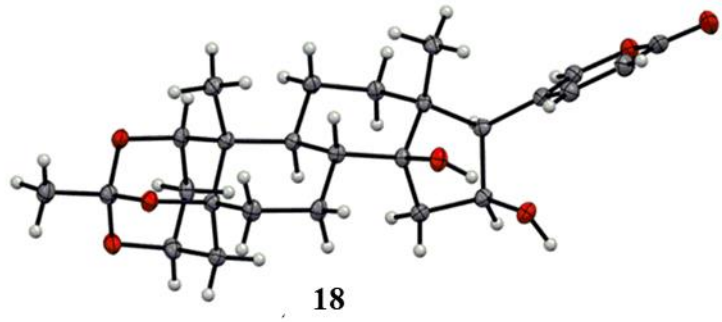

18

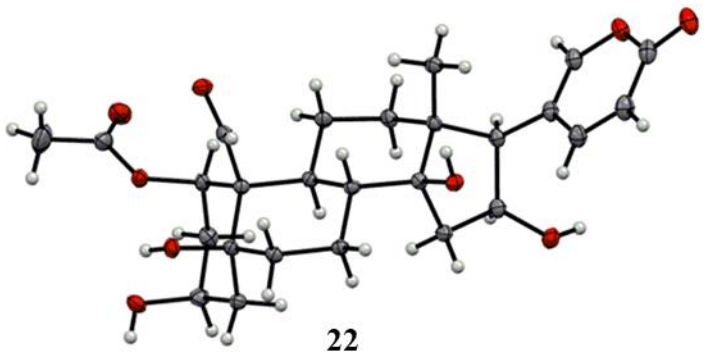

22

Figure 4.8: ORTEP drawing of **17**, **18** and **22.** The ellipsoids are shown at the 50% probability level**.**

Paulliniogenin A (**17)**: $C_{26}H_{32}O_7$ M =456.51 g/mol, monoclinic, space group $P2_1$ (no. 4), a = 12.1262(8) Å, b = 14.4026(7) Å, c = 13.3342(8) Å, β = 105.607(4)°, V = 2242.9(2) Å^3, Z = 4, T = 100.0 K, μ(CuKα) = 0.800 mm^{-1}, *Dcalc* = 1.352 g/cm^3, 41245 reflections measured (6.882° ≤ 2Θ ≤ 149.992°), 9034 unique (R_{int} = 0.0643, R_{sigma} = 0.0477) which were used in all calculations. The final R_1 was 0.0428 (I > 2σ(I)) and wR_2 was 0.1108 (all data).

16β-hydroxybersamagenin 1,3,5-orthoacetate (**18**): $C_{26}H_{34}O_7$ *M* =458.53 g/mol, orthorhombic, space group $P2_12_12_1$ (no. 19), *a* = 10.3562(6) Å, *b* = 10.6612(6) Å, *c* = 19.9903(11) Å, *V* = 2207.1(2) $Å^3$, *Z* = 4, *T* = 100.0 K, μ(CuKα) = 0.813 mm^{-1}, *Dcalc* = 1.380 g/cm^3, 46009 reflections measured (8.846° ≤ 2Θ ≤ 154.856°), 4662 unique (R_{int} = 0.0266, R_{sigma} = 0.0116) which were used in all calculations. The final R_1 was 0.0288 (I > 2σ(I)) and wR_2 was 0.0787 (all data).

16β-hydroxybersaldegenin-1-acetate (**22**): $C_{27}H_{38}O_{10}$ *M* =522.57 g/mol, monoclinic, space group $P2_1$ (no. 4), *a* = 7.1585(3) Å, *b* = 16.5713(8) Å, *c* = 10.8248(4) Å, *β* = 102.657(2)°, *V* = 1252.89(9) $Å^3$, *Z* = 2, *T* = 100.0 K, μ(CuKα) = 0.877 mm^{-1}, *Dcalc* = 1.385 g/cm^3, 42139 reflections measured (8.372° ≤ 2Θ ≤ 149.94°), 5098 unique (R_{int} = 0.0224, R_{sigma} = 0.0107) which were used in all calculations. The final R_1 was 0.0250 (I > 2σ(I)) and wR_2 was 0.0698 (all data).

4.4 Secondary metabolites isolated from the leaves of *B. abyssinica* subsp. *abyssinica*

The MeOH extract of the leaves of *B. abyssinica* subsp. *abyssinica* was subjected to successive column chromatography over silica gel and Sephadex LH-20, followed by preparative HPLC to afford eight compounds **33** – **40**. Compounds **33** – **36** were found to be new while compounds **37** – **40** have been previously reported. The isolated bufadienolides were characterized with formyl group at C-19. Whereas, bufadienolides isolated from *B. abyssinica* subspecies *paullioniodes* have a methyl group at this position (Nyamboki *et al*., 2021).

Compound **33** (figure 4.9) was isolated as colorless powder with a molecular formula $C_{27}H_{30}O_8$, which was determined from its HRESIMS (appendix 106) at *m/z* 483.2016 $[M + H]^+$ (calcd for $C_{27}H_{31}O_8$, 483.2013). IR spectral cm^{-1}: 3435, 2935, 1711, 1627 (appendix 107). The NMR data assignment was done by analysis of 1D and 2D NMR spectra and by comparison with analogues bufadienolides reported in literature data (Bedane *et al*., 2020a). These data (Table 4.7) suggested that **33** has a bufadienolide steroidal structure with α-pyrone ring system. The presence of this characteristic α-pyrone (2H-pyran-2-one) ring was evident from the ^1H NMR data (appendix 108) [δ_H 7.53 (H-21, s), 7.31 (H-22, d, J = 9.6 Hz), and 6.34 (H-23, d, J = 9.6 Hz)] and ^{13}C NMR data (appendix 109) δ_C 153.1 (C-21), 147.8 (C-22) and 116.2 (C-23) (Bedane *et al*., 2020a). Compound **33** also possessed an orthoacetate group in ring A, as confirmed from the presence of a characteristic orthoacetate singlet methyl proton at H_3-26 (δ_H 1.34), which showed a strong HMBC correlation with C-25 (δ_C 112.0) (Bedane *et al*., 2020b). Long-range HMBC

correlations of H-1 (δ_H 4.65) with C-25 (δ_C 112.0) also supporting the presence of the orthoacetate structure in ring A. The complete ^{1}H and ^{13}C NMR signal assignments and connectivity were determined from a combination of ^{1}H-^{1}H COSY (appendix 110), HSQC (appendix 111) and HMBC (appendix 112) data. The COSY correlations of H_2-2 with H-1 and H-3, and H-3 with H-2 and H_2-4 identified the connectivity sequence in the A ring. Signals for 27 carbon atoms were observed in the ^{13}C NMR spectrum. Comparison of its experimental and reported NMR data revealed that **33** has similar NMR values with paulliniogenin B, which has been isolated from the bark *B. abyssinica* subsp. *paullinioides* in this study (Nyamboki *et al*., 2021). The difference being the presence of a formyl group at C-19 in **33**. The presence of α, β-unsaturated carbonyl group in ring D was confirmed from signals at δ_C 162.4 (C-14), δ_C 151.3 (C-15), and δ_C 203.0 (C-16). It was also confirmed by the HMBC correlations of H_3-18 to C-14, H-17 to C-14, C-15 and C-16. Position of the methoxy group (δ_H 3.81, δ_C 59.2) at C-15 was determined by strong HMBC correlations from the OMe-15 methoxy protons to C-15 (δ_C 151.3). HMBC from H-17 (δ_H 3.23) to C-13, C-16, C-18, C-20, C-21, and C-22 were important correlations observed in ring D and confirmed the position of the α-pyrone ring at C-17. A Singlet methyl group at δ_H 0.92 (δ_C 23.2) is typical steroidal methyl group and was assigned to C-18 based on their HMBC correlations, H_3-18 to C-12, C-13, C-14, and C-17. The presence of a formyl group was determined from its proton at δ_H 10.25 (H-19) that showed HSQC correlation with δ_C 208.7 (C-19). HMBC correlation of formyl proton, H-19 with C-10 (δ_C 54.4) confirmed the position of the formyl group at C-10.

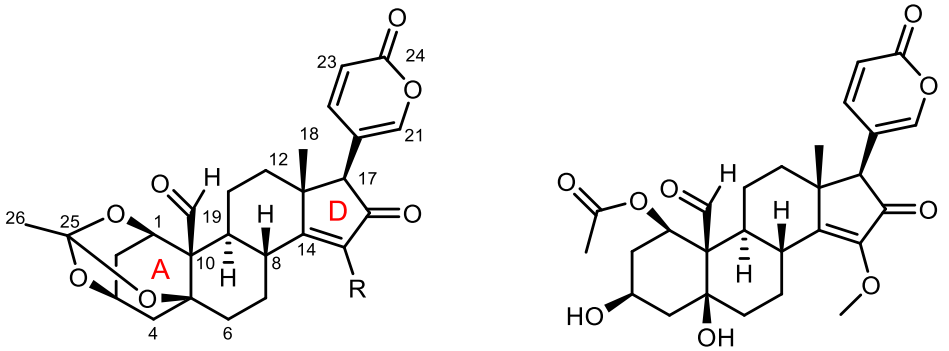

33 R = OCH_3
34 R = H

Figure 4.9: Chemical structures of compounds **33**, **34** and **35**

Table 4.7: ^{1}H and ^{13}C NMR Data[a] of Compound **33–35** in CD_3OD.

no.	**33**[b]		**34**[c]		**35**[c]	
	^{13}C	^{1}H, mult. (*J* in Hz)	^{13}C	^{1}H, mult. (*J* in Hz)	^{13}C	^{1}H, mult. (*J* in Hz)
1α	72.4	4.65, brs	72.4	4.65, brs	72.3	5.75, t (2.7)
2α	28.1	1.85	28.0	1.85	31.7	1.94
2β		2.42		2.42		2.16, m
3α	68.6	4.34, brs	68.6	4.30, brs	67.1	4.27, brs
4α	34.4	2.51	34.4	2.51	38.6	2.41, dd (15.0, 3.4)
4β		1.94, m		1.94, m		1.75, m
5	75.8		75.9		74.8	
6α	33.7	1.41, m	33.3	1.64	36.9	1.80
6β		2.38		2.40		2.35, m
7α	25.5	2.04, m	25.4	2.06, m	27.1	1.97, m
7β		2.51, m		1.81		2.58, m
8β	38.4	2.74, td (12.1, 3.5)	38.1	2.76, m	38.7	2.68, td (12.2, 3.7)
9α	45.2	1.85	45.5	1.81	46.4	1.80
10	54.4		54.3		58.2	
11α	21.1	1.82	21.2	1.84	22.5	1.85
11β		1.64		1.64		1.71
12α	39.4	1.98	39.9	2.04	39.6	2.02
12β		1.48		1.54		1.50, td (13.4, 4.0)
13	44.1		49.0		43.9	
14	162.4		190.4		162.4	
15	151.3		124.9	5.96, s	151.4	
16	203.0		207.5		203.2	
17α	59.2	3.23, s	59.9	3.66, s	59.0	3.21, s
18	23.2	0.92, s	22.7	0.94, s	22.9	0.89, s
19	208.7	10.25, s	208.5	10.23, s	207.5	10.14, s
20	116.3		116.6		116.3	
21	153.1	7.53, s	153.1	7.52, d (2.6)	153.1	7.53, s
22	147.8	7.31, d (9.6)	147.9	7.27, dd (9.6. 2.6)	147.8	7.31, dd (9.6. 2.6)
23	116.2	6.34, d (9.6)	116.3	6.34, d (9.6. 1.2)	116.2	6.35, d (9.6)
24	163.6		163.7		163.6	

25	112.0		112.1			
26	26.1	1.34, s	26.1	1.32, s		
OMe-15	59.2	3.81, s				
1-OC(O)Me					171.9	
1-OC(O)Me					21.3	1.98, s

[a]Signals without multiplicity are overlapping signals deduced from the HSQC spectrum.

[b]Recorded at (^{1}H: 700 MHz, ^{13}C: 175 MHz). [c]Recorded at (^{1}H: 600 MHz, ^{13}C: 150 MHz).

The relative configuration of **33** was defined based on NOESY correlations (appendix 113) and biosynthetic considerations, as it has the same stereogenic centres as paulliniogenin B (Nyamboki *et al*., 2021). The configuration of the formyl group at C-10 assigned β-orientation based on NOESY correlations of H-19/H-8 and H-8/H_3-18. The NOESY correlations between H-19 and H-8 and between H-8 and H_3-18 suggested the β-orientation of H_3-18, H-8, and the formyl group at C-10. Additional NOESY correlations from H_3-18 to H-21 and H-22 confirmed the β-orientation of the α-pyrone ring. Thus, the structure of compound **33** was determined as 10*β*-formylpaulliniogenin A.

Compound **34** (figure 4.9) was isolated as a white powder with a molecular formula $C_{26}H_{28}O_7$, as determined from the HRESIMS (appendix 114) at *m/z* 453.1912 $[M + H]^+$ (calcd for $C_{26}H_{29}O_7$, 453.1907). IR spectral cm^{-1}: 3410, 2934, 2358, 1719, 1594 (appendix 115). Its NMR data (table 4.7) were very similar to those of **33** except the absence of the methoxy signals in **34**, and in effect, the C-15 chemical shift was more upfield (δ_C 124.9) compared to δ_C 151.3 in **33**. The resulting vinylic singlet proton signal δ_H 5.96 (H-15) showed HMBC correlations with C-14, C-15, and C-17. The complete ^{1}H (appendix 116) and ^{13}C NMR (appendix 117) signal assignments and connectivity were determined from a combination of ^{1}H-^{1}H COSY (appendix 118), HSQC (appendix 119), and HMBC (appendix 120) data. The relative configuration of **34** was established from the observed identical coupling constants and NOESY correlations (appendix 121) as in **33**. Comparison of its NMR data with reported data indicated that **34** has similar NMR values with paulliniogenin A except **34** has a formyl group at C-19 (Nyamboki *et al*., 2021). The presence of a formyl group was determined from its proton at δ_H 10.23 (H-19) that showed HSQC correlation with δ_C 208.5 (C-19). HMBC correlation of the formyl proton, H-19 with C-10 (δ_C 54.4) confirmed

the position of the formyl group at C-10. Therefore, the structure of **34** was elucidated as 10*β*-formylpaulliniogenin A.

Compound **35** (figure 4.9) gave a molecular ion at *m/z* 501.2123 for $[M + H]^+$ (calcd for $C_{27}H_{33}O_9$, 501.2119) in the HRESIMS (appendix 122) defined a molecular formula $C_{27}H_{32}O_9$. IR spectral cm^{-1}: 3401, 2931, 2361, 17210, 1592 (appendix 123). The ^1H (appendix 124) and ^{13}C NMR (appendix 125) spectroscopic data (table 4.7) suggested that **35** is also a bufadienolide steroidal structure. Unlike 10*β*-formylpaulliniogenin A (**33**) and10*β*-formylpaulliniogenin A (**34**), **35** has no orthoacetate ring. It possessed an acetoxy group deduced from its carbonyl carbons at δ_C 171.9, and an acetoxy methyl groups at δ_C 21.3 (δ_H 1.98). The COSY correlations (appendix 126) of H-1 to H_2-2, H_2-2 to H-3 and H-3 to H_2-4 identified a connectivity sequence in ring-A. The structure of ring-A and its NMR signals are identical to those reported for bersaldegenin 1-acetate (Moniuszko-Szajwaj *et al*., 2016). HMBC correlation of H-1 (δ_H 5.75) with δ_C 171.9 confirmed the position of the acetoxy group at C-1. The presence of a formyl group was established from its proton at δ_H 10.14 (H-19) that showed HSQC correlation (appendix 127) with δ_C 207.5 (C-19). HMBC correlation (appendix 128) of the formyl proton (H-19) with C-10 (δ_C 58.2) confirmed position of the formyl group at C-10. The remaining rings have identical NMR spectra as in compound **33**. The relative configuration of **35** was defined based on NOESY correlations (appendix 129) and biosynthetic considerations, as it has the same stereogenic centers as **33**. The NOESY correlations of H-19 with H-8, H-8 with H_3-18, and H_3-18 with H-22 suggested the formyl group and the pyrone ring to be *β*-cofacially oriented. Additional NOESY correlations of H-1α (δ_H 5.75) with H-11α (δ_H 1.85) showed that the acetoxy group at C-2 was *β*-oriented. Thus, the new compound (**35**) was identified as 1*β*-acetoxy-3*β*,5*β*-dihydroxy-15-methoxy-16,19-dioxobufa-14(15),20,22-trienolide.

Compound **36** (figure 4.10) was isolated as a yellow powder with a molecular formula $C_{28}H_{26}O_{11}$ that was determined from its HRESIMS (appendix 130) at *m/z* 539.1554 $[M + H]^+$ (calcd for $C_{28}H_{27}O_{11}$, 539.1553). IR spectral cm^{-1}: 3359, 2924, 1699, 1598 (appendix 131). The complete ^1H (appendix 132) and ^{13}C NMR (appendix 133) signal assignments and connectivity were determined from a combination of ^1H-^1H COSY (appendix 134), HSQC (appendix 135) and HMBC (appendix 136) data. A total of 28 carbons were observed on the ^{13}C NMR spectrum (Table 4.8). The shielded aromatic methines at δ_C 98.2 (C-3), δ_C 96.1 (C-5), δ_C 133.5 (C-2' and C-6') and δ_C 115.7 (C-3' and C-5') are typical of phenolic natural compounds. The signal at δ_C 197.5 (C-7)

corresponds to carbonyl of a benzophenone (Rancon *et al*., 2001). Four quaternary carbon signals, C-2 (δ_C 162.6), C-4 (δ_C 158.7), C-6 (δ_C 160.0) and C-4' (δ_C 163.4), correspond to oxygenated aromatic carbons. The NMR of sub structure of **36**, the benzophenone and the sugar moiety, are identical to those of **37**, which has been previously isolated by Rancon *et al*. (2001). The difference being the presence of a cinnamoyl group in **36**. The ^{1}H NMR and the HSQC spectra revealed an anomeric signal (δ_H 4.88, m, H1" and δ_C 101.9, C1") together with a set of signals between δ_H 3.17 – 4.51 in ^{1}H NMR and δ_C 64.8 – 77.8 in ^{13}C NMR, firmly established the presence of a glucopyranose (Dhouafli *et al*., 2019).

The HMBC correlation between the anomeric proton H-1" (δ_H 4.88) and C-4 (δ_C 158.7) indicated 4-O-linkage between the sugar moiety and benzophenone. The cinnamoyl subunit was deduced from aromatic protons (δ_H 7.42 – 7.63) and two olefinic *trans* coupled protons (δ_H 6.60, *d*, J=16.0 Hz and δ_H 7.7, *d*, J=16.0 Hz), correlated in HMBC with carbonyl carbon δ_C 168.5 (C-1'") (Nishimura *et al*., 2016). The HMBC correlation from the methylene proton, H-6" of the sugar moiety to the carbonyl carbon, δ_C 168.5 (C-1'") provided a link between the two subunits. The cinnamoyl fragment ion was also observed in HRMS at *m/z* 131.0493. Further analysis of the HRMS^2 indicated fragment ion at *m/z* 293.1021$[C_{15}H_{17}O_6]^+$ and *m/z* 247.0602 $[C_{13}H_{11}O_5]^+$ due to cleavage of the acetophenone and sugar moiety at 4-O linkage. A combination of ^{1}H-^{1}H COSY, HSQC and HMBC data were used to determine the complete ^{1}H and ^{13}C NMR signal assignments. The type of sugar was deduced from compound **37** which is known (Rancon *et al*., 2001). The main difference between compounds **36** and **37** is the presence of the cinnamoyl group in **36**. The NMR data of the two compounds were also comparable as shown in table 9. The structure of compound **36** was therefore determined as 2,6,4'-trihydroxybenzophenone-4-O-(6'"-cinnamoyl)-β-D-glucoside.

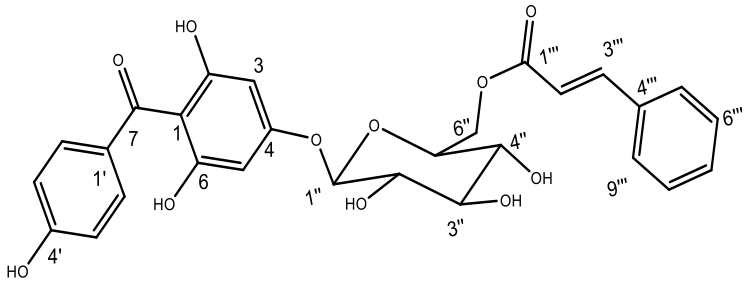

36

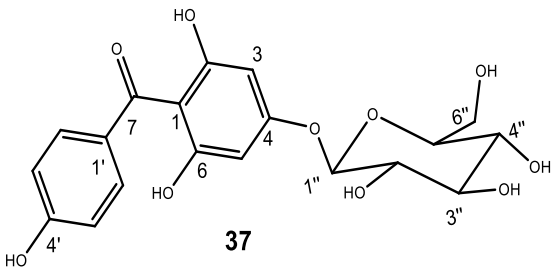

37

Figure 4.10: Chemical structures of compounds **36** and **37**

Table 4.8: ^{1}H NMR (600 MHz) and ^{13}C NMR (150 MHz) Spectroscopic Data of Compounds **36** and **37** in CD3OD

		36		**37**
no.	^{13}C, Type	^{1}H, mult.(*J* in Hz)	^{13}C, Type	^{1}H, mult.(*J* in Hz)
1	110.2, C		108.9, C	
2	162.6, C		158.3, C	
3	98.2, CH	6.06, d (2.0)	96.7, CH	6.09, d (2.1)
4	158.7, C		157.3, C	
5	96.1, CH	6.26, d (2.0)	94.5, CH	6.27, d (2.0)
6	160.0, C		161.1, C	
7	197.5, C		196.1, C	
1'	132.4, C		130.9, C	
2'/6'	133.5, CH	7.67 d (8.6)	132.1, CH	7.70, d (8.7)
3'/5'	115.7, CH	6.77 d (8.6)	114.4, CH	6.80, d (8.7)
4'	163.4, C		162.2, C	
1"	101.9, CH	4.88*	100.9, CH	4.84, d (7.7)
2"	74.6, CH	3.17	73.3, CH	3.11
3"	77.8, CH	3.47	76.4, CH	3.39
4"	71.5, CH	3.37	76.8, CH	3.37
5"	75.6, CH	3.62	69.7, CH	3.29
6"	64.8, CH_2	4.30 dd (11.8, 6.8), 4.51	61.1, CH_2	3.69
		dd (11.8, 2.0)		3.88
1'"	168.5, C			
2'"	118.7, CH	6.60 d (16.0)		
3'"	146.6, CH	7.70 d (16.0)		
4'"	135.8, C			
5'"/9'"	129.4, CH	7.63 m		
6'"/8'"	130.0, CH	7.42 m		
7'"	131.5, CH	7.42 m		

[a]Signals without multiplicity are overlapping signals deduced from the HSQC spectrum.

Compound **37** (figure 4.10) was isolated as a yellow powder with a molecular formula $C_{19}H_{20}O_{10}$ that was determined from its HRESIMS (appendix 137) at *m/z* 409.1131 $[M + H]^+$ (calcd for $C_{19}H_{21}O_{10}$, 409.1135). The complete ^{1}H NMR (appendix 138) and ^{13}C NMR (appendix

139) signal assignments and connectivity were determined from a combination of ^{1}H-^{1}H COSY (appendix 140), HSQC (appendix 141) and HMBC (appendix 142) data. Compound **37** was determined as a known compound and identified as 4-O-*β*-D-glucopyranosyl-2,6,4'-trihydroxybenzophenone (**37**) (Rancon *et al*., 2001). Compound **37** formed a basis for the structure determination of the new compound **36**.

Compound **38** (figure 4.11) was isolated as a yellow powder with a molecular formula $C_{19}H_{20}O_8$ that was determined from its HRESIMS (appendix 143) at *m/z* 399.1051 $[M + Na]^+$ and at *m/z* 377.1231 $[M + H]^+$ (calcd for $C_{19}H_{21}O_8$, 377.1236). The ^{1}H (appendix 144) and ^{13}C NMR (appendix 145) spectra (table 4.9) indicated signals attributable to benzoyl moiety, β-glucopyranosyl moiety, and catechol moiety (Bourjot *et al*., 2012). The ^{1}H NMR data at δ_H 4.77 (H-1', d, J = 7.3 Hz), 3.49 (H-2', m), 3.50 (H-3', m), 3.45 (H-4', m), 3.76 (H-5', ddd, J = 9.7 Hz, 7.6 Hz, 2.2 Hz), and 4.42 (H-6', dd, J = 11.7 Hz, 7.6 Hz);, 4.74 (H-6', dd, J = 11.7 Hz, 2.2 Hz); and from the ^{13}C NMR at δ_C 102.2 (C-1'), δ_C 73.6 (C-2'), δ_C 76.6 (C-3'), δ_C 70.7 (C-4'), δ_C 74.0 (C-5') and δ_C 64.0 (C-6') were attributed to the presence of the β-glucopyranosyl moiety. The complete ^{1}H and ^{13}C NMR signal assignments and connectivity were determined from a combination of ^{1}H-^{1}H COSY (appendix 146), HSQC (appendix 147) and HMBC (appendix 148) data. HMBC correlations from δ_H 4.42, 4.74 (H-6') to the ester carbonyl carbon [δ_C 166.4 (C-7)], indicated the β-glucopyranosyl moiety was attached to the benzoyl moiety through the primary alcohol. Furthermore, the HMBC correlations from δ_H 4.77 (H-1') to δ_C 118.1 (C-2) indicated that the catechol moiety was linked to the glucose through the anomeric carbon. Compound 38 was determined as flacourtoside A, a phenolic glycoside which has been previously reported in a medicinal plant *Flacourtia ramontchi* (Bourjot *et al*., 2012).

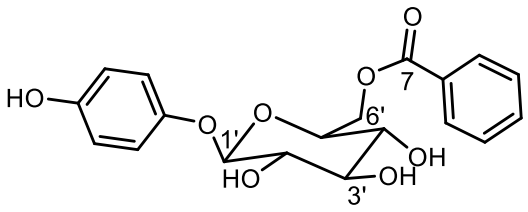

38

Figure 4.11: Chemical structure of compound **38**

Table 4.9: ^{1}H and ^{13}C NMR Data of Compounds **38** in CD_3OD

no.	^{13}C, Type	^{1}H, mult.(*J* in Hz)
1	115.1, CH	6.60, m
2	118.1, CH	6.95, m
3	152.5, C	
4	118.1, CH	6.95, m
5	115.1, CH	6.60, m
6	150.8, C	
2-Glc		
1'	102.2, CH	4.77, d (7.3)
2'	73.6, CH	3.49, m
3'	76.6, CH	3.50, m
4'	70.7, CH	3.45, m
5'	74.0, CH	3.76, ddd (9.7, 7.6, 2.2)
6'	64.0, CH_2	4.43, dd (11.7, 7.6)
		4.74, dd (11.7, 2.2)
6'-Bz		
1	129.9, C	
2	129.2, CH	8.06, m
3	128.2, CH	7.54, t (7.53)
4	133.0, CH	7.66, m
5	128.2, CH	7.54, t (7.53
6	129.2, CH	8.06, m
7	166.4, C	

Compound **39** (figure 4.12) was isolated as a yellow powder with a molecular formula $C_{20}H_{18}O_{11}$ that was determined from its HRESIMS (appendix 149) at *m/z* 435.0918 $[M + H]^+$ (calcd for $C_{28}H_{19}O_{11}$, 435.0927). The NMR data assignment was done by analysis of 1D and 2D NMR spectra (table 4.10) and by comparison with analogues flavonoids reported in literature (Gomes *et al.*, 2019). The ^{1}H NMR (appendix 150) and ^{13}C NMR (appendix 151) spectrum displayed signals at δ_H 5.18 (H-1"), δ_H 3.92 (H-2"), δ_H 3.66 (H-3"), δ_H 3.83 (H-4"), δ_H 3.46, 3.83 (H-5") and δ_C 103.2 (C-1"), δ_C 71.5 (C-2"), δ_C 72.7 (C-3"), δ_C 67.7 (C-4"), δ_C 63.5 (C-5")] which

established the presence of the xylose ring. The quercetin moiety was deduced by the presence of methine signals at δ_H 6.41 (H-6), δ_H 6.22 (H-8), δ_H 7.60 (H-2'), δ_H 6.89 (H-3') in ^{1}H NMR spectrum. ^{13}C NMR spectrum confirmed the presence of methine carbon atoms at δ_C 93.4 (C-6), δ_C 98.6 (C-8), δ_C 121.5 (C-2'), δ_C 114.8 (C-3') and quartenary carbons at δ_C 157.2 (C-2), δ_C 134.2 (C-3), δ_C 178.0 (C-4), δ_C 157.1 (C-5), δ_C 165.0 (C-7), δ_C 161.6 (C-9), δ_C 104.1 (C-10), δ_C 148.6 (C-4') and δ_C 144.6 (C-5'). The complete ^{1}H NMR and ^{13}C NMR signal assignments and connectivity were determined from a combination of ^{1}H-^{1}H COSY (appendix 152), HSQC (appendix 153) and HMBC (appendix 154) data. Further, ^{1}H-^{1}H COSY correlations of H-2′ with H-3′ and those H-1″ with H-2″ were important in establishing the connectivities in compound **39**. The HMBC correlation from δ_H 5.18 (H-1") to δ_C 134.2 (C-3) determined the connectivity between the xylose ring and the quercetin moiety. Compound **39** was determined as quercetin-3-O-xyloside.

Table 4.10: ^{1}H and ^{13}C NMR Data of Compounds **39** and **40** in CD3OD

	39[b]		**40**[b]	
no.	^{13}C, Type	^{1}H, mult.(*J* in Hz)	^{13}C, Type	^{1}H, mult.(*J* in Hz)
2	157.2, C		157.6, C	
3	134.2, C		134.2, C	
4	178.0, C		178.1, C	
5	157.1, C		157.1, C	
6	93.4, CH	6.41	93.3, CH	6.42
7	165.0, C		164.6, C	
8	98.6, CH	6.22	98.5, CH	6.22
9	161.6, C		161.6, C	
10	104.1, C		104.0, C	
1'	121.6, C		121.5, C	
2'	121.5, CH	7.60	121.8, CH	7.61
3'	114.8, CH	6.89	114.6, CH	6.89
4'	148.6, C		148.4, C	
5'	144.6, C		145.5, C	
6'	116.0, CH	7.76	116.1, CH	7.73
1"	103.2, CH	5.18	102.9, CH	5.30
2"	71.5, CH	3.92	74.4, CH	3.50
3"	72.7, CH	3.66	77.0, CH	3.24

4"	67.7, CH	3.83	76.7, CH	3.45
5"	63.5, CH_2	3.46	69.8, CH	3.37
		3.83		
6"			61.1, CH_2	3.59
				3.73

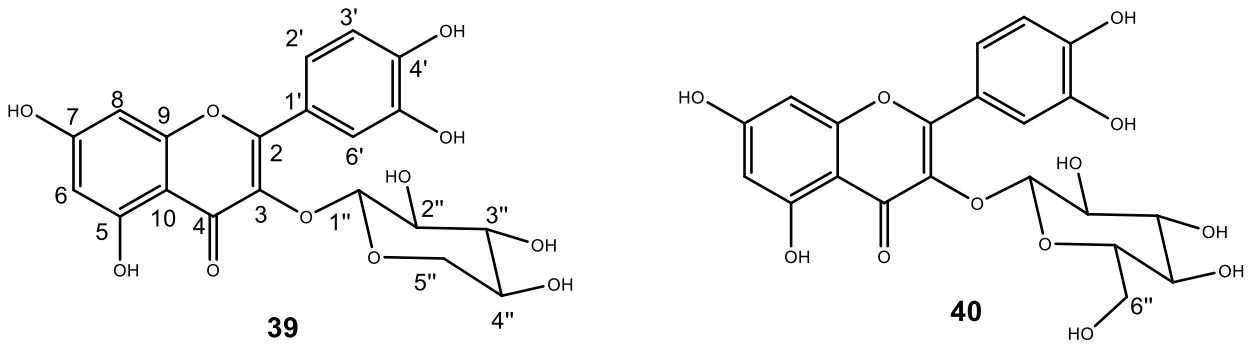

Figure 4.12: Chemical structures of compounds **39** and **40**

Compound **40** (figure 4.12) was isolated as a yellow powder with a molecular formula $C_{21}H_{20}O_{12}$ that was determined from its HRESIMS (appendix 155) at *m/z* 465.1027 $[M + H]^+$ (calcd for $C_{21}H_{21}O_{12}$, 465.0927). Compound **40** was similar to **39** except for the glucose ring in **40** in place of the xylose ring. The NMR data assignment was done by analysis of 1D and 2D NMR spectra (table 4.10) and by comparison with analogues flavonoids reported in literature (Dong *et al*., 2019; Gomes *et al*., 2019). The ^{1}H NMR (appendix 156) and ^{13}C NMR (appendix 157) spectrum displayed signals at [δ_H 5.30 (H-1"), δ_H 3.50 (H-2"), δ_H 3.24 (H-3"), δ_H 3.45 (H-4"), δ_H 3.37 (H-5"), δ_H 3.59, 3.73 (H-6")] and [δ_C 102.9 (C-1"), δ_C 74.4 (C-2"), δ_C 77.0 (C-3"), δ_C 76.7 (C-4"), δ_C 69.8 (C-5"), δ_C 61.1 (C-6")] which established the presence of the glucose ring. The quercetin moiety was deduced by the presence of methine signals at δ_H 6.42 (H-6), δ_H 6.22 (H-8), δ_H 7.61 (H-2'), δ_H 6.89 (H-3') in ^{1}H NMR spectrum. ^{13}C NMR spectrum confirmed the presence of methine carbon atoms at δ_C 93.3 (C-6), δ_C 98.5 (C-8), δ_C 121.8 (C-2'), δ_C 114.6 (C-3') and quartenary carbons at δ_C 157.6 (C-2), δ_C 134.2 (C-3), δ_C 178.1 (C-4), δ_C 157.1 (C-5), δ_C 164.6 (C-7), δ_C 161.6 (C-9), δ_C 104.0 (C-10), δ_C 148.4 (C-4') and δ_C 145.5 (C-5'). The complete ^{1}H NMR and ^{13}C NMR signal assignments and connectivity were determined from a combination of ^{1}H-^{1}H COSY (appendix 158), HSQC (appendix 159) and HMBC (appendix 160) data. Further, ^{1}H-^{1}H COSY correlations of H-2′ with H-3′ and those H-2″ with H-1″ and H-3″ were important in

establishing the connectivities in compound **40**. The HMBC correlation from δ_H 5.30 (H-1") to δ_C 134.2 (C-3) determined the connectivity between the glucose ring and the quercetin moiety. Compound **40** was determined as quercetin-3-O-*β*-D-glucoside **40** (Dong *et al*., 2019).

4.5 Isolation of fungal endophytes

Six endophytic fungal isolates were successfully obtained from surface sterilized fresh leaves and stem bark of *B. abyssinica* subsp. of *abyssinica* and subsp. *paulliniodes*. Pure cultures of fungal endophytes were obtained from subsequent sub-culturing of the isolated strains (figure 4.13).

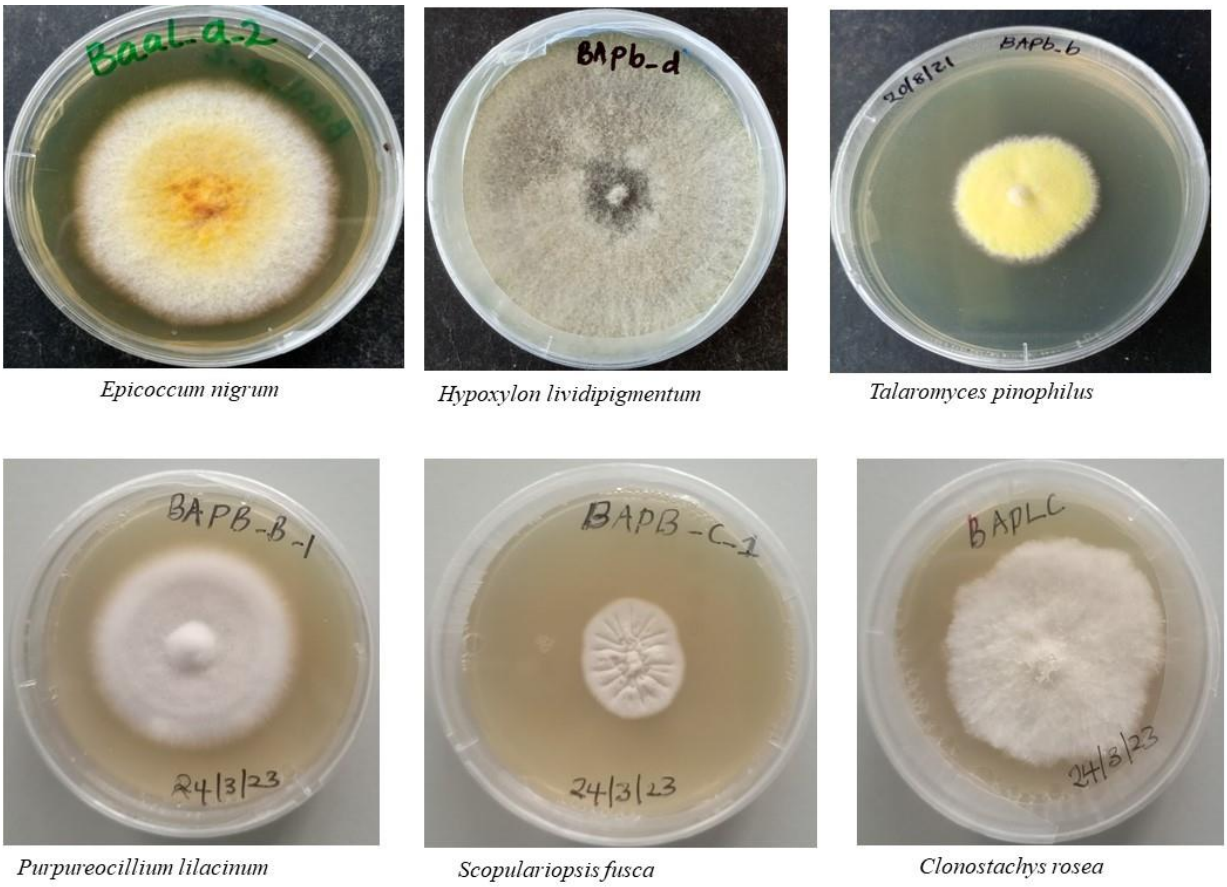

Figure 4.13: Photos of the isolated endophytic fungi

4.6 DNA Extraction and polymerase chain reaction (PCR)

Fungal endophyte DNA extraction was successful and the consensus sequences obtained from the amplification of the internal transcribed spacer (ITS) sequences. The size of the DNA

band obtained from PCR amplification and subsequent agarose gel electrophoresis was 560 base pairs.

4.7 DNA Sequencing

Data from molecular analyses were used to characterize taxonomically the endophytic fungi isolated from the plant tissues of *B. abyssinica* subsp. *abyssinica* and subsp. *paullioniodes*. The ITS1-5.8S-ITS2 consensus sequences (Appendix 161) of the isolates were compared to sequences that are already deposited in the national center for biotechnology information (NCBI) database GenBank. The results generated from ITS sequencing analyses identified six endophytic fungi to the species level. The basic local alignment search tool (BLAST) searches from the NCBI database revealed that the isolated fungal endophytes are *Purpureocillium lilacinum*, *Clonostachys rosea*, *Scopulariopsis fusca*, *Hypoxylon lividipigmentum*, *Talaromyces pinophilus* and *Epicoccum nigrum*. The BLAST searches indicated high sequences similarities (table 12). The endophytic fungi isolates belonged to a diverse group of fungi distributed within the phylum Ascomycota.

Table 4.11: Percentage sequence similarity of representative fungal endophytes from NCBI database

Isolate	Closely related species	Query coverage	Sequence similarity	Accession number
BAPB_2	*Purpureocillium lilacinum*	100%	99.8%	NR165946.1
BAPLC	*Clonostachys rosea*	100%	99.59%	MH864650.1
BAPLC_1	*Scopulariopsis fusca*	100%	99.32%	NR145258.1
BAPB_D	*Hypoxylon lividipigmentum*	100%	93.70%	MG686611.1
BAPB_B	*Talaromyces pinophilus*	99%	100.00%	MF683084.1
BAAL_A2	*Epicoccum nigrum*	100%	99.40%	KX778640.1

4.8 Secondary metabolites and pharmacological activity of the isolated fungi

The isolated endophytic fungi namely; *P. lilacinum*, *C. rosea*, *S. fusca*, *H. lividipigmentum*, *T. pinophilus* and *E. nigrum* have been reported previously to contain a wide range of secondary

metabolites with various pharmacological activities. A study by Henrique *et al*. (2023) evaluated *P. lilacinum* fungus as a biocontrol agent for nematode control. The fungus was found to be a potential control agent for nematodes. The fungus also produces secondary metabolites with bioactivities against pathogenic bacteria and fungi (Wei & Hu, 2022). *C. rosea* is in the genus *Clonostachys*, which is abundant in many classes of secondary metabolites, including alkaloids, polyketides, and terpenoids. Many of these secondary metabolites exhibit biological activities, such as antimicrobial, insecticidal, nematocidal, antiparasitic, phytotoxic and cytotoxic activities (Han *et al*., 2020). The biological activity of secondary metabolites from *H. lividipigmentum* were investigated by Weerasinghe *et al*. (2021). The compounds are reported to show antioxidant, antibacterial, anti-inflammatory, and tyrosinase inhibitory activities. The genus *Hypoxylon* is reported to posses various classes of compounds, mainly sesquiterpenoids with antimicrobial and cytotoxic activities (Basnet *et al*., 2019). Many kinds of compounds are reported in *Talaromyces* sp. including polyketides, steroids, esters, terpenes, alkaloids and anthraquinones, some of which have shown bacteriostatic, antitumor and anti-inflammatory activities (Han *et al*., 2020; Vinale *et al*., 2017). Further, compounds isolated from *Talaromyces* sp. have been reported to exhibit lipid-lowering properties, antitumor and antifungal properties (Rashmi *et al*., 2019). *E. nigrum* is reported to be rich in alkaloids, sesquiterpenes, quinones, peptides, lactones, esters, diterpenes, cytochalasins, and polyketides (Amrani *et al*., 2014; de Fávaro *et al*., 2012; Lee *et al*., 2020; Zhang *et al*., 2007). In the present study *E. nigrum* was subjected to solid state fermentation on rice media leading to the isolation of six polyketides. These polyketides were found to have antibacterial activities, antidermatophytic activities, and cytotoxic activities.

4.9 Secondary metabolites isolated from endophytic fungi *Epicoccum nigrum*

The ethylacetate extract of *E. nigrum* fungus culture on rice media was subjected to successive column chromatography over silica gel and Sephadex LH-20, followed by preparative HPLC to afford six compounds **41** – **46**. Compound **41** is a new compound while **42 - 46** have been previously described. Compound **41** (figure 4.14) was isolated as a yellow amorphous powder with a molecular formula $C_{17}H_{16}O_7$ that was determined from its HRESIMS (appendix 163) at *m/z* 333.0970 $[M + H]^+$ (calcd for $C_{17}H_{17}O_7$, 303.0974). IR spectral cm^{-1}: 3386, 2360, 1719, 1680 (appendix 164). Table 4.12 shows the NMR data of compound **41**. The ^1H NMR spectrum (appendix 165) displayed five signals assignable to two methyl groups at δ_H 1.64 (H_3-16, s) and δ_H 2.21 (H_3-17, s), three methylene groups at δ_H 4.63, 4.83 (H_2-2), δ_H 2.73, 3.62 (H_2-13) and δ_H

3.95, 4.96 (H_2-15). A total of 17 carbons were observed on the ^{13}C NMR spectrum (appendix 166), including two carbonyl groups at δ_c 204.5 (C-5), δ_c 195.9 (C-18); two methyl groups at δ_c 7.4 (C-16) and δ_c 10.4 (C-17); three methylene groups at δ_c 28.1 (C-13), δ_c 72.6 (C-15), and δ_c 63.5 (C-2). Further, twelve quartenary carbons at δ_c 179.3 (C-3), δ_c 130.4 (C-4), δ_c 204.5 (C-5), δ_c 84.3 (C-6), δ_c 123.7 (C-7), δ_c 142.6 (C-8), δ_c 117.5 (C-9), δ_c 139.6 (C-10), δ_c 140.0 (C-11), δ_c 118.4 (C-12), δ_c 52.8 (C-14), and δ_c 195.5 (C-18) were observed.

The complete ^1H and ^{13}C NMR signal assignments and connectivity were determined from a combination of ^1H-^1H COSY (appendix 167), HSQC (appendix 168) and HMBC (appendix 169) data. The HMBC correlations (figure 4.15) from δ_H 4.63, 4.83 (H_2-2) to δ_c 179.3 (C-3), δ_c 130.4 (C-4), δ_c 52.8 (C-14) and δ_c 72.6 (C-15); from δ_H 2.73, 3.62 (H_2-13) to δ_c 179.3 (C-3), δ_c 84.3 (C-6), δ_c 123.7 (C-7), δ_c 140.0 (C-11), δ_c 118.4 (C-12), δ_c 52.8 (C-14) and δ_c 72.6 (C-15); and from δ_H 3.95, 4.96 (H_2-15) to δ_c 63.5 (C-2), δ_c 179.3 (C-3), δ_c 84.3 (C-6), δ_c 52.8 (C-14) and δ_c 72.6 (C-15) were important correlations in the establishment of connectivities in rings B, C and D. Of these, signals at δ_C 179.3 (C-3), δ_C 130.4 (C-4), and δ_C 204.5 (C-5) were due to the presence of α-β unsaturated carbonyl group in ring-C. Further, the HMBC correlations from the methyl protons δ_H 2.21 (H_3-17) to δ_c 123.7 (C-7), δ_c 142.6 (C-8), δ_c 117.5 (C-9) provided the linkage in ring A. The hydroxyl groups were assigned to carbon atoms according to their chemical shifts. Compound **41** was determined as 5a,8,9-trihydroxy-4,6-dimethyl-5-oxo-3,5,5a,10-tetrahydro-1H-benzo[4,5]pentaleno[1,6a-c]furan-7-carboxylic acid.

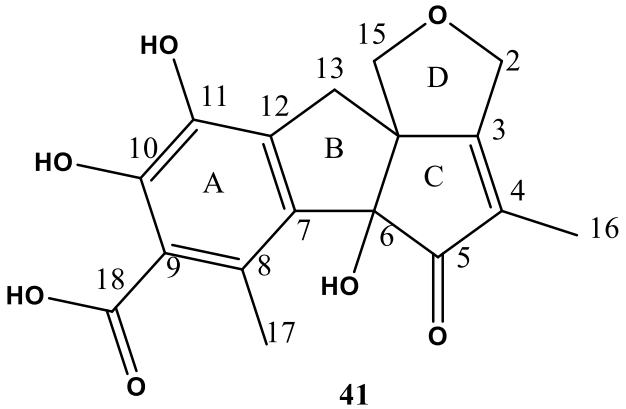

41

Figure 4.14: Chemical structure of compound **41**

Table 4.12: ^{1}H NMR (600 MHz) and ^{13}C NMR (175 MHz) Spectroscopic Data of Compound **41**

no.	^{13}C, Type	^{1}H, mult.(*J* in Hz)	HMBC
2	63.5, CH_2	4.63, d	3, 4, 14, 15
		4.83,	
3	179.3, C		
4	130.4, C		
5	204.5, C		
6	84.3, C		
7	123.7, C		
8	142.6, C		
9	117.5, C		
10	139.6, C		
11	140.0, C		
12	118.4, C		
13	28.1, CH_2	2.73	3, 6, 7, 11, 12, 14, 15
		3.62	
14	52.8, C		
15	72.6, CH_2	3.95	2, 3, 6, 13, 14
		4.96	
16	7.4, CH_3	1.64, s	3, 4, 5
17	10.4, CH_3	2.21, s	7, 8, 9
18	195.9, C		

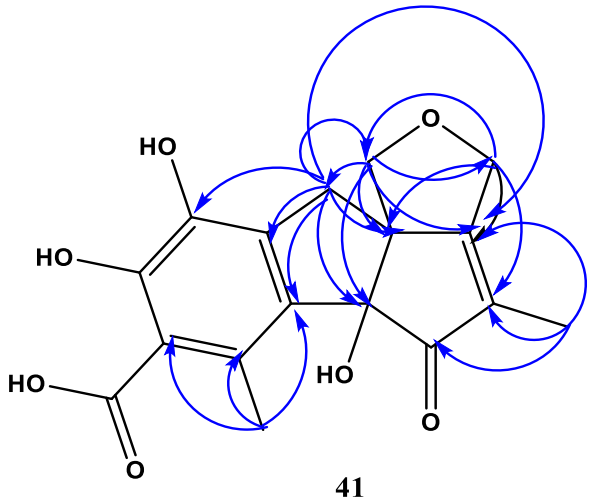

41

HMBC correlations

Figure 4.15: Chemical structure of compound **41** showing HMBC correlations

Compound **42** (figure 4.16) was isolated as a colourless compound. The molecular formula, $C_9H_8O_5$ was deduced using HRESIMS (appendix 170) at *m/z* 197.0446 $[M+H]^+$, (calcd for $C_9H_9O_5$, 197.0444). Table 4.13 shows the ^1H and ^{13}C NMR spectroscopic data. The ^1H NMR spectra (appendix 171) exhibited two singlet signals assigned to one methyl at δ_H 2.43 (H_3-8, s) and one methine at δ_H 5.13 (H_2-3, s). A total of nine carbon atoms were observed in the ^{13}C NMR (appendix 172) spectrum including seven quaternary carbons at δ_c 173.2 (C-1), δ_c 126.5 (C-4a), δ_c 136.6 (C-4), δ_c 140.1 (C-5), δ_c 144.9 (C-6), δ_c 116.9 (C-7) and δ_c 112.6 (C-7a), an oxygenated sp3 hybridized methine carbon at δ_c 66.6 (C-3) and a methyl carbon at δ_c 8.3 (C-8). The complete ^1H and ^{13}C NMR signal assignments and connectivity were determined from a combination of ^1H - ^1H COSY (appendix 173) HSQC (appendix 174) and HMBC (appendix 175) data. The HMBC correlations (figure 4.17) from δ_H 2.43 (H_3-8) to δ_c 149.9 (C-6), δ_c 116.9 (C-7) and δ_c 112.6 (C-7a) led to the establishment of the connectivities in the aromatic ring. Furthermore, HMBC correlations from δ_H 5.13 (H_2-3) to 173.2 (C-1) was important in the determining the position of the carbonyl group in compound **42**. The structure of compound **42** was established by assigning the hydroxyl groups to δ_c 136.6 (C-4), δ_c 140.1 (C-5) and δ_c 144.9 (C-6) according to their chemical shifts. The compound **42** was determined as 4,5,6-trihydroxy-7-methylphthalate with a trivial name, epicoccone. Epicoccone has been previously reported from algicolous marine fungus (Abdel-Lateff *et al*., 2003).

Table 4.13: ^{1}H NMR (700 MHz) and ^{13}C NMR (175 MHz) Spectroscopic Data of Compound **42**

	42			Lit	
no.	^{13}C, Type	^{1}H, mult.(*J* in Hz)	HMBC	^{13}C, Type	^{1}H, mult.(*J* in Hz)
1	173.2, C			174.6, C	
3	66.6, CH_2	5.13	1, 4a, 4, 5,7a	68.0, CH_2	5.16
4	136.6,C			138.1, C	
4a	126.5,C			127.9, C	
5	140.1, C			141.5, C	
6	144.9, C			146.3, C	
7	116.9, C			118.3, C	
7a	112.6, C			113.9, C	
8	8.3, CH_3	2.43, s	6, 7, 7a	9.7, CH_3	2.45, s

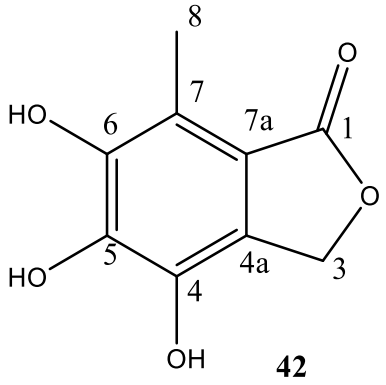

42

Figure 4.16: Chemical structure of compound **42**

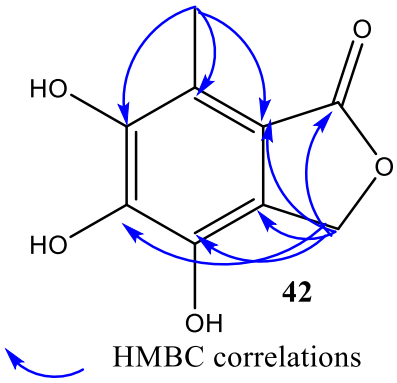

42

Figure 4.17: Chemical structure of compound **42** showing HMBC correlations

Compound **43** (figure 4.18) was isolated as a brown powder. Its molecular formula, $C_{18}H_{14}O_8$ was established from HRESIMS (appendix 176) at *m/z* 359.0762 $[M+H]^+$, (calcd for $C_{18}H_{15}O_8$, 359.0767). The ^1H NMR spectrum (appendix 177) displayed five singlets at δ_H 7.45 (H-3), δ_H 10.45 (H-9), δ_H 9.53 (H_3-15), δ_H 2.11 (H_3-16) and δ_H 2.67 (H-17), which were attributed to two methyl groups, two aldehyde groups and one methine group (table 4.14). Analysis of ^{13}C NMR spectrum (appendix 178) confirmed the presence of two methyl carbons; δ_c 9.53 (C-16) and δ_c 11.4 (C-17), two carbonyl carbons; δ_c 190.4 (C-8) and δ_c 195.0 (C-15), sp^2 hybridized methine carbon; δ_c 109.3 (C-3), and 13 sp^2 hybridized quaternary carbon atoms; δ_c 152.4 (C-2), δ_c 123.3 (C-3a), δ_c 117.3 (C-4), δ_c 127.7 (C-5), δ_c 141.0 (C-6), δ_c 137.1 (C-7), δ_c 142.5 (C-7a), δ_c 125.5 (C-9), δ_c 113.0 (C-10), δ_c 150.0 (C-11), δ_c 132.6 (C-12), δ_c 151.2 (C-13) and δ_c 119.0 (C-14). The NMR data assignment was done by comparison with reported polyketides (Amrani *et al*., 2014; Talontsi *et al*., 2013b) and analysis of ^1H-^1H COSY (appendix 179), HSQC (appendix 180) and HMBC (appendix 181) data.

The HMBC correlations (figure 4.19) from δ_H 2.67 (H_3-17) to δ_c 117.3 (C-4), δ_c 127.7 (C-5) and δ_c 141.0 (C-6) assisted in determining connectivity in ring A. Further, the HMBC correlations from δ_H 7.45 (H-3) to δ_c 123.3 (C-3a), δ_c 142.5 (C-7a), δ_c 152.4 (C-2), and from δ_H 10.45 (H-8) to δ_c 123.3 (C-3a), δ_c 117.3 (C-4), δ_c 127.7 (C-5) and δ_c 141.0 (C-6) led to the establishment of 6,7-dihydroxy-5-methylbenzofuran-4-carbaldehyde subunit. The link between ring B to ring C was determined by HMBC correlation from δ_H 7.45 (H-3) to δ_c 125.5 (C-9). Furthermore, the correlations from the aldehyde proton; δ_H 9.53 (H-15) to δ_c 125.5 (C-9), δ_c 113.0 (C-10), δ_c 150.0 (C-11) and δ_c 132.6 (C-12) and from the methyl protons; δ_H 2.11 (H_3-16) to δ_c 125.5 (C-9), δ_c 151.2 (C-13) and δ_c 119.0 (C-14) provided the linkage in ring C. The structure of compound **43** was determined to be epicoccolide B, a polyketide which has been previously reported from an endophytic fungus *Epicoccum* sp. associated with *Theobroma cacao* (Talontsi *et al*., 2013a) and *Mentha suaveolens* (Amrani *et al*., 2014).

Table 4.14: ^{1}H NMR (700 MHz) and ^{13}C NMR (175 MHz) Spectroscopic Data of Compound **43**

	43			Lit*	
no.	$\delta_{C,}$ Type	$\delta_{H,}$ mult.	HMBC	$\delta_{C,}$ Type	$\delta_{H,}$ mult.
2	152.4, C			151.6, C	
3	109.3, CH	7.45, s	2, 3a, 7a, 9	108.9, CH	7.46, s
3a	123.3, C			122.9, C	
4	117.3, C			117.1, C	
5	127.7, C			127.5, C	
6	141.0, C			141.0, C	
7	137.1, C			136.7, C	
7a	142.5, C			142.4, C	
8	190.4, CH	10.45, s	3a, 4, 5, 7a	190.1, CH	10.41, s
9	125.5, C			124.9, C	
10	113.0, C			112.6, C	
11	150.0, C			150.2, C	
12	132.6, C			132.7, C	
13	151.2, C			151.5, C	
14	119.0, C			118.7, C	
15	195.0, CH	9.53, s	9, 10, 11, 12	194.7, CH	9.48, s
16	11.4, CH_3	2.11, s	9, 13, 14	12.6, CH_3	2.01, s
17	9.7, CH_3	2.67, s	4, 5, 6	11.0, CH_3	2.58, s

*Amrani *et al*.,2014

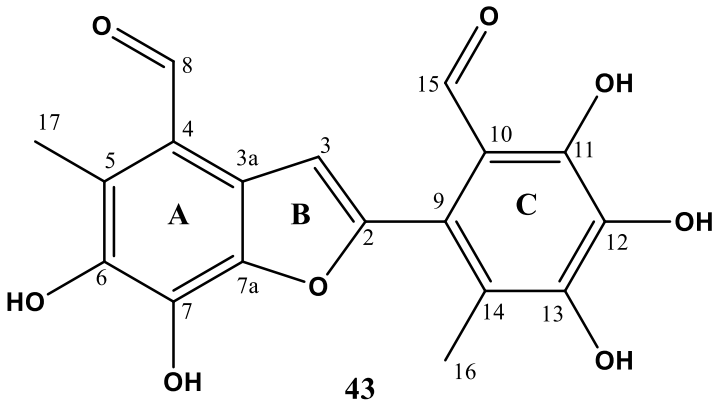

Figure 4.18: Chemical structure of compound **43**

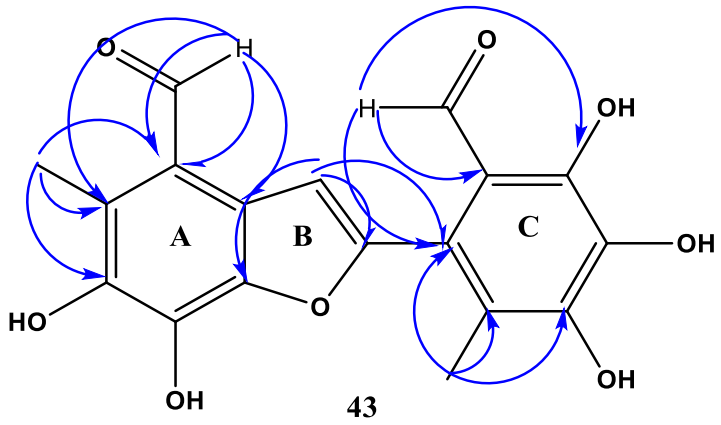

Figure 4.19: Chemical structure of compound **43** showing HMBC correlations

Compound **44** (figure 4.20) was isolated as a brown solid. Its molecular formula, $C_{18}H_{14}O_9$ was deduced by HRESIMS (appendix 182) at *m/z* 375.0712 $[M+H]^+$, (calcd for $C_{18}H_{15}O_9$, 375.0716) implying 12 degrees of unsaturation. The ^{1}H NMR spectrum (appendix 183) exhibited five singlet signals assignable to two methyls, δ_H 2.43 (H_3-17, s) and δ_H 2.33 (H_3-19, s), two oxymethine protons δ_H 6.71 (H-2, s) and δ_H 6.21 (H-10, s) and an aldehydic proton δ_H 10.43 (H-18, s). The ^{13}C NMR spectrum (appendix 184) showed a total of 18 carbon signals (table 4.15). These include two carbonyls at δ_c 197.4 (C-9) and δ_c 191.5 (C-18), two oxygenated sp^3-hybridized carbons at δ_c 90.8 (C-2) and δ_c 69.7 (C-10) and 12 sp^2 hybridized carbon atoms at δ_c 126.9 (C-3), δ_c 115.1 (C-4), δ_c 152.5 (C-5), δ_c 132.3 (C-6), δ_c 148.7 (C-7), δ_c 104.3 (C-8), δ_c 113.1 (C-11), δ_c 121.8 (C-12), δ_c 122.7 (C-13), δ_c 144.0 (C-14), δ_c 138.7 (C-15) and δ_c 135.8 (C-16). The complete ^{1}H and ^{13}C NMR signal assignments and connectivity were determined from a combination of ^{1}H-^{1}H COSY (appendix 185) HSQC (appendix 186) and HMBC (appendix 187) data.

The HMBC correlations (figure 4.21) from the methyl proton, δ_H 2.43 (H_3-17) to δ_c 121.8 (C-12), δ_c 122.7 (C-13) and δ_c 144.0 (C-14), from the aldehyde proton δ_H 10.43 (H-18) to δ_c 113.1 (C-11) and δ_c 122.7 (C-13) and from the oxymethine proton δ_H 6.21 (H-10) to δ_c 90.8 (C-2), δ_c 104.3 (C-8), δ_c 197.4 (C-9), δ_c 113.1 (C-11), δ_c 121.8 (C-12) and δ_c 122.7 (C-13) were some of the important correlations in determining the connectivity in ring A. The HMBC correlations from δ_H 6.71 (H-2) to δ_c 69.7 (C-10) and δ_c 135.8 (C-16), as well as, from δ_H 6.21 (H-10) to δ_c 90.8 (C-2) suggested the presence of two oxygen bridges between δ_c 90.8 (C-2) / δ_c 135.8 (C-16) and δ_c 90.8 (C-2) / δ_c 135.8 (C-16) in ring B. This could explain the downfield shift of signals at δ_H 6.71 (H-2) and δ_c 90.8 (C-2). The HMBC correlation from the oxymethine proton δ_H 6.21 (H-10) to δ_c 104.3 (C-8) and δ_c 197.4 (C-9) suggested the position of the carbonyl group at C-9. Compound **44**

was identified as a highly oxygenated polyketide epicocconigrone A, which has been isolated previously in a study carried out by Amrani *et al*., (2014). Table 16 shows the comparison of the 1D NMR of compound **44** in this study and that reported in literature previously. Epicocconigrone A was previously isolated from endophytic fungus, *Epicoccum sp.* obtained from the leaves of *Mentha suaveoleus*. In the present study, Epicocconigrone A was obtained from the endophytic fungus *E. nigrum* isolated from the leaf tissues of *B. abyssinica* subsp. abyssinica.

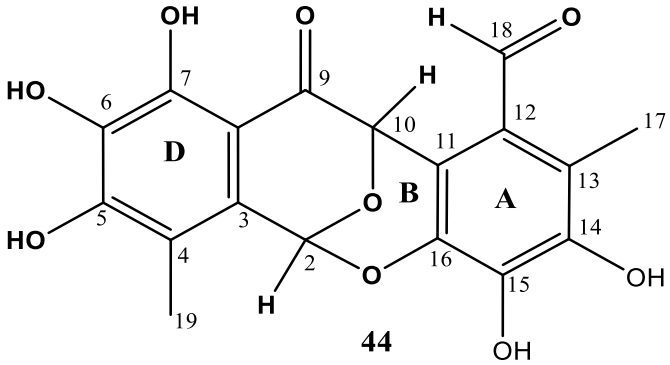

Figure 4.20: Chemical structure of compound **44**

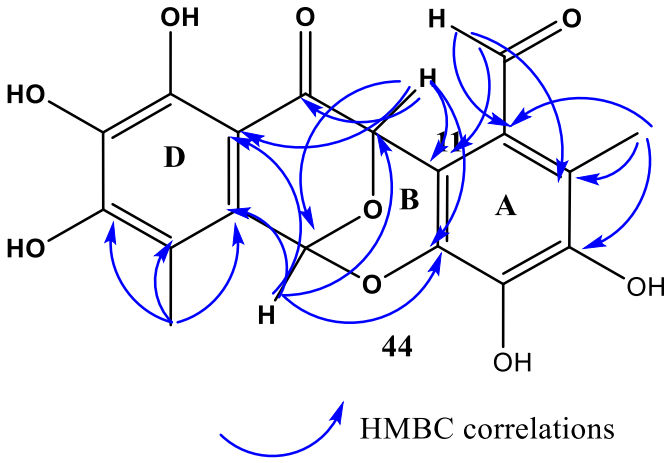

Figure 4.21: Chemical structure of compound **44** showing HMBC correlations

Table 4.15: ^{1}H NMR (600 MHz) and ^{13}C NMR (175 MHz) Spectroscopic Data of Compound **44**

		44[a]		Lit[b]	
no.	^{13}C, Type	^{1}H, mult.(*J* in Hz)	HMBC	^{13}C, Type	^{1}H, mult.(*J* in Hz)
2	90.8, CH	6.71, s	3, 8, 10, 16	90.0, CH	6.35, s
3	126.9, C			126.6, C	
4	115.1, C			115.4, C	
5	152.5, C			153.0, C	
6	132.3, C			132.5, C	
7	148.7, C			148.6, C	
8	104.3, C			104.0, C	
9	197.4, C			196.9, C	
10	69.7, CH	6.21, s		68.7, CH	6.80, s
11	113.1, C			112.9, C	
12	121.8, C			121.6, C	
13	122.7, C			121.6, C	
14	144.0, C			144.2, C	
15	138.7, C			138.4, C	
16	135.8, C			135.8, C	
17	10.5, CH_3	2.43, s	12, 13, 14	11.8, CH_3	2.31, s
18	191.5, CH	10.43, s	11, 12, 13, 14	191.2, CH	10.35, s
19	8.9, CH_3	2.33, s	3, 4, 5	10.1, CH_3	2.25, s

[a]Recorded in MeOD, [b]Recorded at (^{1}H: 600 MHz, ^{13}C: 75 MHz) in DMSO-d_6

Compound **45** (Figure 4.22), was isolated as a yellow amorphous powder. Its molecular formula, $C_{18}H_{16}O_9$ was established from HRESIMS (appendix 188) at *m/z* 377.0865 $[M+H]^+$, implying 11 degrees of unsaturation. Table 4.16 indicate the ^{1}H and ^{13}C NMR spectral data of compound **45**. The ^{1}H NMR spectrum (appendix 189) exhibited four signals assigned to two methyls at H_3-9 (δ_H 2.07, s) and H_3-9' (δ_H 2.05, s) and two methylenes at H_2-1 (δ_H 5.02, 5.15) and H_2-1' (δ_H 4.86, 5.14). ^{13}C NMR spectrum (appendix 190) exhibited a total of 18 carbon atoms which include one carbonyl carbon at δ_c 192.8 (C-8'), two oxygenated sp^3 hybridized methylene carbons at δ_c 72.8 (C-1) and δ_c 60.7 (C-1'); two sp^3 hybridized methyl carbons at δ_c 10.6 (C-9) and δ_c 8.5 (C-9'); and twelve sp^2 hybridized carbons at δ_c 131.6 (C-2), δ_c 108.3 (C-3), δ_c 146.4 (C-4), δ_c 132.8 (C-5), δ_c 139.4 (C-6), δ_c 115.2 (C-7), δ_c 131.7 (C-2'), δ_c 110.9 (C-3'), δ_c 152.7 (C-4'), δ_c

130.2 (C-5'), δ_c 150.2 (C-6') and δ_c 106.5 (C-7'). The structure of compound **45** (Figure 23) was proposed by analysis of ^{1}H and ^{13}C NMR signal assignments and connectivity were determined from a combination of ^{1}H-^{1}H COSY (appendix 191), HSQC (appendix 192) and HMBC (appendix 193) data. The HMBC correlations (figure 28) from δ_H 5.02, 5.15 (H_2-1) to δ_c 131.6 (C-2), δ_c 108.3 (C-3), δ_c 115.2 (C-7) and δ_c 108.1 (C-8) established the presence of 2,7-dihydroisobenzofuran subunit. Correlations from H-1' (δ_H 4.86, 5.14) to δ_c 108.1 (C-8), δ_c 131.7 (C-2'), δ_c 110.9 (C-3'), δ_c 106.5 (C-7') and δ_c 192.8 (C-8') led to the establishment of the other subunit of compound **45**.

The HMBC correlations from H-1 (δ_H 5.02, 5.15) to δ_c 108.1 (C-8), as well as, from H-1' (δ_H 5.02, 5.15) to δ_c 108.1 (C-8) suggested the presence of two oxygen bridges between δ_c 72.8 (C-1) / δ_c 108.1 (C-8) and δ_c 60.7 (C-1') / δ_c 108.1 (C-8) in ring B and ring C (figure 4.23). These correlations were also important in establishing the link between the two subunits. Further, HMBC correlations from H_3-9 (δ_H 2.07) to δ_c 131.6 (C-2), δ_c 108.3 (C-3) and δ_c 146.4 (C-4) determined the connectivity in ring A. The HMBC correlations from H_3-9' (δ_H 2.05) to δ_c 131.7 (C-2'), δ_c 110.9 (C-3') and δ_c 152.7 (C-4') determined the connectivity in ring D. The structure of compound **45** was established by assigning the hydroxyl groups to δ_c 146.4 (C-4), δ_c 132.8 (C-5), δ_c 139.4 (C-6), δ_c 152.7 (C-4') and δ_c 130.2 (C-5') according to the chemical shift (Amrani *et al*., 2014; Luan *et al*., 2014). Thus, compound **45** was established as Eleganketal A.

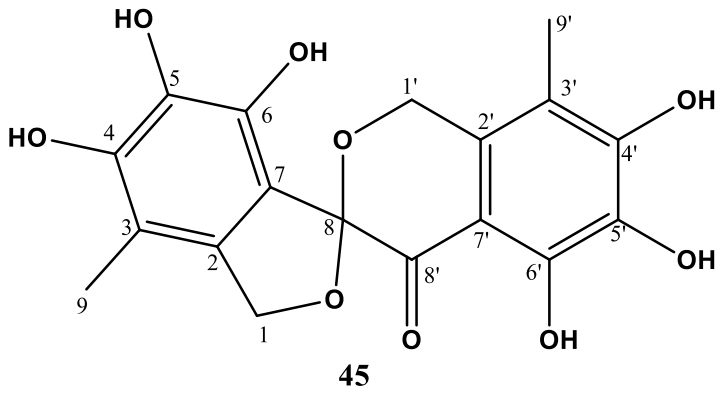

45

Figure 4.22: Chemical structure of compound **45**

Table 4.16: ^{1}H NMR (600 MHz) and ^{13}C NMR (175 MHz) Spectroscopic Data of Compound **45**

		45[a]	Lit [b*]	
no.	^{13}C, Type	^{1}H, mult.(*J* in Hz)	^{13}C, Type	^{1}H, mult.(*J* in Hz)
1	72.8, CH_2	5.02, d (11.8)	72.8, CH_2	5.05, d (12.0)
		5.15		4.93, d (12.0)
2	131.6, C		131.0, C	
3	108.3, C		107.6, C	
4	146.4, C		146.3, C	
5	132.8, C		132.6, C	
6	139.4, C		139.7, C	
7	115.2, C		115.2, C	
8	108.1, C		107.6, C	
9	10.6, CH_3	2.07, s	11.9, CH_3	1.98, s
1'	60.7, CH_2	5.14	60.4, CH_2	5.00, d (15.6)
		4.86		4.81, d (15.6)
2'	131.7, C		131.4, C	
3'	110.9, C		111.0, C	
4'	152.7, C		152.5, C	
5'	130.2, C		130.2, C	
6'	150.2, C		150.0, C	
7'	106.5, C		106.2, C	
8'	192.8, C		192.2, C	
9'	8.5, CH_3	2.05, s	9.7, CH3	1.95, s

[a]Recorded in MeOD, [b]Recorded at (^{1}H: 600 MHz, ^{13}C: 75 MHz) in DMSO-d_6
*Luan *et al*., 2014

Eleganketal A is a highly oxygenated dibenzospiroketal that has been previously reported from *Spicaria elegans* fungus (Luan *et al*., 2014; Talontsi *et al*., 2013a). Eleganketal A was previously isolated from marine-derived fungus *Spicaria elegans*. However, in the present study, Eleganketal A was obtained from endophytic fungus *E. nigrum* isolated from the leaves of *B. abyssinica* subsp. *abyssinica*.

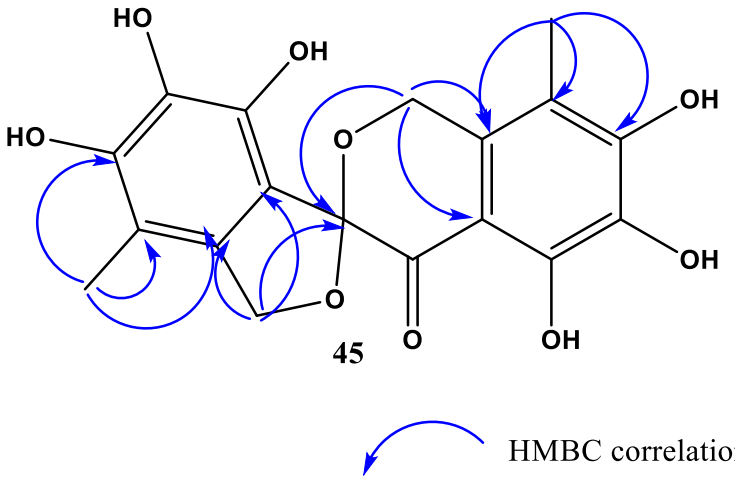

Figure 4.23: Chemical structure of compound **45** showing HMBC correlations

Compound **46** (figure 4.24) was isolated as a yellow powder. Its molecular formula $C_{19}H_{18}O_9$ that was determined from its HRESIMS (appendix 194) at *m/z* 413.0792 $[M + Na]^+$ (calcd for $C_{19}H_{18}O_9$, 406.0900). ^1H NMR spectra (appendix 195) showed two methyl signals at δ_H 2.14 (H_3-9) and δ_H 2.06 (H_3-9'), a methine signal at δ_H 6.16 (H-1, s) and methylene signal at δ_H 4.95, 5.19 (H-1', d, J = 15.4 Hz). A methoxy signal at δ_H 3.37 and δ_c 51.9 for ^1H NMR and ^{13}C NMR respectively were observed. A total of nineteen carbon atoms were observed in the ^{13}C NMR spectra (appendix 196) (table 4.17). The NMR spectral data of compound **46** had close similarity to that of compound **45,** eleganketal A indicating that the two compounds have the same dibenzospiroketal structure. The difference between compounds **45** and **46** is the appearance of an oxygenated methine at δ_c 106.9 (C-1) and a methoxy group at δ_c 51.9 in **46** instead of the oxygenated methylene at δ_c 72.8 (C-1) in **45**. The deshielded movement of the oxygenated methine carbon signal at δ_c 106.9 (C-1) in compound **46** is expected due to the presence of the methoxy group at C-1. The presence of a methoxy group was determined from its proton at δ_H 3.37 that showed HSQC correlation with the carbon at δ_C 51.9. The HMBC correlation from the methoxy protons δ_H 3.37 to δ_c 106.9 (C-1) further confirmed this deduction. On the other hand, the oxygenated methylene carbon δ_c 72.8 (C-1) in **45** is shielded due to the absence of a methoxy group.

The complete ^1H and ^{13}C NMR signal assignments and connectivity were determined from a combination of ^1H-^1H COSY (appendix 197) HSQC (appendix 198) and HMBC (appendix 199) data. Figure 4.25 shows the HMBC correlations that were observed in the HMBC spectra. Furthermore, comparison of the ^1H and ^{13}C NMR data of **46** with literature of that of reported

dibenzospiroketal indicated similar chemical shifts (table 4.17) with aspermicrone B. Thus, compound **46** was established as aspermicrone B, a highly oxygenated dibenzospiroketal that has been previously reported from *Aspergillus micronesiensis* endophytic fungus associated with seaweed (Luyen *et al*., 2019).

Table 4.17: ^{1}H NMR (600 MHz) and ^{13}C NMR (175 MHz) Spectroscopic Data of Compound **46**

		46[a]	Lit [b*]	
no.	^{13}C, Type	^{1}H, mult.(*J* in Hz)	^{13}C, Type	^{1}H, mult.(*J* in Hz)
1	106.9, CH	6.16, s	108.3, CH	6.16, s
2	128.6, C		130.0, C	
3	111.1, C		112.6, C	
4	146.4, C		147.8, C	
5	131.5, C		136.2, C	
6	138.7, C		140.1, C	
7	117.2, C		118.6, C	
8	105.5, C		106.9, C	
9	9.6, CH_3	2.14, s	10.9, CH_3	2.14, s
1'	60.1, CH_2	4.95, d (15.4)	62.4, CH_2	4.95, d (15.5)
		5.19, d (15.4)		5.18, d (15.5)
2'	131.5, C		132.9, C	
3'	110.0, C		112.5, C	
4'	152.2, C		153.7, C	
5'	134.7, C		131.6, C	
6'	149.9, C		151.3, C	
7'	134.8, C		107.9, C	
8'	192.7, C		194.1, C	
9'	8.5, CH_3	2.06, s	9.9, CH_3	2.06, s
1-OCH_3	51.9, CH_3	3.37, s	53.3, CH_3	3.37, s

[a]Recorded in MeOD, [b]Recorded at (^{1}H: 500 MHz, ^{13}C: 125 MHz) in MeOD
*Luyen *et al*., 2019

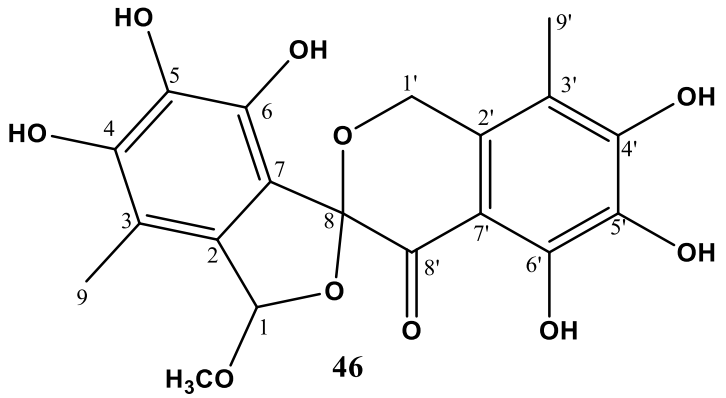

Figure 4.24: Chemical structure of compound **46**

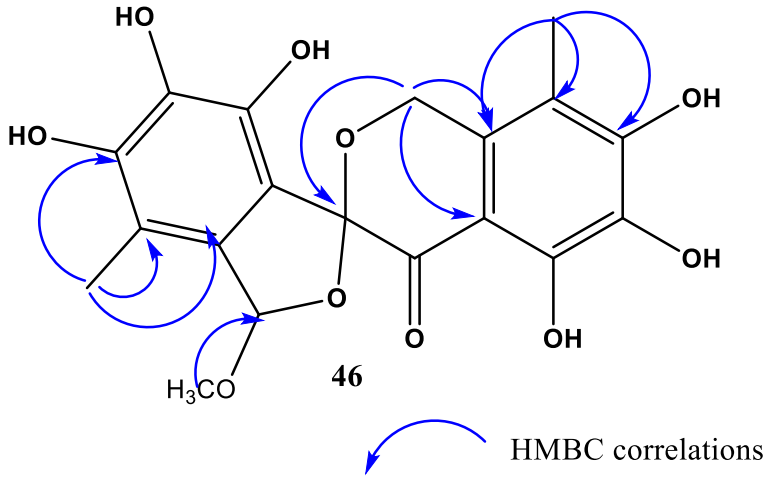

Figure 4.25: Chemical structure of compound **46** showing HMBC correlations

4.10 Biological activities

4.10.1 *In-vitro* Antibacterial assay

Compounds **17**, **18**, **20**-**23**, **24**, **25**, **28**, **33**-**38** and **43**-**45** were tested for antibacterial activity against *E. coli* DSM 1116, *M. smegmatis* DSM ATCC 700084, *S. aureus* DSM 346, and *B. subtilis* DSM 10 (table 4.18). 1,2,6-tri-*O*-galloyl-β-D-glucose (**23**) showed weak activity against *E. coli* with an MIC value of 33.3 µg/mL, which is about the same potency value as reported previously (MIC of 15.5 µg/mL against another *E. coli* strain) (Bag *et al*., 2013). Paulliniogenin A (**17**) and Paulliniogenin B (**18**) exhibited weak activities against *S. aureus* with MIC values of 66.6 µg/mL in each case. Mangiferin (**28**) showed MIC values of 66.7 µg/mL against both *B. subtilis* and *S. aureus*. In previous work, a quinone-like compound showed weak antibacterial activities against *B. subtilis* with MIC value of 66.7 µg/mL (Narmani *et al*., 2019). This MIC range is similar to that

exhibited by **28** in this study. Furthermore, **28** showed weak antibacterial activity against Gram-negative *S. aureus* (Biswas *et al*., 2015).

Epicoccolide B (**43**), exhibited activity against *E. coli* and *B. subtilis* with MIC values of 66.6 and 33.3 µg/mL respectively. Eleganketal A (**45**), exhibited activity with MIC values of 66.6 µg/mL against *E. coli* and *S. aureus*. Further, epicoccolide B (**43**), showed antibacterial activity against *B. subtilis* with an MIC value of 33.3 µg/mL. Compounds **43** and **45** were isolated from endophytic fungus *E. nigrum*. They are polyketides, highly oxygenated spiroketal compounds with reported antimicrobial activities (Fazle & Baek, 2020; Sadorn *et al*., 2016; Zhang *et al*., 2009). In previous studies, Epicoccolide B (**43)** is reported to show weak activity against *S. aureus*, which is in agreement with the findings in this study (Talontsi *et al*., 2013b; Xue *et al*., 2022). No activity was observed for any of all the compounds against *M. smegmatis*. Due to the limited material obtained in each case, compounds **19, 22, 26, 27, 29-32, 36** and **39-42** were not tested.

4.10.2 Cytotoxicity assay

Compounds **17**, **18**, **20-23**, **24**, **25**, **28**, **33**, **34**, **37-40** and **43-45** were tested for cytotoxic effects against the HeLa (KB3.1) and mouse L929 fibroblast cell lines (table 4.19). According to the national cancer institute (NCI) guidelines on cancer studies, a compound is considered cytotoxic if it exhibits an IC_{50} values of less than 10 µM. Paulliniogenin A (**17**) and 16ß-hydroxybersamagenin 1,3,5-orthoacetate (**20**) showed cytotoxicity against the KB3.1 cell line with IC_{50} values of 1.4 ± 0.77 and 1.6 ± 0.81 µM, respectively. Compound **20** has been reported previously to be cytotoxic against the KB3.1 cell line (Kupchan, *et al*., 1971). Compound **33** exhibited significant cytotoxicity against KB3.1 cell line with IC_{50} value of 3.9 ± 0.99 µM. Cytotoxic activity was also observed against KB3.1 cell line with IC_{50} value of 16.35 ± 2.45 µM for compound **38**. Bufadienolides have been reported to be potential anticarcinogenic agents (Supratman *et al*., 2001). Furthermore, other bufadienolides have been reported to be cytotoxic against various cancer cell lines (Bedane *et al*., 2020b).

Table 4.18: MIC values[a] (μg/mL) of the antibacterial assay

	Test organisms			
Compounds	*E.coli*	*S. aureus*	*M. smegmatis*	*B. subtilis*
17	n.i.	66.7	n.i.	n.t
18	n.i.	66.7	n.i.	n.t
20	n.i.	n.i.	n.i.	n.i.
21	n.i.	n.i.	n.i.	n.i.
23	n.i.	n.i.	n.i.	n.t
24	33.3	n.i.	n.i.	n.t
25	n.i.	n.i.	n.i.	n.t
28	n.i.	66.7	n.i	66.7
33	n.i.	n.i.	n.i.	n.t
34	n.i.	n.i.	n.i.	n.t
35	n.i.	n.i.	n.i.	n.t
37	n.i.	n.i.	n.i.	n.t
38	n.i.	n.i.	n.i.	n.t
43	66.7	n.i.	n.i	33.3
44	n.i.	n.i.	n.i.	n.i.
45	66.7	66.7	n.i	33.3
Control[b]	1.7, O	0.4, K	1.7, O	16.7, O

[a] n = 3 independent experiments, n.i = no inhibition, n.t = not tested

[b] Positive control; O Oxytetracyclin 1 μ/mL, K Kanamycin 1 μ/mL

Table 4.19: IC_{50} values[a] (μM) of the cytotoxicity assay

Compounds	Cell lines	
	KB3.1	L929
17	1.4 ± 0.77	n.i
18	14.73 ± 2.42	n.i
20	1.6 ± 0.81	n.i
21	n.i	n.i
23	18.78 ± 12.93	n.i
24	30.49 ± 4.31	35.82 ± 5.40
25	n.i	n.i
28	n.i	n.i
33	3.9 ± 0.99	n.i
34	n.i	n.i
37	n.i	n.i
38	16.35 ± 2.44	n.i
39	n.i	n.i
40	n.i	n.i
43	50.25 ± 7.93	28.63 ± 10.86
44	5.88 ± 1.89	18.45 ± 4.16
45	17.28 ± 0.0	11.7 ± 6.78
Epithilon B[b]	0.000056 ± 000 001	0.001081 ± 0.000 776

[a]Data are expressed as mean ± SD; n = 3 independent experiments, n.i = no inhibition
[b]Positive control.

4.10.3 Antidermatophytic assay

The isolated compounds and crude extracts were tested for antifungal assay against five skin disease causing pathogens namely: *Trichophyton mentagrophytes* CCF 6579, *Trichophyton rubrum* IDE 241/20, *Trichophyton rubrum resistant* LY 8, *Trichophyton benhamiae* var. *luteum* CCF 6474 and *Trichophyton tonsurans* CCIS 5356. The ethyl acetate extract of *E. nigrum* fungus (BAAL_A2), methanol extract of the stem bark of *B. abyssinica* subsp. *paulliniodes* (BEPA_B), the methanol extract of the leaf (BEAA_L), and stem bark (BEAB_B) of *B. abyssinica* subsp. *abyssinica* were tested for activity on these pathogens (table 4.20). All the tested extracts exhibited

activities against the dermatophytic pathogens with minimum inhibitory concentrations ranging from 37.5 μg/mL – 300 μg/mL. The methanol crude extracts of *B. abyssinica* are reported to exhibit antifungal activity against *T. mentagrophytes* (Amuka *et al*., 2015). These findings are in agreement with the results in this study. Further, the ethyl extract of the endophytic fungus, *E. nigrum* (BAAL_A2) was the most active against *T. rubrum* and *T. tonsurans* with MIC value of 37.5 μg/mL. Various studies conducted on *E. nigrum* have indicated strong activities against both pathogenic fungi and yeasts (de Fávaro *et al*., 2012; Lee *et al*., 2020; Zhang *et al*., 2007).

Table 4.20: MIC values[a] (μg/mL) of the antifungal assay of crude extracts

	Test organisms				
Extracts	*T. rubrum*	*T. mentagrophytes*	*T. tonsurans*	*T. benhamiae var. leteum*	*T. rubrum resistant*
BAAL_A2	37.5	150	37.5	150	300
BEPA_B	150	150	150	150	300
BEAB_B	150	150	75	150	300
BEAA_L	300	150	75	150	n.t
Control[b]	1.95	7.81	7.81	7.81	15.63

[a] n = 3 independent experiments, n.t not tested

[b] Positive control. Amphotericin B, 1 μ/mL

Compounds **26** – **32**, **39** and **43 - 45** were also tested for activities against *T. mentagrophytes* CCF 6579, *T. rubrum* IDE 241/20, *T. benhamiae* var. *luteum* CCF 6474 and *T. tonsurans* CCIS 5356 (table 4.21). The compounds exhibited activities with MIC values ranging between 18.75 μg/mL – 300 μg/mL. *T. mentagrophytes* and *T. tonsurans* were more susceptible to the tested compounds. Eleganketal A (**45**), was the most active against *T. tonsurans* with MIC value of 18.75 μg/mL. Furthermore, **45** exhibited activity towards *T. rubrum*, *T. mentagrophytes*, *T. benhamiae* var. *luteum* with MIC values of 37.5 μg/mL, 37.5 μg/mL and 75 μg/mL respectively. Eleganketal A derivatives have been evaluated previously and found to possess antimicrobial properties (Luyen *et al*., 2019). Quercetin-3-O-xyloside (**26**), mangferin (**28**) and apigenin-7,4'-diethylether (**30**) were the most active against *T. mentagrophytes* with an MIC value of 37.5 μg/mL for each case. Genistein (**29**) apigenin-7,4'-diethylether (**30)** formononetin (**31**) and daidzein (**32**) are isoflavone class of compounds. These compounds are previously reported to be

active against both plant and human fungal pathogens (Da Silva *et al*., 2019; Weidenbörner *et al*., 1990; Zhang *et al*., 2022).

Table 4.21: MIC values[a] (μg/mL) of the antifungal assay of compounds

	Test Organisms			
Compounds	*T. rubrum*	*T. mentagrophytes*	*T. tonsurans*	*T. benhamiae* var. *leteum*
26	150	37.5	37.5	n.i
27	n.i	n.i	150	150
28	75	37.5	75	75
29	150	150	75	150
30	150	37.5	75	n.i
31	n.i	n.i	n.i	n.i
32	150	150	150	n.i
39	n.i	75	150	150
43	150	75	75	75
44	150	75	75	300
45	37.5	37.5	18.75	75
Control[b]	1.95	7.81	7.81	7.81

[a] n = 3 independent experiments, n.i no inhibition.

[b] Positive control. Amphotericin B, 1 μ/mL

T. mentagrophytes was susceptible to quercetin-3-O-xyloside (**39**) with an MIC of 75 μg/mL. Further, compound **39** showed activity with an MIC of 150 μg/mL against both *T. tonsurans* and *T. benhamiae* var. *leteum*. Epicoccolide B (**43**) and epicocconigrone A (**44**) showed antifungal activity towards all the tested pathogens with MIC values in the range of 75 μg/mL - 300 μg/mL. All the antidermatophytic activities were compared to those of amphotericin B, an available antifungal drug which was used as a positive control. Dimethyl sulfoxide (DMSO) was used as the negative control.

CHAPTER FIVE

CONCLUSIONS AND RECOMMENDATIONS

5.1 Conclusions

i. Six strains of endophytic fungi *P. lilacinum, C. rosea, S. fusca, H. lividipigmentum, T. pinophilus* and *E. nigrum* were solated and identified by molecular characterization.

ii. Thirty (30) compounds were isolated in this study and structure determination was done using a combination of 1D and 2D nuclear magnetic resonance (NMR) spectroscopic techniques, high resolution electrospray ionization mass spectrometry (HRESIMS) and X-ray diffraction (XRD) analysis.

iii. Eight (8) new compounds namely; paulliniogenin A (**17**), paulliniogenin B (**18**), and 16*β*-formyloxybersamagenin 1,3,5-orthoacetate (**19**), 10*β*-formylpaulliniogenin B (**33**), 10*β*-formylpaulliniogenin A (**34**) and 1*β*-acetoxy-3*β*,5*β*-dihydroxy-15-methoxy-16,19-dioxobufa-14(15),20,22-trienolide (**35**), 2,6,4'-trihydroxybenzophenone-4-O-(6'''-cinnamoyl)-β-D-glucoside (**36**), 5a,8,9-trihydroxy-4,6-dimethyl-5-oxo-3,5,5a,10-tetrahydro-1H-benzo[4,5]pentaleno[1,6a-c]furan-7-carboxylic acid (**41**) were isolated.

iv. Paulliniogenin A (**17**) and 16*β*-hydroxybersamagenin 1,3,5-orthoacetate (**20**) and 1*β*-acetoxy-3*β*,5*β*-dihydroxy-15-methoxy-16,19-dioxobufa-14(15),20,22-trienolide (**35**), showed strong cytotoxic activities against KB3.1 cell lines and therefore form lead molecules for the development of anticancer drugs

v. 1,2,3,6-tetra-*O*-galloyl-β-D-glucose (**24)**, epicoccolide B (**43**) and eleganketal A (**45**) exhibited antibacterial activity against *E. coli* and *B. subtilis* with MIC value of 33.3 µg/mL hence are potential lead compounds for the development of drugs against the bacteria.

vi. *T. mentagrophytes* and *T. tonsurans* was more susceptible to the tested compounds. Moreover, eleganketal A (**45**) was more active against *T. tonsurans* with MIC value of 18.75 µg/mL hence a potential lead compound for the development of antifungal drugs.

5.2 Recommendations

i. Endophytic fungi from the plant tissues of *B. abyssinica* subsp. *abyssinica* and subsp. *paulliniodes* should be explored extensively.

ii. The isolated compounds should be tested for biological activities against other microorganisms.

iii. Specificity and selectivity of Paulliniogenin A (**17**) and 16*β*-hydroxybersamagenin 1,3,5-orthoacetate (**20**) and 1*β*-acetoxy-3*β*,5*β*-dihydroxy-15-methoxy-16,19-dioxobufa-14(15),20,22-trienolide (**35**) should be determined.

iv. Propagation of the medicinal plants *B. abyssinica* subsp. *abyssinica* and subsp. p*aulliniodes* should be carried out to ensure conservation of plants

REFERENCES

Abbott, B. J., Perdue, R. E., & Schepartz, S. A. (1967). Screening Data from the Cancer Chemotherapy National Service Centre Screening Laboratories. XL. Plant Extracts. *Cancer Research*, *27*(2), 190–345. https://doi.org/27/3_Part_2/190/476468

Abdel-Lateff, A., Fisch, K. M., Wright, A. D., & König, G. M. (2003). A New Antioxidant Isobenzofuranone Derivative from the Algicolous Marine Fungus *Epicoccum* sp. *Planta Medica*, *69*(9), 831–834. https://doi.org/10.1055/s-2003-43209

Abushaheen, M. A., Muzaheed, Fatani, A. J., Alosaimi, M., Mansy, W., George, M., Acharya, S., Rathod, S., Divakar, D. D., Jhugroo, C., Vellappally, S., Khan, A. A., Shaik, J., & Jhugroo, P. (2020). Antimicrobial resistance, mechanisms and its clinical significance. *Disease-a-Month*, *66*(6), 100971. https://doi.org/10.1016/j.disamonth.2020.100971

Acker, V. H., Dijck, V. P., & Coenye, T. (2014). Molecular mechanisms of antimicrobial tolerance and resistance in bacterial and fungal biofilms. *Trends in Microbiology*, *22*(6), 326–333. https://doi.org/10.1016/j.tim.2014.02.001

Adelusi, O. A., Gbashi, S., Adebiyi, J. A., Makhuvele, R., Adebo, O. A., Aasa, A. O., Targuma, S., Kah, G., & Njobeh, P. B. (2022). Variability in metabolites produced by *Talaromyces pinophilus* SPJ22 cultured on different substrates. *Fungal Biology and Biotechnology*, *9*(1), 1–9. https://doi.org/10.1186/s40694-022-00145-8

Ahmad, M., & Khan, A. U. (2019). Global economic impact of antibiotic resistance: A review. *Journal of Global Antimicrobial Resistance*, *19*, 313–316. https://doi.org/10.1016/j.jgar.2019.05.024

Ahmad, S., Ahmad, G., & Mohsin, M. (2021). Superficial Dermatophytic Infection Prevention and Its Management: A Review. *International Journal of Research and Review*, *8*(8), 427–439. https://doi.org/10.52403/ijrr.20210859

Akiyama, S. I., Fojo, A. T., Hanover, J. A., Pastan, I., & Gottesman, M. M. (1985). Isolation and genetic characterization of human KB cell lines resistant to multiple drugs. *Somat. Cell Mol. Genet.*, *11*(march), 117–126. https://doi.org/10.1007/BF01534700

Ali, S., Chattopadhyay, T., & Orasugh, D. (2022). "*Bacillus subtilis*-based biofilms." Application of Biofilms in Applied Microbiology, (pp. 93–104). *Academic Press*.

Almagro, L., Fernández-Pérez, F., & Pedreño, M. A. (2015). Indole alkaloids from *Catharanthus roseus*: Bioproduction and their effect on human health. *Molecules*, *20*(2), 2973–3000.

https://doi.org/10.3390/molecules20022973

Almeida, A. M., Queiroz, J. A., Sousa, F., & Sousa, Â. (2019). Cervical cancer and HPV infection: ongoing therapeutic research to counteract the action of E6 and E7 oncoproteins. *Drug Discovery Today*, *24*(10), 2044–2057. https://doi.org/10.1016/j.drudis.2019.07.011

Alqurashi, M. M., Alsaileek, A., Aljizeeri, A., Bamefleh, H. S., & Alenazi, T. H. (2019). *Mycobacterium smegmatis* causing a granulomatous cardiomediastinal mass. *IDCases*, *18*(6), 1–5. https://doi.org/10.1016/j.idcr.2019.e00608

Alshehri, B. A., Alamri, A. M., Rabaan, A. A., & Al-Tawfiq, J. A. (2021). Epidemiology of Dermatophytes Isolated from Clinical Samples in a Hospital in Eastern Saudi Arabia: A 20-Year Survey. *Journal of Epidemiology and Global Health*, *11*(4), 405–412. https://doi.org/10.1007/s44197-021-00005-5

Alvarez-Rivera, G., Ballesteros-Vivas, D., Parada-Alfonso, F., Ibañez, E., & Cifuentes, A. (2019). Recent applications of high resolution mass spectrometry for the characterization of plant natural products. *TrAC - Trends in Analytical Chemistry*, *112*, 87–101. https://doi.org/10.1016/j.trac.2019.01.002

Alves-Silva, J. M., Romane, A., Efferth, T., & Salgueiro, L. (2017). North African Medicinal plants traditionally used in cancer therapy. *Frontiers in Pharmacology*, *8*(JUN), 1–24. https://doi.org/10.3389/fphar.2017.00383

Amaewhule, M. (2022). Prevalence and Pattern of Dermatophytosis in Patients with Human Immunodeficiency Virus Infection Seen in The University of Port Harcourt Teaching Hospital , (UPTH) Port- Harcourt Amaewhule MN Department of Internal Medicine , Rivers State University Te. *Greener Journal of Medical Sciences*, *11*(1), 46–72. https://doi.org/https://gjournals.org/GJMS

Amrani, M. El, Lai, D., Debbab, A., Aly, H. A., Siems, K., Seidel, C., Schnekenburger, M., Gaigneaux, A., Diederich, M., Feger, D., Lin, W., & Proksch, P. (2014). Protein kinase and HDAC inhibitors from the endophytic fungus *epicoccum nigrum*. *Journal of Natural Products*, *77*(1), 49–56. https://doi.org/10.1021/np4005745

Amuka, O., Machocho, A. K., Okemo, P. O., & Mbugua, P. K. (2015). Antifungal and antibacterial activity of crude stem bark extracts' of *Bersama abysinicca* Verdc. and *Faurea saligna* Harr. *Research Journal of Medicinal Plant*, *9*(4), 160–169. https://doi.org/10.3923/rjmp.2015.160.169

Anand, A., Sharma, A., Kaur Saini, H., Sharma, S., Sharma, R., Thakur, C., Priyanka, Atanassova, M., Caruso, G., & Pasdaran, A. (2022). Profiling of Plant Derived Natural Constituents by Using Magnetic Resonance Techniques. *Concepts in Magnetic Resonance Part A: Bridging Education and Research*, *2022*(1), 5705637. https://doi.org/10.1155/2022/5705637

Ashworth, M., & Cloatre, E. (2022). Enacting a depoliticised alterity: law and traditional medicine at the World Health Organization. *International Journal of Law in Context*, *18*(4), 476–498. https://doi.org/10.1017/S1744552322000143

Asres, K., Gibbons, S., & Bucar, F. (2006). Radical scavenging compounds from Ethiopian medicinal plants. *Ethiopian Pharmaceutical Journal*, *24*(1), 23-30. https://doi.org/10.4314/epj.v24i1.35095

Atta-Ur-Rahman, T. I. (2012). *Nuclear magnetic resonance: basic principles*,pp.1-50. Springer Science & Business Media.

Ayush, K., & Schweizer, H. P. (2005). Bacterial resistance to antibiotics: Active efflux and reduced uptake. *Advanced Drug Delivery Reviews*, *57*(10), 1486–1513. https://doi.org/10.1016/j.addr.2005.04.004

Babu, R., Raveendran, P., & Sugathan, S. (2023). Antimicrobial Drugs: Possibilities from Medicinal Plants Part A—Antibacterials and Antivirals. *In: Sukumaran, S.T., T R, K. (eds) Conservation and Sustainable Utilization of Bioresources. Sustainable Developm*. Springer, Singapore. https://doi.org/10.1007/978-981-19-5841-0_22

Baert, F., Lefevere, P., D'Hooge, E., Stubbe, D., & Packeu, A. (2021). A polyphasic approach to classification and identification of species within the *trichophyton benhamiae* complex. *Journal of Fungi*, *7*(8), 602. https://doi.org/10.3390/jof7080602

Bag, A., Bhattacharyya, S. K., & Chattopadhyay, R. R. (2013). Isolation and identification of a gallotannin 1, 2, 6- tri- O- galloyl- β- d- glucopyranose from hydroalcoholic extract of *Terminalia chebula* fruits effective against multidrug- resistant uropathogens. *Journal of Applied Microbiology*, *115*(2), 390–397. https://doi.org/10.1111/jam.12256

Baron, N. C., de Souza Pollo, A., & Rigobelo, E. C. (2020). *Purpureocillium lilacinum* and *Metarhizium marquandii* as plant growth-promoting fungi. *PeerJ*, *2020*(5), 1–25. https://doi.org/10.7717/peerj.9005

Baroni, A., Buommino, E., De Gregorio, V., Ruocco, E., Ruocco, V., & Wolf, R. (2012).

Structure and function of the epidermis related to barrier properties. *Clinics in Dermatology*, *30*(3), 257–262. https://doi.org/10.1016/j.clindermatol.2011.08.007

Barrios-González, J., & Mejía, A. (1996). Production of Secondary Metabolites by Solid-State Fermentation. *Biotechnology Annual Review*, *2*(8), 85–121. https://doi.org/10.1016/S1387-2656(08)70007-3

Baskar, R., Lee, K. A., Yeo, R., & Yeoh, K. W. (2012). Cancer and radiation therapy: Current advances and future directions. *International Journal of Medical Sciences*, *9*(3), 193–199. https://doi.org/10.7150/ijms.3635

Basnet, B. B., Chen, B., Suleimen, Y. M., Ma, K., Guo, S., Bao, L., & Liu, H. (2019). Cytotoxic secondary metabolites from the endolichenic fungus *Hypoxylon fuscum*. *Planta Medica*, *85*(13), 1088–1097. https://doi.org/10.1055/a-0957-3567

Bassetti, M., Carnelutti, A., Castaldo, N., & Peghin, M. (2019). Important new therapies for methicillin-resistant *Staphylococcus aureus*. *Expert Opinion on Pharmacotherapy*, *20*(18), 2317–2334. https://doi.org/10.1080/14656566.2019.1675637

Beceiro, A., Tomás, M., & Bou, G. (2013). Antimicrobial resistance and virulence: A successful or deleterious association in the bacterial world? *Clinical Microbiology Reviews*, *26*(2), 185–230. https://doi.org/10.1128/CMR.00059-12

Bedane, K. G., Brieger, L., Strohmann, C., Seo, E. J., Efferth, T., & Spiteller, M. (2020a). Cytotoxic bufadienolides from the leaves of a medicinal plant *Melianthus comosus* collected in South Africa. *Bioorganic Chemistry*, *102*(February), 104102. https://doi.org/10.1016/j.bioorg.2020.104102

Bedane, K. G., Brieger, L., Strohmann, C., Seo, E. J., Efferth, T., & Spiteller, M. (2020b). Cytotoxic Bufadienolides from the Leaves of *Melianthus major*. *Journal of Natural Products*, *83*(7), 2122–2128. https://doi.org/10.1021/acs.jnatprod.0c00060

Beentje, H., Adamson, J., & Bhanderi, D. (1994). Kenya trees, shrubs, and lianas. pp. 500 -772. National Museums of Kenya.

Bene, K., Guessennd, N. K., Camara, D., Zirihi, G. N., & Dosso, M. (2016). Botanical Study and in vitro Antibacterial Activity of *Bersama abyssinica* Fresen.(Melianthaceae) on Multi-Resistant *Staphylococcus aureus* Strains. *International Journal of Science and Research*, *5*(1), 375-379. DOI:10.21275/v5i1.nov152671

Bernabeu, E., Cagel, M., Lagomarsino, E., Moretton, M., & Chiappetta, D. A. (2017). Paclitaxel: What has been done and the challenges remain ahead. *International Journal of Pharmaceutics*, *526*(1–2), 474–495. https://doi.org/10.1016/j.ijpharm.2017.05.016

Bernardini, S., Tiezzi, A., Laghezza Masci, V., & Ovidi, E. (2018). Natural products for human health: an historical overview of the drug discovery approaches. *Natural Product Research*, *32*(16), 1926–1950. https://doi.org/10.1080/14786419.2017.1356838

Birhanu, Z. (2013). Traditional use of medicinal plants by the ethnic groups of Gondar Zuria district, North-Western Ethiopia. *Journal of Natural Remedies*, *13*(1), 46–53. https://doi.org/10.18311/jnr/2013/117

Biswas, T., Sen, A., Roy, R., Maji, S., & Maji, H. S. (2015). Isolation of mangiferin from flowering buds of *Mangifera indica* L and its evaluation of in vitro antibacterial activity. *Journal of Pharmaceutical Analysis*, *4*(3), 49-56. https://doi.org/https://doi.org/10.3892/mmr.2018.9529

Bitew, A. (2018). Dermatophytosis: Prevalence of Dermatophytes and Non-Dermatophyte Fungi from Patients Attending Arsho Advanced Medical Laboratory, Addis Ababa, Ethiopia. *Dermatology Research and Practice*, 2018 (*10*), 1-6 . https://doi.org/10.1155/2018/8164757

Bitrus, A. A., Peter, O. M., Abbas, M. A., & Goni, M. D. (2018). *Staphylococcus aureus*: A Review of Antimicrobial Resistance Mechanisms. *Veterinary Sciences: Research and Reviews*, *4*(2), 43-54. https://doi.org/10.17582/journal.vsrr/2018/4.2.43.54

Blair, J. M., Richmond, G. E., & Piddock, L. J. (2014). Multidrug efflux pumps in Gram-negative bacteria and their role in antibiotic resistance. *Future Microbiology*, *9*(10), 1165-1177. https://doi.org/https://doi.org/10.2217/fmb.14.66

Blair, J. M., Webber, M. A., Baylay, A. J., Ogbolu, D. O., & Piddock, L. J. (2015). Molecular mechanisms of antibiotic resistance. *Nature Reviews Microbiology*, *13*(1), 42-51. https://doi.org/https://doi.org/10.1038/nrmicro3380

Blome, C., Radtke, M., Eissing, L., & Augustin, M. (2016). Quality of Life in Patients with Atopic Dermatitis: Disease Burden, Measurement, and Treatment Benefit. *American Journal of Clinical Dermatology.*, *17*(2), 163-9. https://doi.org/10.1007/s40257-015-0171-3

Bonfante, P., & Genre, A. (2010). Mechanisms underlying beneficial plant - Fungus interactions in mycorrhizal symbiosis. *Nature Communications*, *1*(4), 1–11. https://doi.org/10.1038/ncomms1046

Bongomin, F., Olum, R., Nsenga, L., & Baluku, J. B. (2020). Burden of *tinea capitis* among children in Africa: protocol for a systematic review and meta-analysis of observational studies, 1990-2020. *BMJ Open*, *10*(9), e041230. https://doi.org/10.1136/bmjopen-2020-041230

Bourjot, M., Leyssen, P., Eydoux, C., Guillemot, J. C., Canard, B., Rasoanaivo, P., Guéritte, F., & Litaudon, M. (2012). Flacourtosides A-F, phenolic glycosides isolated from *Flacourtia ramontchi*. *Journal of Natural Products*, *75*(4), 752–758. https://doi.org/10.1021/np300059n

Bovey, F. A., Mirau, P. A., & Gutowsky, H. S. (1988). Nuclear magnetic resonance spectroscopy, pp. 325-355. Elsevier.

Bruns, T. D., & Gardes, M. (1993). Molecular tools for the identification of ectomycorrhizal fungi—taxon- specific oligonucleotide probes for suilloid fungi. *Molecular Ecology*, *2*(4), 233-242. https://doi.org/https://doi.org/10.1111/j.1365-294X.1993.tb00013.x

Burstein, V. L., Beccacece, I., Guasconi, L., Mena, C. J., Cervi, L., & Chiapello, L. S. (2020). Skin Immunity to Dermatophytes: From Experimental Infection Models to Human Disease. *Frontiers in Immunology*, *11*(December), 1–16. https://doi.org/10.3389/fimmu.2020.605644

Butler, M. S., Robertson, A. A., & Cooper, M. A. (2014). Natural product and natural product derived drugs in clinical trials. *Natural Product Reports*, *31*(11), 1612–1661. https://doi.org/DOI https://doi.org/10.1039/C4NP00064A

Cadagan, D., & Merry, S. (2013). Circumvention of inherent or acquired cytotoxic drug resistance in vitro using combinations of modulating agents. *Anticancer Research*, *33*(10), 4381–4388.

Cañete-Gibas, C., & Wiederhold, N. P. (2023). Mycology of Onychomycosis. *Clinical Microbiology Newsletter*, *45*(2), 11–17. https://doi.org/10.1016/j.clinmicnews.2023.01.002

CDC. (2019). CDC's Antibiotic Resistance Threats in the United States. https://doi.org/https://www.cdc.gov/drugresistance/biggest-threats.html

Chadeganipour, M., Mohammadi, R., & Shahla, S. (2016). "A 10- year study of dermatophytoses in Isfahan, Iran." *Journal of Clinical Laboratory Analysis 3*, *30*(2), 103–107. https://doi.org/https://doi.org/10.1002/jcla.21852

Chahal, K. (2021). Bacteria Emerging As an Opportunistic Pathogen. *International Journal of Current Science Research and Review*, *4*(5), 401-407. https://doi.org/10.47191/ijcsrr/v4-i5-

Chan, C. K., Aimagambetova, G., Ukybassova, T., Kongrtay, K., & Azizan, A. (2019). Human Papillomavirus Infection and Cervical Cancer: Epidemiology, Screening, and Vaccination - Review of Current Perspectives. *Journal of Oncology*, 2019 (10), 2-11. https://doi.org/10.1155/2019/3257939

Chanyachailert, P., Leeyaphan, C., & Bunyaratavej, S. (2023). Cutaneous Fungal Infections Caused by Dermatophytes and Non-Dermatophytes : An Updated Comprehensive Review of Epidemiology , Clinical Presentations , and Diagnostic Testing. *Journal of Fungi*, *9*(6), 669. https://doi.org/https://doi.org/10.3390/ jof9060669 Academic

Chen, H. Y., Liu, T. K., Shi, Q., & Yang, X. L. (2019). Sesquiterpenoids and diterpenes with antimicrobial activity from *Leptosphaeria* sp. XL026, an endophytic fungus in *Panax notoginseng*. *Fitoterapia*, *137*(June), 104243. https://doi.org/10.1016/j.fitote.2019.104243

Chen, X., Dai, X., Yu, Y., Wei, X., Zhang, X., & Li, C. (2019). "Sulfhydryl functionalized graphene oxide for efficient preconcentration and photoablation of pathogenic bacteria." *New Journal of Chemistry*, *43*(2), 917-925. https://doi.org/https://doi.org/10.1039/C8NJ04401E

Chepkirui, C., Yuyama, K. T., Wanga, L. A., Decock, C., Matasyoh, J. C., Abraham, W. R., & Stadler, M. (2018). Microporenic Acids A-G, Biofilm Inhibitors, and Antimicrobial Agents from the *Basidiomycete Microporus* Species. *Journal of Natural Products*, *81*(4), 778–784. https://doi.org/10.1021/acs.jnatprod.7b00764

Chowdhry, P. N., Gupta, S. L., & Anand, N. (2009). Diversity of fungi as human pathogen. *Recent Research in Science and Technology*, *5*(1), 17–20. http://scienceflora.org/journals/index.php/rrst/article/view/1000

Čmoková, A., Kolařík, M., Dobiáš, R., Hoyer, L., Janouškovcová, H., Kano, R., Kuklová, I., Lysková, P., Machová, L., Maier, T., & Mallátová, N. (2020). Resolving the taxonomy of emerging zoonotic pathogens in the *Trichophyton benhamiae* complex. *Fungal Diversity*, *104*(9), 333–387. https://doi.org/https://doi.org/10.1007/s13225-020-00465-3

Colla, G., Rouphael, Y., Di Mattia, E., El-Nakhel, C., & Cardarelli, M. (2015). Co-inoculation of *Glomus intraradices* and *Trichoderma atroviride* acts as a biostimulant to promote growth, yield and nutrient uptake of vegetable crops. *Journal of the Science of Food and Agriculture*, *95*(8), 1706–1715. https://doi.org/10.1002/jsfa.6875

Cong, Y., Yang, S., & Rao, X. (2020). Vancomycin resistant *Staphylococcus aureus* infections: A review of case updating and clinical features. *Journal of Advanced Research*, *21*, 169–176. https://doi.org/10.1016/j.jare.2019.10.005

Costa, L. B., Rangel, D. E. N., & Morandi, M. A. B. (2012). Impact of UV-B radiation on *Clonostachys rosea* germination and growth. *World J Microbiol Biotechnol*, *28*(7), 2497–2504. https://doi.org/https://doi.org/10.1007/s11274-012-1057-7

Cox, G., & Wright, G. D. (2013). Intrinsic antibiotic resistance: Mechanisms, origins, challenges and solutions. *International Journal of Medical Microbiology*, *303*(6–7), 287–292. https://doi.org/10.1016/j.ijmm.2013.02.009

Coyner, K. S. (2019). Bacterial, fungal, oomycete, and algal infections. In *Clinical Atlas of Canine and Feline Dermatology* (pp. 133-198.). Wiley Online Library. https://doi.org/https://doi.org/10.1002/9781119565925.ch37

da Silva, B., Kupski, L., & Badiale-Furlong, E. (2019). Central Composite Design-Desirability Function Approach for Optimum Ultrasound-Assisted Extraction of Daidzein and Genistein from Soybean and Their Antimycotoxigenic Potential. *Food Anal. Methods*, *12*(1), 258–270. https://doi.org/https://doi.org/10.1007/s12161-018-1357-0

Dadgostar, P. (2019). Antimicrobial resistance: implications and costs. *Infection and Drug Resistance*, *12*(2019), 3903–3910. https://doi.org/10.2147/IDR.S234610

Dasbasi, T. (2020). Determination of Isoflavones in Nuts, Dried Fruits and Vegetables by High Performance Liquid Chromatography. *Journal of the Institute of Science and Technology*, *10*(2), 1191–1201. https://doi.org/10.21597/jist.619176

Datta, S., Ramamurthy, P. C., Anand, U., Singh, S., Singh, A., Dhanjal, D. S., Dhaka, V., Kumar, S., Kapoor, D., Nandy, S., Kumar, M., Koshy, E. P., Dey, A., Proćków, J., & Singh, J. (2021). Wonder or evil?: Multifaceted health hazards and health benefits of *Cannabis sativa* and its phytochemicals. *Saudi Journal of Biological Sciences*, *28*(12), 7290–7313. https://doi.org/10.1016/j.sjbs.2021.08.036

de Fávaro, L. C. L., de Sebastianes, F. L. S., & Araújo, W. L. (2012). *Epicoccum nigrum* P16, a sugarcane endophyte, produces antifungal compounds and induces root growth. *PLoS ONE*, *7*(6), 1–10. https://doi.org/10.1371/journal.pone.0036826

Deshmukh, S. K., & Verekar, S. A. (2012). Fungal endophytes: A potential source of antifungal compounds. *Frontiers in Bioscience - Elite*, *4 E*(6), 2045–2070.

https://doi.org/10.2741/e524

Dhouafli, Z., Ben Jannet, H., Mahjoub, B., Leri, M., Guillard, J., Saidani, T. M., Stefani, M., & Hayouni, E. A. (2019). 1,2,4-trihydroxynaphthalene-2- O -β-D-glucopyranoside: A new powerful antioxidant and inhibitor of Aβ42 aggregation isolated from the leaves of *Lawsonia inermis*. *Natural Products Research*, *33*(10), 1406–1414. https://doi.org/https://doi.org/10.1080/14786419.2017.1419229

Dilnessa, T., & Bitew, A. (2016). Prevalence and antimicrobial susceptibility pattern of methicillin resistant *Staphylococcus aureus* isolated from clinical samples at Yekatit 12 Hospital Medical College, Addis Ababa, Ethiopia. *BMC Infectious Diseases*, *16*(1), 1–9. https://doi.org/10.1186/s12879-016-1742-5

Djemgou, P. C., Hussien, T. A., Hegazy, M. E. F., Ngandeu, F., Neguim, G., Tane, P., & Mohamed, A. E. H. H. (2010). C-Glucoside xanthone from the stem bark extract of *Bersama engleriana*. *Pharmacognosy Research*, *2*(4), 229–232. https://doi.org/10.4103/0974-8490.69110

Dolomanov, O. V., Bourhis, L. J., Gildea, R. J., Howard, J. A. K., & Puschmann, H. (2009). OLEX2: a complete structure solution, refinement and analysis program. *Journal of Applied Crystallography*, *42*(2), 339–341. https://doi.org/https://doi.org/10.1107/S0021889808042726

Dong, X., Huang, Y., Wang, Y., & He, X. (2019). Anti-inflammatory and antioxidant jasmonates and flavonoids from lychee seeds. *Journal of Functional Foods*, *54*(August), 74–80. https://doi.org/10.1016/j.jff.2018.12.040

Duan, D., Li, Z., Luo, H., Zhang, W., Chen, L., & Xu, X. (2004). Antiviral compounds from traditional Chinese medicines Galla Chinese as inhibitors of HCV NS3 protease. *Bioorganic and Medicinal Chemistry Letters*, *14*(24), 6041–6044. https://doi.org/10.1016/j.bmcl.2004.09.067

Duarte, B., Galhardas, C., & Cabete, J. (2019). Adult *tinea capitis* and *tinea barbae* in a tertiary Portuguese hospital: A 11- year audit. *Mycoses*, *62*(11), 1079-1083. https://doi.org/https://doi.org/10.1111/myc.12991

Engels, D., & Savioli, L. (2006). Reconsidering the underestimated burden caused by neglected tropical diseases. *Trends in Parasitology*, *22*(8), 363–366. https://doi.org/10.1016/j.pt.2006.06.004

Enioutina, E. Y., Salis, E. R., Job, K. M., Gubarev, M. I., Krepkova, L. V., & Sherwin, C. M. (2017). Herbal Medicines: challenges in the modern world. Part 5. status and current directions of complementary and alternative herbal medicine worldwide. *Expert Review of Clinical Pharmacology*, *10*(3), 327-338. https://doi.org/https://doi.org/10.1080/17512433.2017.1268917

Erb, M., & Kliebenstein, D. J. (2020). Plant Secondary Metabolites as Defenses, Regulators, and Primary Metabolites: The Blurred Functional Trichotomy1[OPEN]. *Plant Physiology*, *184*(1), 39–52. https://doi.org/10.1104/PP.20.00433

Estell, R. E., Fredrickson, E. L., & James, D. K. (2016). Effect of light intensity and wavelength on concentration of plant secondary metabolites in the leaves of *Flourensia cernua*. *Biochemical Systematics and Ecology*, *65*, 108–114. https://doi.org/10.1016/j.bse.2016.02.019

Fares, J., Fares, M. Y., Khachfe, H. H., Salhab, H. A., & Fares, Y. (2020). Molecular principles of metastasis: a hallmark of cancer revisited. *Signal Transduction and Targeted Therapy*, *5*(1). https://doi.org/10.1038/s41392-020-0134-x

Fazle, R. M., & Baek, K. H. (2020). Antimicrobial Activities of Lipopeptides and Polyketides of *Bacillus velezensis* for Agricultural Applications. *Molecules (Basel, Switzerland)*, *25*(21). https://doi.org/10.3390/molecules25214973

Fenetahun, Y., & Eshetu, G. (2017). A review on ethnobotanical studies of medicinal plants use by agro-pastoral communities in, Ethiopia. *Journal of Medicinal Plants Studies*, *5*(1), 33–44. DOI:10.13140/RG.2.2.27572.55689

Fogliani, B., Raharivelomanana, P., Bianchini, J. P., Bouraïma-Madjèbi, S., & Hnawia, E. (2005). Bioactive ellagitannins from Cunonia macrophylla, an endemic Cunoniaceae from New Caledonia. *Phytochemistry*, *66*(2), 241–247. https://doi.org/10.1016/j.phytochem.2004.11.016

Gakuubi, M. M., Ching, K. C., Munusamy, M., Wibowo, M., Liang, Z. X., Kanagasundaram, Y., & Ng, S. B. (2022). Enhancing the Discovery of Bioactive Secondary Metabolites From Fungal Endophytes Using Chemical Elicitation and Variation of Fermentation Media. *Frontiers in Microbiology*, *13*(June). https://doi.org/10.3389/fmicb.2022.898976

Gali-Muhtasib, H., Hmadi, R., Kareh, M., Tohme, R., & Darwiche, N. (2015). Cell death mechanisms of plant-derived anticancer drugs: Beyond apoptosis. *Apoptosis*, *20*(12), 1531–

1562. https://doi.org/10.1007/s10495-015-1169-2

Gnanamani, A., Hariharan, P., & Paul-Satyaseela, M. (2017). Gnanamani, A., Hariharan, P., & Paul-Satyaseela, M. Staphylococcus aureus: Overview of bacteriology, clinical diseases, epidemiology, antibiotic resistance and therapeutic approach. In *Frontiers in Staphylococcus aureus*, 4(28). https://dx.doi.org/10.5772/67338

Gnat, S., Łagowski, D., Dyląg, M., & Nowakiewicz, A. (2022). European Hedgehogs (Erinaceus europaeus L.) as a Reservoir of Dermatophytes in Poland. *Microbial Ecology*, *84*(2), 363–375. https://doi.org/10.1007/s00248-021-01866-w

Gnat, S., Nowakiewicz, A., Lagowski, D., Czyk, A. T., & Zieba, P. (2019). Multiple-strain *trichophyton mentagrophytes* infection in a silver fox (vulpes vulpes) from a breeding farm. *Medical Mycology*, *57*(2), 171–180. https://doi.org/10.1093/mmy/myy011

Gomes, N. G. M., Oliveira, A. P., Cunha, D., Pereira, D. M., Valentão, P., Pinto, E., Araújo, L., & Andrade, P. B. (2019). Flavonoid Composition of *Salacia senegalensis* (Lam.) DC. Leaves, Evaluation of Antidermatophytic Effects, and Potential Amelioration of the Associated Inflammatory Response. *Molecules*, *24*(14), 2530. https://doi.org/doi:10.3390/molecules24142530

Graham, J. G., Quinn, M. L., Fabricant, D. S., & Farnsworth, N. R. (2000). Plants used against cancer - An extension of the work of Jonathan Hartwell. *Journal of Ethnopharmacology*, *73*(3), 347–377. https://doi.org/10.1016/S0378-8741(00)00341-X

Guédé, N. Z., N'guessan, K., Dibié, T. E., & Grellier, P. (2010). Ethnopharmacological study of plants used to treat malaria, in traditional medicine, by Bete Populations of Issia (Côte d'Ivoire). *Journal of Pharmaceutical Sciences Research*, *2*(4), 216-227. https://doi.org/https://doi.org/10.1016/j.jep.2014.05.060

Guilhaumou, R., Benaboud, S., Bennis, Y., Dahyot-Fizelier, C., Dailly, E., Gandia, P., Goutelle, S., Lefeuvre, S., Mongardon, N., Roger, C., Scala-Bertola, J., Lemaitre, F., & Garnier, M. (2019). Optimization of the treatment with beta-lactam antibiotics in critically ill patients - Guidelines from the French Society of Pharmacology and Therapeutics (Société Française de Pharmacologie et Thérapeutique - SFPT) and the French Society of Anaesthesia . *Critical Care*, *23*(1), 1–20. https://doi.org/10.1186/s13054-019-2378-9

Gunatilaka, A. A. L. (2006). Natural products from plant-associated microorganisms: Distribution, structural diversity, bioactivity, and implications of their occurrence. *Journal*

of Natural Products, *69*(3), 509–526. https://doi.org/10.1021/np058128n

Guo, B., Li, H., & Zhang, L. (1998). Isolation of an fungus producting vinbrastine. *Journal of Yunnan University (Natural Sciences)*, *20*(3), 214-215. https://doi.org/10.22108/BJM.2018.107927.1095

Guo, H., Sun, B., Gao, H., Chen, X., Liu, S., Yao, X., Liu, X., & Che, Y. (2009). Diketopiperazines from the Cordyceps-colonizing fungus *Epicoccum nigrum*. *Journal of Natural Products*, *72*(12), 2115–2119. https://doi.org/10.1021/np900654a

Guo, Z. (2017). The modification of natural products for medical use. *Acta Pharmaceutica Sinica B*, *7*(2), 119–136. https://doi.org/10.1016/j.apsb.2016.06.003

Halder, S., Anand, U., Nandy, S., Oleksak, P., Qusti, S., Alshammari, E. M., El-Saber Batiha, G., Koshy, E. P., & Dey, A. (2021). Herbal drugs and natural bioactive products as potential therapeutics: A review on pro-cognitives and brain boosters perspectives. *Saudi Pharmaceutical Journal*, *29*(8), 879–907. https://doi.org/10.1016/j.jsps.2021.07.003

Hammerum, A. M., & Heuer, O. E. (2009). Human health hazards from antimicrobial-resistant *Escherichia coli* of animal origin. *Clinical Infectious Diseases*, *48*(7), 916–921. https://doi.org/10.1086/597292

Han, P., Zhang, X., Xu, D., Zhang, B., Lai, D., & Zhou, L. (2020). Metabolites from clonostachys fungi and their biological activities. *Journal of Fungi*, *6*(4), 1–30. https://doi.org/10.3390/jof6040229

Harwoko, H., Hartmann, R., Daletos, G., Ancheeva, E., Frank, M., Liu, Z., & Proksch, P. (2019). Biotransformation of Host Plant Flavonoids by the Fungal Endophyte Epicoccum nigrum. *ChemistrySelect*, *4*(45), 13054–13057. https://doi.org/10.1002/slct.201903168

Havlickova, B., Czaika, V. A., & Friedrich, M. (2009). Epidemiological trends in skin mycoses worldwide (Mycoses (2008) 51, SUPPL. 4, (2-15)). *Mycoses*, *52*(1), 95. https://doi.org/10.1111/j.1439-0507.2008.01668.x

Hawas, U. W., & Al-Farawati, R. (2017). Chemical constituents and antiviral activity from marine endophytic fungi from red sea alga *Padina pavonica*. *Journal of the Chemical Society of Pakistan*, *39*(3), 478–483. doi:10.3390/microorganisms8121934

Heiman, K. E., Mody, R. K., Johnson, S. D., Griffin, P. M., & Hannah Gould, L. (2015). *Escherichia coli* O157 Outbreaks in the United States, 2003–2012. *Emerging Infectious Diseases*, *21*(8), 1293–1301. https://doi.org/10.3201/eid2108.141364

Helaly, S. E., Thongbai, B., & Stadler, M. (2018). Diversity of biologically active secondary metabolites from endophytic and saprotrophic fungi of the ascomycete order Xylariales. *Natural Product Reports*, *35*(9), 992-1014. https://doi.org/DOI https://doi.org/10.1039/C8NP00010G

Henrique, C., Santos, B., Andrade, L. A. De, & Frezarin, E. T. (2023). *Purpureocillium lilacinum for biocontrol , bioremediation and biofertilization*. *May*. https://doi.org/10.20944/preprints202305.1926.v1

Hernández-Gómez, O., Kimble, S. J. A., Briggler, J. T., & Williams, R. N. (2017). Characterization of the Cutaneous Bacterial Communities of Two Giant Salamander Subspecies. *Microbial Ecology*, *73*(2), 445–454. https://doi.org/10.1007/s00248-016-0859-9

Hölker, U., Höfer, M., & Lenz, J. (2004). Biotechnological advantages of laboratory-scale solid-state fermentation with fungi. *Applied Microbiology and Biotechnology*, *64*(2), 175–186. https://doi.org/10.1007/s00253-003-1504-3

Hölker, Udo, & Lenz, J. (2005). Solid-state fermentation - Are there any biotechnological advantages? *Current Opinion in Microbiology*, *8*(3), 301–306. https://doi.org/10.1016/j.mib.2005.04.006

Hotaka, D., Amnuaykanjanasin, A., Maketon, C., Siritutsoontorn, S., & Maketon, M. (2015). Efficacy of *Purpureocillium lilacinum* CKPL-053 in controlling Thrips palmi (Thysanoptera: Thripidae) in orchid farms in Thailand. *Applied Entomology and Zoology*, *50*(3), 317–329. https://doi.org/10.1007/s13355-015-0339-6

Hridoy, M., Gorapi, M. Z. H., Noor, S., Chowdhury, N. S., Rahman, M. M., Muscari, I., Masia, F., Adorisio, S., Delfino, D. V., & Mazid, M. A. (2022). Putative Anticancer Compounds from Plant-Derived Endophytic Fungi: A Review. *Molecules*, *27*(1). https://doi.org/10.3390/molecules27010296

Huang, L. H., Yuan, M. Q., Ao, X. J., Ren, A. Y., Zhang, H. B., & Yang, M. Z. (2018). Endophytic fungi specifically introduce novel metabolites into grape flesh cells in vitro. *PLoS ONE*, *13*(5), 1–10. https://doi.org/10.1371/journal.pone.0196996

Huang, M., Lu, J. J., & Ding, J. (2021). Natural Products in Cancer Therapy: Past, Present and Future. *Natural Products and Bioprospecting*, *11*(1), 5–13. https://doi.org/10.1007/s13659-020-00293-7

Huang, Z., Guo, Z., Yang, R., Yin, X., Li, X., Luo, W., & Lin, Y. (2009). Chemistry and

cytotoxic activities of polyketides produced by the mangrove endophytic fungus *Phomopsis* sp. ZSU-H76. *Chemistry of Natural Compounds*, *45*(3), 625–628. https://doi.org/https://doi.org/10.1007/s10600-009-9446-3

Hutchings, M., Truman, A., & Wilkinson, B. (2019). Antibiotics: past, present and future. *Current Opinion in Microbiology*, *51*(1), 72–80. https://doi.org/10.1016/j.mib.2019.10.008

Hwang, K. S., Kim, H. U., Charusanti, P., Palsson, B. T., & Lee, S. Y. (2014). Systems biology and biotechnology of *Streptomyces* species for the production of secondary metabolites. *Biotechnology Advances*, *32*(2), 255–268. https://doi.org/10.1016/j.biotechadv.2013.10.008

Hyde, K. D., & Soytong, K. (2008). The fungal endophyte dilemma. *Fungal Diversity*, *33*(11), 163–173. https://www.doi.org/261401775

Ito, A., Chai, H. B., Lee, D., Kardono, L. B. S., Riswan, S., Farnsworth, N. R., Cordell, G. A., Pezzuto, J. M., & Kinghorn, A. D. (2002). Ellagic acid derivatives and cytotoxic cucurbitacins from *Elaeocarpus mastersii*. *Phytochemistry*, *61*(2), 171–174. https://doi.org/10.1016/S0031-9422(02)00232-7

Jian, Z., Zeng, L., Xu, T., Sun, S., Yan, S., Yang, L., Huang, Y., Jia, J., & Dou, T. (2021). Antibiotic resistance genes in bacteria: Occurrence, spread, and control. *Journal of Basic Microbiology*, *61*(12), 1049–1070. https://doi.org/10.1002/jobm.202100201

Jiang, C. X., Li, J., Zhang, J. M., Jin, X. J., Yu, B., Fang, J. G., & Wu, Q. X. (2019). Isolation, Identification, and Activity Evaluation of Chemical Constituents from Soil Fungus *Fusarium avenaceum* SF-1502 and Endophytic Fungus *Fusarium proliferatum* AF-04. *Journal of Agricultural and Food Chemistry*, *67*(7), 1839–1846. https://doi.org/10.1021/acs.jafc.8b05576

Jiang, L., Pu, H., Xiang, J., Su, M., Yan, X., Yang, D., Zhu, X., Shen, B., Duan, Y., & Huang, Y. (2018). Huanglongmycin A-C, cytotoxic polyketides biosynthesized by a putative type II polyketide synthase from *Streptomyces* sp. CB09001. *Frontiers in Chemistry*, *6*(JUN), 1–9. https://doi.org/10.3389/fchem.2018.00254

Jota Baptista, C., Oliveira, P. A., Gonzalo-Orden, J. M., & Seixas, F. (2023). Do Urban Hedgehogs (*Erinaceus europaeus*) Represent a Relevant Source of Zoonotic Diseases? *Pathogens*, *12*(2), 1–12. https://doi.org/10.3390/pathogens12020268

Kamtcha, D. W., Tene, M., Bedane, K. G., Knauer, L., Brieger, L., Strohmann, C., Tane, P., Kusari, S., & Spiteller, M. (2018). Cardenolides and dihydro-β-agarofuran sesquiterpenes

from the seeds of *Salacia staudtiana*. *Fitoterapia*, *131*(October), 174–181. https://doi.org/10.1016/j.fitote.2018.10.025

Kaneria, M. J., Rakholiya, K. D., & Chanda, S. V. (2017). Role of medicinal plants and bioactive compounds against skin disease–causing microbes, with special emphasis on their mechanisms of action. In *The Microbiology of Skin, Soft Tissue, Bone and Joint* (pp. 255–269). Academic Press. https://doi.org/https://doi.org/10.1016/B978-0-12-811079-9.00015-X

Karimkhani, C., Dellavalle, R. P., Coffeng, L. E., Flohr, C., Hay, R. J., Langan, S. M., Nsoesie, E. O., Ferrari, A. J., Erskine, H. E., Silverberg, J. I., Vos, T., & Naghavi, M. (2017). Global skin disease morbidity and mortality an update from the global burden of disease study 2013. *JAMA Dermatology*, *153*(5), 406–412. https://doi.org/10.1001/jamadermatol.2016.5538

Katz, L., & Baltz, R. H. (2016). Natural product discovery: past, present, and future. *Journal of Industrial Microbiology and Biotechnology*, *43*(2–3), 155–176. https://doi.org/10.1007/s10295-015-1723-5

Kaul, S., Gupta, S., Ahmed, M., & Dhar, M. K. (2012). Endophytic fungi from medicinal plants: a treasure hunt for bioactive metabolites. *Phytochemistry Reviews*, *11*, 487-505. https://doi.org/https://doi.org/10.1007/s11101-012-9260-6

Kaul, Sanjana, Gupta, S., Sharma, S., & Dhar, M. K. (2017). *The Fungal Endobiome of Medicinal Plants: A Prospective Source of Bioactive Metabolites*. https://doi.org/10.1007/978-981-10-5978-0_7

Kazan, K., & Manners, J. M. (2011). The interplay between light and jasmonate signalling during defence and development. *Journal of Experimental Botany*, *62*(12), 4087–4100. https://doi.org/10.1093/jxb/err142

Khalid, E. B., Ayman, E. L. M. E. L. K., Rahman, H., Abdelkarim, G., & Najda, A. (2016). Natural products against cancer angiogenesis. *Tumor Biology*, *37*(11), 14513–14536. https://doi.org/10.1007/s13277-016-5364-8

Khare, T., Anand, U., Dey, A., Assaraf, Y. G., Chen, Z. S., Liu, Z., & Kumar, V. (2021). Exploring Phytochemicals for Combating Antibiotic Resistance in Microbial Pathogens. *Frontiers in Pharmacology*, *12*(July), 1–18. https://doi.org/10.3389/fphar.2021.720726

Kharwar, R. N., Mishra, A., Gond, S. K., Stierle, A., & Stierle, D. (2011). Anticancer compounds derived from fungal endophytes: their importance and future challenges.

Natural Product Reports, *28*(7), 1208-1228.

Kifle, Z. D., & Enyew, E. F. (2020). Evaluation of In Vivo Antidiabetic, In Vitro α-Amylase Inhibitory, and In Vitro Antioxidant Activity of Leaves Crude Extract and Solvent Fractions of *Bersama abyssinica* Fresen (Melianthaceae). *Journal of Evidence-Based Integrative Medicine*, *25*, 1–11. https://doi.org/10.1177/2515690X20935827

Koch, A. L. (2002). Control of the bacterial cell cycle by cytoplasmic growth. *Critical Reviews in Microbiology*, *28*(1), 61–77. https://doi.org/10.1080/1040-840291046696

Kokoska, L., Kloucek, P., Leuner, O., & Novy, P. (2019). Plant-derived products as antibacterial and antifungal agents in human health care. *Current Medicinal Chemistry*, *26*(29), 5501-5541. https://doi.org/10.2174/0929867325666180831144344

Kokwaro, J. O. (1993). "Medicinal plants of East Africa,. In *East Africa Literature Bureau, Kampala, Nairobi, and Dar-es-Salaam*, pp. 106–115. East Africa Literature Bureau, Kampala, Nairobi, and Dar-es-Salaam.

Kolařík, M., Spakowicz, D. J., Gazis, R., Shaw, J., Kubátová, A., Nováková, A., Chudíčková, M., Forcina, G. C., Kang, K. W., Kelnarová, I., Skaltsas, D., Portero, C. E., Strobel, S. A., & Narváez-Trujillo, A. (2017). Biatriospora (Ascomycota: Pleosporales) is an ecologically diverse genus including facultative marine fungi and endophytes with biotechnological potential. *Plant Systematics and Evolution*, *303*(1), 35–50. https://doi.org/10.1007/s00606-016-1350-2

Kong, D. X., Li, Y. Q., Wang, M. L., Bai, M., Zou, R., Tang, H., & Wu, H. (2016). Effects of light intensity on leaf photosynthetic characteristics, chloroplast structure, and alkaloid content of *Mahonia bodinieri* (Gagnep.) Laferr. *Acta Physiol Plant*, *38*(120), 1-15. https://doi.org/https://doi.org/10.1007/s11738-016-2147-1

Kopacz, K., & Phadtare, S. (2022). Probiotics for the Prevention of COVID-19 Sequelae. *Archives of Medical Research*, *53*(6), 643. https://doi.org/10.1016/j.arcmed.2022.08.004

Kristensen, K., Ward, L. M., Mogensen, M. L., & Cichosz, S. L. (2023). Using image processing and automated classification models to classify microscopic gram stain images. *Computer Methods and Programs in Biomedicine Update*, *3*(December), 100091. https://doi.org/10.1016/j.cmpbup.2022.100091

Křížová, L., Dadáková, K., Kašparovská, J., & Kašparovský, T. (2019). Isoflavones. *Molecules*, *24*(6), 1076. https://doi.org/10.3390/molecules24061076

Kubo, I, & Matsumoto, T. (1984). Abyssinin, a potent insect antifeedant from an African medicinal plant, *Bersama abyssinica*. *Tetrahedron Letters*, *25*(41), 4601–4604. https://doi.org/https://doi.org/10.1016/S0040-4039(01)91210-9

Kubo, Isao, & Matsumoto, A. (1985a). *"Potent insect antifeedants from the African medicinal plant Bersama abyssinica."* pp. 183-200. ACS Symposium Series. https://doi.org/10.1021/bk-1985-0276.ch012 10.1021/bk-1985-0276.ch012

Kubo, Isao, & Matsumoto, T. (1984). Abyssinin, a potent insect antifeedant from an african medicinal plant, *bersama abyssinica*. *Tetrahedron Letters*, *25*, 4601–4604. https://doi.org/10.1016/S0040-4039(01)91210-9

Kubo, Isao, & Matsumoto, T. (1985b). Potent insect antifeedants from the African medicinal plant *Bersama abyssinica*. *ACS Symposium Series*, *276*, 183–200. https://doi.org/10.1016/S0040-4039(01)91210-9

Kuete, V., Mbaveng, A. T., Tsaffack, M., Beng, V. P., Etoa, F. X., Nkengfack, A. E., Meyer, J. J. M., & Lall, N. (2007). Antitumor, antioxidant and antimicrobial activities of *Bersama engleriana* (Melianthaceae). *Journal of Ethnopharmacology*, *115*(3), 494–501. https://doi.org/10.1016/j.jep.2007.10.027

Kumar, A., Patil, D., Rajamohanan, P. R., & Ahmad, A. (2013). Isolation, Purification and Characterization of Vinblastine and Vincristine from Endophytic Fungus *Fusarium oxysporum* Isolated from *Catharanthus roseus*. *PLoS ONE*, *8*(9). https://doi.org/10.1371/journal.pone.0071805

Kumar, S., Anwer, R., Yadav, M., Sehrawat, N., Singh, M., & Kumar, V. (2021). Molecular Typing and Global Epidemiology of *Staphylococcus aureus*. *Current Pharmacology Reports*, *7*(5), 179–186. https://doi.org/10.1007/s40495-021-00264-7

Kumpitsch, C., Koskinen, K., Schöpf, V., & Moissl-Eichinger, C. (2019). The microbiome of the upper respiratory tract in health and disease. *BMC Biology*, *17*(1), 1–20. https://doi.org/10.1186/s12915-019-0703-z

Kupchan, S. M., Hemingway, R. J., & Hemingway, J. C. (1968). The isolation and characterization of hellebrigenin 3-acetate and hellebrigenin 3, 5-diacetate, bufadienolide tumor inhibitors from *Bersama abyssinica*. *Tetrahedron Letters*, *9*(2), 149-152. https://doi.org/https://doi.org/10.1016/S0040-4039(00)75577-8

Kupchan, S. M., Maniot, J. L., Sigel, C. W., & Hemingway, R. J. (1971). 3-Epiberscillogenin ,

Three New Cytotoxic Bufadienolides from *Bersama abyssinica* of Cytotoxic Extract. *Journal of Organic Chemistry*, *36*(2611–2616). https://doi.org/10.1021/bk-1985-0276.ch012

Kupchan, S. M., Ognyanov, I., & Moniot, J. L. (1971). Tumor inhibitors. LXIV. isolation and structural elucidation of novel bufadienolides, the cytotoxic principles of *Bersama abyssinica*. *Bioorganic Chemistry*, *1*(1–2), 13–31. https://doi.org/10.1016/0045-2068(71)90003-4

Kusari, S., Pandey, S. P., & Spiteller, M. (2013). Untapped mutualistic paradigms linking host plant and endophytic fungal production of similar bioactive secondary metabolites. *Phytochemistry*, *91*, 81–87. https://doi.org/10.1016/j.phytochem.2012.07.021

Lai, D., Wang, A., Cao, Y., Zhou, K., Mao, Z., Dong, X., Tian, J., Xu, D., Dai, J., Peng, Y., Zhou, L., & Liu, Y. (2016). Bioactive Dibenzo-α-pyrone Derivatives from the Endophytic Fungus *Rhizopycnis vagum* Nitaf22. *Journal of Natural Products*, *79*(8), 2022–2031. https://doi.org/10.1021/acs.jnatprod.6b00327

Lambert, P. A. (2002). Cellular impermeability and uptake of biocides and antibiotics in Gram-positive bacteria and mycobacteria. *Journal of Applied Microbiology Symposium Supplement*, *92*(1), 46–54. https://doi.org/10.1046/j.1365-2672.92.5s1.7.x

Lan, D., & Wu, B. (2020). Chemistry and bioactivities of secondary metabolites from the genus *Talaromyces. Chemistry & Biodiversity*, *17*(8), e2000229. https://doi.org/https://doi.org/10.1002/cbdv.202000229

Lavoie, S., Ouellet, M., Fleury, P. Y., Gauthier, C., Legault, J., & Pichette, A. (2016). Complete 1H and 13C NMR assignments of a series of pergalloylated tannins. *Magnetic Resonance in Chemistry*, *54*(2), 168–174. https://doi.org/10.1002/mrc.4328

Lee, A. J., Cadelis, M. M., Kim, S. H., Swift, S., Copp, B. R., & Villas-Boas, S. G. (2020). Epipyrone A, a Broad-Spectrum Antifungal Compound Produced by *Epicoccum nigrum* ICMP 19927. *Molecules*, *25*(24), 5997. https://doi.org/10.3390/25245997

Lee, W. J., Sim, H. B., Jang, Y. H., Lee, S.-J., Kim, D. W., Jun, J. B., & Bang, Y. J. (2016). Skin Infection due to *Trichophyton tonsurans* Still Occurs in People in Korea but not as Outbreaks Weon. *Journal of Korean Medical Science*, *31*(2015), 296–300. http://dx.doi.org/10.3346/

Lefèvre-Utile, A., Braun, C., Haftek, M., & Aubin, F. (2021). Five functional aspects of the

epidermal barrier. *International Journal of Molecular Sciences*, *22*(21), 1–14. https://doi.org/10.3390/ijms222111676

Lei, H., Lei, J., Zhou, X., Hu, M., Niu, H., Song, C., Chen, S., Liu, Y., & Zhang, D. (2019). Cytotoxic polyketides from the marine sponge-derived fungus *pestalotiopsis heterocornis* XWS03F09. *Molecules*, *24*(14), 5–12. https://doi.org/10.3390/molecules24142655

Li, C., Zhao, H., & Wang, B. (2021). Mesenchymal stem/stromal cells: Developmental origin, tumorigenesis and translational cancer therapeutics. *Translational Oncology*, *14*(1) 100948. https://doi.org/10.1016/j.tranon.2020.100948

Li, Q., Lei, S., Du, K., Li, L., Pang, X., Wang, Z., Wei, M., Fu, S., Hu, L., & Xu, L. (2016). RNA-seq based transcriptomic analysis uncovers α-linolenic acid and jasmonic acid biosynthesis pathways respond to cold acclimation in *Camellia japonica*. *Scientific Reports*, *6*(October), 1–13. https://doi.org/10.1038/srep36463

Li, X. B., Chen, G. Y., Liu, R. J., Zheng, C. J., Song, X. M., & Han, C. R. (2017). A new biphenyl derivative from the mangrove endophytic fungus *Phomopsis longicolla* HL-2232. *Natural Product Research*, *31*(19), 2264–2267. https://doi.org/10.1080/14786419.2017.1300799

Li, Z., Z., Hu, X., & Zhang, Q. (2013). Advanced hyphenated chromatographic- mass spectrometry in mycotoxin determination: Current status and prospects. *Mass Spectrometry Reviews*, *32*(6), 420-452. https://doi.org/10.1002/mas.21377

Lima, L. M., Silva, B. N. M. da, Barbosa, G., & Barreiro, E. J. (2020). β-lactam antibiotics: An overview from a medicinal chemistry perspective. *European Journal of Medicinal Chemistry*, *208*, 112829. https://doi.org/10.1016/j.ejmech.2020.112829

Lindahl, J. F., Grace, D., & Strand, T. (2015). The consequences of human actions on risks for infectious diseases: a review. *Infection Ecology and Epidemiology*, *5*(1), 30048. https://doi.org/10.3402/IEE.V5.30048

Liu, L., Johnson, H. L., Cousens, S., Perin, J., Scott, S., Lawn, J. E., Rudan, I., Campbell, H., Cibulskis, R., Li, M., Mathers, C., & Black, R. E. (2012). Global, regional, and national causes of child mortality: An updated systematic analysis for 2010 with time trends since 2000. *The Lancet*, *379*(9832), 2151–2161. https://doi.org/10.1016/S0140-6736(12)60560-1

Liu, S., Liu, X., Guo, L., Che, Y., & Liu, L. (2013). 2H- Pyran- 2- one and 2H- Furan- 2- one Derivatives from the Plant Endophytic Fungus *Pestalotiopsis fici*. *Chemistry & Biodiversity*,

10(11), 2007-2013. https://doi.org/https://doi.org/10.1002/cbdv.201200361

Lock, J. A. (1962). Cardiotonic substances from *Bersama abyssinica* fres. sub. species *abyssinica*. *Journal of Pharmacy and Pharmacology*, *14*, 496–502. https://doi.org/10.1111/j.2042-7158.1962.tb11128.x

Luan, Y., Wei, H., Zhang, Z., Che, Q., Liu, Y., Zhu, T., Mándi, A., Kurtán, T., Gu, Q., & Li, D. (2014). Eleganketal A, a highly oxygenated dibenzospiroketal from the marine-derived fungus *Spicaria elegans* KLA03. *Journal of Natural Products*, *77*(7), 1718–1723. https://doi.org/10.1021/np500458a

Luca, M., Musumeci, M. L., D'Agata, E., & Micali, G. (2020). Depression and sleep quality in psoriatic patients: impact of psoriasis severity. *International Journal of Psychiatry in Clinical Practice*, *24*(1), 102-104. https://doi.org/https://doi.org/10.1080/13651501.2019.1659372

Lulekal, E., Rondevaldova, J., Bernaskova, E., Cepkova, J., Asfaw, Z., Kelbessa, E., Kokoska, L., & Van Damme, P. (2014). Antimicrobial activity of traditional medicinal plants from Ankober District, North Shewa Zone, Amhara Region, Ethiopia. *Pharmaceutical Biology*, *52*(5), 614–620. https://doi.org/10.3109/13880209.2013.858362

Lunardelli, N. de C. P., De, O. S. E., Aparecida, C.-P. D., Honorata, H. L. J., & Ikegaki, M. (2016). Importance and Implications of the Production of Phenolic Secondary Metabolites by Endophytic Fungi: A Mini-Review. *Mini Reviews in Medicinal Chemistry*, *16*(14), 259–271. DOI:10.2174/1389557515666151016123923

Luyen, N. D., Huong, L. M., Thi Hong Ha, T., Cuong, L. H., Thi Hai Yen, D., Nhiem, N. X., Tai, B. H., Gardes, A., Kopprio, G., & Van Kiem, P. (2019). Aspermicrones A-C, novel dibenzospiroketals from the seaweed-derived endophytic fungus *Aspergillus micronesiensis*. *Journal of Antibiotics*, *72*(11), 843–847. https://doi.org/10.1038/s41429-019-0214-8

Lv, L., Shao, X., Chen, H., Ho, C. T., & Sang, S. (2011). Genistein inhibits advanced glycation end product formation by trapping methylglyoxal. *Chemical Research in Toxicology*, *24*(4), 579–586. https://doi.org/10.1021/tx100457h

Madzinga, M., Kritzinger, Q., & Lall, N. (2018). Medicinal plants used in the treatment of superficial skin infections: From traditional medicine to herbal soap formulations. In *In Medicinal plants for holistic health and well-being*, pp. 255–275. Academic Press.

https://doi.org/10.1016/B978-0-12-812475-8.00008-1

Mah, T. F. (2012). Biofilm-specific antibiotic resistance. *Future Microbiology*, *7*(9), 1061-1072. https://doi.org/https://doi.org/10.2217/fmb.12.76

Mahajan, M., Kuiry, R., & Pal, P. K. (2020). Understanding the consequence of environmental stress for accumulation of secondary metabolites in medicinal and aromatic plants. *Journal of Applied Research on Medicinal and Aromatic Plants*, *18*(April), 100255. https://doi.org/10.1016/j.jarmap.2020.100255

Mahomoodally, M. F. (2013). Evidence - Based Complementary and Alternative Medicine Traditional Medicines in Africa : An Appraisal of Ten Potent African Medicinal Plants. *Evidence-Based Complementary and Alternative Medicine*, *2013*, 1–14. https://doi.org/10.1155/2013/617459

Maji, H. S., Chatterjee, R., Das, D., & Maji, S. (2023). *Fungal infection: An unrecognized threat. In Viral, parasitic, bacterial, and fungal infections*, pp. 625–644. Academic Press.

Maldonado, I., Elisiri, M. E., Monaco, M., Hevia, A., Larralde, M., Fox, B., & Fernández-Canigia, L. (2021). *Trichophyton benhamiae*, an emergent zoonotic pathogen in Argentina associated with Guinea pigs. *Revista Argentina de Microbiologia*, *54*(3), 203-208. https://doi.org/10.1016/j.ram.2021.02.004

Manganyi, M. C., & Ateba, C. N. (2020). Untapped potentials of endophytic fungi: A review of novel bioactive compounds with biological applications. *Microorganisms*, *8*(12), 1–25. https://doi.org/10.3390/microorganisms8121934

Martínez, J. L. (2007). Evolution of bacterial opportunistic pathogens. Evolutionary biology of bacterial and fungal pathogens, pp. 85-91. Wiley Online Library. https://doi.org/https://doi.org/10.1128/9781555815639.ch9

Mathewos, A., Feleke, W., Libsu, S., Mamo, F., Endale, M., & 1. (2018). Phytochemical Screening and Antibacterial Activity of Leaves Extract of *Senna*. *Jornal of Advanced Biotechnology and Zoology*, *2*(1), 59–65. https://fjs.fudutsinma.edu.ng/index.php/fjs/article/view/1260

Mattar, C., Edwards, S., Baraldi, E., & Hood, J. (2020). An overview of the global antimicrobial resistance research and development hub and the current landscape. *Current Opinion in Microbiology*, *57*, 56–61. https://doi.org/10.1016/j.mib.2020.06.009

Mccormack, V. A., & Boffetta, P. (2011). Today's lifestyles, tomorrow's cancers: Trends in

lifestyle risk factors for cancer in low- and middle-income countries. *Annals of Oncology*, *22*(11), 2349–2357. https://doi.org/10.1093/annonc/mdq763

McDermott, A. (2022). Drug-resistant fungi on the rise. *Proceedings of the National Academy of Sciences of the United States of America*, *119*(48), 1–5. https://doi.org/10.1073/pnas.2217948119

Meng, F., Lv, R., Cheng, M., Mo, F., Zhang, N., Qi, H., Liu, J., Chen, X., Liu, Y., Ghanizadeh, H., & Wang, A. (2022). Insights into the molecular basis of biocontrol of *Botrytis cinerea* by *Clonostachys rosea* in tomato. *Scientia Horticulturae*, *291*(July 2021), 110547. https://doi.org/10.1016/j.scienta.2021.110547

Mikkelsen, K., & Seberg, O. (2001). Morphometric analysis of the *Bersama abyssinica* Fresen. complex (Melianthaceae) in East Africa. *Plant Syst. Evol.*, *227*, 157–182. https://doi.org/https://doi.org/10.1007/s006060170046

Miller, W. R., Munita, J. M., & Arias, C. A. (2014). Mechanisms of antibiotic resistance in enterococci. *Expert Review of Anti-Infective Therapy*, *12*(10), 1221-1236. https://doi.org/https://doi.org/10.1586/14787210.2014.956092

Mirzaei, R., Mohammadzadeh, R., Sholeh, M., Karampoor, S., Abdi, M., Dogan, E., Moghadam, M. S., Kazemi, S., Jalalifar, S., Dalir, A., Yousefimashouf, R., Mirzaei, E., Khodavirdipour, A., & Alikhani, M. Y. (2020). The importance of intracellular bacterial biofilm in infectious diseases. *Microbial Pathogenesis*, *147*(March), 104393. https://doi.org/10.1016/j.micpath.2020.104393

Mishra, B. B., & Tiwari, V. K. (2011). Natural products: An evolving role in future drug discovery. *European Journal of Medicinal Chemistry*, *46*(10), 4769–4807. https://doi.org/10.1016/j.ejmech.2011.07.057

Mohammed, M. J., Anand, U., Altemimi, A. B., Tripathi, V., Guo, Y., & Pratap-Singh, A. (2021). Phenolic composition, antioxidant capacity and antibacterial activity of white wormwood (Artemisia herba-alba). *Plants*, *10*(1), 1–14. https://doi.org/10.3390/plants10010164

Moniuszko-Szajwaj, B., Pecio, Ł., Kowalczyk, M., & Stochmal, A. (2016). New bufadienolides isolated from the roots of *kalanchoe daigremontiana* (crassulaceae). *Molecules*, *21*(3). https://doi.org/10.3390/molecules21030243

Moore, A., & Pinkerton, R. (2007). Vincristine: Can its therapeutic index be enhanced?.

Pediatric Blood & Cancer, *53*(7), 1180–1187. https://doi.org/https://doi.org/10.1002/pbc.22161

Morris, S., & Cerceo, E. (2020). Trends, epidemiology, and management of multi-drug resistant gram-negative bacterial infections in the hospitalized setting. *Antibiotics*, *9*(4), 1–20. https://doi.org/10.3390/antibiotics9040196

Mossmann, P. B. (1983). Rapid colorimetric assay for cellular growth and survival: application to proliferation and cytotoxicity assays. *Jornal of Immunology Methods*, *65*, 49-53. https://doi.org/1574231874990851840

Moto, J. N., Maingi, J. M., & Nyamache, A. K. (2015). Prevalence of *Tinea capitis* in school going children from Mathare, informal settlement in Nairobi, Kenya. *BMC Research Notes*, *8*(1), 1–4. https://doi.org/10.1186/s13104-015-1240-7

Murata, M., Midorikawa, K., Koh, M., Umezawa, K., & Kawanishi, S. (2004). Genistein and Daidzein Induce Cell Proliferation and Their Metabolites Cause Oxidative DNA Damage in Relation to Isoflavone-Induced Cancer of Estrogen-Sensitive Organs. *Biochemistry*, *43*(9), 2569–2577. https://doi.org/10.1021/bi035613d

Muvea, A. M., Meyhöfer, R., Subramanian, S., Poehling, H. M., Ekesi, S., & Maniania, N. K. (2014). Colonization of onions by endophytic fungi and their impacts on the biology of thrips tabaci. *PLoS ONE*, *9*(9), 1–7. https://doi.org/10.1371/journal.pone.0108242

Nadeem, S. F., Gohar, U. F., Tahir, S. F., Mukhtar, H., Pornpukdeewattana, S., Nukthamna, P., Moula Ali, A. M., Bavisetty, S. C. B., & Massa, S. (2020). Antimicrobial resistance: more than 70 years of war between humans and bacteria. *Critical Reviews in Microbiology*, *46*(5), 578–599. https://doi.org/10.1080/1040841X.2020.1813687

Nagaral, G. V., Veerabhadra Goud, G. K., & Sudha, P. (2018). Prevalence of *tinea corporis* and *tinea cruris* in Chitradurga rural population. *IP Indian J Clin Exp Dermatol*, *4*(3), 221–225.

Nahar, L., Onder, A., & Sarker, D. (2020). A review on the recent advances in HPLC, UHPLC and UPLC analyses of naturally occurring cannabinoids (2010–2019). *Phytochemical Analysis*, *31*(4), 413–457 https://doi.org/10.1002/pca.2906.

Naik, B., Goyal, S. K., Tripathi, A. D., & Kumar, V. (2019). Screening of agro-industrial waste and physical factors for the optimum production of pullulanase in solid-state fermentation from endophytic Aspergillus sp. *Biocatalysis and Agricultural Biotechnology*, *22*(November), 101423. https://doi.org/10.1016/j.bcab.2019.101423

Nandy, S., Mukherjee, A., Pandey, D. K., Ray, P., & Dey, A. (2020). Indian Sarsaparilla (*Hemidesmus indicus*): Recent progress in research on ethnobotany, phytochemistry and pharmacology. *Journal of Ethnopharmacology*, *254*(January), 112609. https://doi.org/10.1016/j.jep.2020.112609

Narmani, A., Teponno, R. B., Arzanlou, M., Surup, F., Helaly, S. E., Wittstein, K., Praditya, D. F., Babai-Ahari, A., Steinmann, E., & Stadler, M. (2019). Cytotoxic, antimicrobial and antiviral secondary metabolites produced by the plant pathogenic fungus Cytospora sp. CCTU A309. *Fitoterapia*, *134*(December), 314–322. https://doi.org/10.1016/j.fitote.2019.02.015

Nascimento, A. M., Conti, R., Turatti, I. C. C., Cavalcanti, B. C., Costa-Lotufo, L. V., Pessoa, C., de Moraes, M. O., Manfrim, V., Toledo, J. S., Cruz, A. K., & Pupo, M. T. (2012). Bioactive extracts and chemical constituents of two endophytic strains of *Fusarium oxysporum*. *Revista Brasileira de Farmacognosia*, *22*(6), 1276–1281. https://doi.org/10.1590/S0102-695X2012005000106

Nedialkov, P. T., & Kitanov, G. M. (2002). Two benzophenone O-arabinosides and a chromone from *Hypericum annulatum*. *Phytochemistry*, *59*(8), 867–871. https://doi.org/10.1016/S0031-9422(01)00484-8

Nenoff, P., Krüger, C., Ginter-Hanselmayer, G., & Tietz, H. J. (2014). Mycology-an update. Part 1: Dermatomycoses: Causative agents, epidemiology and pathogenesis. *JDDG - Journal of the German Society of Dermatology*, *12*(3), 188–210. https://doi.org/10.1111/ddg.12245

Nenoff, P., Uhrlaß, S., Krüger, C., Erhard, M., Hipler, U. C., Seyfarth, F., Herrmann, J., Wetzig, T., Schroedl, W., & Gräser, Y. (2014). *Trichophyton Spezies* von *Arthroderma benhamiae* - Ein neuer Infektionserreger in der Dermatologie. *JDDG - Journal of the German Society of Dermatology*, *12*(7), 571–582. https://doi.org/10.1111/ddg.12390

Newman, D. J., & Cragg, G. M. (2016). Natural Products as Sources of New Drugs from 1981 to 2014. *Journal of Natural Products*, *79*(3), 629–661. https://doi.org/10.1021/acs.jnatprod.5b01055

Nisa, H., Kamili, A. N., Nawchoo, I. A., Shafi, S., Shameem, N., & Bandh, S. A. (2015). Fungal endophytes as prolific source of phytochemicals and other bioactive natural products: A review. *Microbial Pathogenesis*, *82*, 50–59. https://doi.org/10.1016/j.micpath.2015.04.001

Nishimura, E., Murakami, S., Suzuki, K., Amano, K., Tanaka, R., & Shinada, T. (2016).

Structure Determination of monomeric phloroglucinol derivatives with a cinnamoyl group isolated from propolis of the stingless Bee, *Tetragonula carbonaria*. *Asian Journal of Organic Chemistry*, *5*(7), 5, 855–859. https://doi.org/https://doi.org/10.1002/ajoc.201600106

Nishino, K., Yamasaki, S., Nakashima, R., Zwama, M., & Hayashi-Nishino, M. (2021). Function and Inhibitory Mechanisms of Multidrug Efflux Pumps. *Frontiers in Microbiology*, *12*(December), 1–13. https://doi.org/10.3389/fmicb.2021.737288

Nogawa, T., Kamano, Y., Yamashita, A., & Pettit, G. R. (2001). Isolation and structure of five new cancer cell growth inhibitory bufadienolides from the Chinese traditional drug Ch'an Su. *Journal of Natural Products*, *64*(9), 1148–1152. https://doi.org/10.1021/np0101088

Nweze, E. I., & Eke, I. E. (2018). Dermatophytes and dermatophytosis in the eastern and southern parts of Africa. *Medical Mycology*, *56*(1), 13–28. https://doi.org/10.1093/mmy/myx025

Nyamboki, D. K., Bedane, K. G., Hassan, K., Brieger, L., Strohmann, C., Spiteller, M., & Matasyoh, J. C. (2021). Cytotoxic Compounds from the Stem Bark of Two subsp. Of *Bersama abyssinica*. *Journal of Natural Products*, *84*(5), 1453–1458. https://doi.org/10.1021/acs.jnatprod.0c01141

Omwenga, E. O., Hensel, A., Shitandi, A., & Goycoolea, F. M. (2015). Ethnobotanical survey of traditionally used medicinal plants for infections of skin, gastrointestinal tract, urinary tract and the oral cavity in Borabu sub-county, Nyamira county, Kenya. *Journal of Ethnopharmacology*, *176*, 508–514. https://doi.org/10.1016/j.jep.2015.11.032

Pandey, A., Soccol, C. R., & Mitchell, D. (2000). New developments in solid state fermentation: I-bioprocesses and products. *Process Biochemistry*, *35*, 1153–1169. https://doi.org/10.1007/978-1-4020-9942-7_2

Pant, P., Pandey, S., & Dall'Acqua, S. (2021). The Influence of Environmental Conditions on Secondary Metabolites in Medicinal Plants: A Literature Review. *Chemistry and Biodiversity*, *18*(11), e2100345. https://doi.org/10.1002/cbdv.202100345

Parasuraman, S., Rao, A., Balamurugan, S., Muralidharan, S., Jayaraj Kumar, K., & Vijayan, V. (2014). An Overview of Liquid Chromatography-Mass Spectroscopy Instrumentation. *Pharmaceutical Methods*, *5*(2), 47–55. https://doi.org/10.5530/phm.2014.2.2

Parija, S. C. (2023). "Bacillus." Textbook of Microbiology and Immunology, pp. 407-418.

Singapore: *Springer Nature*.

Paterson, I. K., Hoyle, A., Ochoa, G., Baker-Austin, C., & Taylor, N. G. H. (2016). Optimising antibiotic usage to treat bacterial infections. *Scientific Reports*, *6*(November), 1–10. https://doi.org/10.1038/srep37853

Pimentel, M. R., Molina, G., Dionísio, A. P., Maróstica Junior, M. R., & Pastore, G. M. (2011). The Use of Endophytes to Obtain Bioactive Compounds and Their Application in Biotransformation Process. *Biotechnology Research International*, *2011*(9), 1–11. https://doi.org/10.4061/2011/576286

Pirofski, L. A., & Casadevall, A. (2020). The state of latency in microbial pathogenesis. *Journal of Clinical Investigation*, *130*(9), 4525–4531. https://doi.org/10.1172/JCI136221

Pomin, H. V. (2012). Unravelling Glycobiology by NMR Spectroscopy. In *Glycosylation* (Issue September 2012, pp. 63–98). https://doi.org/10.5772/48136

Prabhu, S. R. (2023). Infectious and Communicable Diseases: An Overview. *Textbook of General Pathology for Dental Students*, pp. 63-72. Springer. https://doi.org/https://doi.org/10.1007/978-3-031-31244-1_9

Qiang, Q., Gao, Y., Yu, B., Wang, M., Ni, W., Li, S., Zhang, T., Li, W., & Lin, L. (2020). Elevated CO2 enhances growth and differentially affects saponin content in *Paris polyphylla* var. *yunnanensis*. *Industrial Crops and Products*, *147*(February), 112-124. https://doi.org/10.1016/j.indcrop.2020.112124

Radušienė, J., Karpavičienė, B., & Stanius, Ž. (2013). Effect of External and Internal Factors on Secondary Metabolites Accumulation in St. John's Worth. *Botanica Lithuanica*, *18*(2), 101–108. https://doi.org/10.2478/v10279-012-0012-8

Rahimi, S., & Hasanloo, T. (2016). The effect of temperature and pH on biomass and bioactive compounds production in *Silybum marianum* hairy root cultures. *Research Journal of Pharmacognosy (RJP)*, *3*(2), 53–59. http://rjpharmacognosy.ir

Ramabulana, A. T., Petras, D., Madala, N. E., & Tugizimana, F. (2021). Metabolomics and molecular networking to characterize the chemical space of four momordica plant species. *Metabolites*, *11*(11), 11–14. https://doi.org/10.3390/metabo11110763

Ramakrishna, A., & Ravishankar, G. A. (2011). Influence of abiotic stress signals on secondary metabolites in plants. *Plant Signaling and Behavior*, *6*(11), 1720–1731. https://doi.org/10.4161/psb.6.11.17613

Ramirez, M. S., & Tolmasky, M. E. (2010). Aminoglycoside modifying enzymes. *Drug Resistance Updates*, *13*(6), 151–171. https://doi.org/10.1016/j.drup.2010.08.003

Ramos, S., Silva, V., Dapkevicius, E. M. de L., Caniça, M., Tejedor-Junco, M. T., Igrejas, G., & Patrícia, P. (2020). *Escherichia coli* as Commensal and Pathogenic Bacteria among Food-Producing Animals: Health Implications of Extended Spectrum β-Lactamase (ESBL) Production. *Animals*, *10*(12), 2–15. https://doi.org/10.3390/ani10122239

Rancon, S., Chaboud, A., Darbour, N., Comte, G., Bayet, C., Simon, P. N., Raynaud, J., Di Pietro, A., Cabalion, P., & Barron, D. (2001). Natural and synthetic benzophenones: Interaction with the cytosolic binding domain of P-glycoprotein. *Phytochemistry*, *57*(4), 553–557. https://doi.org/10.1016/S0031-9422(01)00120-0

Randall, C. P., Mariner, K. R., Chopra, I., & O'Neill, A. J. (2013). The target of daptomycin is absent from *Escherichia coli* and other gram-negative pathogens. *Antimicrobial Agents and Chemotherapy*, *57*(1), 637–639. https://doi.org/10.1128/AAC.02005-12

Rashmi, M., Kushveer, J. S., & Sarma, V. V. (2019). Secondary Metabolites Produced by Endophytic Fungi from Marine Environments, Endophytes and Secondary Metabolites, pp. 491-526. Springer international publishing.

Réblová, M., Hubka, V., Thureborn, O., Lundberg, J., Sallstedt, T., Wedin, M., & Ivarsson, M. (2016). From the tunnels into the treetops: New lineages of black yeasts from biofilm in the Stockholm metro system and their relatives among ant-associated fungi in the *chaetothyriales*. *PLoS ONE*, *11*(10), 1–36. https://doi.org/10.1371/journal.pone.0163396

Regassa, R. (2013). Assessment of indigenous knowledge of medicinal plant practice and mode of service delivery in Hawassa city, southern Ethiopia. *Journal of Medicinal Plants Research*, *7*(9), 517–535. https://doi.org/10.5897/JMPR012.1126

Reygaert, W. (2009). Methicillin-resistant *Staphylococcus aureus* (MRSA): molecular aspects of antimicrobial resistance and virulence. *Clinical Laboratory Science*, *22*(2), 115. http://hwmaint.clsjournal.ascls.org/

Reygaert, W. C. (2018). An overview of the antimicrobial resistance mechanisms of bacteria. *AIMS Microbiology*, *4*(3), 482-501. https://doi.org/doi: 10.3934/microbiol.2018.3.482

Robicsek, A., Strahilevitz, J., Jacoby, G. A., Macielag, M., Abbanat, D., Hye Park, C., & Hooper, D. C. (2006). Fluoroquinolone-modifying enzyme: a new adaptation of a common aminoglycoside acetyltransferase. *Nature Medicine*, *12*(1), 83-88.

https://doi.org/https://doi.org/10.1038/nm1347

Robinson, T., Singh, D., & Nigam, P. (2001). Solid-state fermentation: a promising microbial technology for secondary metabolite production. *Applied Microbiology and Biotechnology*, *55*, 284–289. https://doi.org/https://doi.org/10.1007/s002530000565

Romano, C., Gianni, C., & Papini, M. (2001). Tinea capitis in infants less than 1 year of age. *Pediatric Dermatology*, *18*(6), 465-468. https://doi.org/10.1046/j.1525-1470.2001.1861997.x

Rook, K. A., & Abraham, J. L. (2022). Dermatologic Emergencies. In Feline Emergency and Critical Care Medicine, pp. 453–477. Wiley Online Library. https://doi.org/https://doi.org/10.1002/9781119565925.ch37

Rossney, A. S., Shore, A. C., Morgan, P. M., Fitzgibbon, M. M., O'Connell, B., & Coleman, D. C. (2007). The emergence and importation of diverse genotypes of methicillin-resistant *Staphylococcus aureus* (MRSA) harboring the panton-valentine leukocidin gene (pvl) reveal that pvl is a poor marker for community-acquired MRSA strains in Ireland. *Journal of Clinical Microbiology*, *45*(8), 2554–2563. https://doi.org/10.1128/JCM.00245-07

Ruszkowski, J. J., Hetman, M., Turlewicz-Podbielska, H., & Pomorska-Mól, M. (2021). Hedgehogs as a potential source of zoonotic pathogens—a review and an update of knowledge. *Animals*, *11*(6), 1–13. https://doi.org/10.3390/ani11061754

Sadorn, K., Saepua, S., Boonyuen, N. Laksanacharoen, P. Rachtawee, P., & Pittayakhajonwut, P. (2016). Antimicrobial activity and cytotoxicity of polyketides isolated from the mushroom *Xerula* sp. BCC56836. *RSC Advances*, *6*(97), 94510-94523. https://doi.org/DOI https://doi.org/10.1039/C6RA21898A

Sahoo, A., & Mahajan, R. (2016). Management of *tinea corporis*, *tinea cruris*, and *tinea pedis*: A comprehensive review. *Indian Dermatology Online Journal*, *7*(2), 77. https://doi.org/10.4103/2229-5178.178099

Samanta, I. (2015). Veterinary mycology. pp 11606. Springer India. https://doi.org/10.1007/978-81-322-2280-4

Sampaio, B. L., Edrada-Ebel, R., & Da Costa, F. B. (2016). Effect of the environment on the secondary metabolic profile of *Tithonia diversifolia*: A model for environmental metabolomics of plants. *Scientific Reports*, *6*(October), 1–11. https://doi.org/10.1038/srep29265

Sankaranarayanan, R. (2014). Screening for cancer in low- and middle-income countries. *Annals of Global Health*, *80*(5), 412–417. https://doi.org/10.1016/j.aogh.2014.09.014

Scarpa, M. A., Etchecopaz, A. N., Abrantes, R. A., Mas, J. A., Romero Núñez, C., & Miranda Contreras, L. (2021). Dermatophytosis caused by *Trichophyton benhamiae* in a dog. *Veterinary Dermatology*, *32*(3), 297-381. https://doi.org/https://doi.org/10.1111/vde.12944

Schmelzer, G. H., & Gurib-Fakim, A. (2013). Plant resources of tropical Africa. In G. H. Schmelzer & A. Gurib-Fakim (Eds.), *medicinal plants*, pp.384. medicinal plants.

Schwarz, S., Kehrenberg, C., Doublet, B., & Cloeckaert, A. (2004). Molecular basis of bacterial resistance to chloramphenicol and florfenicol. *FEMS Microbiology Reviews*, *28*(5), 519–542. https://doi.org/10.1016/j.femsre.2004.04.001

Sefton, A. (2002). "Mechanisms of antimicrobial resistance: their clinical relevance in the new millennium." *Drugs*, *62*, 557-566. https://doi.org/10.2165/00003495-200262040-00001

Selim, M. S. M., Abdelhamid, S. A., & Mohamed, S. S. (2021). Secondary metabolites and biodiversity of actinomycetes. *Journal of Genetic Engineering and Biotechnology*, *19*(1), 557-566. https://doi.org/10.1186/s43141-021-00156-9

Severi, J. A., Lima, Z. P., Kushima, H., Brito, A. R. M. S., Santos, L. C. Dos, Vilegas, W., & Hiruma-Lima, C. A. (2009). Polyphenols with antiulcerogenic action from aqueous decoction of mango leaves (*Mangifera indica* L.). *Molecules*, *14*(3), 1098–1110. https://doi.org/10.3390/molecules14031098

Seyoum, G., & Zerihun, G. (2014). An ethnobotanical study of medicinal plants in Debre Libanos Wereda, Central Ethiopia. *African Journal of Plant Science*, *8*(7), 366–379. https://doi.org/10.5897/ajps2013.1041

Shahat, A. A., Hassan, R. A., Nazif, N. M., Van Miert, S., Pieters, L., Hammuda, F. M., & Vlietinck, A. J. (2003). Isolation of Mangiferin from *Bombax malabaricum* and Structure Revision of Shamimin. *Planta Medica*, *69*(11), 1068–1070. https://doi.org/10.1055/s-2003-45161

Sharma, A., Malhotra, B., Kharkwal, H., Kulkarni, G. T., & Kaushik, N. (2020). Therapeutic agents from endophytes harbored in Asian medicinal plants. *Phytochemistry Reviews*, *19*(6), 691-720. https://doi.org/10.1007/s11101-020-09683-8

Sharma, S., Walia, S., Rathore, S., Kumar, P., & Kumar, R. (2020). Combined effect of elevated CO2 and temperature on growth, biomass and secondary metabolite of *Hypericum*

perforatum L. in a western Himalayan region. *Journal of Applied Research on Medicinal and Aromatic Plants*, *16*(July 2019), 100239. https://doi.org/10.1016/j.jarmap.2019.100239

Sharquie, K. E., & Jabbar, R. I. (2021). Major Outbreak of Dermatophyte Infections Leading Into Imitation of Different Skin Diseases: *Trichophyton Mentagrophytes* is the Main Criminal Fungus. *Journal of the Turkish Academy of Dermatology*, *15*(4), 91–100. https://doi.org/10.4274/jtad.galenos.2021.83007

Sheldrick, G. M. (2008). A short history of SHELX. *Acta Crystallographica Section A: Foundations of Crystallography*, *64*(1), 112–122. https://doi.org/https://doi.org/10.1107/S0108767307043930

Sheldrick, G. M. (2015). SHELXT–Integrated space-group and crystal-structure determination. *Acta Crystallographica Section A: Foundations and Advances*, *71*(1), 3-8. https://doi.org/https://doi.org/10.1107/S2053273314026370

Shen, A. Q., Munteanu, M., & Khoury, H. J. (2014). Updated Product Label Allows Home Administration of Omacetaxine Mepesuccinate. *The Oncologist*, *19*(11), e14–e14. https://doi.org/10.1634/theoncologist.2014-0230

Shinde, K., Shinde, V., Sharma, K., & Mahadik, K. (2010). Phytochemical and Pharmacological Investigation on *Vitex negundo* Linn. *Planta Medica*, *76*(5), 77. https://doi.org/10.1055/s-0030-1251839

Shinu, P., Al Mouslem, A. K., Nair, A. B., Venugopala, K. N., Attimarad, M., Singh, V. A., Nagaraja, S., Alotaibi, G., & Deb, P. K. (2022). Progress Report: Antimicrobial Drug Discovery in the Resistance Era. *Pharmaceuticals*, *15*(4), 413. https://doi.org/10.3390/ph15040413

Shoeb, M. (2008). Anticancer agents from medicinal plants. *Bangladesh Journal of Pharmacology*, *1*(2), 35–41. https://doi.org/10.3329/bjp.v1i2.486

Shrestha, L. B., Baral, R., & Khanal, B. (2019). Comparative study of antimicrobial resistance and biofilm formation among Gram-positive uropathogens isolated from community-acquired urinary tract infections and catheter-associated urinary tract infections. *Infection and Drug Resistance*, *2019*(12), 957–963. https://doi.org/10.2147/IDR.S200988

Shu, X., Zhang, Y., Guan, L., Chen, Z., Huang, M., Chen, X., & Yuan, C. (2020). Antibacterial secondary metabolites of *Clonostachys rosea*, an endophytic fungus from *Blumea balsamifera* (L.) DC. Sheng wu Gong Cheng xue bao=. *Chinese Journal of Biotechnology*,

36(8), 1650–1658. https://doi.org/10.13345/j.cjb.190555

Siavash, M. S., Ibrahim, R., Damalas, C. A., & Noorhosseini, S. A. (2017). Effects of Gamma Stress and Carbon Dioxide on Eight Bioactive Flavonoids and Photosynthetic Efficiency in *Centella asiatica*. *Journal of Plant Growth Regulation*, *36*(4), 957–969. https://doi.org/10.1007/s00344-017-9700-z

Silva-Hughes, A. F., Wedge, D. E., Cantrell, C. L., Carvalho, C. R., Pan, Z., Moraes, R. M., Madoxx, V. L., & Rosa, L. H. (2015). Diversity and antifungal activity of the endophytic fungi associated with the native medicinal cactus *Opuntia humifusa* (Cactaceae) from the United States. *Microbiological Research*, *175*(6), 67–77. https://doi.org/10.1016/j.micres.2015.03.007

Silva, D. A. F., Liotti, R. G., Ana Paula deAraújo, B., De Melo Reis, É., Passos, M. B. S., Dos Santos, E. L., Sampaio, O. M., Januário, A. H., Branco, C. L. B., Da Silva, G. F., De Mendonça, E. A. F., & Soares, M. A. (2018). Diversity of cultivable fungal endophytes in *Paullinia cupana* (Mart.) Ducke and bioactivity of their secondary metabolites. In *PLoS ONE*, *13*(4), e0195874. https://doi.org/10.1371/journal.pone.0195874

Sinan, K. I., Chiavaroli, A., Orlando, G., Bene, K., Zengin, G., Cziáky, Z., Jekő, J., Mahomoodally, M. F., Picot-Allain, M. C. N., Menghini, L., Recinella, L., Brunetti, L., Leone, S., Ciferri, M. C., Di Simone, S., & Ferrante, C. (2020). Biopotential of *Bersama abyssinica* fresen stem bark extracts: UHPLC profiles, antioxidant, enzyme inhibitory, and antiproliferative propensities. *Antioxidants*, *9*(2), 163. https://doi.org/10.3390/antiox9020163

Sinan, K. I., Kouadio, B., Gokhan, Z., Alina, D., József, J., Cziáky, Z., Carene, M. N. P.-A., Adriano, M., Kannan, R. R., & Fawzi, M. M. (2021). A comparative study of the HPLC-MS profiles and biological efficiency of different solvent leaf extracts of two African plants: *Bersama abyssinica* and *Scoparia dulcis*. *International Journal of Environmental Health Research*, *31*(3), 285-297. https://doi.org/https://doi.org/10.1080/09603123.2019.1652885

Sivars, L., Palsdottir, K., Crona Guterstam, Y., Falconer, H., Hellman, K., & Tham, E. (2023). The current status of cell-free *human papillomavirus* DNA as a biomarker in cervical cancer and other HPV-associated tumors: A review. *International Journal of Cancer*, *152*(11), 2232–2242. https://doi.org/10.1002/ijc.34333

Soltani, S., Emamie, A., Dastranj, M., Farahani, A., Abolfazl, D., & Parviz, M. (2018). “Role of

toxins of uropathogenic *Escherichia coli* in development of urinary tract infection." *Journal of Pharmaceutical Research International*, *21*(1), 1-11. DOI: 10.9734/JPRI/2018/39188

Soto, S. M. (2013). Role of efflux pumps in the antibiotic resistance of bacteria embedded in a biofilm. *Virulence*, *4*(3), 223–229. https://doi.org/10.4161/viru.23724

Sousa, C. P. (2006). The Versatile Strategies of *Escherichia coli* Pathotypes: A Mini Review. *J. Venom. Anim. Toxins Incl. Trop. Dis.*, *12*(3), 363–373. https://doi.org/10.1590/S1678-91992006000300002

Spanamberg, A., Ravazzolo, A., Araujo, R., Tomazi, N., Fuentes, B., & Ferreiro, L. (2023). Molecular detection and species identification of dermatophytes by SYBR-Green real-time PCR in-house methodology using hair samples obtained from dogs and cats. *Medical Mycology Mycol. ., 61*(5), 1–6. https://doi.org/10.1093/mmy/myad047.

Steyn, P. S., & Van Heerden, F. R. (1998). Bufadienolides of plant and animal origin. *Natural Product Reports*, *15*(4), 397-413. https://doi.org/10.1039/A815397Y

Steyn, Pieter. S, & van Heerden, F. R. (1998). Bufadienolides of plant and animal origin. *Natural Product Reports*, *15*(4), 397–413. DOI: 10.1039/A815397Y

Strobel, G., & Daisy, B. (2003). Bioprospecting for microbial endophytes and their natural products. *Microbiology and Molecular Biology Reviews*, *67*(4), 491–502. https://doi.org/10.55734/nbujps.2015.v09i01.001

Subban, K., Subramani, R., & Johnpaul, M. (2013). A novel antibacterial and antifungal phenolic compound from the endophytic fungus *Pestalotiopsis mangiferae*. *Natural Product Research*, *27*(16), 1445-1449. https://doi.org/https://doi.org/10.1080/14786419.2012.722091

Subramaniyam, R., & Vimala, R. (2012). Solid State and Submerged Fermentation for the Production of Bioactive Substances *: a Comparative Study*. *3*(3), 480–486. https://doi.org/10.1016/j.biotechadv.2011.01.008

Sun, R. R., Miao, F. P., Zhang, J., Wang, G., Yin, X. L., & Ji, N. Y. (2013). Three new xanthone derivatives from an algicolous isolate of *Aspergillus wentii*. *Magnetic Resonance in Chemistry*, *51*(1), 65-68. https://doi.org/https://doi.org/10.1002/mrc.3903

Supratman, U., Fujita, T., Akiyama, K., Hayashi, H., Murakami, A., Sakai, H., & Ohigashi, H. (2001). Anti-tumor Promoting Activity of Bufadienolides from *Kalanchoe pinnata* and *K. daigremontiana* butiflora. *Bioscience, Biotechnology, and Biochemistry*, *65*(4), 947-949.

https://doi.org/https://doi.org/10.1271/bbb.65.947

Supratman, U., Suzuki, T., Nakamura, T., Yokoyama, Y., Harneti, D., Maharani, R., & Shiono, Y. (2019). New metabolites produced by endophyte *Clonostachys rosea* B5− 2. *Natural Product Research*, *35*(9), 1525-1531. https://doi.org/https://doi.org/10.1080/14786419.2019.1656629

Suresh, J. I., & Sona, N. M. (2021). Fungal endophytes, biodiversity and biopotential applications. In *Fungi Bio-Prospects in Sustainable Agriculture, Environment and Nano-Technology*, pp. 107–115. Academic Press. https://doi.org/https://doi.org/10.1016/B978-0-12-821394-0.00005-6

Syed, Y. Y. (2021). Cefiderocol: A Review in Serious Gram-Negative Bacterial Infections. *Drugs*, *81*(13), 1559–1571. https://doi.org/10.1007/s40265-021-01580-4

Talib, W. H., Daoud, S., Mahmod, A. I., Hamed, R. A., Awajan, D., Abuarab, S. F., Odeh, L. H., Khater, S., & Al Kury, L. T. (2022). Plants as a Source of Anticancer Agents: From Bench to Bedside. *Molecules*, *27*(15), 4818. https://doi.org/10.3390/molecules27154818

Talontsi, F. M., Dittrich, B., Schüffler, A., Sun, H., & Laatsch, H. (2013a). Epicoccolides: Antimicrobial and antifungal polyketides from an endophytic fungus *Epicoccum* sp. associated with *Theobroma cacao*. *European Journal of Organic Chemistry*, 2013(*15*), 3174–3180. https://doi.org/10.1002/ejoc.201300146

Talontsi, F. M., Dittrich, B., Schüffler, A., Sun, H., & Laatsch, H. (2013b). Epicoccolides: Antimicrobial and antifungal polyketides from an endophytic fungus Epicoccum sp. associated with *Theobroma cacao*. *European Journal of Organic Chemistry*, *2013*(15), 3174–3180. https://doi.org/10.1002/ejoc.201300146

Tamura, Y. (2010). Current Approach to Rodents as Patients. *Journal of Exotic Pet Medicine*, *19*(1), 36–55. https://doi.org/10.1053/j.jepm.2010.01.014

Tang, C., Kong, X., Ahmed, S. A., Thakur, R., Chowdhary, A., Nenoff, P., Uhrlass, S., Verma, S. B., Meis, J. F., Kandemir, H., Kang, Y., & de Hoog, G. S. (2021). Taxonomy of the *Trichophyton mentagrophytes*/*T. interdigitale* Species Complex Harboring the Highly Virulent, Multiresistant Genotype *T. indotineae*. *Mycopathologia*, *186*(3), 315–326. https://doi.org/10.1007/s11046-021-00544-2

Tanvir, R., Javeed, A., & Bajwa, A. G. (2017). Endophyte bioprospecting in South Asian medicinal plants: an attractive resource for biopharmaceuticals. *Applied Microbiology and*

Biotechnology, *101*, 1831-1844. https://doi.org/10.1007/s00253-017-8115-x

Tariq, A., Sadia, S., Pan, K., Ullah, I., Mussarat, S., Sun, F., Abiodun, O. O., Batbaatar, A., Li, Z., Song, D., Xiong, Q., Ullah, R., Khan, S., Basnet, B. B., Kumar, B., Islam, R., & Adnan, M. (2017). A systematic review on ethnomedicines of anti-cancer plants. *Phytotherapy Research*, *31*(2), 202–264. https://doi.org/10.1002/ptr.5751

Thakur, V., Uniyal, A., & Tiwari, V. (2021). A comprehensive review on pharmacology of efflux pumps and their inhibitors in antibiotic resistance. *European Journal of Pharmacology*, *903*(May), 174151. https://doi.org/10.1016/j.ejphar.2021.174151

Tian, H. Y., Wang, L., Zhang, X. Q., Zhang, D. M., Wang, Y., Liu, J. S., Jiang, R. W., & Ye, W. C. (2010). New bufadienolides and C23 steroids from the venom of Bufo bufo gargarizans. *Steroids*, *75*(12), 884–890. https://doi.org/10.1016/j.steroids.2010.05.013

Tiwari, S., Nanda, M., Pattanaik, S., Shivakumar, G. C., Sunila, B. S., Cicciù, M., & Minervini, G. (2023). Analytical Study on Current Trends in the Clinico-Mycological Profile among Patients with Superficial Mycoses. *Journal of Clinical Medicine*, *12*(9), 3051. https://doi.org/10.3390/jcm12093051

Topcu, G., & Ulubelen, A. (2007).. Structure elucidation of organic compounds from natural sources using 1D and 2D NMR techniques *Journal of Molecular Structure*, *834*(5) 57–73. https://doi.org/10.1016/j.molstruc.2006.12.001

Ullrich, S. F., Rothauer, A., Hagels, H., & Kayser, O. (2017). Influence of light, temperature, and macronutrients on growth and scopolamine biosynthesis in Duboisia species. *Planta Medica*, *83*(11), 937-945. https://doi.org/10.1055/s-0043-106435

UNICEF. (2004). *The state of the World's children 2005. Childhood under the threat of internet.* https://doi.org/https://www.unicef.org/publications/index_24432.html

Uttpal, A., Jacobo-Herrera, N., Altemimi, A., & Lakhssassi, N. (2019). A comprehensive review on medicinal plants as antimicrobial therapeutics: Potential avenues of biocompatible drug discovery. *Metabolites*, *9*(11), 1–13. https://doi.org/10.3390/metabo9110258

Uttpal, A., Tudu, C. K., Nandy, S., Sunita, K., Tripathi, V., Loake, G. J., Dey, A., & Proćków, J. (2022). Ethnodermatological use of medicinal plants in India: From ayurvedic formulations to clinical perspectives – A review. *Journal of Ethnopharmacology*, *284*(2), 114744. https://doi.org/10.1016/j.jep.2021.114744

Vasundhara, M., Kumar, A., & Reddy, M. S. (2016). Molecular approaches to screen bioactive

compounds from endophytic fungi. *Frontiers in Microbiology*, *7*(11), 1–12. https://doi.org/10.3389/fmicb.2016.01774

Venkatesan, G., Singh, A. J. A. R., Murugesan, A. G., Janaki, C., & Gokul Shankar, S. (2007). *Trichophyton rubrum*-the predominant etiological agent in human dermatophytoses in Chennai, India. *African Journal of Microbiology Research*, *1*(1), 9–12. http://www.academicjournals.org/ajmr

Ververidis, F., Trantas, E., Douglas, C., Vollmer, G., Kretzschmar, G., & Panopoulos, N. (2007). Biotechnology of flavonoids and other phenylpropanoid- derived natural products. Part I: Chemical diversity, impacts on plant biology and human health. *Biotechnology Journal: Healthcare Nutrition Technology*, *2*(10), 1214-1234. https://doi.org/https://doi.org/10.1002/biot.200700084

Villagra, N. A., Fuentes, J. A., Jofré, M. R., Hidalgo, A. A., García, P., & Mora, G. C. (2012). The carbon source influences the efflux pump-mediated antimicrobial resistance in clinically important Gram-negative bacteria. *Journal of Antimicrobial Chemotherapy*, *67*(4), 921–927. https://doi.org/10.1093/jac/dkr573

Vinale, F., Nicoletti, R., Lacatena, F., Marra, R., Sacco, A., Lombardi, N., d'Errico, G., Digilio, M. C., Lorito, M., & Woo, S. L. (2017). Secondary metabolites from the endophytic fungus *Talaromyces pinophilus*. *Natural Product Research*, *31*(15), 1778–1785. https://doi.org/10.1080/14786419.2017.1290624

Visalakchi, S., & Muthumary, J. (2010). Taxol (anticancer drug) producing endophytic fungi: an overview. *International Journal of Pharma and Bio Sciences*, *1*(3), 0975–6299. https://www.cabidigitallibrary.org/doi/full/10.5555/20113372357

Wang, C., Song, Y., Li, T., Hu, J., Chen, X., & Li, H. (2022). *Mycobacterium smegmatis* Skin Infection Following Cosmetic Procedures: Report of Two Cases. *Clinical, Cosmetic and Investigational Dermatology*, *15*(3), 535–540. https://doi.org/10.2147/CCID.S359010

Wang, J. M., Ding, G. Z., Fang, L., Dai, J. G., Yu, S. S., Wang, Y. H., Chen, X. G., Ma, S. G., Qu, J., Xu, S., & Du, D. (2010). Thiodiketopiperazines produced by the endophytic fungus *Epicoccum nigrum*. *Journal of Natural Products*, *73*(7), 1240–1249. https://doi.org/10.1021/np1000895

Wayne, P. (2008). Clinical and Laboratory Standards Institute: Reference method for broth dilution antifungal susceptibility testing of yeasts; approved standard. *CLSI Document M27-*

A3 and Supplement, *48*(5), 6-12. https://doi.org/10.1128/jcm.02316-09

Weaver, B. A. (2014). How Taxol/paclitaxel kills cancer cells. *Molecular Biology of the Cell*, *25*(18), 2677–2681. https://doi.org/10.1091/mbc.E14-04-0916

Weerasinghe, R. H., Maduranga, K., Attanayake, R. N., Shevkar, C., Kate, A. S., Weerakoon, G., Kalia, K., & Paranagama, P. A. (2021). Bioactive Properties and Metabolite Profiles of Endolichenic Fungi in Mangrove Ecosystem of Negombo Lagoon, Sri Lanka. *Natural Product Communications*, *16*(10), 1934578X211048652. https://doi.org/10.1177/1934578X211048652

Weerasinghe, W. R. H., Shevkar, C. D., De Silva, R. S., Attanayake, R. N., Weerakoon, G., Kate, A. S., Kalia, K., & Paranagama, P. A. (2021). Bioactive properties and metabolite profile of an endolichenic fungus, *Hypoxylon lividipigmentum*. *International Conference on Applied and Pure Sciences*, *2021*(1), 219. http://repository.kln.ac.lk/handle/123456789/24076

Wei, C., & Hu, Q. (2022). Secondary metabolites of *purpureocillium lilacinum*. *Molecules*, *27*(1), 18. https://doi.org/10.3390/molecules27010018

Weidenbörner, M., Hindorf, H., Chandra Jha, H., Tsotsonos, P., & Egge, H. (1990). Antifungal activity of isoflavonoids in different reduced stages on *Rhizoctonia solani* and *Sclerotium rolfsii*. *Phytochemistry*, *29*(3), 801–803. https://doi.org/10.1016/0031-9422(90)80022-9

White, T. J., Bruns, T., Lee, S., & Taylor, J. W. (1990). "Amplification and direct sequencing of fungal ribosomal RNA genes for phylogenetics" in "PCR Protocols: A Guide to Methods and Applications" pp. 315–322*Academic Press, Inc., New York*.

WHO. (2017). Prioritization of pathogens to guide discovery, research and development of new antibiotics for drug-resistant bacterial infections including tuberculosis. https://doi.org/https://www.who.int/medicines/areas/rational_use/PPLreport_2017_09_19.pdf?ua=1

Wink, M. (2015). Modes of Action of Herbal Medicines and Plant Secondary Metabolites. *Medicines*, *2*(3), 251–286. https://doi.org/10.3390/medicines2030251

Wink, M., & Schimmer, O. (2010). Molecular modes of action of defensive secondary metabolites. In *Functions and Biotechnology of Plant Secondary Metabolites* (pp. 21-161.). Annual Plant Reviews. https://doi.org/10.1002/9781444318876.ch2

Wood, A. J., Rowinsky, E. K., & Donehower, R. C. (1995). Paclitaxel (taxol). *New England*

Journal of Medicine, *332*(15), 1004-1014. https://doi.org/10.1056/NEJM199504133321507

Water, W. C .(2019). World Meteorological Organization Greenhouse Gas Bulletin. *World Meteorological Organization, pp. 1-11 Geneva, Switzerland*.

Wu, L. S., Jia, M., Chen, L., Zhu, B., Dong, H. X., Si, J. P., Peng, W., & Han, T. (2016). Cytotoxic and antifungal constituents isolated from the metabolites of endophytic fungus DO14 from *dendrobium officinale*. *Molecules*, *21*(1), 1–14. https://doi.org/10.3390/molecules21010014

Xiao, Z., Morris- Natschke, S. L., & Lee, K. H. (2016). Strategies for the optimization of natural leads to anticancer drugs or drug candidates. *Medicinal Research Reviews*, *36*(1), 32–91. https://doi.org/https://doi.org/10.1002/med.21377

Xu, X., van Galen, L. S., Koh, M. J. A., Bajpai, R., Thng, S., Yew, Y. W., Ho, V. P. Y., Alagappan, U., Järbrink, K. S. A., & Car, J. (2019). Factors influencing quality of life in children with atopic dermatitis and their caregivers: a cross-sectional study. *Scientific Reports*, *9*(1), 1–10. https://doi.org/10.1038/s41598-019-51129-5

Xue, Y. H., Li, A., Li, H., Liu, C., Luo, H. J., Liu, C. X., Chen, J. F., Zou, K., & Liu, S. P. (2022). Metabolite profiling reveals comprehensive effects of *Chaetomium globosum* on citrus preservation. *Food Chemistry*, *369*(August). https://doi.org/10.1016/j.foodchem.2021.130959

Yahia, Y., Benabderrahim, M. A., Tlili, N., Bagues, M., & Nagaz, K. (2020). Bioactive compounds, antioxidant and antimicrobial activities of extracts from different plant parts of two Ziziphus Mill. species. *PLoS ONE*, *15*(5), 1–16. https://doi.org/10.1371/journal.pone.0232599

Yang, L., Wen, K. S., Ruan, X., Zhao, Y. X., Wei, F., & Wang, Q. (2018). Response of plant secondary metabolites to environmental factors. *Molecules*, *23*(4), 1–26. https://doi.org/10.3390/molecules23040762

Yao, H., Liu, J., Xu, S., Zhu, Z., & Xu, J. (2017). "The structural modification of natural products for novel drug discovery." *Expert Opinion on Drug Discovery*, *12*(2), 21-140. https://doi.org/https://doi.org/10.1080/17460441.2016.1272757

Ye, G., Peng, H., Fan, M., & Huang, C. G. (2007). Ellagic acid derivatives from the stem bark of *Dipentodon sinicus*. *Chemistry of Natural Compounds*, *43*(3), 125-127. https://doi.org/https://doi.org/10.1007/s10600-007-0060-y

Yi, Y., Adrjan, B., Li, J., Hu, B., & Roszak, S. (2019). NMR studies of daidzein and puerarin: active anti-oxidants in traditional Chinese medicine. *Journal of Molecular Modeling*, *25*(7). https://doi.org/10.1007/s00894-019-4090-8

Yoder, J. A., Fisher, K. A., & Dobrotka, C. J. (2018). A report on *Purpureocillium lilacinum* found naturally infecting the predatory mite, *Balaustium murorum* (Parasitengona: Erythraeidae). *International Journal of Acarology*, *44*(4–5), 139–145. https://doi.org/10.1080/01647954.2018.1487996

Zekeya, N., Chacha, M., Shahada, F., & Kidukuli, A. (2014). Analysis of phytochemical composition of *Bersama abyssinica* by gas chromatography–mass spectrometry. *Life Sciences and Bio-Engineering*, *3*(4): 246-252. https://dspace.nm-aist.ac.tz/handle/20.500.12479/1131

Zhang, C., Yang, D., Liang, Z., Liu, J., Yan, K., Zhu, Y., & Yang, S. (2019). Climatic factors control the geospatial distribution of active ingredients in Salvia miltiorrhiza Bunge in China. *Scientific Reports*, *9*(1), 1–11. https://doi.org/10.1038/s41598-018-36729-x

Zhang, J., Liu, L., Wang, J., Ren, B., Zhang, L., & Li, W. (2018). Formononetin, an isoflavone from Astragalus membranaceus inhibits proliferation and metastasis of ovarian cancer cells. *Journal of Ethnopharmacology*, *221*(April), 91–99. https://doi.org/10.1016/j.jep.2018.04.014

Zhang, W., Zhang, F., Li, Z., Miao, X., Meng, Q., & Zhang, X. (2009). Investigation of bacteria with polyketide synthase genes and antimicrobial activity isolated from South China Sea sponges. *Journal of Applied Microbiology*, *107*(2), 567–575. https://doi.org/10.1111/j.1365-2672.2009.04241.x

Zhang, Y. J., Pang, Y. B., Wang, X. Y., Jiang, Y. H., Herrera- Balandrano, D. D., Jin, Y., & Laborda, P. (2022). Exogenous genistein enhances soybean resistance to Xanthomonas axonopodis pv. glycines. *Pest Management Science*, *78*(8), 3664-3675. https://doi.org/https://doi.org/10.1002/ps.7009

Zhang, Y., Liu, S., Che, Y., & Liu, X. (2007). Epicoccins A-D, epipolythiodioxopiperazines from a Cordyceps-colonizing isolate of *Epicoccum nigrum*. *Journal of Natural Products*, *70*(9), 1522–1525. https://doi.org/10.1021/np070239u

Zielińska, A., Paradowska, K., Jakowski, J., & Wawer, I. (2008). 13C CP MAS NMR and GIAO-CHF/DFT calculations of flavonoids: Morin, kaempferol, tricin, genistein,

formononetin and 3,7-dihydroxyflavone. *Journal of Molecular Structure*, *873*(1–3), 109–116. https://doi.org/10.1016/j.molstruc.2007.03.009

Zinniel, D. K., Lambrecht, P., Harris, N. B., Feng, Z., Kuczmarski, D., Higley, P., Ishimaru, C. A., Arunakumari, A., Barletta, R. G., & Vidaver, A. K. (2002). Isolation and characterization of endophytic colonizing bacteria from agronomic crops and prairie plants. *Applied and Environmental Microbiology*, *68*(5), 2198–2208. https://doi.org/10.1128/AEM.68.5.2198-2208.2002

Żwawiak, J., & Zaprutko, L. (2014). A brief history of taxol. *Journal of Medical Science*, *83*(1), 47–52. https://doi.org/10.20883/medical.e43

APPENDICES

Appendix 1: HRESIMS of **17**

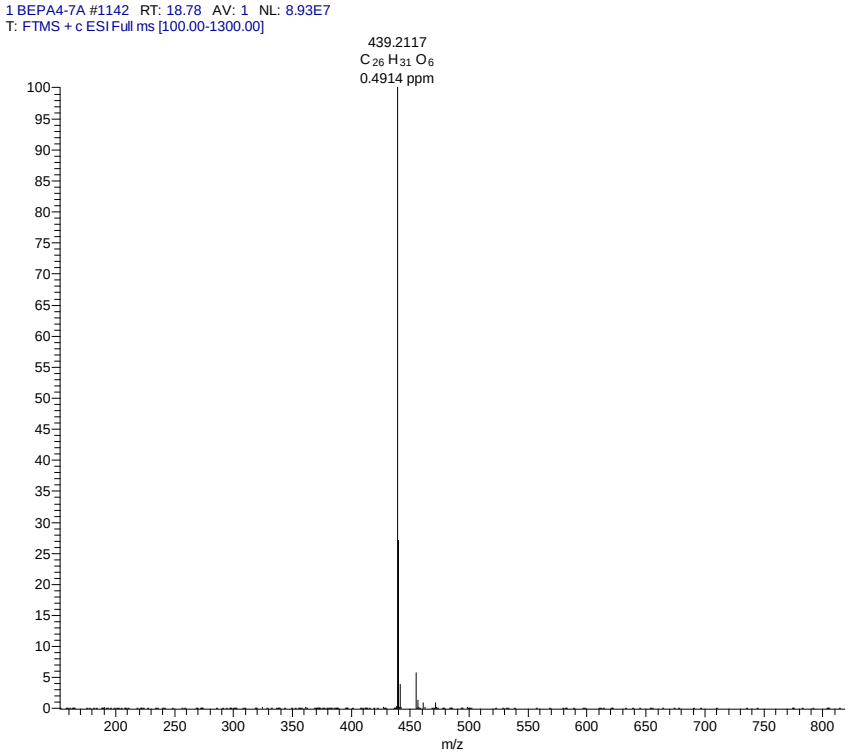

Appendix 2: Infrared spectrum of **17**

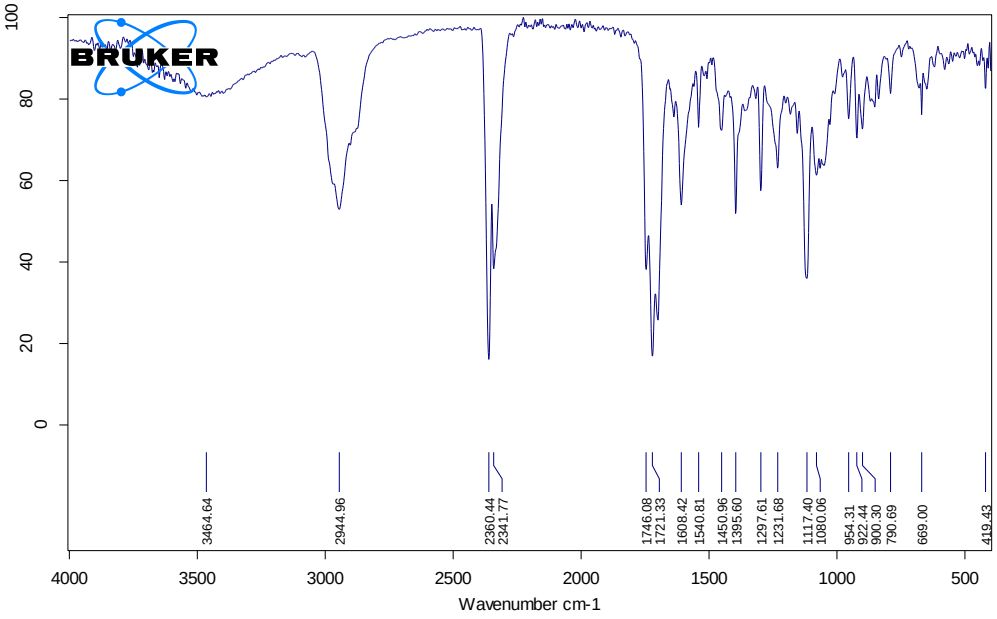

C:\Messungen\INFU\BEPA\3 BEPA4-7A.0000	3 BEPA4-7A	Liquid	03.12.2019

Seite 1 von 1

Appendix 3: ^{1}H NMR (700 MHz, $CDCl_3$) spectrum of **17**

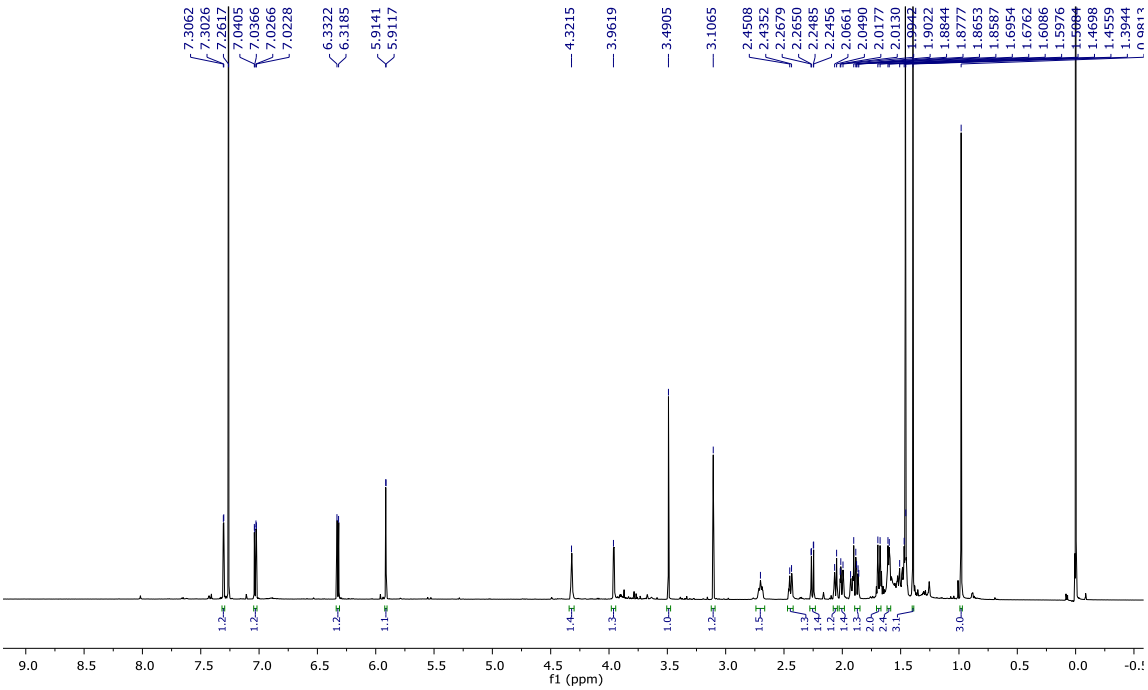

Appendix 4: ^{13}C NMR (175 MHz, $CDCl_3$) spectrum of **17**

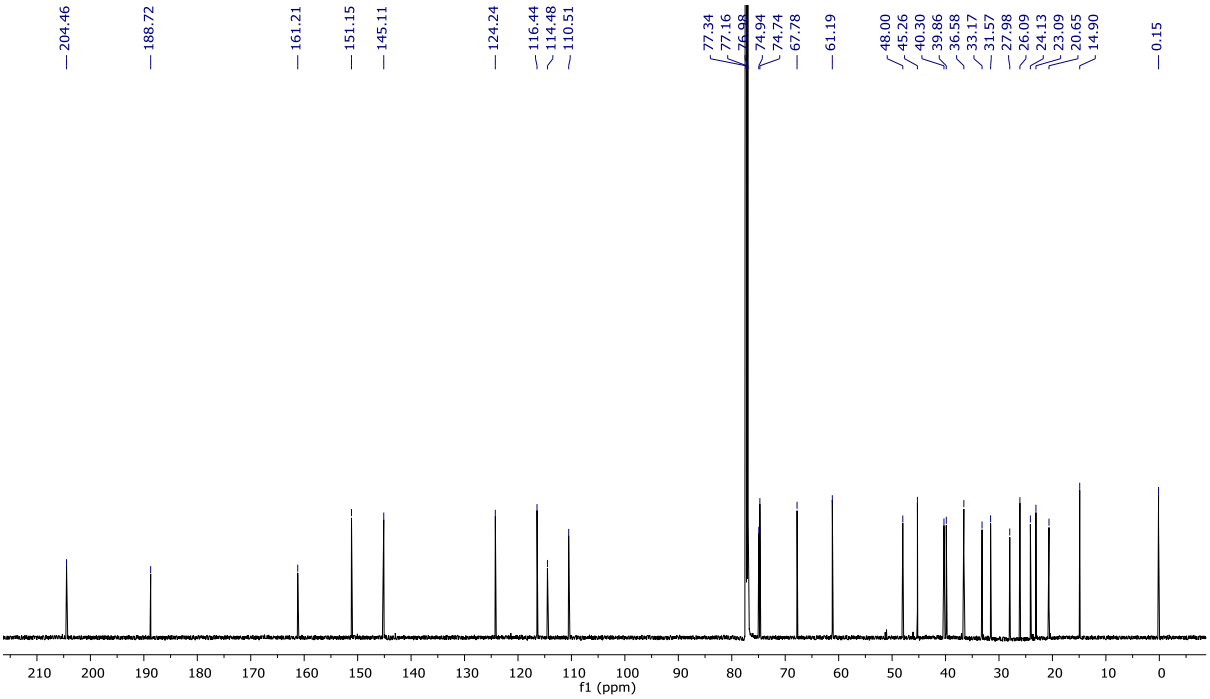

Appendix 5: COSY (700 MHz, $CDCl_3$) spectrum of **17**

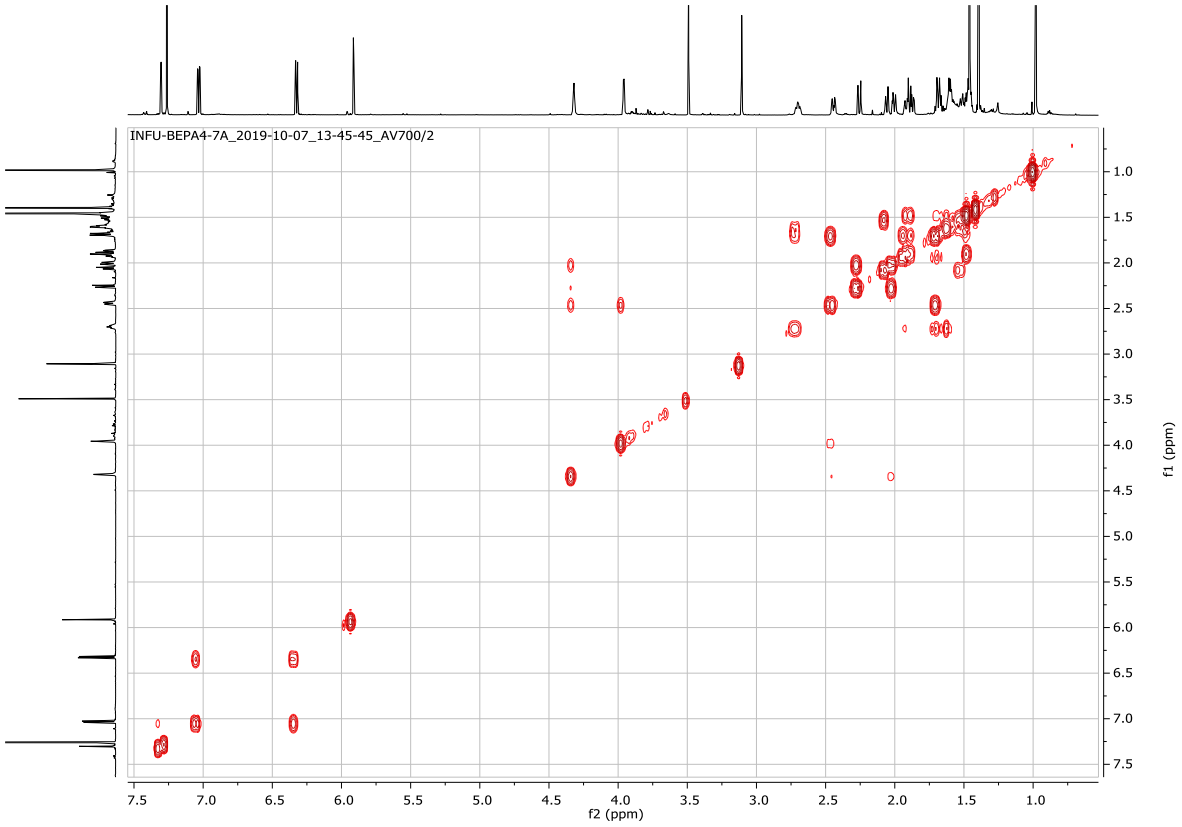

Appendix 6: HSQC ($CDCl_3$) spectrum of **17** (^1H: 700 MHz, ^{13}C: 175 MHz)

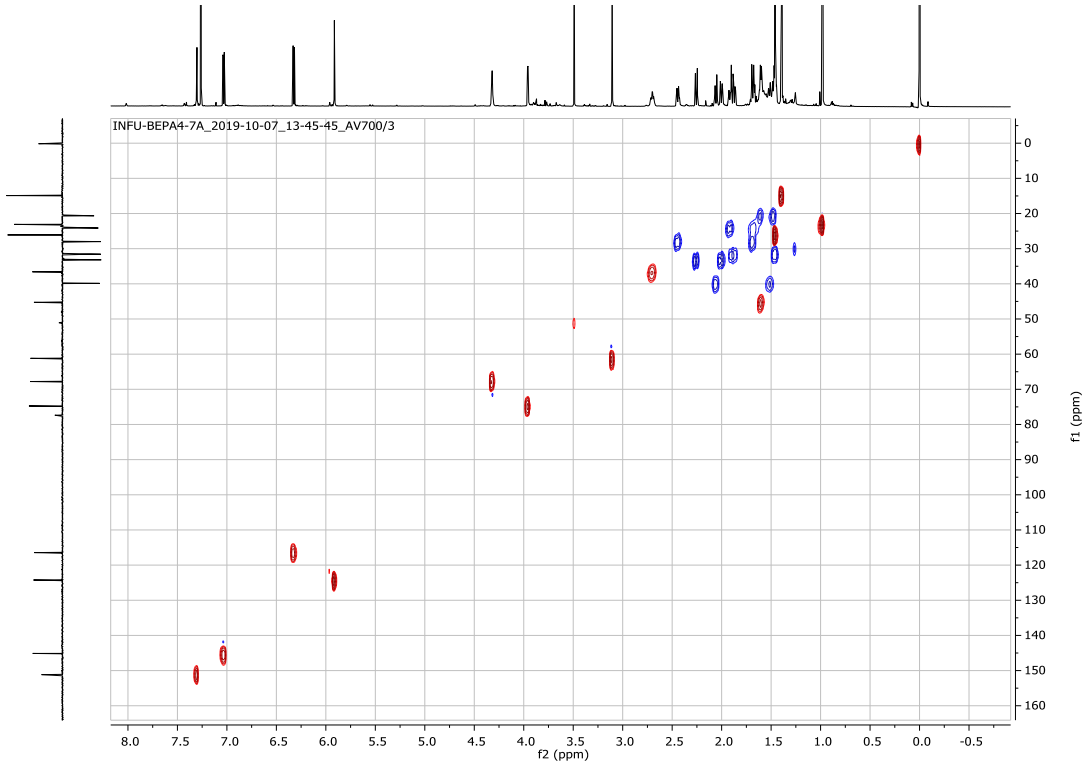

Appendix 7: HMBC ($CDCl_3$) spectrum of **17** (^1H: 700 MHz, ^{13}C: 175 MHz)

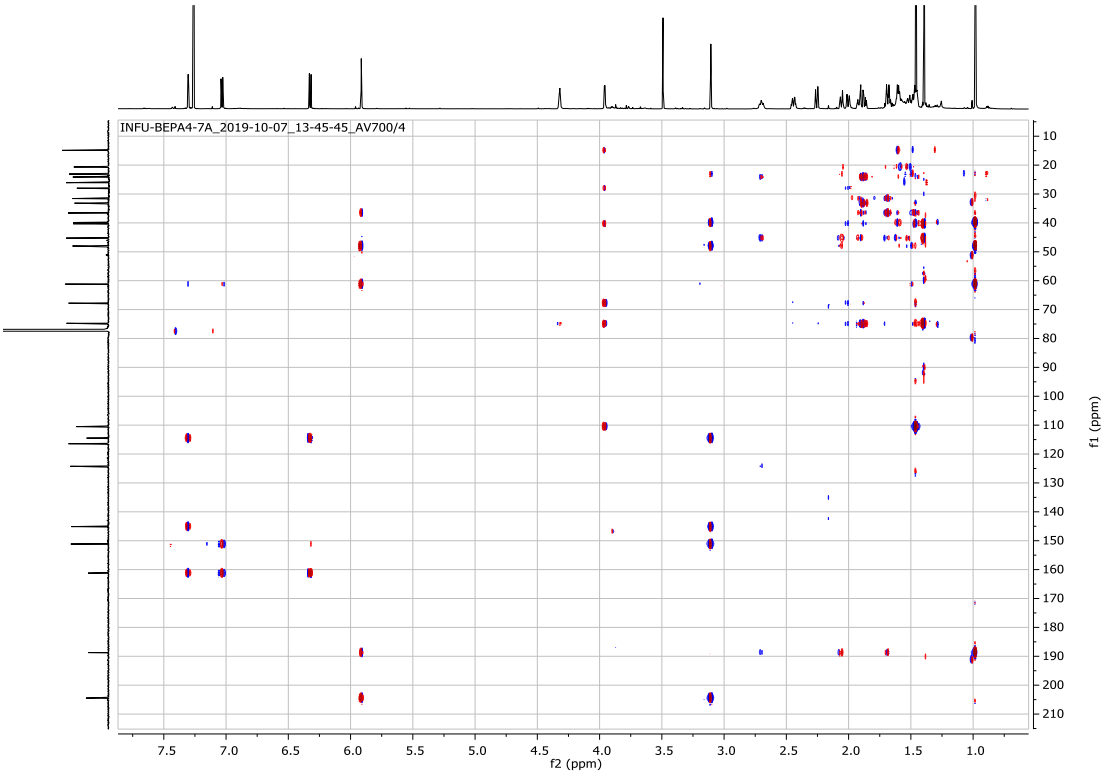

Appendix 8: NOESY (700MHz, $CDCl_3$) spectrum of **17**

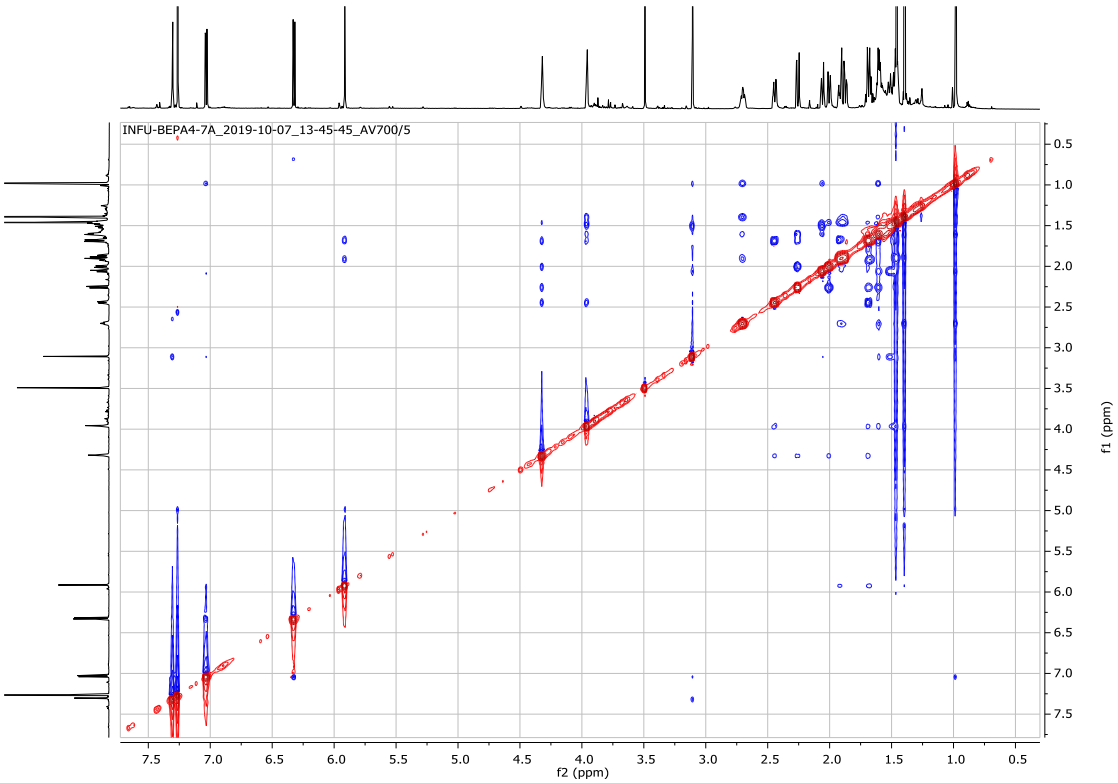

Appendix 9: HRESIMS of **18**

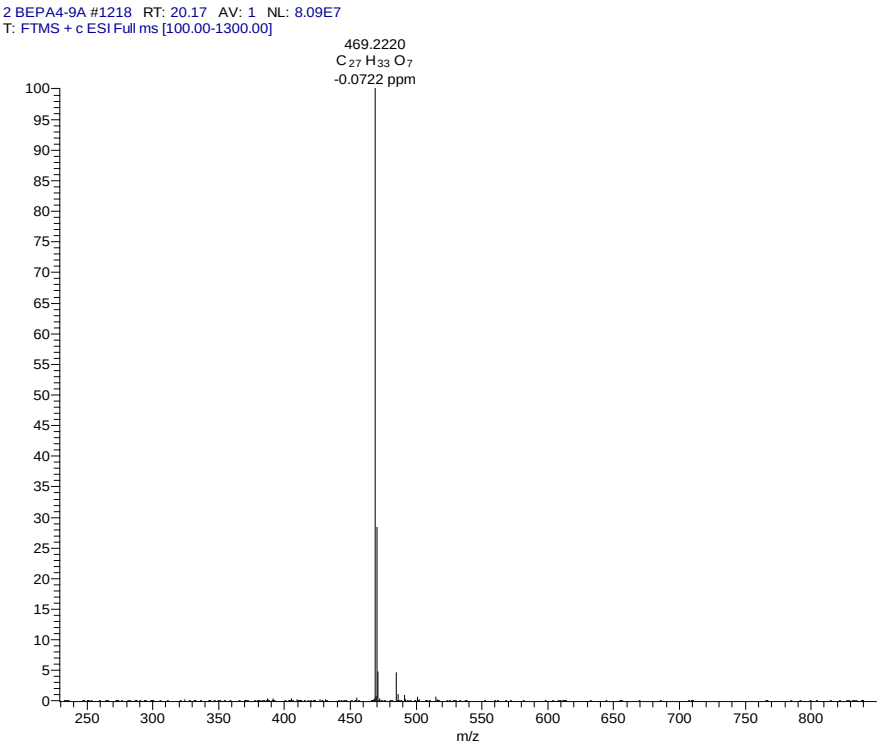

Appendix 10: Infrared spectrum of **18**

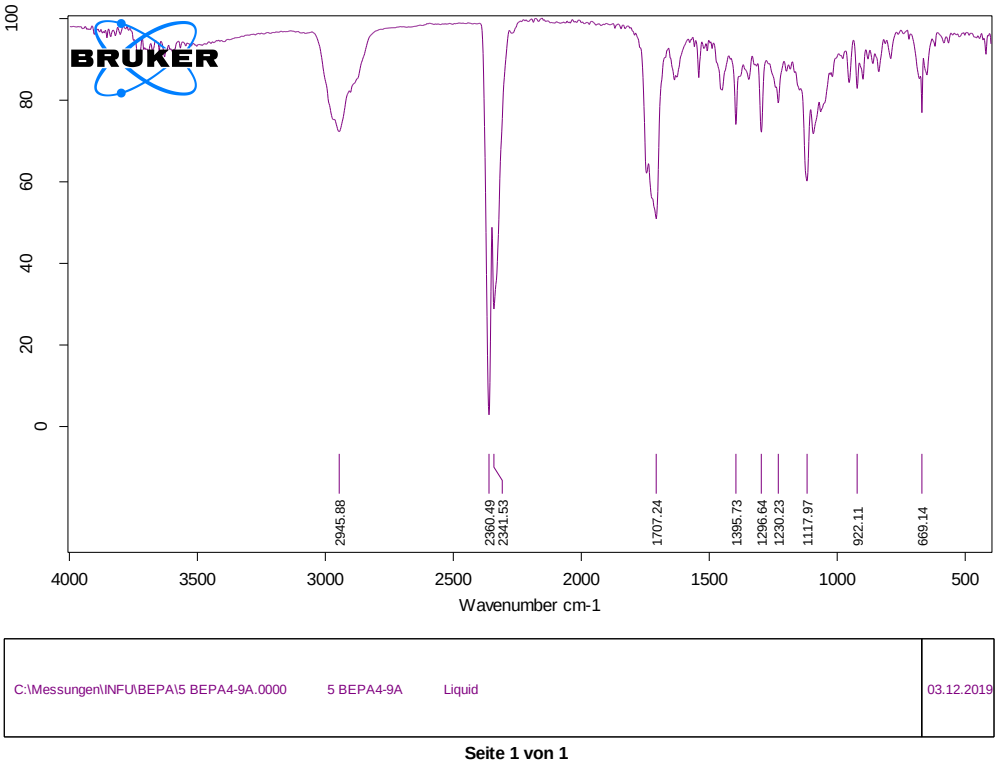

Appendix 11: ^{1}H NMR (700 MHz, $CDCl_3$) spectrum of **18**

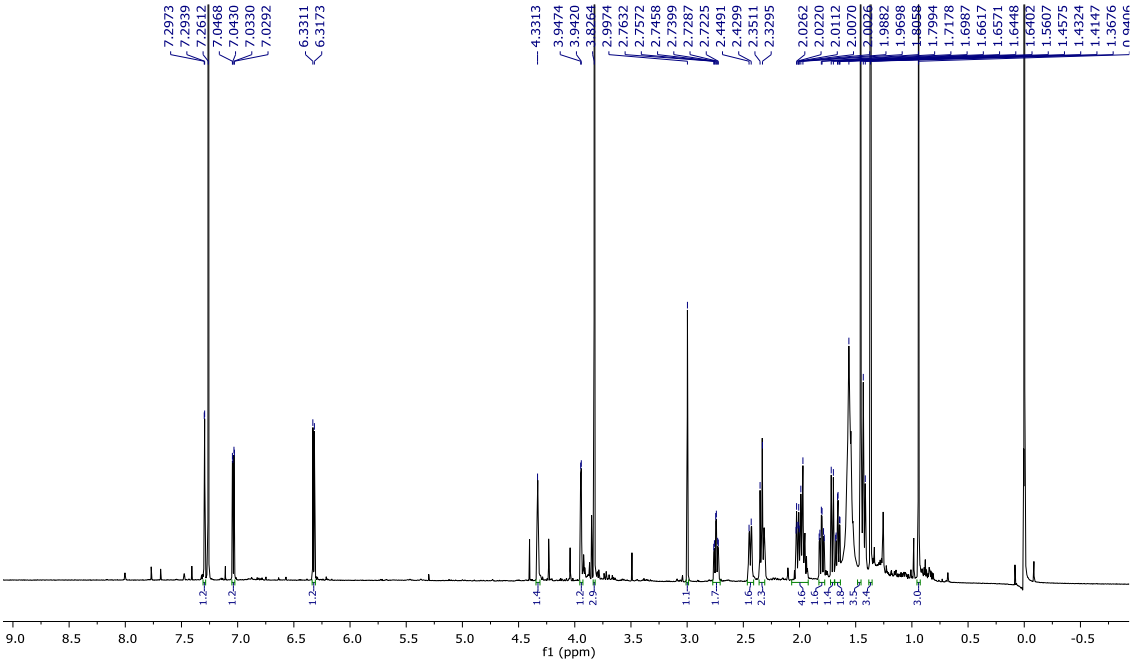

Appendix 12: ^{13}C NMR (175 MHz, $CDCl_3$) spectrum of **18**

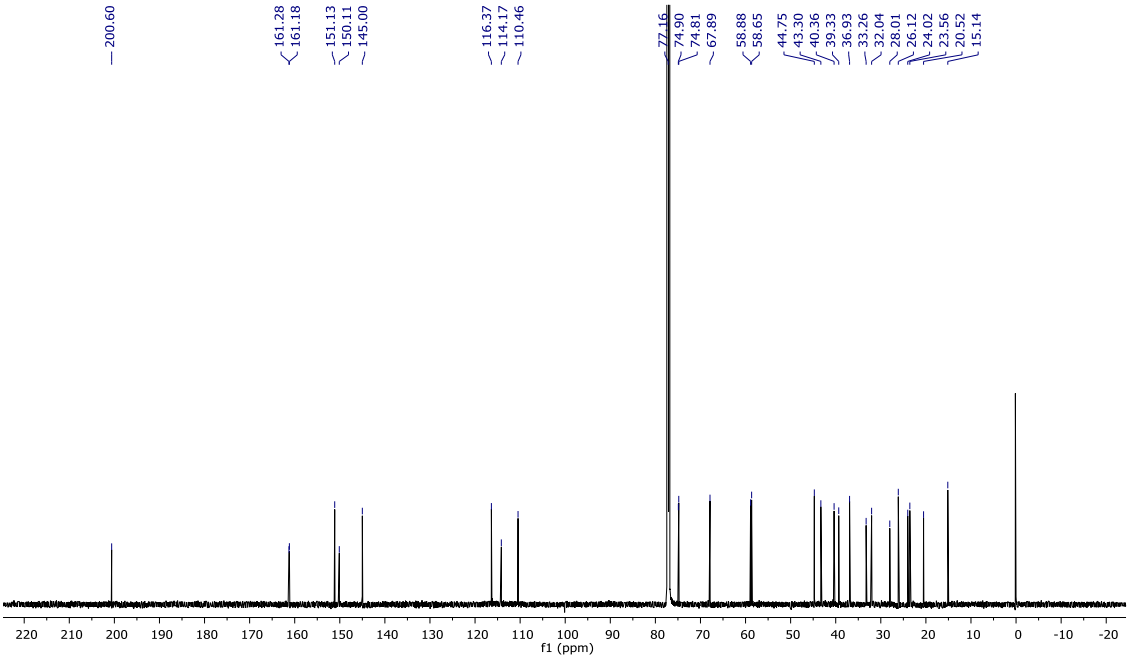

Appendix 13: COSY (700 MHz, $CDCl_3$) spectrum of **18**

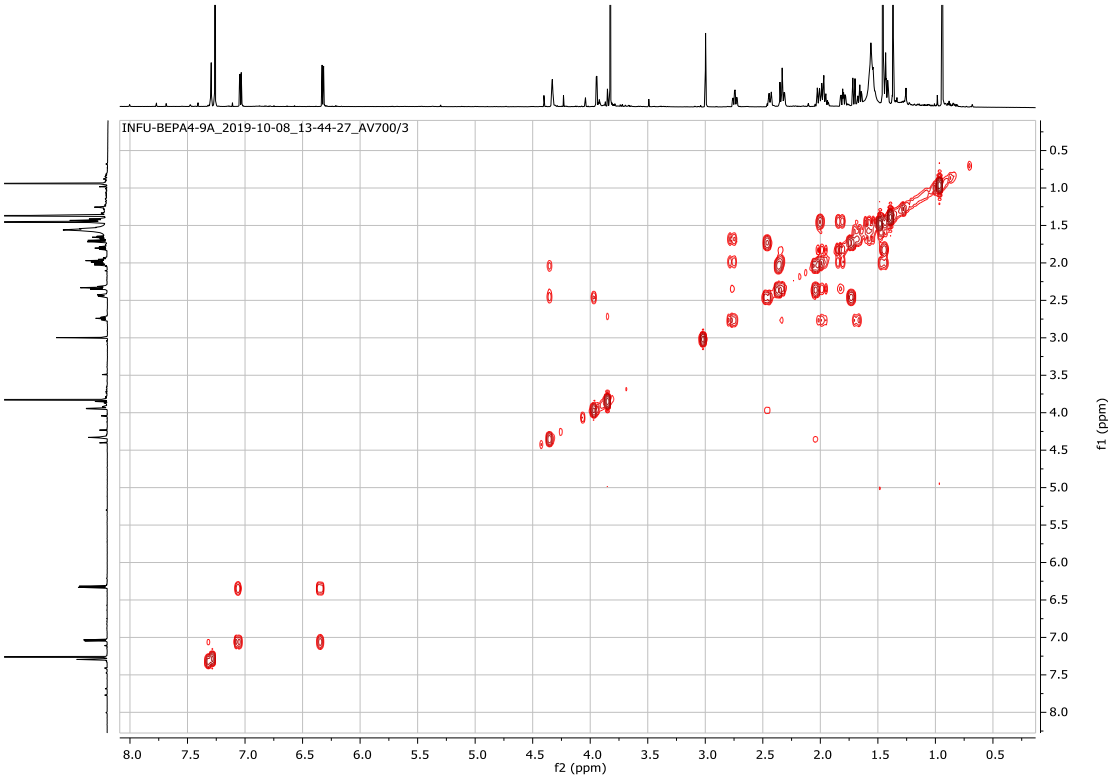

Appendix 14: HSQC ($CDCl_3$) spectrum of **18** (^1H: 700 MHz, ^{13}C: 175 MHz)

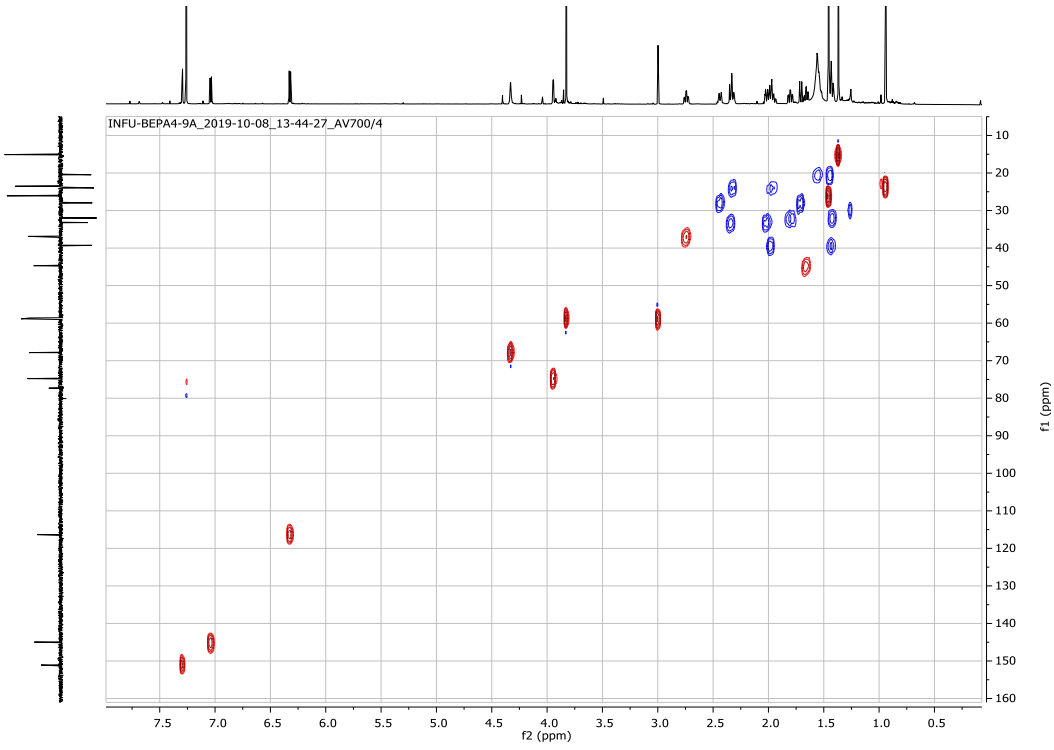

Appendix 15: HMBC ($CDCl_3$) spectrum of **18** (^1H: 700 MHz, ^{13}C: 175 MHz)

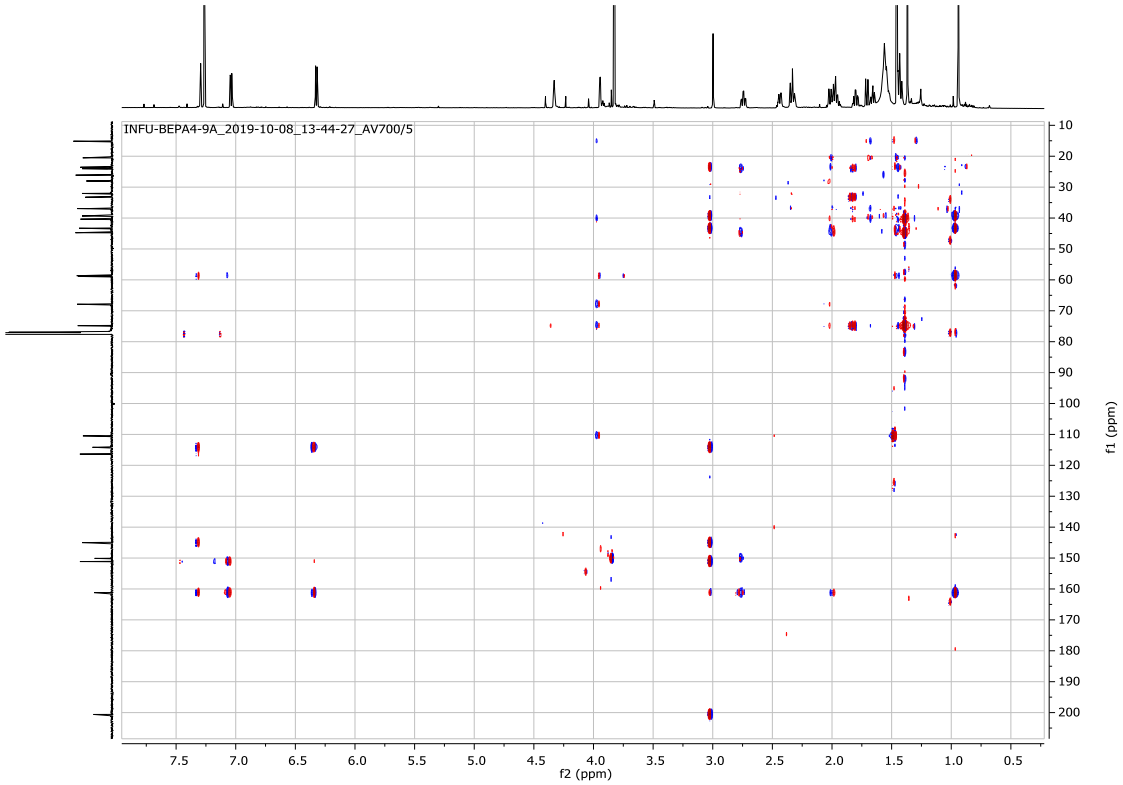

Appendix 16: NOESY (700MHz, $CDCl_3$) spectrum of **18**

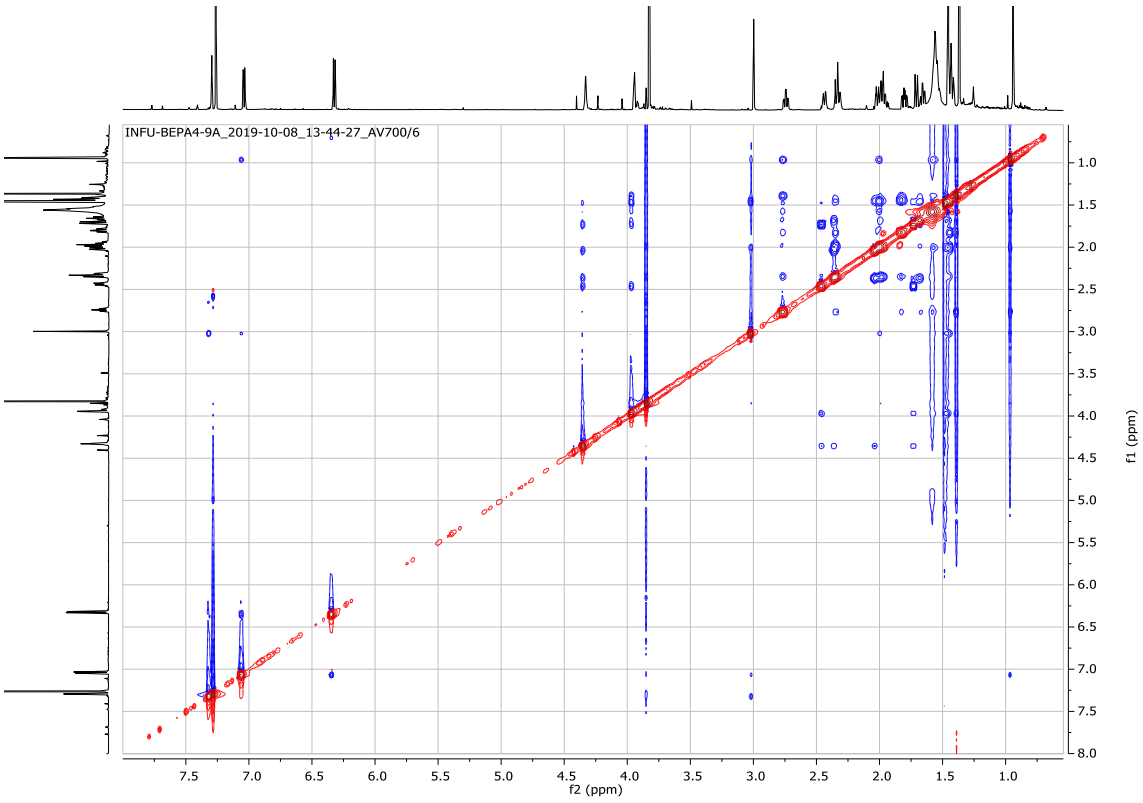

Appendix 17: HRESIMS of **19**

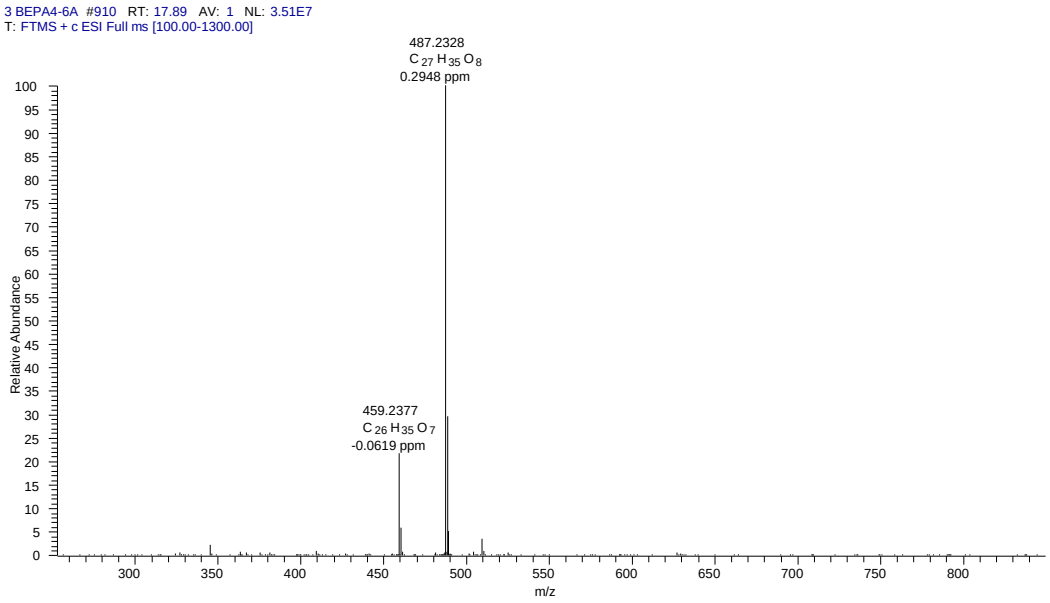

Appendix 18: Infrared spectrum of **19**

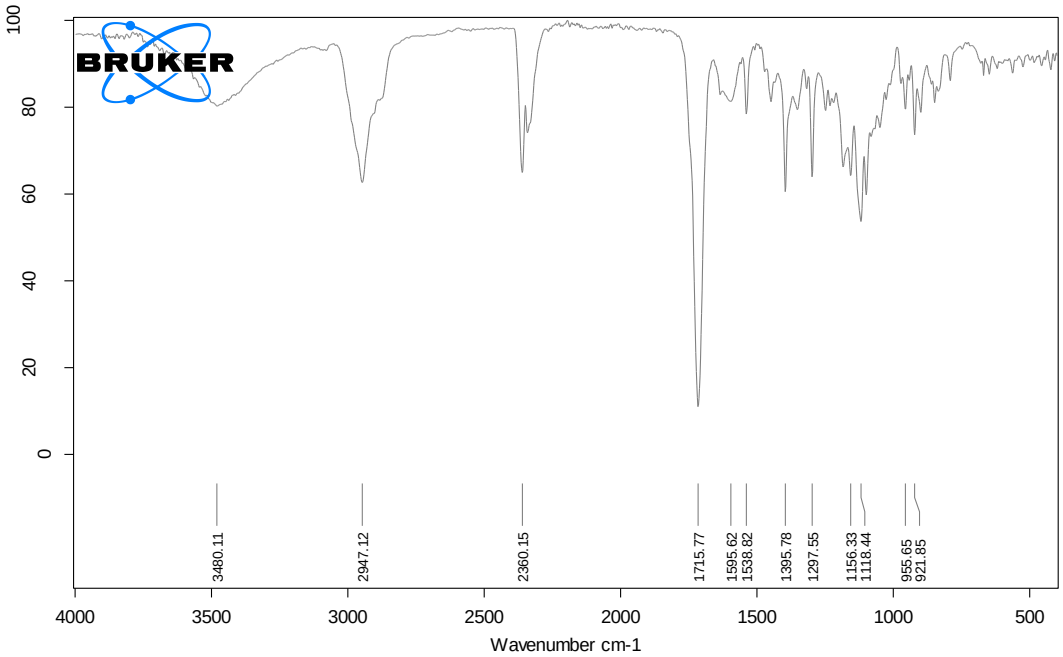

C:\Messungen\INFU\BEPA\1 BEPA4-6A.0002	1 BEPA4-6A	Liquid	03.12.2019

Seite 1 von 1

Appendix 19: ^{1}H NMR (700 MHz, DMSO-d_6) spectrum of **19**

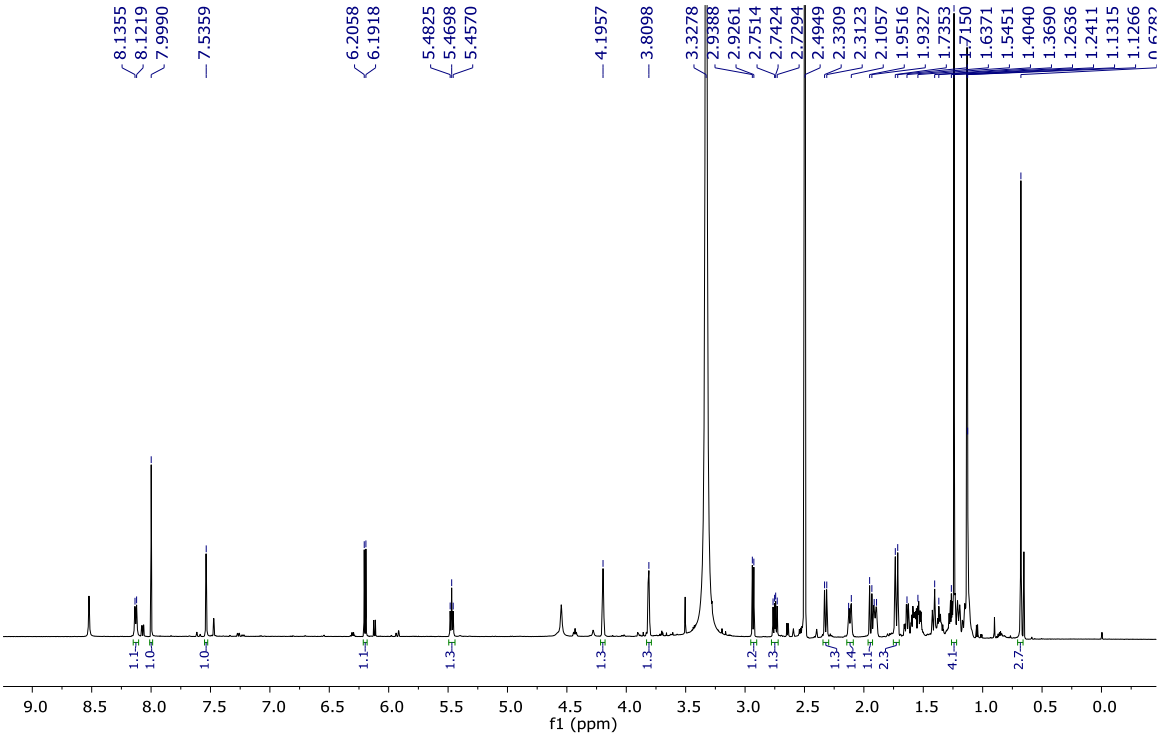

Appendix 20: ^{13}C NMR (175 MHz, DMSO-d_6) spectrum of **19**

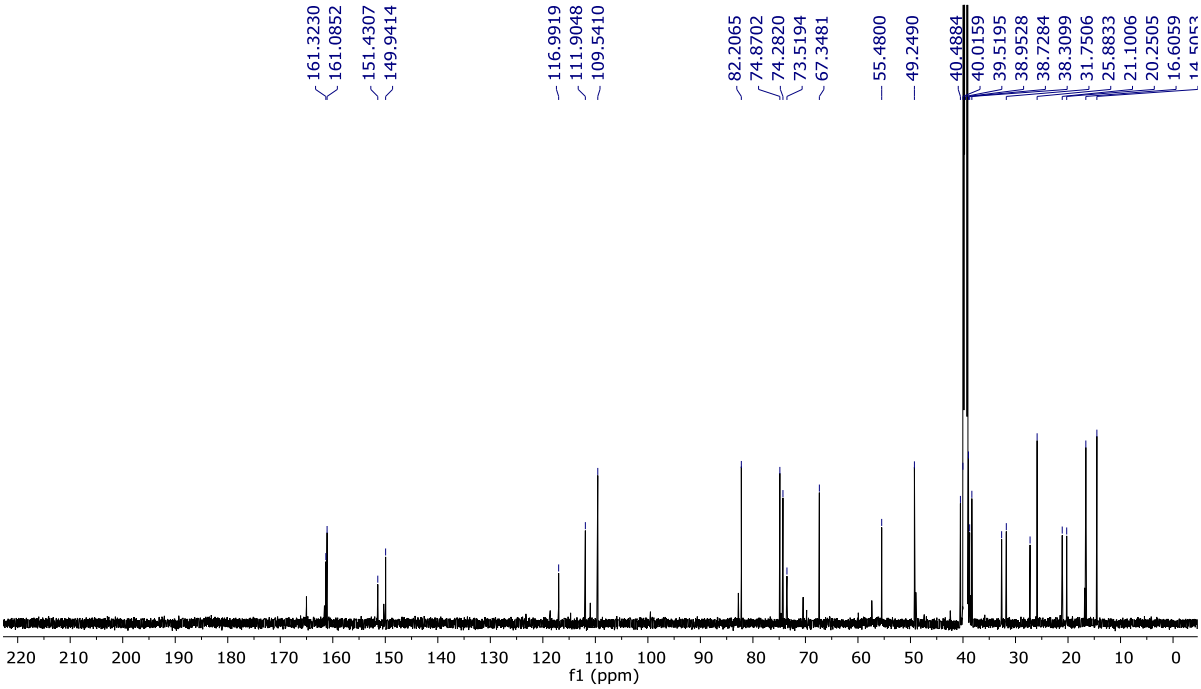

Appendix 21: COSY (700 MHz, DMSO-d_6) spectrum of **19**

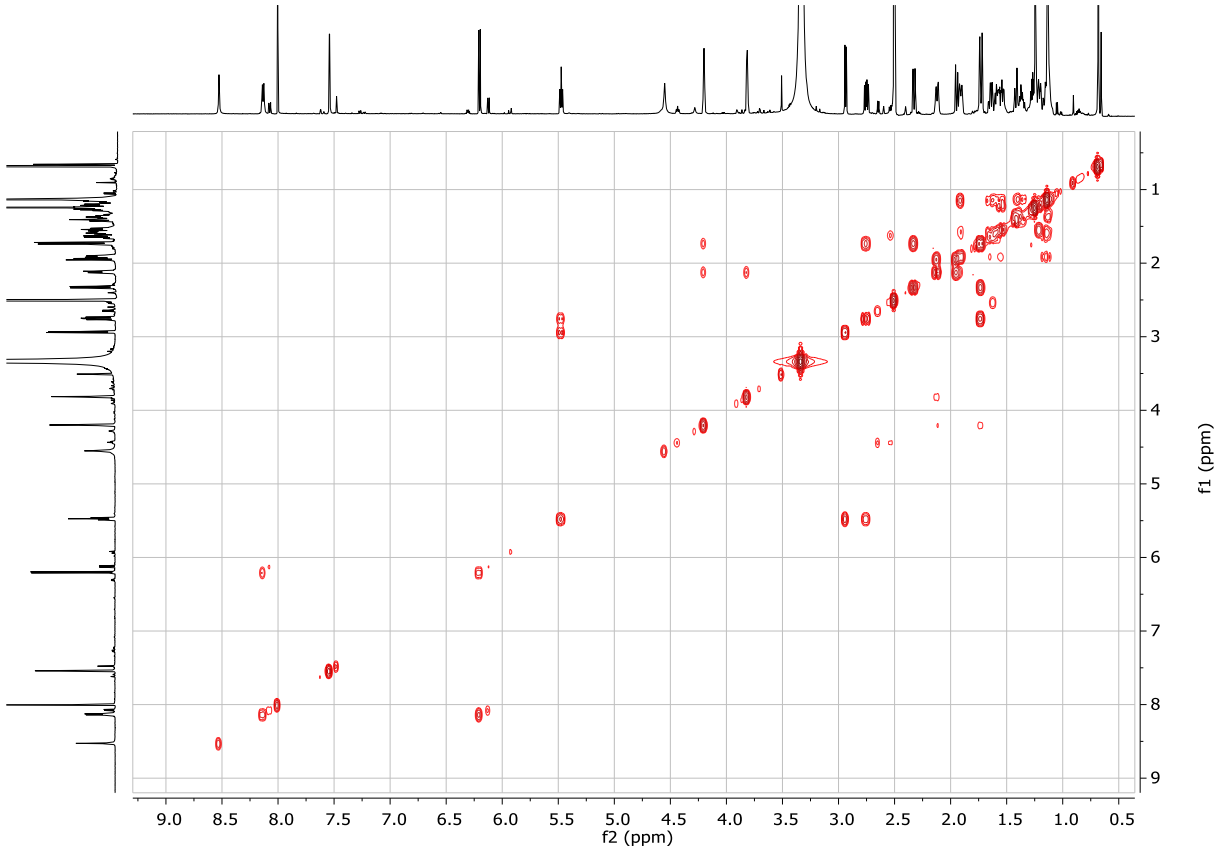

Appendix 22: HSQC (DMSO-d_6) spectrum of **19** (^{1}H: 700 MHz, ^{13}C: 175 MHz)

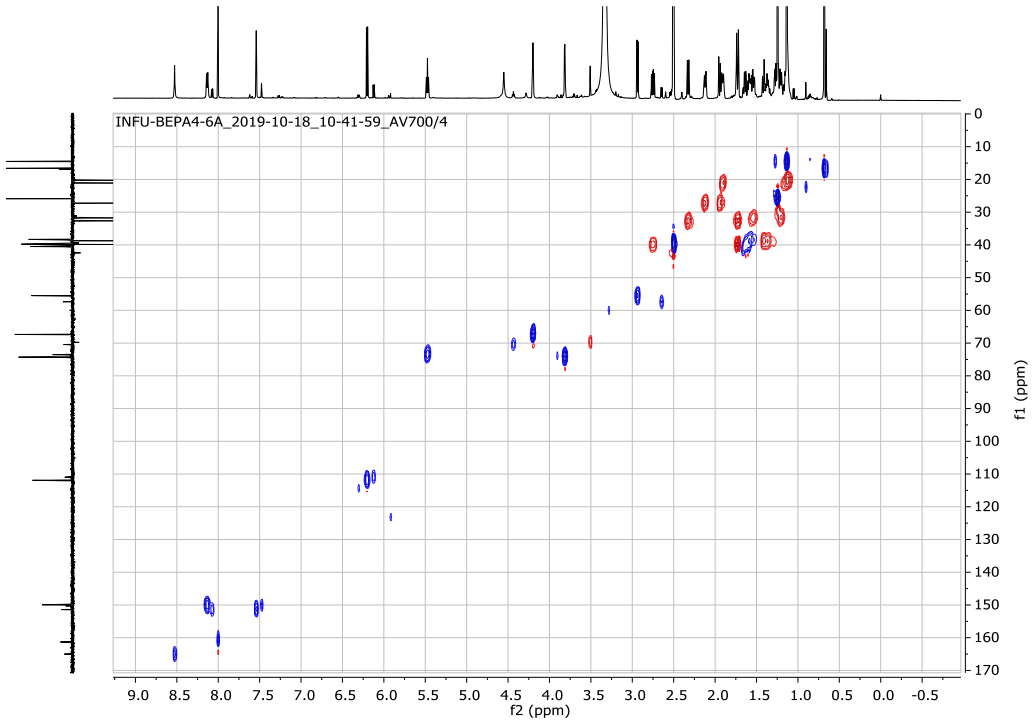

Appendix 23: HMBC (DMSO-d_6) spectrum of **19** (^{1}H: 700 MHz, ^{13}C: 175 MHz)

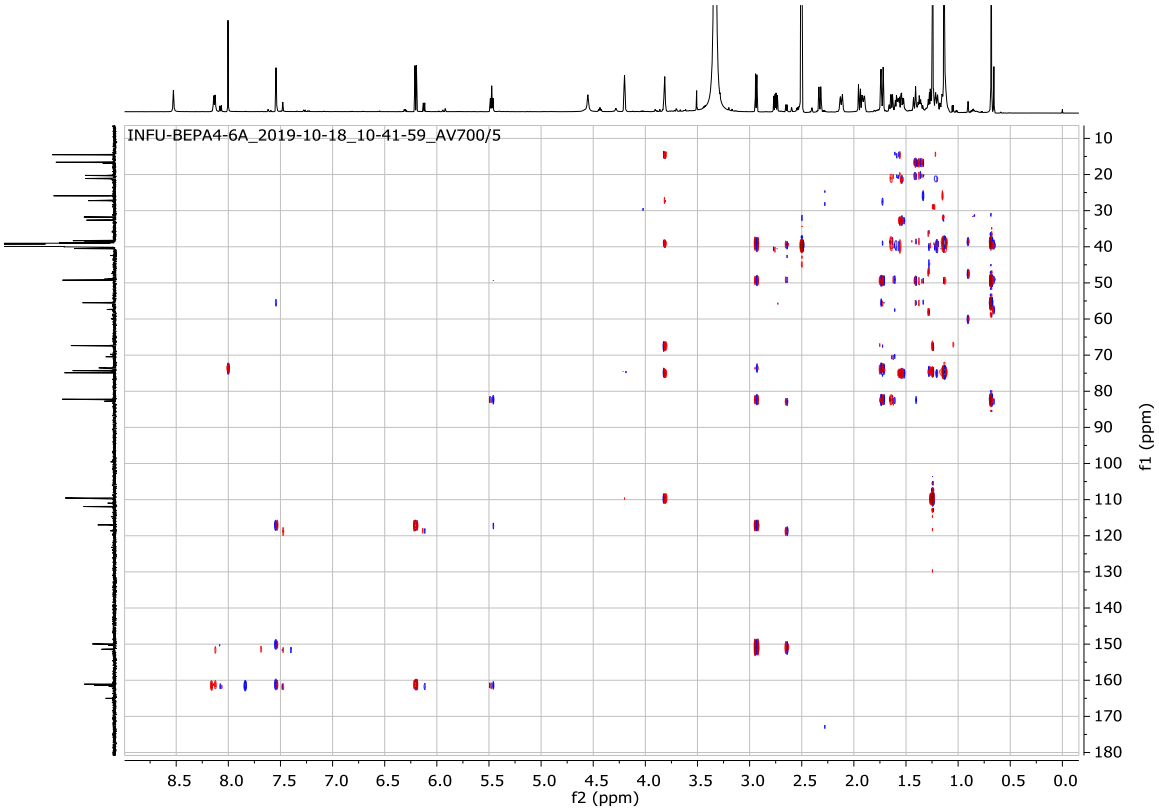

Appendix 24: HRESIMS of **20**

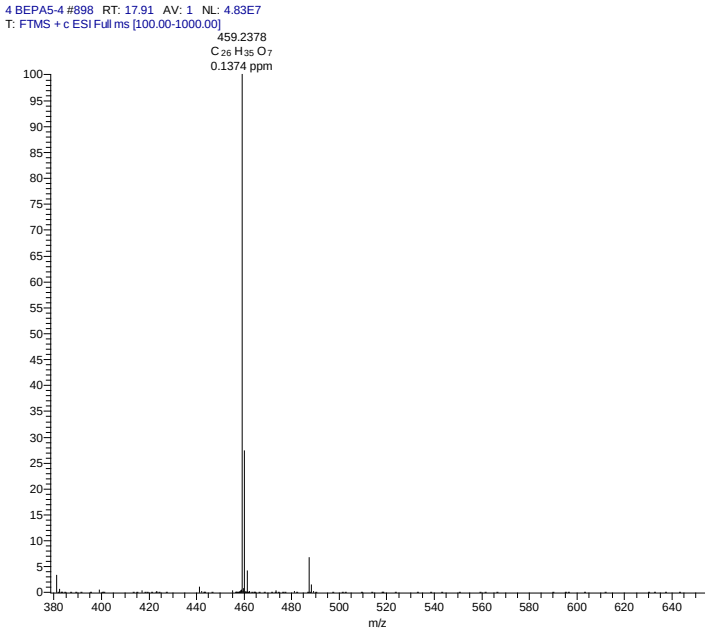

Appendix 25: Infrared spectrum of **20**

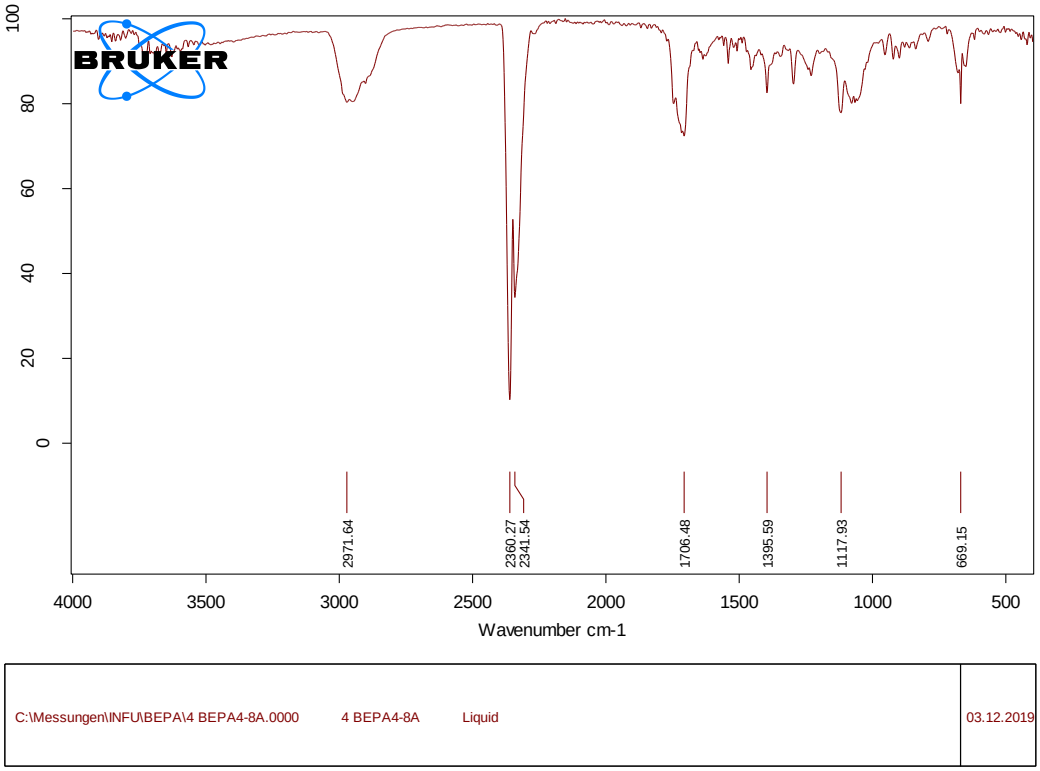

Seite 1 von 1

Appendix 26: ^{1}H NMR (700 MHz, DMSO-d_6) spectrum of **20**

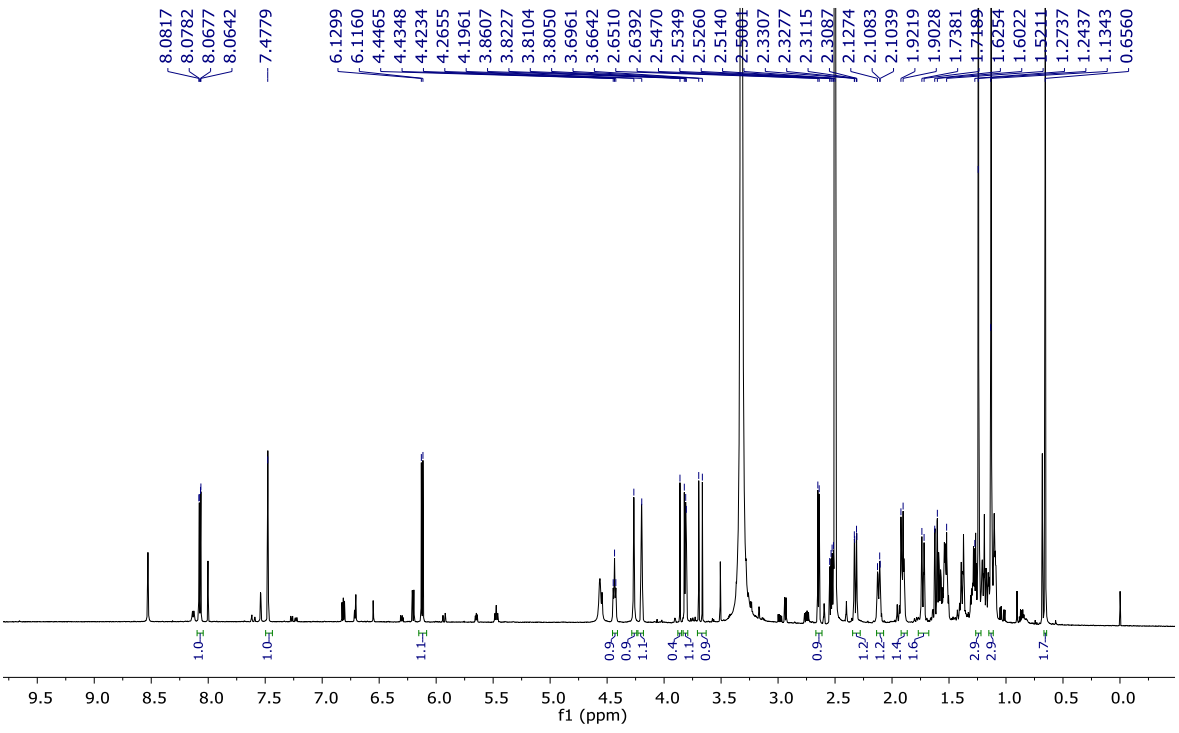

Appendix 27: ^{13}C NMR (175 MHz, DMSO-d_6) spectrum of **20**

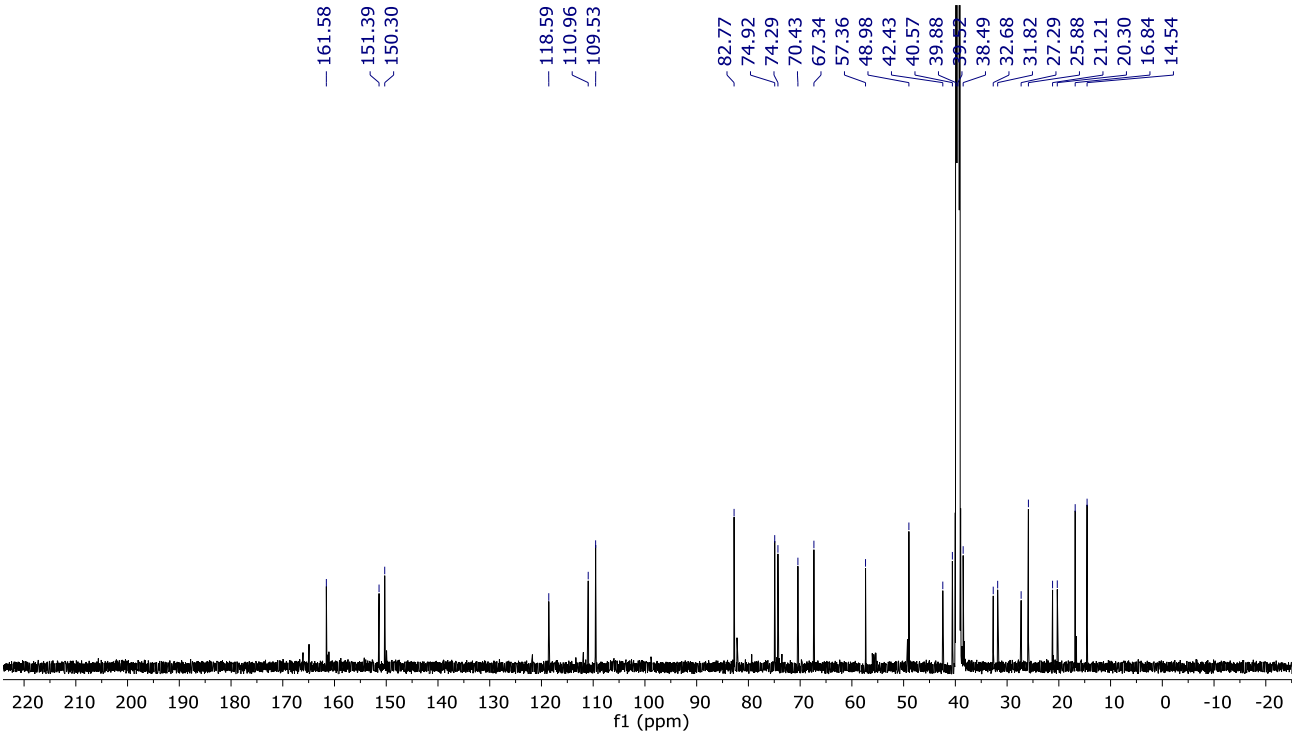

Appendix 28: COSY (700 MHz, DMSO-d_6) spectrum of **20**

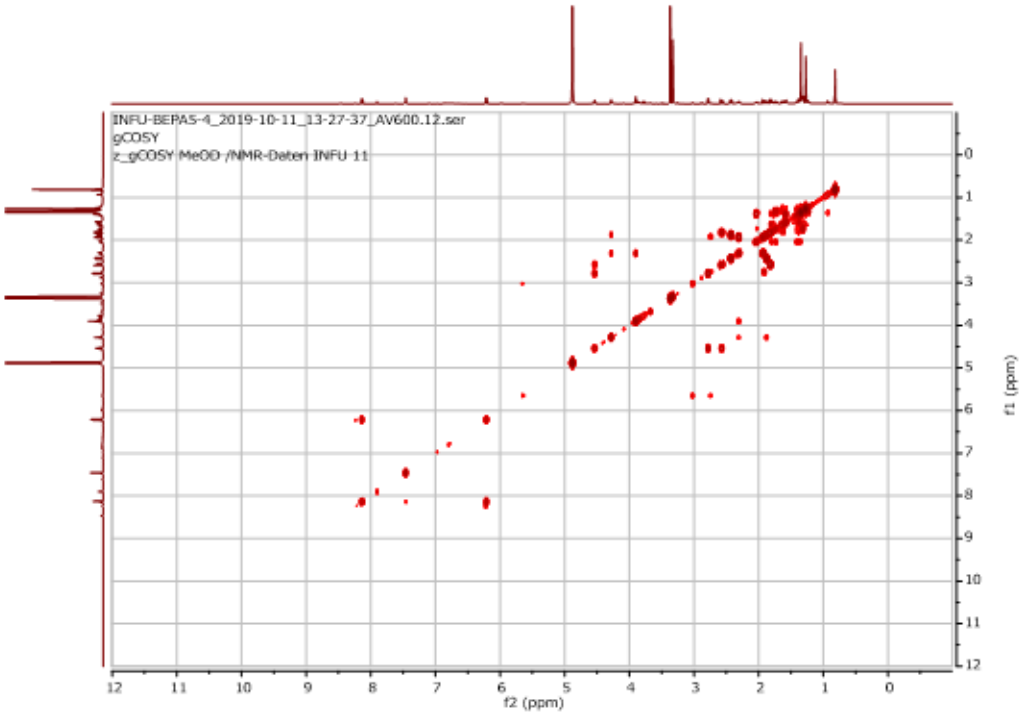

Appendix 29: HSQC (DMSO-d_6) spectrum of **20** (^{1}H: 700 MHz, ^{13}C: 175 MHz)

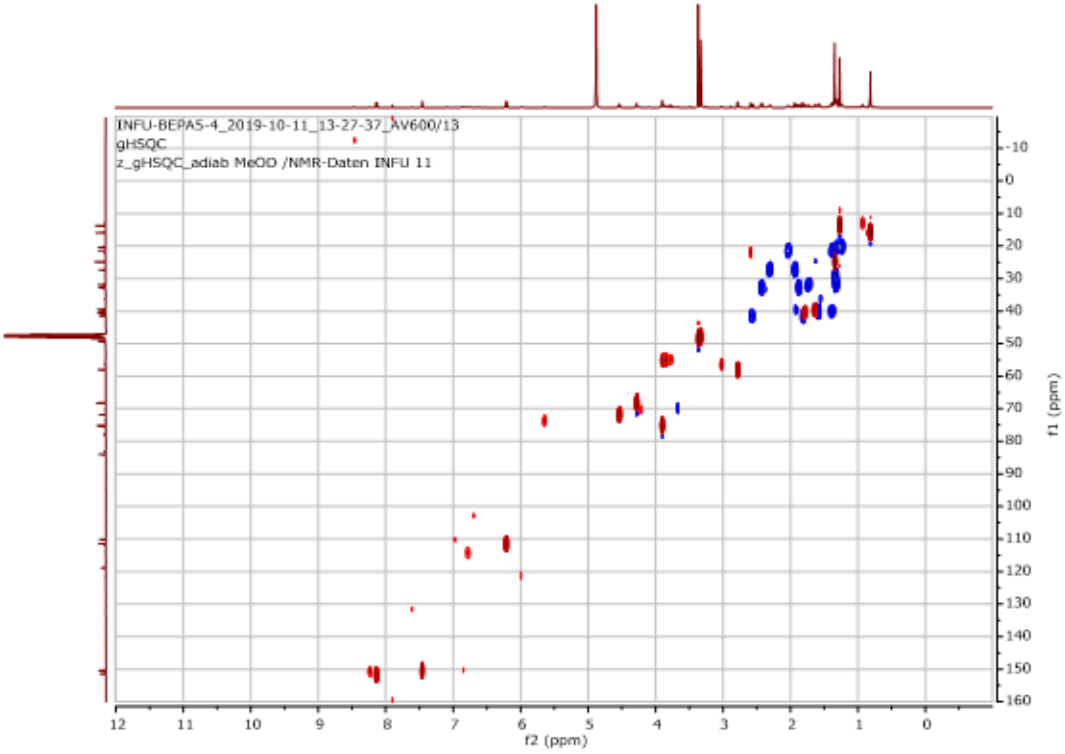

Appendix 30: HMBC (DMSO-d_6) spectrum of **20** (^{1}H: 700 MHz, ^{13}C: 175 MHz)

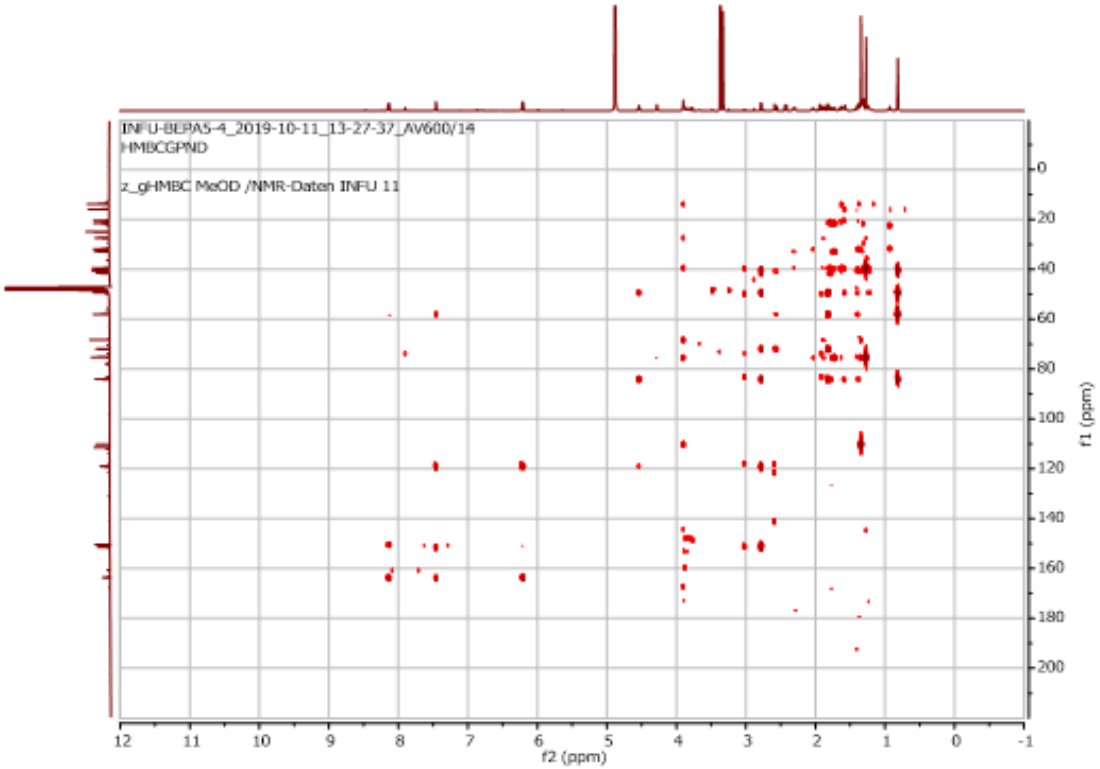

Appendix 31: NOESY (700MHz, DMSO-d_6) spectrum of **20**

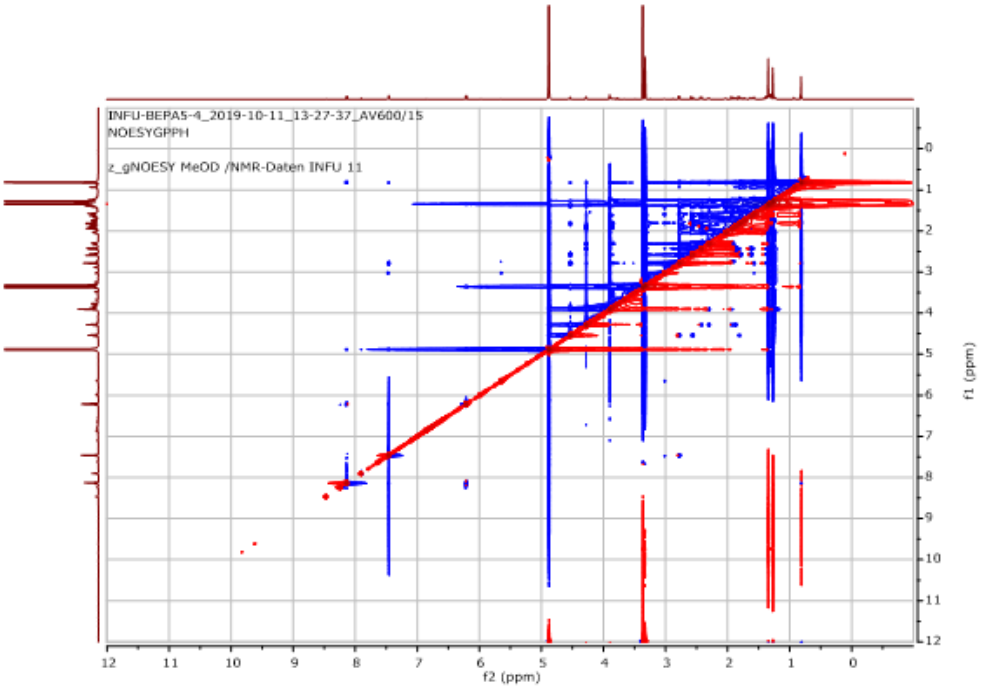

Appendix 32: HRESIMS of **21**

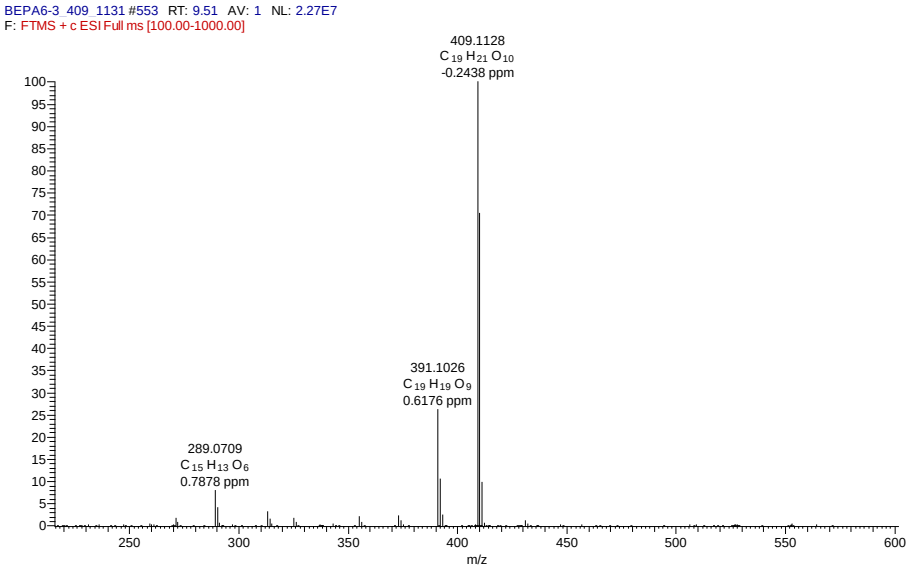

Appendix 33: ^{1}H NMR (600 MHz, MeOD) spectrum of **21**

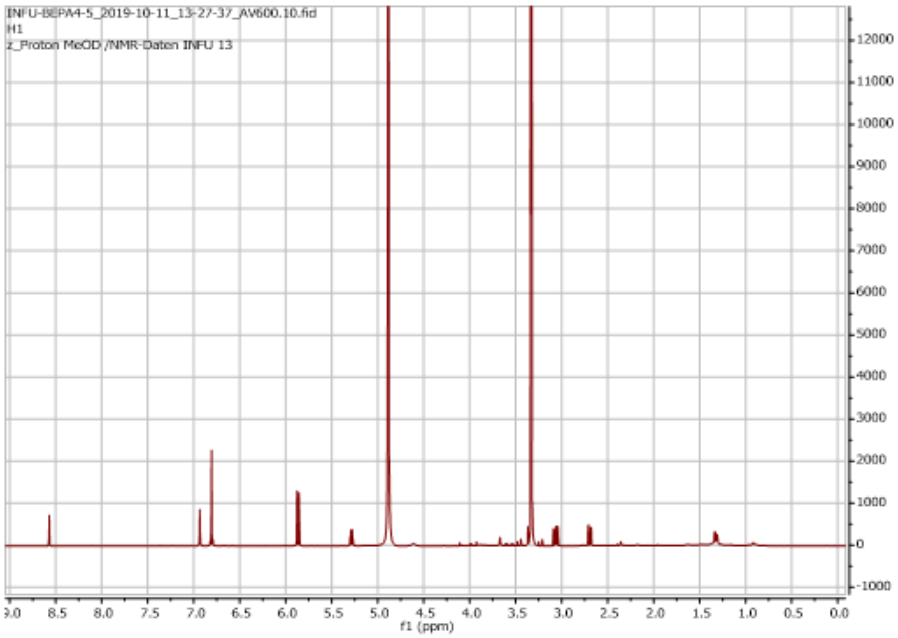

Appendix 34: ^{13}C NMR (175 MHz, MeOD) spectrum of **21**

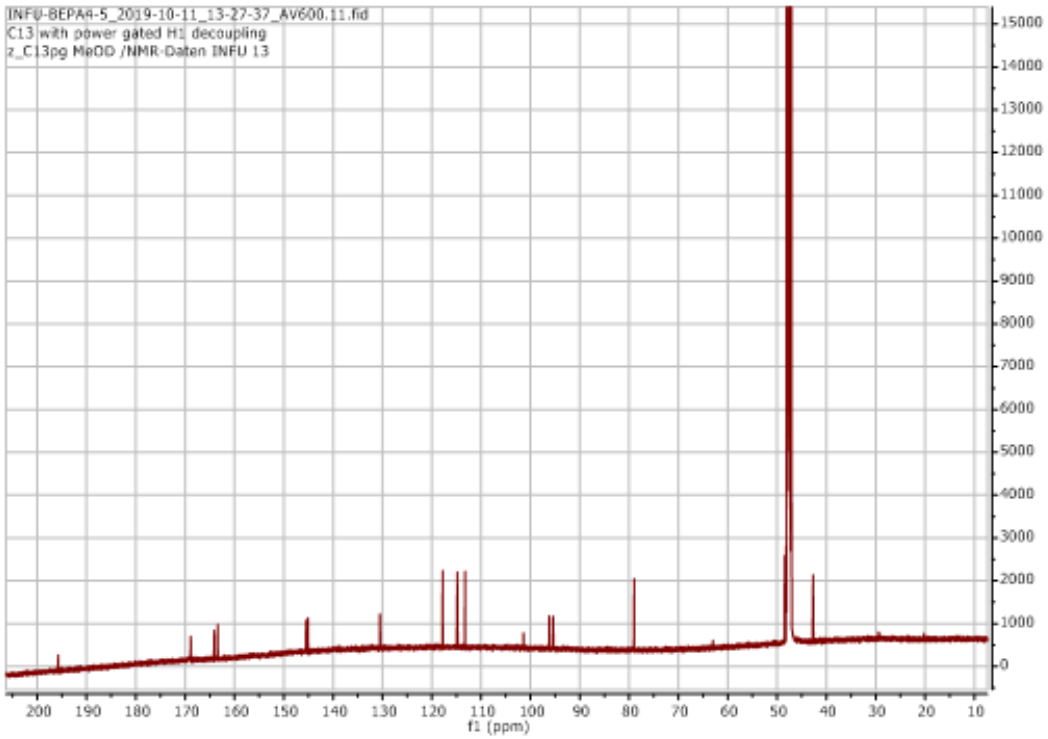

Appendix 35: COSY (600 MHz, MeOD) spectrum of 21

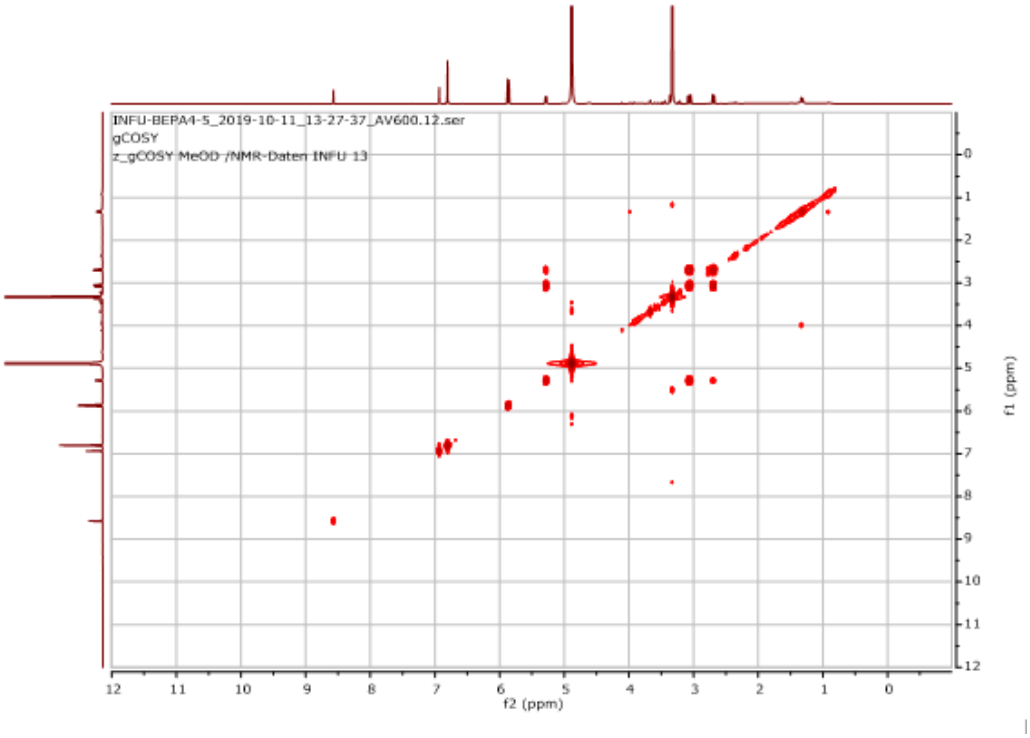

Appendix 36: HSQC (MeOD) spectrum of **21** (^{1}H: 600 MHz, ^{13}C: 175 MHz)

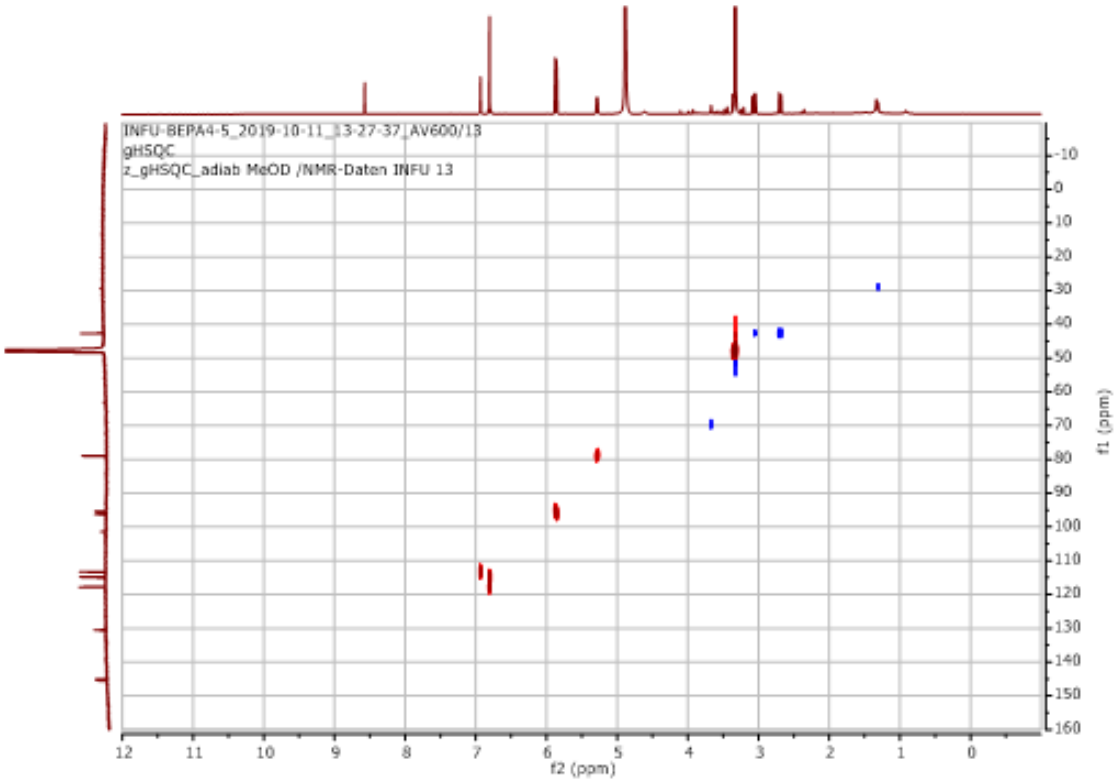

Appendix 37: HMBC (MeOH) spectrum of **21** (^{1}H: 600 MHz, ^{13}C: 175 MHz)

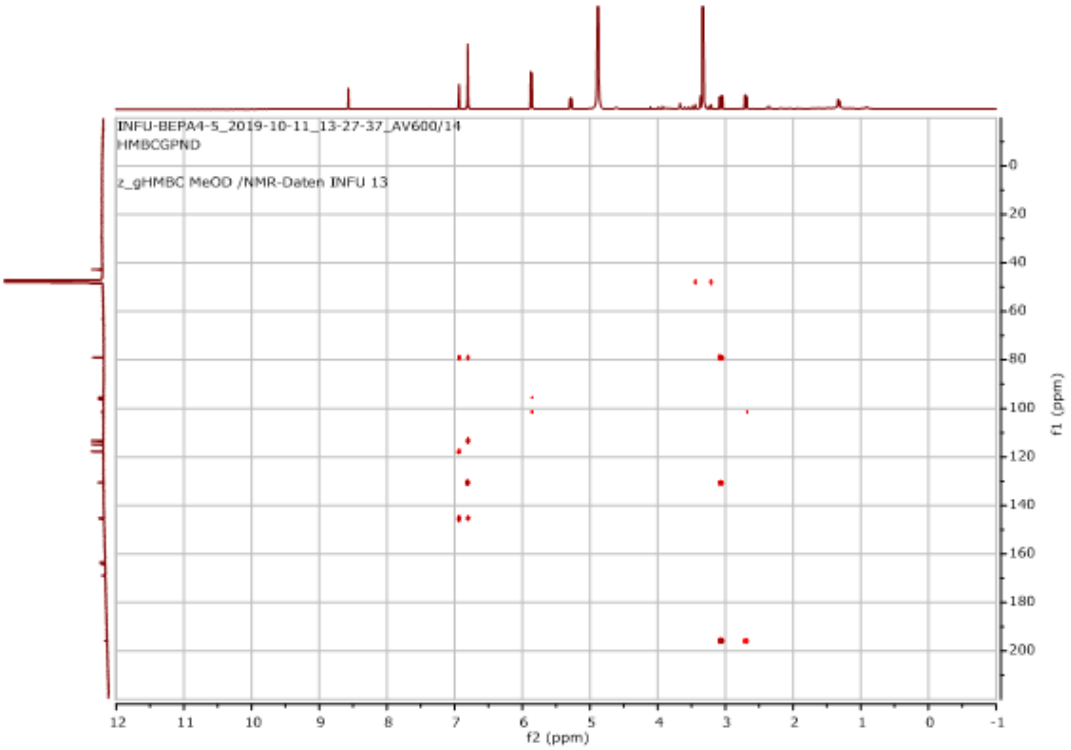

Appendix 38: NOESY (600 MHz, MeOD) spectrum of **21**

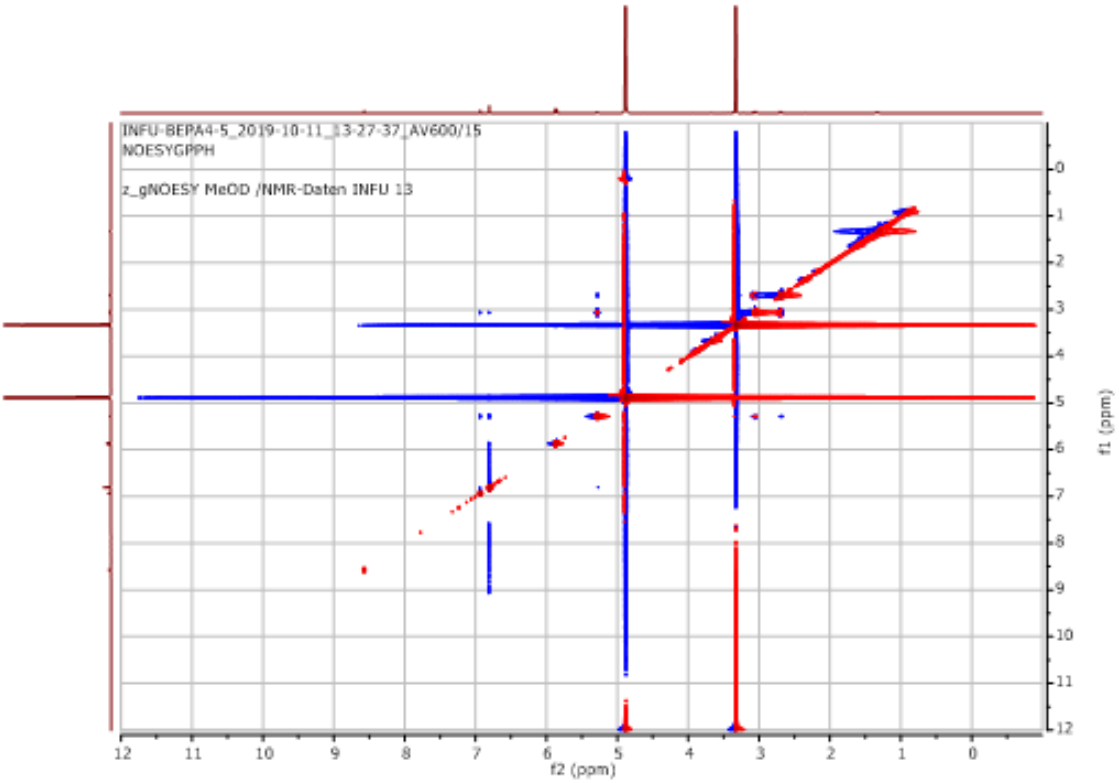

Appendix 39: HRESIMS spectrum of **22**

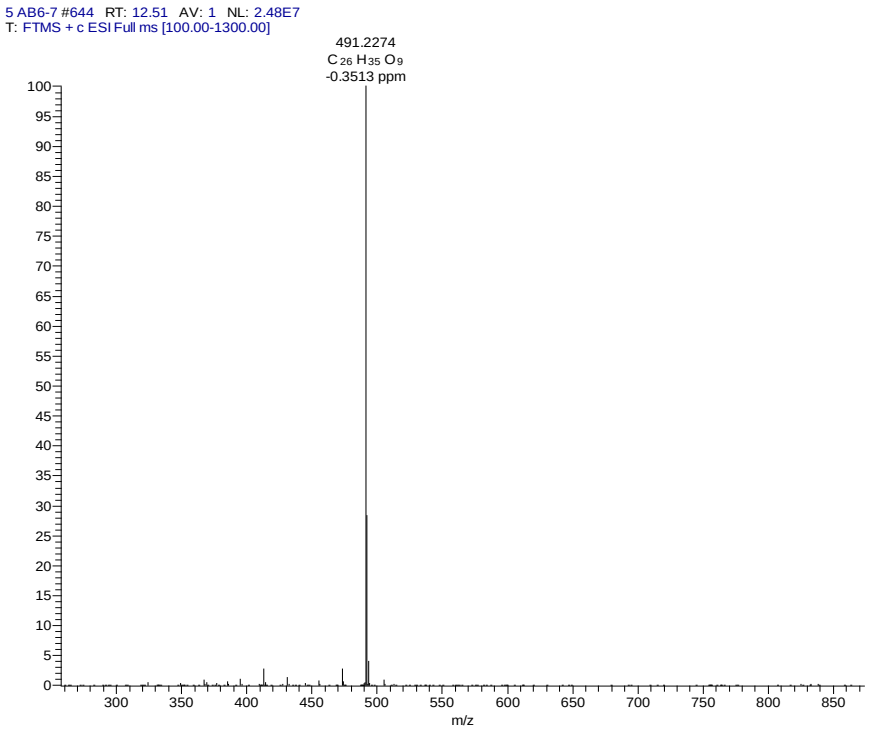

Appendix 40: Infrared spectrum of **22**

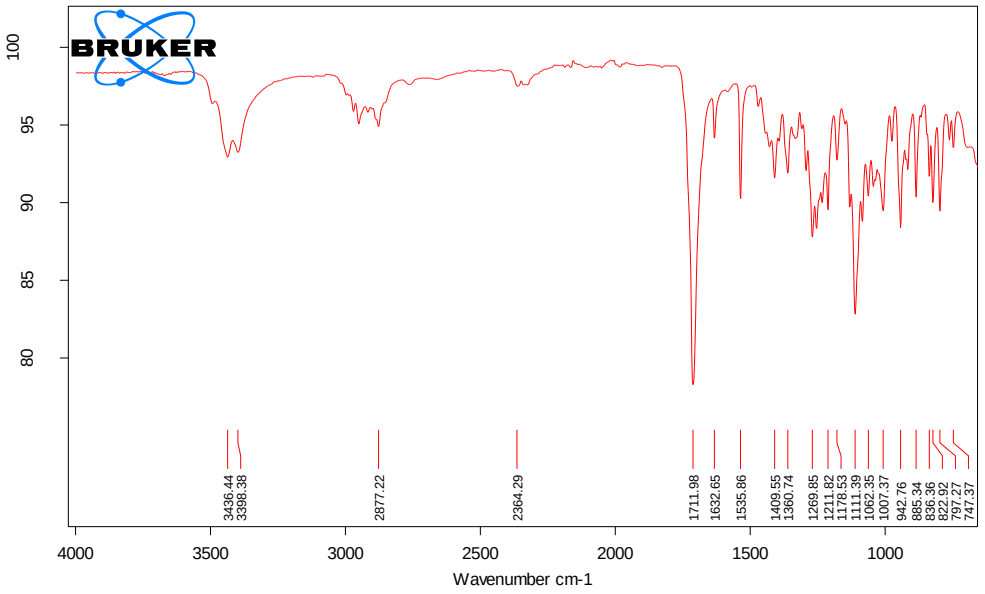

C:\Messungen\INFU\BEPA\AB6-7.0000 AB6-7 Solid 03.12.2019

Seite 1 von 1

Appendix 41: ^{1}H NMR (600 MHz, DMSO-d_6) of spectrum **22**

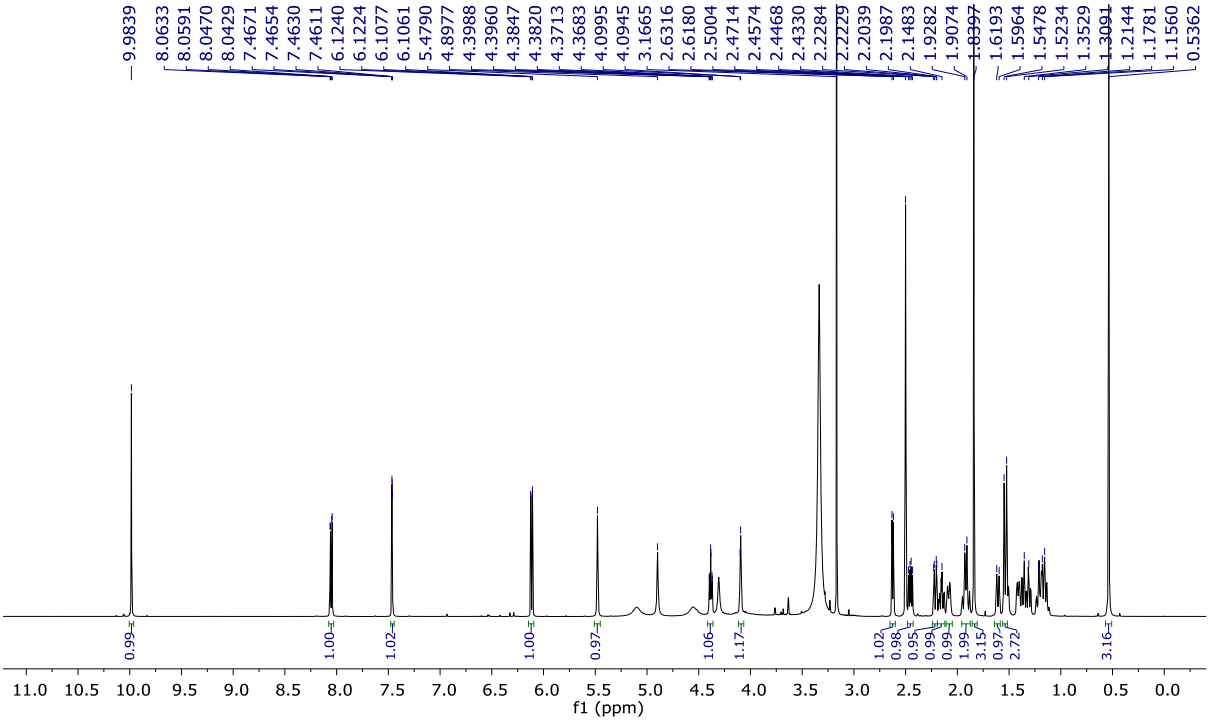

Appendix 42: ^{13}C NMR (175 MHz, DMSO-d_6) of spectrum **22**

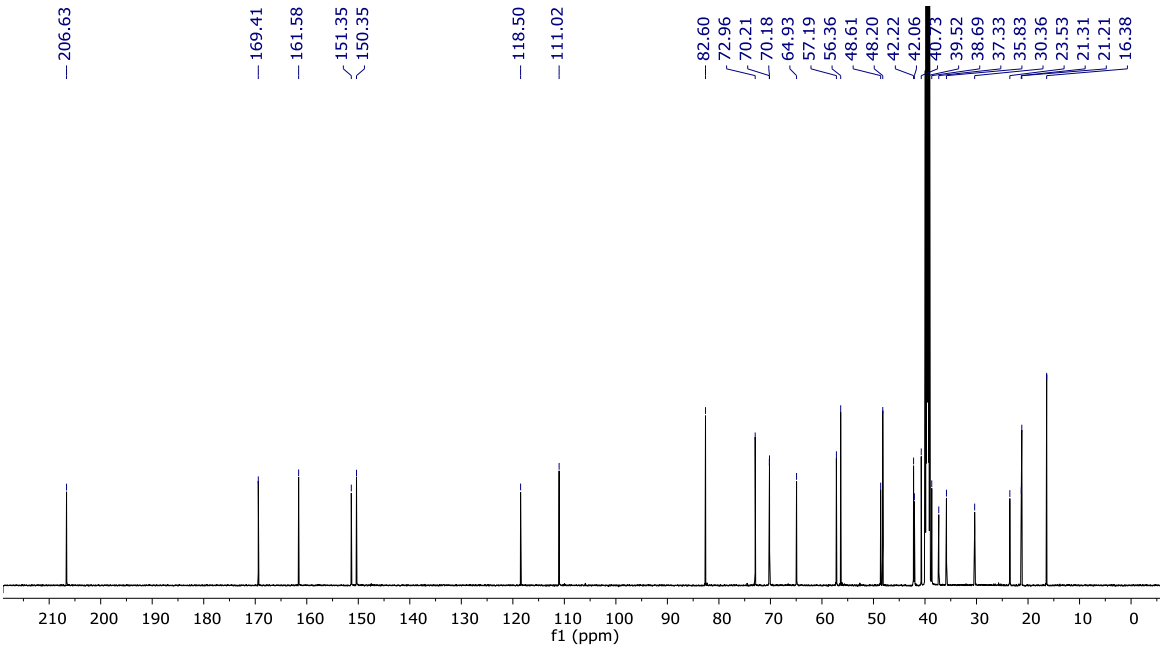

Appendix 43: COSY (600 MHz, DMSO-d_6) spectrum of **22**

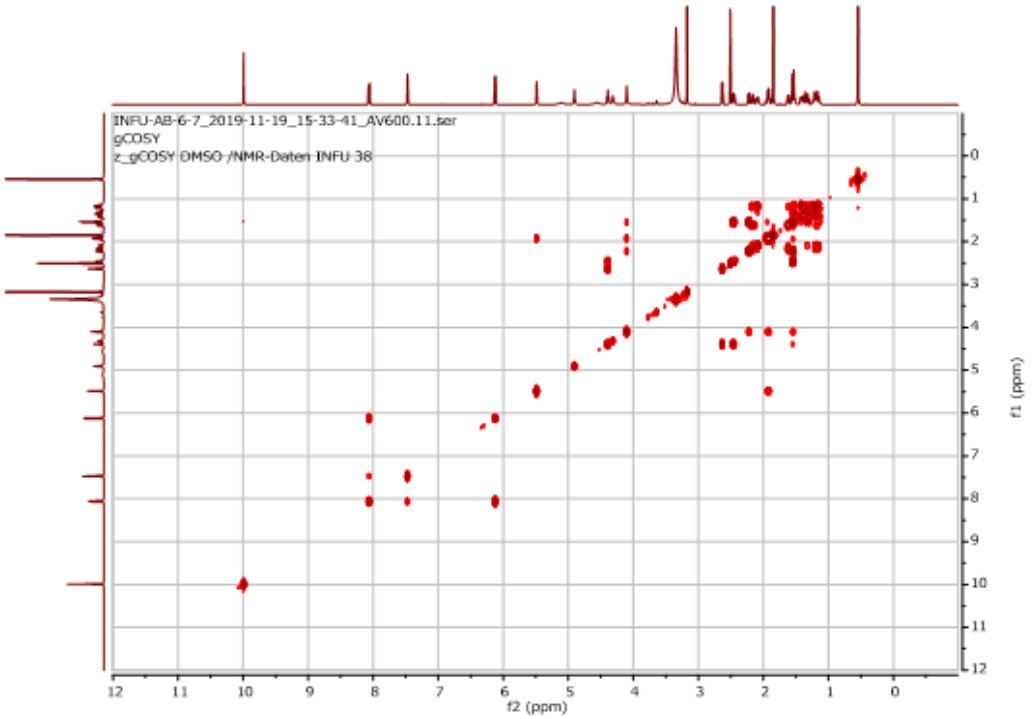

Appendix 44: HSQC (DMSO-d6) spectrum of **22** (1H: 600 MHz, 13C: 175 MHz)

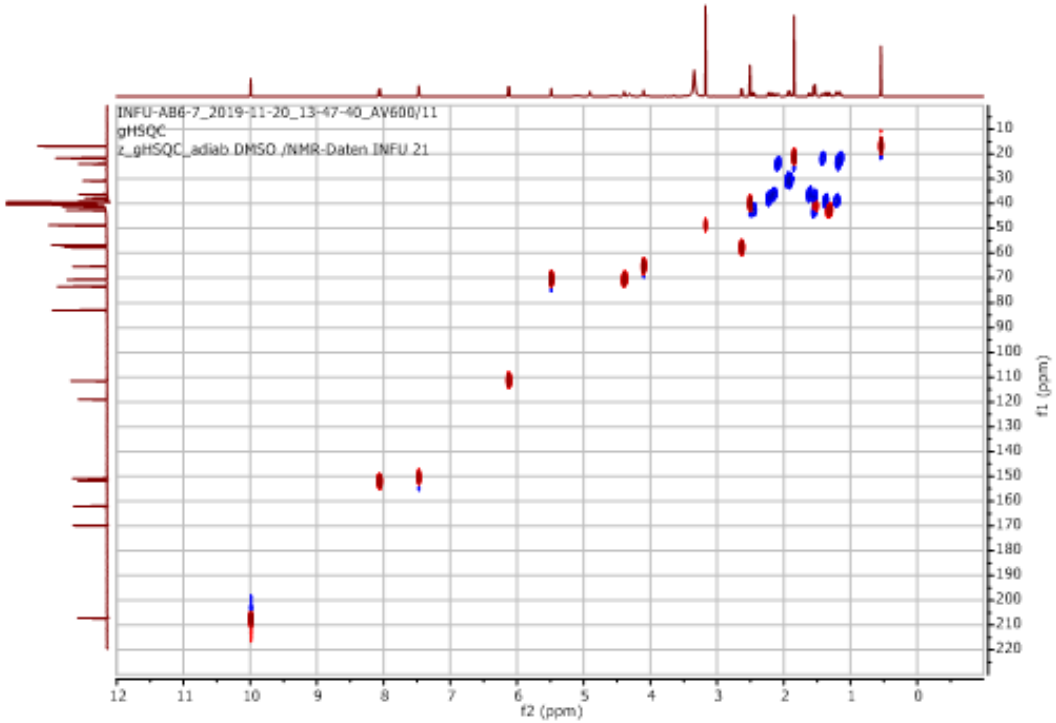

Appendix 45: HMBC (DMSO-d6) spectrum of **22** (1H: 600 MHz, 13C: 175 MHz)

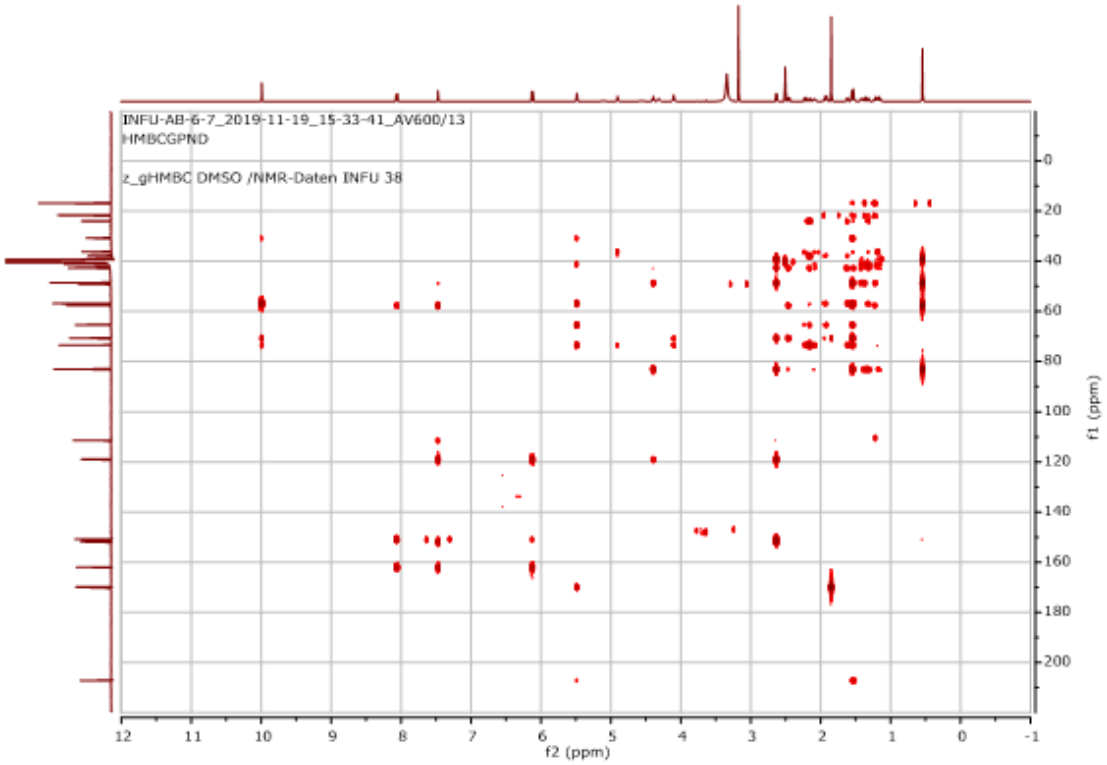

Appendix 46: HRESIMS of **23**

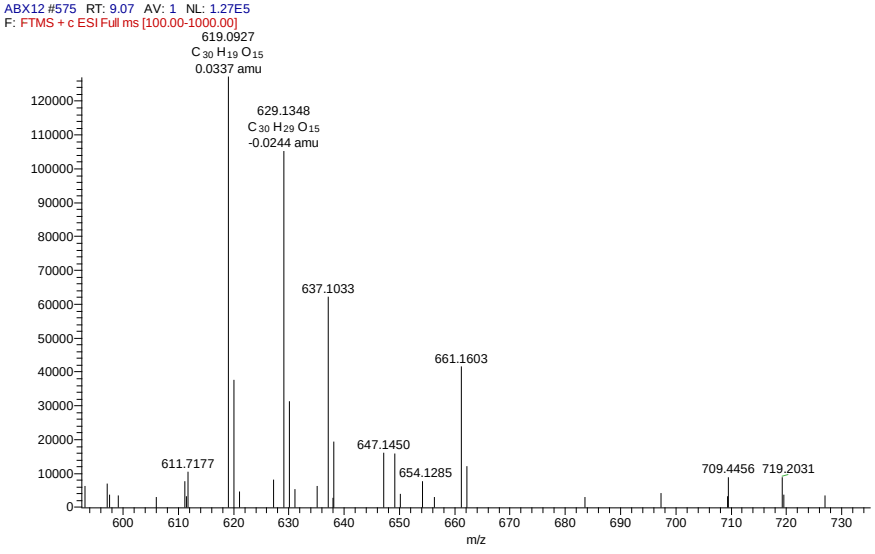

Appendix 47: ^{1}H NMR (600 MHz, DMSO-d_6) spectrum of **23**

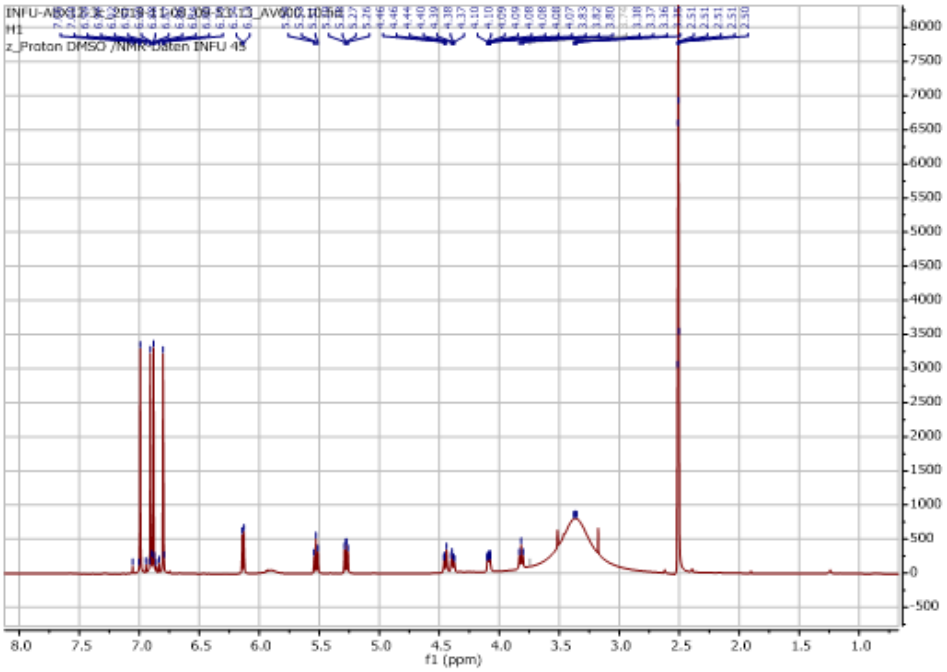

Appendix 48: ^{13}C NMR (175 MHz, DMSO-d_6) spectrum of **23**

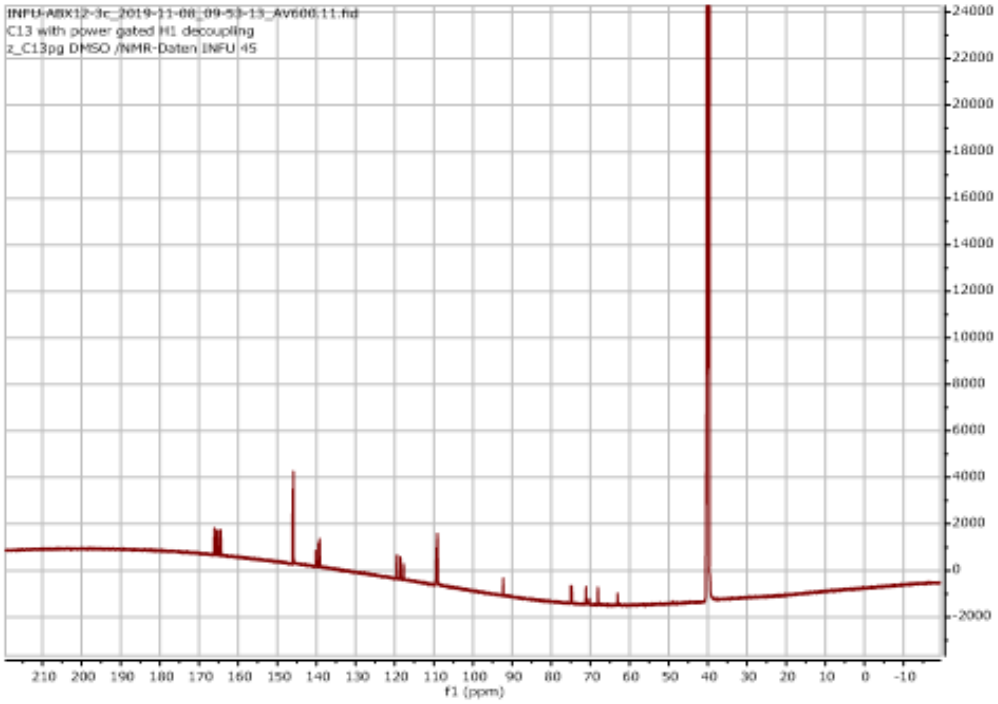

Appendix 49: COSY (600 MHz, DMSO-d_6) spectrum of **23**

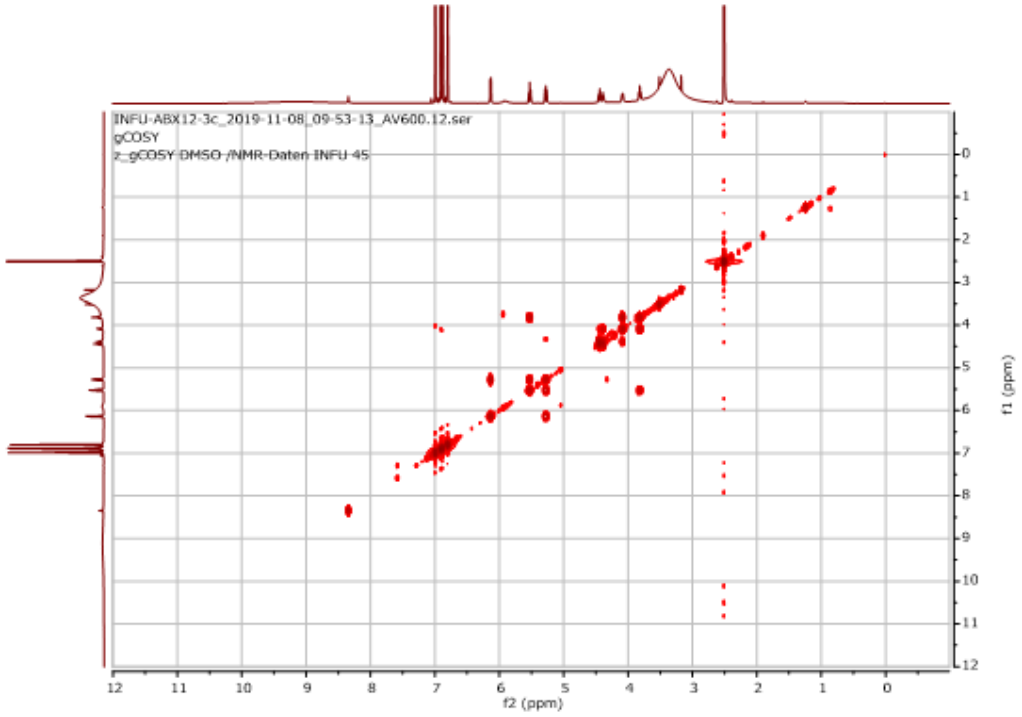

Appendix 50: HSQC (DMSO-d_6) spectrum of **23** (^{1}H: 600 MHz, ^{13}C: 175 MHz)

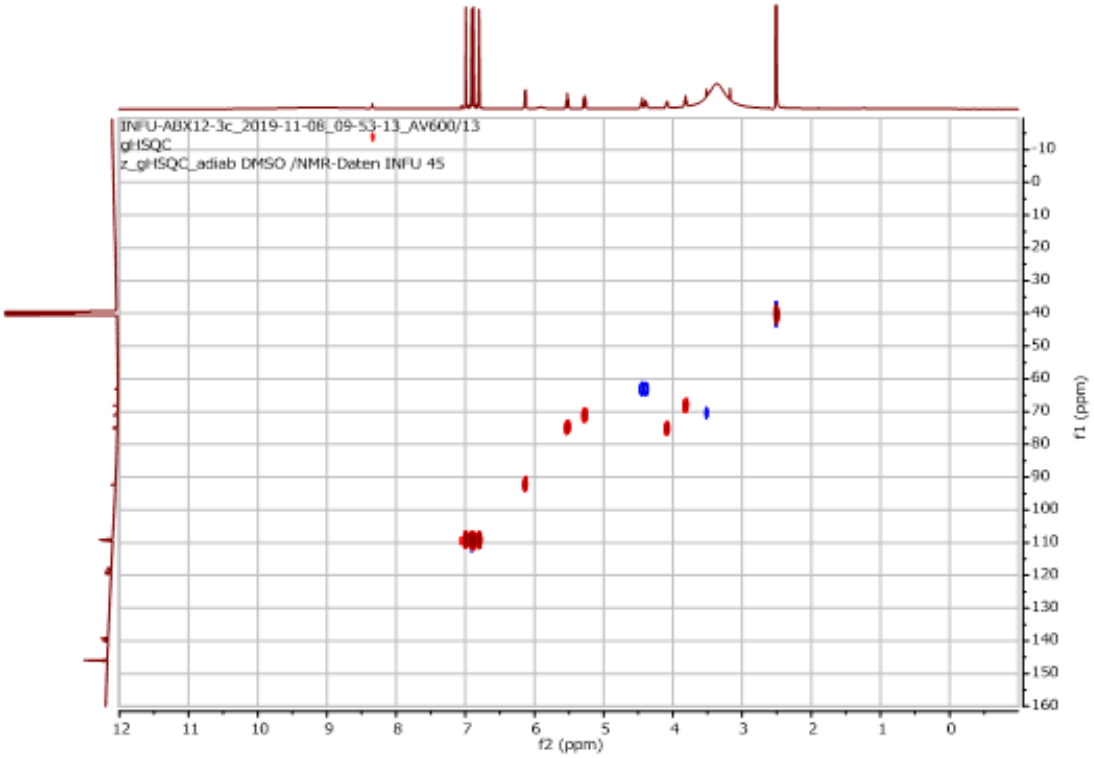

Appendix 51: HMBC (DMSO-d_6) spectrum of **23** (^{1}H: 600 MHz, ^{13}C: 175 MHz)

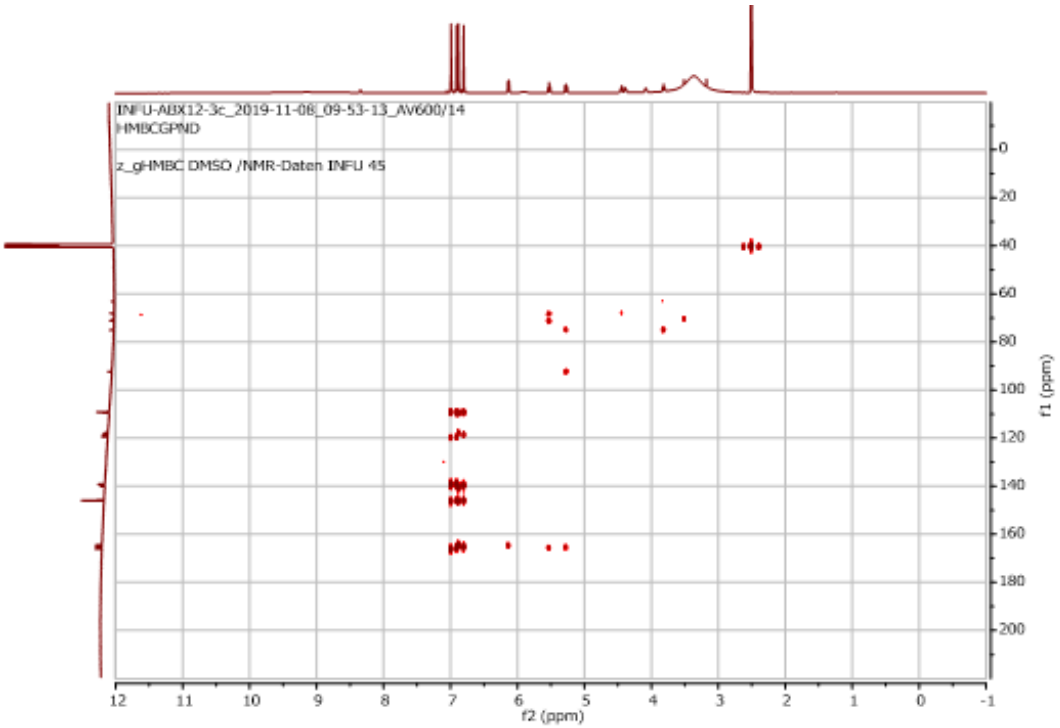

Appendix 52: HRESIMS of **24**

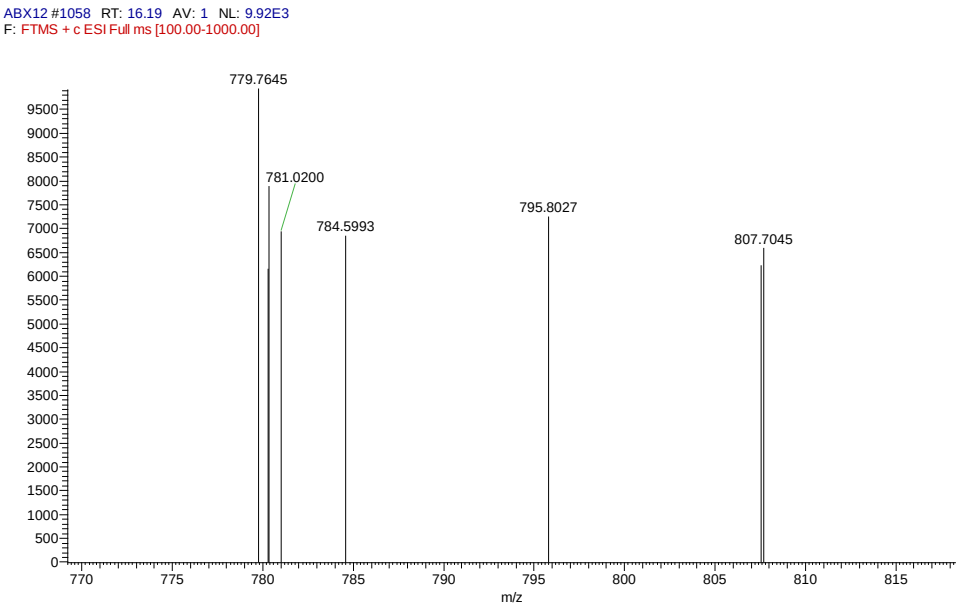

Appendix 53: ^{1}H NMR (600 MHz, DMSO-d_6) spectrum of **24**

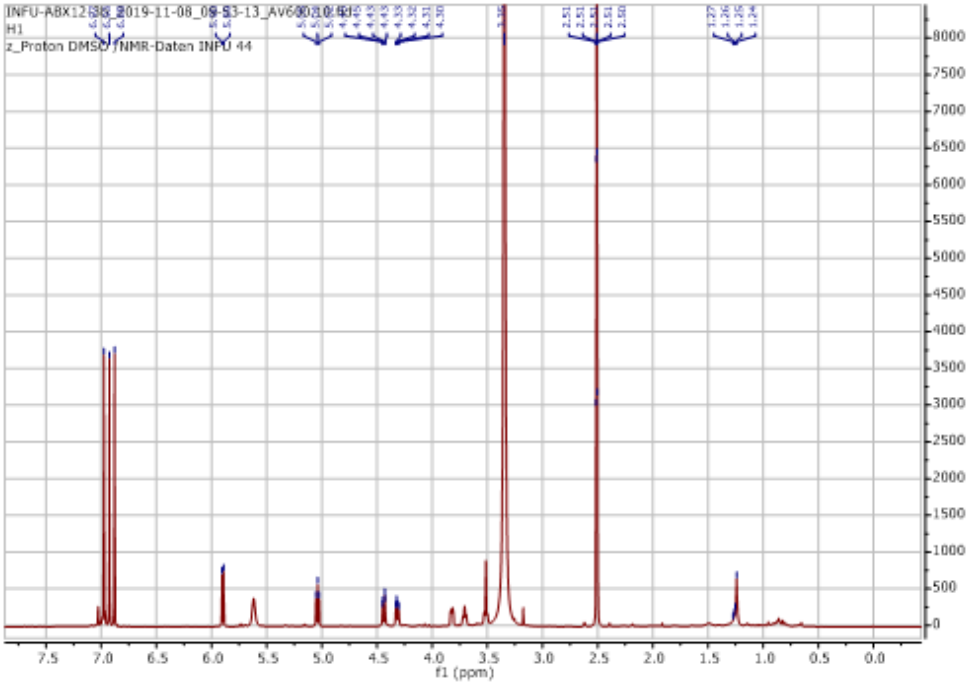

Appendix 54: ^{13}C NMR (175 MHz, DMSO-d_6) spectrum of **24**

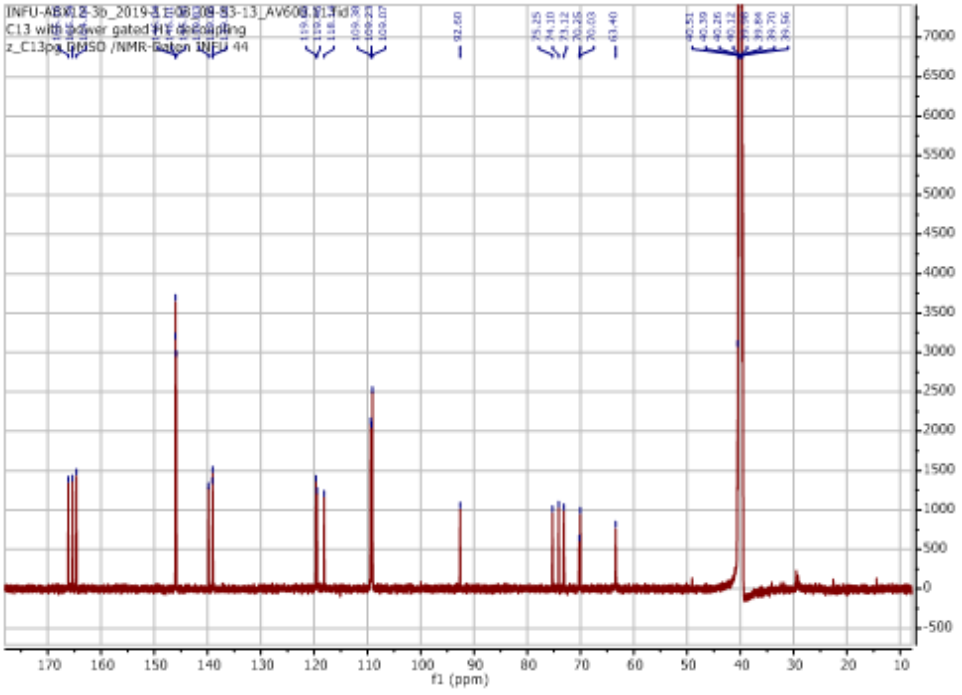

Appendix 55: COSY (600 MHz, DMSO-d_6) spectrum of **24**

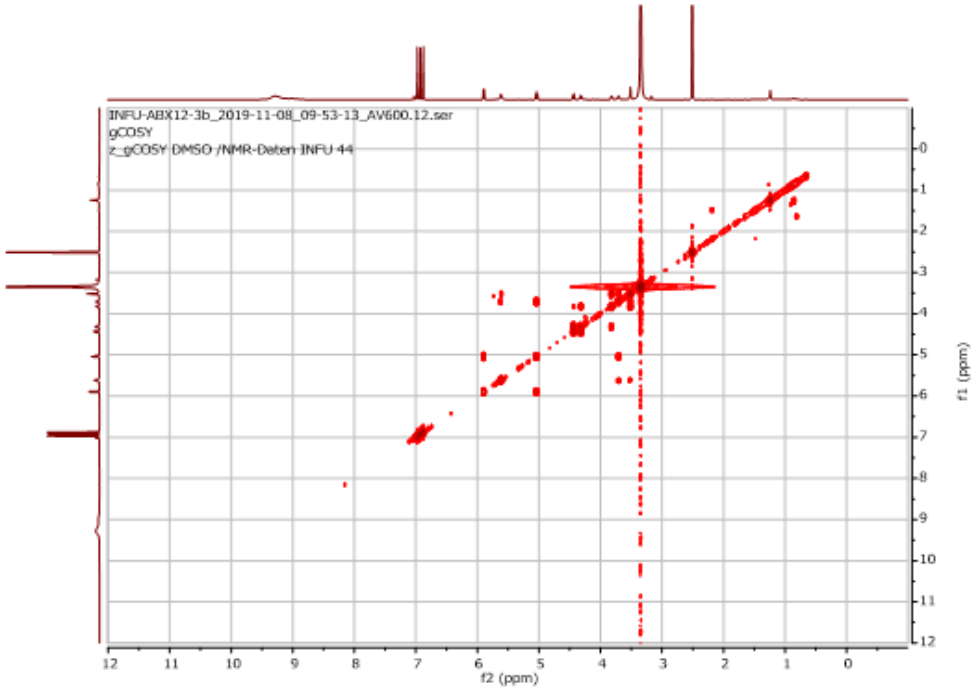

Appendix 56: HSQC (DMSO-d_6) spectrum of **24** (^{1}H: 600 MHz, ^{13}C: 175 MHz)

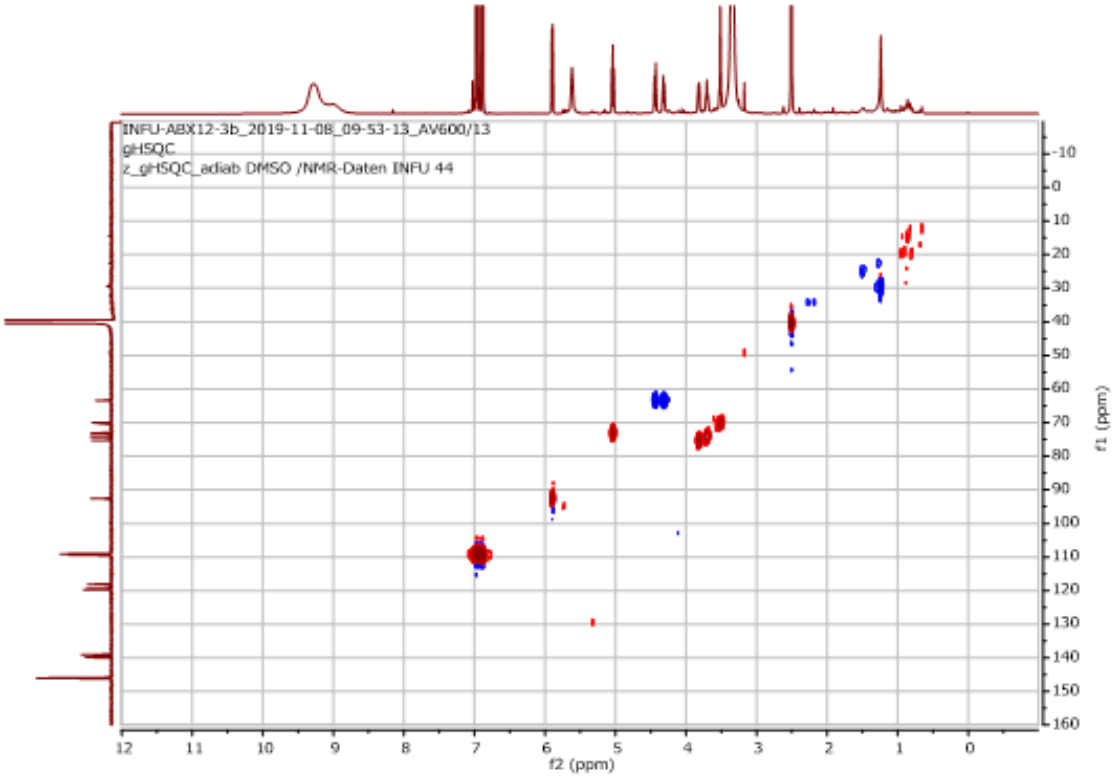

Appendix 57: HMBC (DMSO-d_6) spectrum of **24** (^{1}H: 600 MHz, ^{13}C: 175 MHz)

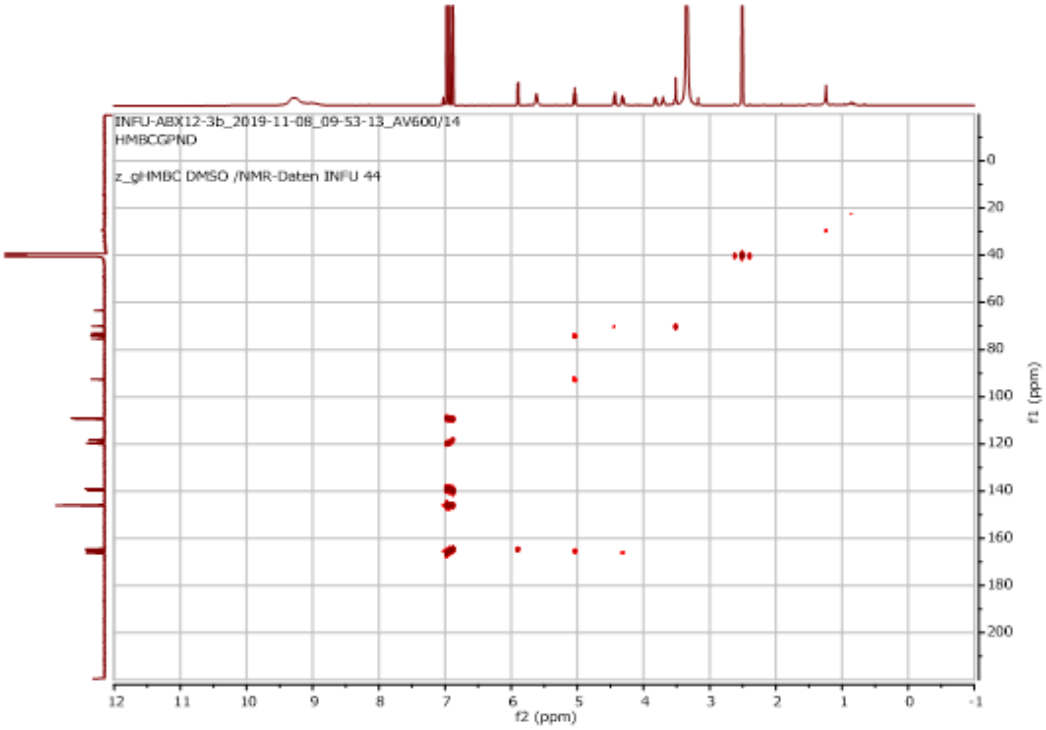

Appendix 58: HRESIMS of **25**

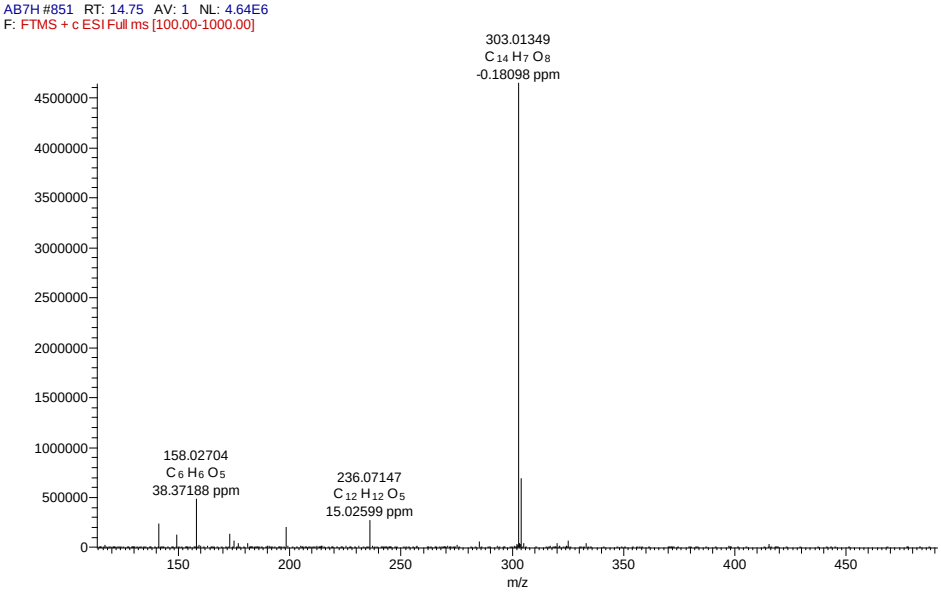

Appendix 59: ^{1}H NMR (600 MHz, DMSO-d_6) spectrum of **25**

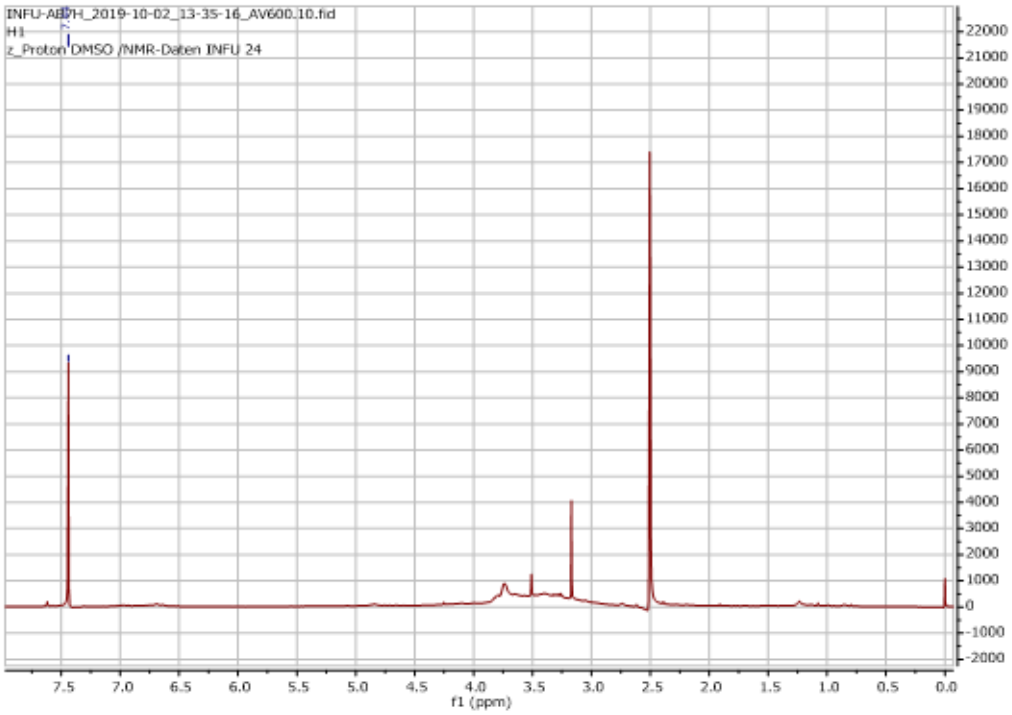

Appendix 60: ^{13}C NMR (175 MHz, DMSO-d_6) spectrum of **25**

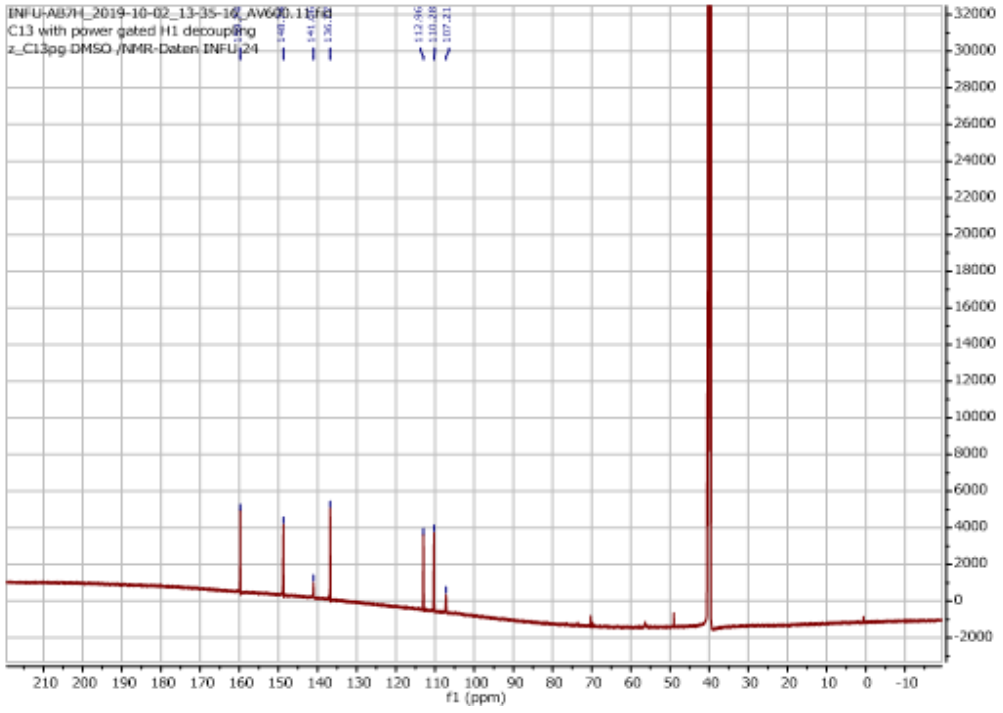

Appendix 61: COSY (600 MHz, DMSO-d_6) spectrum of **25**

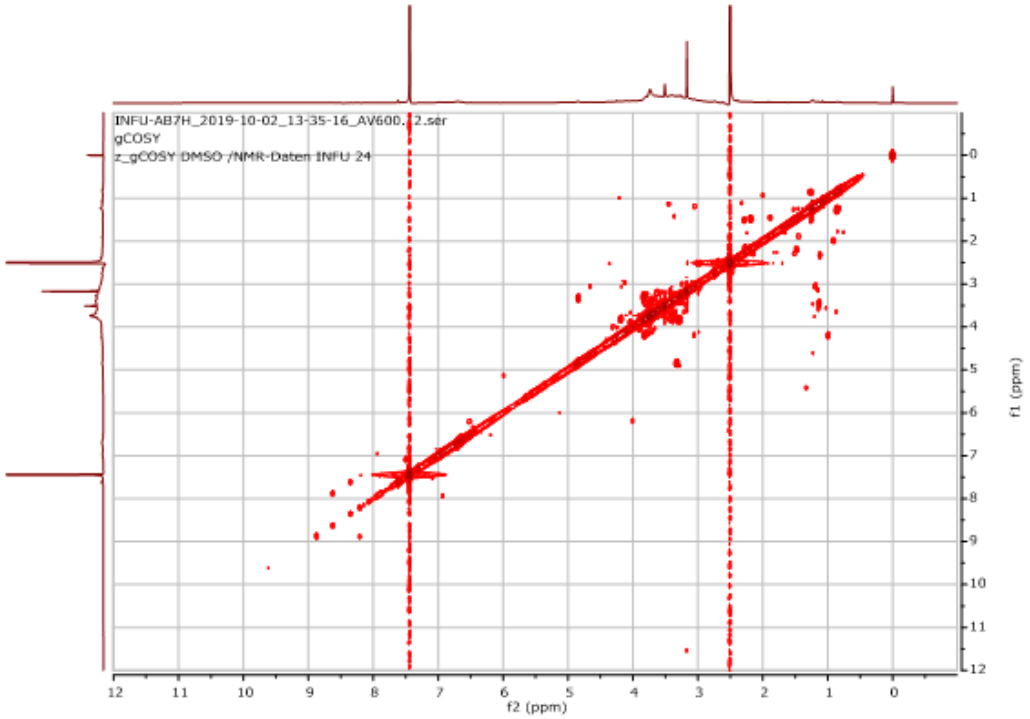

Appendix 62: HSQC (DMSO-d6) spectrum of **25** (1H: 600 MHz, 13C: 175 MHz)

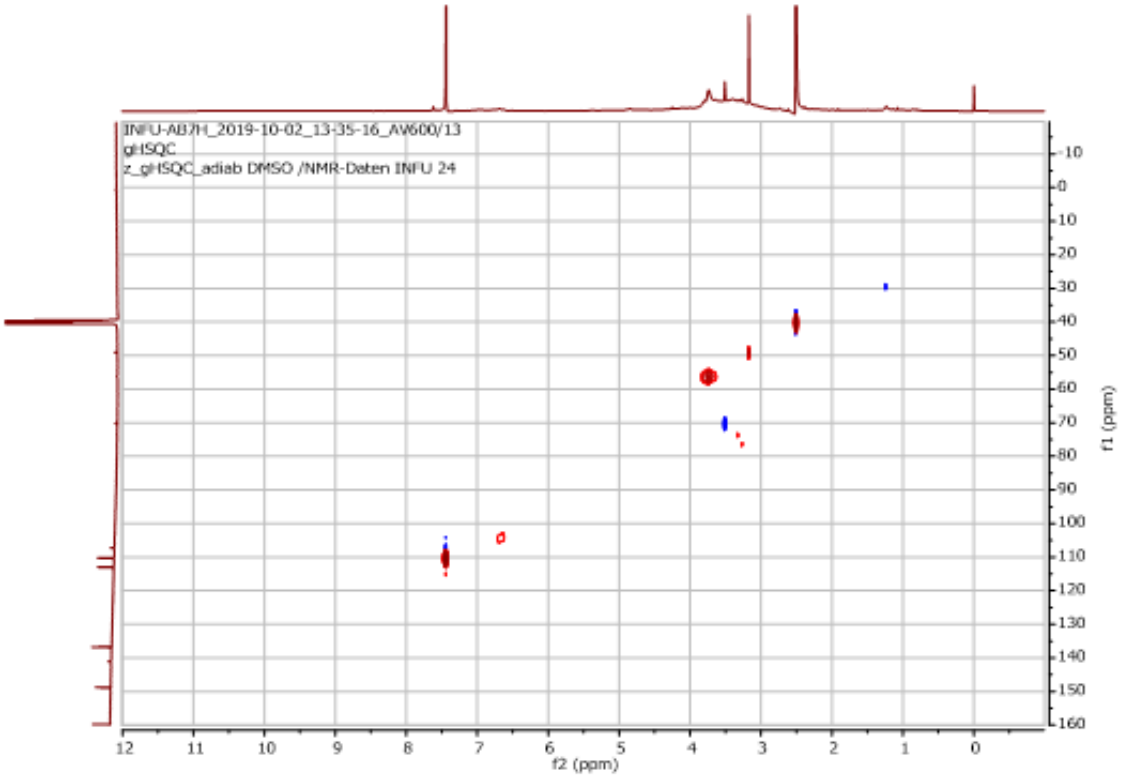

Appendix 63: HMBC (DMSO-d_6) spectrum of **25** (^{1}H: 600 MHz, ^{13}C: 175 MHz)

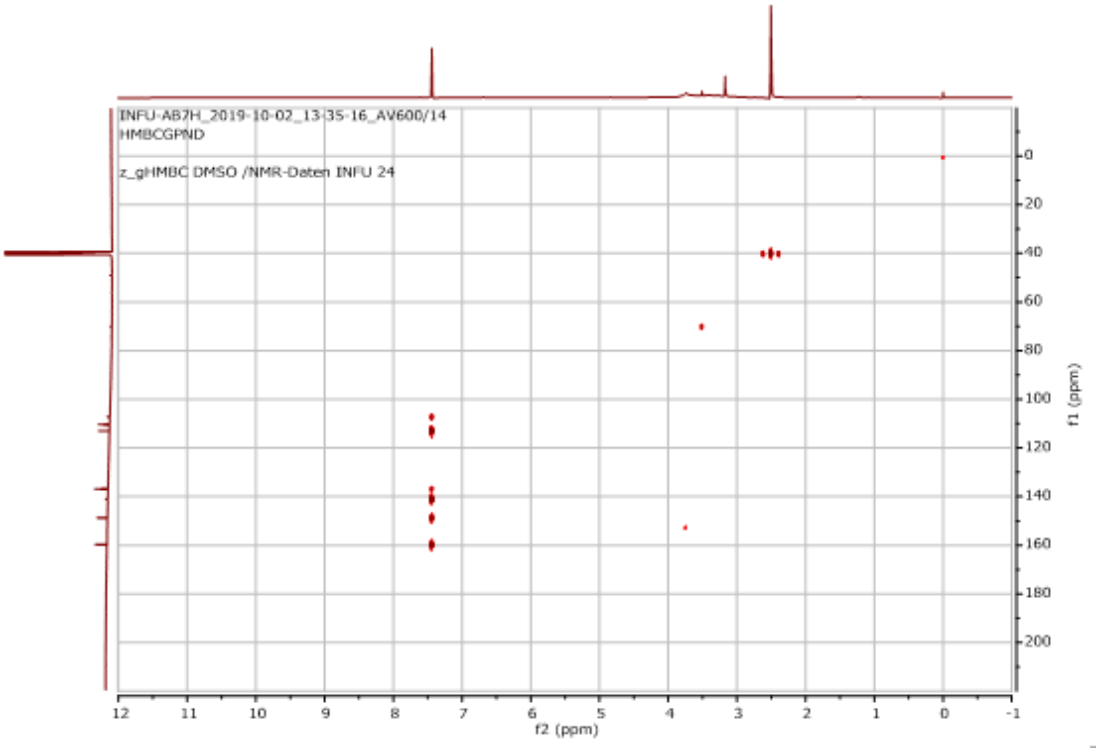

Appendix 64: HRESIMS of 26

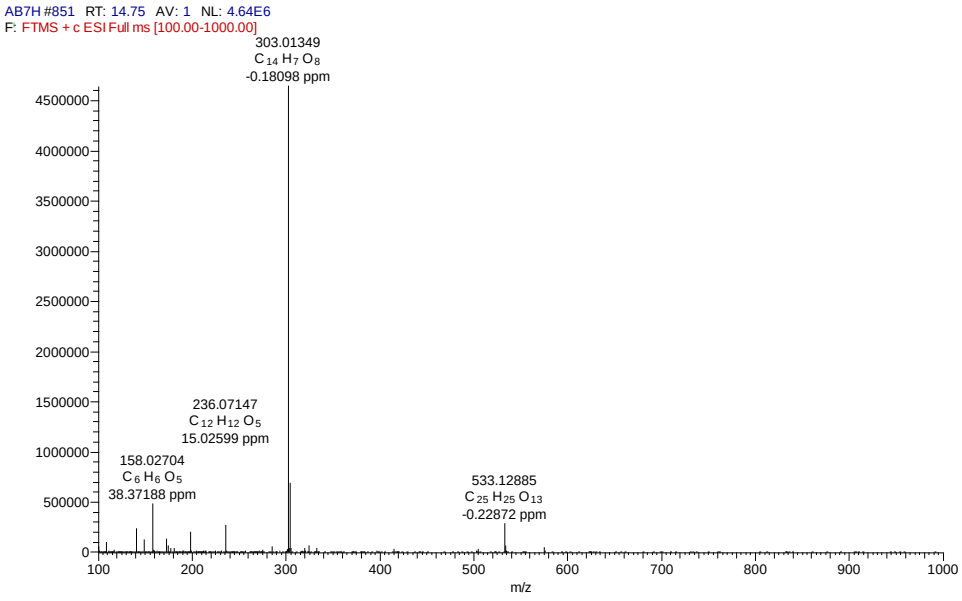

Appendix 65: ^{1}H NMR (700 MHz, DMSO-d_6) spectrum of **26**

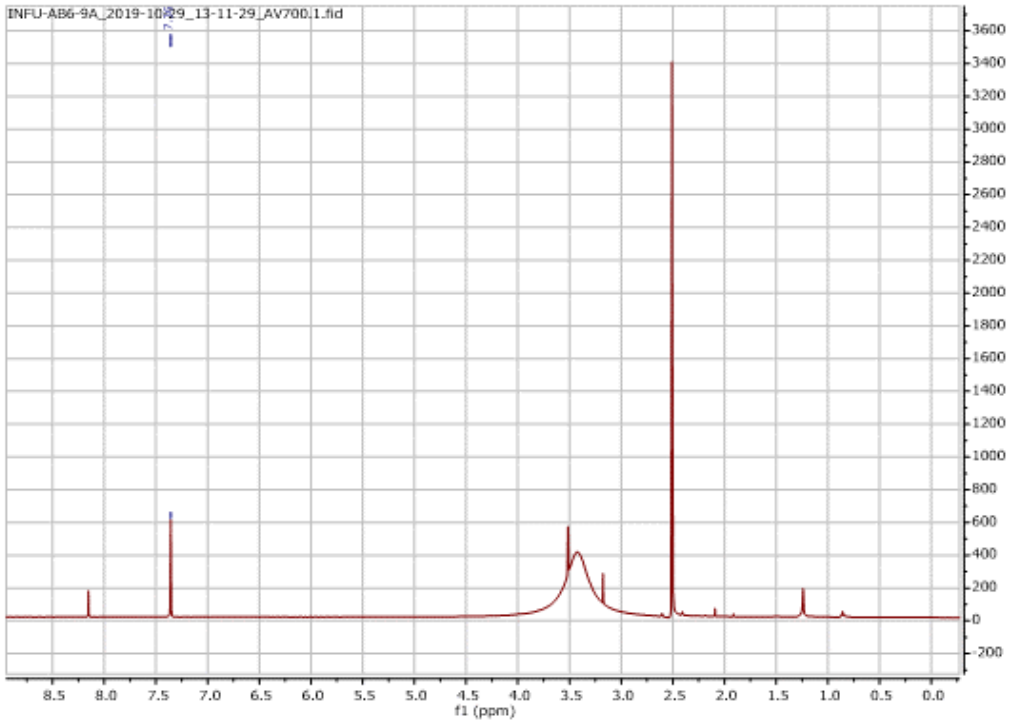

Appendix 66: ^{13}C NMR (175 MHz, DMSO-d_6) spectrum of **26**

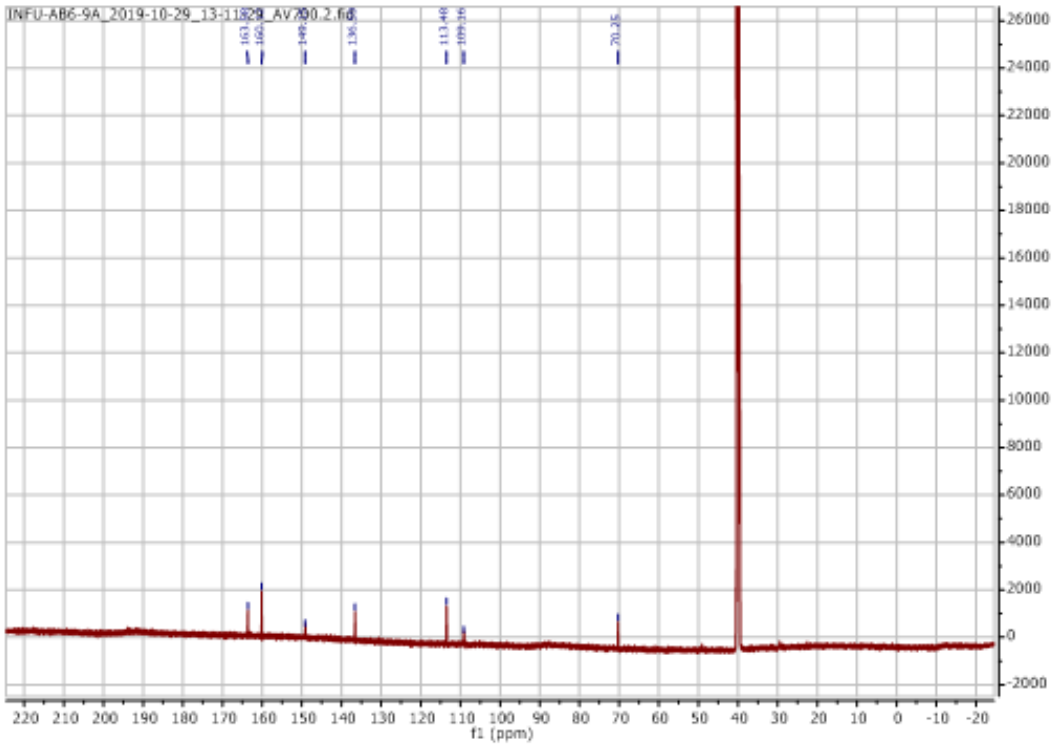

Appendix 67: COSY (700 MHz, DMSO-d_6) spectrum of **26**

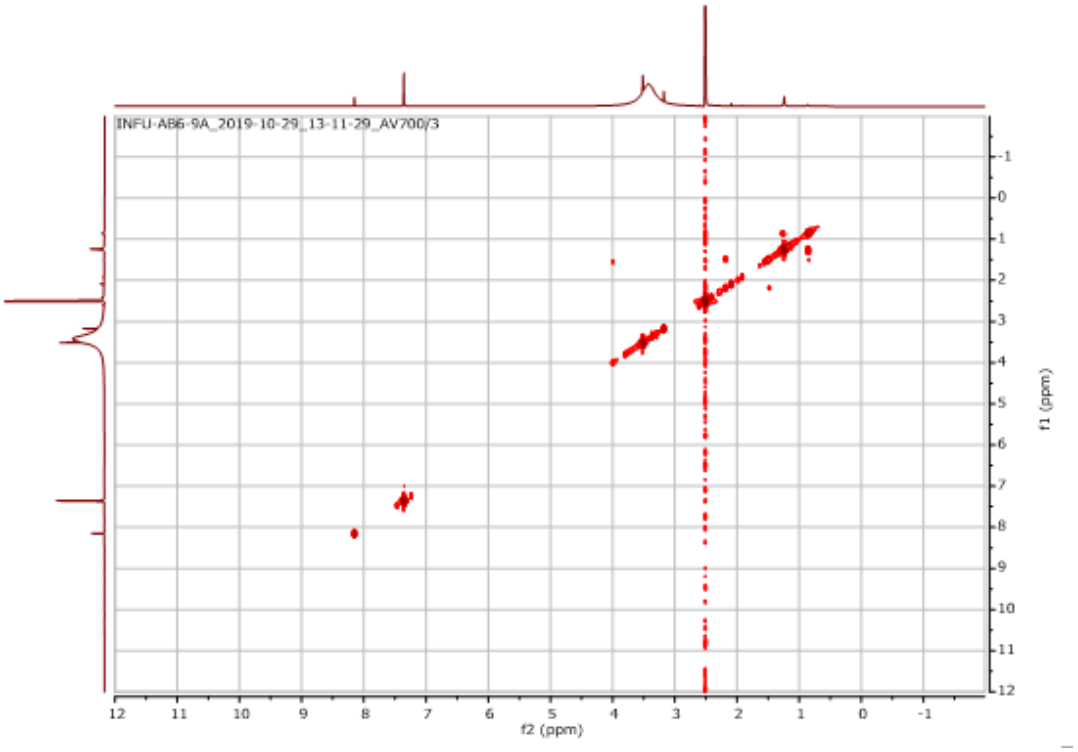

Appendix 68: HSQC (DMSO-d_6) spectrum of **26** (^{1}H: 700 MHz, ^{13}C: 175 MHz)

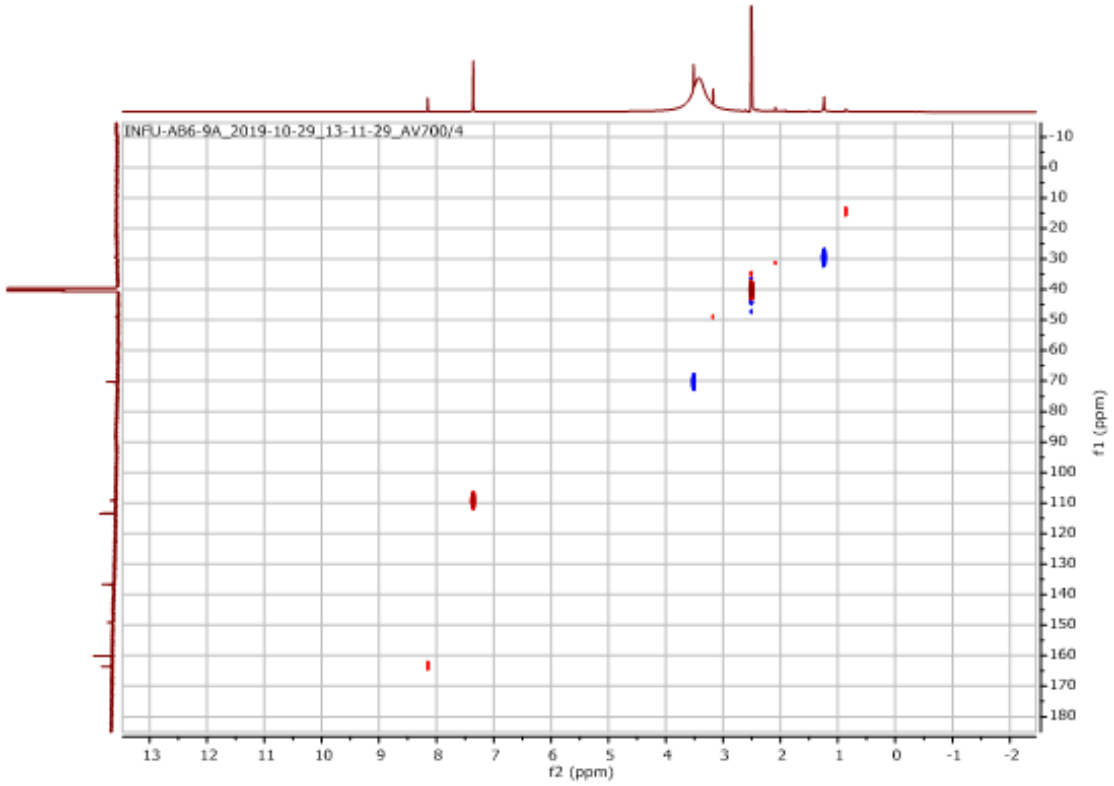

Appendix 69: HMBC (DMSO-d_6) spectrum of **26** (^{1}H: 700 MHz, ^{13}C: 175 MHz)

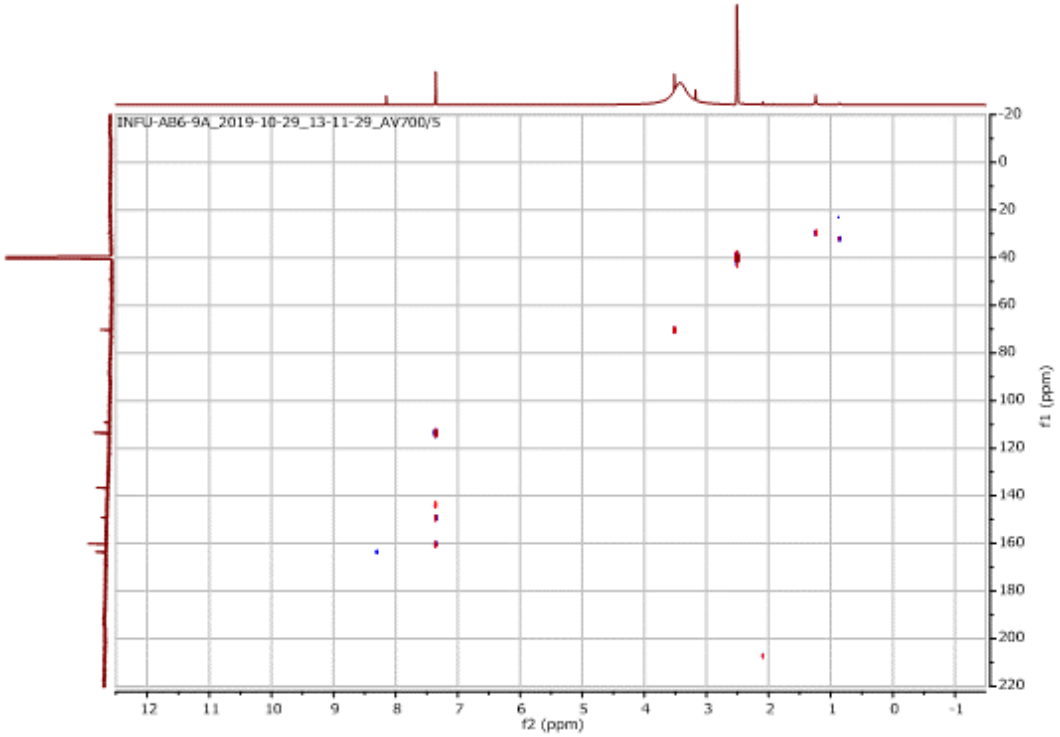

Appendix 70: HRESIMS of **27**

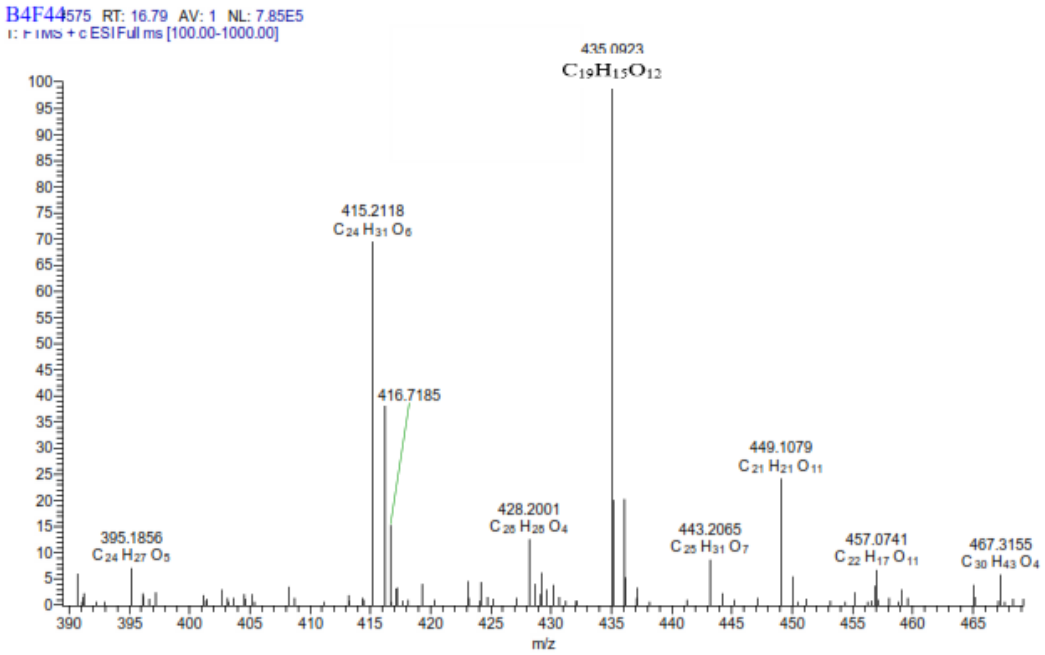

Appendix 71: ^{1}H NMR (600 MHz, DMSO-d_6) spectrum of **27**

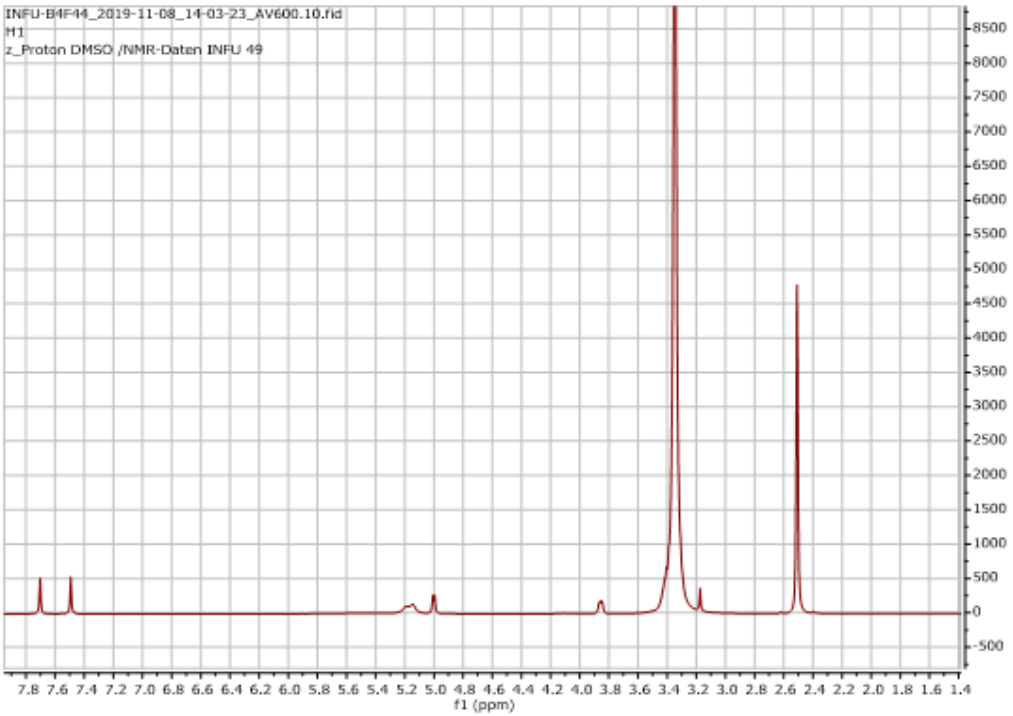

Appendix 72: ^{13}C NMR (175 MHz, DMSO-d_6) spectrum of **27**

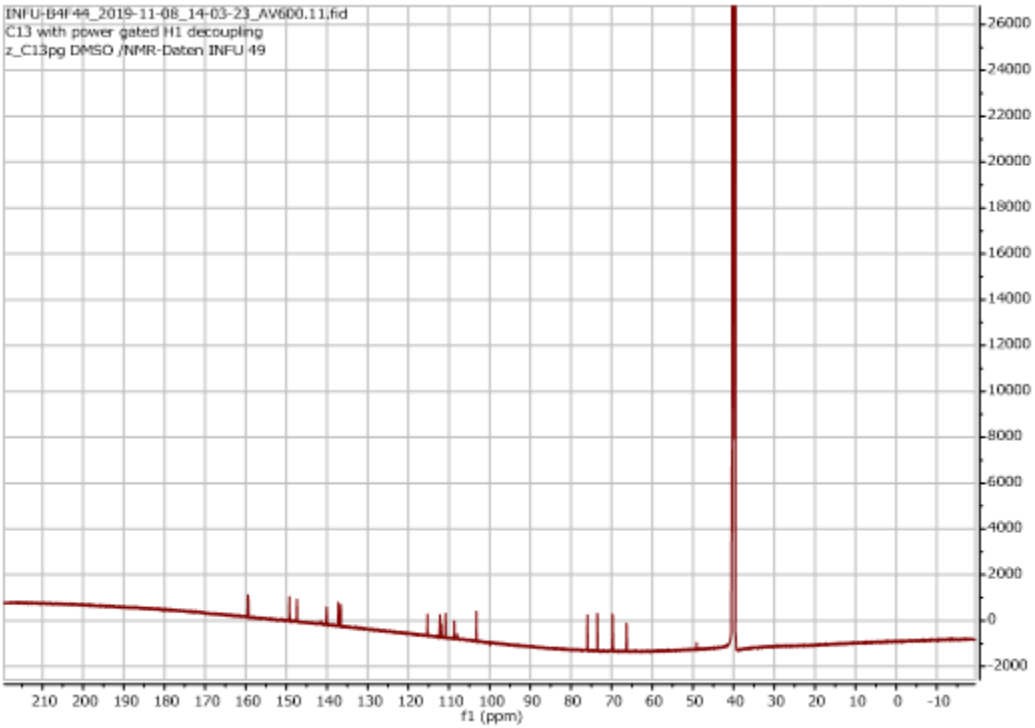

Appendix 73: COSY (600 MHz, DMSO-d_6) spectrum of **27**

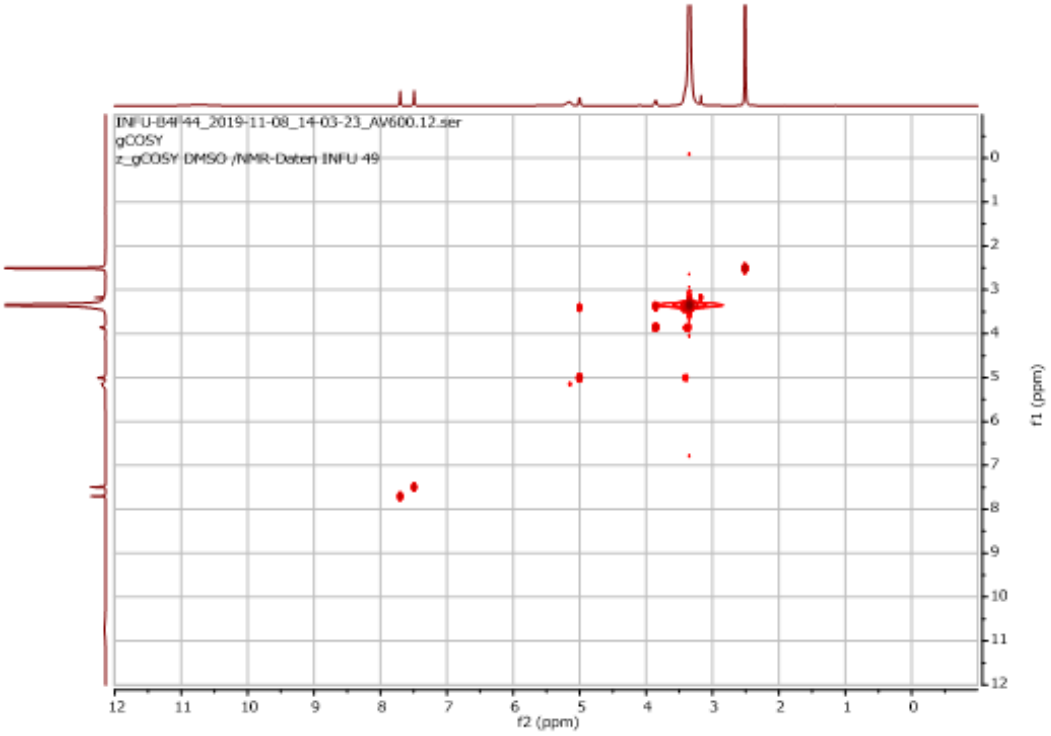

Appendix 74: HSQC (DMSO-d_6) spectrum of **27** (^{1}H: 600 MHz, ^{13}C: 175 MHz)

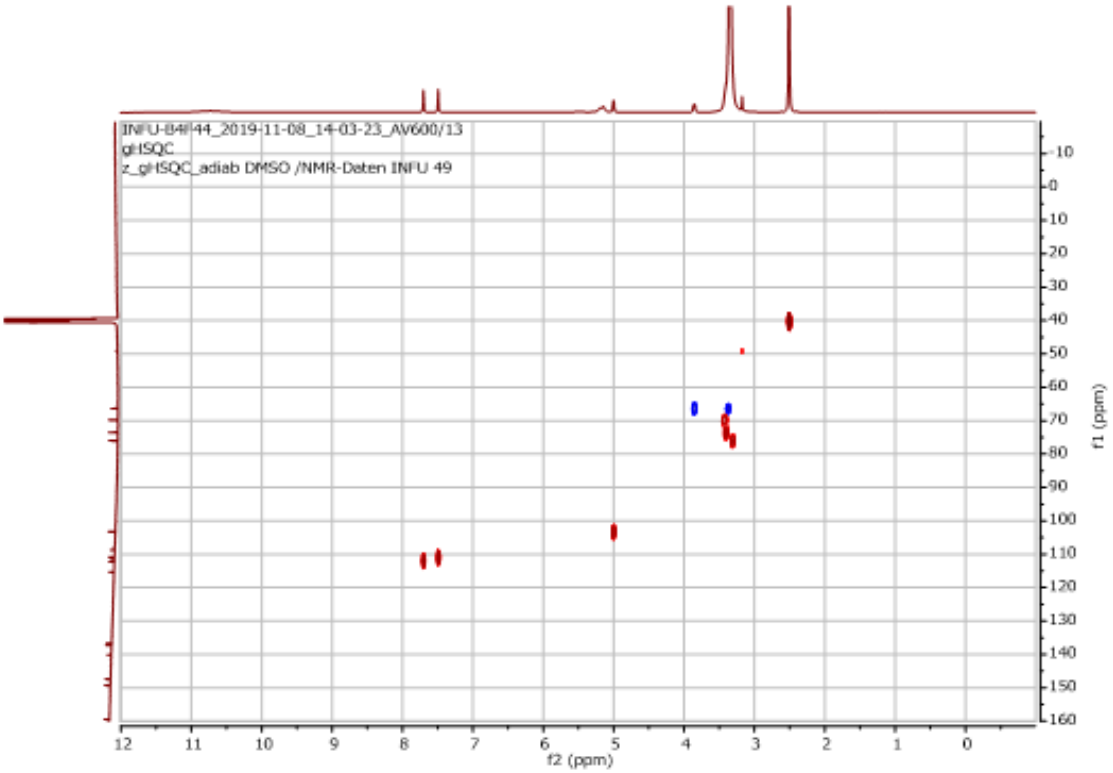

Appendix 75: HMBC (DMSO-d_6) spectrum of **27** (^{1}H: 600 MHz, ^{13}C: 175 MHz)

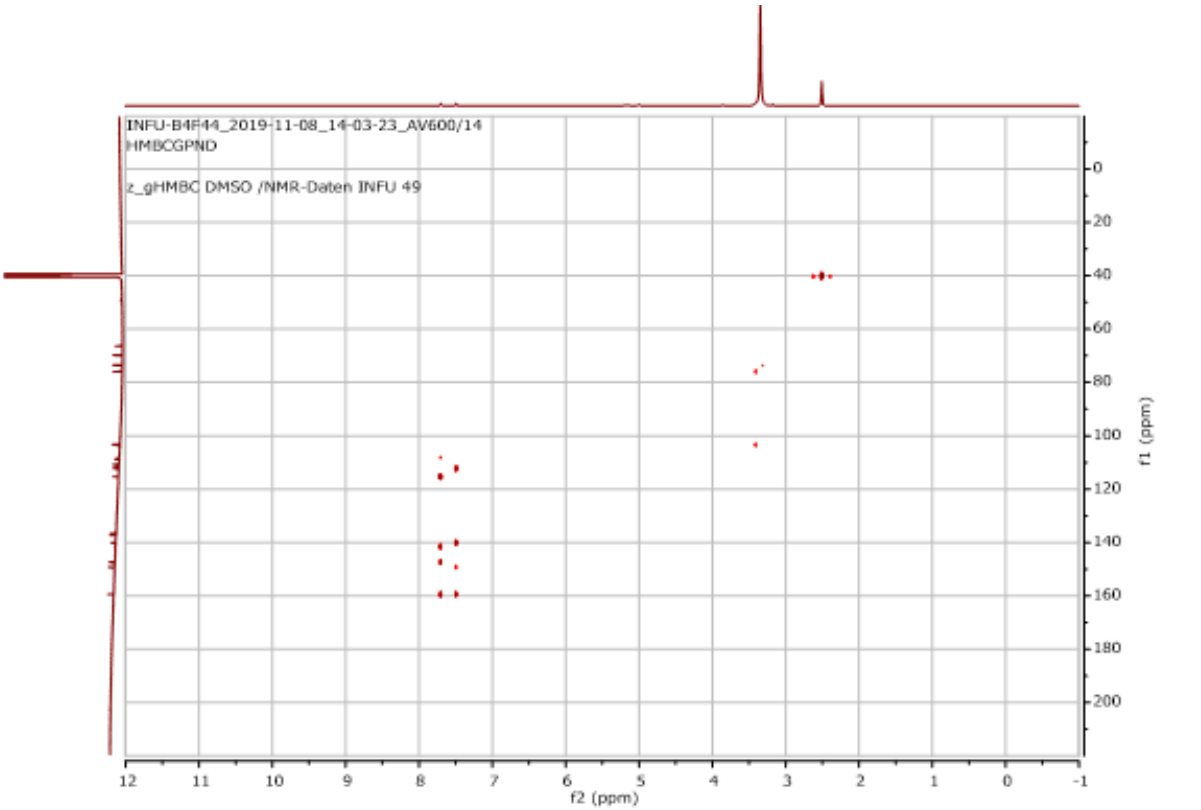

Appendix 76: HRESIMS of **28**

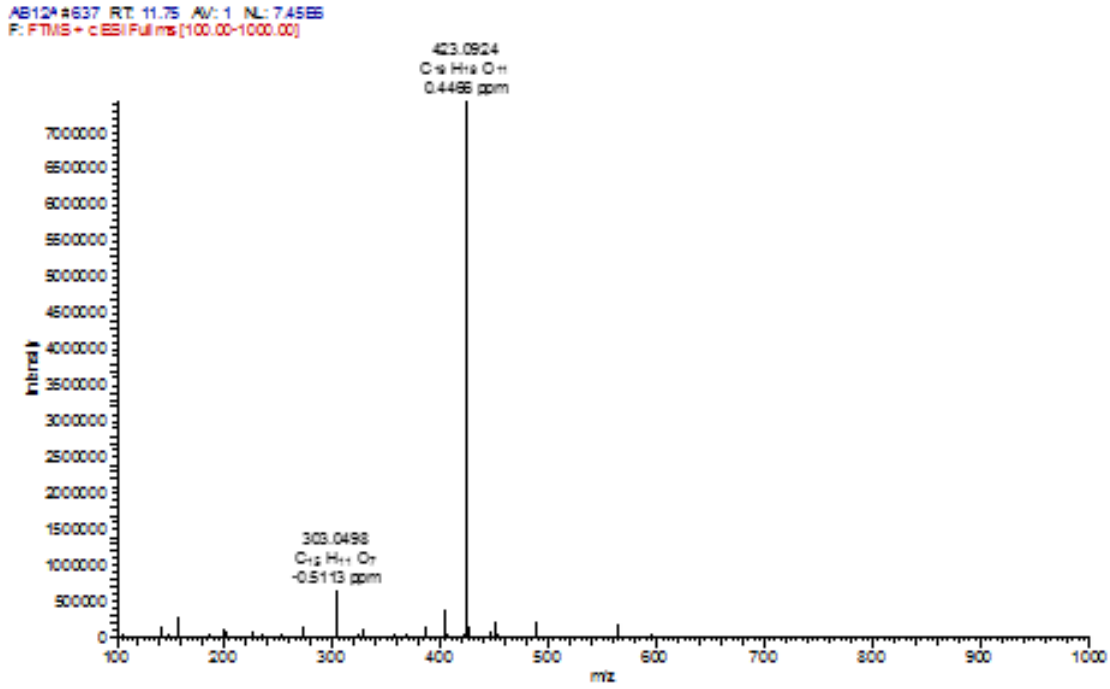

Appendix 77: ^{1}H NMR (600 MHz, DMSO-d_6) spectrum of **28**

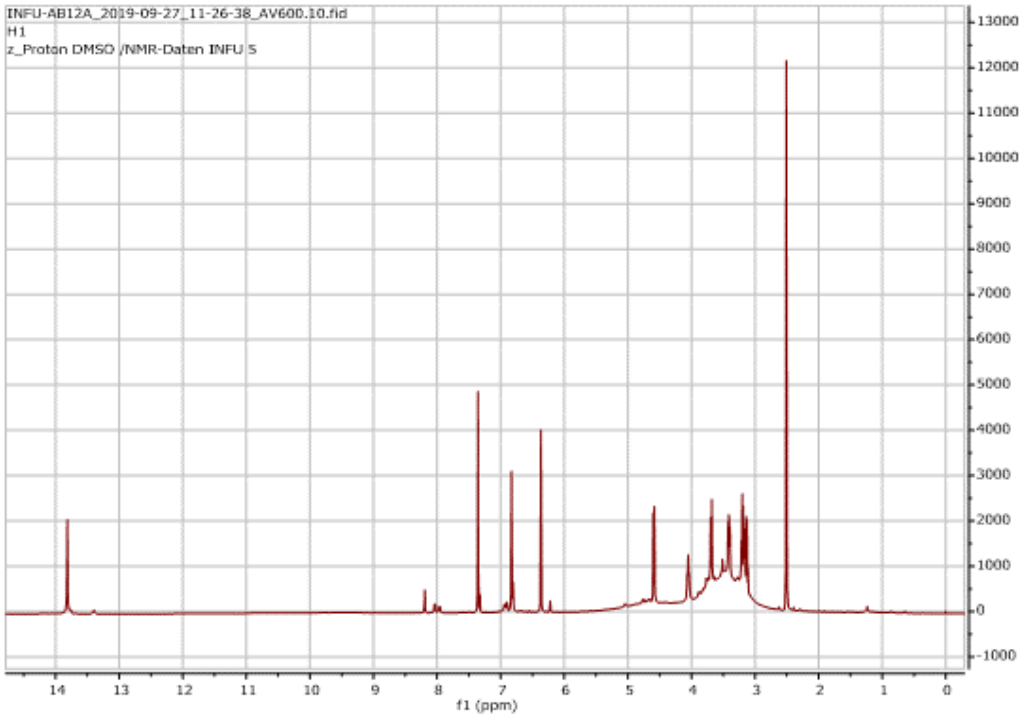

Appendix 78: ^{13}C NMR (175 MHz, DMSO-d_6) spectrum of **28**

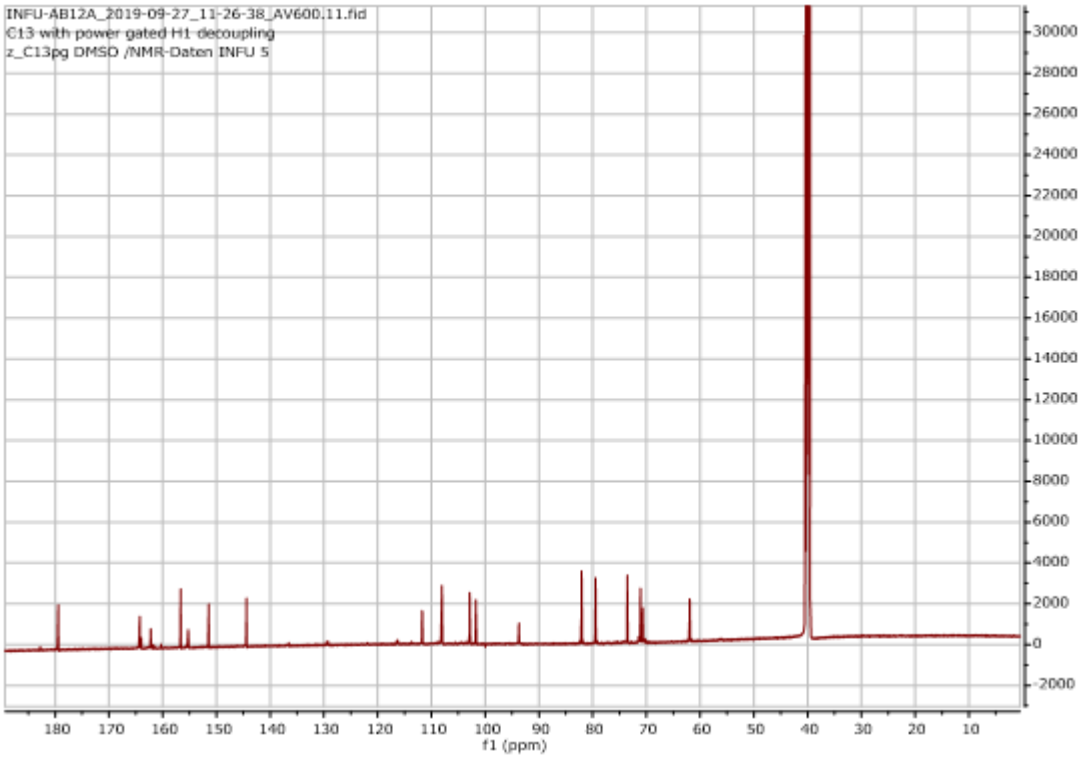

Appendix 79: COSY (600 MHz, DMSO-d_6) spectrum of **28**

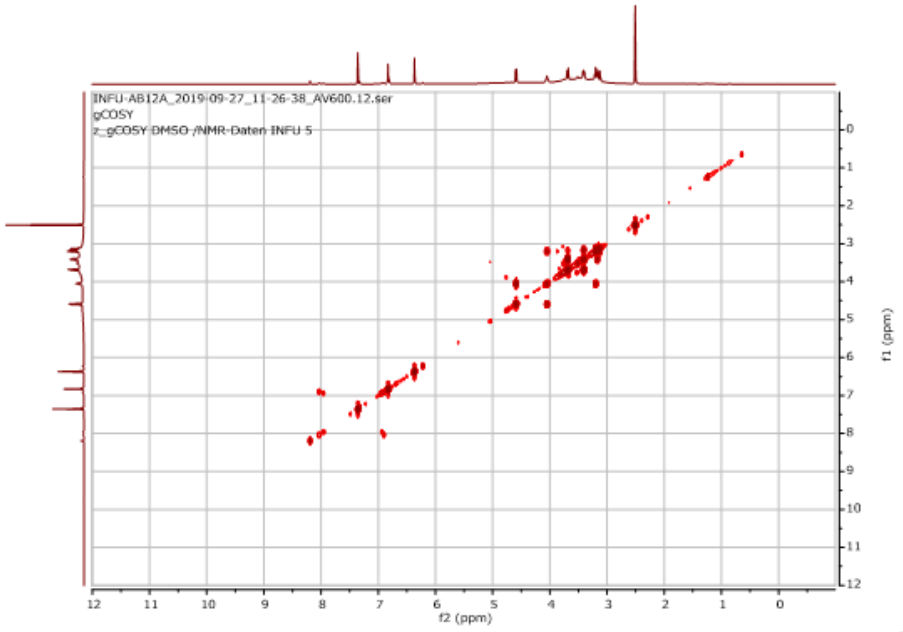

Appendix 80: HSQC (DMSO-d_6) spectrum of **28** (^{1}H: 600 MHz, ^{13}C: 175 MHz)

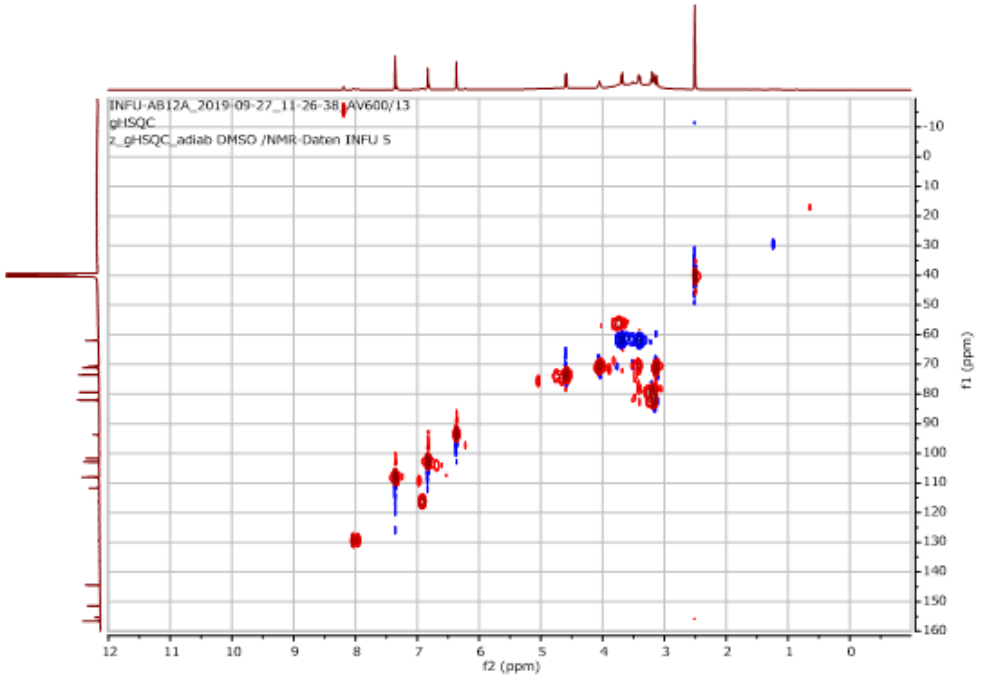

Appendix 81: HMBC (DMSO-d_6) spectrum of **28** (^{1}H: 600 MHz, ^{13}C: 175 MHz)

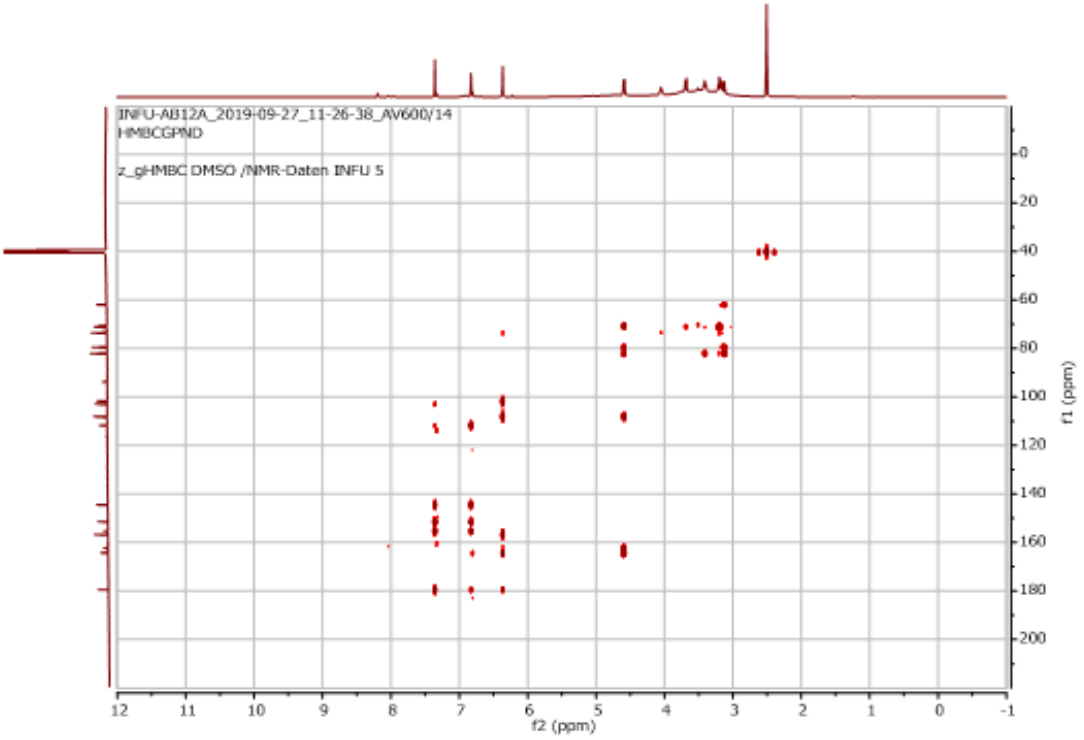

Appendix 82: HRESIMS of **29**

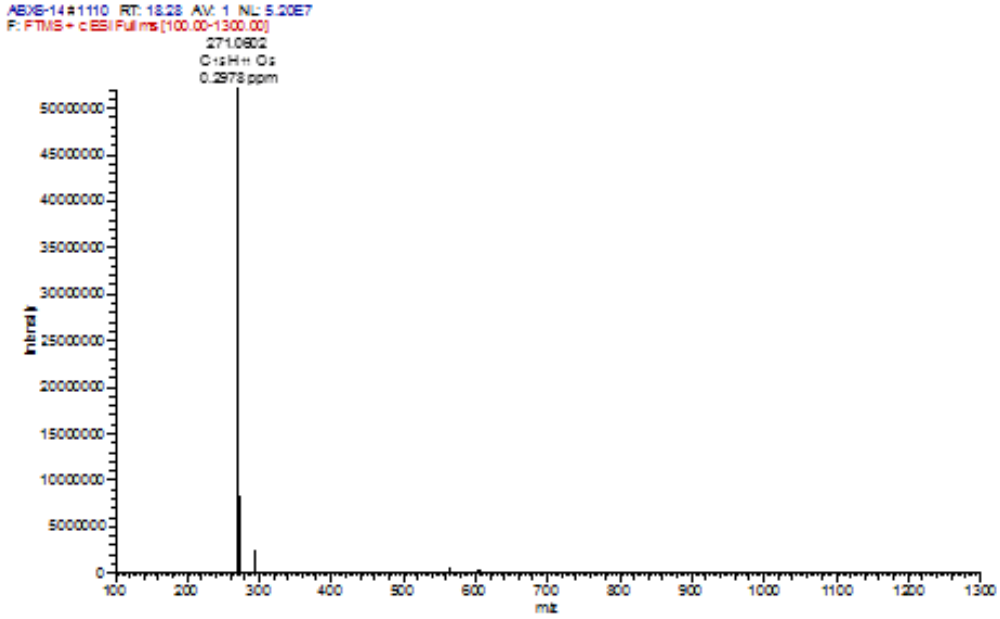

Appendix 83: ^{1}H NMR (600 MHz, DMSO-d_6) spectrum of **29**

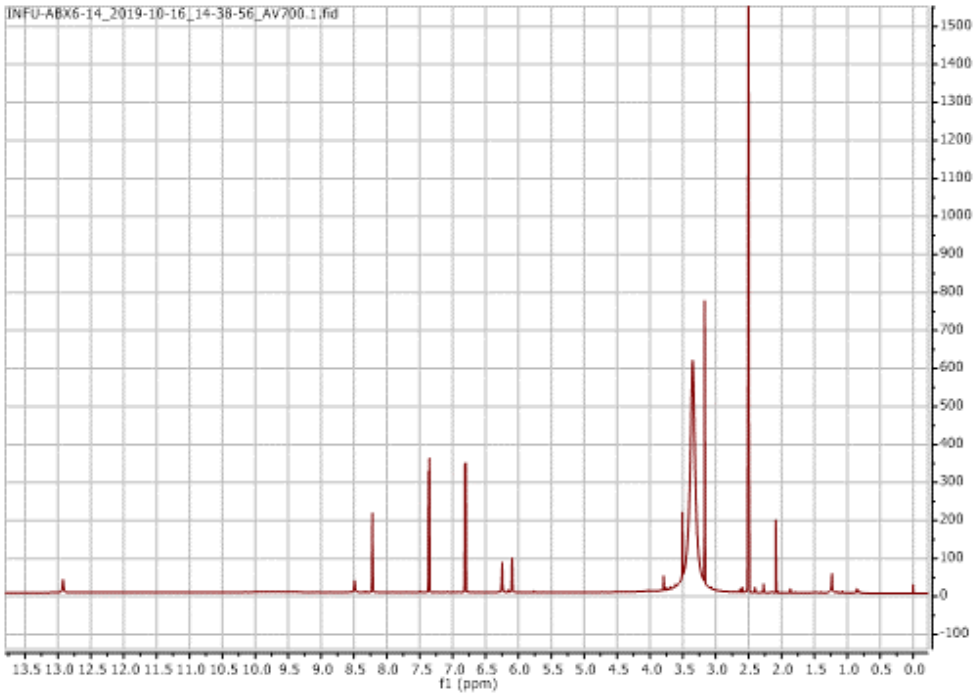

Appendix 84: ^{13}C NMR (175 MHz, DMSO-d_6) spectrum of **29**

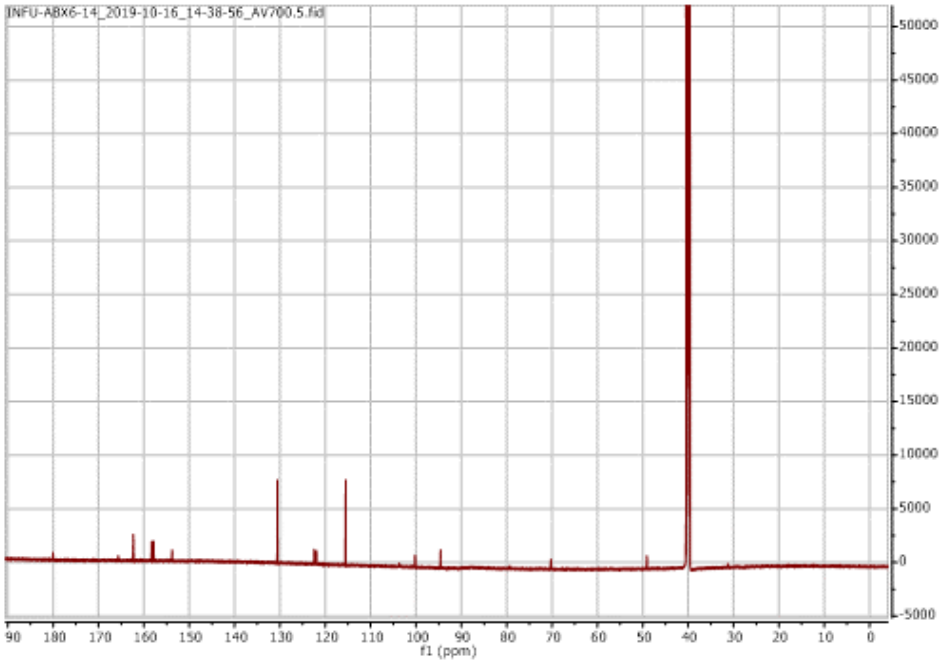

Appendix 85: COSY (600 MHz, DMSO-d_6) spectrum of **29**

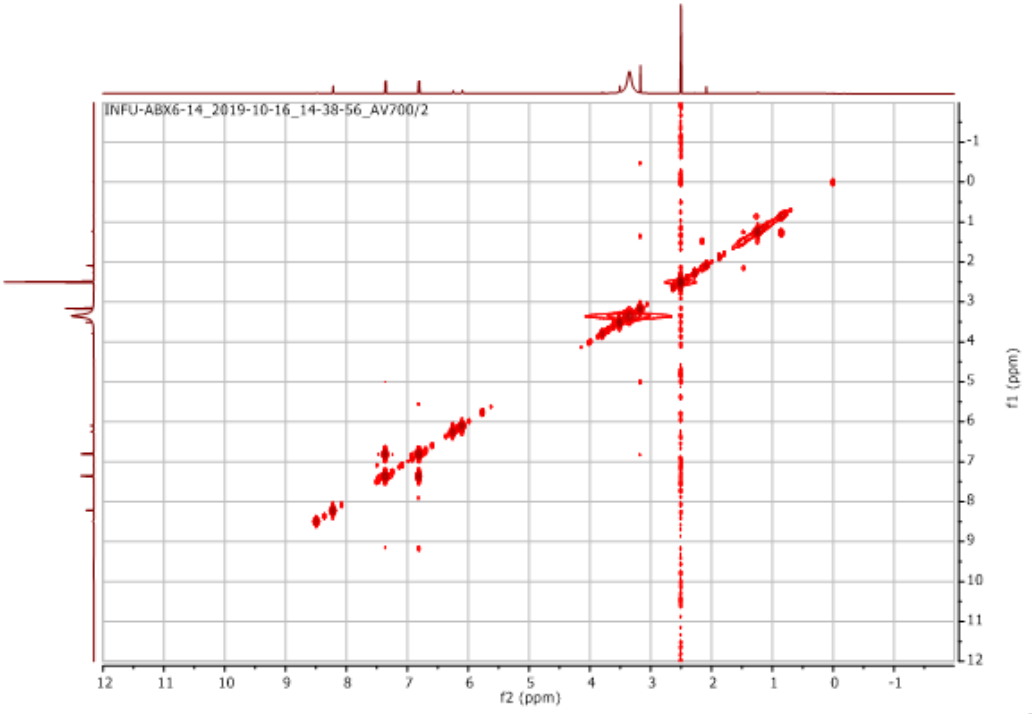

Appendix 86: HSQC (DMSO-d_6) spectrum of **29** (^{1}H: 600 MHz, ^{13}C: 175 MHz)

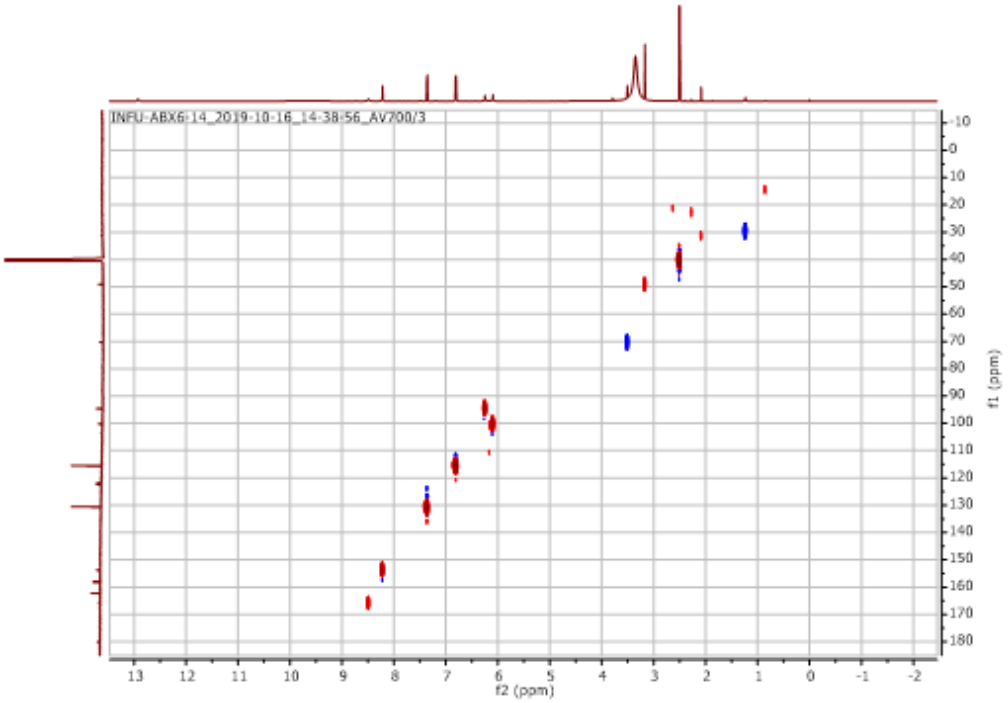

Appendix 87: HMBC (DMSO-d_6) spectrum of **29** (^{1}H: 600 MHz, ^{13}C: 175 MHz)

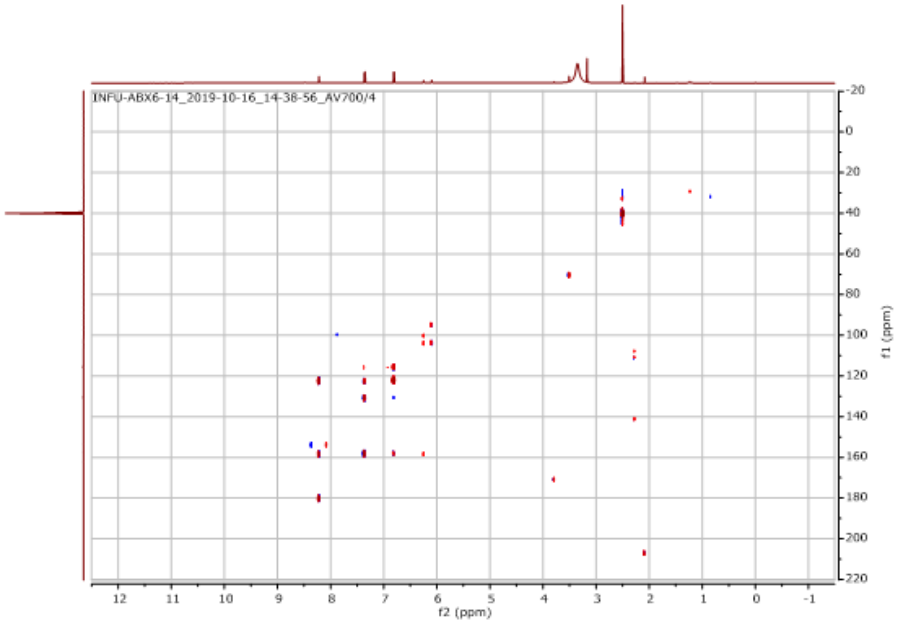

Appendix 88: HRESIMS of **30**

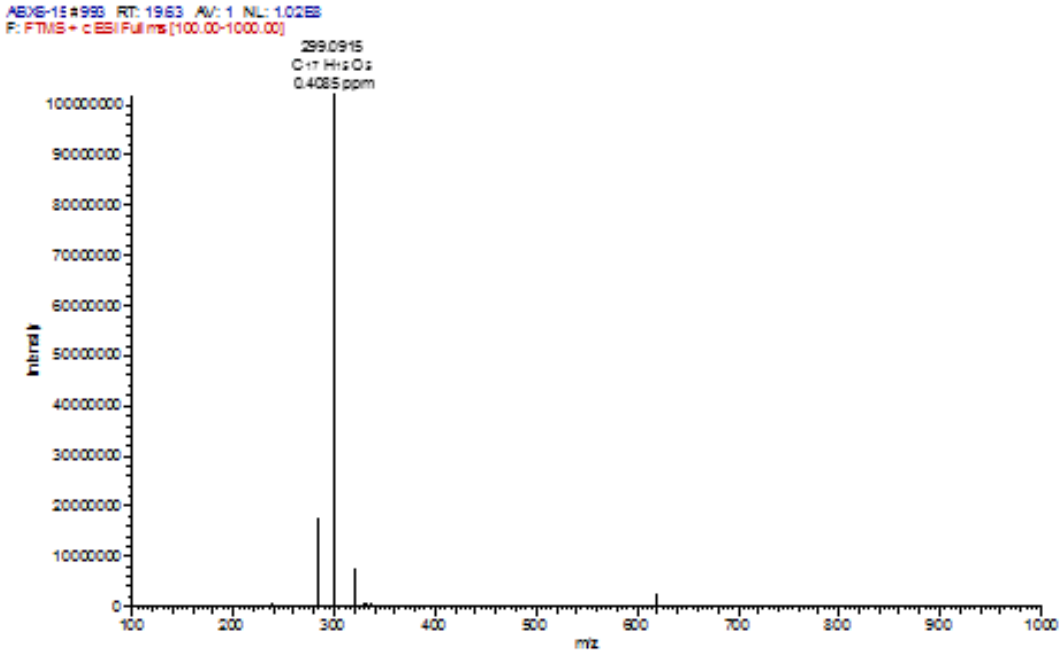

Appendix 89: ^{1}H NMR (600 MHz, DMSO-d_6) spectrum of **30**

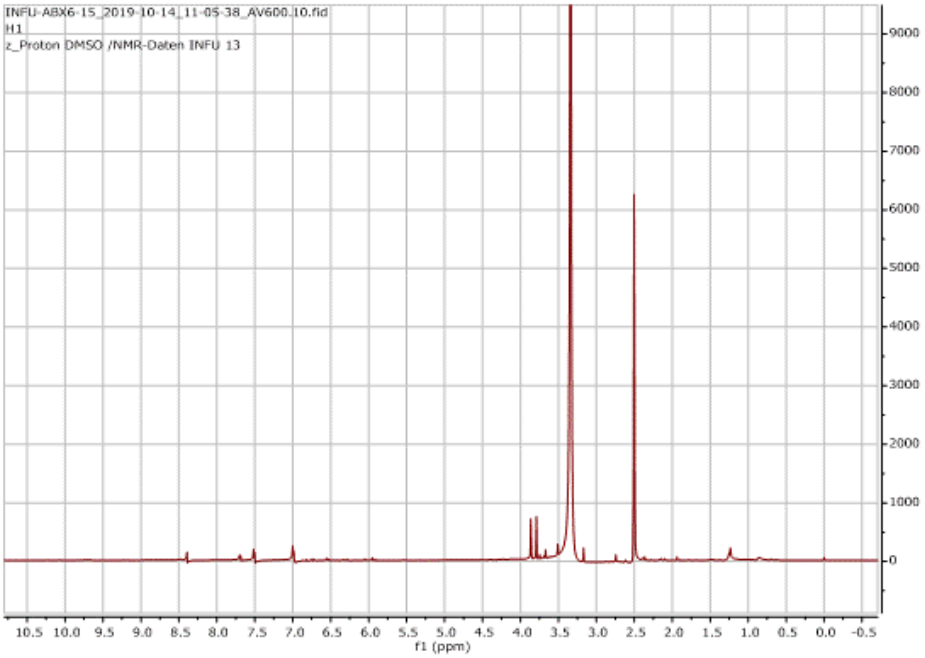

Appendix 90: ^{13}C NMR (175 MHz, DMSO-d_6) spectrum of **30**

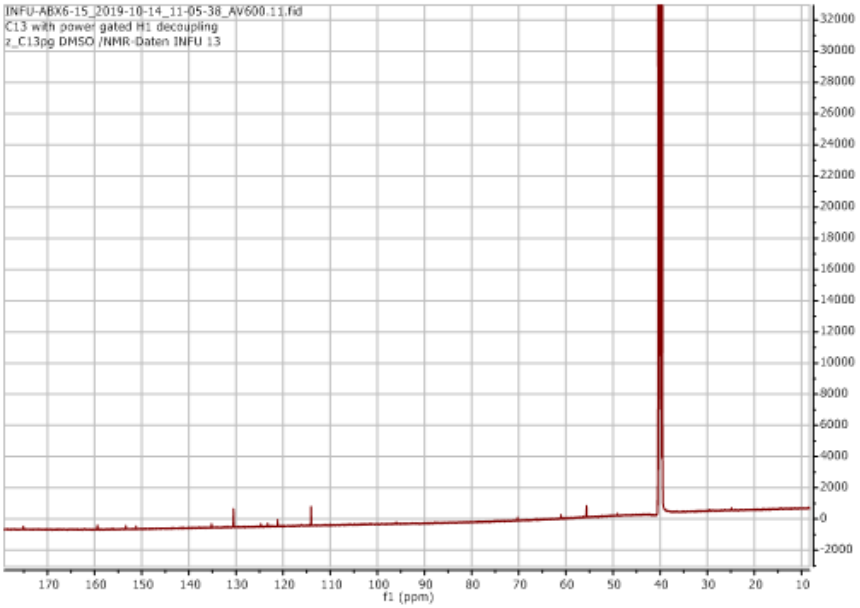

Appendix 91: COSY (600 MHz, DMSO-d_6) spectrum of **30**

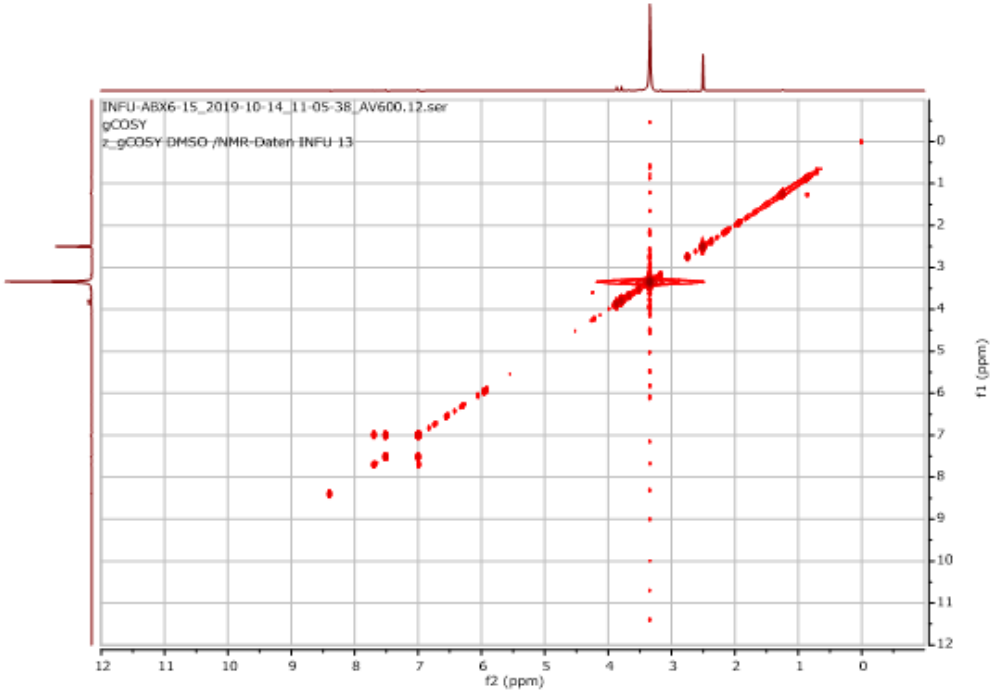

Appendix 92: HSQC (DMSO-d_6) spectrum of **30** (^{1}H: 600 MHz, ^{13}C: 175 MHz)

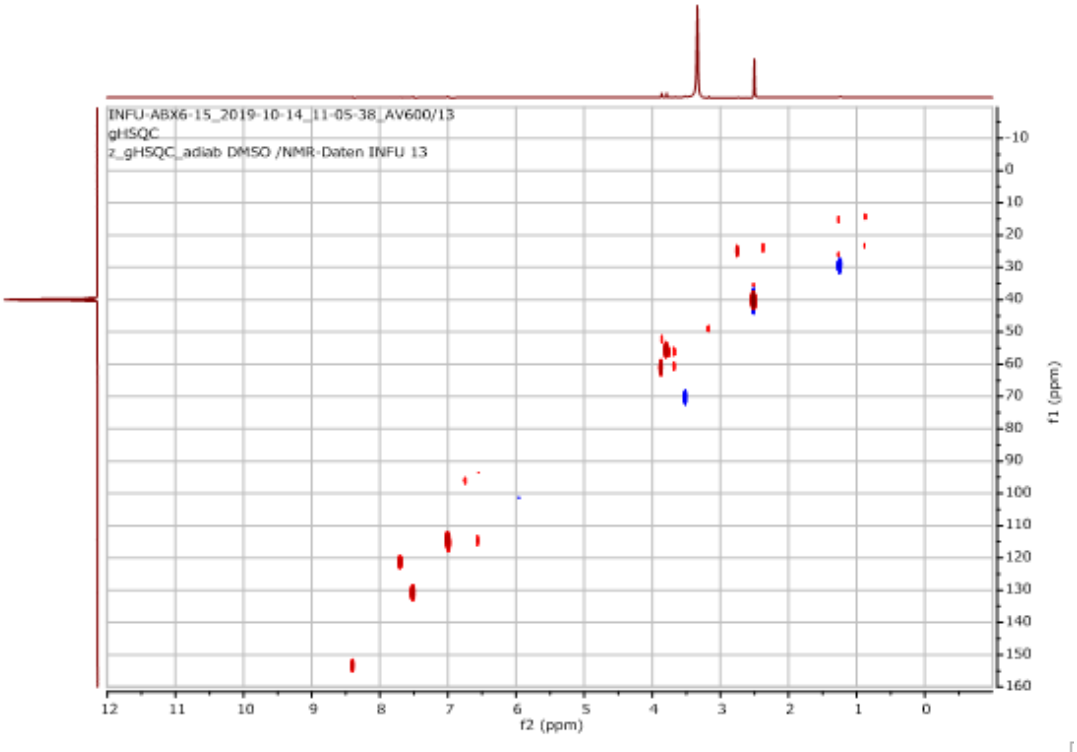

Appendix 93: HMBC (DMSO-d_6) spectrum of **30** (^{1}H: 600 MHz, ^{13}C: 175 MHz)

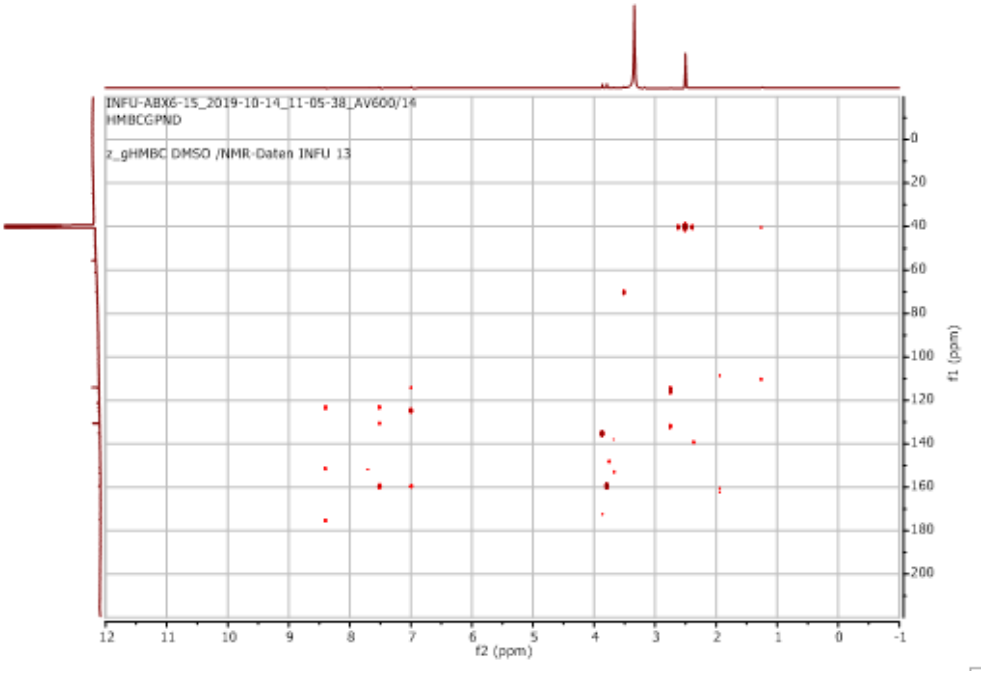

Appendix 94: HRESIMS of **31**

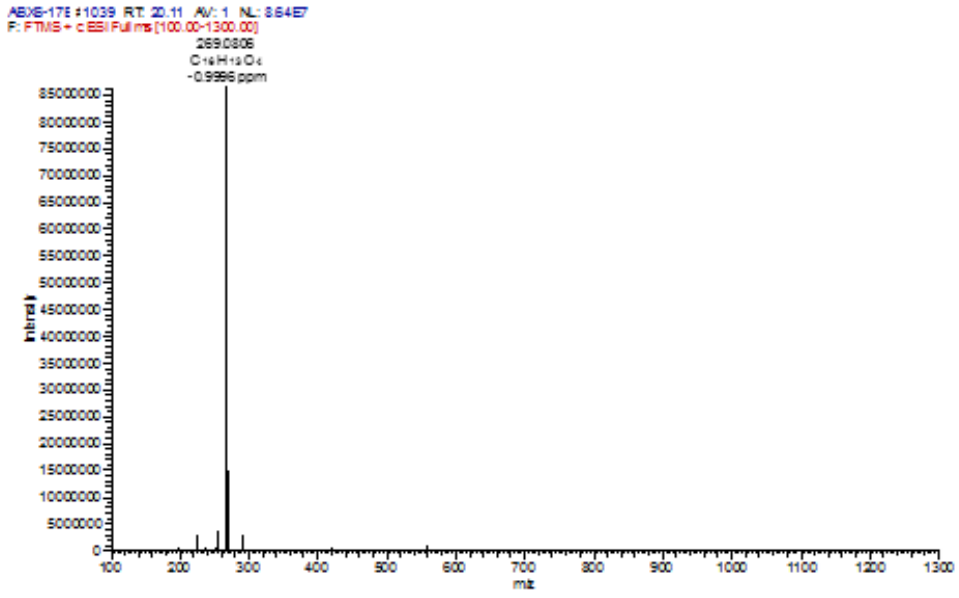

Appendix 95: ^{1}H NMR (600 MHz, DMSO-d_6) spectrum of **31**

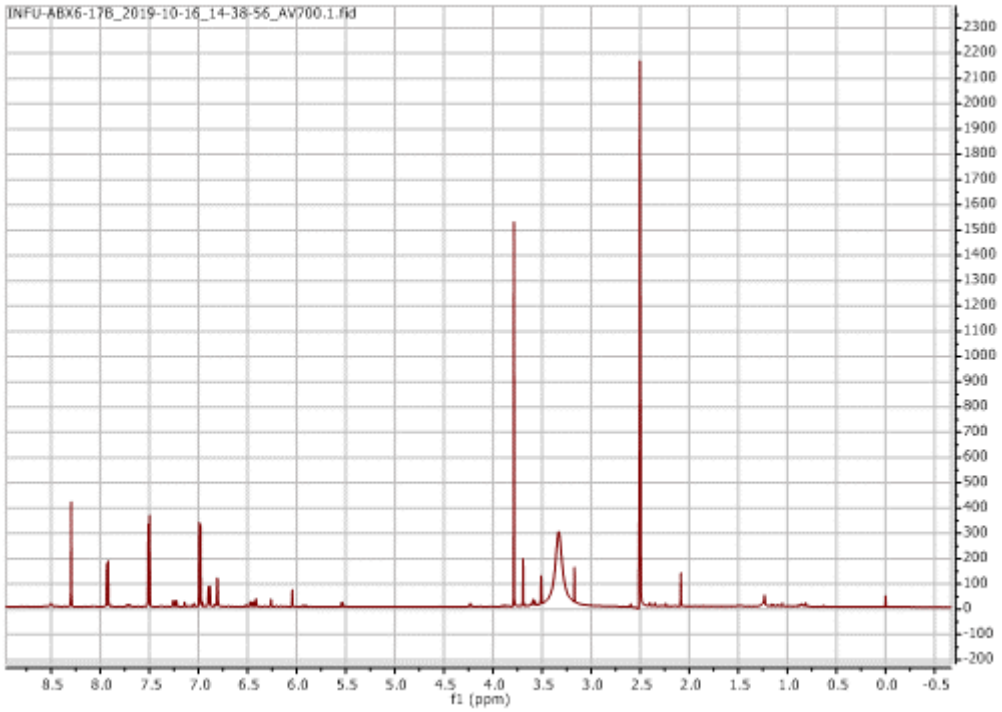

Appendix 96: ^{13}C NMR (175 MHz, DMSO-d_6) spectrum of **31**

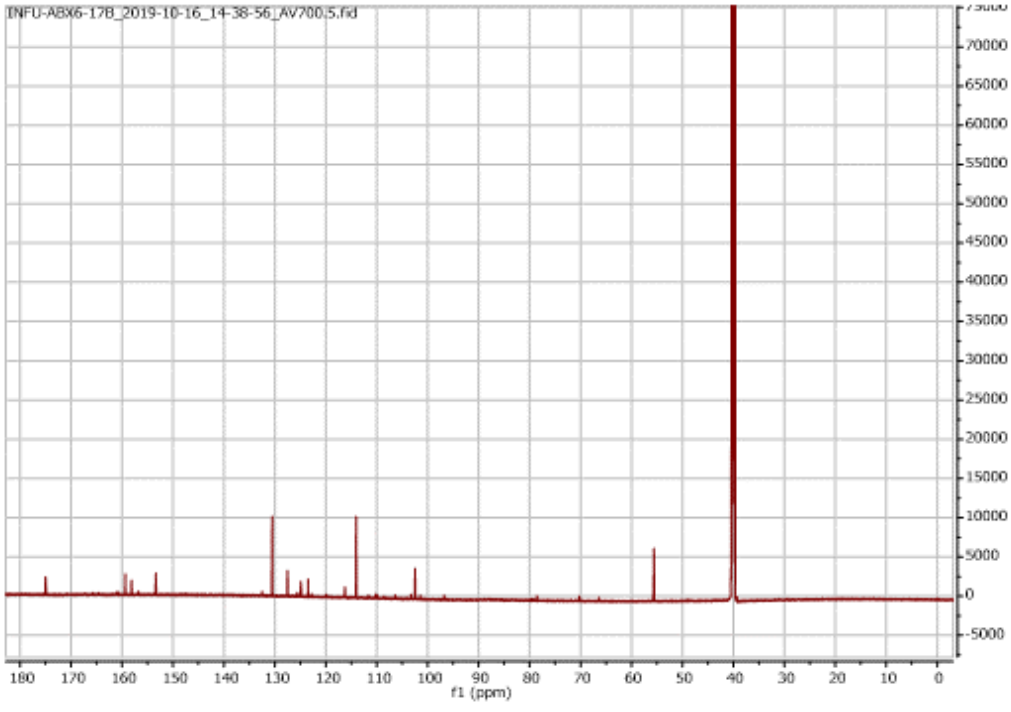

Appendix 97: COSY (600 MHz, DMSO-d_6) spectrum of **31**

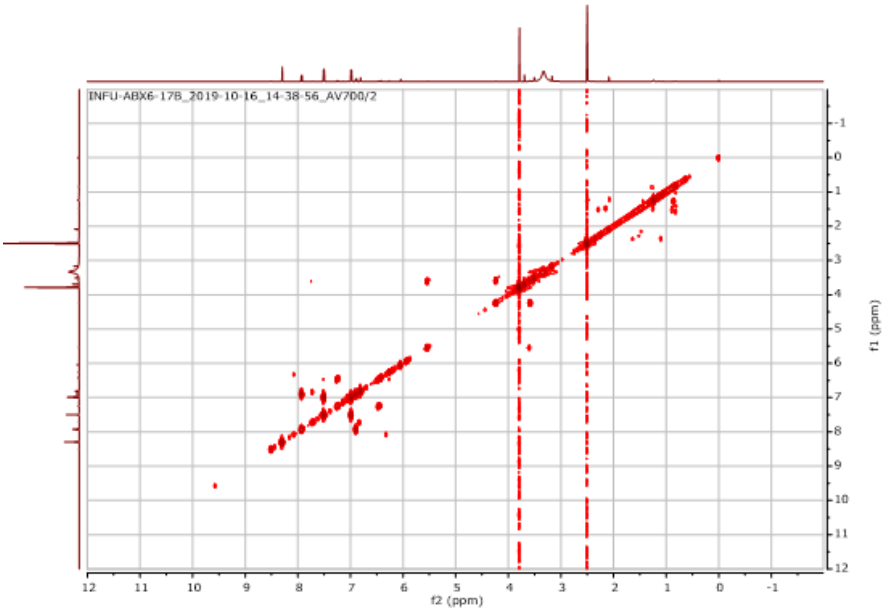

Appendix 98: HSQC (DMSO-d_6) spectrum of **31** (^{1}H: 600 MHz, ^{13}C: 175 MHz)

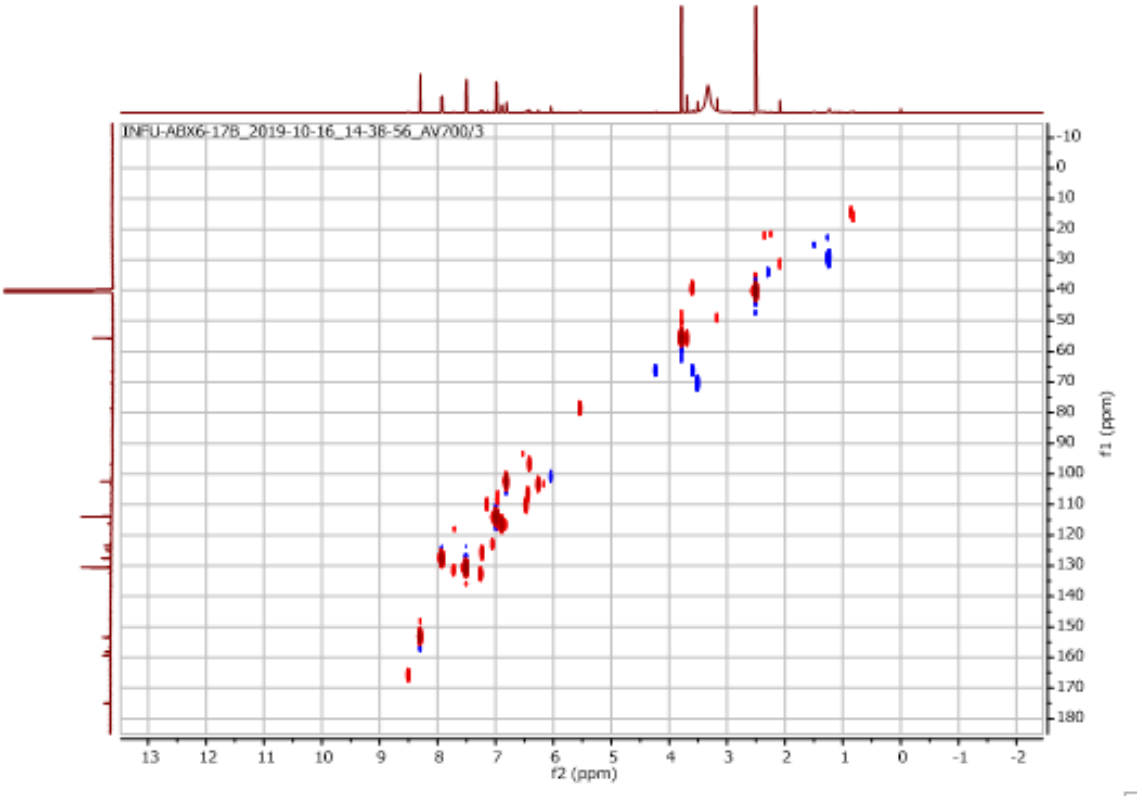

Appendix 99: HMBC (DMSO-d_6) spectrum of **31** (^{1}H: 600 MHz, ^{13}C: 175 MHz)

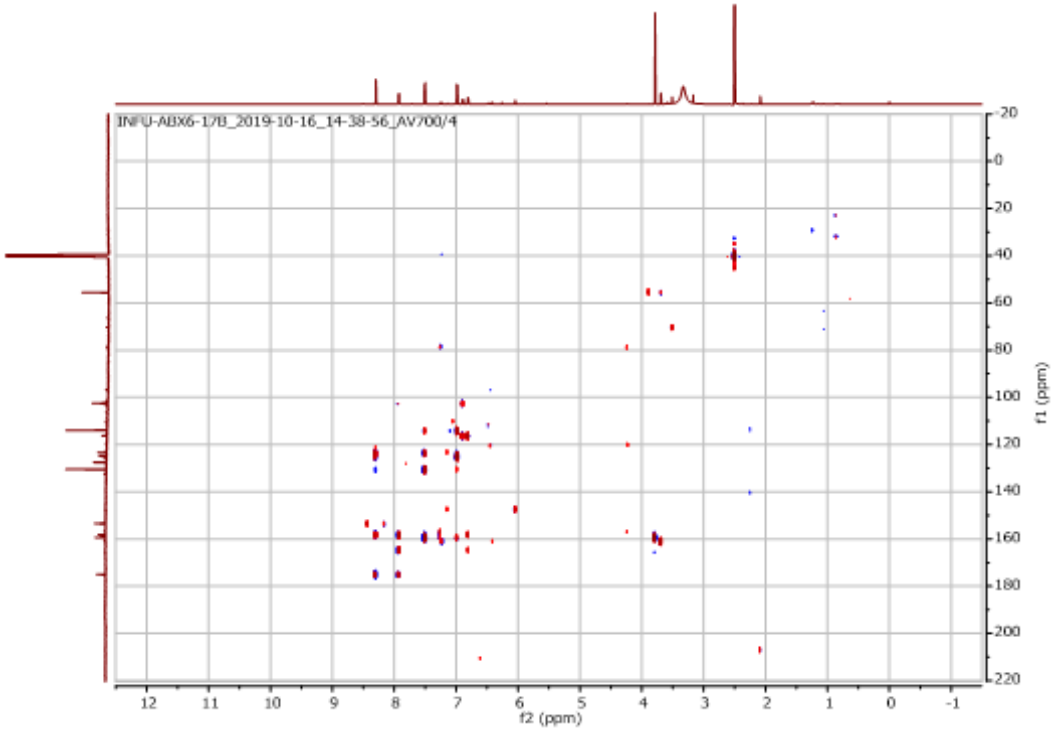

Appendix 100: HRESIMS of **32**

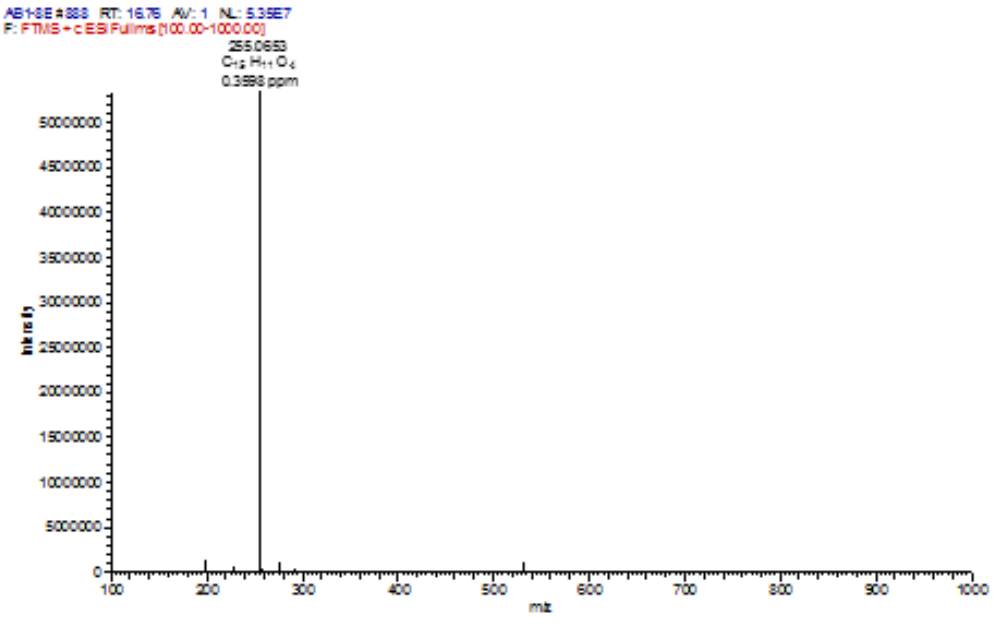

Appendix 101: ^{1}H NMR (600 MHz, DMSO-d_6) spectrum of **32**

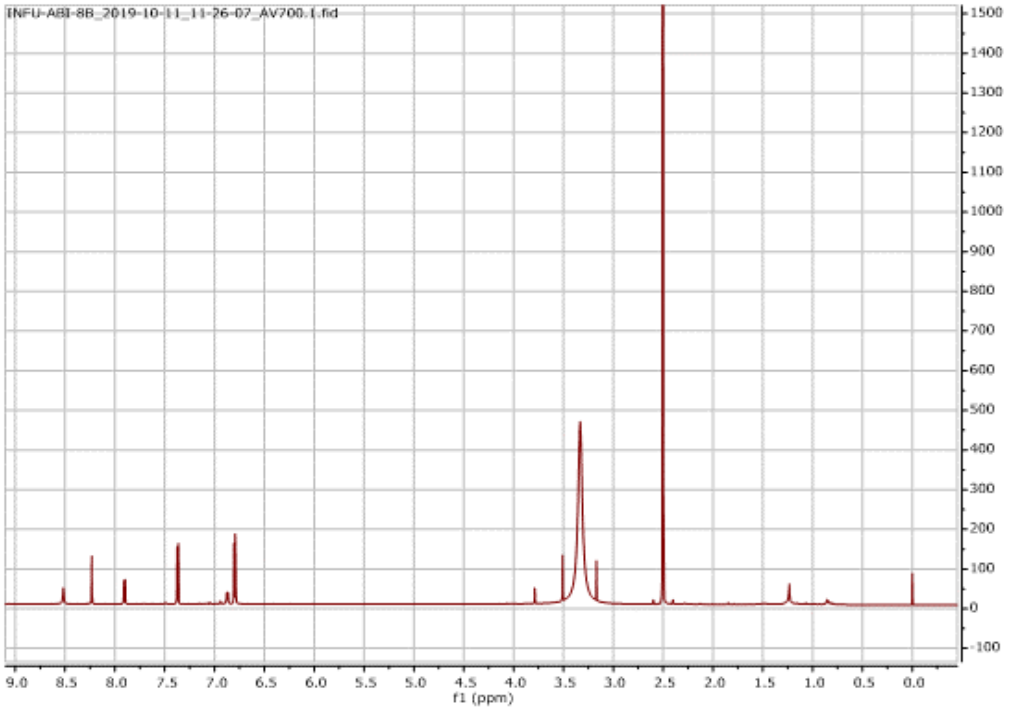

Appendix 102: ^{13}C NMR (175 MHz, DMSO-d_6) spectrum of **32**

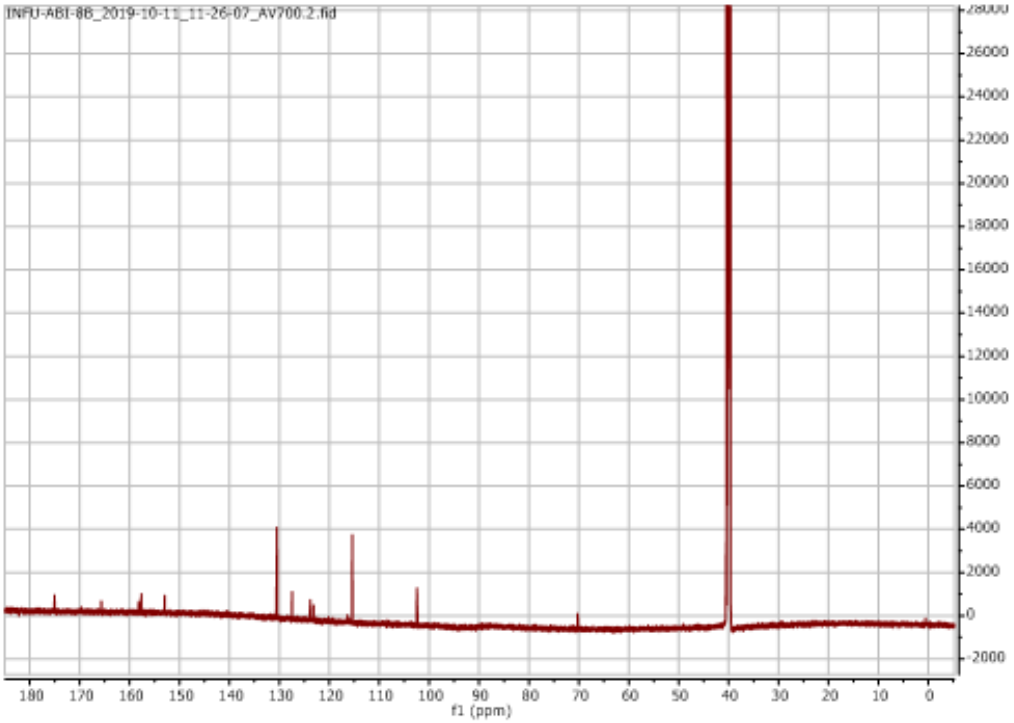

Appendix 103: COSY (600 MHz, DMSO-d_6) spectrum of **32**

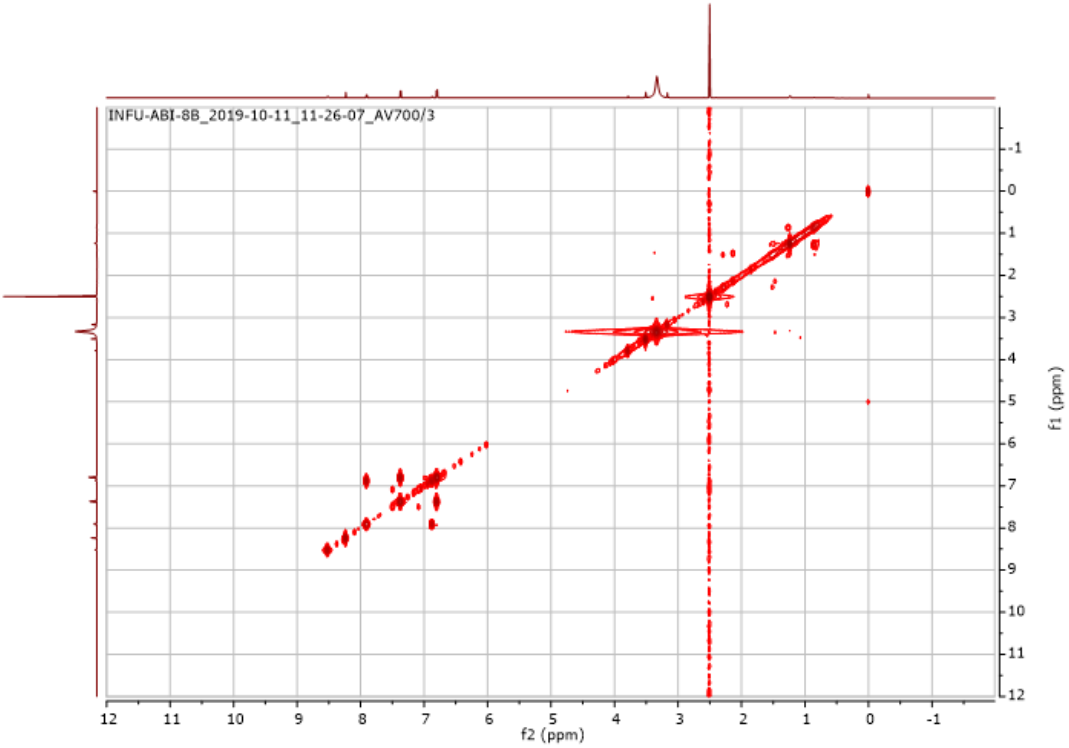

Appendix 104: HSQC (DMSO-d_6) spectrum of **32** (^{1}H: 600 MHz, ^{13}C: 175 MHz)

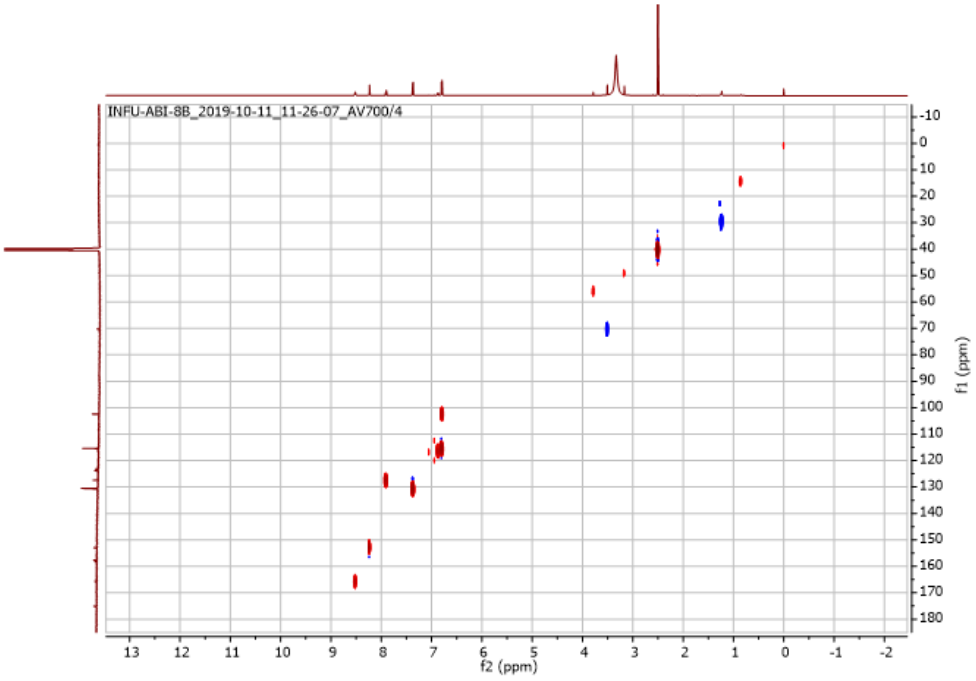

Appendix 105: HMBC (DMSO-d_6) spectrum of **32** (^{1}H: 600 MHz, ^{13}C: 175 MHz)

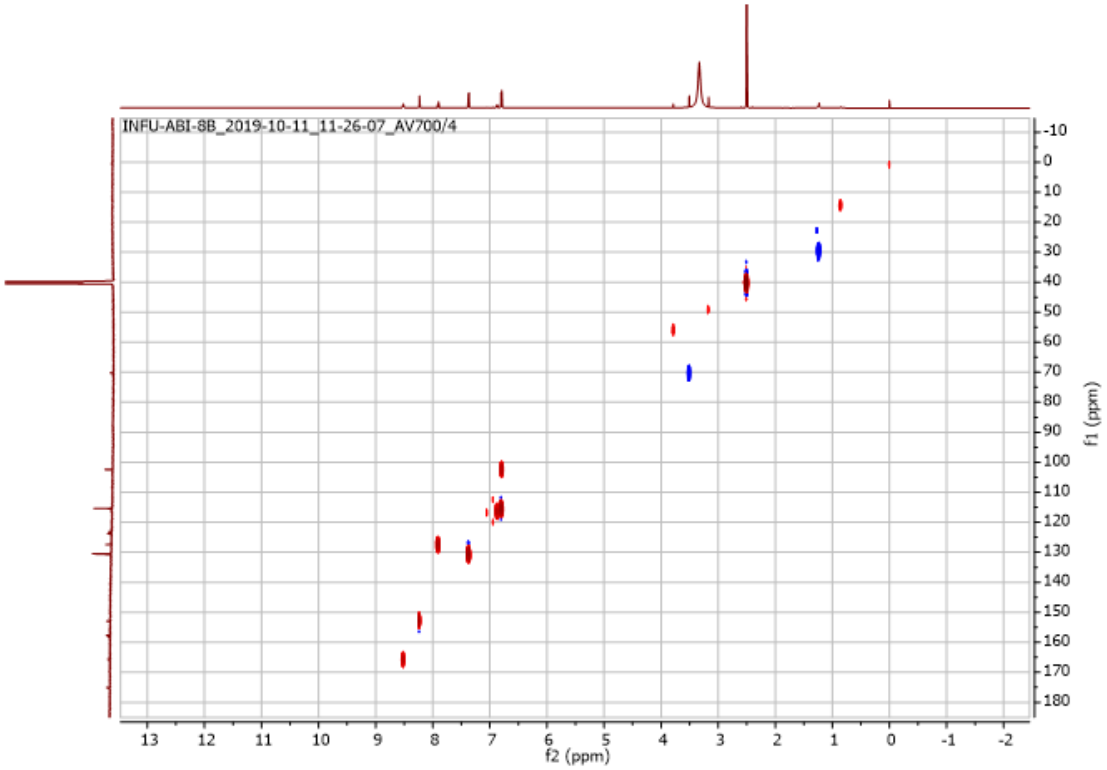

Appendix 106: HRESIMS of **33**

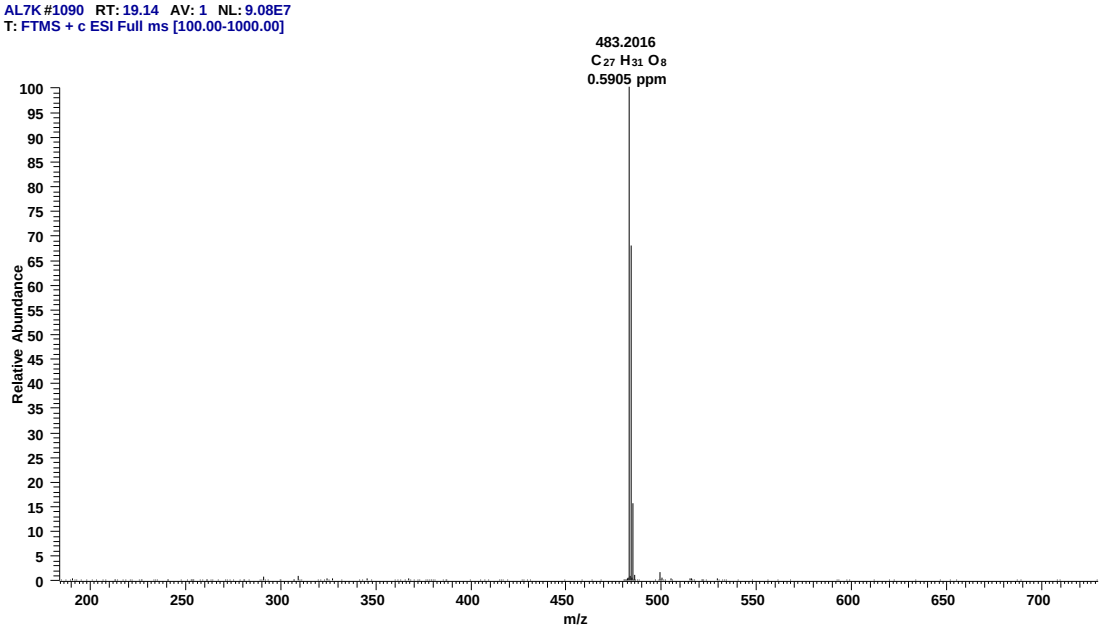

Appendix 107: Infrared spectrum of **33**

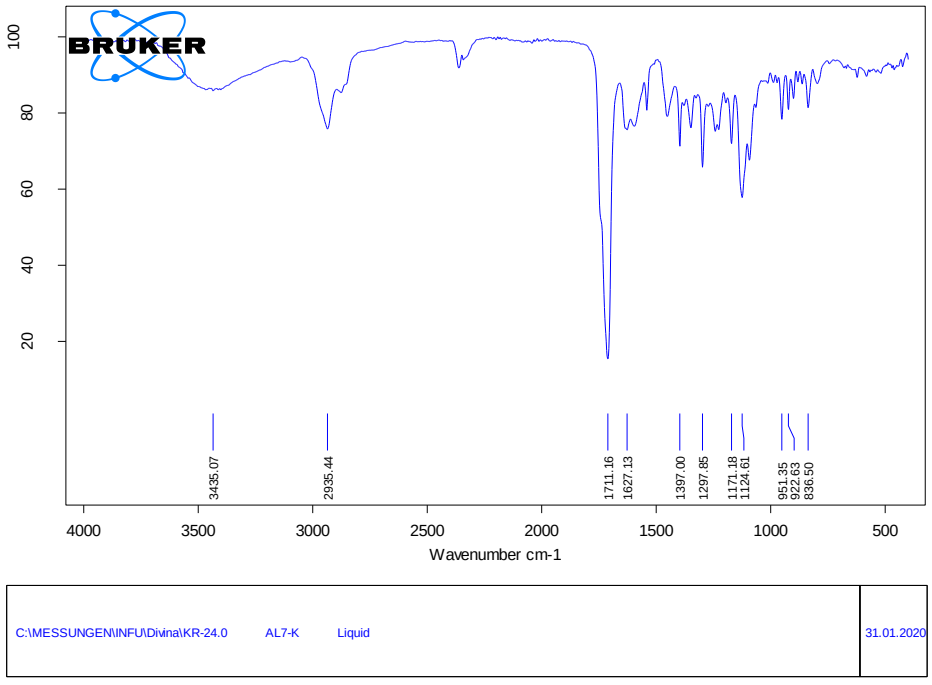

Seite 1 von 1

Appendix 108: ^{1}H NMR (700 MHz, CD_3OD) spectrum of **33**

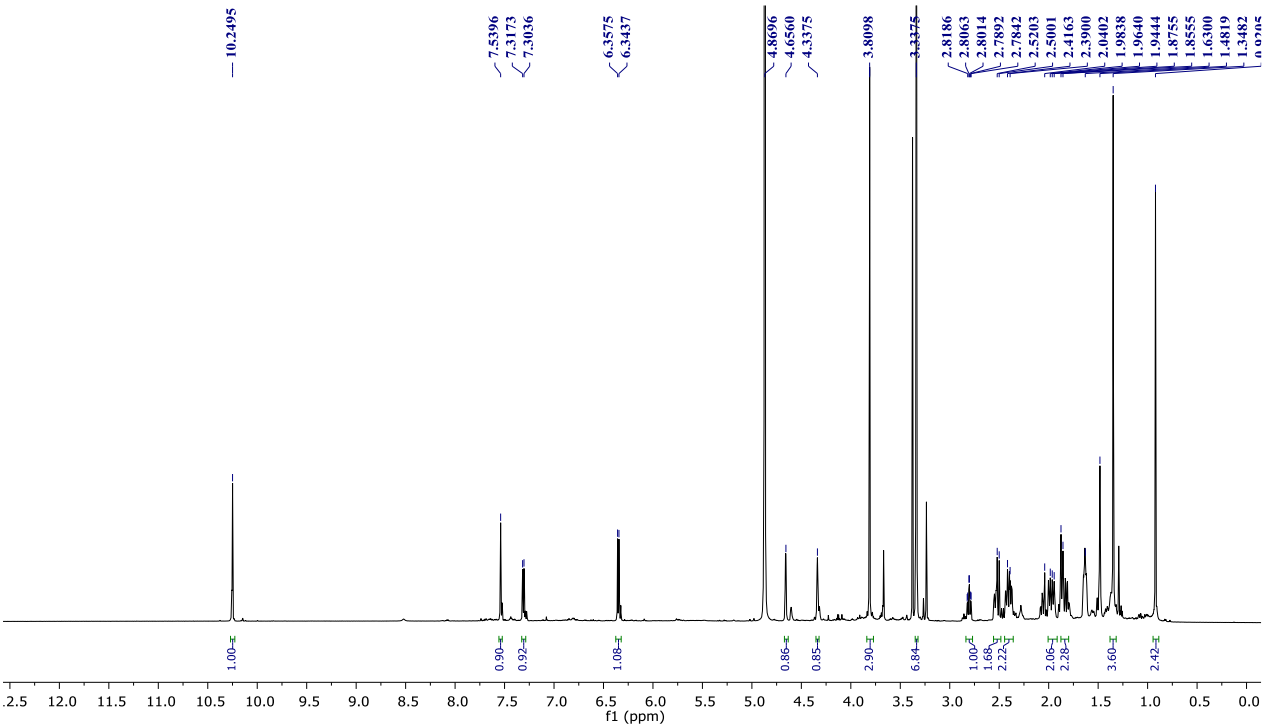

Appendix 109: ^{13}C NMR (175 MHz, CD_3OD) spectrum of **33**

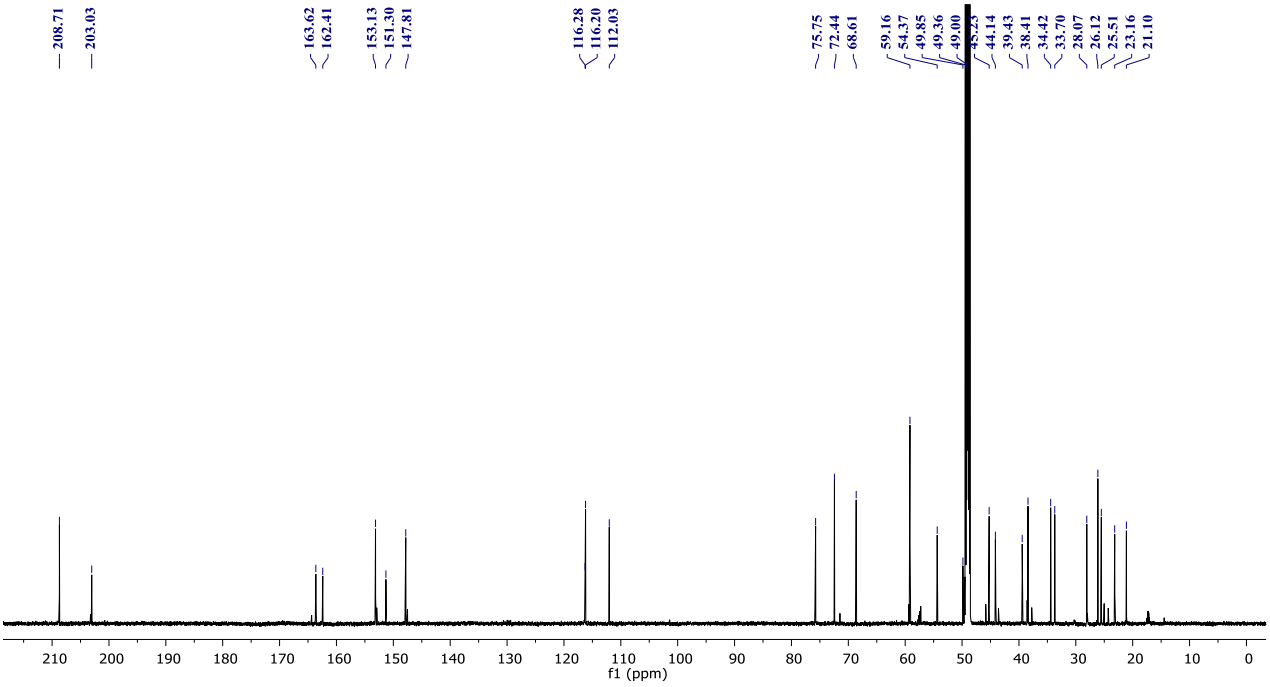

Appendix 110: COSY (CD_3OD) spectrum of **33**

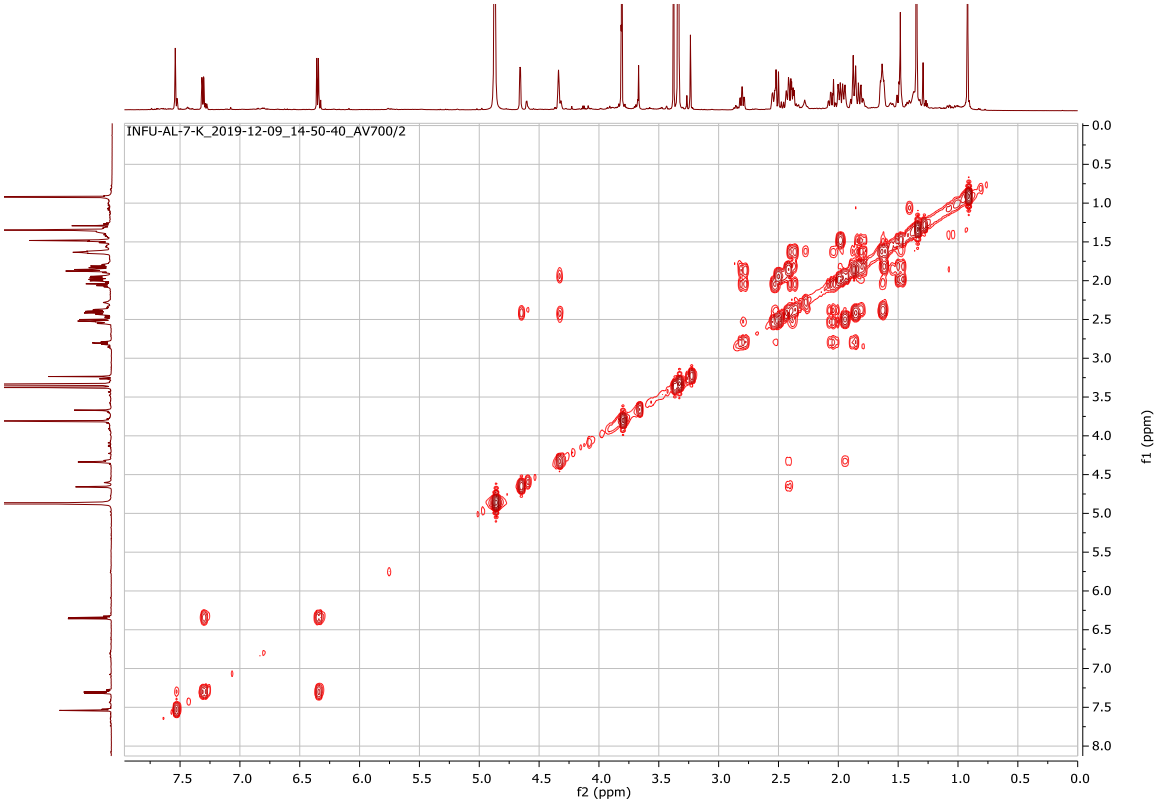

Appendix 111: HSQC (CD_3OD) spectrum of **33**

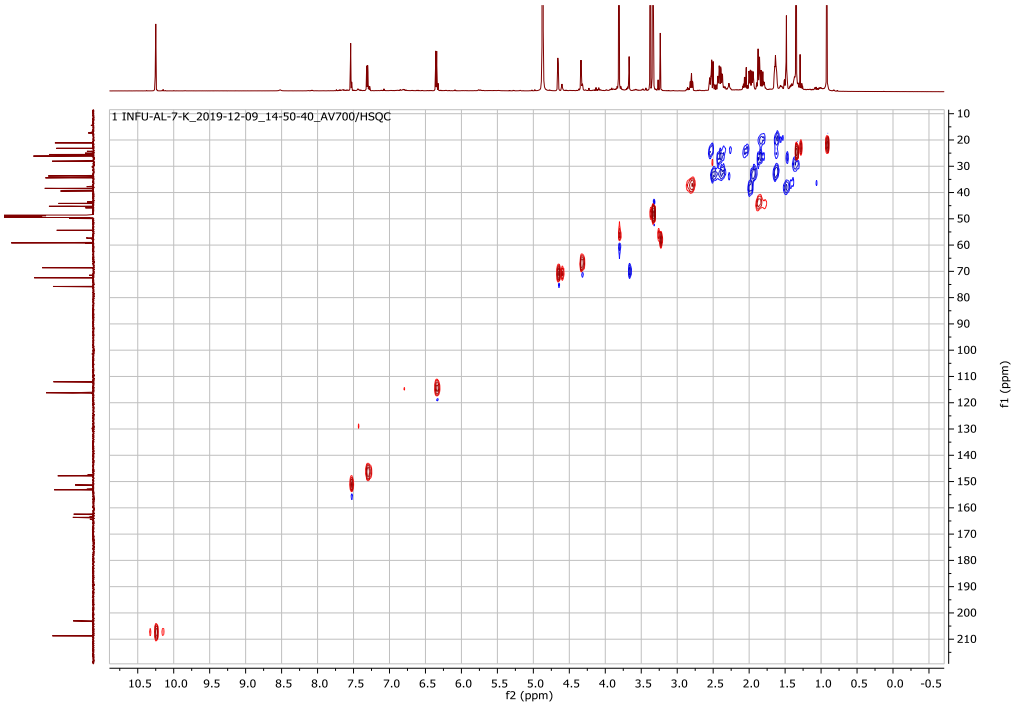

Appendix 112: HMBC (CD3OD) spectrum of **33**

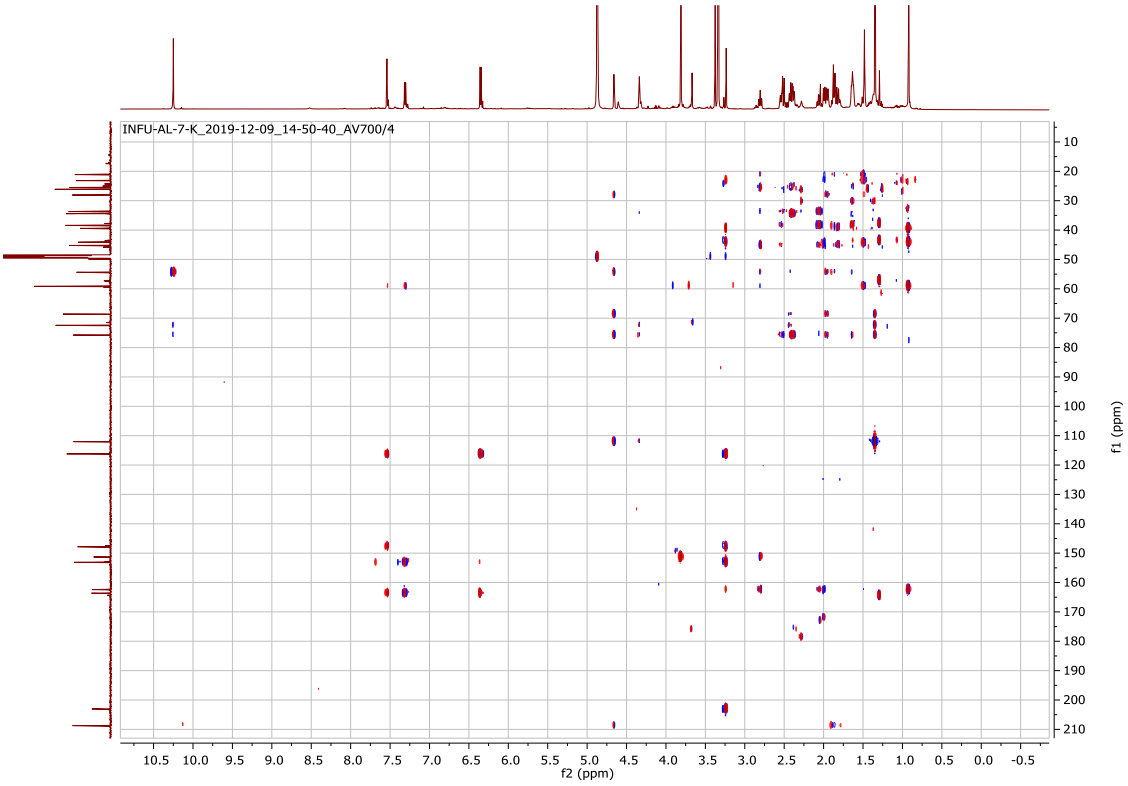

Appendix 113: NOESY spectrum of **33**

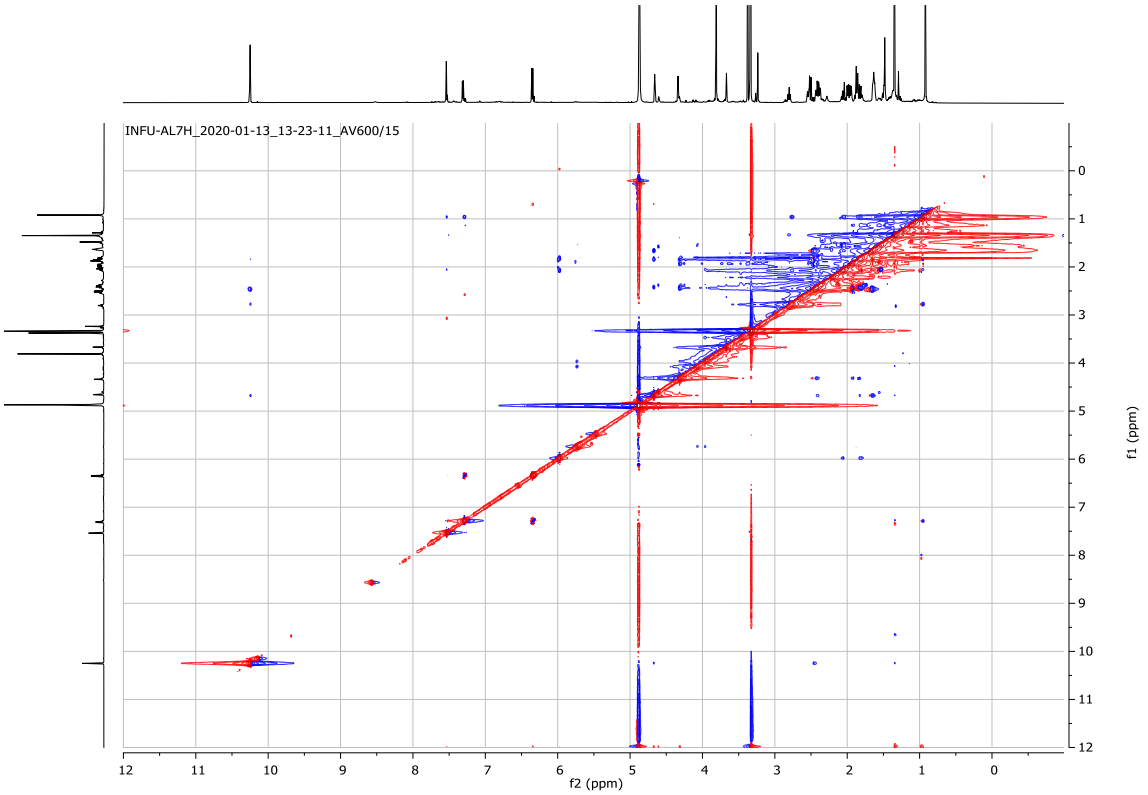

Appendix 114: HRESIMS of **34**

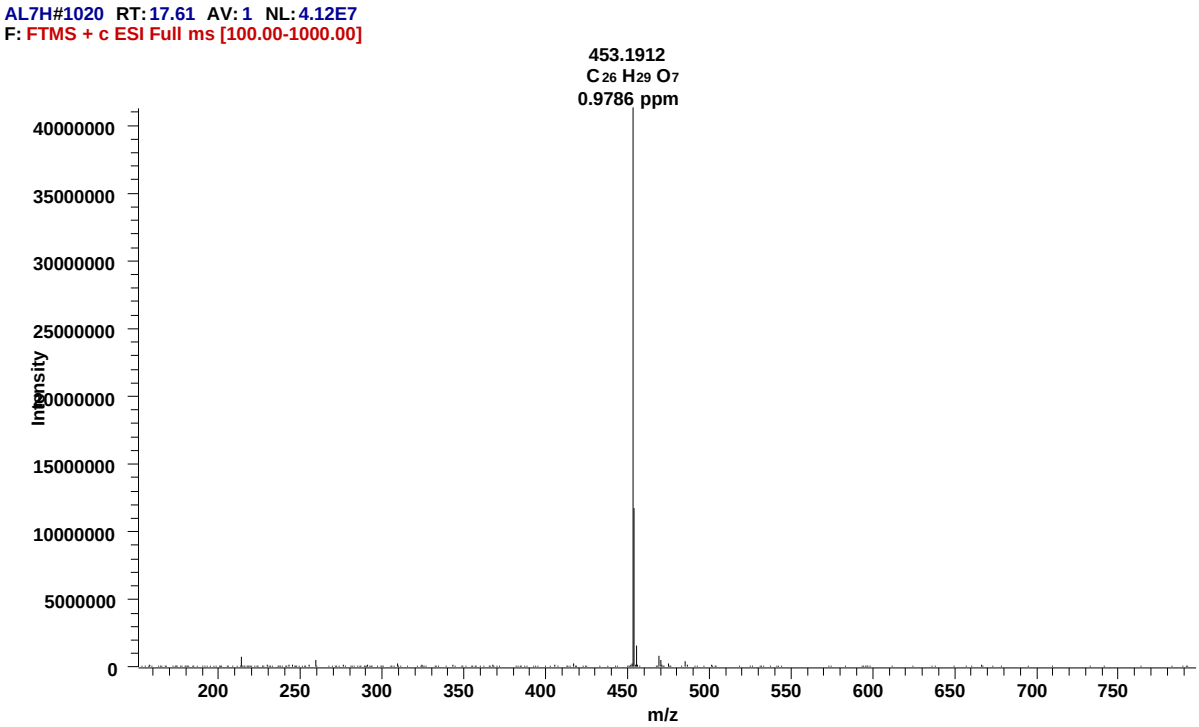

Appendix 115: Infrared spectrum of **34**

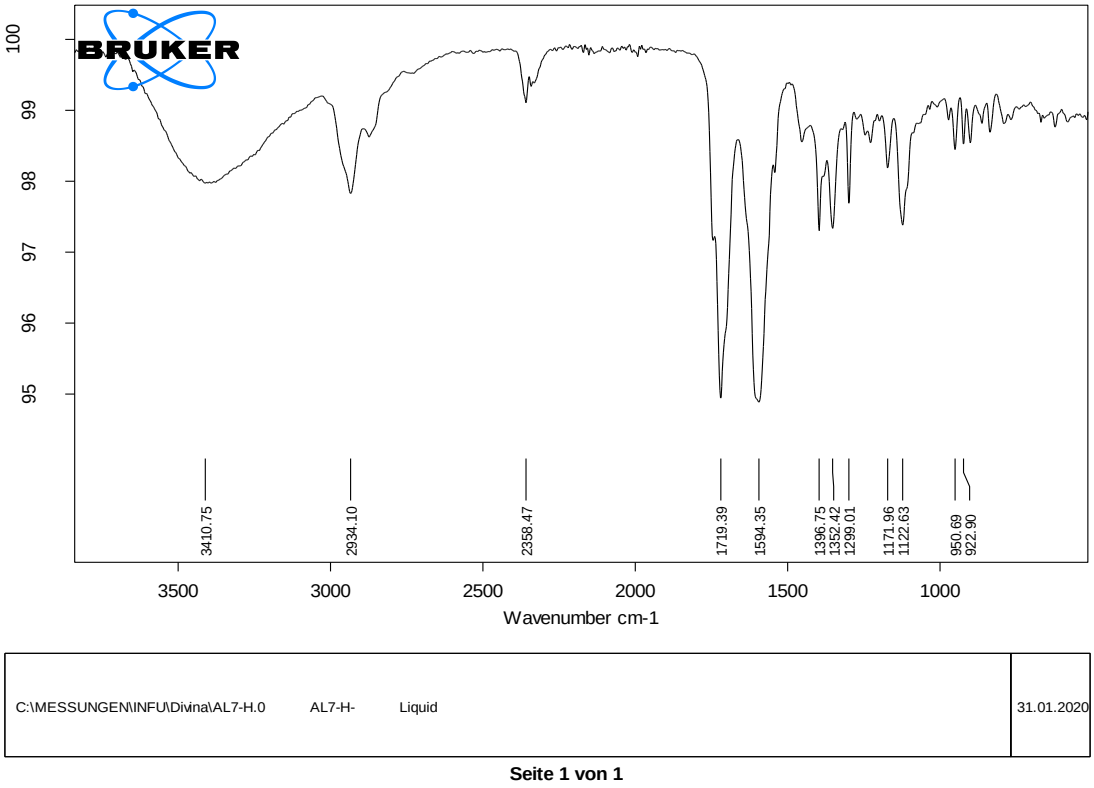

Seite 1 von 1

Appendix 116: ^{1}H NMR (700 MHz, CD_3OD) spectrum of **34**

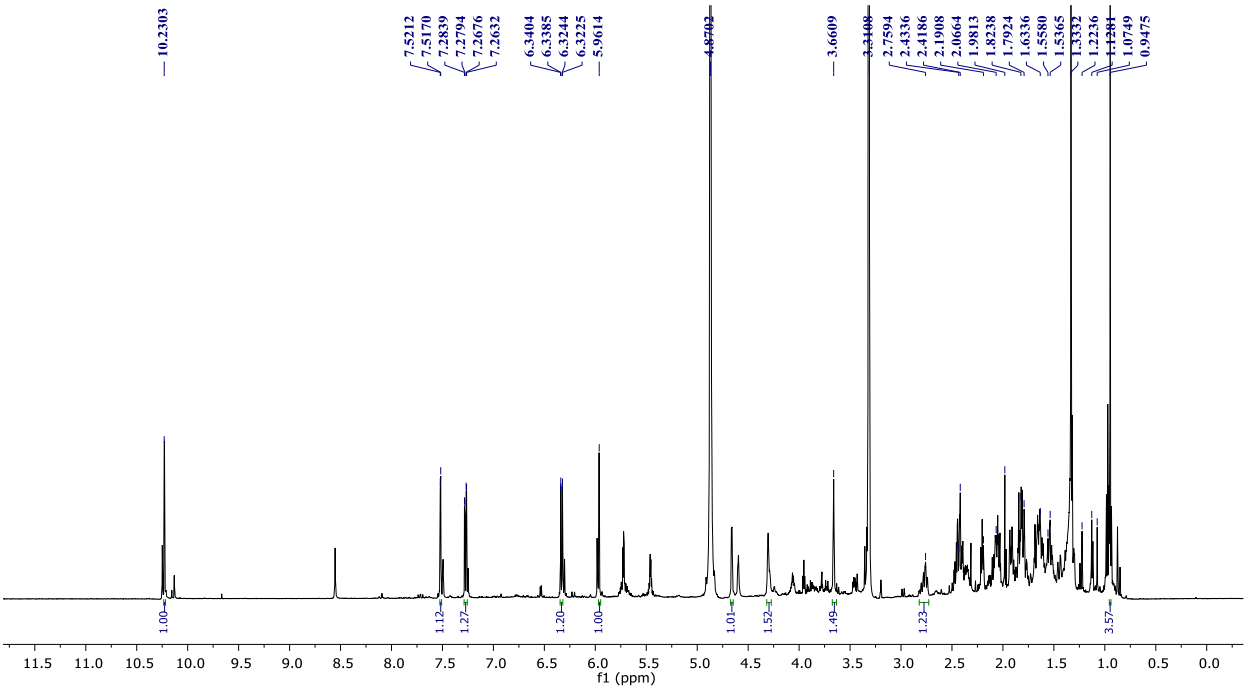

Appendix 117: ^{13}C NMR (175 MHz, CD_3OD) spectrum of **34**

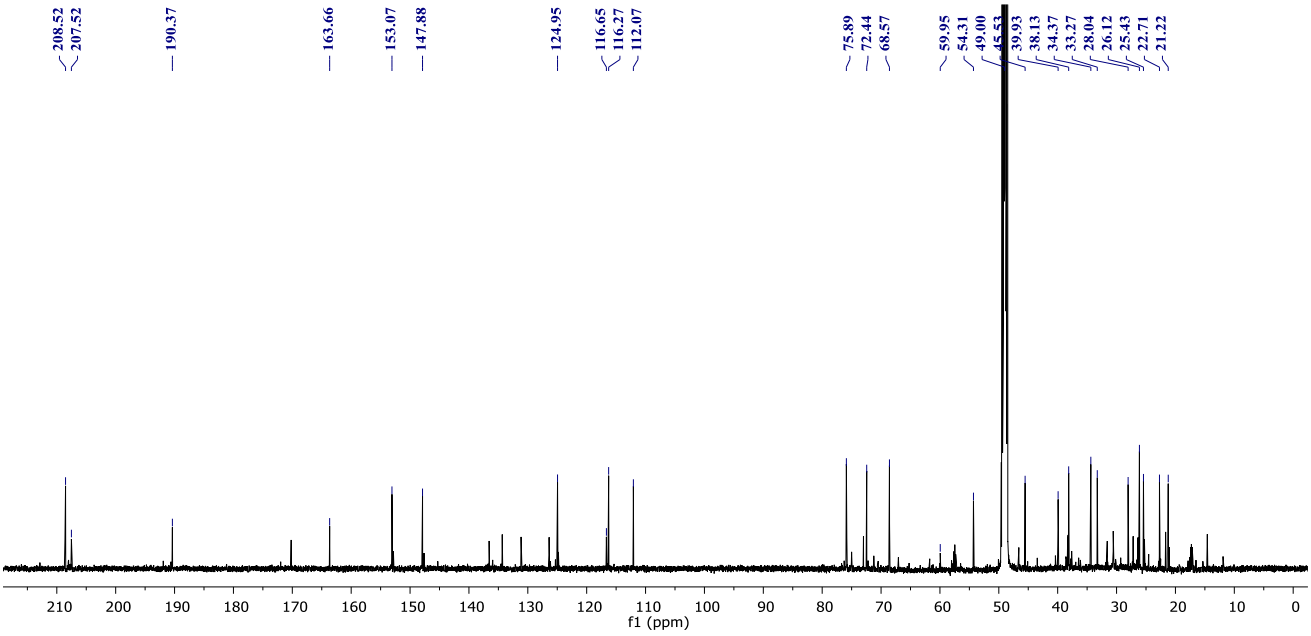

Appendix 118: COSY (CD_3OD) spectrum of **34**

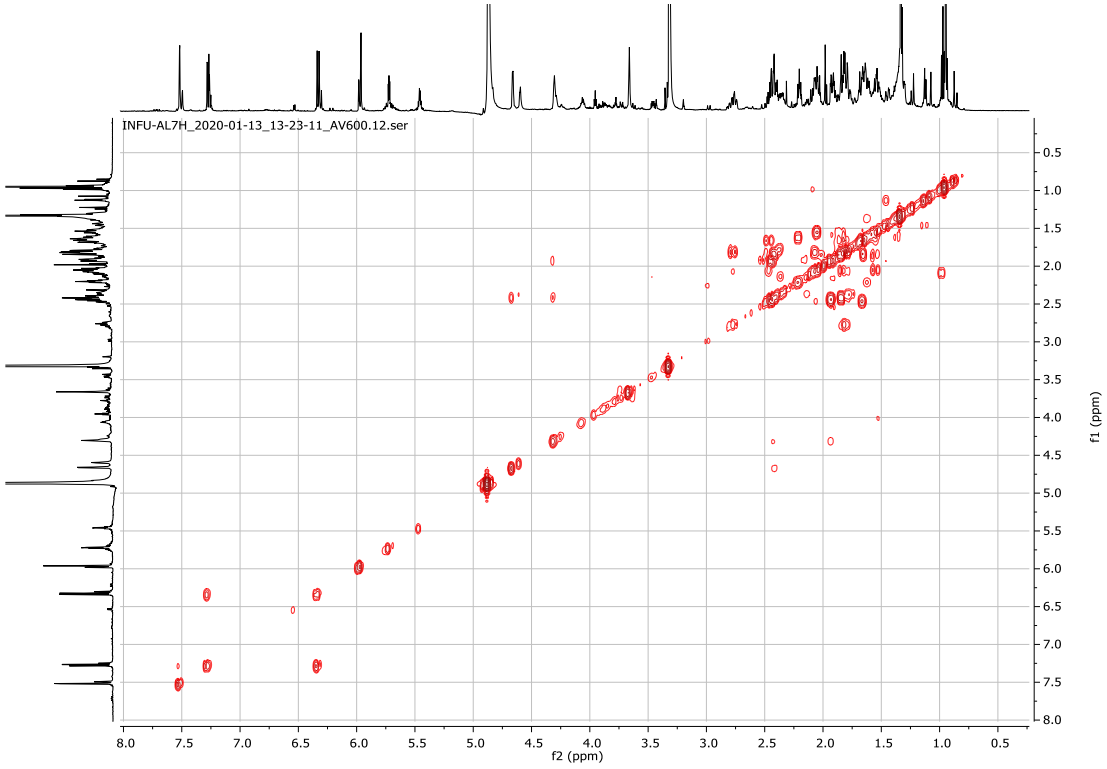

Appendix 119: HSQC (CD_3OD) spectrum of **34**

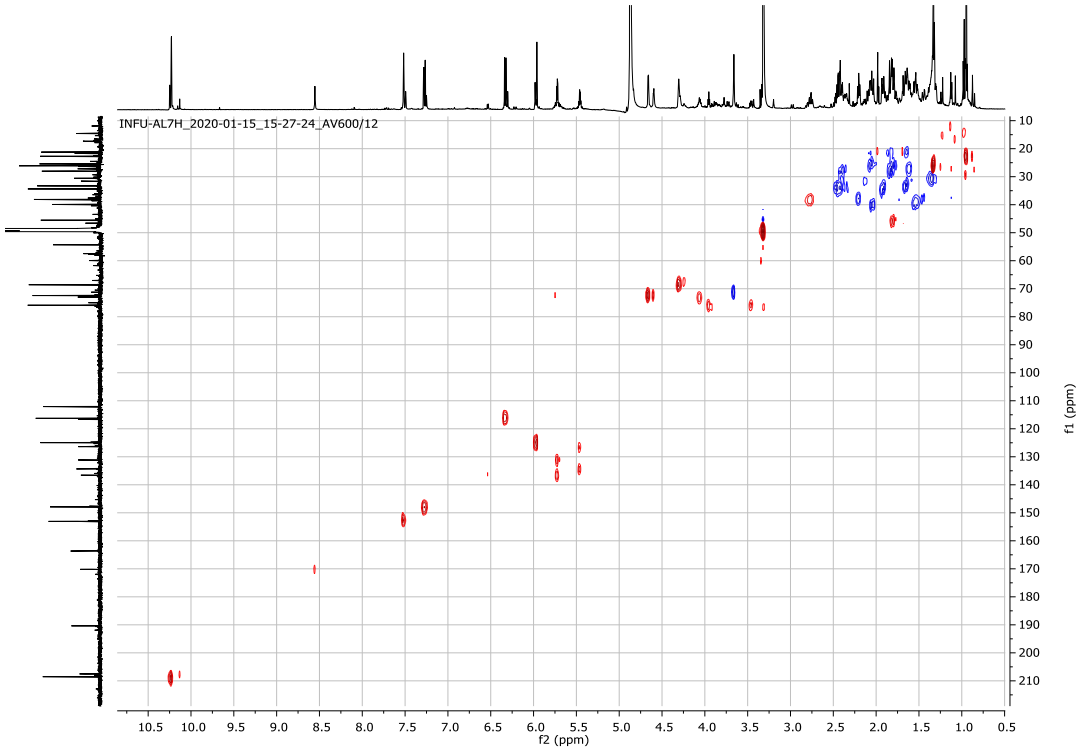

Appendix 120: HMBC (CD_3OD) spectrum of **34**

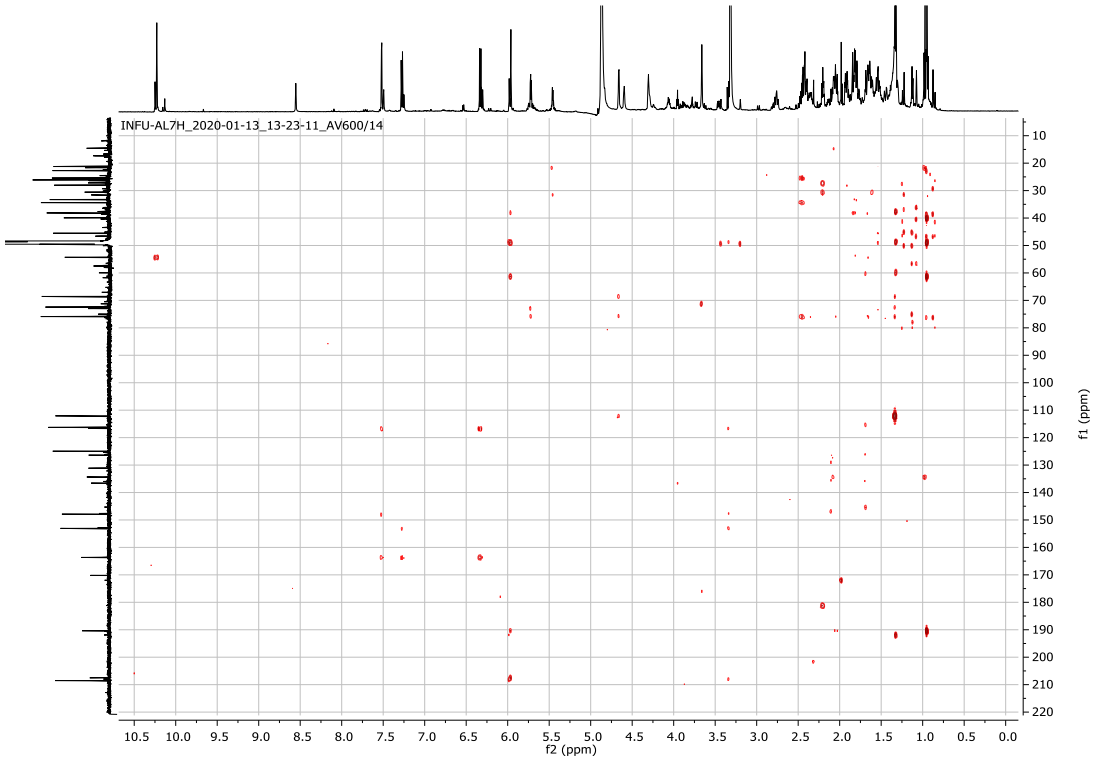

Appendix 121: NOESY (CD_3OD) spectrum of **34**

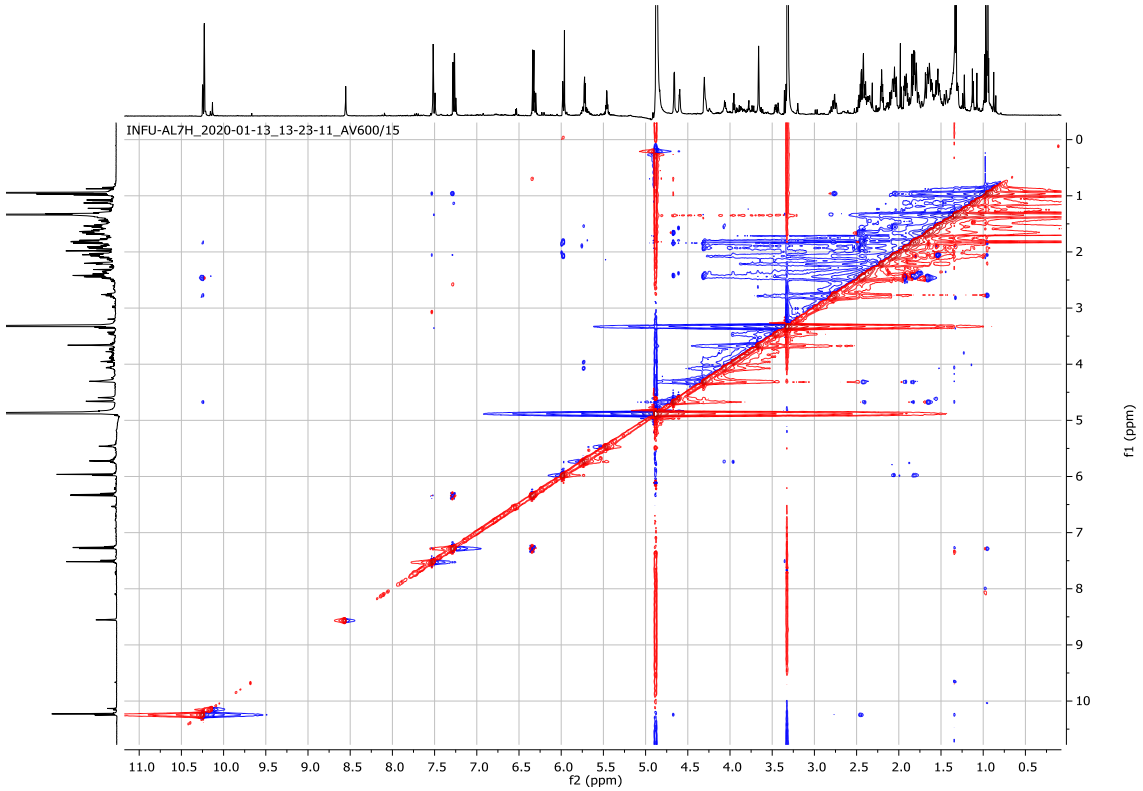

Appendix 122: HRESIMS of **35**

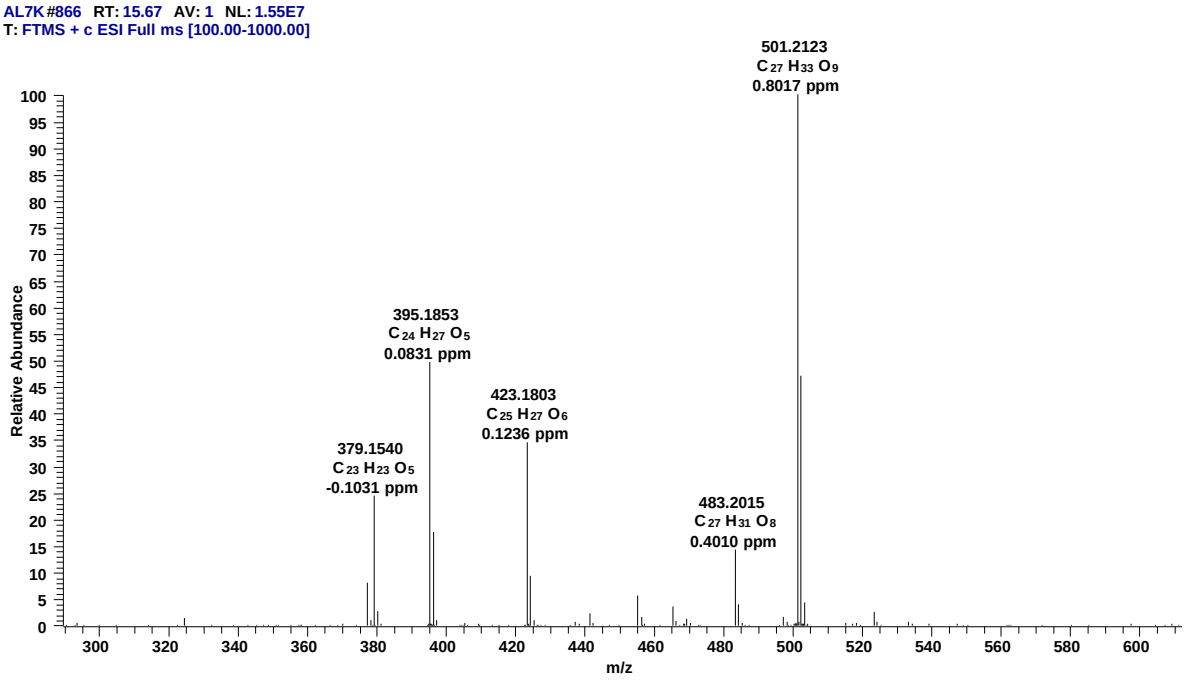

Appendix 123: Infrared spectrum of **35**

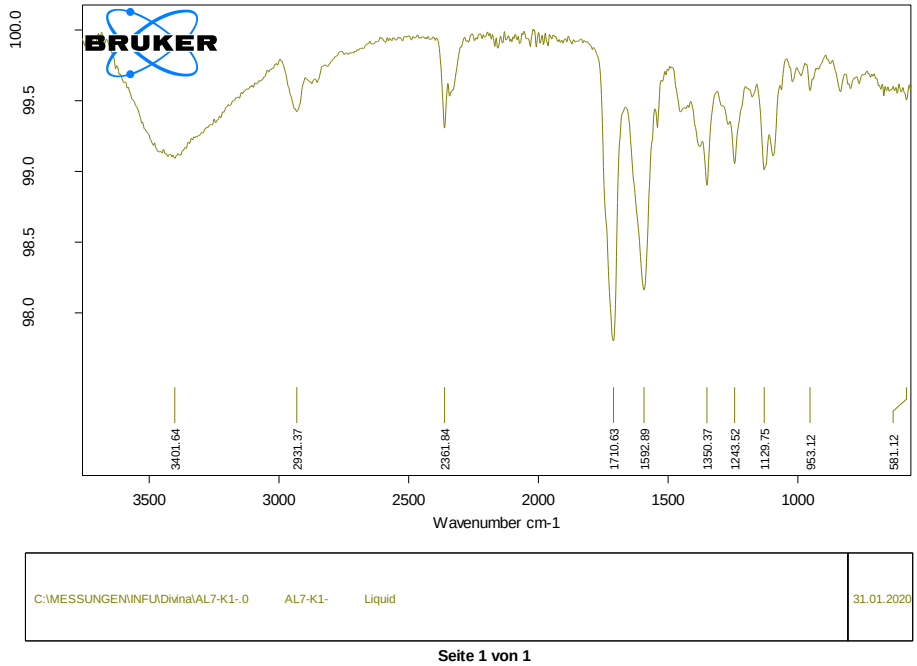

Appendix 124: ^{1}H NMR (600 MHz, CD_3OD) spectrum of **35**

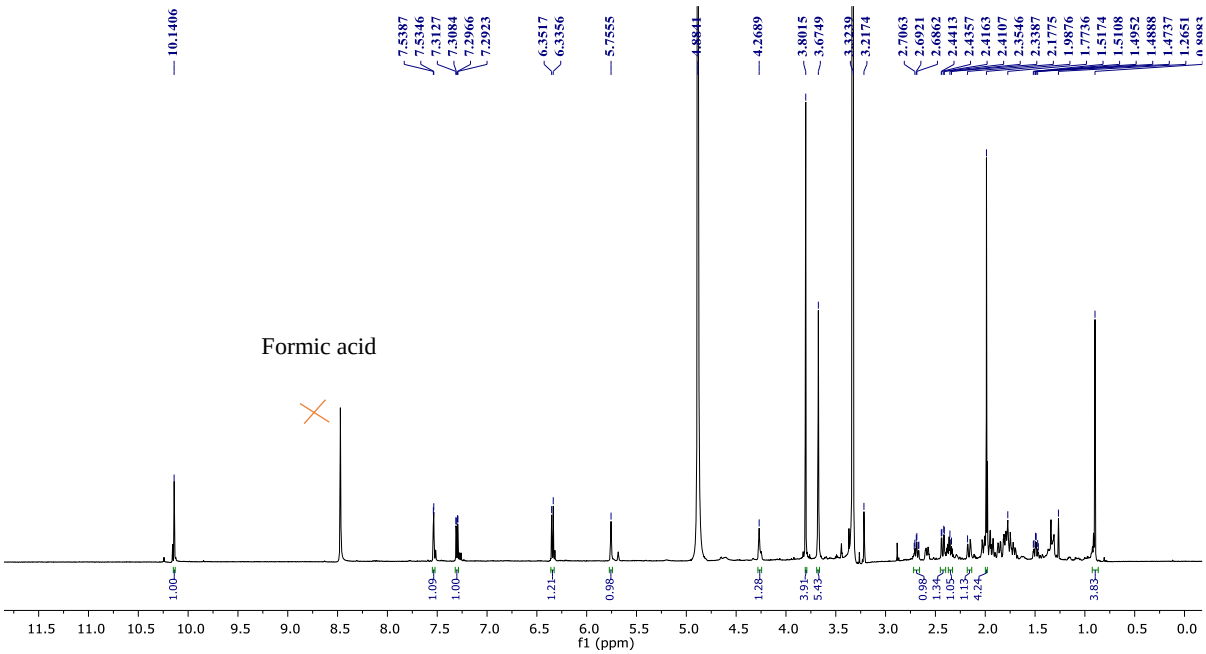

Appendix 125: ^{13}C NMR (150 MHz, CD_3OD) spectrum of **35**

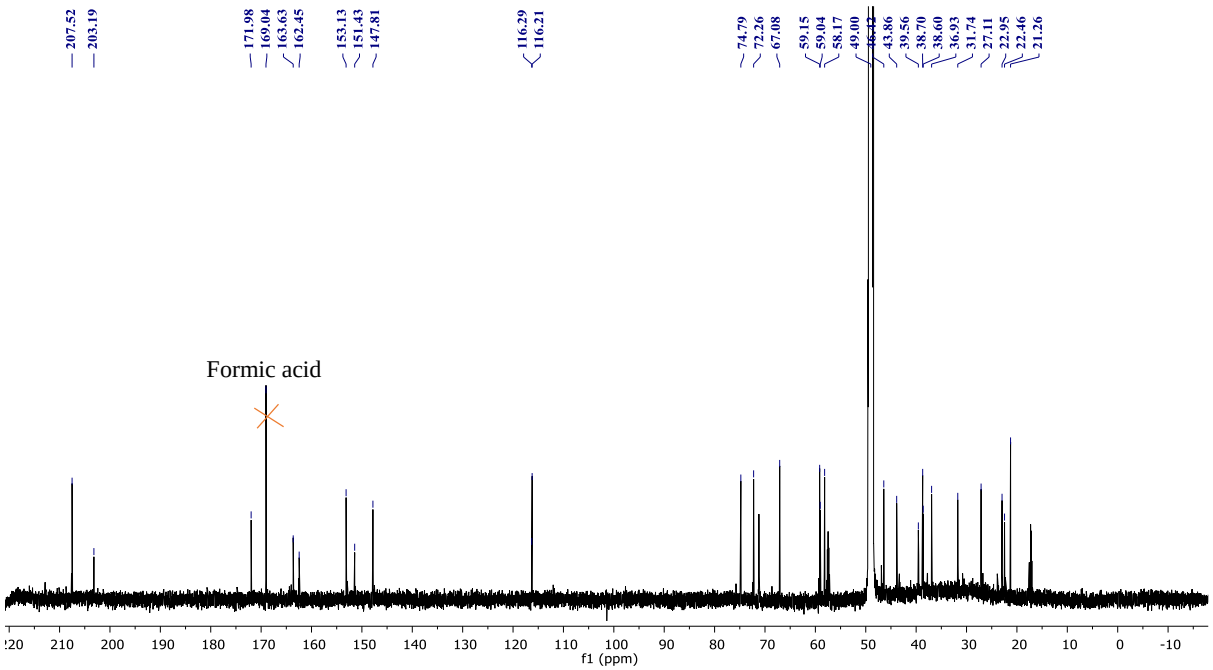

Appendix 126: COSY (600 MHz, CD_3OD) spectrum of **35**

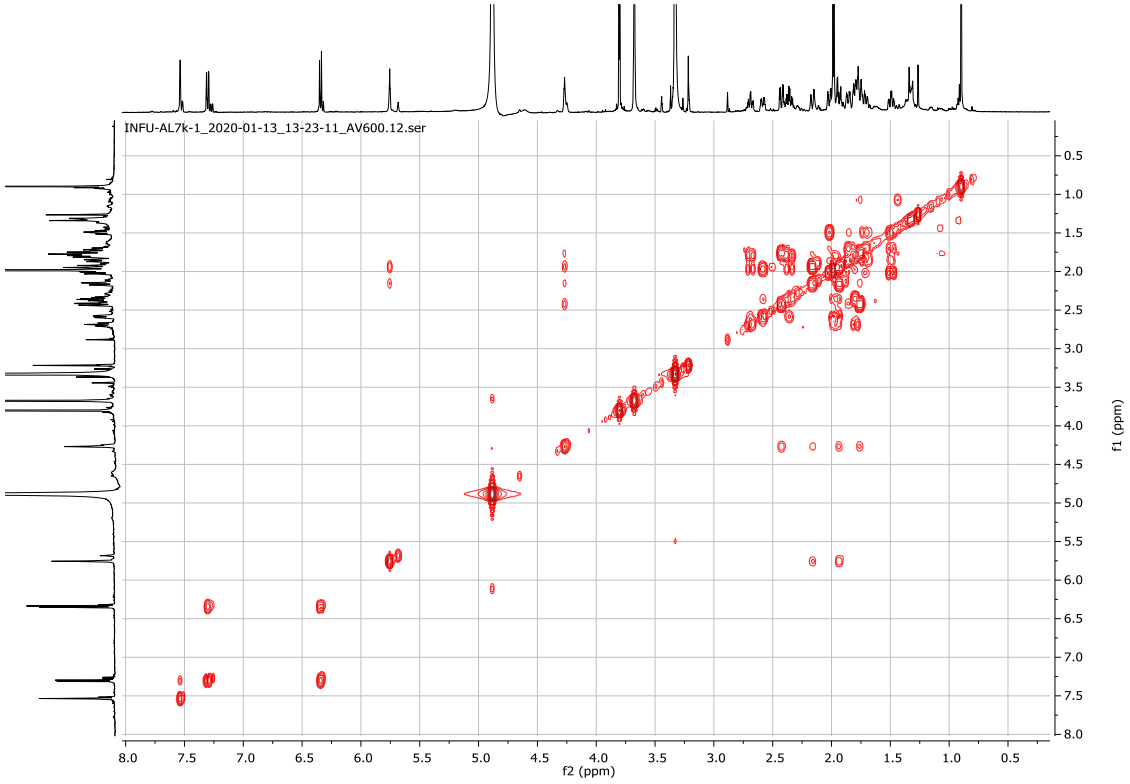

Appendix 127: HSQC (CD_3OD) spectrum of **35**

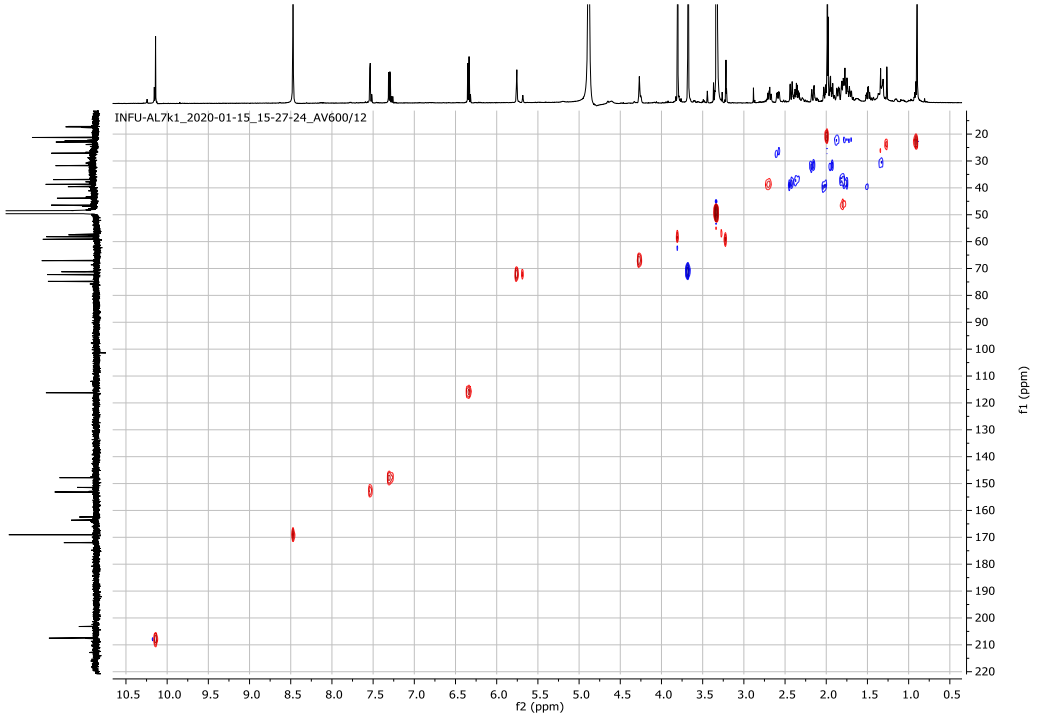

Appendix 128: HMBC (CD3OD) spectrum of **35**

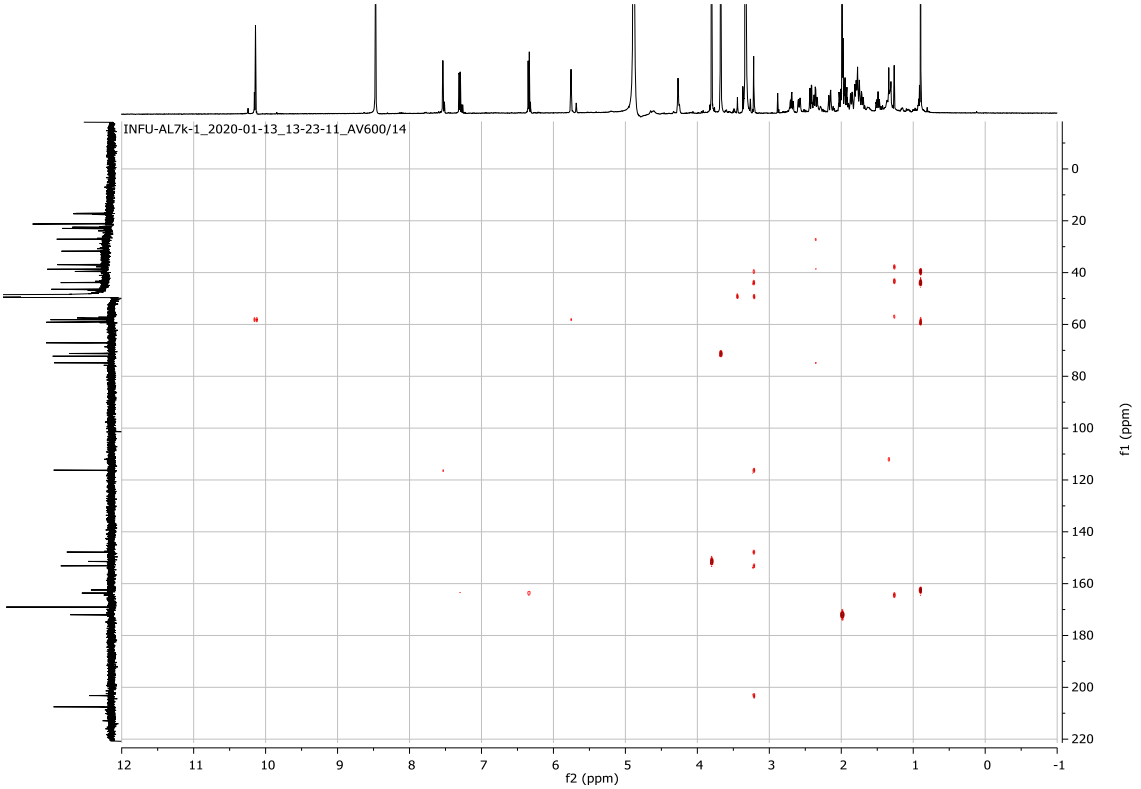

Appendix 129: NOESY (600MHz, CD_3OD) spectrum of **35**

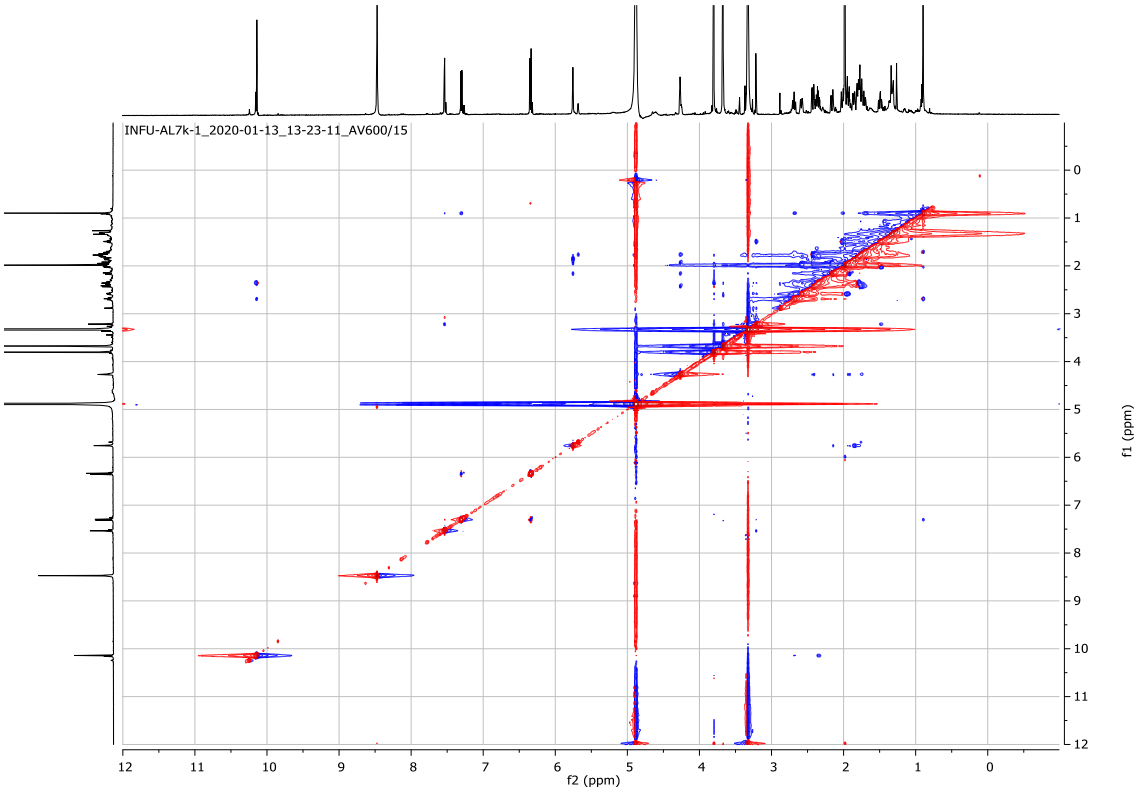

Appendix 130: HRESIMS of **36**

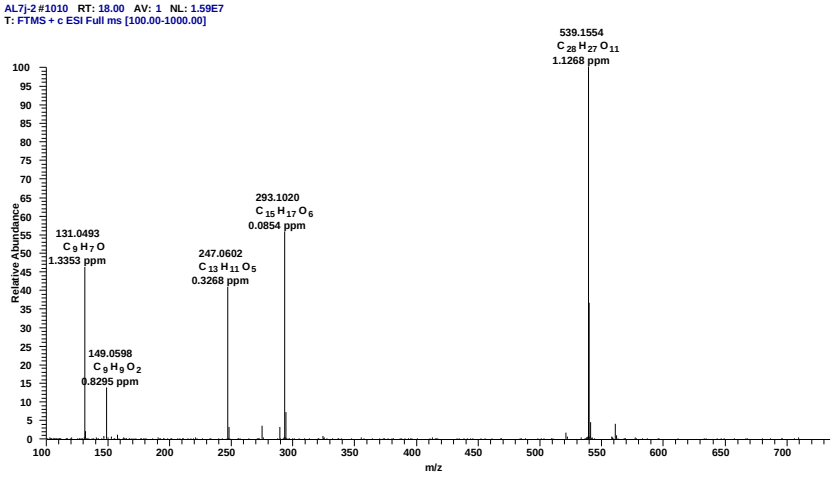

Appendix 131: Infrared spectrum of **36**

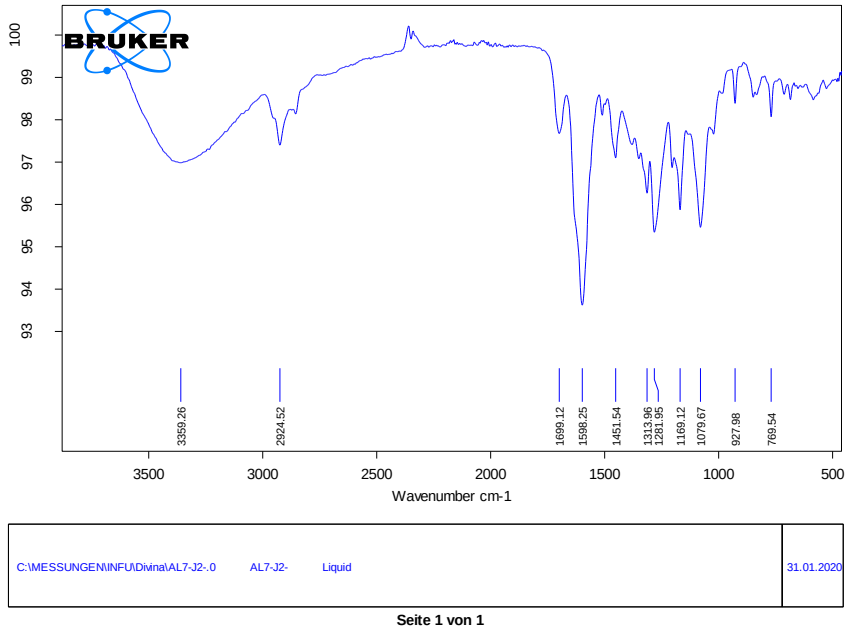

Appendix 132: ^{1}H NMR (600 MHz, CD_3OD) spectrum of **36**

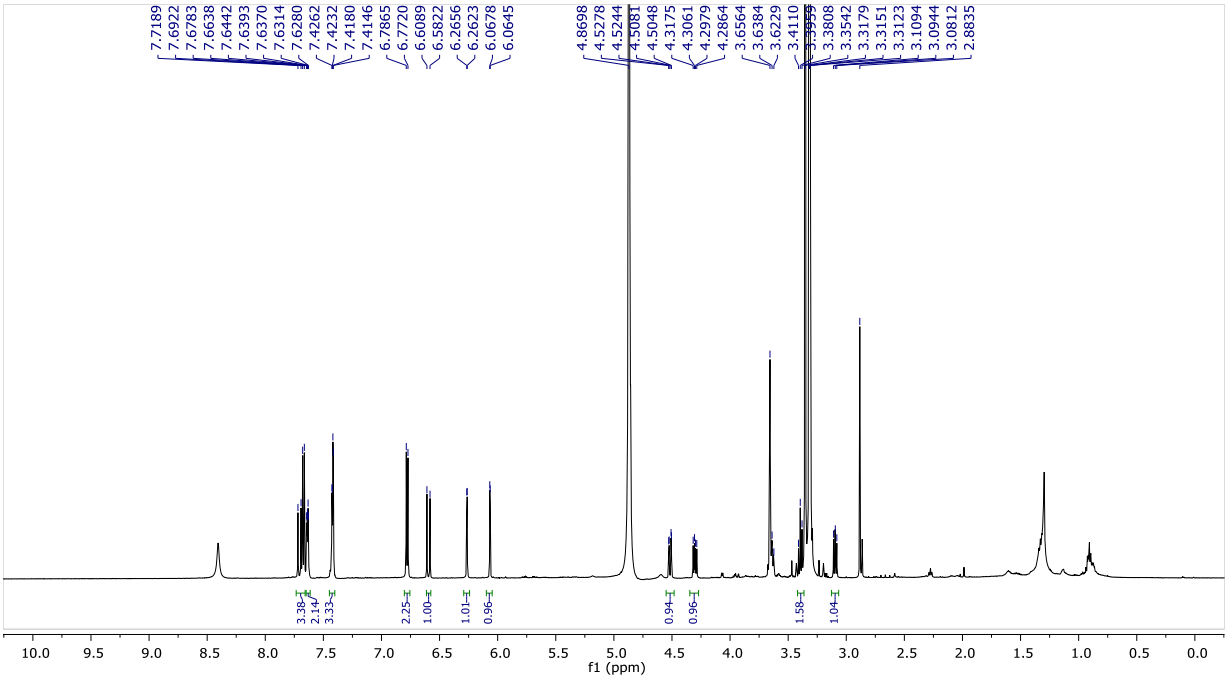

Appendix 133: ^{13}C NMR (150 MHz, $CDCl_3$) spectrum of **36**

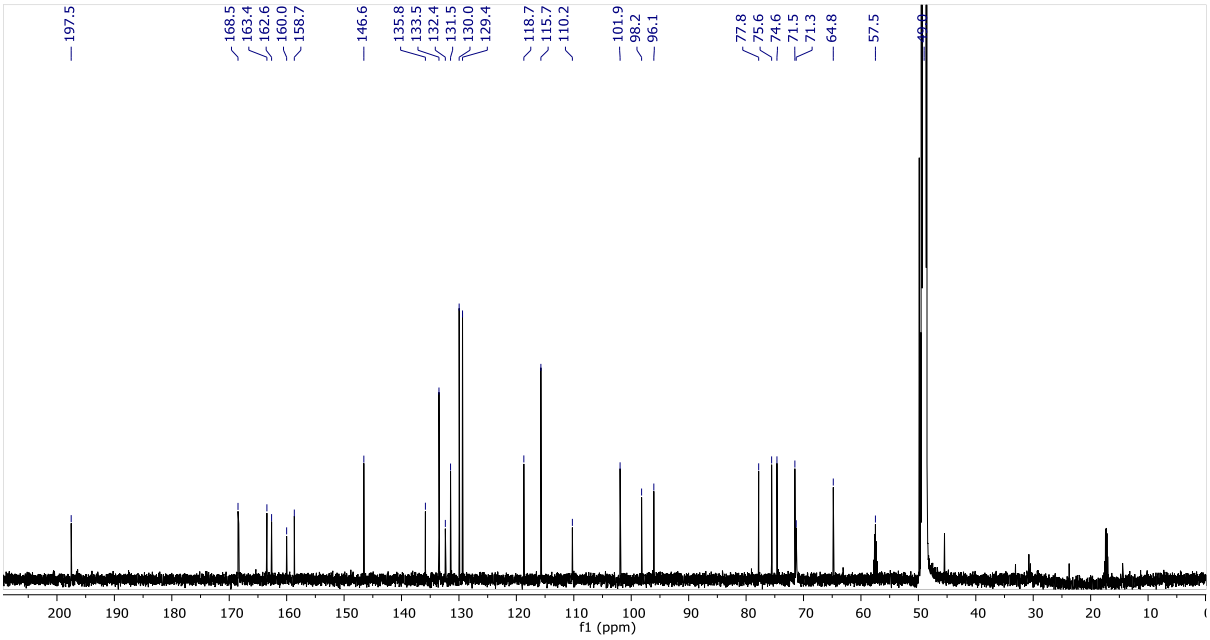

Appendix 134: COSY (600 MHz, CD3OD) spectrum of **36**

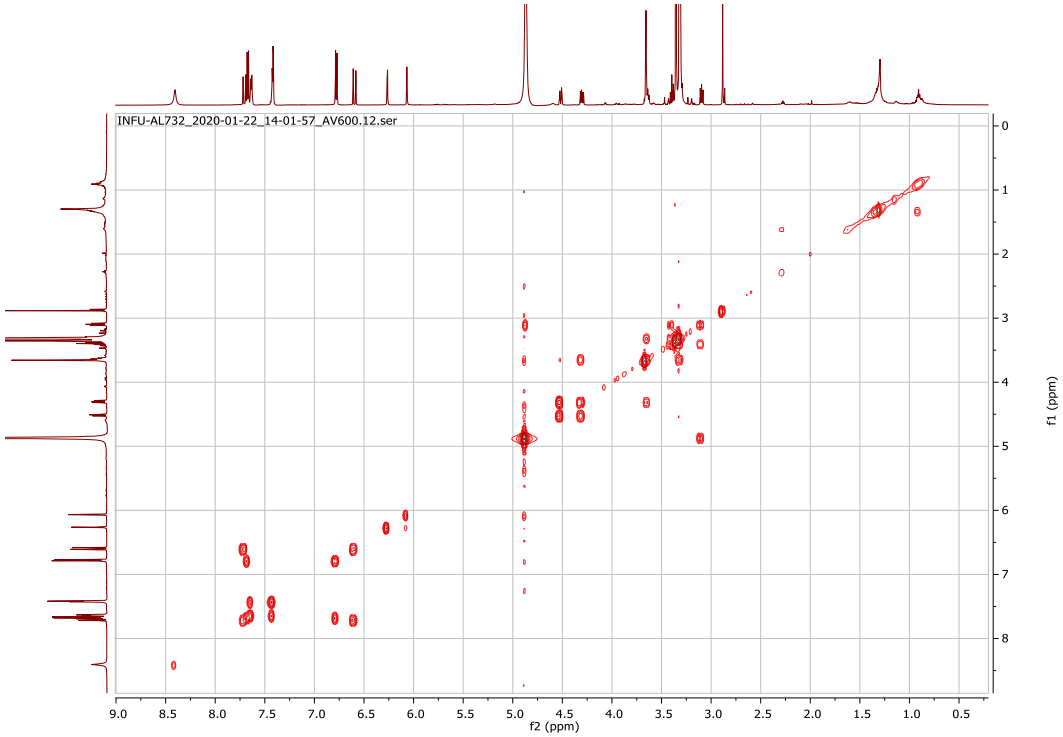

Appendix 135: HSQC (CD_3OD) spectrum of **36**

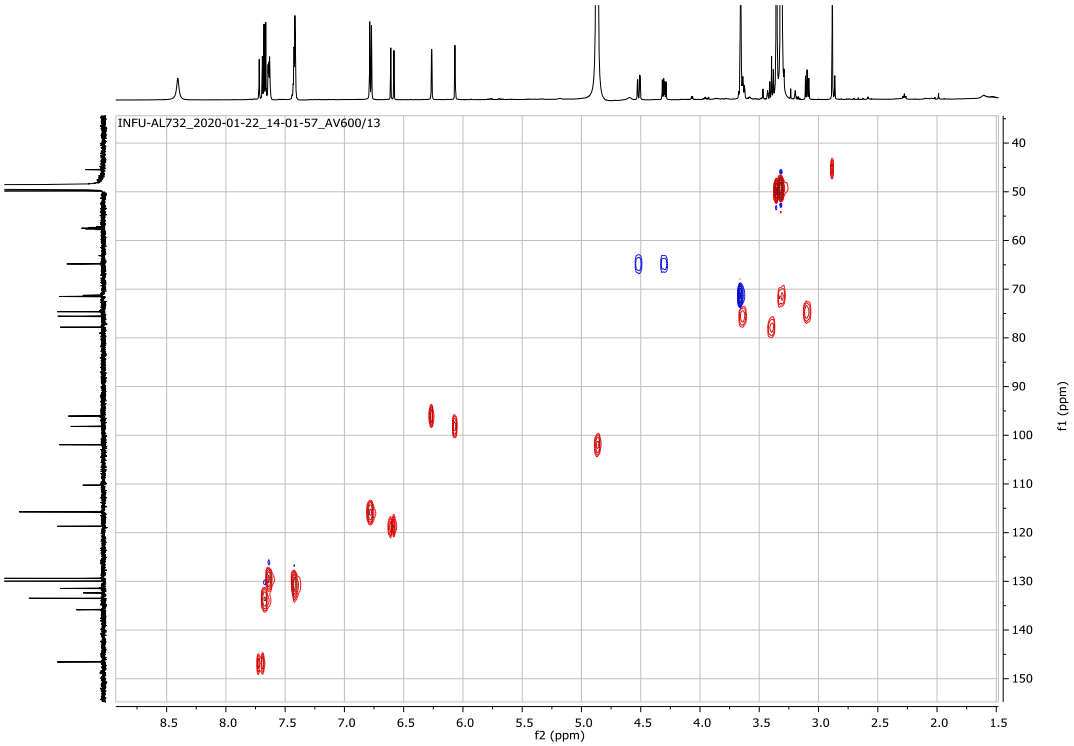

Appendix 136: HMBC (CD_3OD) spectrum of **36**

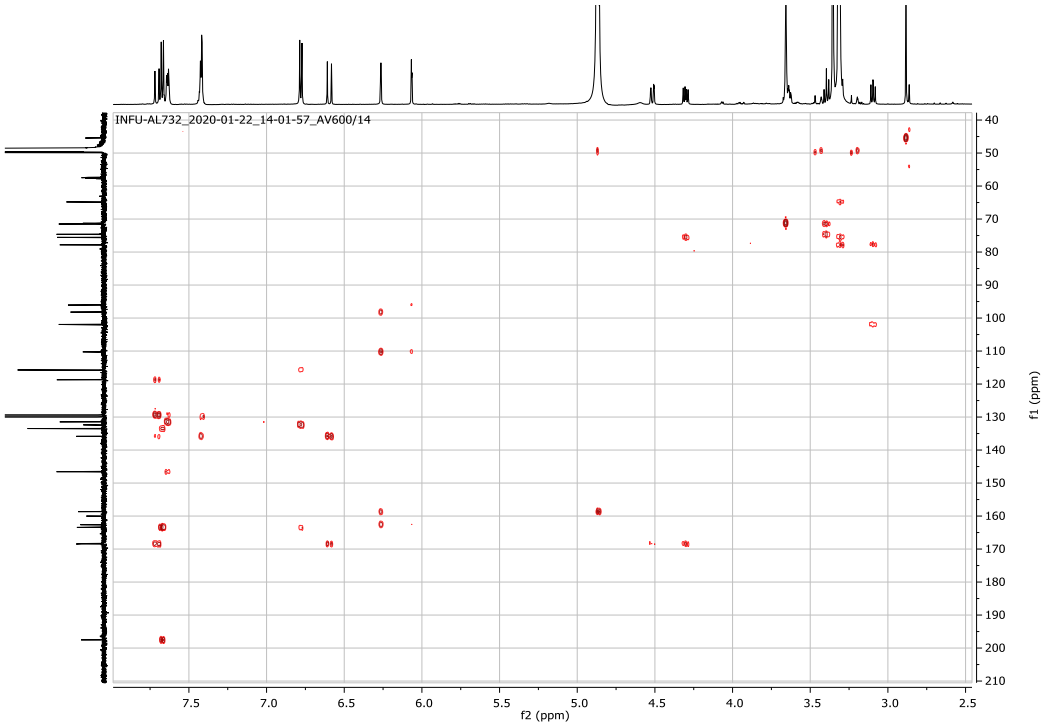

Appendix 137: HRESIMS of **37**

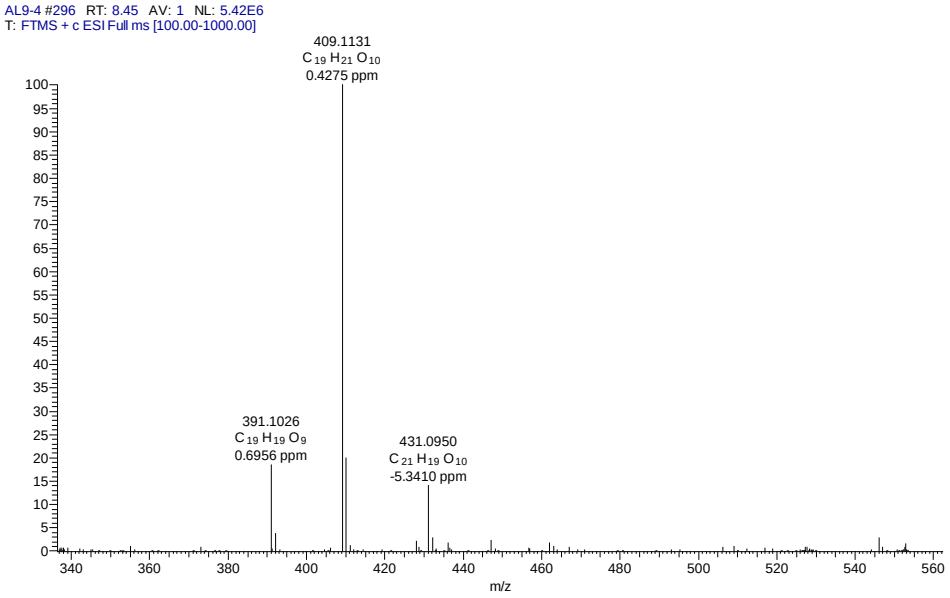

Appendix 138: ^{1}H NMR (600 MHz, MeOD-d_4) spectrum of **37**

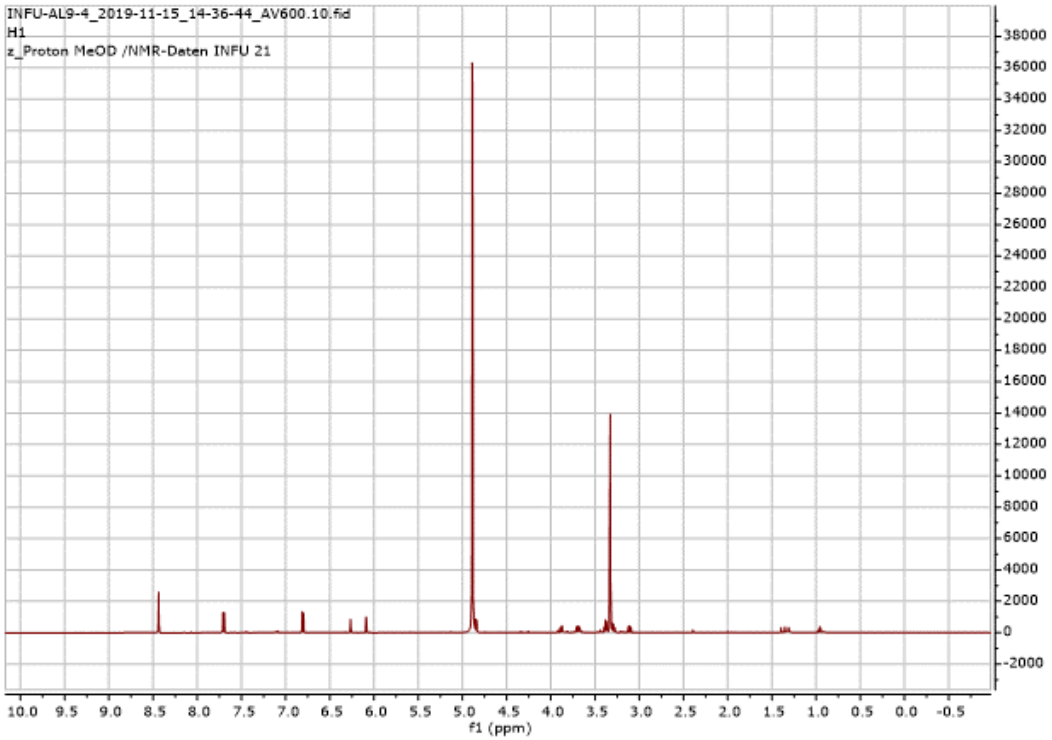

Appendix 139: ^{13}C NMR (175 MHz, MeOD-d_4) spectrum of **37**

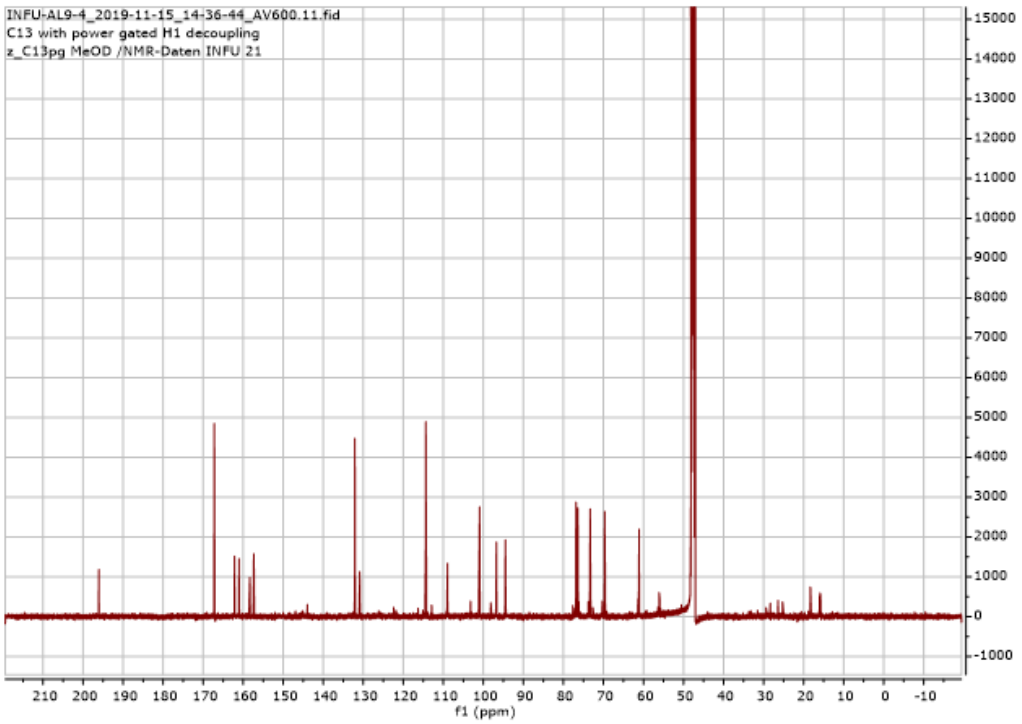

Appendix 140: COSY (600 MHz, MeOD-d_4) spectrum of **37**

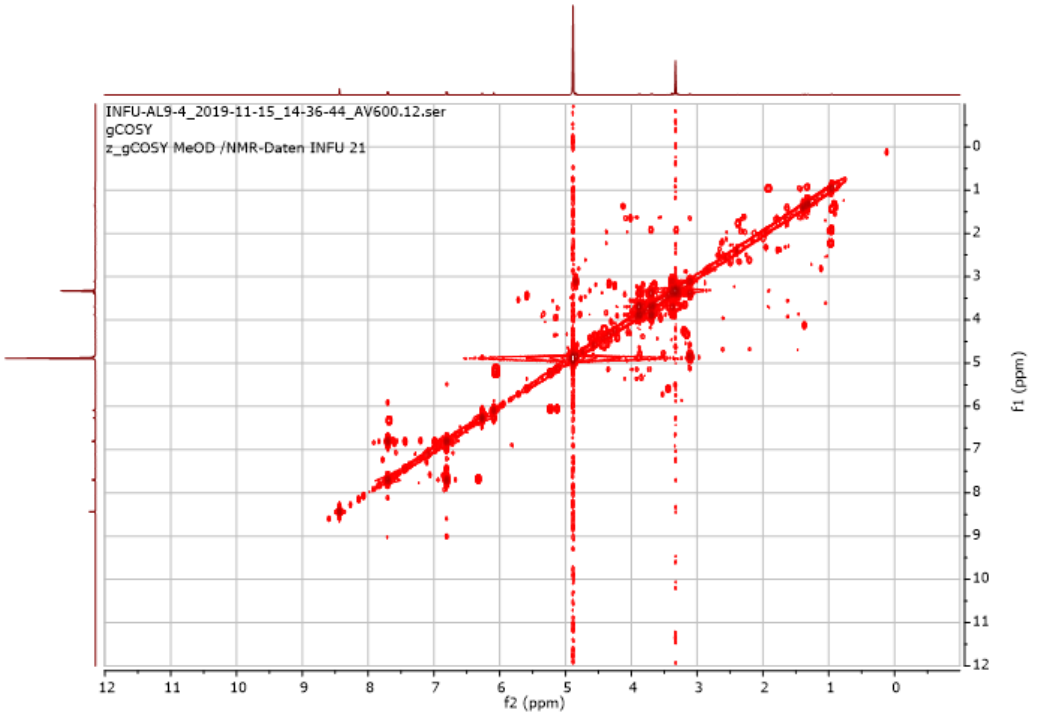

Appendix 141: HSQC (MeOD-d_4) spectrum of **37** (^{1}H: 600 MHz, ^{13}C: 175 MHz)

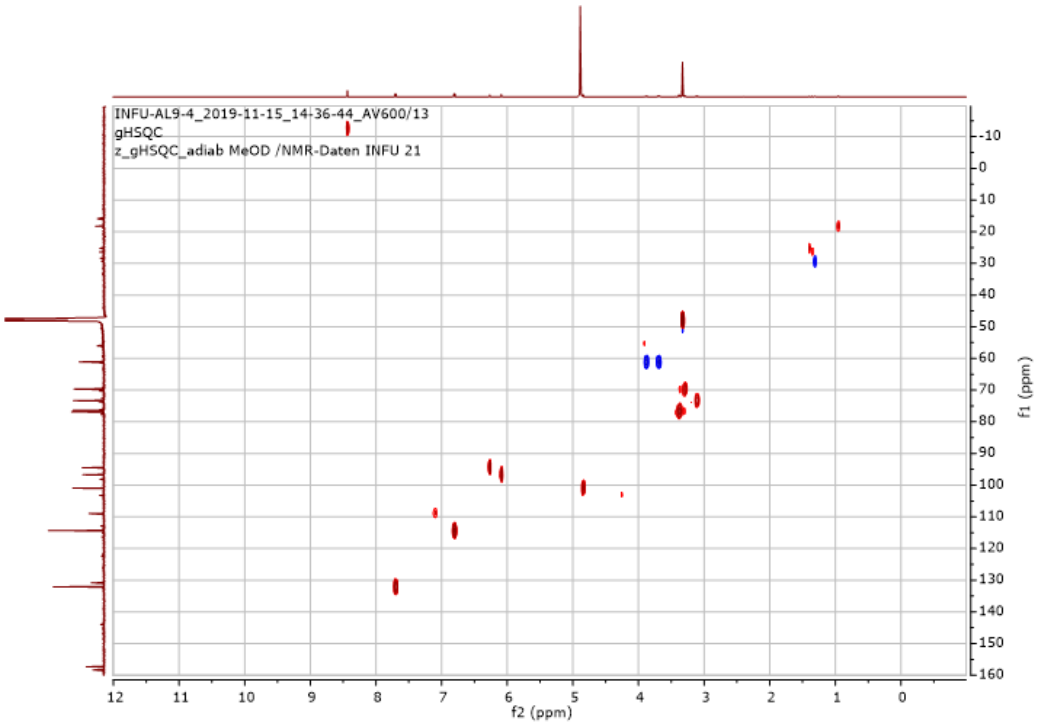

Appendix 142: HMBC (MeOD-d_4) spectrum of **37** (^{1}H: 600 MHz, ^{13}C: 175 MHz)

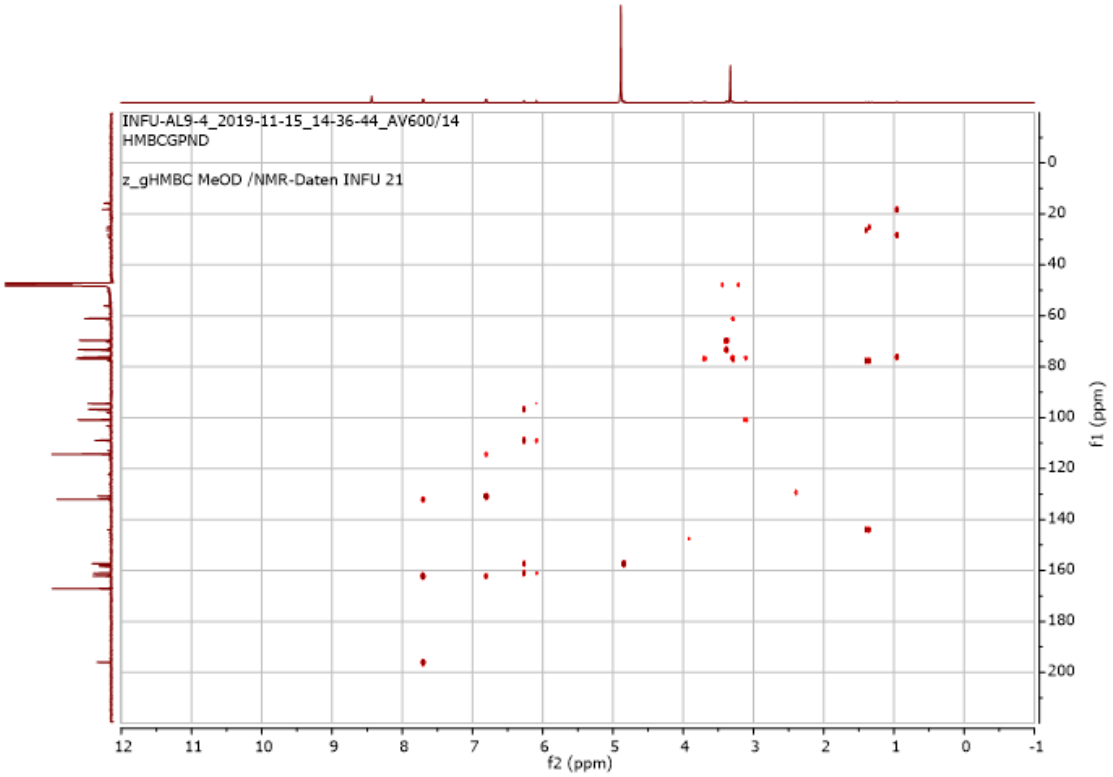

Appendix 143: HRESIMS of **38**

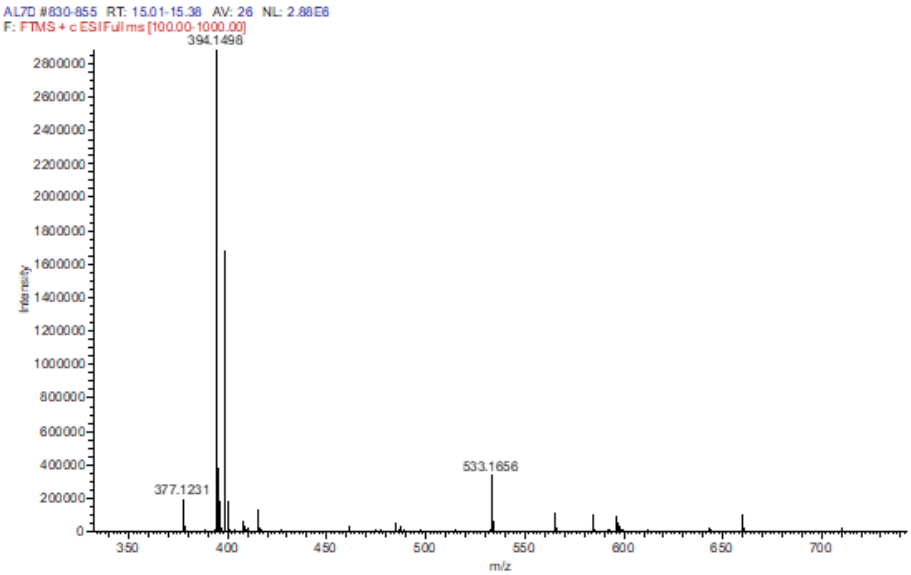

Appendix 144: ^{1}H NMR (600 MHz, MeOD-d4) spectrum of **38**

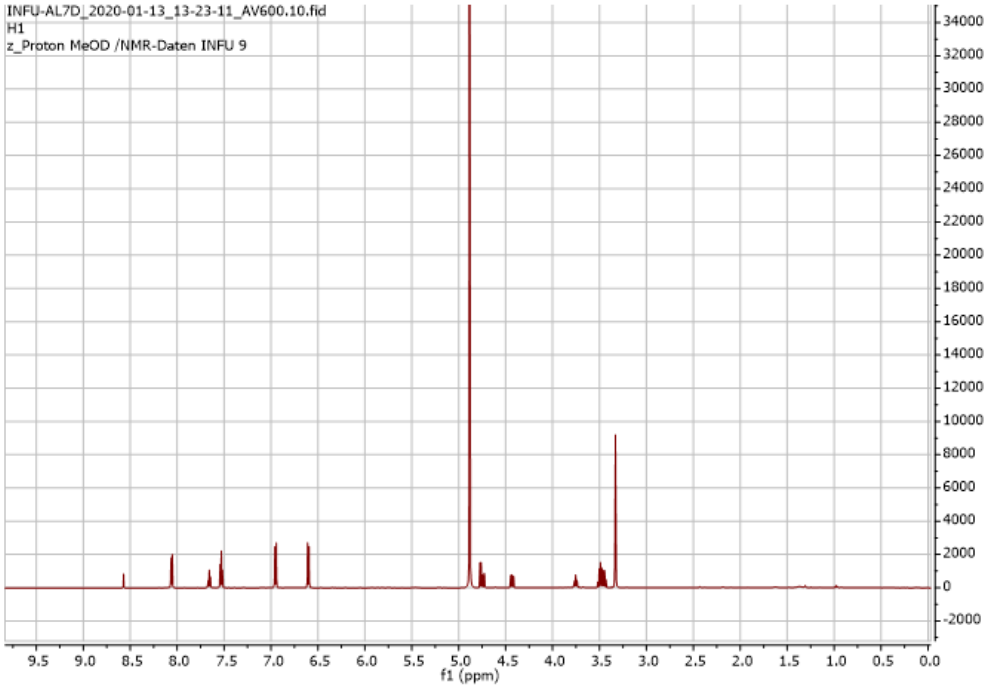

Appendix 145: ^{13}C NMR (175 MHz, MeOD-d_4) spectrum of **38**

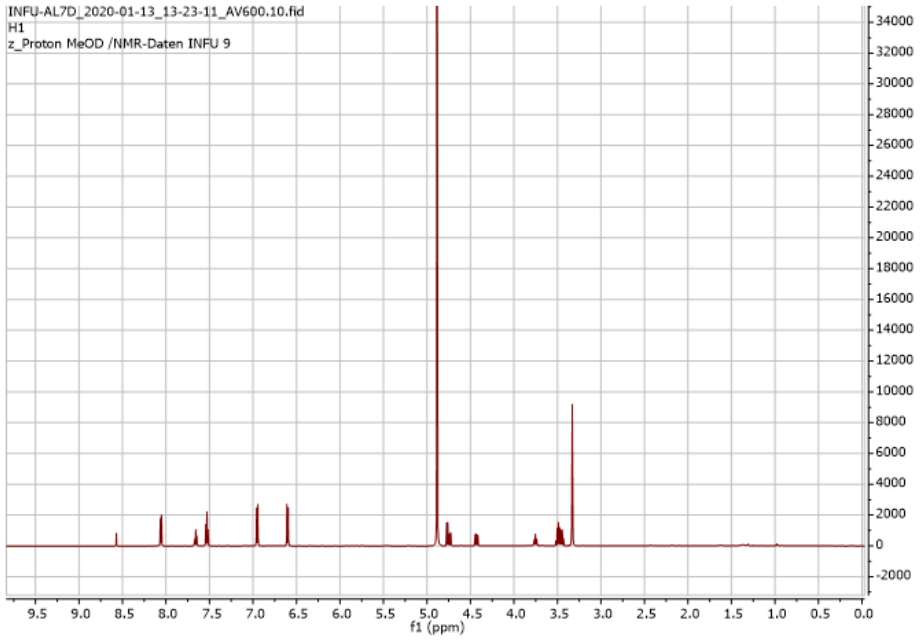

Appendix 146: COSY (600 MHz, MeOD-d4) spectrum of **38**

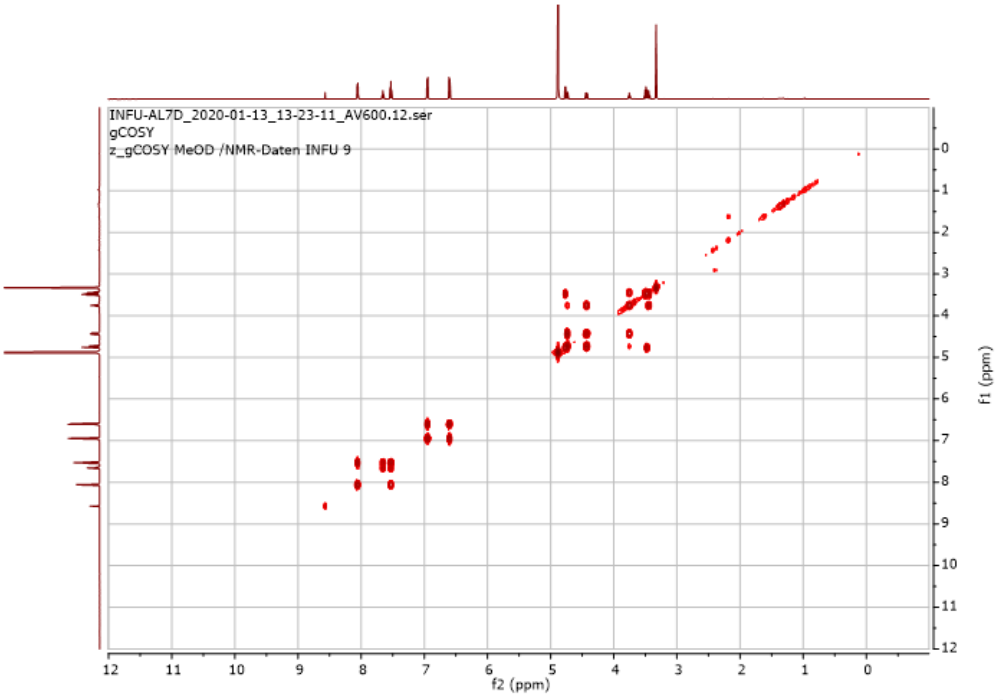

Appendix 147: HSQC (MeOD-d_4) spectrum of **38** (^{1}H: 600 MHz, ^{13}C: 175 MHz)

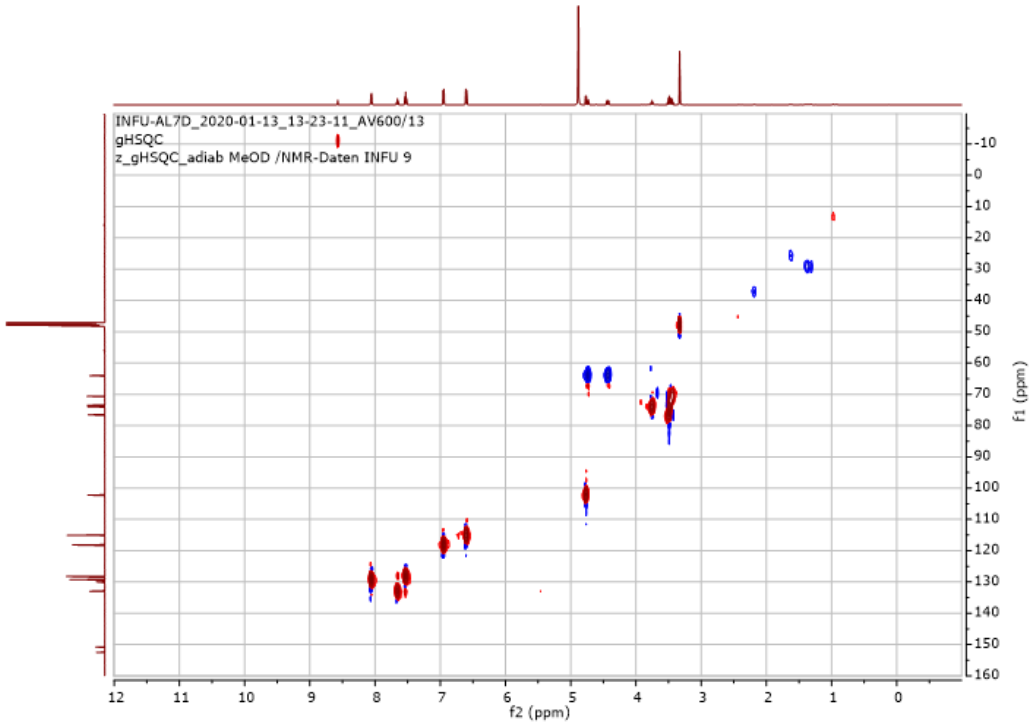

Appendix 148: HMBC (MeOD-d_4) spectrum of **38** (^{1}H: 600 MHz, ^{13}C: 175 MHz)

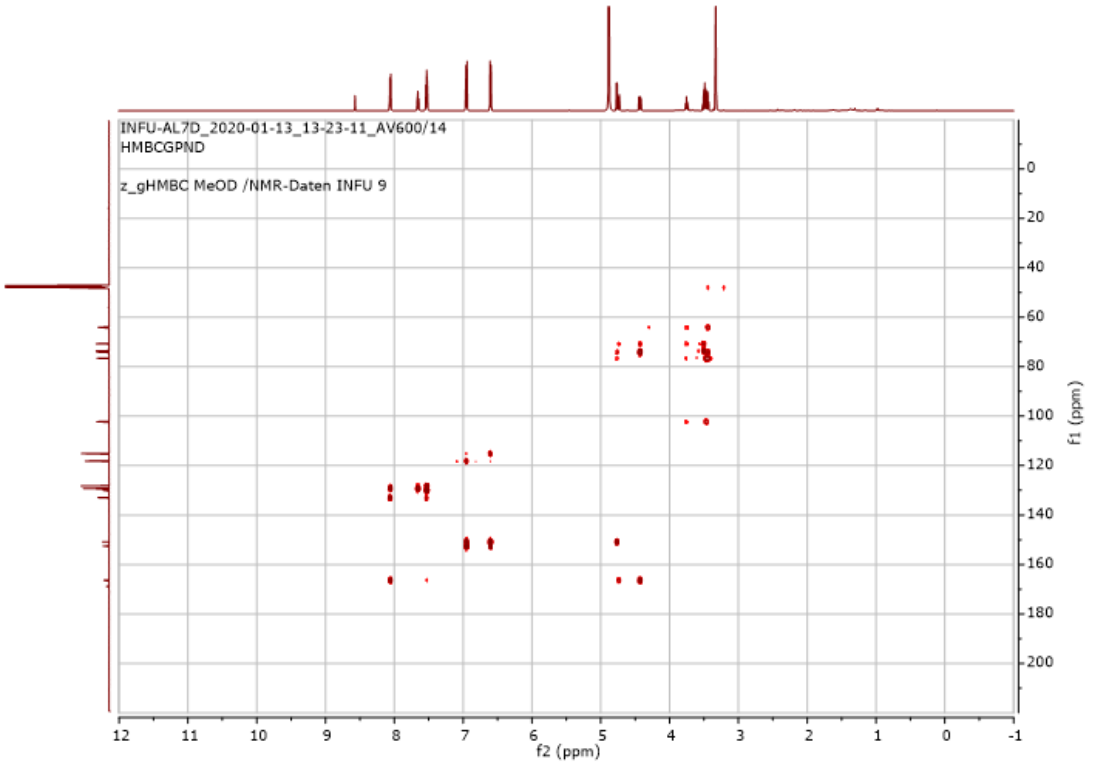

Appendix 149: HRESIMS of **39**

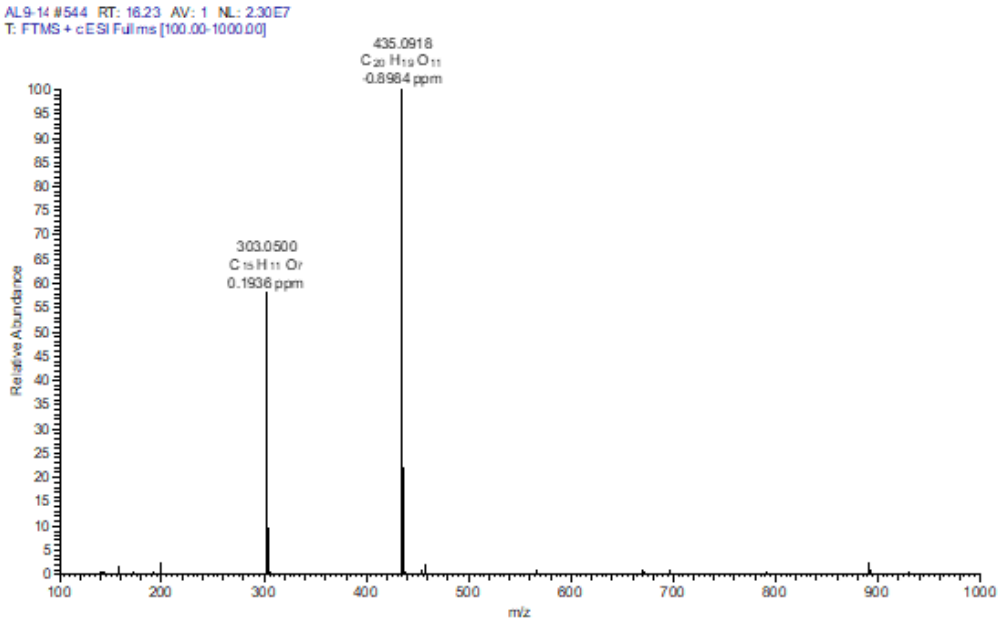

Appendix 150: ^{1}H NMR (600 MHz, MeOD-d_4) spectrum of **39**

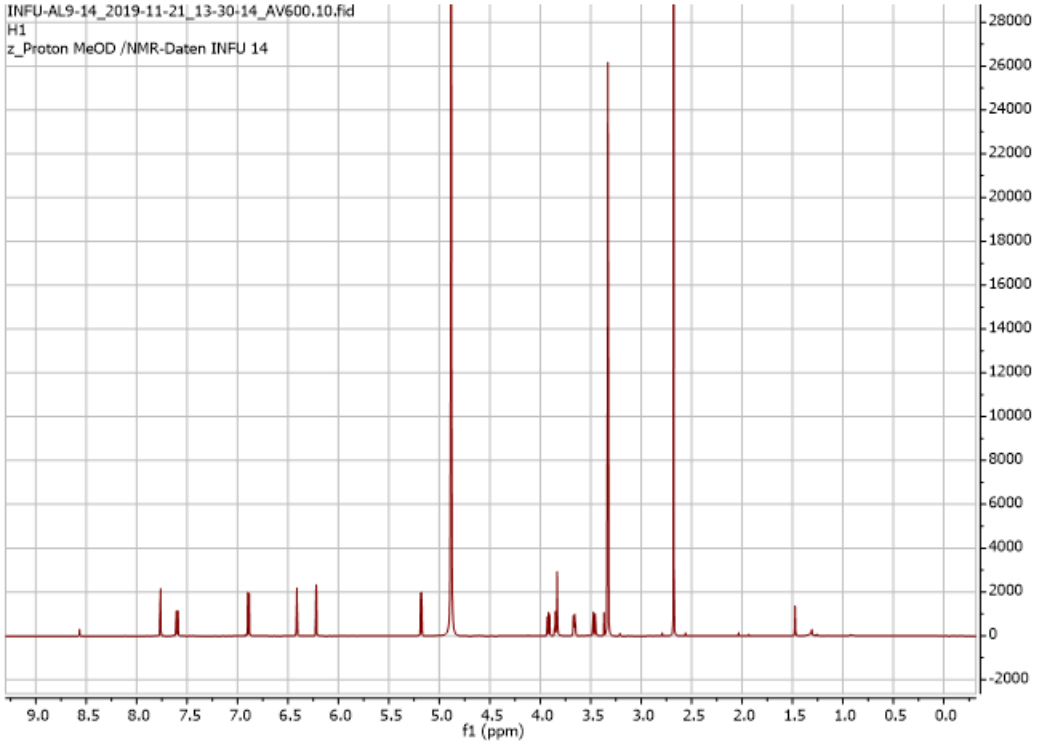

Appendix 151: ^{13}C NMR (175 MHz, MeOD-d_4) spectrum of **39**

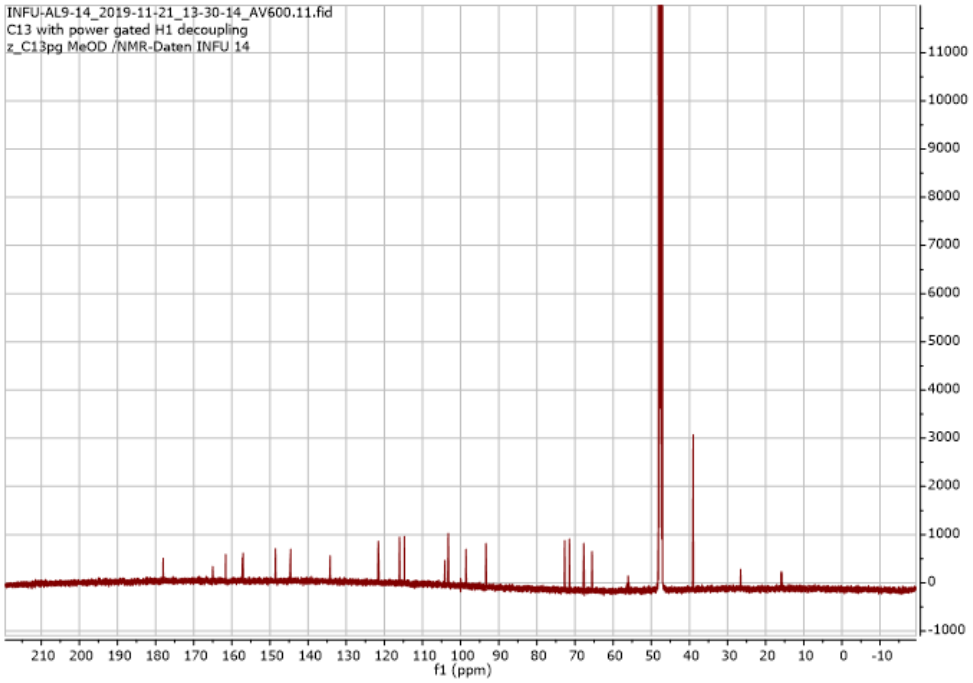

Appendix 152: COSY (600 MHz, MeOD-d_4) spectrum of **39**

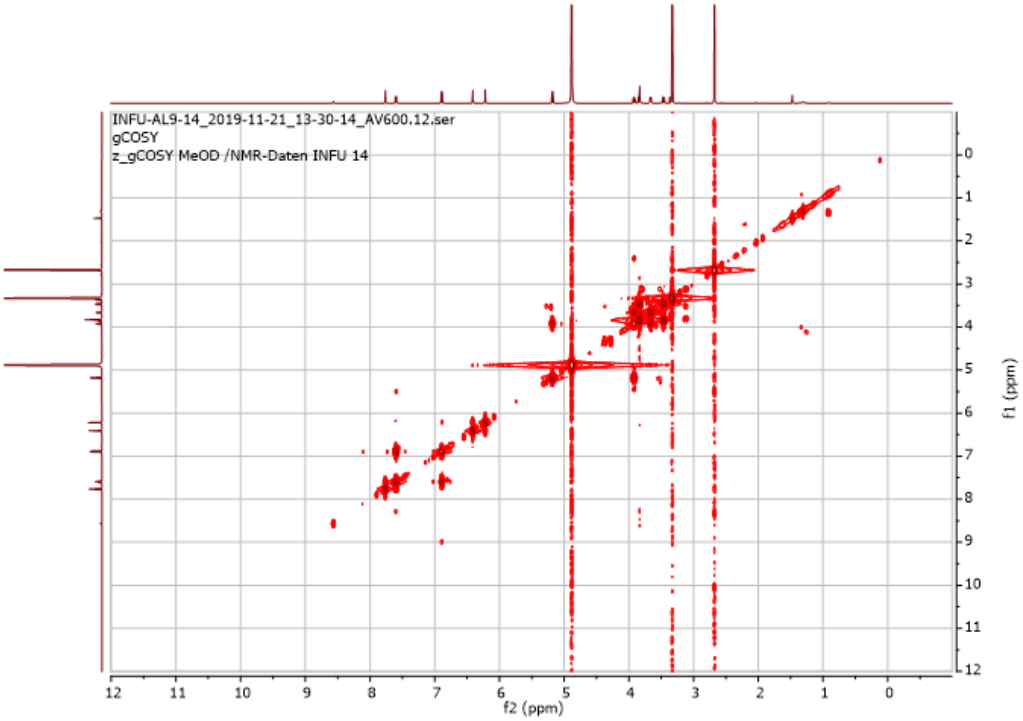

Appendix 153: HSQC (MeOD-d_4) spectrum of **39** (^{1}H: 600 MHz, ^{13}C: 175 MHz)

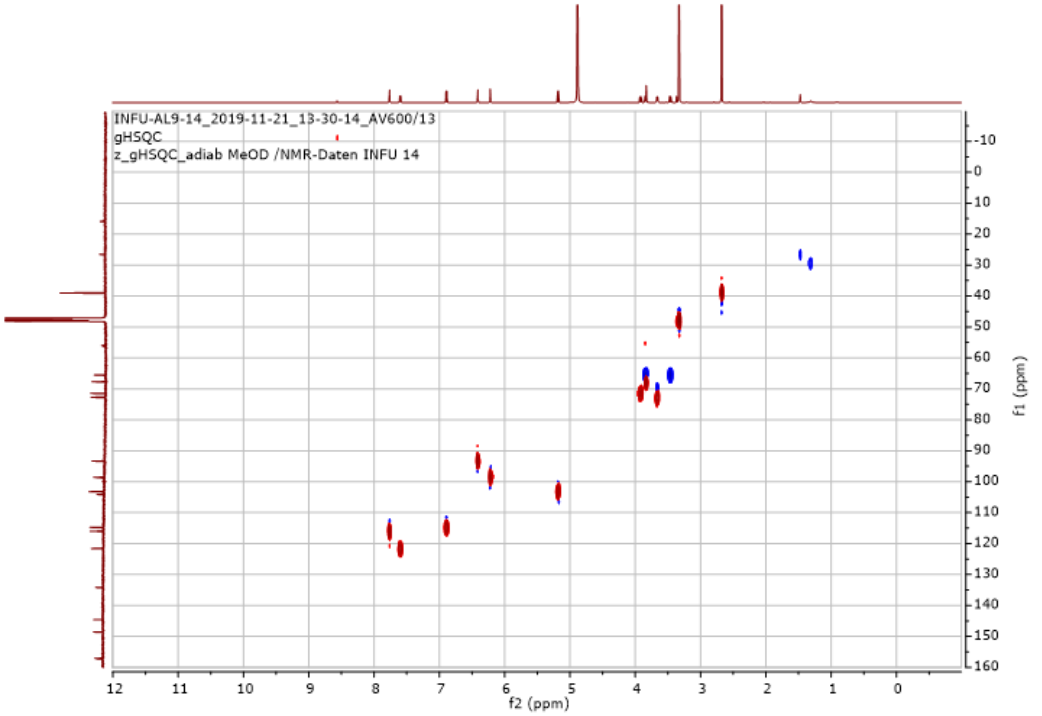

Appendix 154: HMBC (MeOD-d_4) spectrum of **39** (^{1}H: 600 MHz, ^{13}C: 175 MHz)

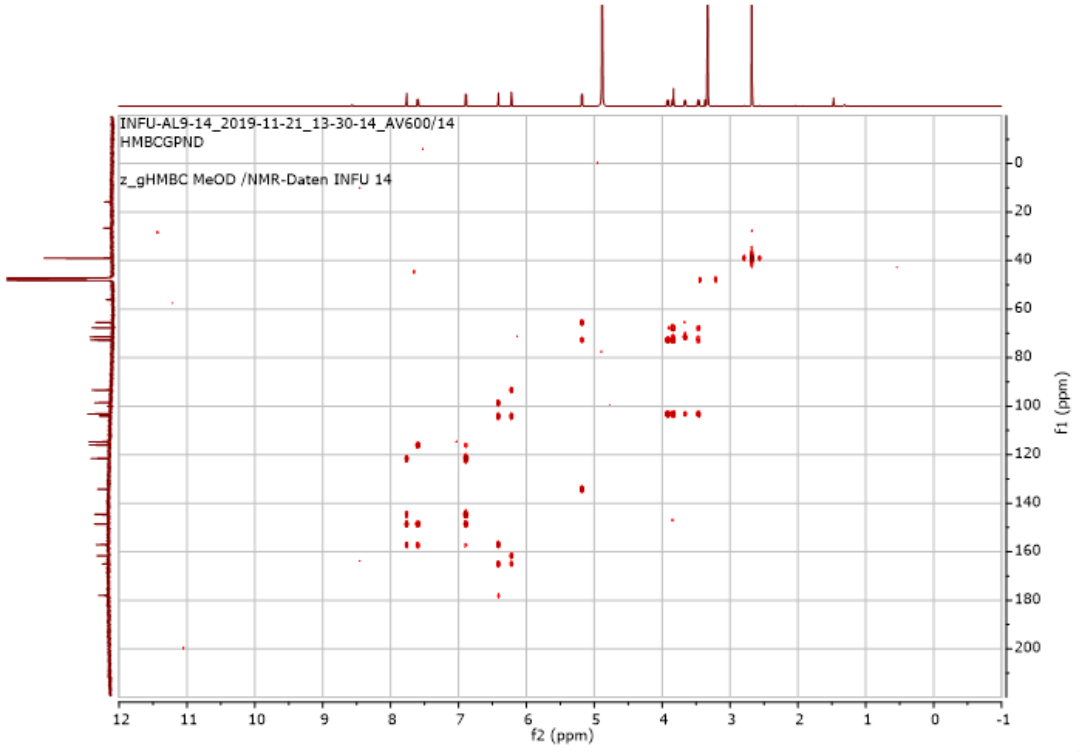

Appendix 155: HRESIMS of **40**

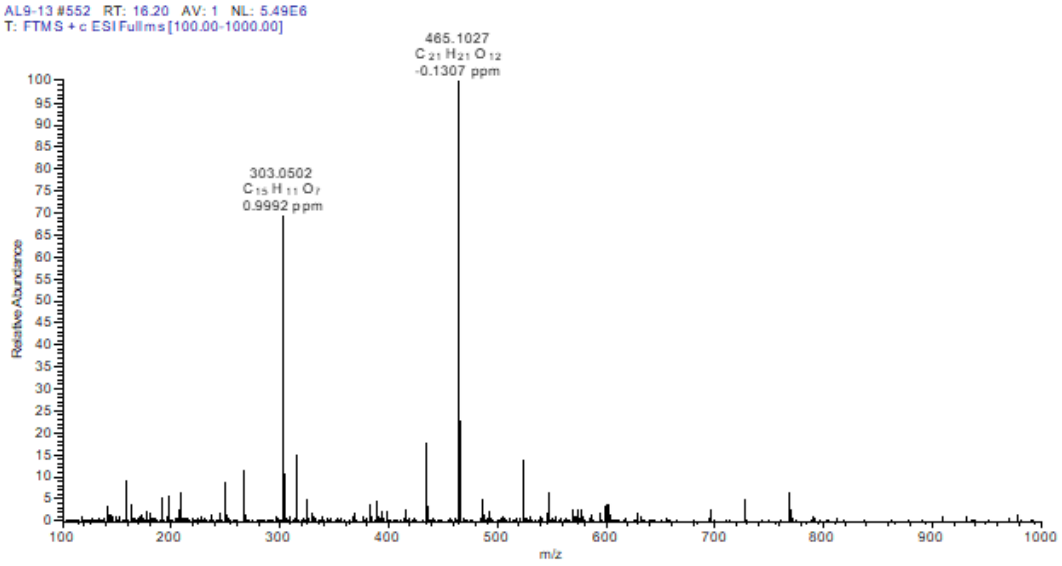

Appendix 156: ^{1}H NMR (600 MHz, MeOD-d_4) spectrum of **40**

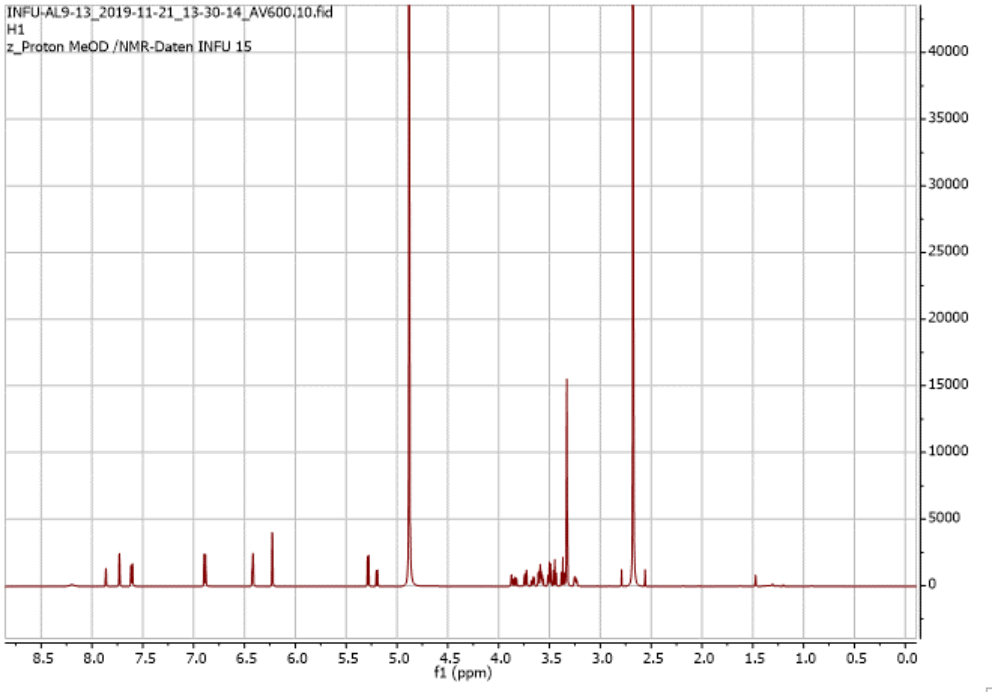

Appendix 157: ^{13}C NMR (175 MHz, MeOD-d_4) spectrum of **40**

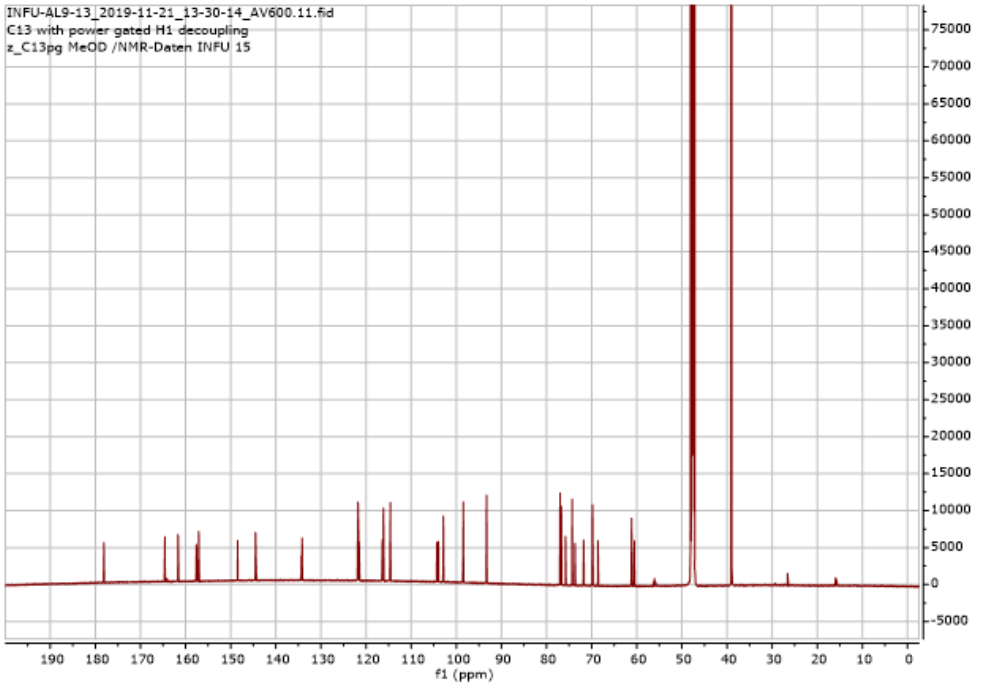

Appendix 158: COSY (600 MHz, MeOD-d_4) spectrum of **40**

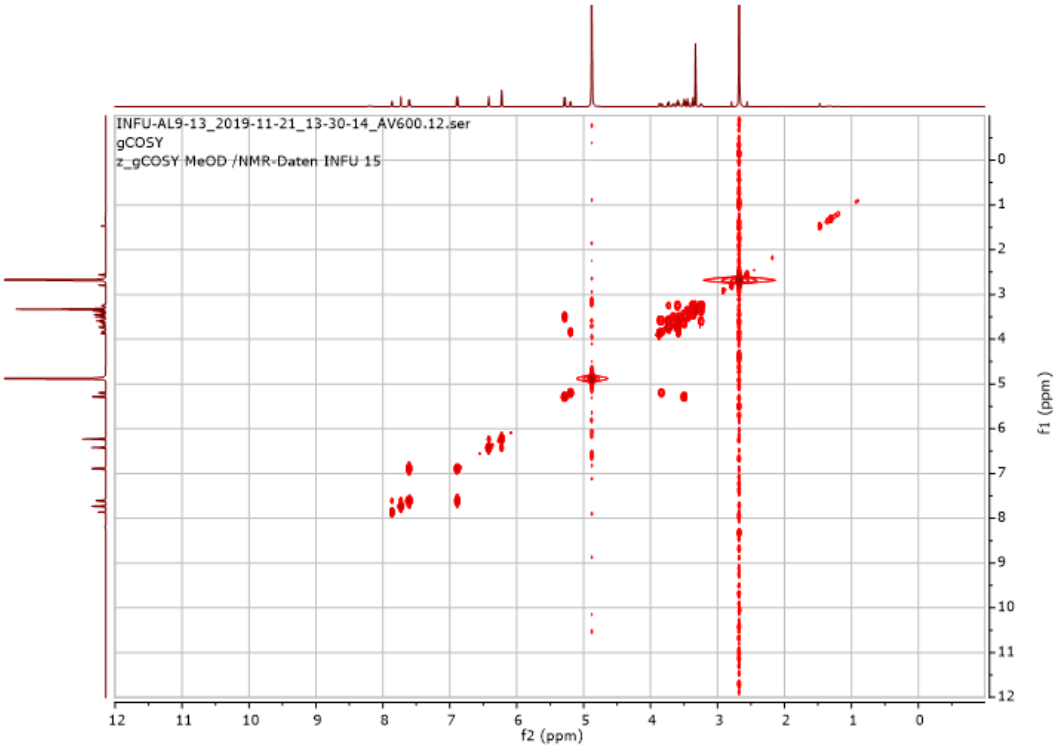

Appendix 159: HSQC (MeOD-d_4) spectrum of **40** (^{1}H: 600 MHz, ^{13}C: 175 MHz)

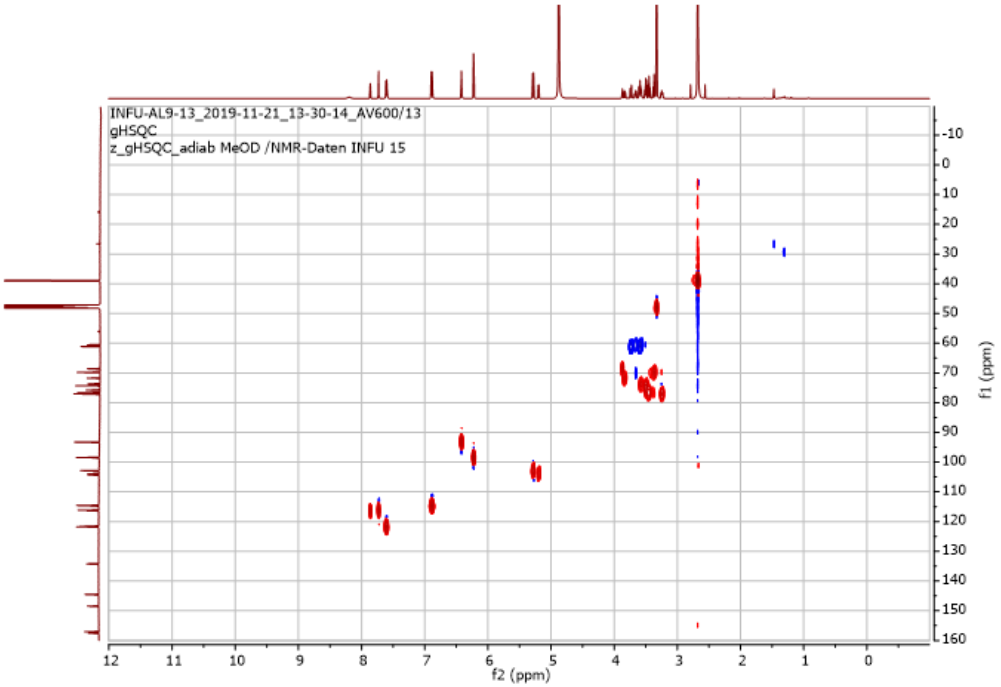

Appendix 160: HMBC (MeOD-d_4) spectrum of **40** (^{1}H: 600 MHz, ^{13}C: 175 MHz)

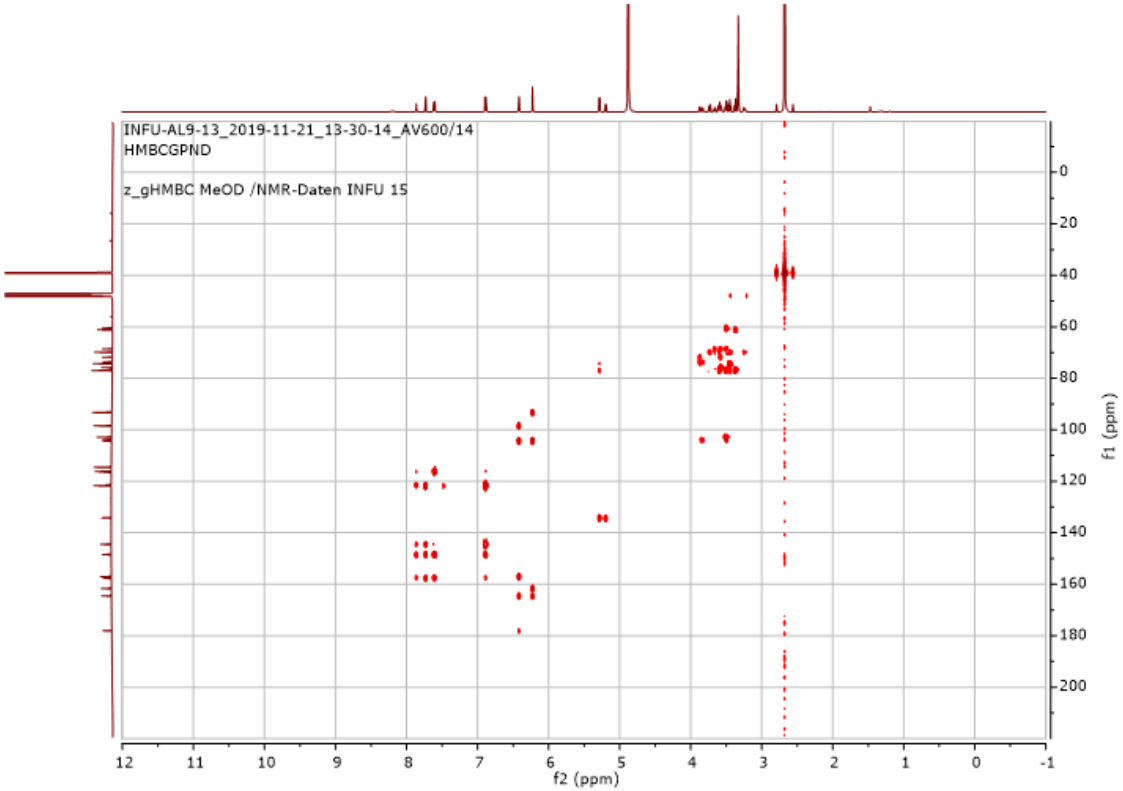

Appendix 161: Sequences and blast search hits of fungal endophyte

Strain code	ITS_consensus_sequence	Best blast hit	Species
BAPB_2	GGAtCATTACCGAGTTATACAACTCCC AAACCCACTGTGAACCTTACCTCAGTT GCCTCGGCGGGAACGCCCCGGCCGCC TGCCCCCGCGCCGGCGCCGGACCCAG GCGCCCGCCGCAGGGACCCCAAACTC TCTTGCATTACGCCCAGCGGGCGGAaT TTCTTCTCTGAGTTGCACAAGCAAAAA CAAATGAATCAAAACTTTCAACAACG GATCTCCTTGGTTCTGGCATCGATGAA GAACGCAGCGAAATGCGATAAGTAAT GTGAATTGCAGAATTCAGTGAATCAT CGAATCTTTGAACGCACATtGCGCCCG CCAGCATTCTGGCGGGCATGCCTGTTC GAGCGTCATTTCAACCCTCGAGCCCCC CCGGGGGCCTCGGTGTTGGGGGACGG CACACCAGCCGCCCCCGAAATGCAGT GGCGACCCCGCCGCAGCCTCCCCTGC GTAGTAGCACACACCTCGCACCGGAG CGCGGAGGCGGTCACGCCGT	NR165946.1 *Purpureocillium lilacinum* 100% coverage, 99.80% similarity	*Purpureocillium lilacinum*
BAPLC	TCATTACCGAGTTTACAACTCCCAAAC CCATGTGAACATACCTATTGTTGCTTC GGCGGGATTGCCCCGGGCGCCTCGTG TGCCCCGGATCAGGCGCCCGCCTAGG AAACTTAACTCTTGTTTTATTTTGGAA TCTTCTGAGTAGTTTTTACAAATAAAT AAAAACTTTCAACAACGGATCTCTTG GTTCTGGCATCGATGAAGAACGCAGC GAAATGCGATAAGTAATGTGAATTGC AGAATTCAGTGAATCATCGAATCTTTG AACGCACATTGCGCCCGCCAGTATTCT GGCGGGCATGCCTGTCTGAGCGTCATT TCAACCCTCATGCCCCTAGGGCGTGGT GTTGGGGATCGGCCAAAGCCCGCGAG GGACGGCCGGCCCCTAAATCTAGTGG CGGACCCGTCGTGGCCTCCTCTGCGAA GTAGTGATATTCCGCATCGGAgAgCGA CgAGCCCCTGCCGTTAAACCCCCAACT TTC	MH864650.1 *Clonostachys rosea* 100% coverage, 99.59%, similarity	*Clonostachys rosea*
BAPLC_1	TCATTACCGAAGTTACCCTTCTAAACC CATTGTGAACCTTACCTCTTGCCGCGC GTTGCCTCGGCGGGGAGGCGGGGGTG GGTCGGCGCGCCCCTCTGCGGGCCGC CGTCCCCGCCACCGTCCCCGCCGGCCG CGCCAAACTCTAAATTTGCAAAGCGG	NR145258.1 *Scopulariopsis fusca* 100% coverage 99.32% similarity	*Scopulariopsis fusca*

	ACTGCATGTTCTGATTTAAAACAAAA AACAAGTAAAAACTTTTAACAACGGA TCTCTTGGTTCTGGCATCGATGAAGAA CGCAGCGAAATGCGATAAGTAATGTG AATTGCAGAATTCAGTGAATCATCGA ATCTTTGAACGCACATTGCGCCCGGCA GCAATCTGCCGGGCATGCCTGTCCGA GCGTCATTTCTCCCCTCGAGCGCGGCT AGCCCTACGGGGCCTGCCGCCGCCCG GTGTTGGGGCTCTACGGGTGGGGCTC GTCCCCCCCGCAGTCCCCGAAATGTA GTGGCGGTCCAGCCGCGGCGCCCCCT GCGTAGTAGATCCTACATCTCGCATCG GGTCCCGGCGAAGGCCAGCCGTCGAA CCTTCTTACTCATGGTTTGACCTCGGA TCAGGTAGGGTTACCCGCTGAACTTA AGCATAT		
BAPB-B	ATCGTAACAAGGTTTCCGTAGGTGAA CCTGCGGAAGGATCATTACCGAGTGC GGGCCCTCGCGGCCCAACCTCCCACC CTTGTCTCTATACACCTGTTGCTTTGG CGGGCCCACCGGGGCCACCTGGTCGC CGGGGGACGCACGTCTCCGGGCCCGC GCCCGCCGAAGCGCTCTGTGAACCCT GATGAAGATGGGCTGTCTGAGTACTG TGAAAATTGTCAAAACTTTCAACAAT GGATCTCTTGGTTCCGGCATCGATGAA GAACGCAGCGAAATGCGATAAGTAAT GTGAATTGCAGAATTCCGTGAATCATC GAATCTTTGAACGCACATTGCGCCCCC TGGCATTCCGGGGGGCATGCCTGTCC GAGCGTCATTTCTGCCCTCAAGCACGG CTTGTGTGTTGGGTGTGGTCCCCCCGG GGACCTGCCCGAAAGGCAGCGGCGAC GTCCGTCTGGTCCTCGAGCGTATGGGG CTCTGTCACTCGCTCGGGAAGGACCTG CGGGGGTTGGTCACCACCATGTTTTAC CACGGTTGACCTCGGATCAGGTAGGA GTTACCCGCTGAACTTAAGCATATCAA A	MF683084.1 *Talaromyces pinophilus* 99% coverage 100.00% similarity	*Talaromyces pinophilus*
BAPB-D	>Consensus ACGTAACAAGGTCTCCGTTGGTGAAC CAGCGGAGGGATCATTACCGAGTGTT AAAAAACTCCCAAAACCCTATGTGAA CATACCGCAGTTGCCTCGGCGTGAGC CGCACTGCCCTGTGGCCGCCCCCCTT	MG686611.1 ***Hypoxylon lividipigmentum*** 99% coverage, 93.70% similarity	***Hypoxylon lividipigmentum***

	CGGGAGGGGGCGGACGCCTGGCAGCG CACTTCAAGGCCCGCCGAAGGACCGC CAAAAACTCTTGTTTTAAATATAACGT TTCTCTGAATGCTTCAAACTAAAATAA GTTAAAACTTTCAACAACGGATCTCTT GGTTCTGGCATCGATGAAGAACGCAG CGAAATGCGATAAGTAATGTGAATTG CAGAATTCAGTGAATCATCGAATCTTT GAACGCACATTGCGCCCATTAGTATTC TAGTGGGCATGCCTATTCGAGCGTCAT TTCAACCCCTTAAGCCCCTGTTGCTTA GCGTTGGGAGTCTACCAGGCCTTCGG CCGCGTAGTTCCTTAAAATCAGTGGCG GAGCGCAGCGTGCCGCGAGCGTAGTA AAACATACACCTCGCTTTTGCAGTGCA CTGTGTTGCCGGCCGTAAAACACCCCC CTAAATTATAGTGGTTGACCTCGGATT AGGTAGGAATACCCGCTGAACTTAAG CATATCAAA		
BAAL_A2	ATGGCTTTCTCCTATACAAATTTCTTTT GAGTACCTTCGTTTCCTCGGCGGTCCG CCCGCCGATTGGACAACATTCAAACC CTTTGCAGTTGCAATCAGCGTCTGAAA AAACATAATAGTTACAACTTTCAACA ACGGATCTCTTGGTTCTGGCATCGATG AAGAACGCAGCGAAATGCGATAAGTA GTGTGAATTGCAGAATTCAGTGAATC ATCGAACTTTGAACGCACATTGCGCCC CTTGGTATTCCATGGGGCATGCCTGTT CGAGCGTCATTGTACCTTCAAGCTCTG CTTGGTGTTGGGTGTTTGTCTCGCCTC TGCGTGTAGACTCGCCTTAAAACAATT GGCAGCCGGCGTATTGATTTCGGAGC GCAGTACATCTCGCGCTTTGCACTCAT AACGACGACGTCCAAAAGTACATTTT TACACTCTTGACCTCGGATCAGGTAGG GATACCCGCTGAACTTAAGCATATCA ATAAGCG GAGGAAAA	KX778640.1 *Epicoccum nigrum* 100% coverage, 99.40% similarity	***Epicoccum nigrum***

Appendix 163: HRESIMS of **41**

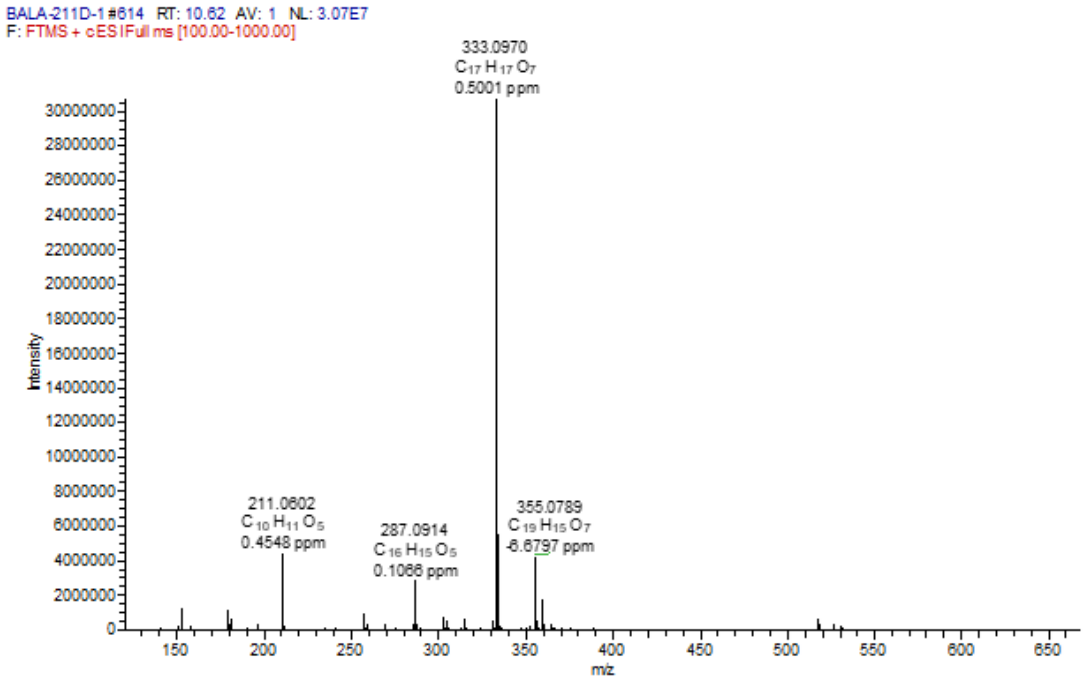

Appendix 164: Infrared spectrum of **41**

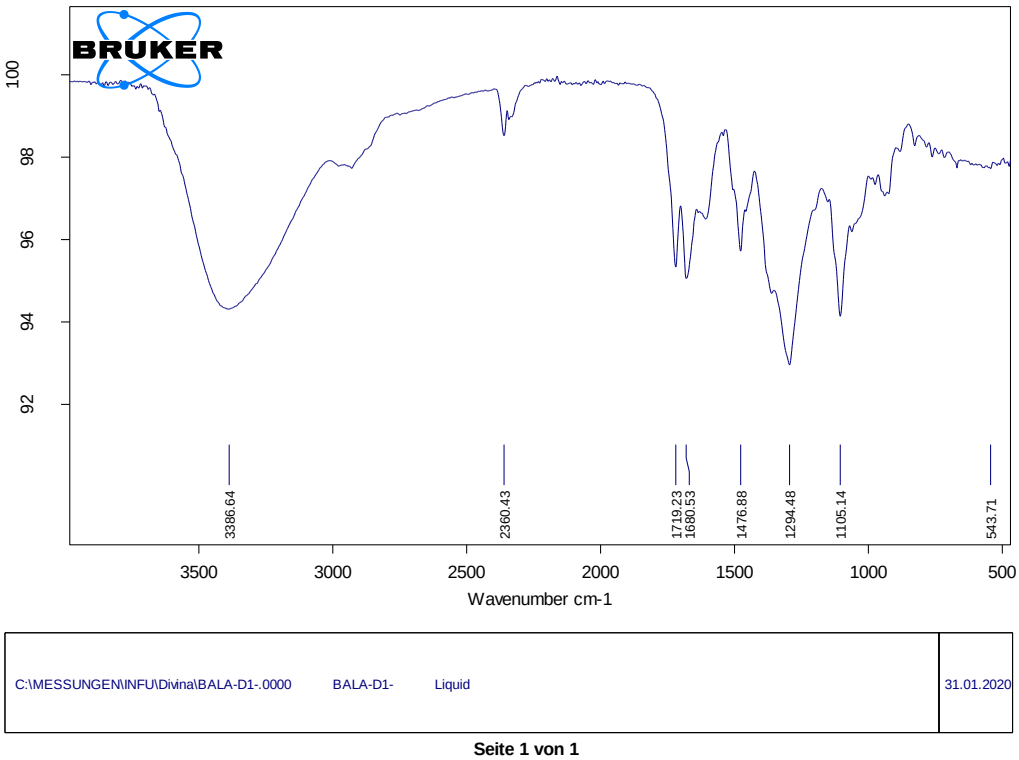

C:\MESSUNGEN\INFU\Divina\BALA-D1-.0000 BALA-D1- Liquid 31.01.2020

Seite 1 von 1

Appendix 165: ^{1}H NMR (600 MHz, MeOD-d_4) spectrum of **41**

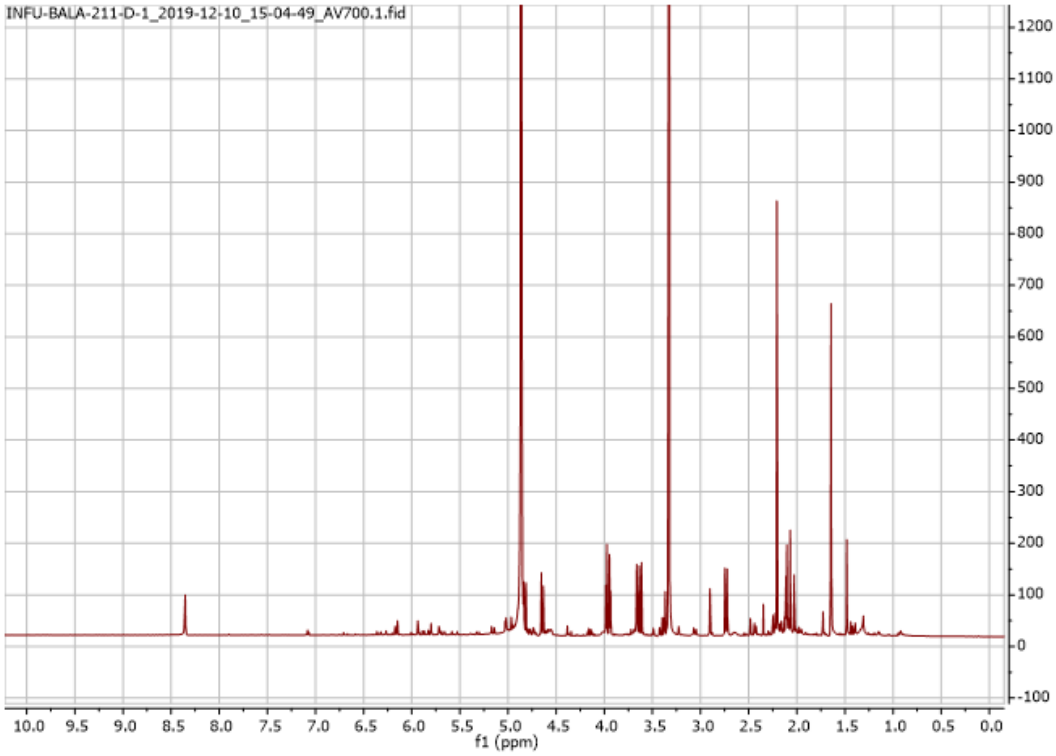

Appendix 166: ^{13}C NMR (175 MHz, MeOD-d_4) spectrum of **41**

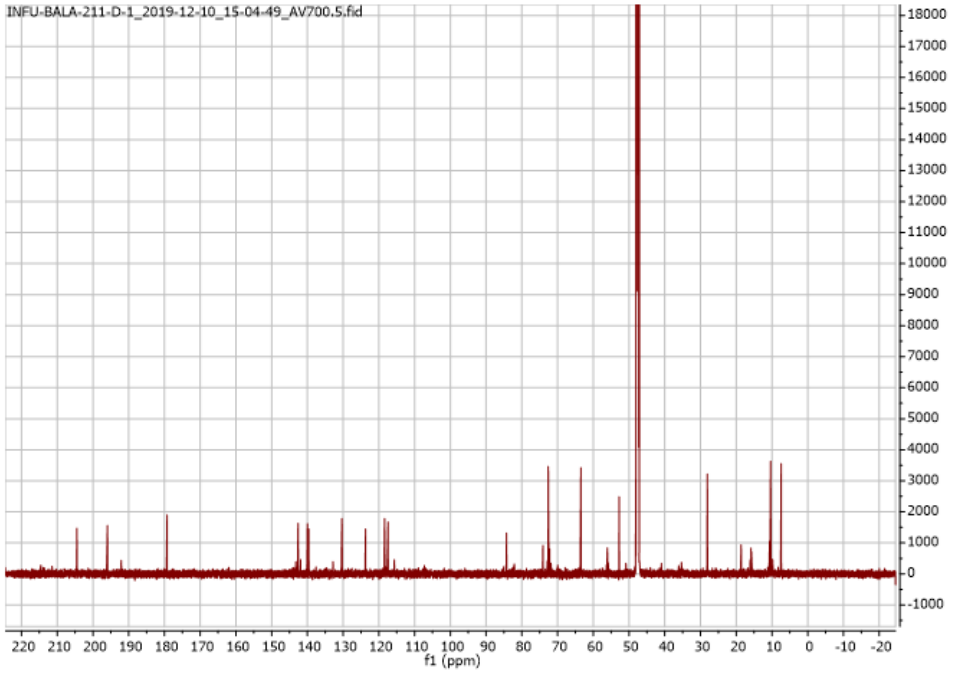

Appendix 167: COSY (600 MHz, MeOD-d_4) spectrum of **41**

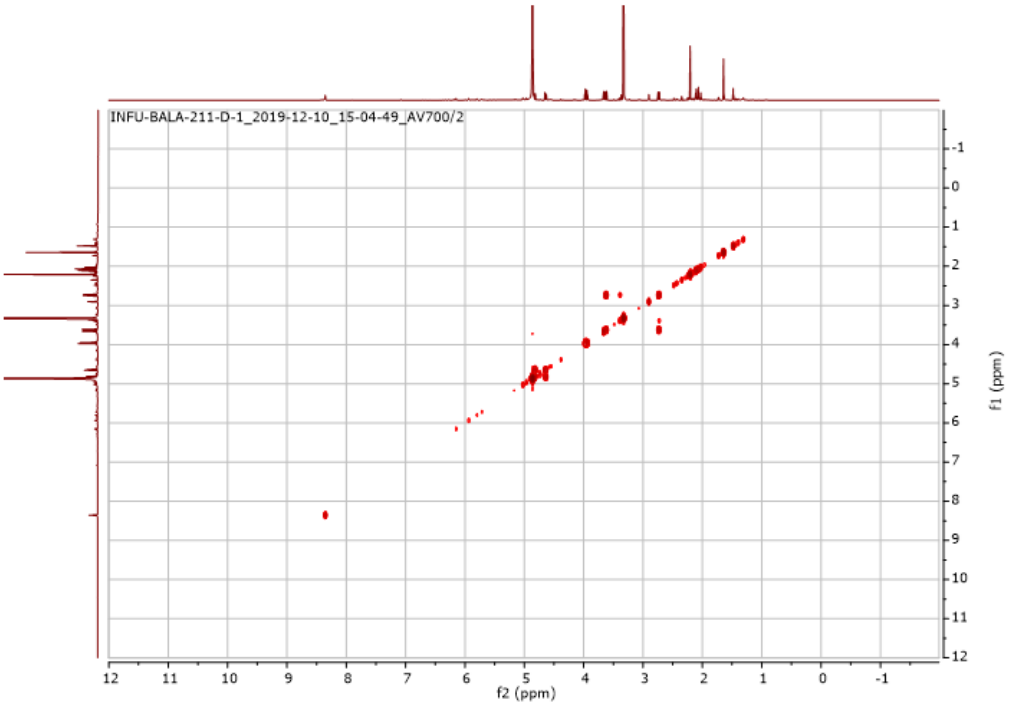

Appendix 168: HSQC (MeOD-d_4) spectrum of **41** (^{1}H: 600 MHz, ^{13}C: 175 MHz)

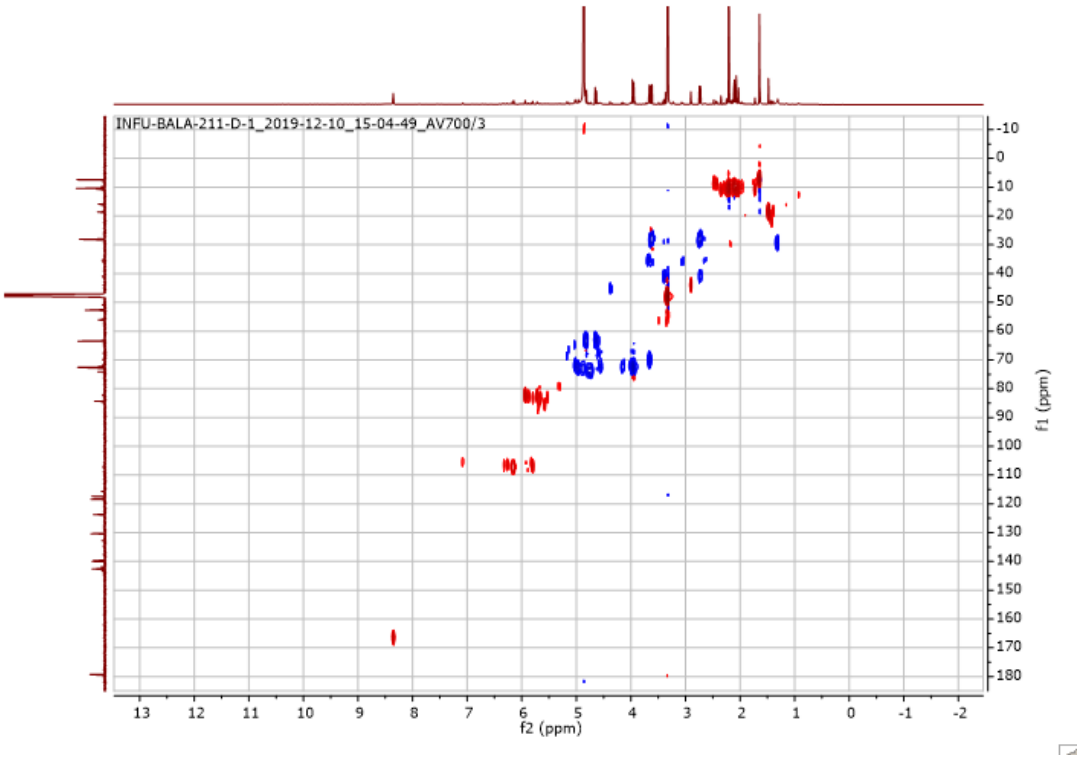

Appendix 169: HMBC (MeOD-d_4) spectrum of **41** (^{1}H: 600 MHz, ^{13}C: 175 MHz)

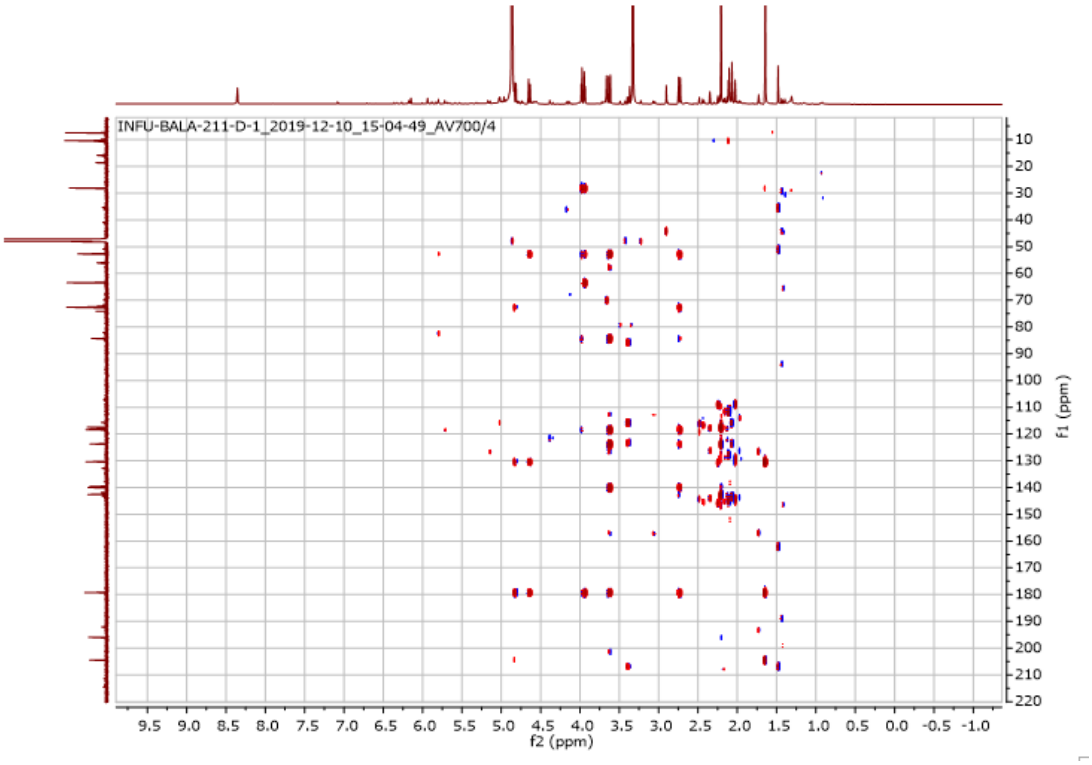

Appendix 170: HRESIMS of **42**

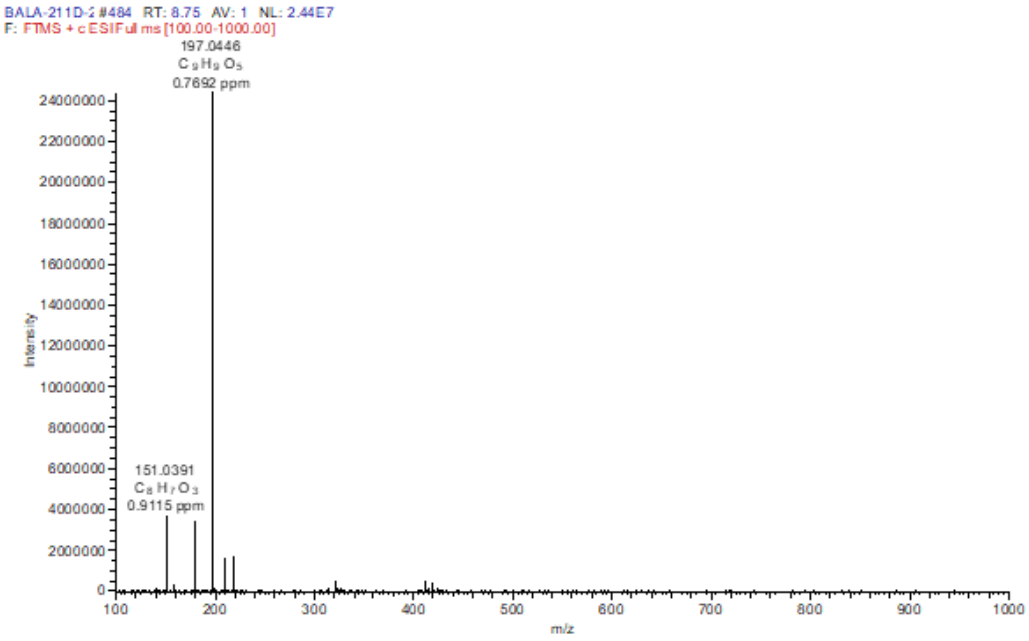

Appendix 171: ^{1}H NMR (600 MHz, MeOD-d_4) spectrum of **42**

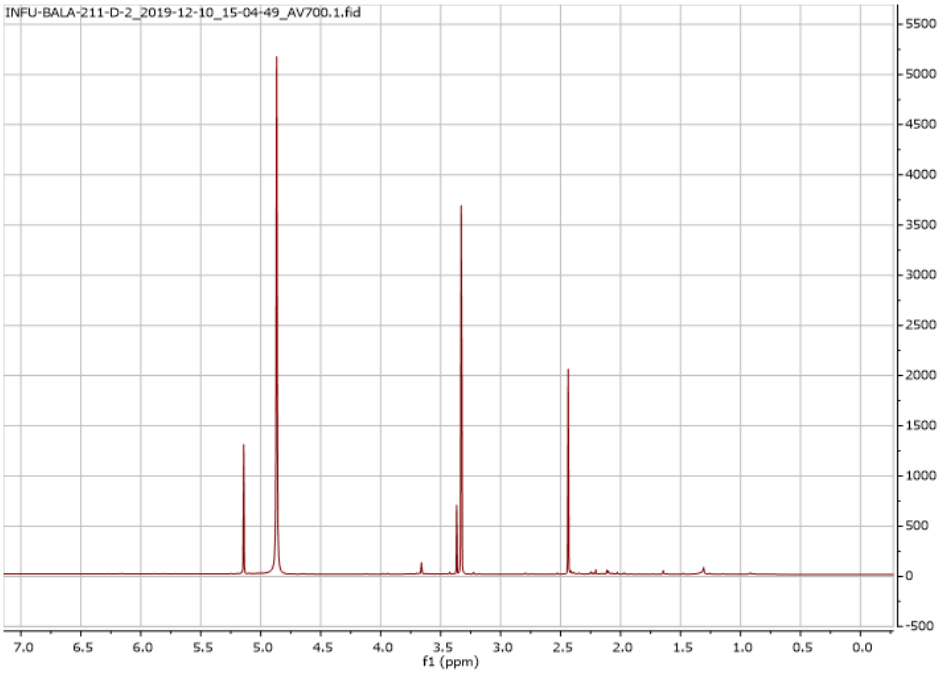

Appendix 172: ^{13}C NMR (175 MHz, MeOD-d_4) spectrum of **42**

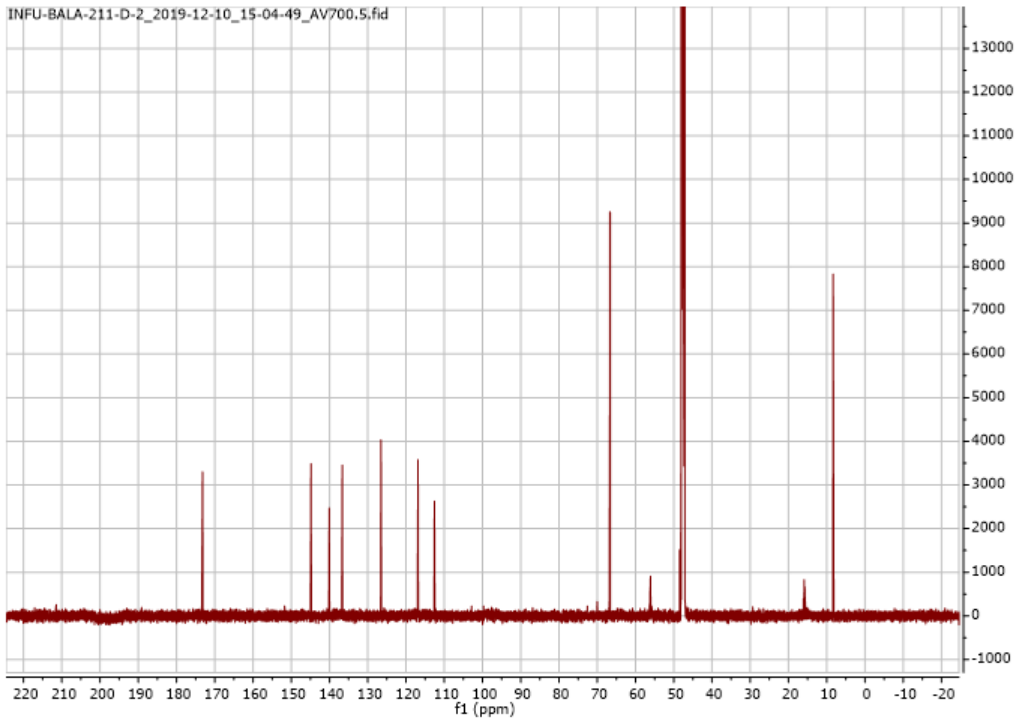

Appendix 173: COSY (600 MHz, MeOD-d_4) spectrum of **42**

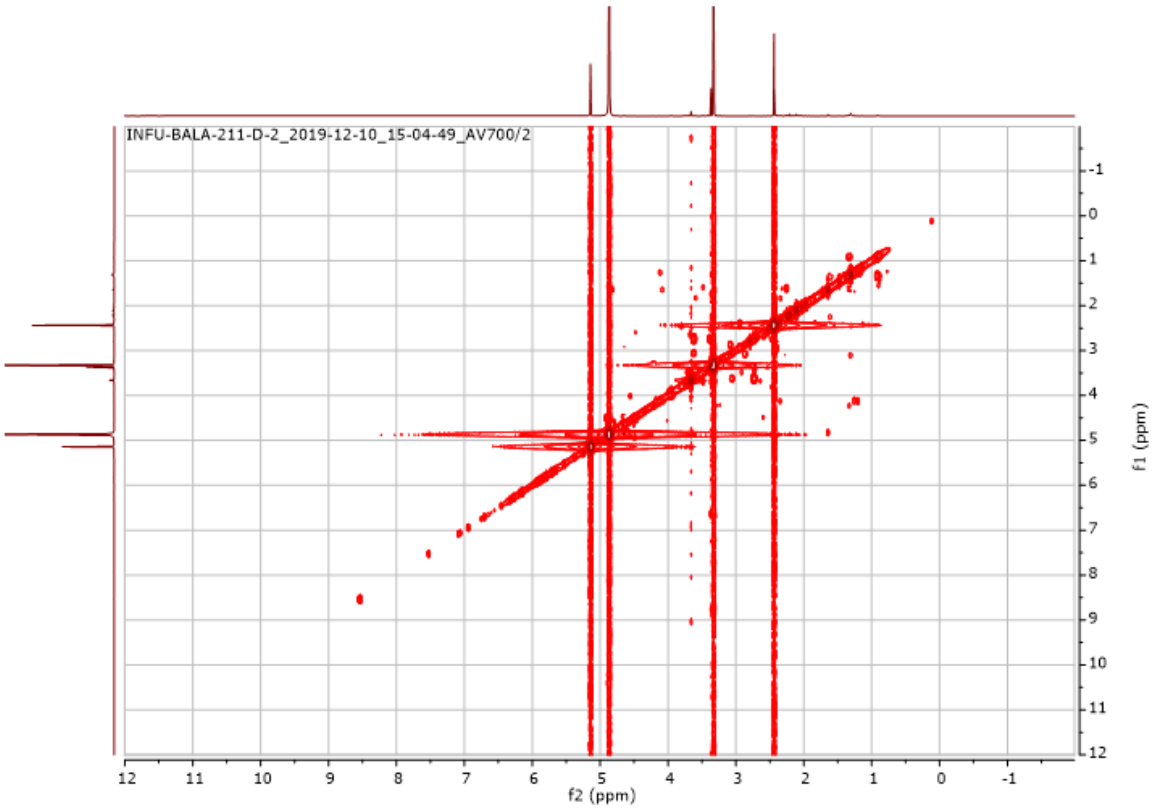

Appendix 174: HSQC (MeOD-d_4) spectrum of **42** (^{1}H: 600 MHz, ^{13}C: 175 MHz)

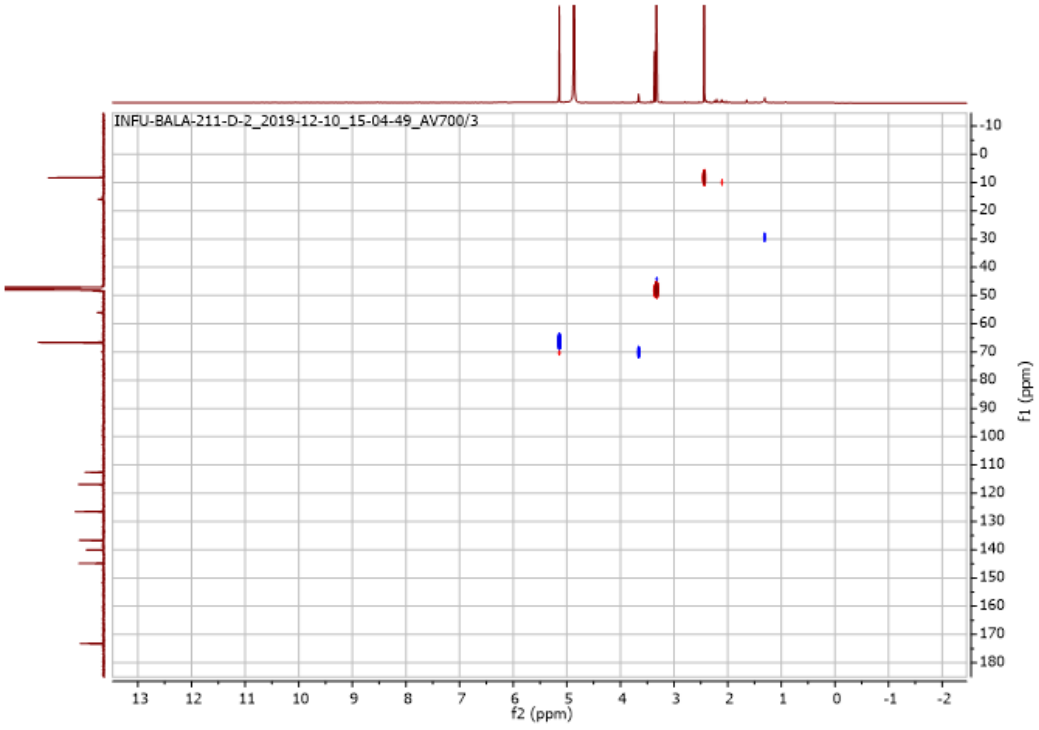

Appendix 175: HMBC (MeOD-d_4) spectrum of **42** (^{1}H: 600 MHz, ^{13}C: 175 MHz)

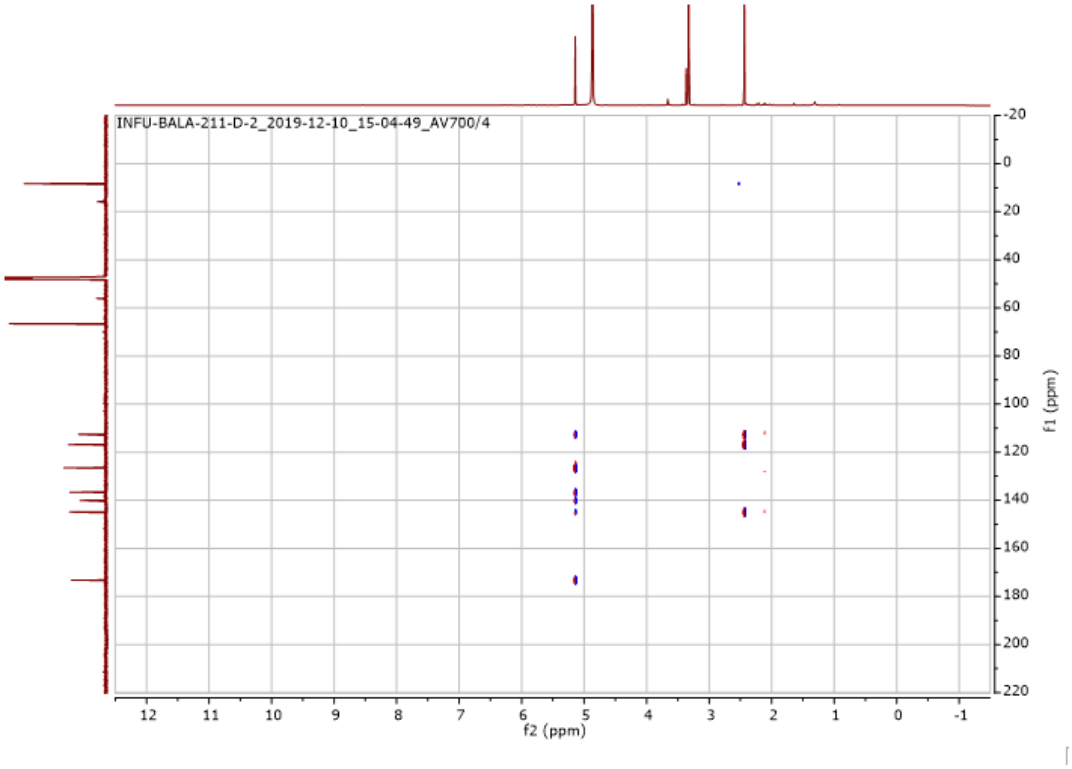

Appendix 176: HRESIMS of **43**

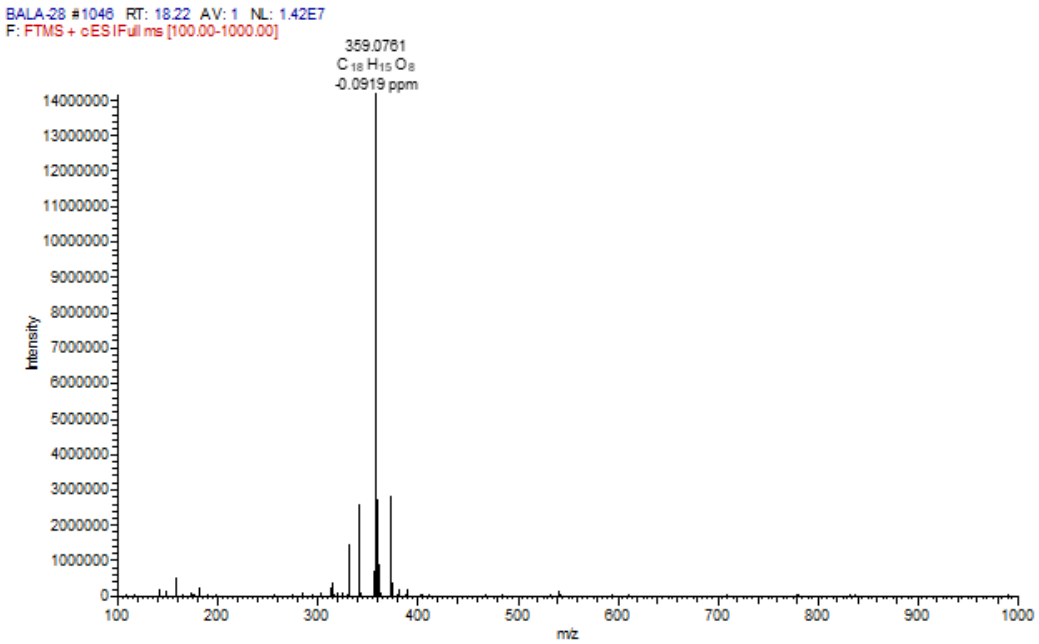

Appendix 177: ^{1}H NMR (700 MHz, MeOD-d_4) spectrum of **43**

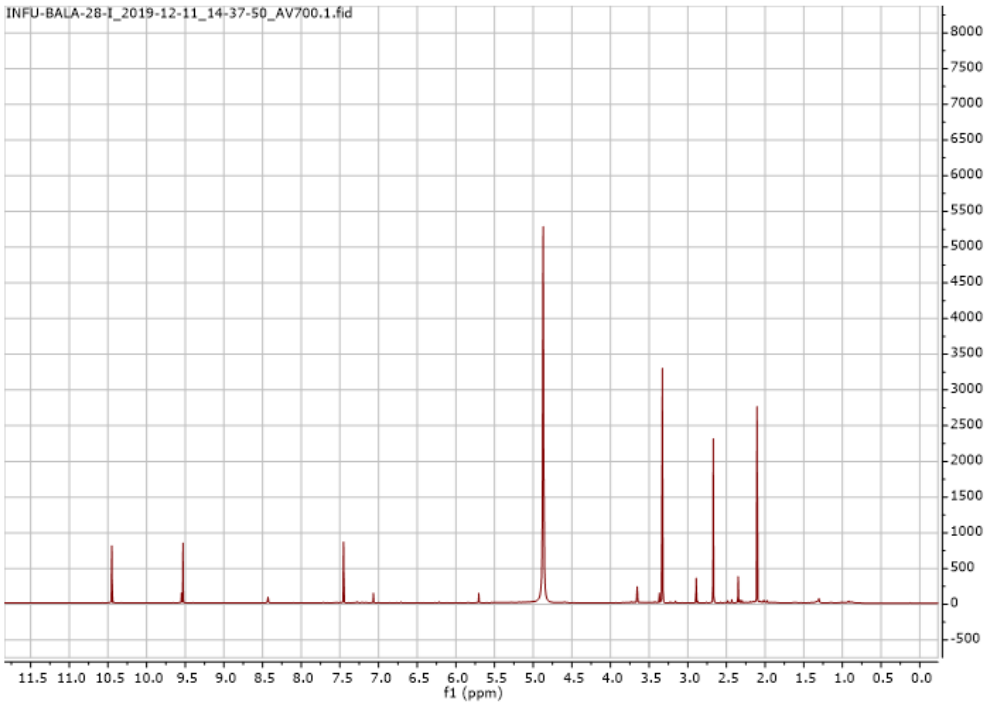

Appendix 178: ^{13}C NMR (175 MHz, MeOD-d_4) spectrum of **43**

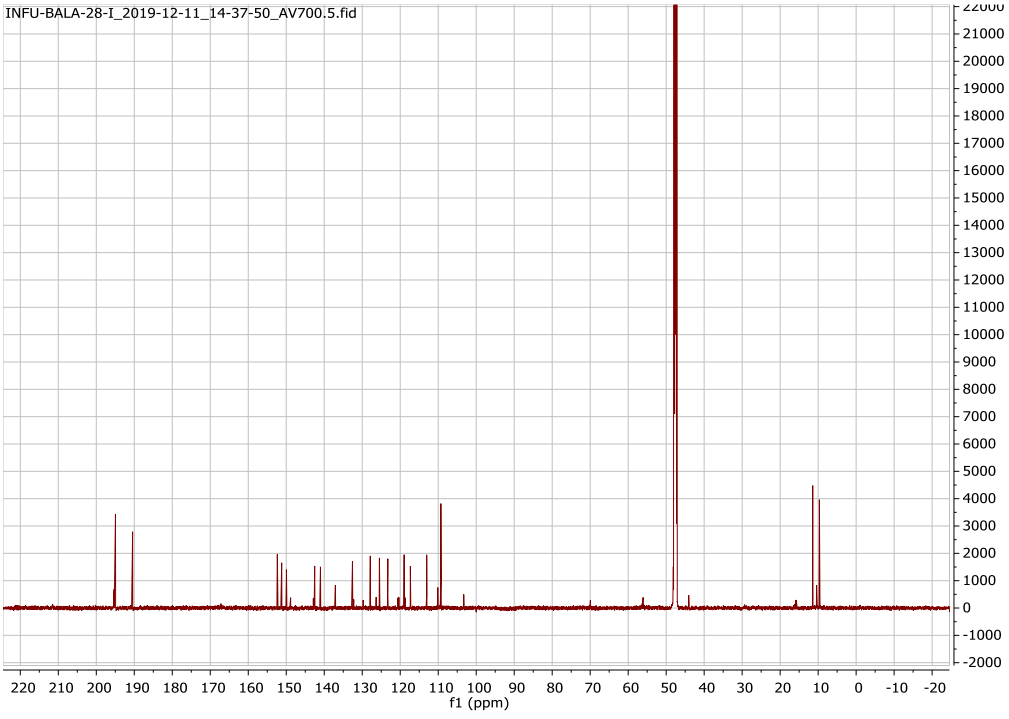

Appendix 179: COSY (700 MHz, MeOD-d_4) spectrum of **43**

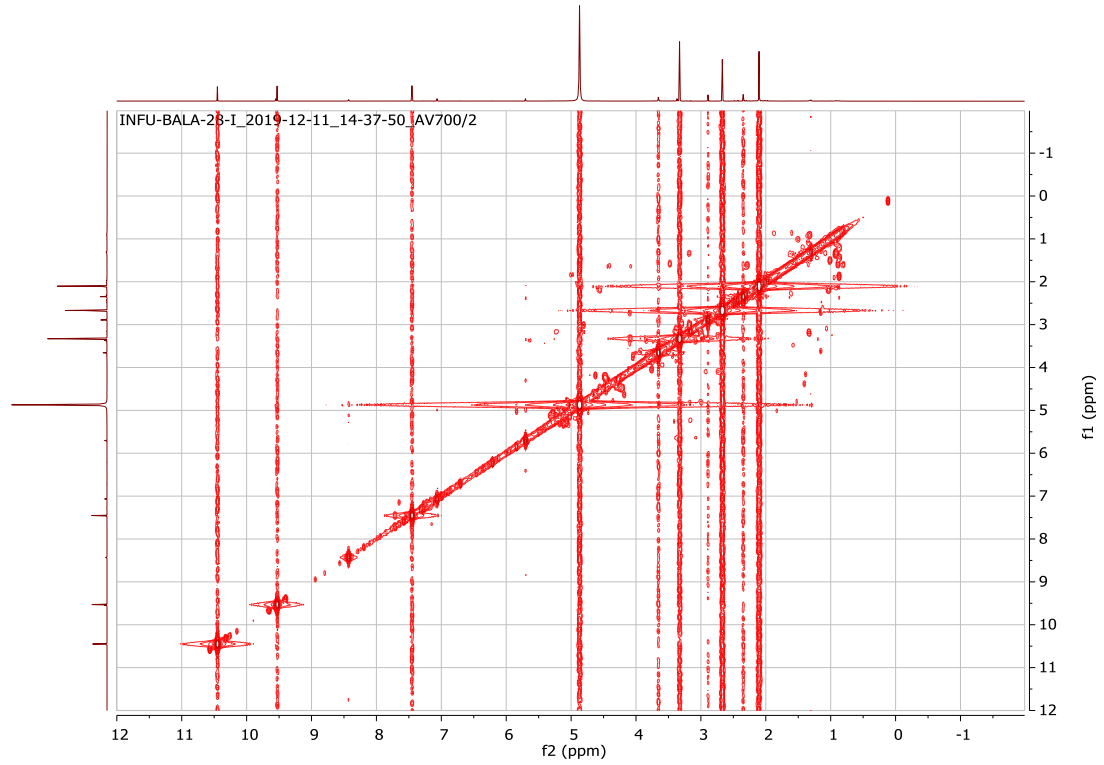

Appendix 180: HSQC (MeOD-d_4) spectrum of **43** (^{1}H: 700 MHz, ^{13}C: 175 MHz)

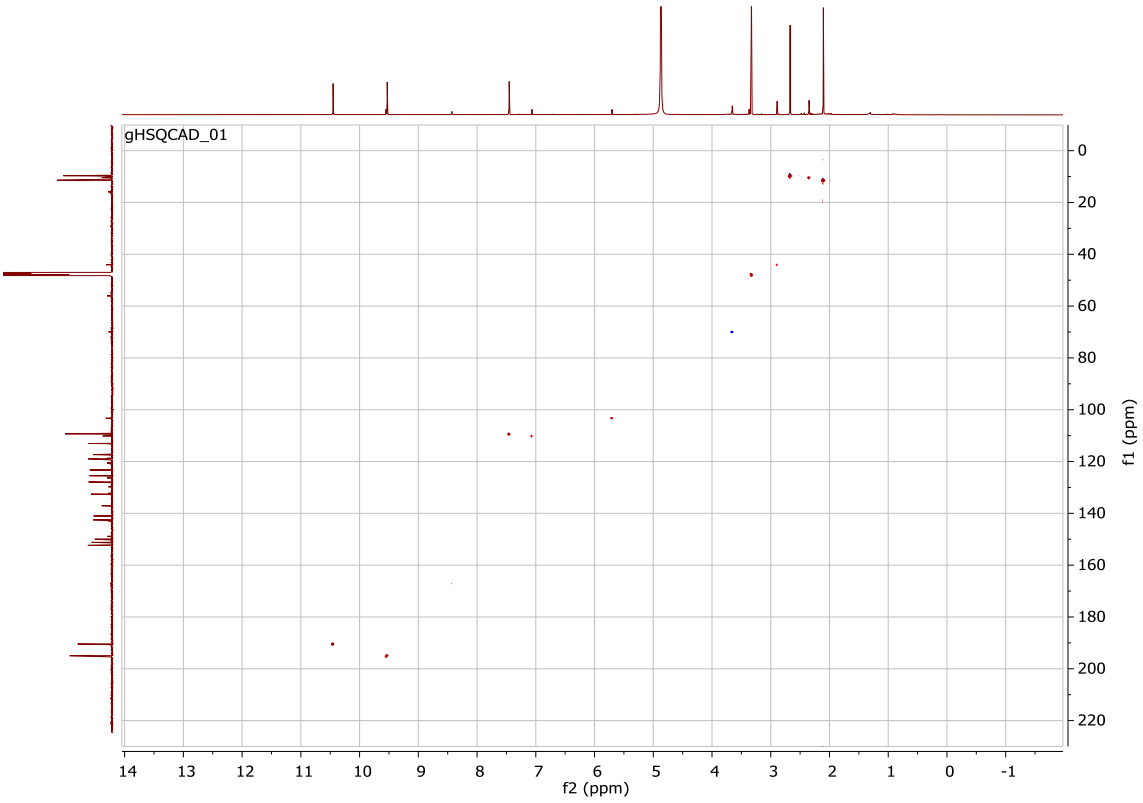

Appendix 181: HMBC (MeOD-d_4) spectrum of **43** (^{1}H: 700 MHz, ^{13}C: 175 MHz)

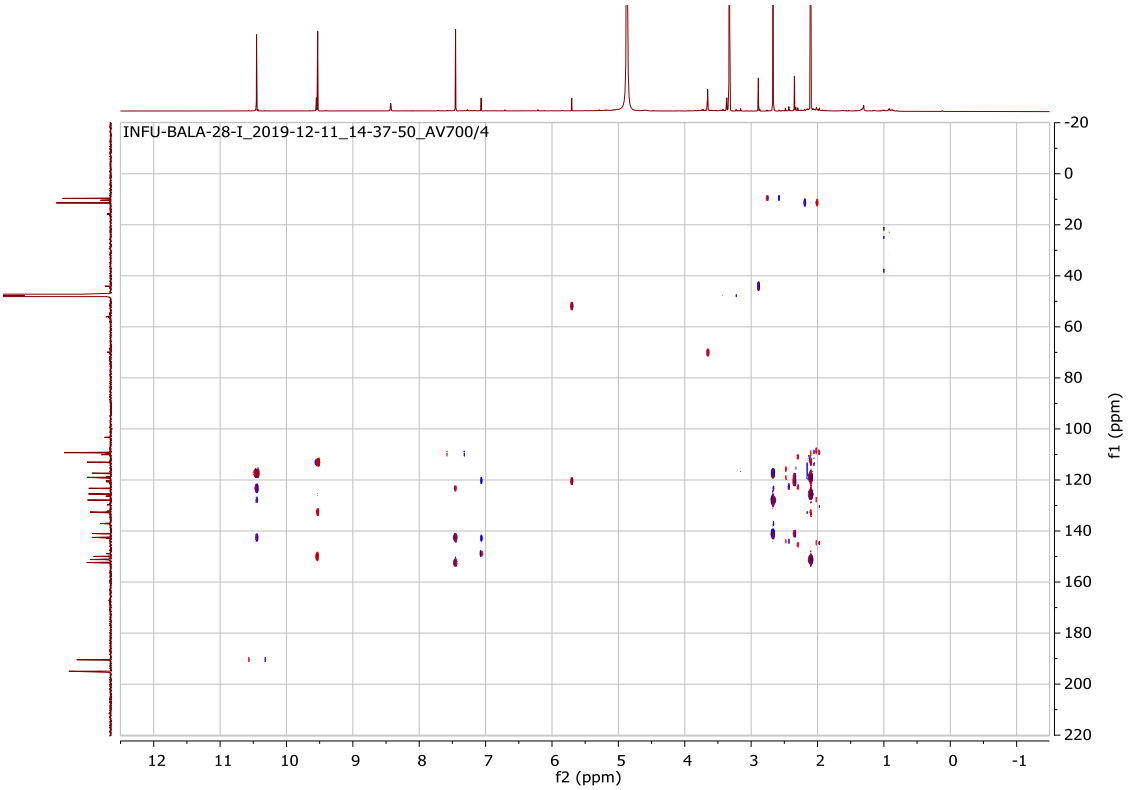

Appendix 182: HRESIMS of **44**

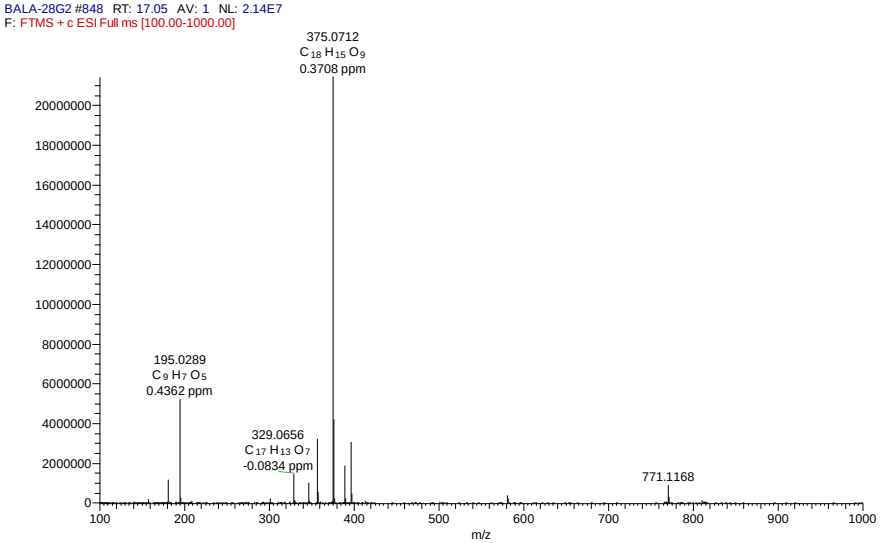

Appendix 183: ^{1}H NMR (600 MHz, MeOD-d_4) spectrum of **44**

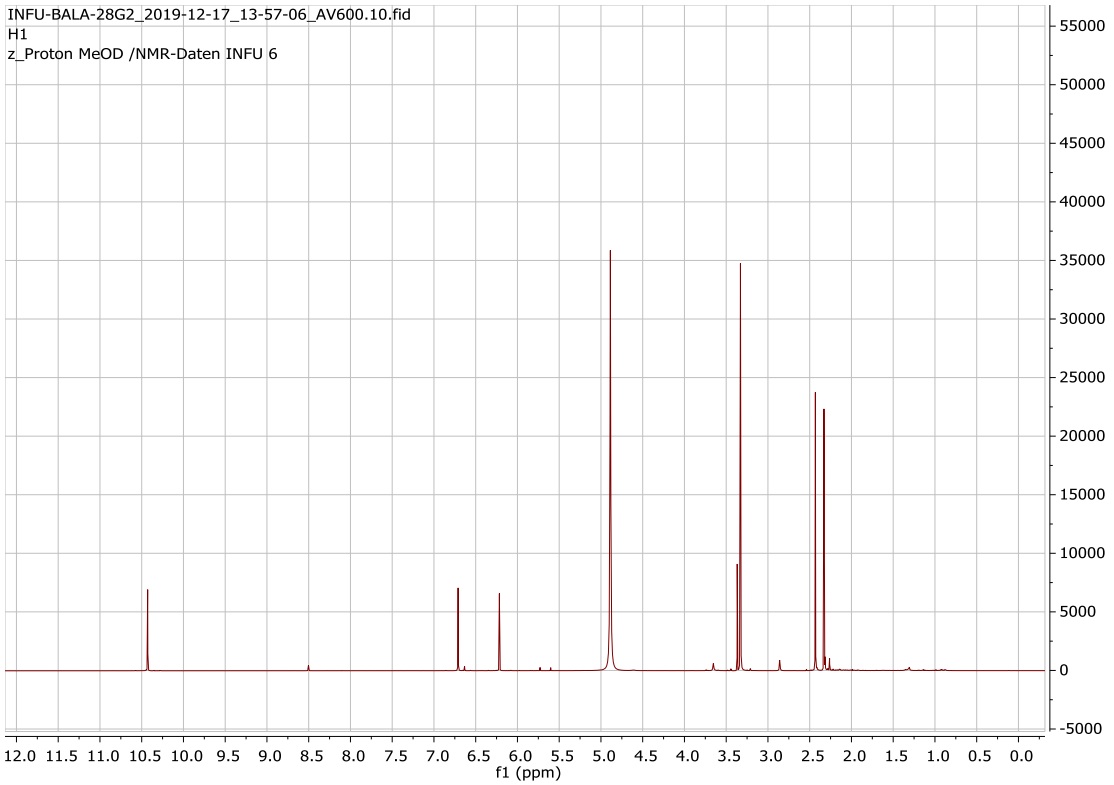

Appendix 184: ^{13}C NMR (175 MHz, MeOD-d_4) spectrum of **44**

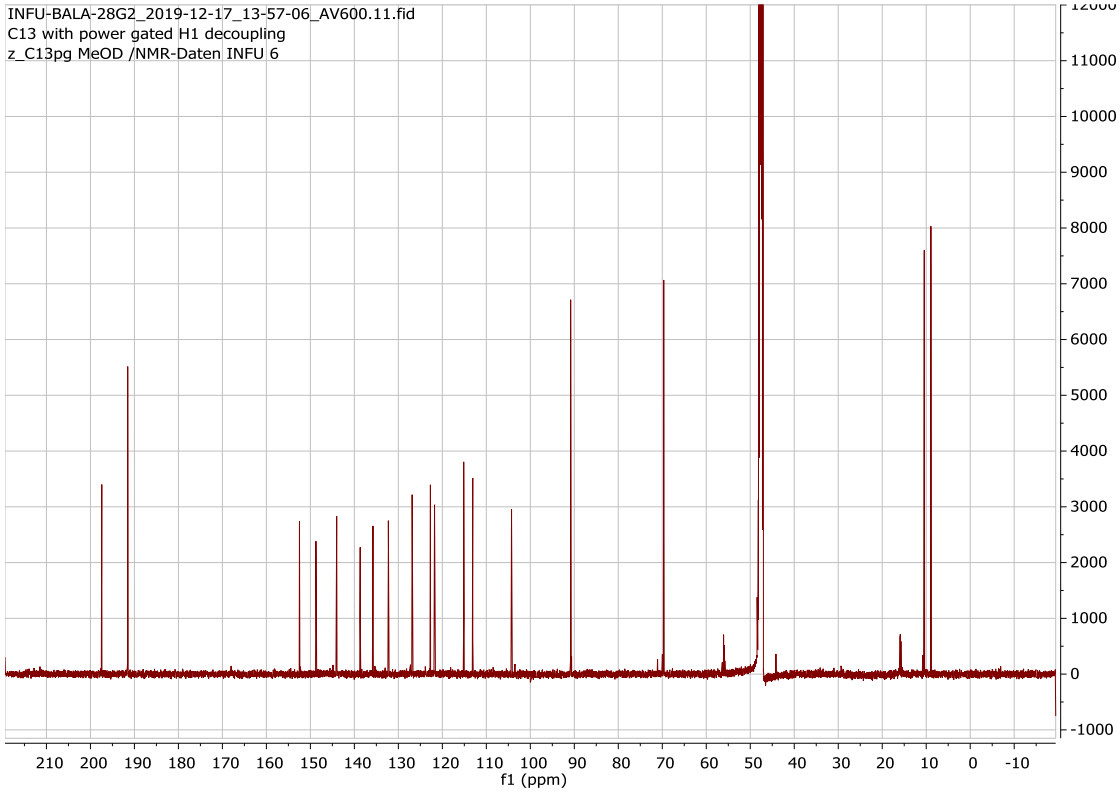

Appendix 185: COSY (600 MHz, MeOD-d4) spectrum of **44**

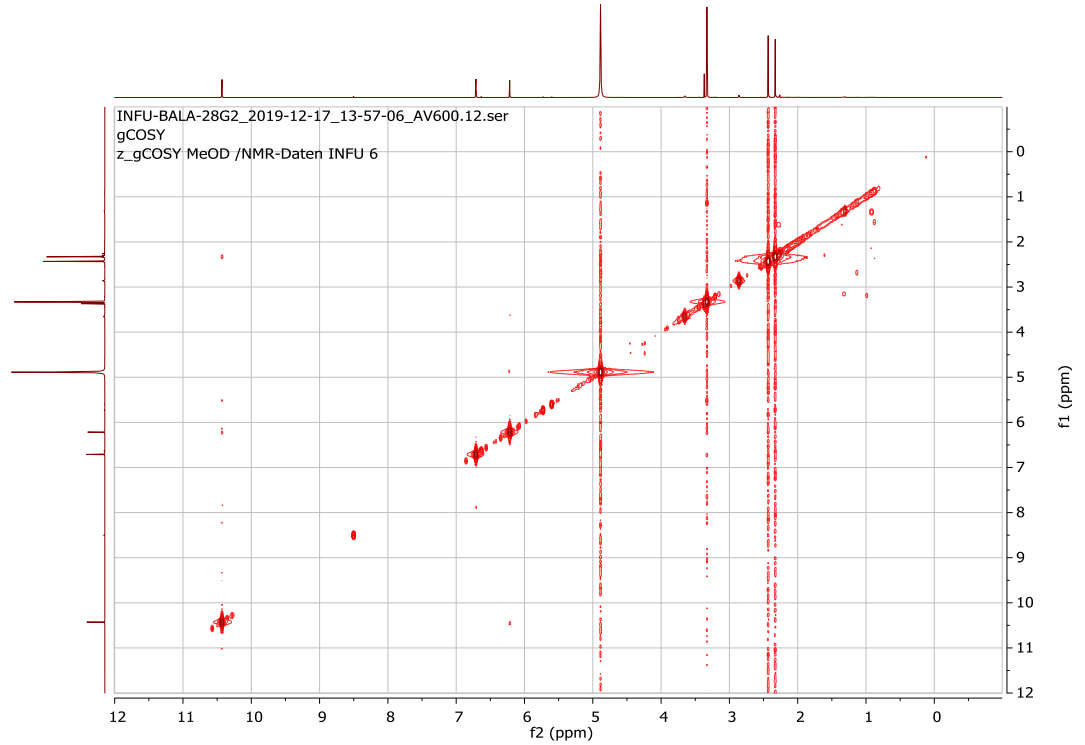

Appendix 186: HSQC (MeOD-d_4) spectrum of **44** (^{1}H: 600 MHz, ^{13}C: 175 MHz)

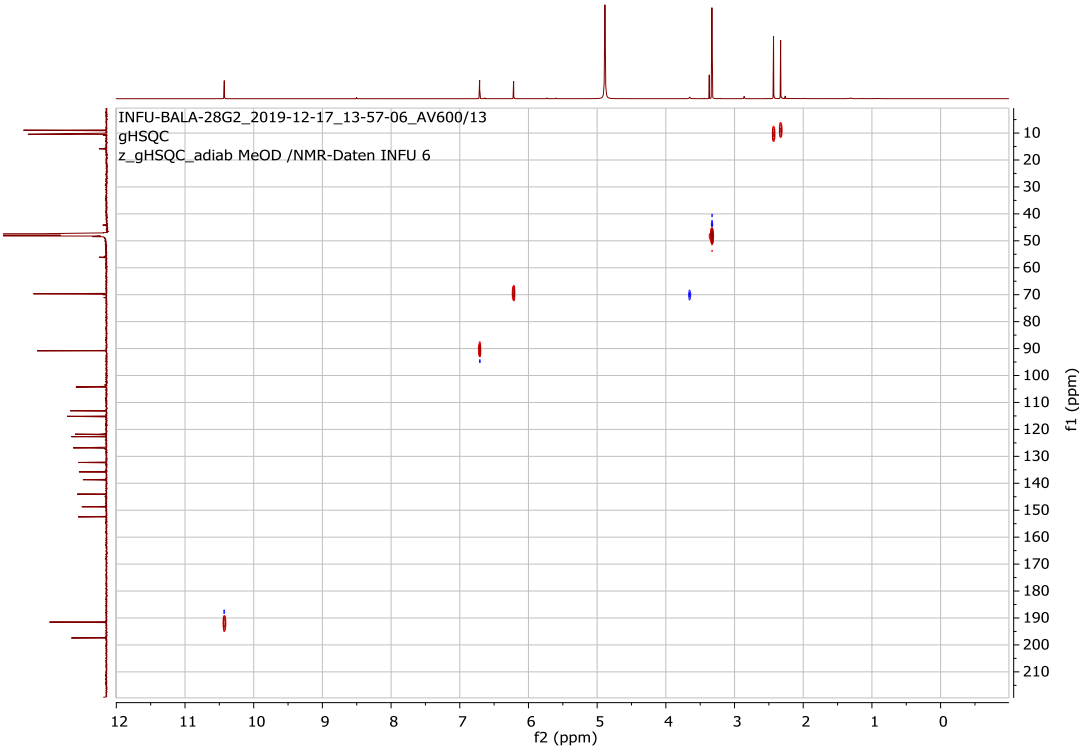

Appendix 187: HMBC (MeOD-d_4) spectrum of **44** (^{1}H: 600 MHz, ^{13}C: 175 MHz)

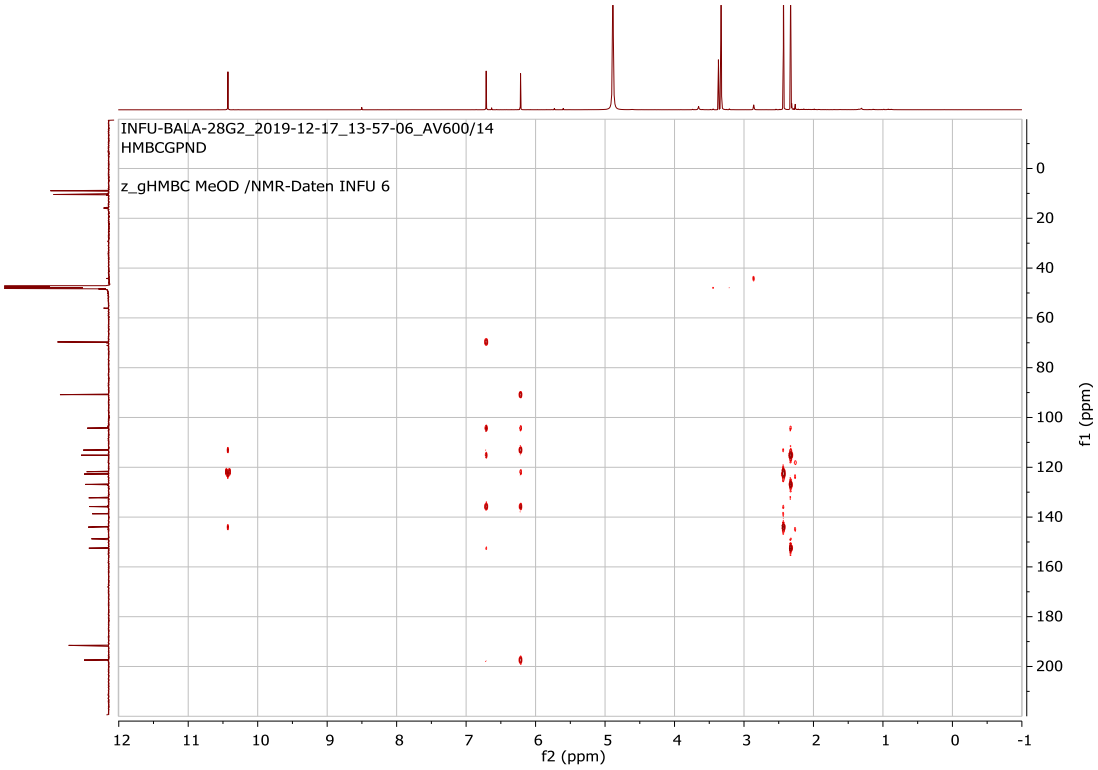

Appendix 188: HRESIMS of **45**

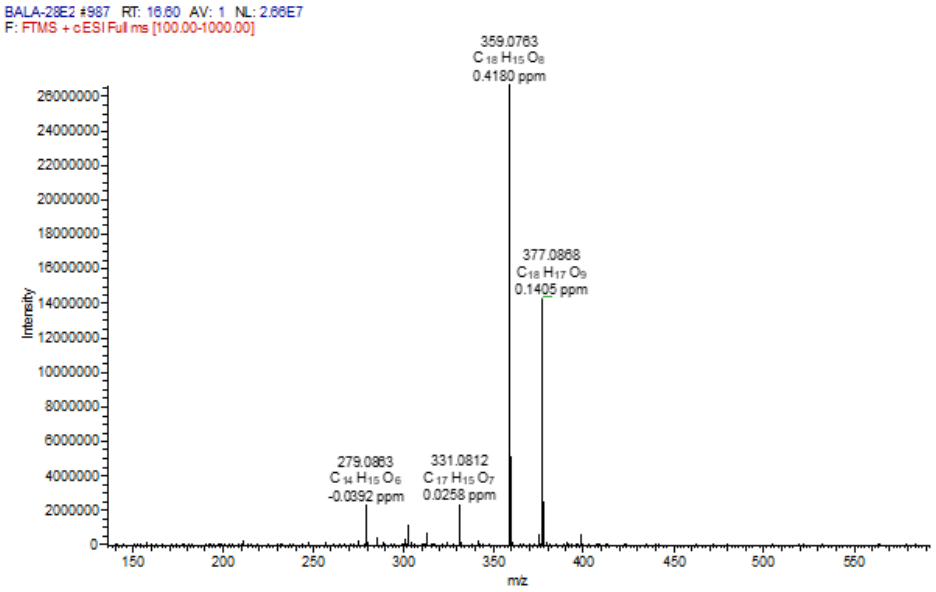

Appendix 189: ^{1}H NMR (600 MHz, MeOD-d_4) spectrum of **45**

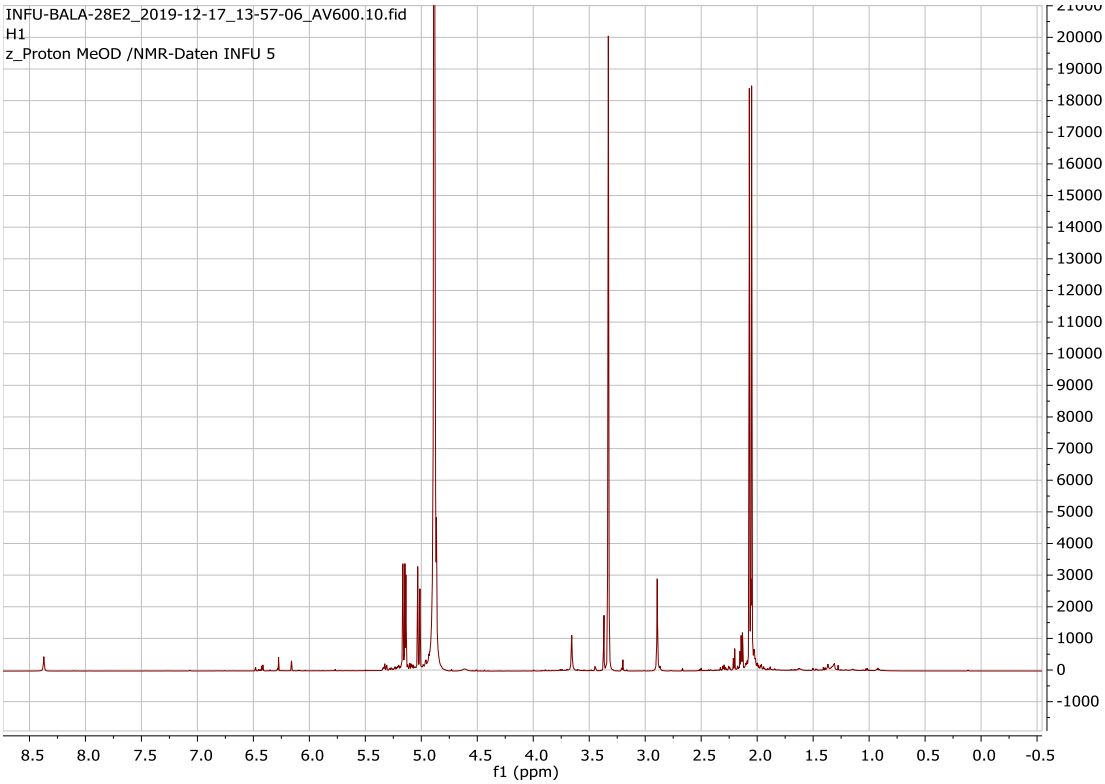

Appendix 190: ^{13}C NMR (175 MHz, MeOD-d_4) spectrum of **45**

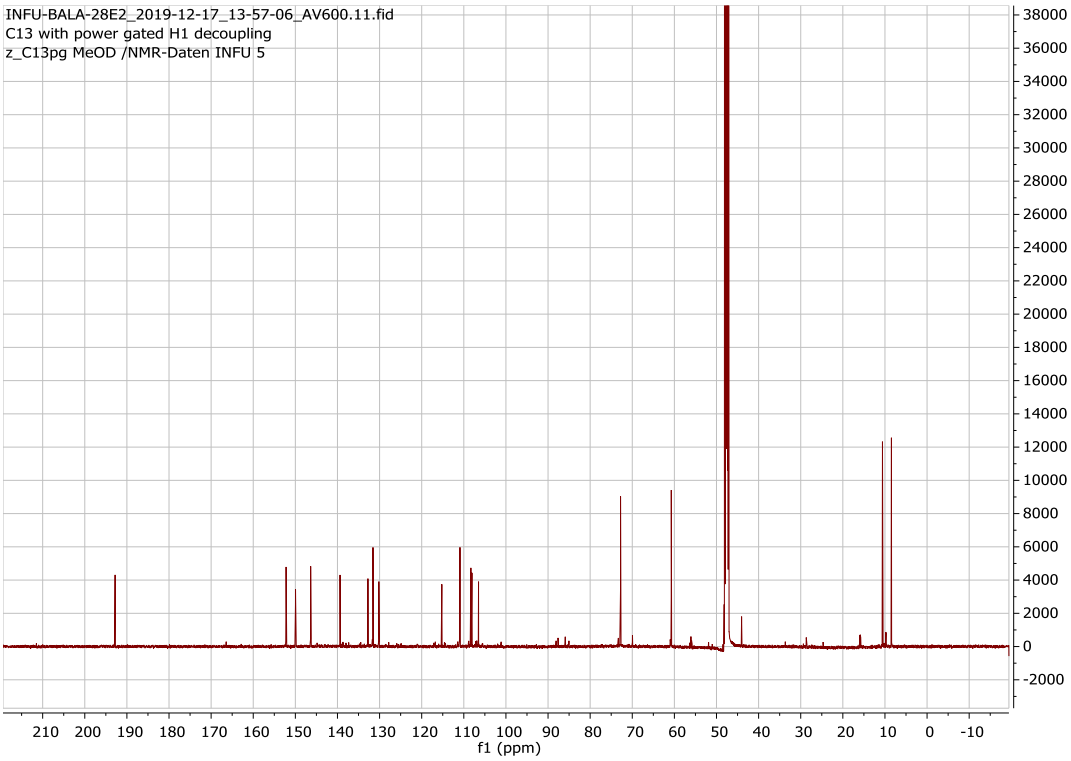

Appendix 191: COSY (600 MHz, MeOD-d_4) spectrum of **45**

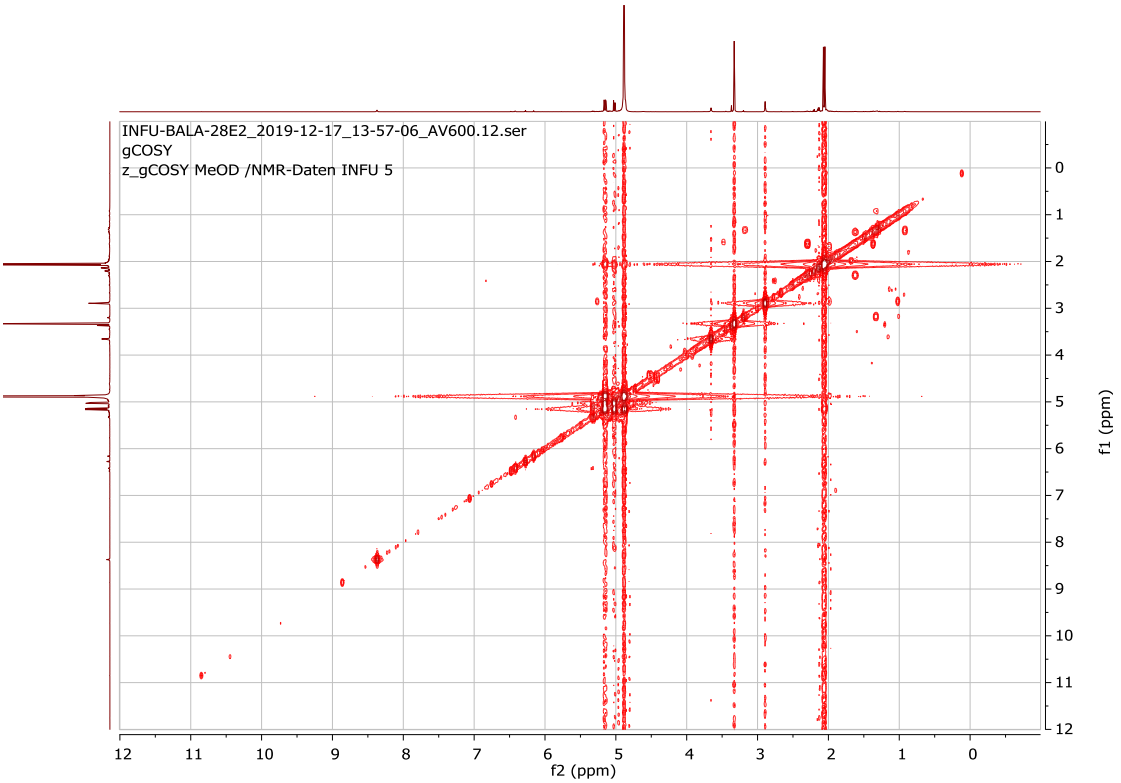

Appendix 192: HSQC (MeOD-d_4) spectrum of **45** (^{1}H: 600 MHz, ^{13}C: 175 MHz)

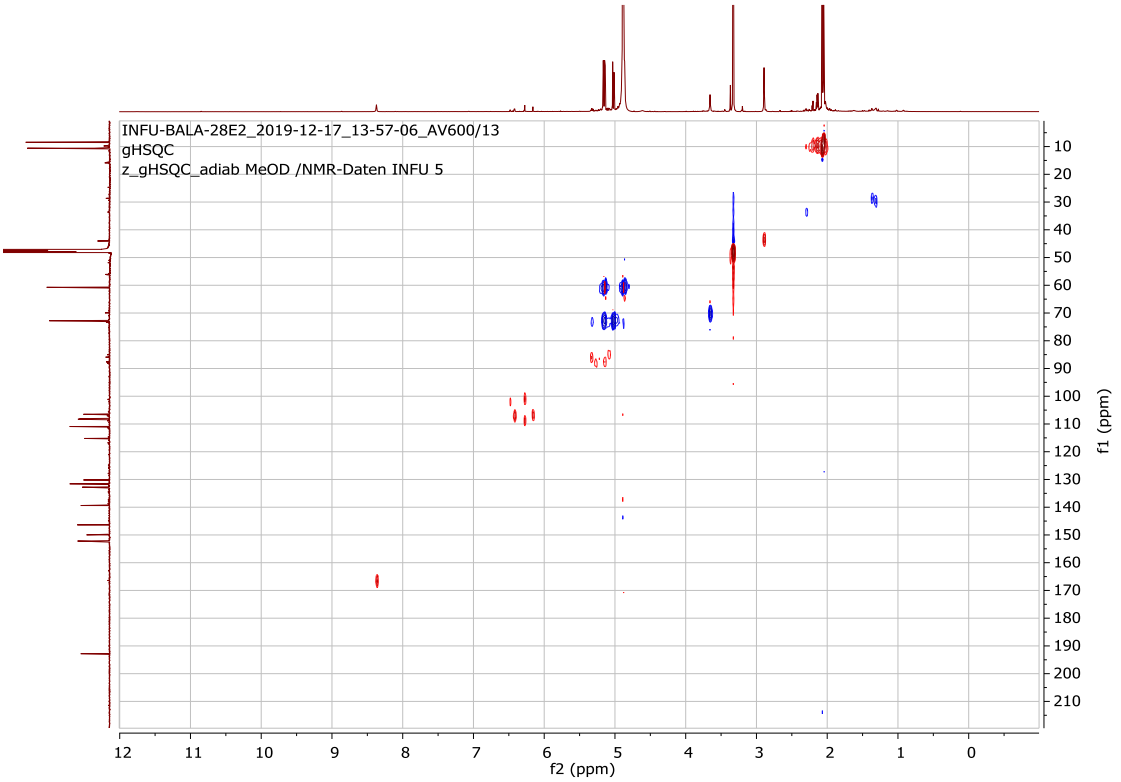

Appendix 193: HMBC (MeOD-d_4) spectrum of **45** (^{1}H: 600 MHz, ^{13}C: 175 MHz)

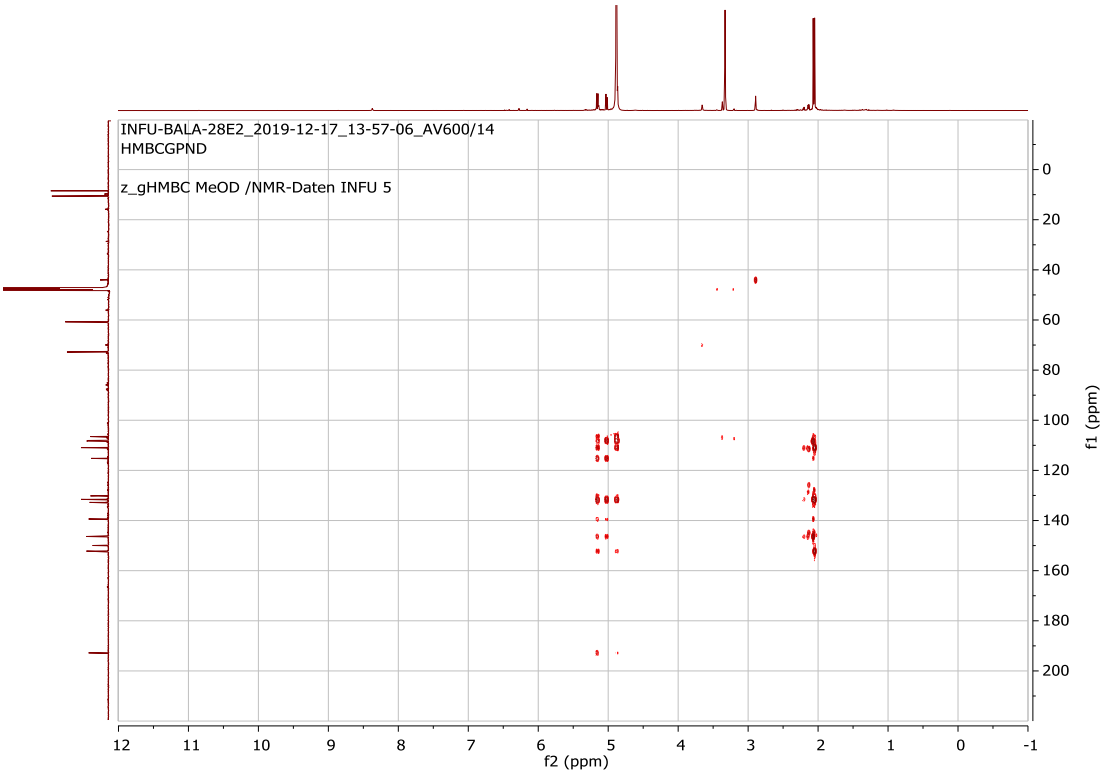

Appendix 194: HRESIMS of **46**

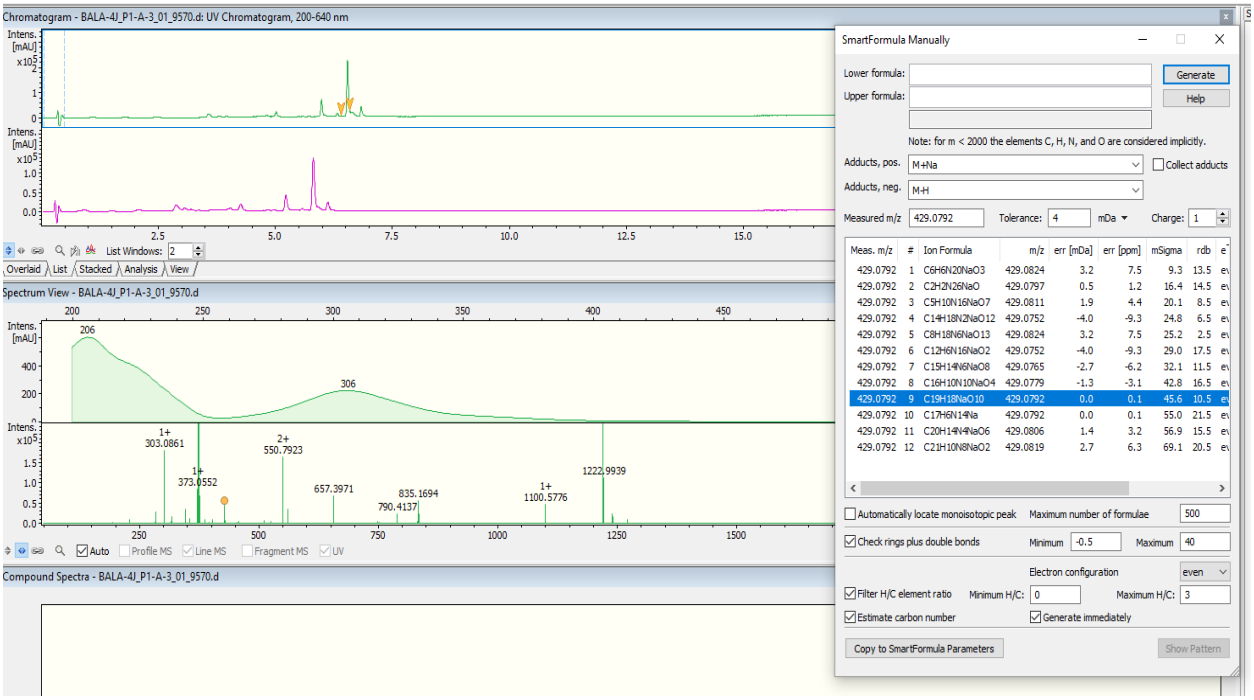

Appendix 195: ^{1}H NMR (600 MHz, MeOD-d_4) spectrum of **46**

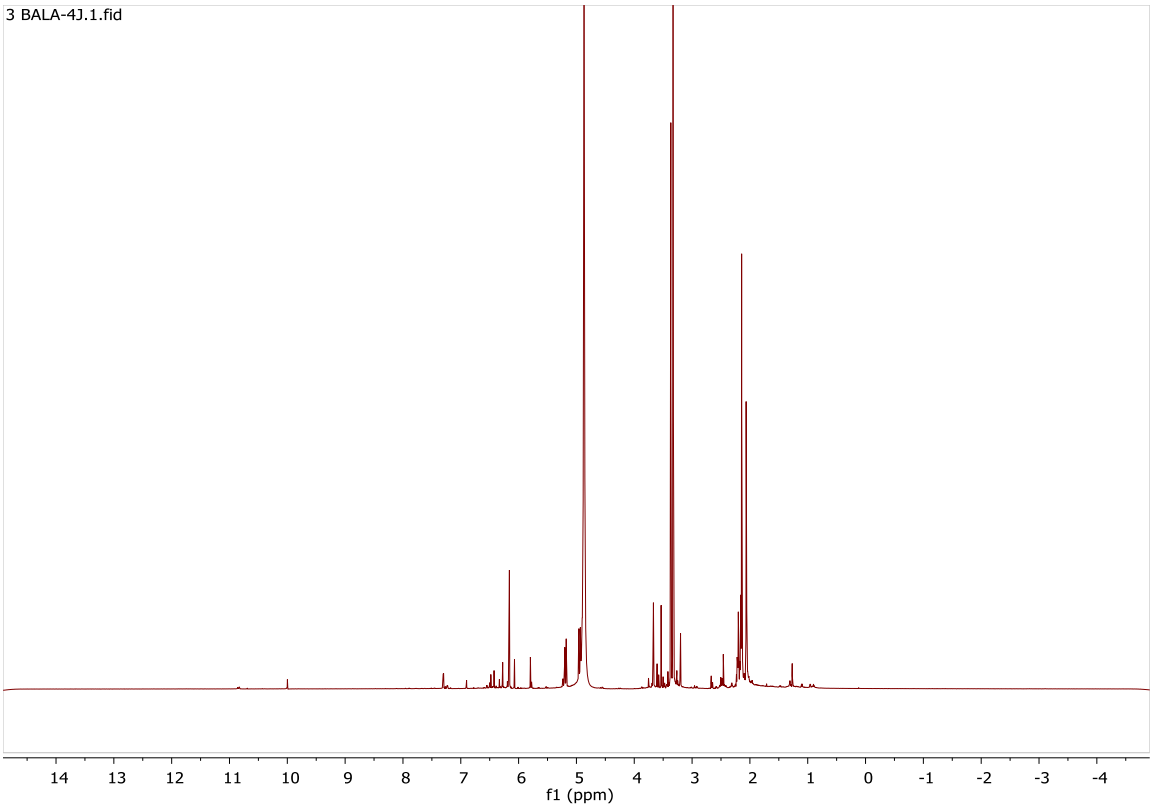

Appendix 196: ^{13}C NMR (175 MHz, MeOD-d_4) spectrum of **46**

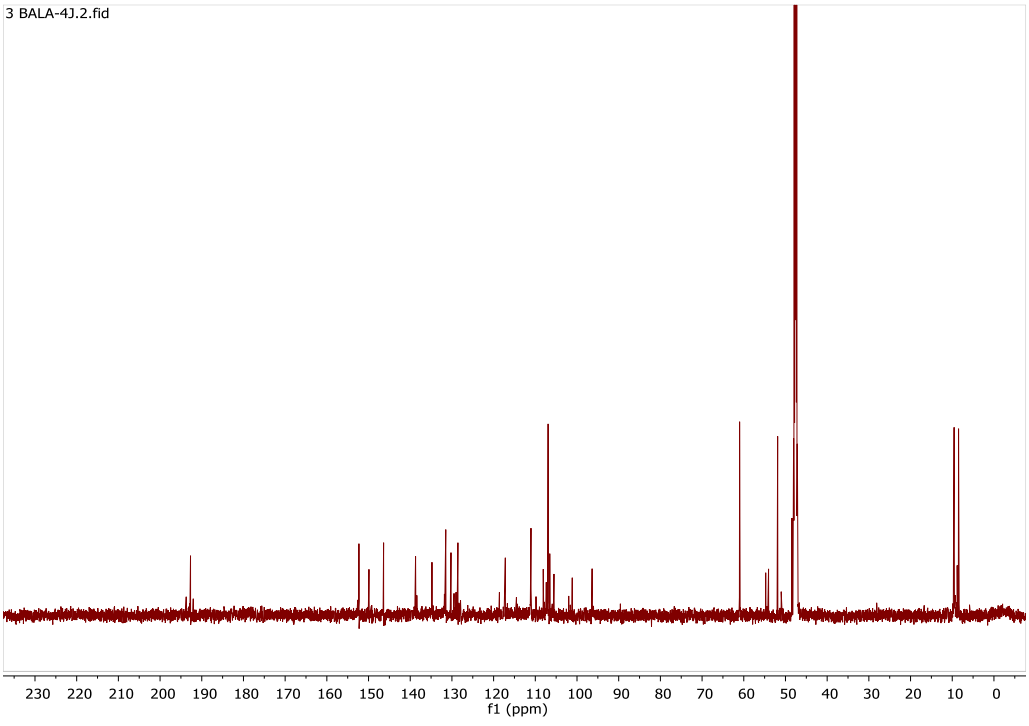

Appendix 197: COSY (600 MHz, MeOD-d_4) spectrum of **46**

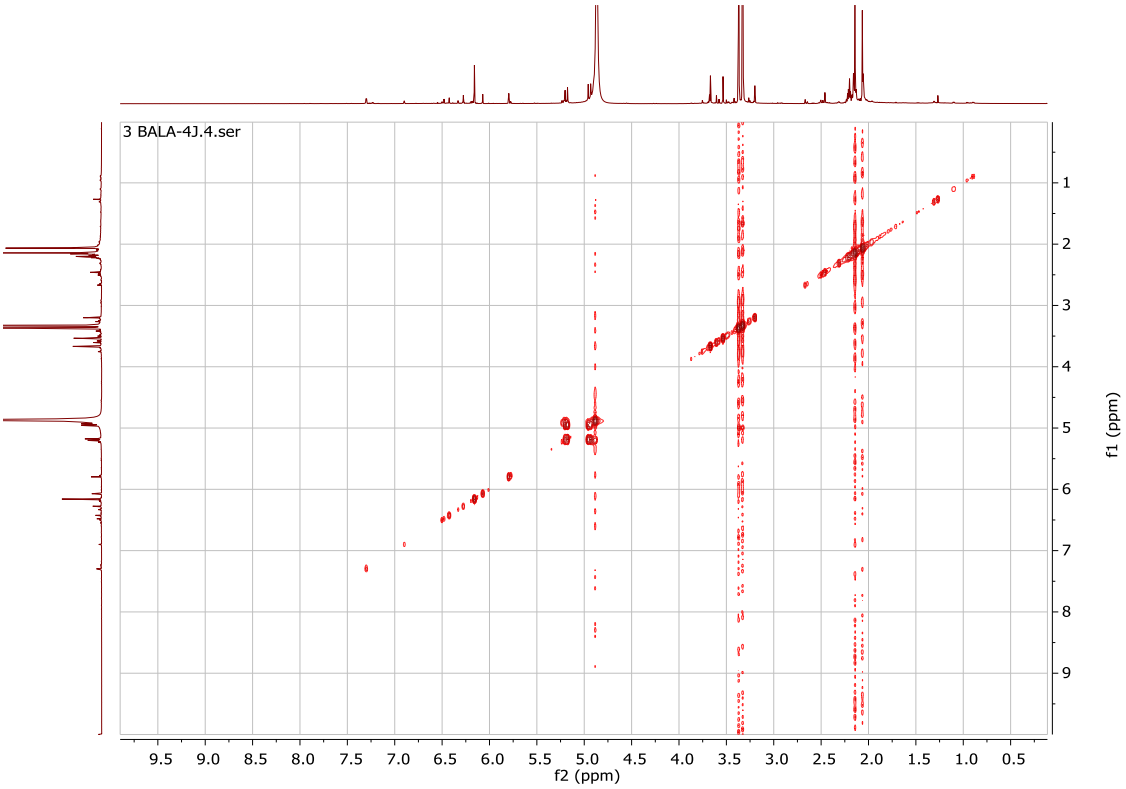

Appendix 198: HSQC (MeOD-d_4) spectrum of **46** (^{1}H: 600 MHz, ^{13}C: 175 MHz)

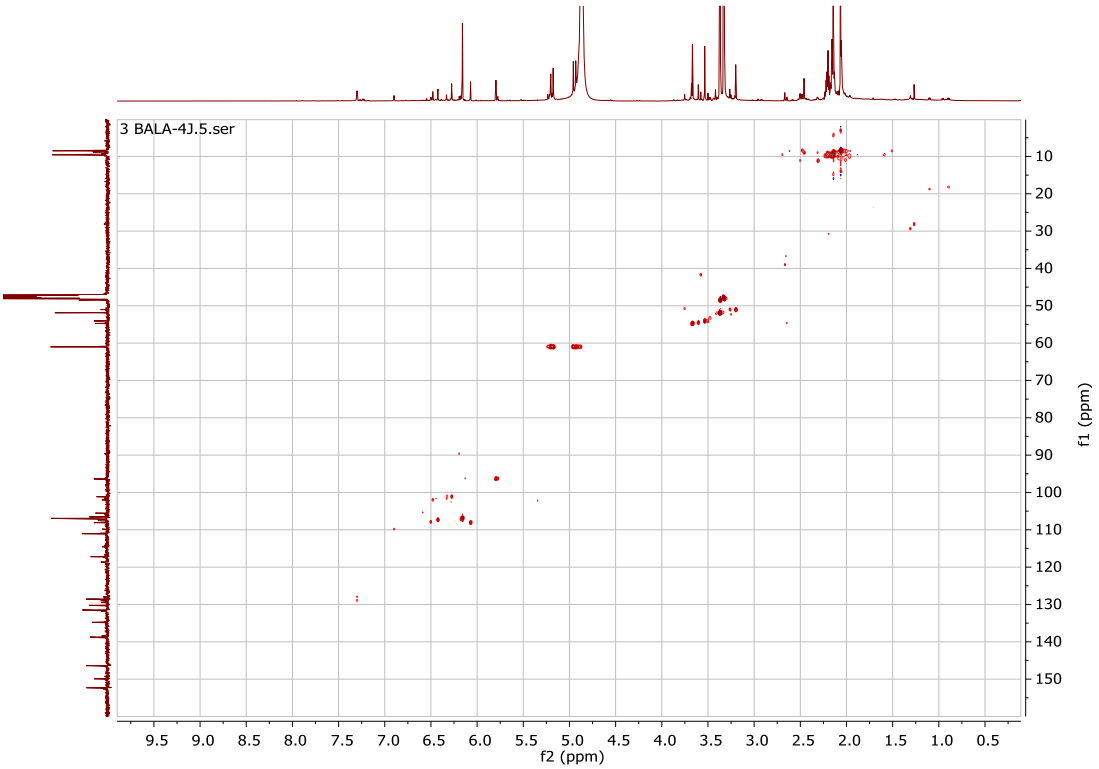

Appendix 199: HMBC (MeOD-d_4) spectrum of **46** (^{1}H: 600 MHz, ^{13}C: 175 MHz)

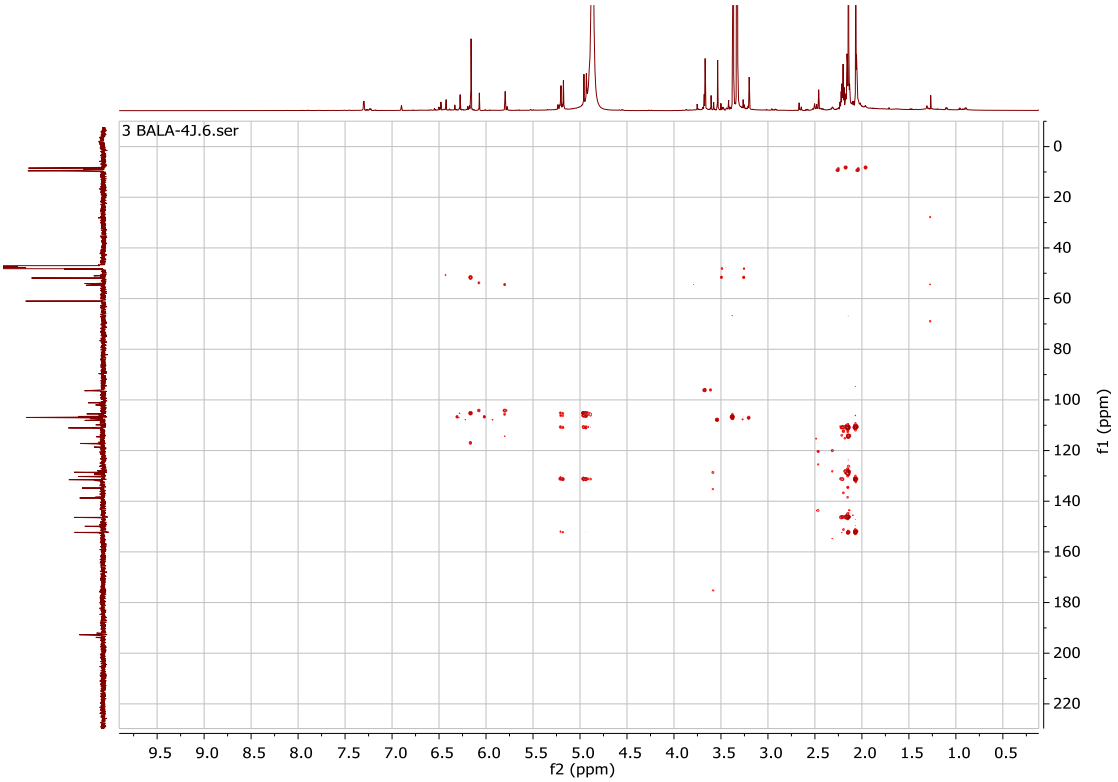

Appendix 200: Publication 1

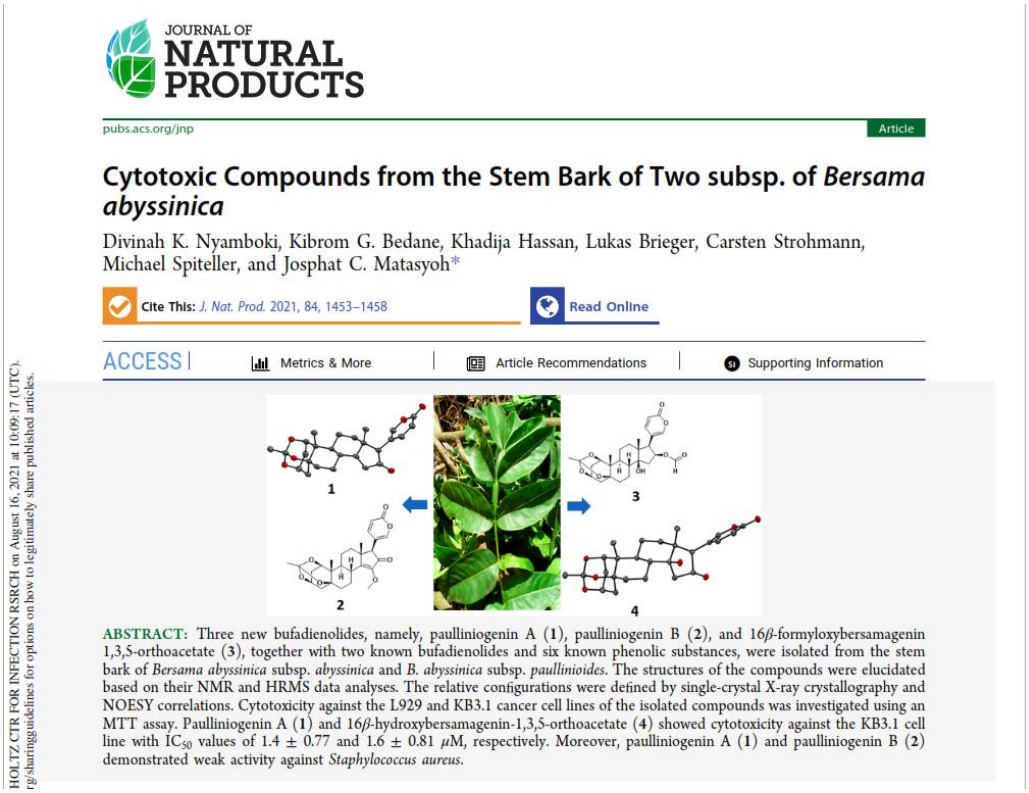

JOURNAL OF NATURAL PRODUCTS

pubs.acs.org/jnp Article

Cytotoxic Compounds from the Stem Bark of Two subsp. of *Bersama abyssinica*

Divinah K. Nyamboki, Kibrom G. Bedane, Khadija Hassan, Lukas Brieger, Carsten Strohmann, Michael Spiteller, and Josphat C. Matasyoh*

Cite This: *J. Nat. Prod.* 2021, 84, 1453−1458 Read Online

ACCESS | Metrics & More | Article Recommendations | Supporting Information

ABSTRACT: Three new bufadienolides, namely, paulliniogenin A (**1**), paulliniogenin B (**2**), and 16β-formyloxybersamagenin 1,3,5-orthoacetate (**3**), together with two known bufadienolides and six known phenolic substances, were isolated from the stem bark of *Bersama abyssinica* subsp. *abyssinica* and *B. abyssinica* subsp. *paullinioides*. The structures of the compounds were elucidated based on their NMR and HRMS data analyses. The relative configurations were defined by single-crystal X-ray crystallography and NOESY correlations. Cytotoxicity against the L929 and KB3.1 cancer cell lines of the isolated compounds was investigated using an MTT assay. Paulliniogenin A (**1**) and 16β-hydroxybersamagenin-1,3,5-orthoacetate (**4**) showed cytotoxicity against the KB3.1 cell line with IC_{50} values of 1.4 ± 0.77 and 1.6 ± 0.81 μM, respectively. Moreover, paulliniogenin A (**1**) and paulliniogenin B (**2**) demonstrated weak activity against *Staphylococcus aureus*.

Appendix 201: Publication 2

Phytochemistry 198 (2022) 113153

Contents lists available at ScienceDirect

Phytochemistry

journal homepage: www.elsevier.com/locate/phytochem

Cytotoxic compounds from the leaf of *Bersama abyssinica* subspecies *abyssinica*

Divinah Kwamboka Nyamboki [a,d], Kibrom Gebreheiwot Bedane [a,e], Khadija Hassan [b,c], Michael Spiteller [a], Josphat Clement Matasyoh [a,d,*]

[a] Institute of Environmental Research (INFU), Department of Chemistry and Chemical Biology, TU Dortmund, Otto-Hahn-Straße 6, 44227, Dortmund, Germany
[b] Department of Microbial Drugs, Helmholtz Centre for Infection Research, 38124, Braunschweig, Germany
[c] German Centre for Infection Research (DZIF), Partner Site Hannover-Braunschweig, 38124, Braunschweig, Germany
[d] Department of Chemistry, Faculty of Sciences, Egerton University, P.O. Box 536, 20115, Egerton, Kenya
[e] Department of Chemistry, Addis Ababa University, P.O. Box 33658, Addis Ababa, Ethiopia

ARTICLE INFO

Keywords:
Bersama abyssinica
Melianthaceae
Cytotoxicity
Bufadienolides
KB3.1 cell lines

ABSTRACT

From the leaves of Kenyan medicinal plant *Bersama abyssinica* Subspecies *abyssinica*, four previously undescribed compounds namely, three bufadienolides, 10β-formylpaulliniogenin B, 10β-formylpaulliniogenin A and 1β-acetoxy-3β,5β-dihydroxy-15-methoxy-16,19-dioxobufa-14(15),20,22-trienolide, and a phenolic compound 2,6,4′-trihydroxybenzophenone-4-O-(6‴-cinnamoyl)-β-D-glucoside were isolated together with four known compounds. The structural elucidation of the compounds was based on 1D and 2D NMR spectroscopy and HRMS data analyses. The relative configurations were defined by NOESY correlations. Cytotoxic activities on L929 and KB3.1 cell lines of the isolated compounds were investigated using MTT assay. The 1β-acetoxy-3β,5β-dihydroxy-15-methoxy-16,19-dioxobufa-14(15),20,22-trienolide showed significant cytotoxic activity against KB3.1 cell lines with IC_{50} of 3.9 ± 0.99 μM.

Appendix 202: NACOSTI permit

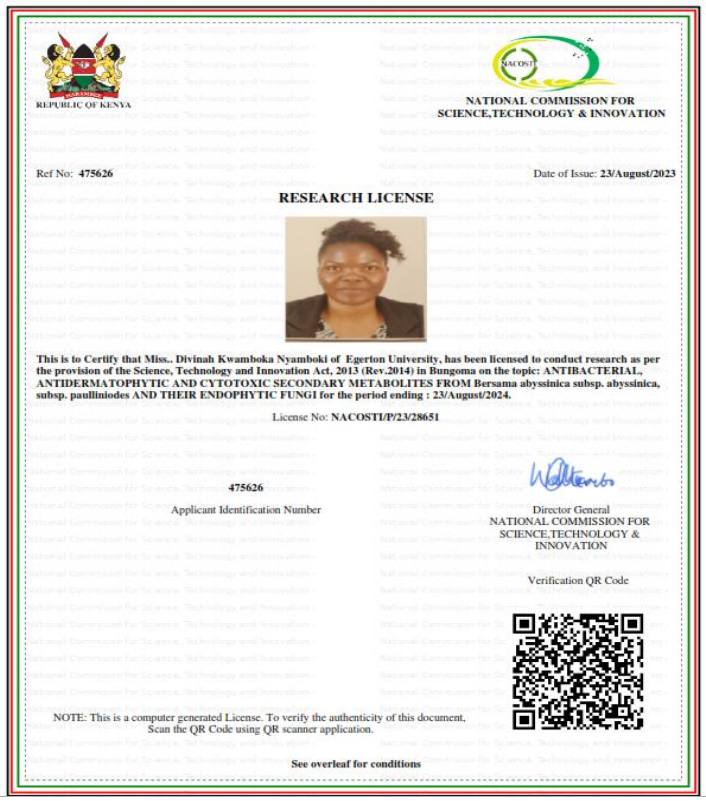

REPUBLIC OF KENYA

NATIONAL COMMISSION FOR SCIENCE,TECHNOLOGY & INNOVATION

Ref No: **475626**

Date of Issue: **23/August/2023**

RESEARCH LICENSE

This is to Certify that Miss., Divinah Kwamboka Nyamboki of Egerton University, has been licensed to conduct research as per the provision of the Science, Technology and Innovation Act, 2013 (Rev.2014) in Bungoma on the topic: ANTIBACTERIAL, ANTIDERMATOPHYTIC AND CYTOTOXIC SECONDARY METABOLITES FROM Bersama abyssinica subsp. abyssinica, subsp. paulliniodes AND THEIR ENDOPHYTIC FUNGI for the period ending : 23/August/2024.

License No: **NACOSTI/P/23/28651**

475626

Applicant Identification Number

Director General
NATIONAL COMMISSION FOR SCIENCE,TECHNOLOGY & INNOVATION

Verification QR Code

NOTE: This is a computer generated License. To verify the authenticity of this document, Scan the QR Code using QR scanner application.

See overleaf for conditions